



NRL/MR/6180--99-8337

Tests of Alternative Fire Protection Method for USAF Hangars

S. A. HILL
J. L. SCHEFFEY

*Hughes Associates, Inc.
Baltimore, Maryland*

F. WALKER

*Air Force Civil Engineering Support Agency
Tyndall Air Force Base, Florida*

F. W. WILLIAMS

*Navy Technology Center for Safety and Survivability
Chemistry Division*

February 8, 1999

Approved for public release; distribution unlimited.

19990218012

REPORT DOCUMENTATION PAGE

Form Approved
OMB No. 0704-0188

Public reporting burden for this collection of information is estimated to average 1 hour per response, including the time for reviewing instructions, searching existing data sources, gathering and maintaining the data needed, and completing and reviewing the collection of information. Send comments regarding this burden estimate or any other aspect of this collection of information, including suggestions for reducing this burden, to Washington Headquarters Services, Directorate for Information Operations and Reports, 1215 Jefferson Davis Highway, Suite 1204, Arlington, VA 22202-4302, and to the Office of Management and Budget, Paperwork Reduction Project (0704-0188), Washington, DC 20503.

1. AGENCY USE ONLY (Leave Blank)		2. REPORT DATE February 8, 1999		3. REPORT TYPE AND DATES COVERED	
4. TITLE AND SUBTITLE Tests of Alternative Fire Protection Methods for USAF Hangars				5. FUNDING NUMBERS N28 FY98 00204	
6. AUTHOR(S) S.A. Hill,* J.L. Scheffey,* and F. Walker,† and F.W. Williams					
7. PERFORMING ORGANIZATION NAME(S) AND ADDRESS(ES) Naval Research Laboratory Washington, DC 20375-5320				8. PERFORMING ORGANIZATION REPORT NUMBER NRL/MR/6180--99-8337	
9. SPONSORING/MONITORING AGENCY NAME(S) AND ADDRESS(ES) U.S. Air Force, HQ AFCEA/CESM (F. Walker) 139 Barnes Drive, Suite 1 Tyndall AFB, FL 32403-5319				10. SPONSORING/MONITORING AGENCY REPORT NUMBER	
11. SUPPLEMENTARY NOTES *Hughes Associates, Inc., Baltimore, MD †Air Force Civil Engineering Support Agency, Arlington, VA					
12a. DISTRIBUTION/AVAILABILITY STATEMENT Approved for public release; distribution unlimited.				12b. DISTRIBUTION CODE A	
13. ABSTRACT (Maximum 200 words) The use of AFFF in overhead suppression systems in aircraft hangars continues to create problems as a result of false discharges and environmental concerns. Two replacement concepts are proposed: the use of water suppression systems to control JP-8 fires and limit fire growth to an acceptable level; and the use of a Mobile Compressed Air Foam Fire Suppression System (MCAFFSS) to protect aircraft in a hangar. Water suppression systems were tested to determine the impact on flame spread and fire growth of the spill fire. The variables investigated included sprinkler application rate and time of sprinkler water discharge. The results showed that the water sprinklers were not capable of preventing flame spread and fire growth on a JP-8 fuel spill. The MCAFFSS unit tested consisted of a premixed AFFF discharged through an oscillating monitor nozzle. Included was a combination UV/IR optical fire detector designed to sense a fuel fire when it is relatively small. Variables evaluated included actuation time, effect of foam aspiration, effect of discharge methods and effect of obstructions. The unit was able to detect and control/extinguish JP-8 spill fires. Tests conducted with obstructions, indicate that obstructions affect the performance of the unit. The technique of targeting the foam at an area in front of the hazard (aircraft) being protected and pushing the foam across the floor, was shown to be the most effective. Non-air aspirated foam was shown to be as effective as air aspirated foam. The location of the fire detector with respect to the fire and obstructions had an effect on detection time.					
14. SUBJECT TERMS Aviation fuel Spill fires Hangar protection				15. NUMBER OF PAGES 385	
				16. PRICE CODE	
17. SECURITY CLASSIFICATION OF REPORT UNCLASSIFIED	18. SECURITY CLASSIFICATION OF THIS PAGE UNCLASSIFIED	19. SECURITY CLASSIFICATION OF ABSTRACT UNCLASSIFIED	20. LIMITATION OF ABSTRACT UL		

NSN 7540-01-280-5500

Standard Form 298 (Rev. 2-89)
Prescribed by ANSI Std Z39-18
298-102

CONTENTS

EXECUTIVE SUMMARY	ix
1.0 INTRODUCTION	1
1.1 Background	1
1.2 Factory Mutual Research Corporation Tests	1
1.3 Spill Sizes and Scenarios	2
2.0 OBJECTIVE	3
3.0 APPROACH	3
4.0 TEST SETUP AND PROCEDURES	4
4.1 Test Facility	4
4.2 Instrumentation	4
4.2.1 Thermocouples	4
4.2.2 Calorimeters	10
4.2.3 Flowmeters	10
4.2.4 Sprinkler System Pressure Transducers	10
4.2.5 Bidirectional Velocity Probes	10
4.2.6 Video Cameras	10
4.2.7 Photographic Cameras	12
4.2.8 Visual Aids	12
4.3 Background Burns	12
4.4 Overhead Sprinkler System Testing	12
4.5 MCAFFSS Testing	13
4.5.1 MCAFFSS	13
4.5.2 Obstructions	15
4.5.3 Pad Modifications	20
4.5.4 Reignition Test Procedures	20
4.6 Test Procedures	25
4.6.1 Fuel Dump Apparatus and Ignition Procedure	25
4.6.2 General Test Procedures	25
5.0 MEASURES OF PERFORMANCE	27
6.0 RESULTS	27
6.1 Background Burns	27
6.1.1 Results of Diesel Spill Fire Tests (BB1-BB5)	29
6.1.2 Results of Test BB6	29

6.1.3	Results of Test BB7	30
6.1.4	Results of Test BB8	30
6.2	Sprinkler Tests	30
6.2.1	Results of Test S1	33
6.2.2	Results of Test S2	33
6.2.3	Results of Test S3	35
6.2.4	Results of Test S4	35
6.2.5	Results of Test S5	36
6.2.6	Results of Test S6	36
6.2.7	Results of Test S7	36
6.3	MCAFFSS Tests	37
6.3.1	Results of Test F1	39
6.3.2	Results of Test F2	39
6.3.3	Results of Test F3	39
6.3.4	Results of Test F4	40
6.3.5	Results of Test F5	41
6.3.6	Results of Test F6	44
6.3.7	Results of Test F7	44
6.3.8	Results of Test F8	46
6.3.9	Results of Test F9	47
7.0	DISCUSSION	48
7.1	Background Burns	48
7.1.1	Effects of Pad Temperature on Fire Spread and Size	48
7.2	Overhead Sprinkler Tests	48
7.2.1	Performance of Overhead Sprinkler Systems	49
7.3	MCAFFSS Tests	52
7.3.1	Performance of Fire Detector	52
7.3.2	Air Aspirated vs. Non-air Aspirated AFFF	53
7.3.3	Effect of Nozzle Orientation on Effectiveness of MCAFFSS	54
7.3.4	Effect of Obstructions on Effectiveness of MCAFFSS	55
7.3.5	Effect of Turret Oscillation Angle on Effectiveness of MCAFFSS	55
7.3.6	Effect of Off-Axis Location on Effectiveness of MCAFFSS	56
8.0	ENGINEERING ANALYSIS OF MCAFFSS	56
8.1	Technical Requirements	56
8.1.1	Existing Design Basis	57
8.1.2	Redefined Technical Requirement	58
8.2	Performance Evaluation	59
8.2.1	Detection	59
8.2.2	Fire Suppression	60
8.2.2.1	Application Rate	60
8.2.2.2	Foam Duration	60

8.2.2.3	Pattern/coverage	63
8.2.2.4	MCAFFSS Hardware Design	64
9.0	CONCLUSIONS	65
9.1	Water Sprinkler System	65
9.2	MCAFFSS	66
10.0	ACKNOWLEDGMENTS	67
11.0	REFERENCES	67
APPENDIX A - Results of JP-8 Background Burns (Tests BB6-BB8)		A-1
APPENDIX B - Overhead Sprinkler System Test Data		B-1
APPENDIX C - MCAFFSS Test Data		C-1
APPENDIX D - Concept Package For The Use of a Mobile Automatic Fire Extinguisher In Aircraft Hangars		D-1

FIGURES

Figure 1 – Test area	5
Figure 2 – Cement board barrier	6
Figure 3 – Backup AFFF system	7
Figure 4 – Instrumentation key	8
Figure 5 – Instrumentation layout	9
Figure 6 – Overhead sprinkler locations	11
Figure 7 – MCAFFSS unit	14
Figure 8 – MCAFFSS and pad configuration for Tests F1-F8	16
Figure 9 – MCAFFSS and pad configuration for Test F9	17
Figure 10 – Obstruction layout for Tests F3-F5	18
Figure 11 – Obstructions used for Tests F3-F5	19
Figure 12 – Obstructions layout for Tests F6-F9	21
Figure 13 – Elevation view of drywall addition to simulated fuselage	22
Figure 14 – Drywall addition to simulated fuselage (Tests F6-F9)	23
Figure 15 – MIL SPEC burnback pan	24
Figure 16 – Fuel dump apparatus	26
Figure 17 – Fully involved spill fire in Test BB8	31
Figure 18 – Fire growth in Test S2	34
Figure 19 – Foam spray over obstruction in Test F4	42
Figure 20 – Sustained reignition in Test F5	43
Figure 21 – Foam spray in Test F7	45
Figure 22 – Fire control and extinguishing times as a function of solution application rate using AFFF at 250, 400, and 800 gpm on 743 m ² (8000 ft ²) JP-4 fuel fires [21] ...	61
Figure 23 – AFFF control time as a function of application rate [22]	62

TABLES

Table 1. Summary of Diesel Background Burns (Tests BB1-BB5)	28
Table 2. Results of JP-8 Background Burns (Tests BB6-BB8)	28
Table 3. Results of Overhead Sprinkler System Tests	32
Table 4. MCAFFSS Test Results	38
Table 5. Average Flame Spread Rates Before and After Sprinkler System Activation	50
Table 6. Summary of Fire Detector Performance Data	52

EXECUTIVE SUMMARY

The use of Aqueous Film Forming Foam (AFFF) in overhead suppression systems in aircraft hangars continues to create problems as a result of false discharges and environmental concerns. The U.S. Air Force (USAF) is conducting research and development to address these issues. As part of this R&D, two concepts were proposed: the use of water suppression systems to control JP-8 fires and limit fire growth to an acceptable level; and, the use of a Mobile Compressed Air Foam Fire Suppression System (MCAFFSS) to protect aircraft in a hangar. This report describes the results of test and evaluation of these two concepts.

Fire tests were conducted in the large-scale fire test facility located at the Underwriters Laboratories complex in Northbrook, IL. The facility ceiling was set to a height of 15 m (48 ft). A temporary concrete pad was constructed on which JP-8 fuel was spilled and ignited. The spill scenario involved 114 L (30 gal) of JP-8 fuel, which was ignited immediately after it was dumped. Without suppression systems, the fire grew at a constant rate and peaked at a maximum free-burn size of 37 m² (400 ft²) 75 seconds after ignition. The total burn time was on the order of 2 minutes.

Water suppression systems were tested to determine the impact on flame spread and fire growth. The suppression systems were designed to represent actual USAF hangar installations. The variables investigated included sprinkler application rate (6.9 and 10.2 Lpm/m² (0.17 and 0.25 gpm/ft²)) and time of sprinkler water discharge. Deluge (open-head) sprinklers were activated immediately after ignition and 30 and 80 seconds after ignition, quick response closed-head sprinklers were also investigated. The results showed that the water sprinklers were not capable of preventing flame spread and fire growth on a JP-8 fuel spill. Fires typically grew to the full free-burn size 37 m² (400 ft²) even with suppression systems activated. If JP-8 ignites, water suppression systems of the magnitude used in these tests cannot be relied upon to prevent continued fire growth. The fire will likely grow to the size of the spill.

The MCAFFSS unit tested included a 454 L (120 gal) tank of premixed AFFF discharged through an oscillating monitor nozzle. Included was a combination UV/IR optical fire detector designed to sense a fuel fire when it is relatively small. The unit is intended to be located in a hangar to protect target hazard areas, e.g., areas in, around and under parked aircraft. The breadboard unit was tested using the same spill fire scenario as in the sprinkler tests. Variables evaluated included actuation time (with the unit set in the automatic and manual modes), effect of foam aspiration, effect of discharge methods ("targeting" a hazard compared to "pushing" foam along a hangar floor), and effect of obstructions (simulated aircraft frames and equipment).

The breadboard MCAFFSS unit evaluated in these tests would not meet current military and national consensus standards as a one-to-one replacement for fixed hangar fire protection systems. Within the parameters tested, the MCAFFSS can detect and operate to control/extinguish JP-8 fuel spill fires. Obstructions which might be found in a hangar have an impact on performance. It was found that the current USAF fire protection design approach for floor nozzle orientation is the appropriate approach. The best results were obtained when agent

was discharged on the floor at the edge of the hazard and the nozzle stream allowed to push the agent below and around obstructions. It was found that a commercial-off-the-shelf (COTS), non-air aspirating nozzle was as effective as the air aspirating nozzle; air injection for aeration is unnecessary. Obstructions and alignment affected detection time, but the times were within acceptable limits. Placement of the MCAFFSS as currently designed would likely be more dependent on nozzle spray pattern characteristics than on detection range limitations. Placement of the units with respect to fuel spill hazards, ignition sources, spray pattern area and aircraft/maintenance obstructions requires careful consideration if the units are designed to "target" hazards and not provide total floor area coverage.

A preliminary engineering evaluation of the MCAFFSS concept was performed. Significant operational and logistical questions remain regarding the feasibility of fielding the unit. Although intended to replace fixed detection and suppression systems, the level of fire protection which would be provided by the system as currently designed is not equivalent to that established by USAF design guidelines. The system should be assessed in terms of providing a similar level of established protection. Alternately, the technical requirements which have led to the established design criteria should be reassessed to consider changes in the fire hazard, environmental impact of suppression systems and the acceptable risk posture of management. In terms of the MCAFFSS concept, a significant unknown is related not to its fire performance capability, but operational viability. Because the feasibility of the MCAFFSS concept is in question, this element of a technical requirements review should be a high priority in any advancement of the concept.

Since a number of aspects related to current design requirements have been raised (e.g., impact of JP-8 replacement of JP-4, detector actuation in high-bay spaces, environmental impact of foam and optical detector performance and reliability), a complete reassessment of the hangar technical requirements appears to be warranted. A key element of this assessment would be the quantification of the acceptable level of risk (i.e., damage to aircraft and structure) consistent with the expected performance of the protection system. A fire hazard analysis could be used to quantify the risk and system performance.

TESTS OF ALTERNATIVE FIRE PROTECTION METHODS FOR USAF HANGARS

1.0 INTRODUCTION

1.1 Background

The use of Aqueous Film Forming Foam (AFFF) in overhead suppression systems in aircraft hangars continues to create problems as a result of false discharges and environmental concerns. The US Air Force (USAF) proposed a potential approach that would utilize only water sprinklers in the overhead of a hangar. It has been stated [1] that deluge sprinkler systems can effectively deal with fires less than 37 m² (400 ft²) based on Factory Mutual Research Corporation (FM) tests [2]. Based on this position, it was proposed that water-based systems might have the potential to:

- (1) Control JP-8 and JP-5 fires without irreparable damage to the incident aircraft until extinguishment by fire department personnel; and
- (2) Prevent JP-8 and JP-5 fires from involving more than 37 m² (400 ft²) of continuous fuel surface.

An additional potential solution would utilize a Mobile Compressed Air Foam Fire Suppression System (MCAFFSS) to protect aircraft in a hangar. In the past when fuels of greater volatility were used, a fuel spill fire would grow to its full extent within a few seconds after ignition. As a result, overhead fire suppression systems were designed to deluge large areas as soon as possible. Given the slower propagation of JP-8 fires, it was proposed that mobile suppression systems protecting a single aircraft may potentially control and extinguish a fuel spill fire before it becomes a threat.

1.2 Factory Mutual Research Corporation Tests

The basis for the 37 m² (400 ft²) limitation was tests conducted by Factory Mutual Research Corporation (FM) [2]. In pool and running fuel fire tests with deluge water sprinkler systems in a 60 ft (18 m) high test building, the most serious fire situations occurred where fires formed a single, strong turbulent plume. These conditions were observed with large (> 37 m² (400 ft²)) pool fires, and in some cases with spill fires (created by continuously flowing jet fuel) where ambient conditions (e.g., no wind) allowed the formation of a single plume. In many cases with the spill fire and deluge sprinkler operation, multiple plumes were formed. This resulted in a less severe fire since flames did not extend to the roof and radiation feed back to the pool surface was interrupted. It was observed during the spill fire tests that fuel floating on water was easily disrupted by winds and drafts and often broke up into small pools. In all of the fires with multiple plume formation and in the 37 m² (400 ft²) pool fires, water deluge systems at 6.9 and

10.2 Lpm/m² (0.17 and 0.25 gpm/ft²) densities provided adequate protection for the building and structural steel specimens. The measure of performance for the FM tests was the temperature of critical structural roof steel elements. No assessment of the impact of fires on adjacent targets (i.e., non-intimate aircraft) was performed. Under certain conditions (pool fires larger than 37 m² (400 ft²) and spill fires where a single plume was formed), water deluge systems discharging at densities up to 10.2 Lpm/m² (0.25 gpm/ft²) did not provide adequate protection to the roof steel.

During the FM tests it was observed that several conditions were required in order for a single, turbulent fire plume to exist:

- (1) First, relatively quiescent ambient conditions so that strong drafts would not disrupt plume formation or cause excessive heat loss in the lower portion of the plume through rapid entrainment of air;
- (2) Second, a fire area of sufficient size so that the mixing of fuel vapors and air would be inefficient near the pool interface and an excess of fuel vapors would be present in the plume and
- (3) Finally, a pool of sufficient depth to provide a continuous, uninterrupted liquid fuel source.

1.3 Spill Sizes and Scenarios

Anecdotal data on spills in USAF hangars indicates that continuous fuel-fed spill scenarios are very rare. The more likely scenario would involve a dump of a fuel cell that results in a pool of fuel [3]. For a given quantity of fuel, the pool spreads to its maximum size based on governing hydrodynamics, including fuel viscosity and surface tension and the roughness and sloping of the floor.

The USAF conducted an investigation of JP-4 fuel spills on a level concrete runway [4]. These tests were used to investigate the area of spills both before and after ignition. It was found that the area of fire likely to occur from a fuel spill is a function of the quantity of fuel spilled and the time allowed for the fuel to spread. It was also found that the area of coverage per gallon decreased considerably as the quantity of fuel spilled increased. It was also found that the size of the spill increased after ignition. For example, the area covered per gallon before ignition averaged 2.9 m² (31 ft²) when only 3.8 L (1 gal) was spilled. When 76 L (20 gal) were spilled, the average coverage area was 0.37 m²/L (15 ft²/gal). Likewise, after ignition, the average coverage area was 1.0 m²/L (41 ft²/gal) when only 3.8 L (1 gal) was spilled. When 76 L (20 gal) were spilled the average was about 0.51 m²/L (21 ft²/gal). The spill size increased on the order of 20 to 50 percent after the spill was ignited. The spills burned out between 42 and 120 seconds. For spills allowed to spread the longest time (2 min), the fire duration was on the order of 1 minute.

The minimum area covered by 3.8 L (1 gal) was 1.2 m² (13 ft²), which corresponds to a fuel layer 3.1 mm (0.123 in.) thick. The maximum area per gallon was 4.5 m² (48 ft²) or a film thickness of 0.8 mm (0.033 in.). The thicker fuel layers did not burn longer than thinner films,

but burn times were generally longer when the fuel had less time to spread out. It was observed that for this to happen, the fuel must have been consumed at different rates.

The Naval Research Laboratory (NRL) has quantified the flame spread across jet fuels [5]. At 27°C (80°F) the flame spread of JP-8 (10.1 cm/s (4.0 in./s)) is roughly equivalent to JP-5 (8.1 cm/s (3.2 in./s)). At 49°C (120°F), the flame spread rate of JP-8 is 27.0 cm/s (10.6 in./s). Flame spread on both fuels are an order of magnitude less than JP-4 (190 cm/s (75 in./s)). For a 37 m² (400 ft²) JP-8 fire, total involvement of the pool area, using ambient temperature flame spread rates, would be estimated on the order of 1 minute.

2.0 OBJECTIVE

The objective of this fire test series was to determine whether the use of deluge or closed head sprinkler systems could control static JP-8 pool fires. The use of a mobile compressed air foam fire suppression system (MCAFFSS) was also evaluated. Data on JP-8 static fuel spills, currently not documented in the literature, were collected. This data will be useful in assessing the overall risk to aircraft.

Control was defined in terms of disrupting the fire so that a single, turbulent plume was not established, stopping or significantly reducing flame spread across the fuel surface area, limiting building structural steel temperatures below critical values and limiting heat flux to adjacent targets (simulating adjacent aircraft).

3.0 APPROACH

Spill fire tests were conducted in accordance with the test plan [6] to assess the impact of water sprinklers and MCAFFSS on spill fire growth. Background tests were conducted with spills of various quantities of diesel and JP-8 to develop the design fire and to establish the baseline threat. These tests were used to quantify the size of the spill before ignition, the speed of flame spread and the duration of the burn. Temperature and heat flux measurements were taken at various locations in the test area to quantify the threat to the structural roof steel and adjacent aircraft.

The spill scenarios were repeated using the best-case sprinkler suppression scenario: deluge sprinklers operating immediately after fire ignition. The impact of the sprinklers in controlling the fire was assessed. Deluge sprinkler tests were then conducted with 30 and 80 second time delays before activation. Closed head sprinkler tests were also conducted. Two water densities were evaluated for both the deluge and closed head system tests.

The MCAFFSS has been proposed for use as a cost-effective alternative to low level AFFF suppression systems. To date, demonstrations have been conducted which indicate that the unit can detect a fire and discharge foam to extinguish a static aviation fuel fire. There are numerous design/installation issues related to the potential use of the portable MCAFFSS unit in a hangar. These issues are discussed in detail later in this report. During this test series, the need

to use compressed air foam, in place of non-air aspirated AFFF, was evaluated. The detection capability of the unit in an off-axis configuration (i.e., detector not located directly in front of the fire) was also evaluated. Obstructions were added during the MCAFFSS tests to simulate equipment found in a hangar. These tests were used to evaluate different discharge tactics. Tests were also conducted to evaluate the effect of varying the effective application rate of the agent.

4.0 TEST SETUP AND PROCEDURES

4.1 Test Facility

The tests were conducted in the large-scale fire test facility located at the Underwriters Laboratories complex in Northbrook, IL. The facility was 36 m (120 ft) x 36 m (120 ft) x 17 m (55 ft) high. The facility was equipped with a 30 m (100 ft) x 30 m (100 ft) moveable ceiling. The ceiling height was adjustable from 1.8 m (6 ft) to 15 m (48 ft). For this test series, the ceiling of the test facility was set at the maximum height of 15 m (48 ft). The facility was configured as shown in Figure 1 (pad viewed from West). A temporary concrete pad measuring 8.5 m (28 ft) by 9.1 m (30 ft) and 20 cm (8 in.) thick was installed in the center of the facility. The slab was constructed using 1.2 m (4 ft) x 4.6 m (15 ft) x 20 cm (8 in.) thick spancrete slab sections. The interface cracks were filled and smoothed. Every effort was made to keep the pad as level as possible, but it did have noticeable high and low spots. Barriers were located around the perimeter of the North, East and South edges of the pad. The barrier consisted of 2.4 m (8 ft) x 0.6 m (2 ft) sections of cement board positioned such that the barrier was 0.6 m (2.0 ft) high (Figure 2). Cement blocks were used to hold the cement board in place against the edge of the temporary pad. The interface between the cement board and the temporary pad was sealed with aluminum tape to prevent leakage from the temporary pad. The West edge of the temporary pad remained open to act as a drain area.

A fixed, low-level AFFF system, shown in Figure 3, was installed around the pad to act as a safety suppression system. The system consisted of two nozzles (Bete Model NF80) supplied by a 2.5 cm (1.0 in.) diameter pipe network. The piping was connected to a 3.8 cm (1.5 in.) diameter fire hose. The fire hose was connected to an eductor which was supplied by a 208 L (55 gal) drum of 3% MIL SPEC AFFF [7]. Water was supplied to the system via an existing fire hose connection in the test area. In addition to the low-level AFFF system, there were two hoselines charged and positioned at opposite ends of the test area.

4.2 Instrumentation

4.2.1 Thermocouples

Thermocouples were installed to measure ceiling gas temperatures, steel temperatures and concrete temperatures. An instrumentation key is provided in Figure 4 and the instrumentation layout is shown in Figure 5. A total of 33 air thermocouples were installed below the ceiling. These thermocouples were positioned 15 cm (6 in.) below the ceiling above the center of the pad and in three concentric rings around the center. The rings had diameters of 3.0 m (10 ft), 4.6 m (15 ft), and 7.6 m (25 ft). The rings had 7, 8 and 16 thermocouples positioned around the

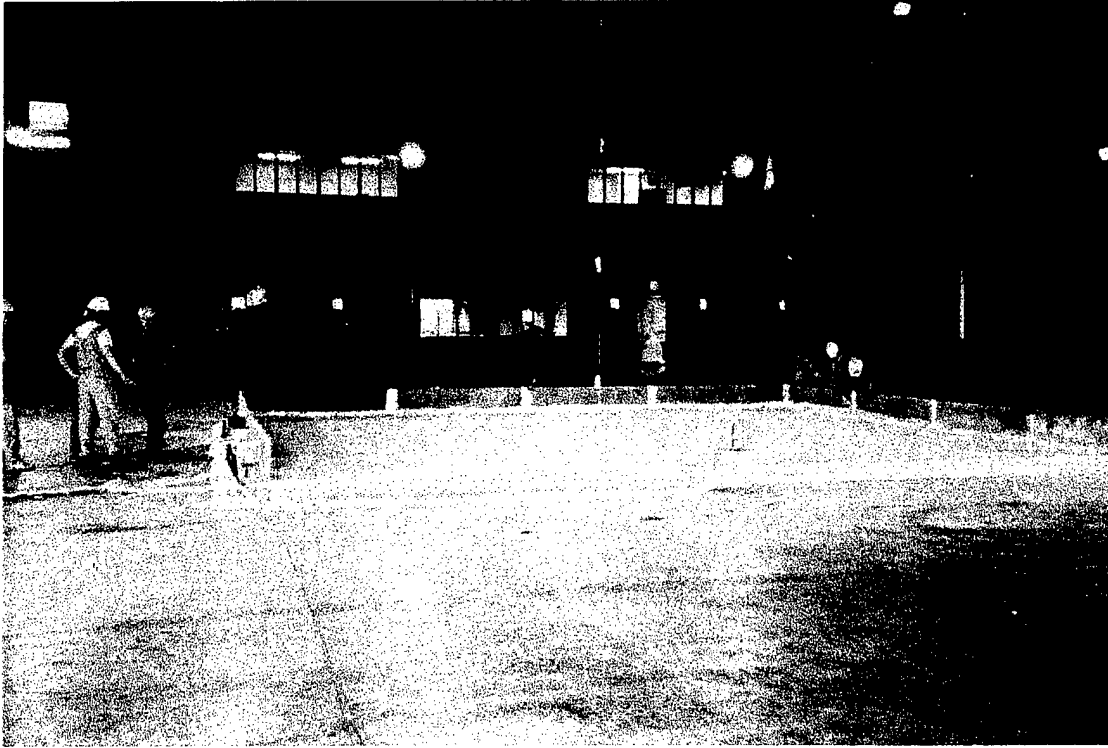


Figure 1 — Test area



Figure 2 — Cement board barrier

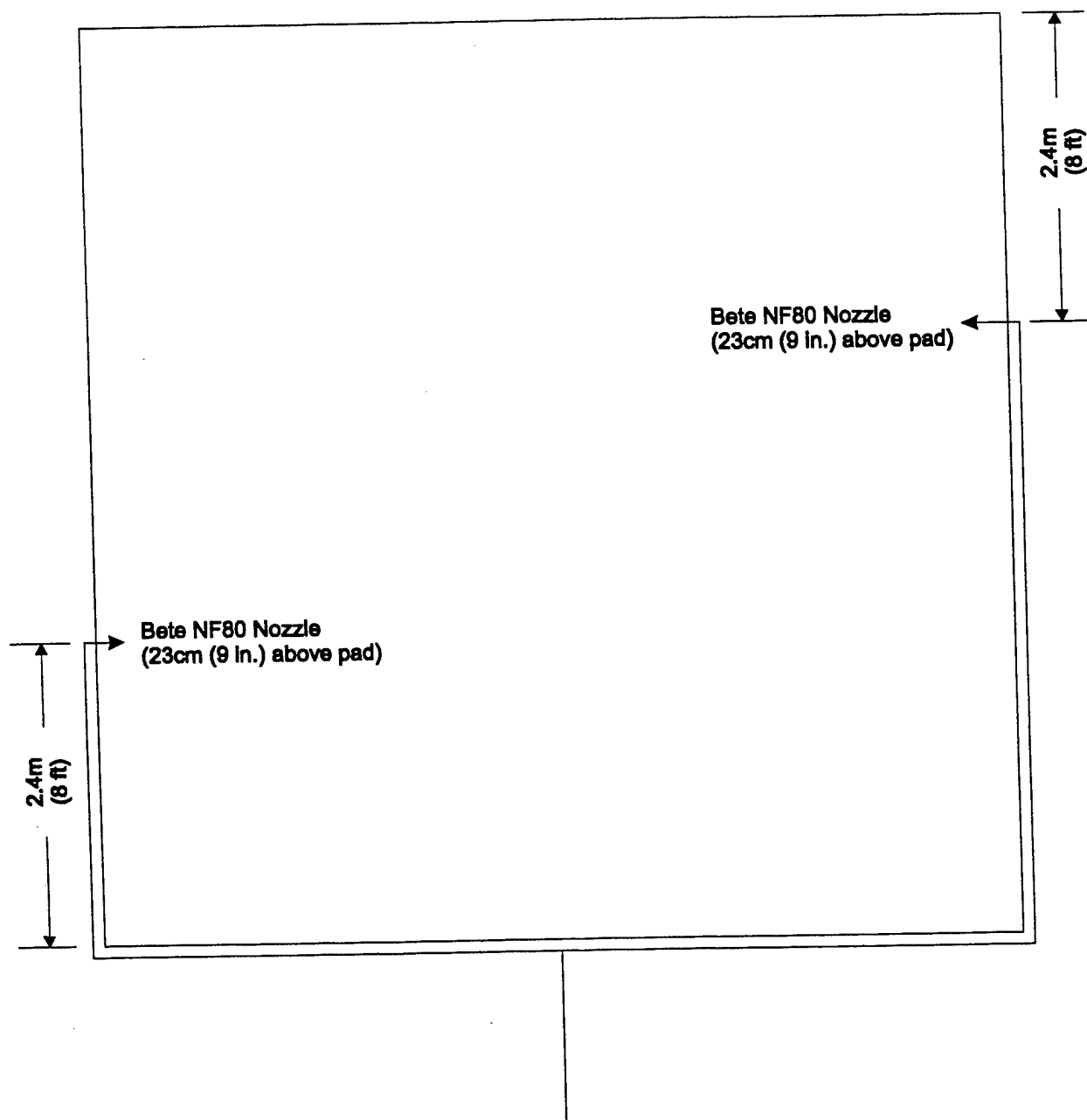


Figure 3 — Backup AFFF system

LEGEND

<hr/> S	Steel Temperatures
(B _h)	Horizontal Bi-Flow positioned 0.3m (12 in.) below ceiling
(B _v)	Vertical Bi-Flow positioned 1.5cm (6 in.) below ceiling
(C)	Calorimeter positioned 0.5m (1.7 ft.) above temporary pad
(T _a)	Air thermocouple positioned 15cm (6 in.) below ceiling
(T _c)	(2) Concrete TCs: (1) below surface and (1) 1.3cm (0.5 in.) below surface
(P)	Firemain pressure

Figure 4 — Instrumentation key

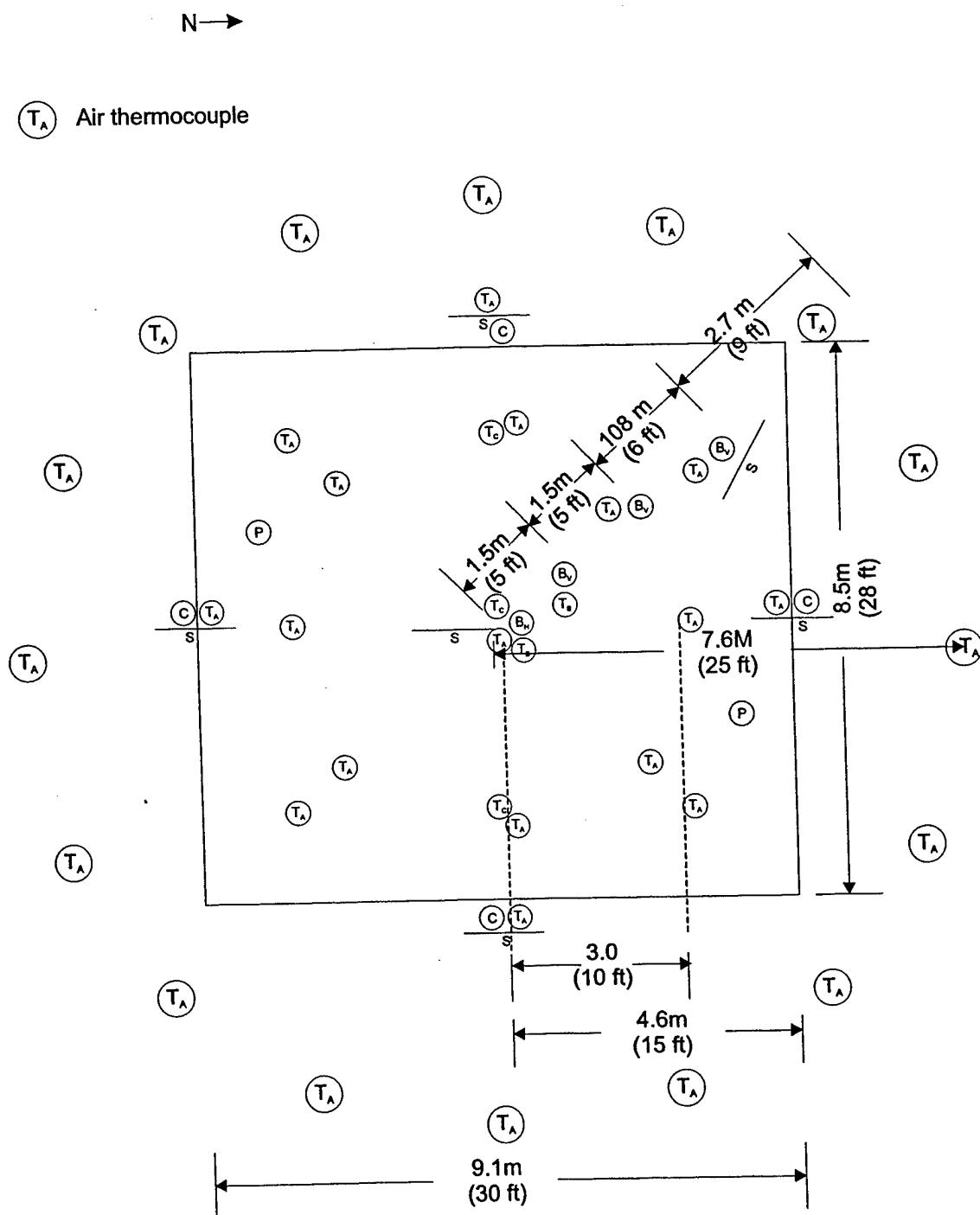


Figure 5 — Instrumentation layout

perimeter, respectively. One thermocouple was positioned above the center of the pad. Three pairs of inconel-sheathed Type K thermocouples were used to measure the concrete temperature at three locations. Measurements were made at the center of the pad and at two locations 10 ft (3 m) from the center of the pad. These measurements were made at two depths (flush with the surface and at a depth of 1.25 cm (0.5 in.)). Type K thermocouples were installed at five locations on six steel beams located at the ceiling. The steel beams were 1.3 m (4.2 ft) long and had five Type K inconel-sheathed thermocouples mechanically staked on 24 cm (9.6 in.) centers. Four of the beams were centered 4.6 m (15 ft) from the center of the pad and positioned such that the length of the beam was in the North-South direction. One beam was located above the center of the pad and positioned in the same manner described above. The sixth beam was located on an angle near the Northwest corner of the pad. Type K thermocouples (1.6 mm (0.06 in.) diameter) were also installed adjacent to each of the 36 water sprinklers to measure the hot gas temperatures during the test and record sprinkler activation time. The sprinkler locations are shown in Figure 6.

4.2.2 Calorimeters

Four calorimeters were installed to measure the potential exposure to adjacent aircraft resulting from the fire. Schmidt Boelter type calorimeters manufactured by Medtherm Company with a full-scale range of 0-50 kW/m² and a 180° view angle were used. The calorimeters were installed in the center of each side of the spill area facing the fire (see Figures 2 and 5). All four calorimeters were water-cooled. The calorimeters were installed 0.3 m (1 ft) above the surface of the temporary concrete pad and aimed horizontally.

4.2.3 Flowmeters

Two flowmeters were used to measure water flow in the water sprinkler systems. Fisher Porter Model X33115DD17 - 15 cm (6 in.) and Fischer Porter Model X3311SFD20 - 30 cm (12 in.) magnetic flowmeters were used. The ranges of these instruments were 0-3028 Lpm (0-800 gpm) and 0-12112 Lpm (0-3200 gpm), respectively.

4.2.4 Sprinkler System Pressure Transducers

Bristol Babcock Model 250815B pressure transducers were used to measure sprinkler riser pressure and sprinkler end-head pressure. The instruments had a range of 0-6.9 bar (0-100 psi).

4.2.5 Bidirectional Velocity Probes

Plume and ceiling jet velocity were measured using MKS Instruments Baratron Model pressure transducers with a range of 0-1 torr. The plume velocity was measured 0.3 m (1 ft) below the ceiling over the center of the spill. The ceiling jet velocity was measured at four locations 0.3 m (1 ft) below the ceiling. Each of these locations is shown in Figure 5.

4.2.6 Video Cameras

A total of seven video cameras were used to simultaneously record each test. Visual cameras were positioned at the center of each side of the pad. The cameras were positioned

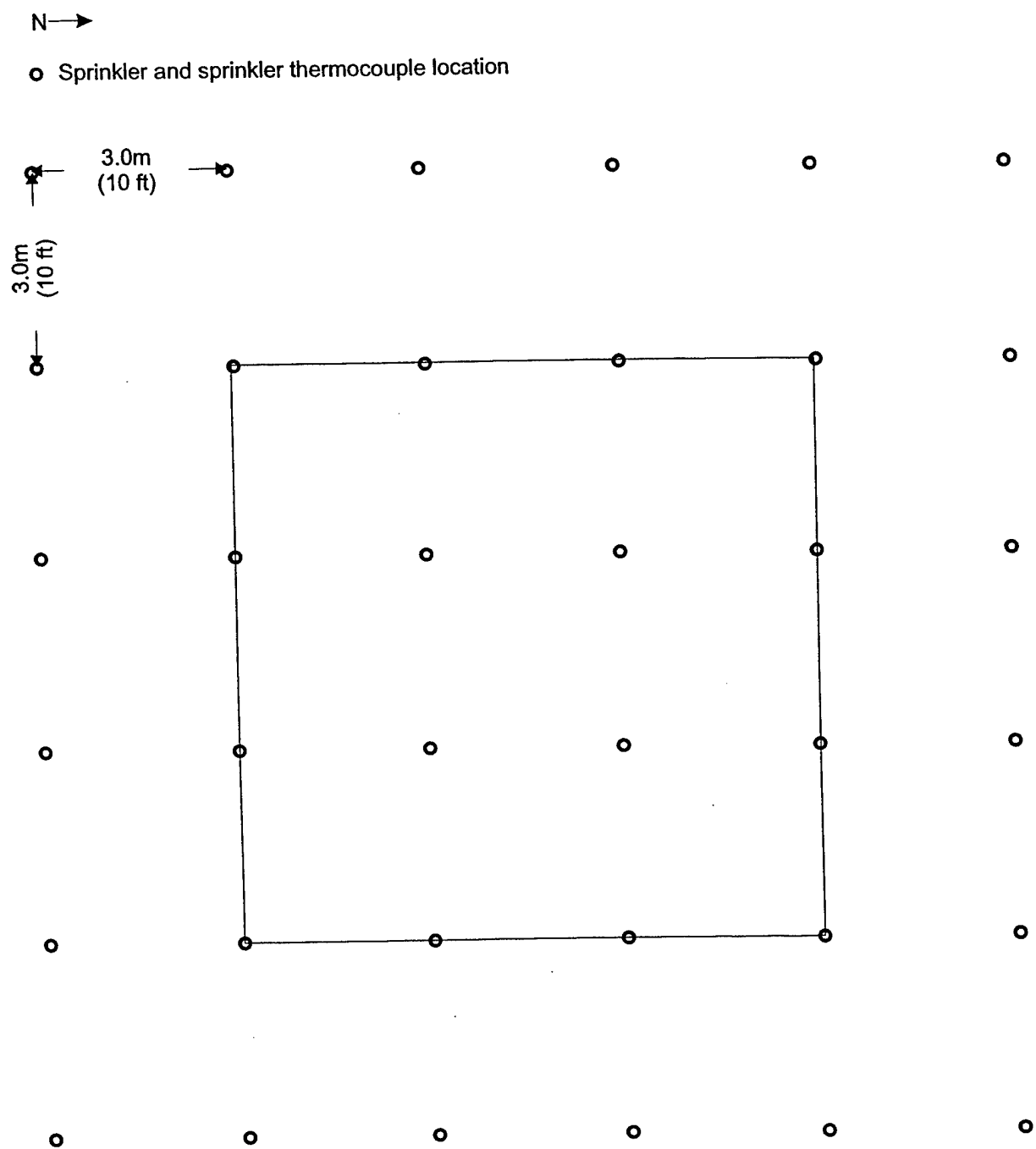


Figure 6 — Overhead sprinkler locations

approximately 7.6 m (25 ft) from the edge of the pad. Two infrared cameras were also installed. One IR was used to monitor the plume and the other was focused on the pad to monitor fire size. A handheld video camera was also used to record each test.

4.2.7 Photographic Cameras

Pre-fire and post-fire photographs were made of each test as well as continual photographic documentation during each test.

4.2.8 Visual Aids

Visual aids were added to aid in the determination of the fire size during the test. These consisted of a vertical chain positioned at the center of the fuel spill area to aid in the estimation of flame height and a painted grid on the test floor to aid in the estimation of burning surface area. The chain was marked with aluminum tape at 1.5 m (5.0 ft) increments from the ceiling down. The tape was replaced between tests as needed. In addition to the painted grid, a series of 6 ft (1.8 m) high pieces of all-thread-rod were positioned around the edge of the pad to aid in the estimation of burning surface area. The rods were spaced every 1.5 m (5.0 ft) along the East edge and every 1.2 m (4.0 ft) along the North edge. The spacing of the painted grid was the same as that of the rod markers, and extended across the surface of the pad.

4.3 **Background Burns**

Background burns were conducted to refine the design fire scenario and to establish the baseline threat. The pad was configured as shown in Figure 1. Spills of various quantities of diesel and JP-8 were evaluated. Diesel was used in some of the background burns due to the unavailability of JP-8. Different ignition sources were also evaluated.

The drum was positioned on the pad prior to filling. For the smaller fuel quantities, the drum was filled by using a small container and a funnel. For the larger quantities the dump apparatus was filled by pumping fuel out of a 208 L (55 gal) drum. The quantity of fuel was determined using the weight of fuel removed from the reservoir. Once the test configuration was verified the fuel was dumped and the igniter was positioned and ignited. The size of the spill at ignition was noted. During the test, the flame spread and maximum fire size were observed.

4.4 **Overhead Sprinkler System Testing**

Sprinkler protection was provided in accordance with the USAF Engineering Technical Letter 98-7 (ETL) [8] and MIL Handbook 1008C [9]. Sprinklers were positioned at a nominal 3 m (10 ft) x 3 m (10 ft) spacing, as shown in Figure 6, to provide an application rate of 6.9 or 10.2 Lpm/m² (0.17 or 0.25 gpm/ft²). For the sprinkler tests, 12.7 mm (0.50 in.) orifice upright sprinklers were used to provide 6.9 Lpm/m² (0.17 gpm/ft²) and 13.5 mm (0.53 in.) orifice upright sprinklers were used to provide 10.2 Lpm/m² (0.25 gpm/ft²). The 6.9 Lpm/m² (0.17 gpm/ft²) application rate was based on previous requirements of NFPA 409. Prior to requiring foam systems in hangars, NFPA 409 required deluge systems that delivered water at this application rate. The 10.2 Lpm/m² (0.25 gpm/ft²) application rate was considered to be a reasonable design

that could be accommodated by most sprinkler systems. In addition to the deluge system tests, closed-head sprinkler scenarios were also evaluated. For the closed-head system tests, the sprinklers were 79°C (175°F) quick response (QR) upright sprinklers. For the deluge and closed-head tests the sprinkler operating area was 334 m² (3,600 ft²).

Draft curtains are normally installed to decrease sprinkler operating times in hangars. The USAF ETL [8] requires draft curtains for each sprinkler zone, up to 1,394 m² (15,000 ft²). Since the test facility area was 1,338 m² (14,400 ft²), which was less than the 1,394 m² (15,000 ft²) limit, draft curtains were not installed.

For the deluge system tests, the fire pump was allowed to operate and pump 397 Lpm (105 gpm) through a bypass line. The pump speed was increased to provide the appropriate flow rate for the design density being used. The flow was set at 3406 Lpm (900 gpm) to provide 10.2 Lpm/m² (0.25 gpm/ft²) and 2316 Lpm (612 gpm) to provide 6.9 Lpm/m² (0.17 gpm/ft²). These flowrates do not include the initial bypass flow. The pump activation sequence was practiced several times prior to each test to make sure the sprinkler system was delivering the design density at the desired activation time. For the closed-head sprinkler system tests, the pump was activated and the system was charged prior to each test. As each sprinkler operated, it immediately began to flow water. There was no bypass flow for the closed-head tests.

4.5 MCAFFSS Testing

4.5.1 MCAFFSS

The mobile compressed air foam fire suppression system (MCAFFSS) evaluated in this test series was designed to automatically detect and extinguish liquid fuel fires. It was a portable, wheeled unit that has been proposed for possible use as a low level detection and suppression system for USAF hangars. Specifications for the COTS unit, shown in Figure 7, are contained in Reference [6]. The unit used a compressed air foam system that was designed to provide air aspiration of foam plus energy to propel the foam. A bleeder valve allowed the expansion ratio to be varied from 5:1 to 20:1 or more. AFFF solution, premixed using three percent MIL SPEC AFFF, was stored in a 454 L (120 gal) tank. Compressed air was stored in two - 11.3 m³ (400 ft³) cylinders. Each cylinder was capable of one complete premix discharge.

Two nozzles were used with the MCAFFSS unit. The unit was originally equipped with a 3.492 cm (1.375 in.) diameter smooth bore straight tip nozzle. This nozzle, designated as the "CAFS" nozzle for these tests, discharged a nominal 265 Lpm (70 gpm) for these tests. The pressure to the system was adjusted to 1034 kPa (150 psi) to achieve this flow rate. Compressed air was discharged into the foam solution just upstream of the nozzle to aerate the foam. The effective stream reach of agent from this nozzle was 15-18 m (50-60 ft).

A non-air aspirating AFFF nozzle was also used in this evaluation. A variable flow, variable stream handline nozzle (Akron style 1720) was set to 227 Lpm (60 gpm). The compressed air pressurizing the system was set to 1379 kPa (200 psi), which resulted in a nominal flow rate from the nozzle of 257 Lpm (68 gpm). In this configuration, compressed air

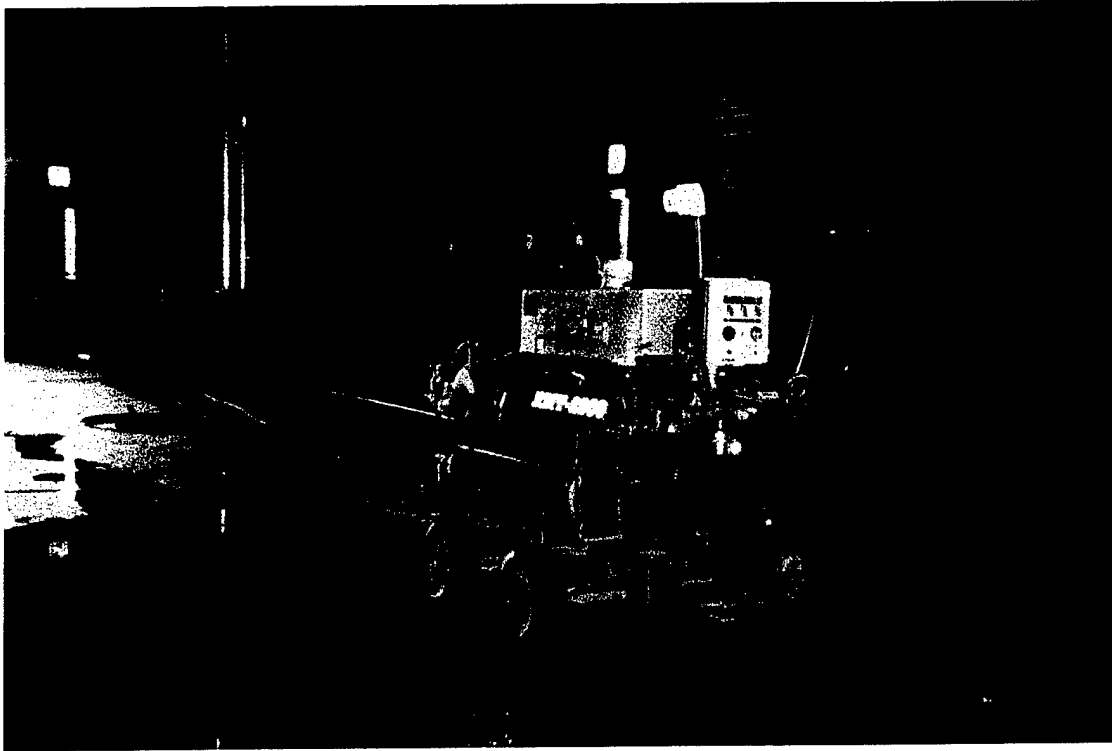


Figure 7 — MSAFFSS unit

was not discharged directly into the solution stream, so that the foam was non-air aspirated. This nozzle was designated as the "AFFF" nozzle during these tests.

Expansion and drainage tests were conducted in accordance with NFPA 412, 1998 Edition [10] Method A for the air aspirated and the non-air aspirated AFFF. For the air aspirated AFFF, the average expansion ratio was 11:0:1 and the average 25% drainage time was 5 minutes and 28 seconds. The average expansion ratio for the non-air aspirated AFFF was 3.2:1. The 25% drainage time was determined to be 54 seconds in one test, but could not be determined in the second test.

The fire sensor was a Meggitt Model 850 UV/IR detector with a horizontal field of view of 120 degrees. In the automatic mode, the agent was discharged through the pneumatic, automatic oscillating turret when the UV/IR sensor detected a fire. A number of tests were conducted with the unit in manual mode. In these cases, the unit was activated at predetermined times following ignition. The turret oscillated automatically in the automatic and manual modes. The turret operating speed and horizontal sweep angle were adjustable. Both 60° and 90° sweep angles were used in this test series. For the 60° oscillation angle, the turret speed was set such that a complete sweep (from one side to the other) took 3 seconds. For the 90° oscillation angle, a complete sweep took 4.5 seconds. The turret operating speed was not varied during the test series. The vertical angle of the nozzle was also adjustable. This angle was set prior to each test and was not adjusted during the test.

The MCAFFSS unit was evaluated at two locations. For Tests F1-F8 the unit was located perpendicular to the center of the West edge of the pad ("CW" location), as shown in Figure 8. The unit was positioned 8.8 m (29 ft) from the edge of the concrete pad (5.2 m (17 ft) from the edge of the temporary cement board pad). In Test F9 two units were positioned perpendicular to the West edge of the pad, as shown in Figure 9 (NW and SW locations). One unit was positioned 4.6 m (15 ft) South of the South edge and 9.4 m (31 ft) away from the West edge of the concrete pad. The second unit was positioned 2.1 m (7 ft) North of the North edge and 9.4 m (31 ft) away from the West edge of the concrete pad.

Two foam discharge concepts were evaluated during this test series: push and throw. The push concept involved directing the foam at the leading (West) edge of the concrete pad and pushing the foam across the pad. The throw concept consisted of directing the foam at the center of the pad and dropping the foam on top of the fire.

4.5.2 Obstructions

During the course of the MCAFFSS testing, obstructions were added to the test area to simulate items that might be found in an aircraft hangar. For Tests F3 through F5 the obstructions were configured as shown in Figure 10. A 6.4 m (21 ft) long piece of 3.18 mm (1.25 in.) diameter pipe was positioned 0.46 m (1.5 ft) from the West edge of the pad to simulate a cable laying on the deck. A fuselage mockup, shown in Figure 11, was positioned 2.4 m (8 ft) from the West edge of the pad. The simulated fuselage was created using four 208 L (55 gal) steel drums. The drums were positioned horizontally and supported 0.6 m (24 in.) above the pad by a series of concrete blocks. A third obstruction was added to simulate a tool cabinet and was

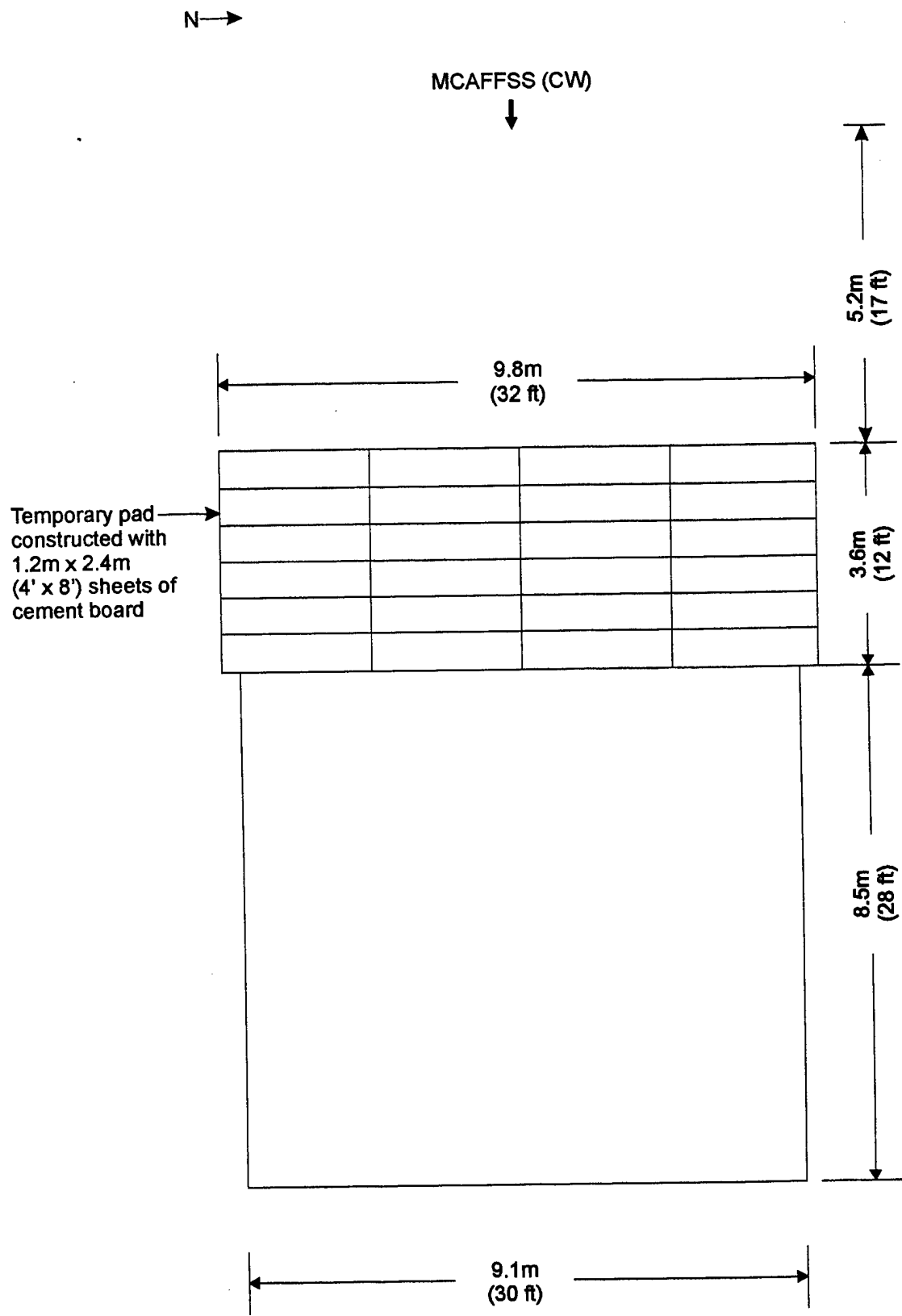


Figure 8 — MCAFFSS and pad configuration for Tests F1-F8

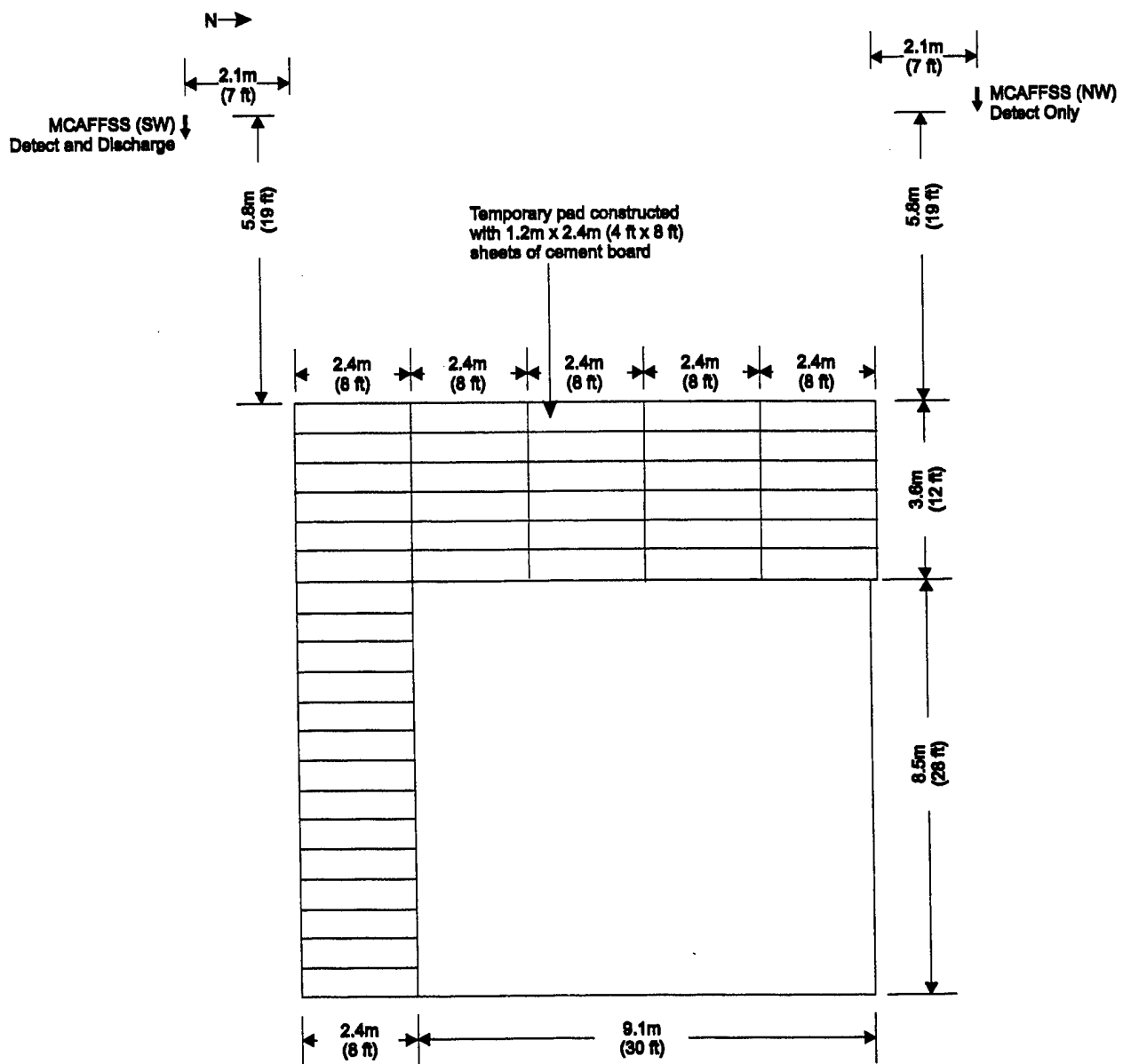


Figure 9 — MCAFFSS and pad configuration for Test F9



Figure 11 — Obstructions used for Tests F3 – F5

positioned approximately 3 m (10 ft) from the East edge and 1.4 m (4.5 ft) from the South edge. The simulated tool cabinet, also shown in Figure 11, was constructed using sheet steel and was 0.9 m (3.1 ft) by 0.7 m (2.2 ft). The bottom of the cabinet was open and approximately 15 cm (6 in.) above the pad. The top of the cabinet was closed and about 1 m (3.4 ft) above the pad.

For Tests F6 through F9, the obstructions were configured as shown in Figure 12. The only change for these tests was the addition of two sheets of drywall to the simulated fuselage. The drywall, shown in Figures 13 and 14, was added to simulate a larger profile aircraft. Two sheets of 1.2 m (4 ft) x 2.4 m (8 ft) x 13 mm (0.5 in.) thick drywall were positioned horizontally such that the top edge of the drywall was 1.8 m (6 ft) above the pad.

4.5.3 Pad Modifications

For Tests F1 through F8 the pad was configured as shown in Figure 8. The pad was expanded for the foam tests to allow the foam to be directed at the West edge of the concrete pad for the "push" scenarios. The pad was extended 3.6 m (12 ft) to the West using a series of 0.6 m (2 ft) by 2.4 m (8 ft) pieces of cement board. The cement board was positioned on top of cement blocks such that the top of the cement board was about 20 cm (8 in.) above the ground, level with the existing pad. The joints between the individual pieces of cement board were not sealed, but no significant amount of foam leakage through the cracks was observed.

For Test F9 the pad was configured as shown in Figure 9. For this test the pad was extended 2.4 m (8 ft) to the South using a series of cement boards. The pad was extended to the South so that the MCAFFSS unit located in the Southwest corner would be able to direct foam onto the pad. To allow the foam to flow across the cement boards and onto the concrete pad the cement board barrier along the South edge was removed.

4.5.4 Reignition Test Procedures

It was planned to conduct 25% burnback tests in accordance with MIL SPEC F-24385F [7] following agent discharge. However, since there was not enough residual fuel to sustain burning, a modified burnback approach was used. The method used sustained reignition of the residual fuel as a measure of burnback performance.

Reignition tests were conducted after agent discharge was complete in five of the MCAFFSS tests. In three of the tests (F3-F5) a burnback pan 0.3 m (1 ft) in diameter and 5 cm (2 in.) deep was used as the reignition source. This pan, shown in Figure 15, is used for MIL SPEC burnback resistance testing [7]. After the discharge was complete, the pan was filled with gasoline and placed on the pad within the foam blanket. This was accomplished within 90 seconds of the termination of agent discharge. Care was taken not to spill gasoline as the pan was positioned. The pan was ignited with a propane torch and allowed to burn until sustained reignition of the surrounding fuel occurred.

In each of the MCAFFSS tests the paper towel ignition source, discussed in Section 4.6.1, continued to burn after agent discharge was complete. In Tests F7 and F8, this ignition source was used as the igniter to measure sustained reignition of the residual fuel.

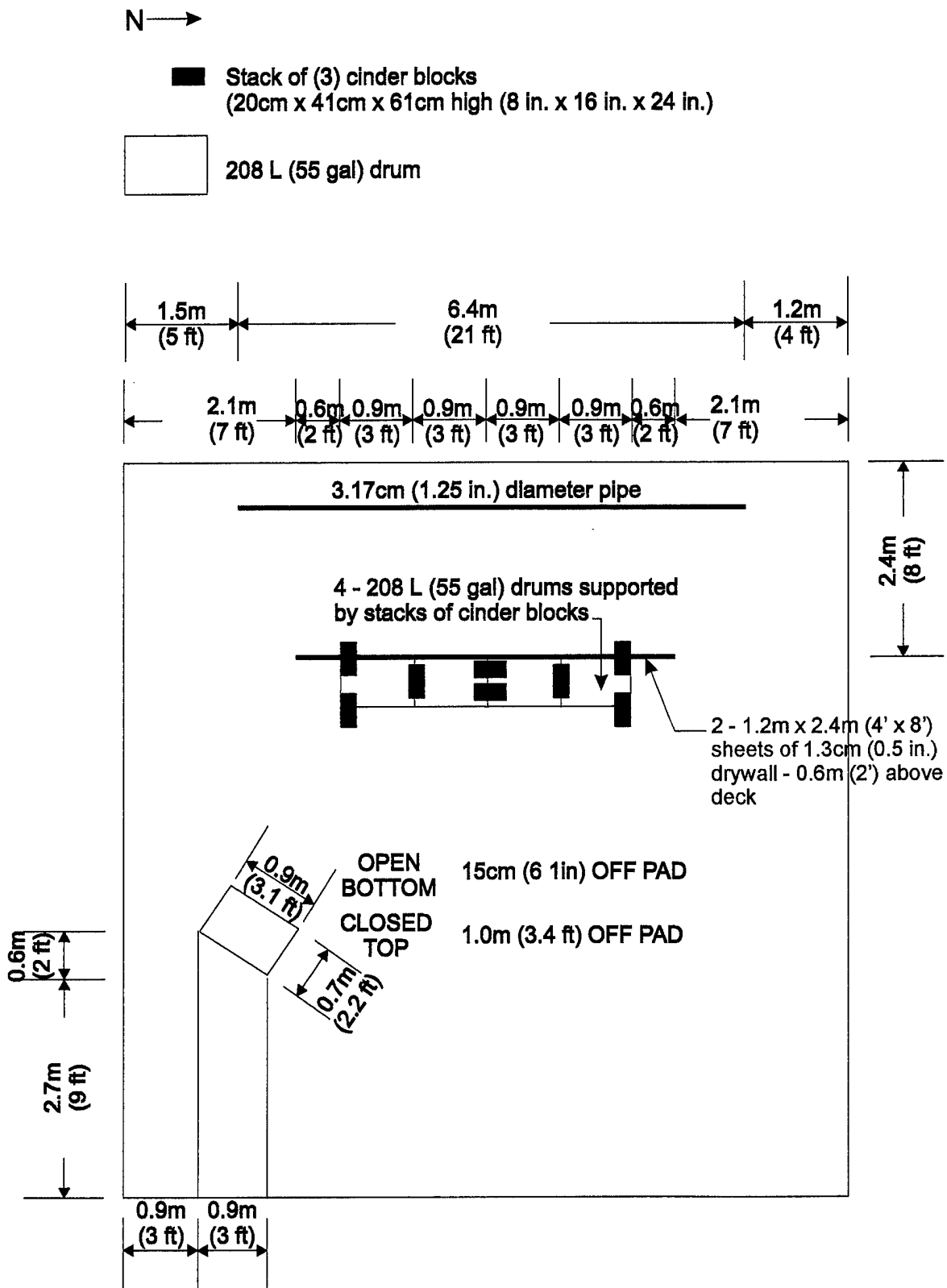


Figure 12 — Obstruction layout for Tests F6-F9

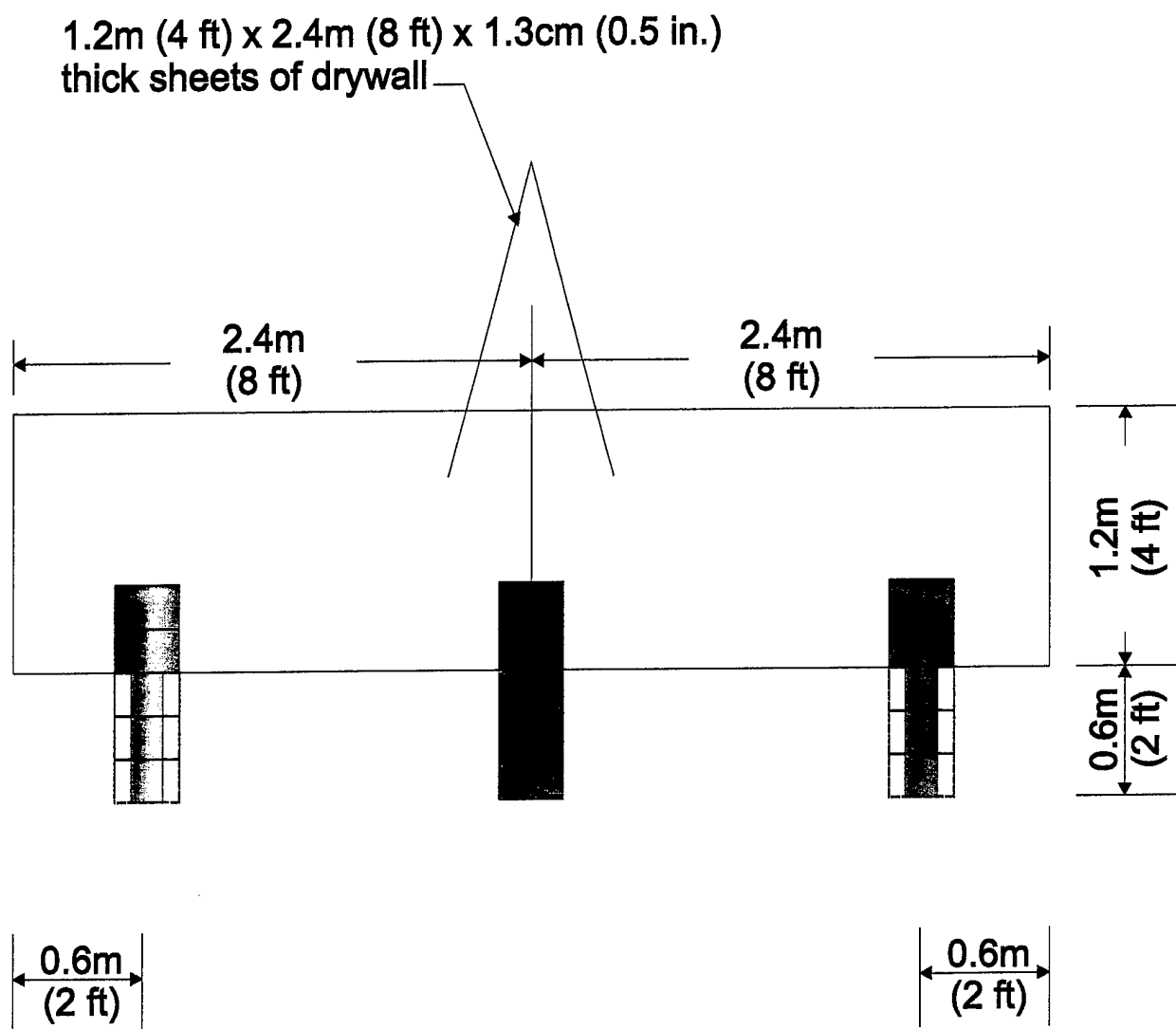


Figure 13 — Elevation view of drywall addition to simulated fuselage



Figure 14 — Drywall addition to simulated fuselage (Tests F6–F9)

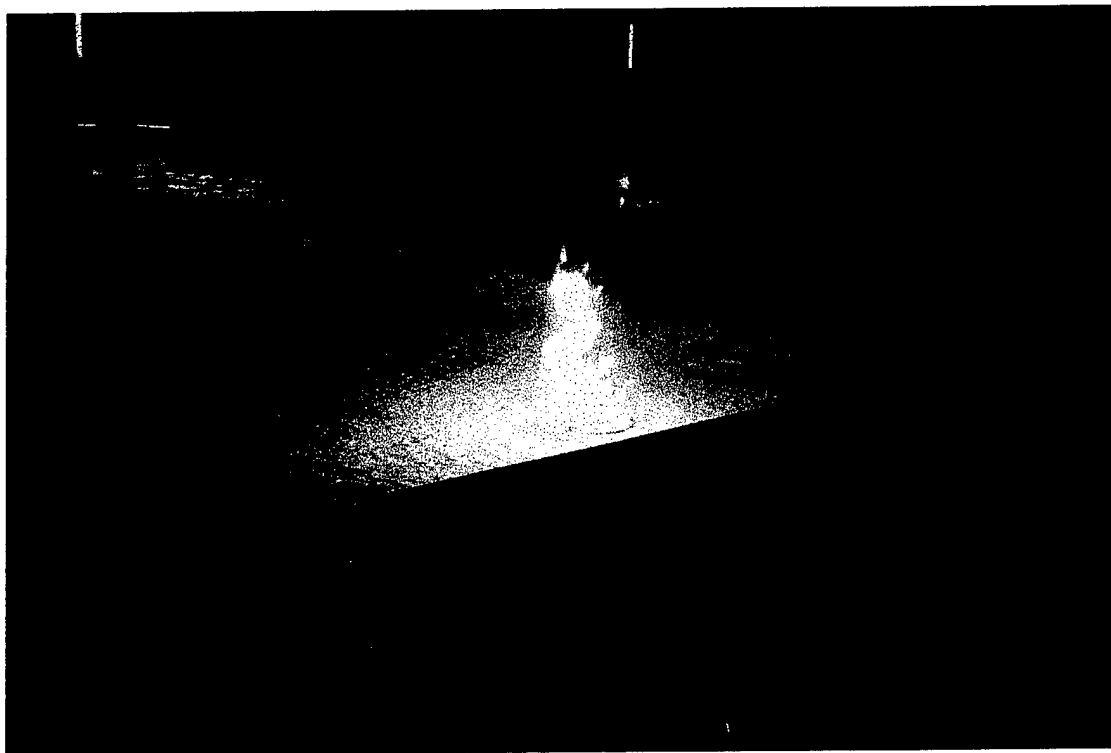


Figure 15 — MIL SPEC burnback pan

4.6 Test Procedures

4.6.1 Fuel Dump Apparatus and Ignition Procedure

The fuel used for each of the sprinkler and MCAFFSS tests was JP-8 with an open cup flashpoint of 54°C (129°F). Diesel fuel was used for some of the preliminary background burns.

The fuel dump apparatus consisted of a 208 L (55 gal) drum with a 2.5 cm (1.0 in.) wide slit cut in the side. The slit was 0.64 m (25 in.) long and centered along the side of the drum. To ensure that all of the fuel would be removed from the drum, a 2.5 cm (1.0 in.) wide slit was cut perpendicular to the center of the first slit. The second slit extended 5.1 cm (2.0 in.) on each side from the center of the slit. The drum and slit configuration are shown in Figure 16.

For fueling purposes, the drum was positioned horizontally on the pad with the slit facing up. The drum was then filled with the appropriate amount of fuel. The amount of fuel was determined by measuring the weight of fuel removed from the reservoir. For each of the sprinkler and MCAFFSS tests a total of 114 L (30 gal) of JP-8 was used. To release the fuel onto the pad the drum was rolled forward until the slit was facing downward. After conducting several tests with water and a series of background burns, it was determined that rolling the drum from South to North and dumping the fuel in the center of the pad provided a large spill with relatively uniform depth. This configuration was used for each of the sprinkler and MCAFFSS tests. When all of the fuel was removed from the drum, the drum was removed from the test area. As the drum was removed the ignition source was placed in the center of the pad and ignited with a propane torch.

For all of the sprinkler and MCAFFSS tests, the ignition source consisted of a roll of paper towels, 1.9 L (0.5 gal) of gasoline and two plastic bags. The roll of paper towels was placed in a plastic bag with 0.95 L (0.25 gal) of gasoline. A second plastic bag containing 0.95 L (0.25 gal) of gasoline was positioned next to the bag containing the paper towels. A propane torch was used to ignite the two plastic bags.

4.6.2 General Test Procedures

Prior to each test, the test configuration and procedures were reviewed with the test team. Before each of the sprinkler tests, the sprinkler type, orifice size, flowrate and sprinkler system activation timing (for deluge system tests) were all verified. Prior to each MCAFFSS test, the nozzle type, the oscillation angle and speed, the vertical angle of the nozzle and the location of the unit with respect to the pad were all verified. For all of the tests, the quantity of fuel, the location of the dump apparatus, the ignition source and safety equipment were checked. Once the initial test conditions were verified, the video recorders were started. The data acquisition system was activated at the same time that the fuel dump began. The fuel was dumped and ignited within 20 to 30 seconds of beginning the fuel dump. The size of the spill at the time of ignition was estimated. The spread of the fire across the surface of the spill was observed and then the suppression system was activated (manually or automatically). Observations of the effect of the suppression system on the fire were recorded. The test was terminated when the fire



Figure 16 — Fuel dump apparatus

was extinguished, fuel burn-out occurred or there was a minimal amount of residual fire. During some of the MCAFFSS tests, reignition tests were conducted following agent discharge.

5.0 MEASURES OF PERFORMANCE

The measures of performance for the overhead sprinkler tests included: ceiling gas and steel temperatures; heat flux exposures at targets adjacent to the spill area; flame spread rate and fire growth over the fuel area after sprinkler activation and discharge and establishment or prevention of a single turbulent plume. A critical steel beam temperature of 538°C (1000°F) was used based on the criteria in ASTM E-119 [11]. The flame spread rate and fire growth were based on visual observations, using the aids described in Section 4.2.8 as references. The flame spread rate was calculated by determining the time required for the flame front to pass the markers located around the North and East edges of the pad. This time and the distance between the markers was used to determine the flame spread rate.

The measures of performance for the MCAFFSS tests were fire control and extinguishment times. NFPA 409 requires that hangar systems be capable of controlling fires within 30 seconds from activation and be able to extinguish fires within 60 seconds. Time when the fuel reignited after extinguishment was assessed in some of the tests. Detection time and fire size at detection were used to evaluate the fire sensor included with the MCAFFSS unit.

6.0 RESULTS

6.1 Background Burns

A series of eight background burns were conducted to establish the baseline threat, refine the design fire and finalize the fuel dump and ignition procedures. The type and amount of fuel as well as the type and location of the ignition source were all varied during the background burns. Tests BB1-BB5 were conducted using diesel fuel and Tests BB6-BB8 were conducted using JP-8.

The configuration and general results for the diesel fuel tests (Tests BB1-BB5) are summarized in Table 1. This Table includes descriptions of the type and quantity of fuel and the type and location of the ignition source.

Table 2 summarizes the configuration and results for the JP-8 tests (Tests BB6-BB8). The Table indicates the type and quantity of fuel, the type and location of the ignition source and summarized data. The maximum average air temperatures over the center of the pad and around the three concentric rings of thermocouples (3.0 m, 4.6 m, and 7.6 m) were determined by using the average of all the thermocouples for each group. The maximum average heat flux was calculated by using the average of the three lowest heat flux measurements. In some of the tests, the fire spread to an area immediately in front of the instrument, which resulted in extremely high heat fluxes measured at a single calorimeter. The calorimeter measuring the highest heat flux was excluded from the averaging to provide a more realistic value. The spill size at ignition,

Table 1. Summary of Diesel Background Burns (Tests BB1-BB5)

Test	Fuel	Fuel Qty (L (gal))	Ignition Source	Igniter Location	Comments
BB1	Diesel	19 (5)	15 cm (6 in.) rolled gauze with 118 mL (4 oz) of gasoline in a plastic bag	1.8 m (6 ft) East and 0.8 m (2.5 ft) South of pad center	Igniter was unable to ignite spill. A second gauze igniter with 237 mL (8 oz) of gasoline was able to ignite spill
BB2	Diesel	38 (10)	15 cm (6 in.) rolled gauze with 237 mL (8 oz) of gasoline in a plastic bag	1.8 m (6 ft) East and 0.8 m (2.5 ft) South of pad center	Unable to ignite spill. Need to repeat with a larger igniter source.
BB3	Diesel	38 (10)	Paper towel ignition source (see Section 4.6.1)	1.8 m (6 ft) East of pad center	Ignited, but did not fully involve spill
BB4	Diesel	76 (20)	Paper towel ignition source (see Section 4.6.1)	1.2 m (6 ft) East and 2.3 m (7.5 ft) South of pad center	Ignited, but did not fully involve spill
BB5	Diesel	76 (20)	Paper towel ignition source (see Section 4.6.1)	Center of pad	Better fire spread than previous tests

Table 2. Results of JP-8 Background Burns (Tests BB6-BB8)

Test	Fuel	Fuel Qty (L (gal))	Ignition Source	Igniter Location	Maximum Average Air Temperatures (°C)			Maximum Average Heat Flux (kW/m ²) ¹	Spill Size at Ignition (m ² (ft ²))	Maximum Fire Size (m ² (ft ²))	Maximum Flame Height (m ² (ft ²))	Average Flame Spread Rate (cm/s (in./s))	First Standard Deviation (cm/s (in./s))
					Center (10 ft)	3.0 m (10 ft)	4.6 m (15 ft)	7.6 m (25 ft)					
BB6	JP-8	95 (25)	Paper towel (see Section 4.6.1)	Center of pad	160	135	115	90	12	34 (370)	32 (350)	7.1 (2.8)	2.5 (1.0)
BB7	JP-8	95 (25)	Paper towel (see Section 4.6.1)	Center of pad	108	88	76	62	5 ²	31 (335)	28 (300)	3.0 (1.2)	0.8 (0.3)
BB8	JP-8	114 (30)	Paper towel (see Section 4.6.1)	Center of pad	172	138	119	107	10	33 (360)	37 (400)	4.1 (1.6)	1.0 (0.4)

¹ Average of lowest three (out of four) values.² All four instruments used to determine average.

maximum fire size, and maximum flame height were determined using the visual aids described in Section 4.2.8.

6.1.1 Results of Diesel Spill Fire Tests (BB1-BB5)

Table 1 summarizes the configuration and general results for Tests BB1-BB5. Small quantities of fuel and small ignition sources were used initially. In Tests BB1 and BB2, ignition sources consisting of rolled gauze and a small amount of gasoline (118 mL in Test BB1 and 237 mL in Test BB2) in a plastic bag were used. These ignition sources were unable to ignite diesel spills of 19 L (5 gal) and 38 L (10 gal). In Test BB3 a larger ignition source, consisting of a paper towel roll and 1.9 L (0.5 gal) of gasoline, was used. The paper towel ignition source is described in detail in Section 4.6.1. The 38 L (10 gal) diesel fuel spill ignited, but was never fully involved. The flame spread appeared to be limited by high spots on the pad. During the fuel dump, the diesel fuel spread across the pad and settled into low spots on the pad. When the fuel dump was completed the fuel ran off of the high spots, leaving these areas relatively dry of fuel. As the fire spread, it reached areas of the pad where there was not enough fuel to allow the fire to spread. In Test BB4, the quantity of fuel was increased to 76 L (20 gal) to overcome the irregularities of the pad surface. The location of the ignition source was also changed so that it was in a low spot on the pad. As in the previous test, the fuel spill ignited, but did not fully involve the spill. In this case the fuel near the ignition source burned out before the fire had spread across the surface of the spill. In Test BB5, the location of the ignition source was changed to the center of the pad. This location resulted in better flame spread than in the previous tests. Based on the results of these tests, the center of the pad was selected as the igniter location and the ignition source (paper towel source with 1.9 L (0.5 gal) of gasoline was standardized for the remainder of the tests. In Tests BB1-BB5, the drum was rolled from North to South.

6.1.2 Results of Test BB6

Test BB6 was the first test using JP-8 as the fuel. A total of 95 L (25 gal) of JP-8 was used. The drum was rolled from North to South. The spill size at ignition was 34 m² (370 ft²). The maximum fire size and flame height occurred approximately 1 minute and 15 seconds after ignition and were 32 m² (350 ft²) and 10 m (33 ft), respectively. The average flame spread rate was 7.1 cm/s (2.8 in./s). The maximum average heat flux was 12 kW/m² (South calorimeter excluded). The maximum average air temperatures above the center of the pad and 3.0 m (10 ft), 4.6 m (15 ft), and 7.6 m (25 ft) from the center of the pad were 160°C, 135°C, 115°C, and 90°C, respectively. The fire in the center of the pad began to burnout 1 minute and 30 seconds after ignition. The maximum steel beam temperature was 59°C. The initial concrete pad temperature was 32°C. The maximum average heat flux and air temperatures occurred at about the same time as the maximum observed fire size and flame height. The thermocouples 7.6 m (25 ft) away from the center reached their maximum values slightly after the thermocouples around the inner rings. The data for this test are shown in Appendix A (Figures A1-A15).

6.1.3 Results of Test BB7

It was suggested that the initial temperature of the deck might have an effect on the spill fire dynamics. Test BB7 was a repeat of Test BB6 with a cool deck (i.e., first test of the day). For Test BB7 the initial concrete pad temperature was 24°C compared to 32°C for Test BB6. The spill size at ignition was 31 m² (335 ft²). The maximum fire size of 28 m² (300 ft²) occurred approximately 1 minute and 45 seconds after ignition. The maximum flame height of 7 m (23 ft) was reached about 1 minute after ignition and remained relatively constant for another minute. The average flame spread rate was 3.0 cm/s (1.2 in./s). The maximum average heat flux was 5 kW/m². There was not a significant difference between the measurements of the four calorimeters, so all of the values were used in determining the maximum average heat flux. The maximum average air temperatures above the center of the pad and 3.0 m (10 ft), 4.6 m (15 ft) and 7.6 m (25 ft) from the center of the pad were 108°C, 88°C, 76°C and 62°C, respectively. Again the fire in the center of the pad began to burnout approximately 1 minute and 30 seconds after ignition. The maximum steel beam temperature was 43°C. The maximum average heat flux and air temperatures occurred about the same time the maximum fire size was observed (1 minute and 45 seconds after ignition). The data for this test are shown in Appendix A (Figures A16-A30).

6.1.4 Results of Test BB8

In Test BB8 the quantity of fuel was increased to 114 L (30 gal) and the drum was rolled from South to North instead of North to South. The fuel quantity was increased to provide the potential for larger spill and fire sizes. The data for this test are shown in Appendix A (Figures A31-A45). The spill size at ignition was 33 m² (360 ft²). The maximum fire size and flame height occurred approximately 1 minute and 15 seconds after ignition and were 37 m² (400 ft²) and 10 m (33 ft), respectively. Figure 17 shows the fully involved spill fire in Test BB8. The average flame spread rate was 4.1 cm/s (1.6 in./s). The maximum average heat flux was 10 kW/m² (North calorimeter excluded). The maximum average air temperatures above the center of the pad and 3.0 m (10 ft), 4.6 m (15 ft), and 7.6 m (25 ft) from the center of the pad were 172°C, 138°C, 119°C and 107°C, respectively. The maximum steel beam temperature was 61°C. The maximum average heat flux and air temperatures occurred at about the same time as the maximum observed fire size and flame height. Approximately 1 minute and 30 seconds after ignition the fuel at the center of the pad was consumed and there was only fire around the perimeter of the spill. This scenario (114 L (30 gal) JP-8, drum rolled from South to North, paper towel ignition source) was standardized for the remainder of the tests.

6.2 Sprinkler Tests

The results of the overhead sprinkler system tests are summarized in Table 3. Included in this Table are details of the sprinkler system configuration and a summary of key temperature, heat flux and fire size data. The average temperature data were calculated by averaging all of the instruments at the specified time. The average heat flux data were calculated using the three lowest values at each time. In some of the tests, the fire spread to an area immediately in front of an instrument, which resulted in extremely high heat fluxes measured at a single calorimeter. The highest heat flux was excluded from the averaging to provide a more realistic value.



Figure 17 — Fully involved spill fire in Test BB8

Table 3. Results of Overhead Sprinkler System Tests

Test ID	S1	S2	S3	S4	S5	S6	S7
Sprinkler type	deluge	deluge	deluge	closed	closed	closed	deluge
Orifice Size (mm (in.))	13.5 (0.53)	13.5 (0.53)	13.5 (0.53)	13.5 (0.53)	13.5 (0.53)	12.7 (0.5)	12.7 (0.5)
Density (Lpm/m ² (gpm/ft ²))	10.2 (0.25)	10.2 (0.25)	10.2 (0.25)	10.2 (0.25)	10.2 (0.25)	6.9 (0.17)	6.9 (0.17)
Sprinkler system activation delay (sec after ignition)	6	32	80	60	58	58	31
Spill Size at ignition (m ² (ft ²))	32 (350)	30 (320)	31 (340)	26 (280)	32 (350)	32 (350)	31 (340)
Fire size at activation (m ² (ft ²)) ¹	0.6 (7)	10 (113)	41 (440)	29 (315)	29 (315)	29 (315)	9 (95)
Flame height at activation (m ² (ft ²)) ¹	0.9 (3)	6 (20)	10 (33)	10 (33)	10 (33)	10 (33)	5 (18)
Average heat flux at activation (kW/m ²)	0.1	5	43	8	10	7	3
Average heat flux 15 sec after activation (kW/m ²)	3	26	8	12	16	25	14
Average heat flux 30 sec after activation (kW/m ²)	4	13	5	5	5	5	11
Air temperature at activation (°C)							
Center	27	56	265	144	122	142	44
10 ft radius	27	53	220	110	104	115	41
15 ft radius	27	47	200	94	88	98	38
25 ft radius	27	39	160	72	64	76	32
Air temperatures 15 sec after activation (°C)							
Center	50	406	265	244	406	442	200
10 ft radius	41	270	200	137	216	297	154
15 ft radius	35	198	190	159	191	243	128
25 ft radius	27	126	165	125	132	174	87
Air temperatures 30 sec after activation (°C)							
Center	83	352	130	57	254	258	403
10 ft radius	64	208	125	71	89	181	260
15 ft radius	61	188	110	88	104	172	214
25 ft radius	44	139	105	79	90	146	150

¹ Tests S4-S6, Activation is the time when first sprinkler operated.

Tests S1, S2, S3 and S7 were tests of deluge systems. Tests S4, S5 and S6 were tests of closed head sprinkler systems. For the closed-head tests, the time that the first head operated was considered the activation time. Two different water densities were evaluated: 0.2 Lpm/m² (0.25 gpm/ft²) for Tests S1-S5 and 6.9 Lpm/m² (0.17 gpm/ft²) for Tests S6 and S7. Three different deluge system activation times were evaluated in this test series: no delay (Test S1), 30 second delay (Tests S2 and S7) and an 80 second delay (Test S3). Activation of the sprinkler system immediately after ignition provided the best-case scenario. The 30 and 80 second delay times provided more realistic scenarios. Tests with closed-head systems were also conducted to determine if fewer sprinklers could be used to control JP-8 spill fires. In the three closed head tests, all of the heads were open by about 1 minute after ignition. The specific results of each of the sprinkler tests are discussed in the following sections. Graphs of the heat flux, air temperature, steel temperature, concrete temperature and plume and ceiling jet velocities for each test are contained in Appendix B.

6.2.1 Results of Test S1

Test S1 evaluated the best-case deluge sprinkler scenario (i.e., high density with no delay in sprinkler activation). At ignition, the spill covered approximately 32 m² (350 ft²). There was a 6 second difference between the time of ignition and the time required to flow through the deluge system. The fire was relatively small (0.6 m² (7 ft²)) when the sprinkler system began discharging. At activation, the average heat flux and air temperatures showed no significant change from ambient conditions. After sprinkler system activation, the fire continued to grow. At 30 seconds after activation, the fire size was 17 m² (180 ft²), and the flame height was 7 m (23 ft). The fire size and flame height remained relatively constant for 1 minute and 30 seconds at which time the fire began to burn out. The average heat flux was 0.1 kW/m², and the average air temperature around each thermocouple ring was 27°C. The average heat flux 15 and 30 seconds after system activation were 3 kW/m² and 4 kW/m², respectively. At 15 seconds after ignition, the average air temperatures above the center of the pad and 3.0 m (10 ft), 4.6 m (15 ft) and 7.6 m (25 ft) from the center of the pad were 50°C, 41°C, 35°C and 27°C, respectively. At 30 seconds after activation, the average air temperatures were 83°C, 64°C, 61°C and 44°C, respectively. The maximum steel beam temperature was 54°C. The data for this test are shown in Appendix B (Figures B1-B17).

6.2.2 Results of Test S2

Test S2 was a repeat of Test S1 with a 32 second delay in sprinkler system activation. The 13.5 mm (0.53 in.) orifice sprinklers were used to deliver 10.2 Lpm/m² (0.25 gpm/ft²) through a deluge system. At ignition, the spill was 30 m² (320 ft²). At activation, the fire was 10 m² (113 ft²) and had a flame height of 6 m (20 ft). At activation, the average heat flux was 5 kW/m², and the average air temperatures above the center of the pad and 3.0 m (10 ft), 4.6 m (15 ft) and 7.6 m (25 ft) from the center of the pad were 56°C, 53°C, 47°C and 39°C, respectively. After activation, the fire size and flame height increased significantly. Figure 18 shows the fire size immediately after, approximately 15 seconds after and approximately 1 minute after sprinkler system activation. At 15 seconds after activation, the flame height had increased from 5 m (18 ft), at activation, to 15 m (48 ft). The fire began to burn out about 1 minute after ignition. At 35 seconds after activation, the flame height was 8 m (28 ft). The average heat flux



At sprinkler system activation



Approximately 30 seconds
after activation



Approximately 60 seconds
after activation

Figure 18 — Fire growth in Test S2

average heat flux and air temperatures increased significantly after the sprinkler system was activated. At 15 seconds after ignition, the average heat flux was 26 kW/m^2 and the average air temperatures above the center of the pad and 3.0 m (10 ft), 4.6 m (15 ft) and 7.6 m (25 ft) from the center of the pad were 406°C , 270°C , 198°C and 126°C , respectively. At 30 seconds after activation, the temperature and heat flux began to decrease. The average heat flux at 30 seconds was 13 kW/m^2 , and the average air temperatures above the center of the pad and 3.0 m (10 ft), 4.6 m (15 ft) and 7.6 m (25 ft) from the center of the pad were 352°C , 208°C , 188°C and 139°C , respectively. The maximum steel beam temperature was 82°C . The data for this test are shown in Appendix B (Figures B18-B34).

6.2.3 Results of Test S3

Test S3 was a repeat of Tests S1 and S2 with an 80 second delay in system activation. At ignition, the spill was 31 m^2 (340 ft^2). At activation, the fire was 41 m^2 (440 ft^2) and had a flame height of 10 m (33 ft). At activation, the average heat flux was 22 kW/m^2 and the average air temperatures above the center of the pad and 3.0 m (10 ft), 4.6 m (15 ft) and 7.6 m (25 ft) from the center of the pad were 265°C , 220°C , 200°C and 160°C , respectively. After activation, there was a quick increase in the size of the fire and the measured heat flux. The fire then began to decrease in size. At 15 seconds after ignition, the average heat flux was 8 kW/m^2 , and the average air temperatures above the center of the pad and 3.0 m (10 ft), 4.6 m (15 ft) and 7.6 m (25 ft) from the center of the pad were 265°C , 200°C , 190°C and 165°C , respectively. The significant decrease in heat flux was due to fuel depletion. At 30 seconds after activation, the temperature and heat flux continued to decrease. The average heat flux at 30 seconds was 5 kW/m^2 , and the average air temperatures above the center of the pad and 3.0 m (10 ft), 4.6 m (15 ft) and 7.6 m (25 ft) from the center of the pad were 130°C , 125°C , 110°C and 105°C , respectively. The maximum steel beam temperature was 83°C . The data for this test are shown in Appendix B (Figures B35-B51).

6.2.4 Results of Test S4

Test S4 was the first closed-head sprinkler system test where 10.2 Lpm/m^2 (0.25 gpm/ft^2) was delivered. The initial temperature of the pad was approximately 30°C . At ignition, the spill was 26 m^2 (280 ft^2). Since the system used closed heads, the sprinklers opened individually. The first sprinkler operated 60 seconds after ignition and the last sprinkler opened 1 minute and 15 seconds after ignition. When the first head opened, the fire was 29 m^2 (315 ft^2) and had a flame height of 10 m (33 ft). The average heat flux was 8 kW/m^2 , and the average air temperatures above the center of the pad and 3.0 m (10 ft), 4.6 m (15 ft) and 7.6 m (25 ft) from the center of the pad were 144°C , 110°C , 94°C and 72°C , respectively. After activation, the fire size and flame height increased significantly. The flame height quickly increased from 10 m (33 ft) to 15 m (48 ft). At 15 seconds after activation, the heat flux and temperature had increased. The average heat flux was 12 kW/m^2 , and the average air temperatures were 244°C , 137°C , 159°C and 125°C , respectively. About 20 seconds after activation, the fire began to decrease in size and intensity. At 30 seconds after activation, the temperature and heat flux had decreased significantly. The average heat flux was 5 kW/m^2 , and the average air temperatures were 57°C , 71°C , 88°C and 79°C , respectively. The maximum steel beam temperature was

70°C. Fire continued to burn along the North edge 90 seconds after activation. The data for this test are shown in Appendix B (Figures B52-B68).

6.2.5 Results of Test S5

Test S5 was a repeat of Test S4 with a cold deck. This test was conducted to evaluate the effects of a cold deck on the effectiveness of the overhead sprinkler system on a spill fire. The initial temperature of the concrete pad was 26°C. At ignition, the spill was 32 m² (350 ft²). The first sprinkler operated 58 seconds after ignition, and the last sprinkler operated 1 minute and 18 seconds after ignition. When the first sprinkler operated, the fire was 29 m² (315 ft²) and had a flame height of 10 m (33 ft). The average heat flux was 10 kW/m², and the average air temperatures above the center of the pad and 3.0 m (10 ft), 4.6 m (15 ft) and 7.6 m (25 ft) from the center of the pad were 122°C, 104°C, 88°C and 64°C, respectively. After activation, the fire size and flame height continued to increase. At 15 seconds after activation, the heat flux and temperature had increased. The average heat flux was 16 kW/m², and the average air temperatures were 406°C, 216°C, 191°C and 132°C, respectively. At 30 seconds after activation, the size and intensity of the fire had decreased, and the temperature and heat flux had decreased significantly. The average heat flux was 5 kW/m², and the average air temperatures were 254°C, 89°C, 104°C and 90°C, respectively. The fire separated into two pool fires 1 minute and 27 seconds after ignition. It appeared that the fuel in the center of the pad had been consumed. The maximum steel beam temperature was 80°C. The data for this test are shown in Appendix B (Figures B69-B85).

6.2.6 Results of Test S6

Test S6 was a repeat of Tests S4 and S5 with a lower water density, 6.9 Lpm/m² (0.17 gpm/ft²). At ignition, the spill was 32 m² (350 ft²). The first sprinkler operated 58 seconds after ignition and the last sprinkler operated 1 minute and 19 seconds after ignition. At activation (first sprinkler operated), the fire was 29 m² (315 ft²) and had a flame height of 10 m (33 ft). The average heat flux was 7 kW/m² and the average air temperatures above the center of the pad and 3.0 m (10 ft), 4.6 m (15 ft) and 7.6 m (25 ft) from the center of the pad were 142°C, 115°C, 98°C and 76°C, respectively. After activation, the fire increased in size and intensity. At 15 seconds after activation, the heat flux and temperature had increased significantly. The average heat flux was 25 kW/m², and the average air temperatures were 442°C, 297°C, 243°C and 174°C, respectively. About 25 seconds after activation, the fire was fully involved. At 30 seconds after activation, the temperature and heat flux had decreased. The average heat flux was 5 kW/m², and the average air temperatures were 258°C, 181°C, 172°C and 146°C, respectively. Multiple pool fires were formed approximately 1 minute and 21 seconds after ignition. About 45 seconds after activation, the fire formed multiple plumes and began to burn out. The maximum steel beam temperature was 86°C. The data for this test are shown in Appendix B (Figures B86-B102).

6.2.7 Results of Test S7

Test S7 was a repeat of Test S2 with a reduced density. The sprinklers (12.7 mm (0.5 in.) orifice) were setup to provide 6.9 Lpm/m² (0.17 gpm/ft²) through a deluge system. The system was activated 31 seconds after ignition. At ignition, the spill was 31 m² (340 ft²). At activation,

the fire was 9 m² (95 ft²) and had a flame height of 5 m (18 ft). The average heat flux was 3 kW/m², and the average air temperatures above the center of the pad and 3.0 m (10 ft), 4.6 m (15 ft) and 7.6 m (25 ft) from the center of the pad were 44°C, 41°C, 38°C and 32°C, respectively. At 15 seconds after activation, the heat flux and temperature had increased significantly. The average heat flux was 14 kW/m², and the average air temperatures were 200°C, 154°C, 128°C and 87°C, respectively. At 30 seconds after activation, the temperature had continued to increase and the heat flux had decreased slightly. The average heat flux was 11 kW/m², and the average air temperatures were 403°C, 260°C, 214°C and 150°C, respectively. The maximum steel beam temperature was 83°C. The data for this test are shown in Appendix B (Figures B103-B119).

6.3 MCAFFSS Tests

The results of the MCAFFSS tests are summarized in Table 4. Included in this Table are details of the MCAFFSS configuration and a summary of key fire control and extinguishment times. For Tests F1-F8 a single unit was used at the center-west location (CW) which was located perpendicular to the center of the West edge of the pad. For Test F9 two units were used and positioned off-center of the fire area (NW and SW). The locations of the units are described in detail in Section 4.5.1. The activation mode is identified as either manual or automatic. In the automatic mode the system was allowed to discharge when the fire detector sensed the fire. In the manual mode the fire detector was allowed to sense the fire, but the unit was activated manually at predetermined times as noted in the table. The type of nozzle used is identified as either CAFS or AFFF. The CAFS nozzle provided air aspirated foam and the AFFF nozzle provided non-air aspirated foam as described in Section 4.5. The non-air aspirated foam was used to provide a direct comparison with the performance of the air aspirated. The discharge characteristics are identified as either throw or push. Throw indicates that the foam was directed across the pad and allowed to strike on the center of the pad (i.e., "targeted" to a specific location). Push indicates that the foam was directed at the leading edge of the pad and pushed across the fuel surface. This is the technique currently specified in the ETL. Two different oscillation angles were evaluated: 60 and 90 degrees. The 60 degree setting was used for the majority of the tests. The 90 degree setting was used to evaluate a reduced effective application rate, i.e., larger sweep area with the same flow rate. Beginning with Test F3, obstructions were added to the pad area to simulate shielded situations which can occur in aircraft hangars. The obstructions are described in detail in Section 4.5.2. The detection time indicates the time that the system fire detector alarmed as well as the time that the system was activated for the manual activation tests. The control and extinguishment times were based on visual observations which were refined during post-test review of the recorded video. For tests where the fire was not extinguished, estimates of residual burning are noted. Reignition tests of the air aspirated and the non-air aspirated foam were conducted. For three of the tests (F3-F5) a burnback pan was used as the fire source. For two of the tests (F7 and F8) the paper towel ignition source was used to evaluate the reignition potential. The specific procedures for the reignition tests are described in Section 4.5.4.

The specific results of each of the MCAFFSS tests are discussed in the following sections. Graphs of the heat flux, air temperature, steel temperature, concrete temperature and plume and ceiling jet velocities for each MCAFFSS test are provided in Appendix C.

Table 4. MCAFFSS Test Results

Test No.	No. of Units	Location of Unit ¹	Detection/Activation	Nozzle	Disch. Char.	Oscillation Angle	Obstructions	Detection ² Time (min:sec)	50% Control (min:sec)	90% Control (min:sec)	Exting. ³ Time (min:sec)	Reignite ⁴ Time (min:sec)	Comments
F1	1	CW	Automatic	CAFS	Throw	60°	No	A-0:04	0:05	0:12	0:16	–	Baseline test with throw, no obstructions, automatic mode, rapid control of fire
F2	1	CW	Automatic	CAFS	Push	60°	No	A-0:04	0:17	0:30	0:49	–	Repeat F1 with "push," rapid control of fire, but longer than F1 "throw"
F3	1	CW	Manual	CAFS	Push	60°	Yes	A-0:07 M-1:00	0:11	0:23	<1 ft ² still burning	B-11:12	One minute delay time to test against fully involved spill fire
F4	1	CW	Manual	CAFS	Throw	60°	Yes	A-0:20 M-1:00	0:11	0:22	1:26	B-9:48	Repeat F3 with "throw" characteristics; no significant difference in CAFS throw vs. push; foam bounced over obstruction; higher obstruction would have affected results (see Test F6)
F5	1	CW	Manual	AFFF ⁵	Push	60°	Yes	A-0:46 M-1:37	0:13	0:28	2 ft ² still burning	B-8:03	Repeat F3 with AFFF nozzle; delayed involvement of ignition accelerator and growth of floor fire; no significant differences between CAFS and AFFF push
F6	1	CW	Manual	CAFS	Throw	60°	Yes with increased obstruction	A-0:18 M-1:00	0:34	1:42	4 ft ² still burning	–	80-90% of fire area extinguished in 1:42 – fuel burnout was occurring; larger obstruction reduced "throw" effectiveness
F7	1	CW	Manual	CAFS	Push	90°	Yes with increased obstruction	A-0:20 M-0:45	0:41	1:35	15 ft ² still burning	I-5:41	Reduced manual activation time from 1:00 to 0:45 to allow more residual fuel; 90° angle selected to reduce effective application rate; 90° angle increased control time and increased residual burning remaining at the conclusion of agent discharge
F8	1	CW	Manual	AFFF ⁵	Push	90°	Yes with increased obstruction	A-0:17 M-0:45	0:38	1:03	4 ft ² still burning	I-7:57	Repeat F7 with AFFF; reach slightly better than F7 test, which resulted in less residual fire at the end of agent discharge; no significant difference between CAFS and AFFF
F9	2	NW ⁶ and SW	Automatic	CAFS	Push	60°	Yes with increased obstruction	A-0:44 (north) A-0:54 (south)	Not achieved	Not achieved	98 ft ² still burning	–	North side still burning; second nozzle system would be required
Notes: 1 CW – center of fire area; NW, SW – off-center 2 A – automatic, M – manual 3 Extinguishment time – excluding rolled paper towel ignition source 4 Reignition time – time when sustained fire ignited outside burnback pan (B) or roll paper towel ignition source (I) 5 Non-air aspirated 6 No foam discharge from north MCAFFSS system													

6.3.1 Results of Test F1

Test F1 evaluated a single unit in automatic mode with no obstructions. The unit was positioned perpendicular to the center of the West edge of the pad. The CAFS nozzle was used and set to throw the foam into the center of the fire. The oscillation angle was set at 60 degrees. The spill size at ignition was approximately 32 m² (340 ft²). The fire was detected 4 seconds after ignition and the system activated automatically. The fire was approximately 0.6 m² (7 ft²) and had a flame height of 1.2 m (4 ft). At this point the fire probably was due more to the gasoline from the ignition source than burning JP-8. The 50% and 90% control times were 5 and 12 seconds. The fire was completely extinguished in 16 seconds.

The data from this test are shown in Appendix C (Figures C1-C15). The air temperatures, steel beam temperatures, heat flux, and concrete temperatures (3.0 m (10 ft) from the center) did not change significantly as a result of the fire. The surface temperature of the concrete at the center of the pad increased slightly, approximately 10°C.

6.3.2 Results of Test F2

Test F2 was a repeat of Test F1 with the MCAFFSS system set to push the foam across the pad. The spill size at ignition was approximately 32 m² (340 ft²). The fire was detected in 4 seconds and the system began to discharge. At activation, the fire was approximately the same size as in Test F1. The fire was approximately 0.6 m² (7 ft²) and had a flame height of 1.2 m (4 ft). The 50% and 90% control times were 17 and 30 seconds. The extinguishment time was 49 seconds. In this configuration the system was able to control and extinguish the fire quickly. However, the control and extinguishment times were longer than those recorded in Test F1. This was due to the additional time required to push the foam across the pad and cover the fuel surface.

The data from this test are shown in Appendix C (Figures C16-C30). The air, steel beam and concrete temperatures and the heat flux did not change significantly due to the fire. The highest heat flux was 1.8 kW/m² and was measured by the calorimeter located on the East edge of the pad.

6.3.3 Results of Test F3

Test F3 was designed to test the ability of the system to extinguish a fully involved JP-8 spill fire. The MCAFFSS unit was configured the same as in Test F2, except that the unit was activated manually 1 minute after ignition instead of automatically. The delay in activation provided the time required for the fire to become more fully involved. Obstructions were also added to simulate items (cable, tool cabinet and fuselage) that would be found in a hangar (see Figure 10). Details of these obstructions are included in Section 4.5.2. The spill size at ignition was approximately 32 m² (340 ft²). The fire was detected 7 seconds after ignition, but the unit was not activated until 1 minute after ignition. At detection, the fire was only about 0.9 m (3 ft) in diameter and had a flame height of 1.2 m (4 ft). At activation, the fire covered approximately 41 m² (440 ft²) of floor area. The flame height at activation, was approximately 15 m (48 ft). The fire was controlled rapidly, but was not completely extinguished. The 50% and 90% control

times were 11 and 23 seconds, respectively. A small strip along the East edge of the spill continued to burn after the agent discharge was complete. The unit was not able to push the foam to cover the entire spill area, resulting in burning along the East edge of the spill. After the discharge was complete, a re-ignition test was conducted. The burnback pan was used as the fire source. Re-ignition of the fuel spill occurred in 11 minutes and 22 seconds after the burnback pan was placed in the test area.

The data from this test are shown in Appendix C (Figures C31-C45). Due to the delay in system activation, the fire was able to grow to a significant size causing noticeable changes in the temperatures and heat fluxes measured around the test area. The concrete temperature measured at the surface in the center of the pad increased from 29°C to 56°C. The temperature measured 13 mm below the surface in the center of the pad did not change significantly. The concrete temperatures measured 3.0 m (10 ft) East of the center of the pad were higher than those measured in the center of the pad. The peak temperatures at the surface and 13 mm below the surface were 110°C and 46°C, respectively. The concrete temperatures measured 3.0 m (10 ft) West of the pad did not change significantly. This lack of change is supported by visual observations of the Westward fire spread being contained to a point less than 3.0 m (10 ft) from the center. The highest heat fluxes were measured by the calorimeter located along the East edge of the pad. The heat flux measured by the North, South and West calorimeters increased slightly before beginning to decrease after the system was activated. After activation, the North and South calorimeters increased from 12 kW/m² and 9 kW/m² to 20 kW/m² and 12 kW/m², respectively. The heat flux measured by these two calorimeters then decreased rapidly. The heat flux measured by the East calorimeter increased from 24 kW/m² to about 70 kW/m² after the system was activated. The fire being pushed toward the East by the foam caused the increase. The heat flux measured by the East calorimeter decreased quickly (about 15 seconds) after the increase. The air temperature over the center of the pad reached a peak value of 340°C and decreased immediately after system activation. The average maximum temperatures measured 3.0 m (10 ft), 4.6 m (15 ft) and 7.6 m (25 ft) from the center of the pad were 205°C, 168°C and 122°C, respectively. The maximum steel beam temperature measured was 70°C.

6.3.4 Results of Test F4

Test F4 was a repeat of Test F3 with the system configured to throw the foam onto the fire. The spill size at ignition was approximately 32 m² (340 ft²). The fire was detected in 20 seconds, but the system was activated manually 1 minute after ignition. At detection, the fire covered approximately 4.4 m² (48 ft²) of floor area and had a flame height of 2.4 m (8 ft). At activation, the fire covered approximately 43 m² (460 ft²) of floor area and had a flame height of about 15 m (48 ft). The 50% and 90% control times were 11 and 22 seconds. The fire was extinguished in 1 minute and 26 seconds. After the discharge was complete, a re-ignition test was conducted using the burnback pan. Re-ignition of the fuel spill occurred in 9 minutes and 48 seconds.

The data from this test are shown in Appendix C (Figures C46-C60). The temperature and heat flux data from Test F4 was similar to that recorded in Test F3. Only the center and East concrete temperatures increased. The West concrete temperatures did not change. This was also verified by visual observations of the fire spread. There was a small increase in the flux

measured by the East calorimeter after activation of the system. The heat flux increased from 30 kW/m² to 36 kW/m² after activation and then decreased rapidly. The increase is believed to be the result of the fire being pushed closer to the East edge by the foam. The fact that the increase is significantly less than that measured in Test F3 is probably due to the fact that in Test F3 the foam was pushed into the fire compared to being thrown into the center of the fire in Test F4. The average maximum air temperatures measured over the center of the pad and 3.0 m (10 ft), 4.6 m (15 ft) and 7.6 m (25 ft) from the center of the pad were 268°C, 215°C, 170°C and 125°C, respectively. The temperature measured over the center of the pad in Test F4 was significantly less than that measured in Test F3. The air temperatures measured 3.0 m (10 ft), 4.6 m (15 ft) and 7.6 m (25 ft) from the center of the pad were similar. The steel beam temperatures were also similar to those measured in Test F3 and were far below the critical steel beam temperature. During this test it was observed that the foam was able to bounce over the simulated fuselage (see Figure 19). Given the actual shape of an aircraft, this was not considered as a challenging enough scenario, given the potential for large silhouette aircraft with wing tanks. Increased obstructions were added in a repeat test, Test F6.

6.3.5 Results of Test F5

Test F5 was a repeat of Test F3 using non-air aspirated foam. The spill size at ignition was approximately 32 m² (340 ft²). The fire was detected 46 seconds after ignition, but the system was not activated until 1 minute and 37 seconds after ignition. The activation was delayed longer than 1 minute after ignition to compensate for the slow initial fire growth caused by the slow involvement of the ignition source and fuel spill. At detection, the fire involved 5.0 m² (54 ft²) of floor area and had a flame height of 2.4 m (8 ft). At activation the fire involved approximately 33 m² (360 ft²) of floor area and had a flame height of about 12 m (38 ft). The fire was controlled quickly, but it was not completely extinguished. The 50% and 90% control times were 13 and 28 seconds, but there was 0.2 m² (2 ft²) of residual burning in the Southeast corner of the pad. After the discharge was complete, a reignition test was conducted using the burnback pan as the fire source. Reignition of the fuel spill occurred in 8 minutes and 3 seconds (see Figure 20).

The data from this test are shown in Appendix C (Figures C61-C75). The concrete pad temperatures were similar to those measured in Tests F3 and F4 in that only the center and East pad temperatures increased. The West pad temperatures did not increase. In the center of the pad the peak surface temperature was 56°C and occurred prior to system activation. The peak temperature measured 13 mm below the surface was 44°C and was not measured until well after the fire had been controlled. The peak concrete temperatures measured 3.0 m (10 ft) East of the center of the pad were 103°C at the surface and 55°C 13 mm below the surface. The peak surface temperature occurred prior to system activation and the peak temperature 13 mm below the surface occurred after the fire was under control. The heat flux measured by the East calorimeter was 26 kW/m² prior to system activation. This increased to a peak of 48 kW/m² 15 seconds after the system was activated. The heat flux measured by the North and South calorimeters was 10 kW/m² prior to activation and both decreased quickly to less than 2 kW/m² after the system was activated. The different responses of the calorimeters were believed to be the result of the fire being pushed in the direction of the East calorimeter. The average maximum air temperatures measured over the center of the pad and 3.0 m (10 ft), 4.6 m (15 ft) and 7.6 m (25 ft) from the center of the pad were 205°C, 165°C, 136°C and 102°C, respectively. These

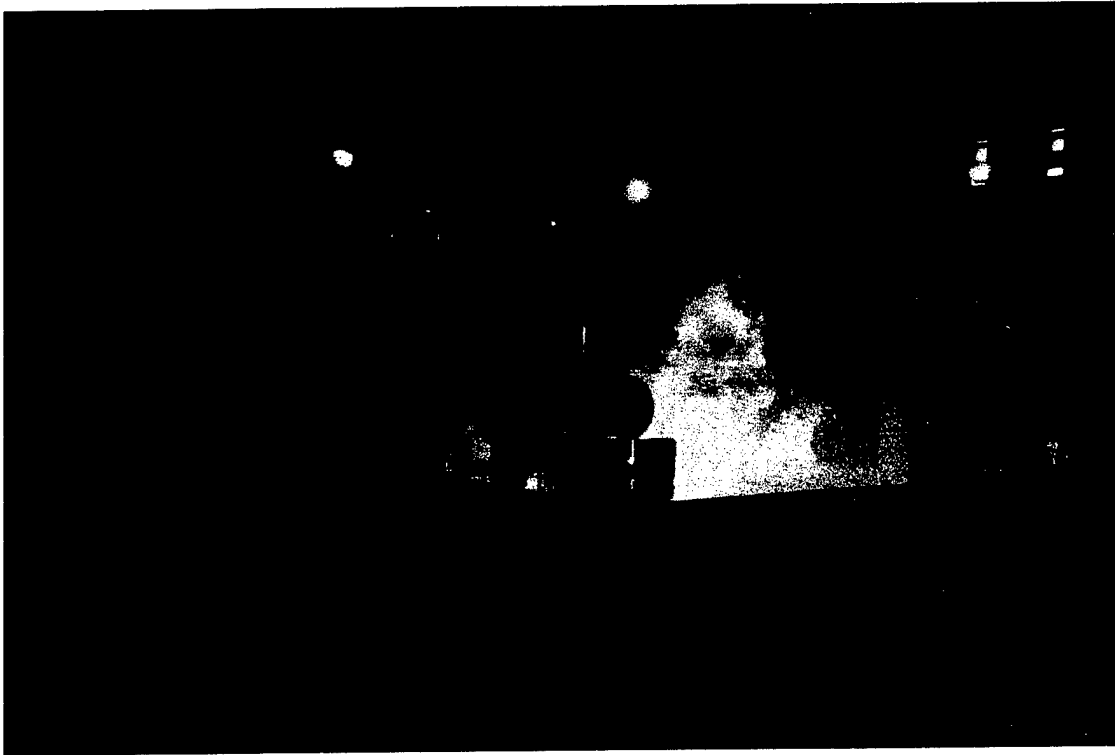


Figure 19 — Foam spray over obstruction in Test F4



Figure 20 — Sustained reignition in Test F5

temperatures are much lower than those measured in Test F3. This was probably due to the fact that in Test F5 the fire grew slower initially and was not as large when the system was activated as the fire in Test F3. The steel beam temperatures were similar to those measured in Test F3 and were far below the critical steel beam temperature.

6.3.6 Results of Test F6

Test F6 was a repeat of Test F4 (CAFS nozzle throw configuration, manual activation) with increased obstructions. The fuselage mockup was modified as shown in Figures 12 through 14. At ignition the fuel spill covered approximately 32 m² (350 ft²). The unit detected the fire 18 seconds after ignition, but was activated manually 60 seconds after ignition. At detection, the fire involved 3.0 m² (32 ft²) and had a flame height of 1.8 m (6 ft). At activation the fire involved approximately 42 m² (450 ft²) and had a flame height of 15 m (48 ft). The 50% and 90% control times were 34 seconds and 1 minute and 42 seconds. The fire was not completely extinguished. After the fire was 90% controlled, the fuel began to burnout.

The data from this test are shown in Appendix C (Figures C76-C90). The concrete pad temperatures were similar to those measured in previous tests in that only the center and East pad temperatures increased. The West pad temperatures did not increase. In the center of the pad the peak surface temperature was 55°C and occurred prior to system activation. The peak temperature measured 13 mm below the surface was 40°C and was not measured until well after the fire had been controlled. The peak concrete temperatures measured 3.0 m (10 ft) East of the center of the pad were 112°C at the surface and 56°C 13 mm below the surface. The peak surface temperature occurred prior to system activation and the peak temperature 13 mm below the surface occurred after the fire was under control. The heat flux measured by the East calorimeter was 24 kW/m² prior to system activation. This increased to a peak of 56 kW/m² 15 seconds after the system was activated. The heat flux measured by the North and South calorimeters was 12 kW/m² prior to activation and increased to 22 kW/m² after the system was activated. The measurements of both calorimeters then decreased quickly to less than 2 kW/m² after the system was activated. The different responses of the calorimeters were believed to be the result of the fire being pushed in the direction of the East calorimeter. The average maximum air temperatures measured over the center of the pad and 3.0 m (10 ft), 4.6 m (15 ft) and 7.6 m (25 ft) from the center of the pad were 240°C, 190°C, 160°C and 120°C, respectively. These temperatures are about the same as those measured in Test F4. However, the differences in the initial knockdown and control times between Tests F4 and F6 can be seen in the amount of time required to reduce the air temperatures and the heat flux. The steel beam temperatures were similar to those measured in previous tests and were far below the critical steel beam temperature.

6.3.7 Results of Test F7

Test F7 was a repeat of F3 (CAFS nozzle, manual activation, push) with an increased oscillation angle and a reduced system activation time. The oscillation angle was increased from 60 to 90 degrees. The activation time was reduced from 60 seconds (Test F3) to 45 seconds to allow more residual fuel. Since the system was configured to push the foam across the pad, there were no differences in the foam distribution across the pad caused by the increased obstruction (see Figure 21). At ignition, the spill covered approximately 31 m² (330 ft²). The fire was



Figure 21 — Foam spray in Test F7

detected in 20 seconds, but the unit was activated manually 45 seconds after ignition. At detection the fire involved 3.7 m^2 (40 ft^2) and had a flame height of 2.4 m (8 ft). At activation, the fire involved 25 m^2 (270 ft^2) and had a flame height of 12 m (38 ft). Due to the reduced activation time, the fire was much smaller at system activation than in previous tests. The 50% and 90% control times were 41 seconds and 1 minute and 35 seconds. There was approximately 1.4 m^2 (15 ft^2) of burning area remaining after the discharge was complete. The burning was occurring in areas that were not covered with foam. After the discharge was complete a reignition test was conducted using the paper towel igniter as the fire source. Sustained reignition occurred in 5 minutes and 41 seconds.

The data from this test are shown in Appendix C (Figures C91-C105). The concrete pad temperatures were similar to those measured in previous tests in that only the center and East pad temperatures increased. The West pad temperatures did not increase. In the center of the pad the peak surface temperature (prior to reignition) was 54°C and occurred after system activation. The peak temperature (prior to reignition) measured 13 mm below the surface was 40°C . The peak concrete temperatures measured 3.0 m (10 ft) East of the center of the pad were 90°C at the surface and 56°C 13 mm below the surface. The peak surface temperature occurred prior to system activation and the peak temperature 13 mm below the surface occurred after the fire was under control. The heat fluxes measured by the North, South and West calorimeters were less than 10 kW/m^2 prior to system activation. The heat flux measured by the East calorimeter was about 20 kW/m^2 prior to system activation. After the system was activated the heat fluxes measured by the North, South and East calorimeters increased to peak values of 12, 8 and 77 kW/m^2 , respectively. The heat flux measured by the West calorimeter did not increase significantly after the system was activated. The average maximum air temperatures measured over the center of the pad and 3.0 m (10 ft), 4.6 m (15 ft) and 7.6 m (25 ft) from the center of the pad were 138°C , 127°C , 110°C and 90°C , respectively. These temperatures are significantly less than those measured in Test F3. This was due to the reduced system activation time and not superior performance of the system. The steel beam temperatures were similar to those measured in previous tests and were far below the critical steel beam temperature.

6.3.8 Results of Test F8

Test F8 was a repeat of Test F7 using non-air aspirated AFFF. The oscillation angle and activation times were the same as those in Test F7. At ignition, the spill covered approximately 32 m^2 (340 ft^2). The fire was detected in 17 seconds, but the unit was activated manually 45 seconds after ignition. At detection the fire involved 3.7 m^2 (40 ft^2) and had a flame height of 2.4 m (8 ft). At activation, the fire involved 24 m^2 (260 ft^2) and had a flame height of 12 m (38 ft). This is about the same size as in Test F7 at activation. The 50% and 90% control times were 38 seconds and 1 minute and 3 seconds. These times were about the same as those recorded in Test F7. There was approximately 0.4 m^2 (4 ft^2) of burning area remaining after the discharge was complete. The burning occurred in areas that were not covered with foam. After the discharge was complete a reignition test was conducted using the paper towel igniter as the fire source. Sustained reignition occurred in 7 minutes and 57 seconds.

The data from this test are shown in Appendix C (Figures C106-C120). The concrete pad temperatures were similar to those measured in Test F8. The center and East pad temperatures

increased whereas the West pad temperatures did not increase. In the center of the pad the peak surface temperature (prior to reignition) was 60°C and occurred after system activation. The peak temperature (prior to reignition) measured 13 mm below the surface was 42°C. The peak concrete temperatures measured 3.0 m (10 ft) East of the center of the pad were 85°C at the surface and 62°C 13 mm below the surface. The peak surface temperature occurred prior to system activation and the peak temperature 13 mm below the surface occurred after the fire was under control. The heat fluxes measured by the North, South and West calorimeters were less than 10 kW/m² prior to system activation. The heat flux measured by the East calorimeter was approximately 22 kW/m² prior to system activation. After the system was activated the heat fluxes measured by the North and South calorimeters increased slightly to peak values of 14 and 10 kW/m², respectively. The West calorimeter did not increase after the system was activated. After the system was activated the heat flux measured by the East calorimeter increased to 68 kW/m² and then decreased. The average maximum air temperatures measured over the center of the pad and 3.0 m (10 ft), 4.6 m (15 ft) and 7.6 m (25 ft) from the center of the pad were 195°C, 160°C, 140°C and 110°C, respectively. These temperatures are similar to those recorded in Test F7. The steel beam temperatures were similar to those measured in previous tests and were far below the critical steel beam temperature.

6.3.9 Results of Test F9

Test F9 was conducted to evaluate the capability of the MCAFFSS unit to detect and control a fire from an off-axis location. The test was also designed to determine the lateral spread of foam outside the range of the oscillation angle. Two MCAFFSS units were positioned as shown in Figure 9. The unit located in the Southwest corner was setup to detect and discharge agent using a pushing action. The Northwest corner was setup only to detect the fire. The pad was modified as described in Section 4.5.3 to increase the floor surface area for "pushing" the AFFF. At ignition the spill covered 31 m² (330 ft²) of floor area. The Northwest unit detected the fire 44 seconds after ignition. The fire was approximately 8.4 m² (90 ft²) and had a flame height of 4.0 m (13 ft). The Southwest unit detected the fire 54 seconds after ignition and began to discharge foam. At activation, the fire was relatively small compared to previous tests. At activation, the fire involved 13 m² (140 ft²) and had a flame height of 5.5 m (18 ft). After agent discharge, there were two areas of residual burning: 0.2 m² (2 ft) behind the cabinet and 9.9 m² (96 ft) in the Northeast corner. The burning in the Northeast corner occurred outside of the turret oscillation angle. The Southwest unit was able to control the fire within the turret oscillation angle.

The data from this test are shown in Appendix C (Figures C121-C135). The results of this test were different than those in previous tests because the MCAFFSS unit did not control the fire outside of the oscillation range. The absence of rapid decreases in the temperatures and heat fluxes demonstrates this. The concrete temperature measured in the center of the pad increased to 44°C at the surface and increased only slightly 13 mm below the surface. The peak surface temperature occurred after the system was activated. The East pad temperatures increased to 52°C and 45°C at the surface and 13 mm below the surface, respectively. The peak surface temperature occurred after the system was activated. The peak temperature 13 mm below the surface occurred after the agent discharge was complete. The West pad temperatures did not increase significantly. The calorimeter located at the South edge of the pad was removed prior to

this test. The heat flux measured by the East calorimeter was similar to that measured in previous tests. Prior to system activation the heat flux was 10 kW/m^2 . The heat flux increased to a peak value of 71 kW/m^2 after the Southwest MCAFFSS unit began to discharge and then began to decrease. As the unit discharged the fire spread toward the North edge of the pad. When the system was activated the heat flux measured by the North calorimeter was about 4 kW/m^2 . However, approximately 45 seconds later the heat flux increased to 54 kW/m^2 . This flux was sustained for another 45 seconds before beginning to decrease as the fuel was consumed. The average maximum air temperatures measured over the center of the pad and 3.0 m (10 ft), 4.6 m (15 ft) and 7.6 m (25 ft) from the center of the pad were 117°C , 110°C , 105°C and 95°C , respectively. The steel beam temperatures were similar to those measured in previous tests and were far below the critical steel beam temperature.

7.0 DISCUSSION

7.1 Background Burns

7.1.1 Effects of Pad Temperature on Fire Spread and Size

Comparisons between Tests BB6 and BB7 illustrate the effect that the initial pad temperature had on a spill fire. Tests BB6 and BB7 were identical tests, except that Test BB6 was conducted at the end of a test day, and Test BB7 was conducted at the beginning of a test day. This was done to evaluate the effect of the concrete pad temperature on the fire growth. In Test BB6 (warm deck), the initial concrete pad temperature was 32°C compared to 24°C in Test BB7 (cold deck). There were significant differences between these two tests. In Test BB6, the size of the spill at ignition was 34 m^2 (370 ft^2) compared to 31 m^2 (335 ft^2). The visual measurements of maximum fire size, maximum flame height and flame spread rate were all higher for Test BB6 (warm deck) than Test BB7 (cold deck). The maximum fire size and maximum flame height were 32 m^2 (350 ft^2) and 10 m (33 ft) for Test BB6 and 28 m^2 (300 ft^2) and 7 m (23 ft) for Test BB7. The flame spread rate was 7.1 cm/s (2.8 in/s) in Test BB6 and 3.0 cm/s (1.2 in./s) in Test BB7. The larger fire size observed in Test BB6 resulted in higher temperature and heat flux measurements than Test BB7. The maximum average heat flux was 12 kW/m^2 in Test BB6 and 5 kW/m^2 in Test BB7. For Test BB6, the maximum average air temperatures above the center of the pad and 3.0 m (10 ft), 4.6 m (15 ft) and 7.6 m (25 ft) from the center of the pad were 160°C , 135°C , 115°C and 90°C , respectively. For Test BB7, the maximum average air temperatures were 108°C , 88°C , 76°C and 62°C , respectively.

7.2 Overhead Sprinkler Tests

Several sprinkler system configurations were evaluated in this test series. Deluge and closed-head systems were evaluated at two densities (10.2 Lpm/m^2 (0.25 gpm/ft^2) and 6.9 Lpm/m^2 (0.17 gpm/ft^2)). The deluge system was evaluated using three different activation times (no delay, 30 seconds and 80 seconds).

7.2.1 Performance of Overhead Sprinkler Systems

The objective of the overhead sprinkler system tests was to determine if either closed-head or deluge systems could control static JP-8 spill fires. For these tests, control was defined as disrupting the fire so that a single, turbulent plume was not established, stopping or significantly reducing flame spread across the fuel surface area, limiting building structural steel temperatures below critical values and limiting heat flux to adjacent targets (simulating adjacent aircraft). Based on the results of the background burns (BB6-BB8) and the sprinkler system tests, the steel temperature was not a factor for these tests. The maximum steel temperature measured in Test BB8 (with no suppression) was 61°C. During the sprinkler tests, steel temperatures greater than 61°C were observed in several tests, but the maximum steel temperature for any test was only 86°C. These temperatures are far below the failure criteria of 538°C identified in Section 5.0. Evaluation of structural steel would be a more significant issue for spills of greater depth and size (i.e., longer duration) and large, uncontrolled three dimensional fires. The remaining measures of performance (preventing the formation of a single plume, reducing flame spread across the fuel surface, and limiting heat flux to adjacent targets) were used to evaluate the performance of the overhead sprinkler system.

In all tests the sprinkler system was unable to prevent the formation of a single plume. This conclusion was based on visual observations of the fires. In Tests S5 and S6 multiple pools were not observed until approximately 1 minute and 20 seconds after ignition. This was about the time that the fuel in the center of the pad began to burn out. In Test BB8 (with no suppression), the fire at the center of the pad began to burn out in approximately 1 minute and 30 seconds.

The average flame spread rate before and after sprinkler activation are summarized in Table 5. In some of the tests, there was a significant amount of variability in the calculated flame spread rate. However, the data in this Table show that the overhead sprinkler systems were not able to reduce the flame spread across the fuel surface. The flame spread rates under free burning conditions were less than published data. In previous testing by the Naval Research Laboratory, the flame spread rate of JP-8 was determined to be 10 cm/s (4 in./s) [5]. The causes for the differences in the flame spread rate are unclear, but may be due to the thickness of the fuel layer. It has been demonstrated that the depth of the fuel layer has an effect on the flame spread [12]. An in-depth analysis of the causes for the changes in the flame spread rate is beyond the scope of this report. In most cases, the flame spread rate increased significantly (2-4 times) after sprinkler system activation. In Test BB8 (with no sprinkler activation) the average flame spread rate was 4 cm/s (1.6 in./s). This is significantly less than the flame spread rates observed after sprinkler activation in Test S2 and Tests S4-S7. In Test S1 (deluge system, no activation delay), the flame spread rate after activation was limited to 7.4 cm/s (2.9 in./s). This was the lowest post-sprinkler system activation flame spread rate for all of the sprinkler system tests, but the test scenario was not realistic. From a practical standpoint, an installed deluge system would not activate and discharge water the moment that ignition occurs. In Test S3, there were no data for flame spread following the activation of the sprinkler system. Due to the long delay in activation (80 seconds), the fire had grown very large and began to burn out in the center of the pad at activation.

Table 5. Average Flame Spread Rates Before and After Sprinkler System Activation

Test	Before Sprinkler Activation		After Sprinkler Activation	
	Average Flame Spread (cm/s (in./s))	First Standard Deviation	Average Flame Spread Rate (cm/s (in./s)) ¹	First Standard Deviation
S1	No Data	No Data	7.4 (2.9)	8.3 (1.3)
S2	4.6 (1.8)	0.5 (0.1)	17.3 (6.8)	8.1 (3.2)
S3	7.9 (3.1)	3.0 (1.2)	No Data	No Data
S4	6.1 (2.4)	2.8 (1.1)	10.7 (4.2)	3.0 (1.2)
S5	5.6 (2.2)	2.0 (0.8)	12.2 (4.8)	2.0 (0.8)
S6	5.8 (2.3)	2.8 (1.1)	12.2 (4.8)	0.8 (0.3)
S7	5.6 (2.2)	2.0 (0.8)	14.2 (5.6)	3.6 (1.4)
BB8 ²	4.1 (1.6)	1.0 (0.4)		

¹ For closed-head tests activation was time first sprinkler operated.

² No sprinkler activation for background tests.

In each of the sprinkler system tests, with the exception of Test S3, the heat flux at the adjacent targets increased after the system was activated. In Test S3, the heat flux decreased after activation, but this was due to fuel depletion. In Test S1, the sprinkler system was able to limit the fire size and the resulting heat fluxes. In the other tests, the heat flux increased significantly after the sprinkler system was activated. With the exception of Test S1, the average heat flux measured 30 seconds after activation was less than that measured 15 seconds after activation. In Test S1, the heat flux measured 30 seconds after activation was about the same as that measured 15 seconds after activation. This was probably due to the differences in the sprinkler system activation times. With delays in activation, there was less fuel remaining at activation than with no delay. As a result the fuel was beginning to burn out during the 30 seconds following activation.

A detailed analysis of the threat to aircraft located near the fire source is beyond the scope of this report. However, in a previous study [13] critical heat fluxes for ignition of several advanced composite materials typically used in aircraft were identified. The materials evaluated included two graphite/epoxy based and one Kevlar[®] honeycomb composite. The first graphite/epoxy based material (G/E1) consisted of graphite layers rotated 45° with respect to the previous layer and bonded with an epoxy resin. The majority of the G/E1 composites were 48 ply. The second graphite/epoxy based composite (G/E2) was composed of a short fiber mat then a metal-coated fabric followed by a fabric layer. The next six layers consisted of fabric followed by a layer of Teflon[®] coated glass. Each of the layers was bonded by an epoxy resin.

The Kevlar[®] based composite samples were taken from a concave shaped structure. The tapered sections consisted of an aluminum mesh followed by an unknown matrix of Kevlar[®] based layers. The honeycomb sections (Kevlar[®]-H) of the composite were composed of an aluminum mesh followed by Kevlar[®] layers. The inner layer was a brown honeycomb followed by more Kevlar[®] layers. The thickness of the Kevlar[®] based composite varied from 3 to 12 mm.

The critical heat fluxes for ignition (i.e., the heat flux which would cause the material to ignite) for the G/E1, G/E2, Kevlar® and Kevlar®-H materials were 40 kW/m², 36 kW/m², 24 kW/m² and 14 kW/m², respectively. These heat flux values correspond to ignition of the material. Irreparable damage will most likely occur at lower heat fluxes. Comparing the critical fluxes for ignition with the average heat fluxes measured 4.6 m (15 ft) from the center of the fire during the sprinkler system tests indicate that in most of the test scenarios, these materials would ignite if positioned the same distance from the fire. Tests S1 and S4 were the only tests where the average heat flux did not exceed the lowest critical heat flux of 14 kW/m² (Kevlar®-H). However, in both of these tests individual calorimeters recorded values in excess of 14 kW/m². Moreover, the average heat flux 15 seconds after activation for Test S4 was 12 kW/m², which is not significantly less than the critical ignition flux for Kevlar®-H. Test S3 was the only test in which the measured heat flux (43 kW/m²) exceeded the critical fluxes for the two graphite/epoxy materials (40 kW/m² and 36 kW/m²). These data indicate that for a 114 L (30 gal) JP-8 spill fire the heat flux 4.6 m (15 ft) from the center of the fire would be sufficient to ignite the Kevlar®-H composite. Based on the results of Test S3, if the fire were allowed to grow freely (i.e., no suppression system activation) or if suppression system activation were significantly delayed, the heat flux 4.6 m (15 ft) from the center of the fire would be sufficient to ignite both Kevlar® and the two graphite/epoxy composites.

Tests S1-S3 evaluated deluge systems with different activation times. With almost no delay (6 seconds) in activation (Test S1), the system was able to limit the size of the fire to 17 m² (180 ft²). The heat flux and temperatures after activation remained relatively low. With a 32 second delay (Test S2), the fire increased significantly in size and intensity after activation. At 20 seconds after activation, the fire began to decrease in size. With an 80 second delay in activation (Test S3), the fuel was being depleted at about the same time as the system was being activated.

Test S2 and S7 evaluated deluge systems with approximately 30 second activation delays using two different densities. Test S2 used 10.2 Lpm/m² (0.25 gpm/ft²) and Test S7 used 6.9 Lpm/m² (0.17 gpm/ft²). The fire increased in size and intensity quicker at the higher density (Test S2). At the lower density (Test S7), the fire also increased in size, but required more time to do so.

There did not appear to be a significant difference between the performance of the deluge and closed-head systems. Both types of systems were evaluated at 6.9 Lpm/m² (0.17 gpm/ft²) (Tests S6 and S7) and at 10.2 Lpm/m² (0.25 gpm/ft²) (Tests S2 and S4). For both types of systems the fire continued to grow after activation. For the closed-head tests all of the sprinklers were open in less than 20 seconds after the first sprinkler opened. There are differences in the heat flux and temperature measurements as shown in Table 3, but these are likely due to the differences in activation times for the systems.

7.3 MCAFFSS Tests

7.3.1 Performance of Fire Detector

An Omniguard Model 850 UV/IR fire detector was used to detect the fire and activate the MCAFFSS units. The USAF ETL [8] currently requires the use of Listed dual-spectrum (UV/IR) optical detectors. The detectors are also required to be able to detect a fully developed 3 m (10 ft) by 3 m (10 ft) JP-4, JP-8, or JET-A fuel fire at a minimum distance of 45 m (150 ft) within 5 seconds. It is important to point out that the fire detector in these tests was about 14 m (45 ft) from the center of the concrete pad, which was the point of ignition. In Test F9, the detector was 16 m (54 ft) away from the center of the pad. In Test F9 the detector was 14 m (46 ft) West and 9 m (29 ft) South of the center of the pad. After Test F2, obstructions were positioned in the test area, which blocked the field of view of the detector.

Table 6 summarizes the detection times and fire size at detection for each of the MCAFFSS tests. There was only one instance where a fire grew to the size specified in the USAF ETL prior to detection. However, the detector was in an off-axis location, which is not part of the ETL criteria. The Southwest unit in Test F9 did not detect the fire until it had grown to 13 m² (140 ft²). The Northwest unit detected the fire 10 seconds earlier and the fire was 8.4 m² (90 ft²), which is smaller than the design fire. To determine if the Southwest unit detected the fire within 5 seconds after the fire reached 9 m² (100 ft²) requires more precision than visual observations allow. Conservatively, the fire was detected in less than 10 seconds after reaching the design fire size.

Table 6. Summary of Fire Detector Performance Data

Test	Detector Location	Obstruction	Detector Time (sec)	Fire Size at Detection (m ² (ft ²))	Flame Height at Detection (m (ft))
F1	Center	No	4	0.6 (7)	1.2 (4)
F2	Center	No	4	0.6 (7)	1.2 (4)
F3	Center	Yes	7	0.6 (7)	1.2 (4)
F4	Center	Yes	20	4.4 (48)	2.4 (8)
F5	Center	Yes	46 ¹	5.0 (54)	2.4 (8)
F6	Center	Yes with Increased Obstruction	18	3.0 (32)	1.8 (6)
F7	Center	Yes with Increased Obstruction	20	3.7 (40)	2.4 (8)
F8	Center	Yes with Increased Obstruction	17	3.7 (40)	2.4 (8)
F9	Center	Yes with Increased Obstruction	44 and 54	8.4 (90) and 13 (140)	4.0 (13) and 5.5 (18)

¹ Increased detection time due to slow initial fire growth.

The addition of obstructions increased the detection time and resulting fire size at the time of detection. With no obstructions (Tests F1 and F2), the fire was detected in 4 seconds when the fire was only 0.6 m² (7 ft²) with a flame height of 1.2 m (4 ft). With the addition of obstructions to the test area (see Figure 10), the detection time increased. For Tests F3 through F5, a fuselage mockup was positioned between the detector and the ignition point of the fire. For Tests F3 through F5, there was a very wide range of detection times (7 to 46 seconds). The

46 second detection time in Test F6 was due to the slow initial fire growth, which was caused by the delay in burning the small bag of gasoline adjacent to the paper towel. Based on the similarities in the size of the fire at detection in Tests F4 and F5, the detection time in Test F5 would probably have been similar to that of Test F4. The 7 second detection time in Test F3 may have been due to reflection off the fuel or pad surface or some other transient condition not experienced in the other obstructed tests. The increased obstruction configuration used in Tests F6-F8 did not have a significant effect on the detection time or fire size at detection. In each of these tests, the fire was detected in about 20 seconds with a fire size of about 3.7 m² (40 ft²).

The position of the fire detectors relative to the fire had a significant effect on the detection time and the fire size at detection. In Test F9, two MCAFFSS units were positioned in off-axis locations as shown in Figure 9. The detection time and fire size at detection increased more than 100% compared to Tests F6-F8 with the detector positioned along the center of the pad. The Northwest and Southwest units alarmed in 44 and 54 seconds, respectively. The fire sizes at detection were 8.4 m² (90 ft²) for the Northwest unit and 13 m² (140 ft²) for the Southwest unit.

7.3.2 Air Aspirated vs. Non-air Aspirated AFFF

Tests were conducted to compare the effectiveness of the air aspirated and non-air aspirated foam. Tests F3 and F5 evaluated air aspirated and non-air aspirated foam respectively in the push configuration with an oscillation angle of 60 degrees. Obstructions were in place for both tests (see Figure 10). In both tests the system was activated manually. In Test F3 the fire was allowed to burn for 1 minute before the system was activated. In Test F5 the system was activated 1 minute and 37 seconds after ignition. Additional preburn time was allowed in Test F5 to compensate for the slow growth of the fire initially. The fire size at activation was smaller for Test F5 than F3. In addition the detection time was longer in Test F5 than in Test F3, indicating slower fire growth. The differences in activation time did not appear to have a significant effect on the control or extinguishment of the fire. The 50% control times were 11 and 13 seconds for the air aspirated and the non-air aspirated AFFF, respectively. There was also little difference in the 90% control times (23 seconds for air aspirated and 28 seconds for non-air aspirated foam). In both tests the fire was not completely extinguished. In Test F3, there was residual burning along the East edge of the spill, beyond the foam blanket. In Test F5, there was residual burning in the Southeast corner. The data for Tests F3 and F5 can be normalized to account for the effect of the slightly different nozzle flow rates and fire sizes at agent activation. Foam control density (L/m², gal/ft²) is a measure of agent used to achieve 90 percent control over the area of fire involvement. The control densities for Tests F3 and F5 were 2.48 L/m² (0.061 gal/ft²) and 3.58 L/m² (0.088 gal/ft²) respectively.

Tests F7 and F8 evaluated air aspirated and non-air aspirated foam respectively using the push technique with an increased turret oscillation angle. The detection and control times were essentially the same for Tests F7 and F8. The fire was detected in 20 seconds in Test F7 and 17 seconds in Test F8. The 50% and 90% control times were 41 seconds and 1 minute and 35 seconds in Test F7, and 38 seconds and 1 minute and 3 seconds in Test F8. In both tests, the fire was not extinguished. In Test F7, there was approximately 1.4 m² (15 ft²) of residual

burning. In Test F8, there was 0.4 m² (4 ft²) of residual burning. The control density for the CAFS (Test F7) was 16.7 L/m² (0.41 gpm/ft²) compared to 11.4 L/m² (0.28 gal/ft²) for the AFFF (Test F8).

The reignition potential did not vary significantly in the tests with different nozzles. In Tests F3 and F5, reignition times using the MIL SPEC burnback pan were 11 minutes and 12 seconds and 8 minutes and 3 seconds for the CAFS and AFFF nozzles respectively. In Tests F7 and F8, reignition times using the ignition source were 5 minutes and 41 seconds and 7 minutes and 57 seconds for CAFS and AFFF, respectively. The reignition time decreased for the decreased effective application rate in Tests F7 and F8, as expected. In this situation, the AFFF nozzle showed a modest advantage. With the higher application rate tests (F3 and F5), the CAFS nozzle showed a modest advantage. Any differences in these times is probably within the range of expected experimental error.

There does not appear to be a significant difference between the effectiveness of the air aspirated and non-air aspirated foam. The control times and extinguishment capability were essentially the same for air aspirated and the non-air aspirated foam. Foam control density slightly favored the CAFS in the 60 degree push tests but favored the AFFF in the 90 degree tests. Reignition times were similar. These results were expected since the expansion ratio and drainage rate characteristics of the CAFS nozzle were adjusted to be similar to the AFFF nozzle (see Section 4.5.1).

7.3.3 Effect of Nozzle Orientation on Effectiveness of MCAFFSS

Tests were conducted to evaluate the performance of the MCAFFSS unit in the throw and push modes. With no obstructions in place, the control and extinguishment times in the push mode (Test F2) were higher than for the throw scenario (Test F1). This was expected since the throw was targeted to the center of the pad. Beginning with Test F3, obstructions were added to simulate items that might be found in an aircraft hangar (see Section 4.5.2). For the CAFS nozzle Tests F3 (push) and F4 (throw) the obstructions were configured as shown in Figure 10. The 50% and 90% control times for these tests were essentially the same. The control density for Test F3 was 2.48 L/m² (0.061 gal/ft²), which was essentially the same as the control density for Test F4 (2.28 L/m² (0.056 gal/ft²)). However, it was observed that in Test F4 the foam was striking the side of the fuselage mockup, bouncing over the top and landing on the fire. A larger obstruction was used beginning with Test F6. Comparing Tests F3 (push) and F6 (throw) also demonstrates the differences between the effectiveness of the push and throw scenarios using the CAFS nozzle. For the throw scenario, the 50% and 90% control times were 34 seconds and 1 minute and 42 seconds. These were higher than those for the push scenario, which were 11 and 23 seconds. In the push scenario there was only a minimal amount of residual burning. In the throw scenario, however, there was a much larger area, approximately 3.7 m² (40 ft²), burning after the discharge was complete. Based on the results of these tests, the push scenario was the more effective method for extinguishing obstructed fires. The data support the philosophy used in the ETL which recommends a "push" technique. Agent can be effectively "targeted" to a pool fire hazard only if there are limited obstructions. Since this is not the case in most hangar scenarios, the ETL approach to "push" foam is appropriate.

7.3.4 Effect of Obstructions on Effectiveness of MCAFFSS

Tests were conducted with different obstruction configurations to evaluate the ability of the MCAFFSS unit to control and extinguish spill fires in realistic hangar scenarios. Tests F1 and F2 were conducted with no obstructions. Obstructions were added for Tests F3-F9 to provide more realistic scenarios (see Section 4.5.2). For Tests F3-F5, the obstructions were configured as shown in Figure 10. For Tests F6-F9, the obstructions were modified as shown in Figure 12. The results of Tests F1, F4, and F6 show the effect of obstructions on the effectiveness of the MCAFFSS unit configured for throw. In Test F1 (no obstruction) the 50% and 90% control times were 5 and 12 seconds. The extinguishment time was 16 seconds. In Test F4, with the addition of the obstructions, the control times increased slightly and the extinguishment time increased significantly. The 50% and 90% control times were 11 and 22 seconds and the fire was extinguished in 1 minute and 26 seconds. There was residual burning under the simulated tool cabinet after agent discharge. In Test F4, it was observed that the foam was striking and bouncing over the simulated fuselage and on the fire. This is not likely to occur if the foam hits the side of an aircraft with a large silhouette and the fire is on the other side of the aircraft. The fuselage mockup was modified for Tests F6 to create a more realistic scenario. In Test F6, the 50% and 90% control times were significantly higher than those observed in Tests F1 and F4. For Test F6, the 50% and 90% control times were 34 seconds and 1 minute and 42 seconds. The modified fuselage obstruction prevented the foam from bouncing over the mockup and on the fire, which increased the control times.

7.3.5 Effect of Turret Oscillation Angle on Effectiveness of MCAFFSS

Tests were conducted with different turret oscillation angles to evaluate the effects of reducing the effective application rate on the control and extinguishment capabilities of the MCAFFSS unit. Test F7 was a repeat of Test F3 with an increased turret oscillation angle using the CAFS nozzle (air aspirated foam). In Test F3 the angle was set at 60 degrees and in Test F7 the angle was increased to 90 degrees. In both tests, the push technique was used. The control times were significantly higher for the 90 degree configuration than for the 60 degree. For the 60 degree oscillation angle (Test F3), the 50% and 90% control times were 11 and 23 seconds, respectively. For the 90 degree oscillation angle (Test F7), the control times were 41 seconds and 1 minute and 35 seconds. After the discharge was complete in Test F3, there was only a small strip of residual burning (less than 0.1 m^2 (1 ft^2)). In Test F7, there was a significant amount of residual burning (1.4 m^2 (15 ft^2)). During Test F7 it was observed that the foam blanket did not cover as much of the concrete pad surface as in Test F3. This was caused by the reduced reach of the foam after contact with the pad. In Test F3 the foam blanket was able to extend 7.6 m (25 ft) from the point of contact at the West edge of the pad. In Test F7 this distance was reduced to 6.1 m (20 ft). This was the cause of the increased residual burning area in Test F7.

Test F8 was a repeat of Test F5 with an increased turret oscillation angle using the non-air aspirated AFFF. In Test F5 the angle was set at 60 degrees and in Test F8 the angle was increased to 90 degrees. In both tests, the push technique was used. The results of these two tests were similar to Tests F3 and F7. The 50% and 90% control times for Test F8 were longer than Test F5. The 50% and 90% control times were 13 and 28 seconds in Test F5 and 38 seconds and

1 minute and 3 seconds in Test F8. There was slightly less residual burning in Test F5 (0.2 m² (2 ft²)) than in Test F8 (0.4 m² (4 ft²)). In Tests F5 and F8, the foam covered approximately the same amount of pad area, but in Test F8 it required more time. The ability of the foam to cover the same amount of area with a larger turret oscillation angle is due to the fluidity of the non-air aspirated foam.

7.3.6 Effect of Off-Axis Location on Effectiveness of MCAFFSS

Test F9 was conducted to evaluate the capability of the MCAFFSS unit to detect and control a fire from an off-axis location. Two MCAFFSS units were positioned as shown in Figure 9. One unit was setup to detect and discharge (Southwest) and the other unit was only setup to detect the fire (Northwest). The effect of the off-axis location on the detection time is discussed in Section 7.3.1. After agent discharge there was significant residual burning. There was 0.2 m² (2 ft²) burning behind the simulated tool cabinet and 8.9 m² (96 ft²) burning in the Northeast corner of the pad. The burning in the Northeast corner occurred outside of the turret oscillation angle. There was only a small area of residual burning (behind tool cabinet) within the oscillation angle. The MCAFFSS unit was able to control the fire within the area it covered. In this scenario a second unit would be required to control and extinguish the fire that could not be reached by the first unit.

8.0 ENGINEERING ANALYSIS OF MCAFFSS

The MCAFFSS has been proposed for use as a cost-effective alternative to low level AFFF suppression systems. To date, demonstrations have been conducted which indicate that the unit can detect a fire and discharge foam to extinguish an aviation fuel pool fire. The tests conducted in this test series were used to gather additional information related to the characteristics of the foam agent, discharge characteristics of the nozzle and detection capabilities. Specifically, the need to use compressed air foam in place of non-air aspirated AFFF was evaluated, along with the effects of obstructions. The detection capability of the unit was also evaluated in an off-axis configuration. As noted in the project test plan, there are numerous design/installation issues related to the potential use of the portable MCAFFSS unit in a hangar. A detailed engineering analysis of the MCAFFSS is beyond the scope of this fire test report. A preliminary analysis has been performed to provide the Air Force with the parameters and design issues which need to be considered before field implementation of the MCAFFSS.

8.1 Technical Requirements

As currently envisioned, MCAFFSS is proposed as a one-to-one replacement for detection and foam suppression systems currently installed to protect USAF hangars. Two presumptions related to the technical requirements for hangar protection can be made: the system currently specified for hangars in the ETL [8] other military handbooks [9] and commercial consensus standards [14] reflects the level of protection which is consistent with operational requirements and an acceptable level of risk; or, fundamental changes have occurred (e.g., in terms of hazard and environmental considerations) which result in a need to readdress the technical requirements and resulting designed level of protection and risk posture. This

analysis does not prejudice which is appropriate, but outlines the associated performance parameters by which MCAFFSS should then be evaluated.

8.1.1 Existing Design Basis

Current design specifications require one of three protection systems:

- conventional wet-pipe sprinkler system (8.0 Lpm/m² over 1400 m² [0.2 gpm/ft² over 15000 ft²]) and one of the following low-level fuel spill fire suppression systems:
 - High-expansion foam system providing a minimum foam depth of 1.0 m (3 ft) over the entire aircraft servicing area and adjacent undivided areas.
 - Low level foam-water nozzle system providing 4.0 Lpm/m² (0.1 gpm/ft²) over the aircraft servicing area.
- A closed-head (wet pipe or pre-action) foam-water sprinkler (6.5 Lpm/m² over 1400 m² [0.16 gpm/ft² over 15,000 ft²]) when the maximum floor to ceiling height is 12 m (40 ft) or less.
- A closed-head (wet pipe or pre-action) foam-water sprinkler system (6.5 Lpm/m² over 465 m² [0.16 gpm over 5000 ft²]) and a low-level foam-water nozzle system (4.0 Lpm/m² [0.1 gpm/ft²] over the aircraft servicing area) when the floor to ceiling height is greater than 12 m (40 ft).

The system selection is based on an economic and mission analysis, subject to approval by the Major Command (MAJCOM). Overhead system pre-action deluge valves are tripped by ceiling thermal detectors. Closed-head wet pipe systems are activated by melting of the sprinkler fusible links. Low level systems are activated by ceiling sprinkler operation or manual alarm pull stations installed specifically for that purpose. Optical detectors are provided for alarm purposes only and may be deleted at the discretion of the MAJCOM fire protection engineer. Optical detector alarm signals no longer automatically activate low level systems because of historical problems associated with false activation and system discharges.

The total required foam discharge time is 10 minutes. Low-level foam nozzles are limited to 1900 Lpm (500 gpm) maximum to assure that the loss or obstruction of a single nozzle does not significantly reduce the total floor area coverage. In designing underwing pattern discharge coverage, credit is given to the "pushing" characteristics of AFFF (see Section A3.4.3 of the ETL). Nozzles are designed to apply AFFF no closer than 3 m (10 ft) from the edge of an aircraft shadow area and push the AFFF under the aircraft. Coverage is based on twice the throw distance by the width at the widest point of the pattern. The application rate of 4.0 Lpm/m² (0.10 gpm/ft²) must be maintained throughout the pattern area.

8.1.2 Redefined Technical Requirement

It may be appropriate to redefine the technical requirements associated with hangar fire protection and resulting level of installed protection. In particular, environmental concerns are resulting in the restricted discharge of AFFF systems. This is already reflected in the elimination of AFFF from overhead sprinklers in some situations in the new ETL. To a large extent, JP-4 fuel has been replaced by JP-8, which results in a reduced ignition hazard and a slower flame spread [18]. It may be appropriate to readdress the technical requirements which are reflected in the level of protection in a USAF hangar as now specified in the ETL. The risk posture and the operational requirements document (ORD) are considered when establishing the technical requirements. Assuming that the ORD remains unchanged, the risk is assessed in terms of a fire hazard analysis which considers the following:

1. Spill and ignition scenarios
 - a. Impact of JP-8 change-out (Ref [18])
 - b. Loss history
 - c. Maximum spill size/thickness
 - d. Three-dimensional scenarios
2. Probability of ignition
3. Mitigation strategies (including the impact of recent research and environmental restrictions)
 - a. Removal of AFFF from overhead
 - b. Likelihood of thermal detection at roof
4. Cost of mitigation strategies
 - a. Construction costs
 - b. Life cycle costs
5. Consequences of protection
 - a. Direct and indirect fire loss consequences
 - b. Environmental impact
 - (1) Fire
 - (2) Protection systems
6. Overall risk profile
 - a. Probability of event
 - b. Ability of systems to protect assets/limit damage
 - c. Reliability of systems
7. Development of technical requirements to meet ORD, consistent with acceptable level of risk

This results in an overall risk-benefit analysis with associated costs, which allows the "owner" to select an optimized level of protection.

As an example, the impact of replacing JP-4 with JP-8 in terms of reducing the hangar fire hazard needs to be thoroughly assessed. The work conducted by AFCESA at Tyndall AFB [15] supplements previous analysis [5] of the flash point differences and reduction in flame spread rate of JP-8 compared to JP-4. Spill scenarios are evaluated in terms of likely fuel depths (which impact on fire duration). It was recommended that, even though it has been determined that JP-8 provides greater fire safety than JP-4, it is prudent to determine the most cost effective intervention method should an inadvertent or accidental fire occur.

This approach should be invoked if the MCAFFSS is used as-is, since its use would result in an inherent change in the current level of protection (e.g., lower application rates and discharge times). The following sections outline the differences between the existing ETL criteria (and other nationally recognized standards) and the expected performance of the MCAFFSS. These differences may be entirely acceptable, but the rationale and associated fire hazard analyses should be prepared to support this decision.

RECOMMENDATION - Establish whether the MCAFFSS fire protection performance should be equal or similar to that established by the ETL. Alternately, conduct a fire hazard analysis to determine the risk/benefit associated with the performance of the MCAFFSS in its current configuration. A blueprint for a technical requirements analysis is provided by a similar analysis recently performed for USAF Hush Houses [16]. Since a number of aspects related to the ETL have been questioned, a reassessment of the technical requirements appears to be warranted.

8.2 Performance Evaluation

8.2.1 Detection

The optical fire detector used on the MCAFFSS unit performed well in the tests. Fires were detected in times ranging from 4-54 seconds. Optical detector performance was only assessed to the extent that the units could view a fire within the range of the AFFF monitor nozzle. To a large degree, the discharge characteristics of the AFFF nozzle appear to be the limiting factor in terms of area of coverage, as opposed to the sensor range.

The unit selected is typical of those currently used in USAF hangars. False alarm/inadvertent suppression system discharge from fielded optical detectors resulted in changes to the ETL. Combination UV/IR detectors are explicitly specified. Optical detectors no longer are used to trip low level system deluge valves, but are used for alarm purposes only. The MCAFFSS design would revert to the earlier system activation concept, i.e., activation using the optical sensor. Without design improvements, it is likely that problems previously encountered with fixed system activations would also be associated with a mobile unit. In terms of reliability, the MCAFFSS would represent a return to a level of performance which has been deemed unacceptable, albeit with potentially less impact (i.e., less foam discharged inadvertently).

Optical detector placement and design have the potential to be improved. As noted in the test plan [6], a detailed detection and reliability performance evaluation of the MCAFFSS optical sensor was well beyond the scope of these tests. Detection parameters would include field of view, distance from fire source, size of fires detected (which is a function of fuel), spacing,

height and the impact of obstructions. Likewise, false alarm and reliability testing involves a wide range of potential spurious signals. Preliminary results from ongoing tests will become available shortly. These tests, recently completed by the Naval Facilities Engineering Command (NAVFAC), the Naval Research Laboratory (NRL) and the National Research Council of Canada (NRC) [17], indicate that different units have different detection sensitivities and resilience to optical stresses. Data from these tests can be used to develop an improved performance specification for optical detectors used in hangars.

Optical detector placement may not be optimized if each foam unit has a sensor, but multiple units are needed to protect an aircraft. In other words, the coverage from the foam nozzle may result in more sensors than would normally be required.

RECOMMENDATION - Reference and use the NAVFAC optical detector test data to improve performance if it is desired to use these devices for system activation. The characteristics of the optical detector should be consistent with the spacing/placement of MCAFFSS units for fire suppression as described in Section 8.2.2.3 below.

8.2.2 Fire Suppression

8.2.2.1 Application Rate

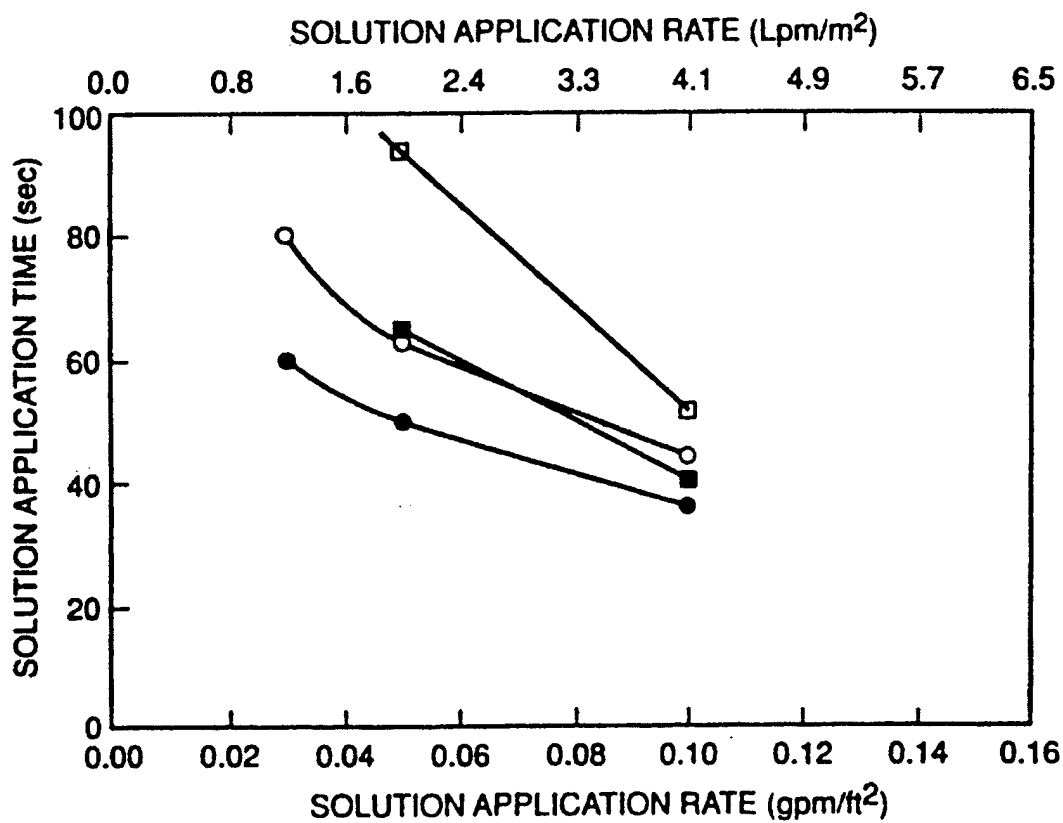
A low-level application rate of 4.0 Lpm/m² (0.10 gpm/ft²) is specified in the ETL. The MCAFFSS provides an effective spray pattern coverage area on the order of 112 m² (1200 ft²) with the 60-degree pattern setting and the nozzle angled for 18 m (60 ft) reach. With a nozzle flow of 265 Lpm (70 gpm), this results in an effective application rate of about half of the ETL criteria, 2.04 Lpm/m² (0.05 gpm/ft²). Data from the literature indicates that aviation fuel fires can be extinguished using rates of this magnitude [18]. For example, the U.S. Navy uses an 2.45 Lpm/m² (0.06 gpm/ft²) discharge rate for AFFF flowing from flush deck nozzles on aircraft carrier flight decks [19]. The 4.0 Lpm/m² (0.10 gpm/ft²) low-level application rate is recognized in the MIL Handbook 1008C [9] and NFPA 409 [17] and provides a safety factor over the minimum rate required for control/extinguishment. Lower rates may result in longer extinguishment times (see Figures 22 and 23).

The reduced effective application rate in Test F8 with a 90-degree nozzle pattern was at least partially responsible for the increased control time (63 seconds) compared to a similar test, Test F5. In Test F5, the effective application rate was greater due to a narrower discharge pattern. This resulted in a quicker control time, 28 seconds.

RECOMMENDATION - If the MCAFFSS is used, the foam duration should be increased. Alternately, the allowance of 2 minutes foam supply should be established in a redefined technical requirement.

8.2.2.2 Foam Duration

The ETL specifies a duration of 10 minutes for low level systems. This is consistent with the MIL Handbook and NFPA 409. The MCAFFSS has a duration of about 2 minutes in its



Note: No fire control or extinguishment at 0.03 gpm/ft²

- CONTROL TIME - AGENT A
- FIRE EXTINGUISHING TIMES - AGENT A
- CONTROL TIME - AGENT B
- FIRE EXTINGUISHING TIMES - AGENT B

Figure 22 — Fire control and extinguishing times as a function of solution application rate using AFFF at 250, 400, and 800 gpm on 743 m² (8000 ft²) JP-4 fuel fires [21]

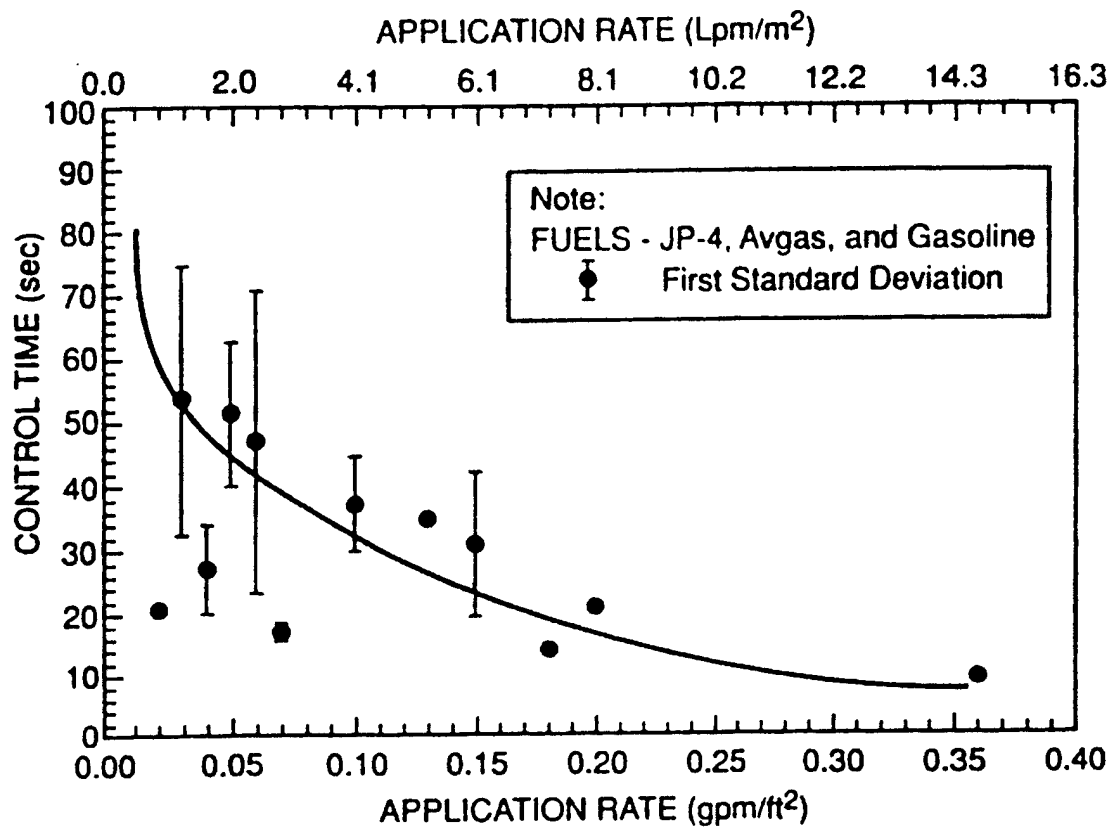


Figure 23 — AFFF control time as a function of application rate [22]

present configuration. Low level systems are designed to control a fire in 30 seconds and extinguish a fire in 60 seconds (NFPA 409 performance objectives). The remaining foam is designed for protection against persistent fires (e.g., three-dimensional fires not completely extinguished by the low level system) and to provide protection against burnback. Recent tests by the Naval Facilities Engineering Command [20] indicate that in a facility with floor drains, burnback from a high-intensity, unextinguished exposure fire can occur relatively quickly after the foam supply is depleted. This implies that there is a significant difference in burnback resistance between the proposed MCAFFSS and the existing ETL design criteria. One method to assess this performance difference is to evaluate the potential response of personnel after the fire is detected. In the case of the ETL, the design allows for a potential response of up to 10 minutes for fire department personnel to respond and use manual fire fighting equipment. In the current MCAFFSS design, this response time is potentially reduced to 2 minutes.

RECOMMENDATION - If the MCAFFSS is used, the foam duration should be increased. Alternately, the allowance of 2 minutes foam supply should be established in a redefined technical requirement.

8.2.2.3 Pattern/coverage

The current ETL concept of "pushing" AFFF was described in Section 8.1.1 above. The data from the tests indicate that where there is the potential for obstructions, the push technique is more effective compared to AFFF that is "thrown" and may be obstructed (see Section 7.3.4). If the pattern is increased to include a wider protected area, the effective fire extinguishment throw distance may be reduced (see Section 7.3.5). Test F9 demonstrated that it is unlikely that any significant lateral area outside the pattern coverage area will be rapidly controlled by a single nozzle. All of these data indicate that positioning/spotting of the existing MCAFFSS unit is critical for adequate coverage. The ETL approach of placing monitors near the hangar wall is unacceptable with the current MCAFFSS design because of flow and reach limitations. An aircraft fuselage and wing tank profile may result in a significant obstruction to any spray pattern. It is intended that the MCAFFSS be manually positioned based on the hazard to be protected.

A complete analysis of spotting criteria and parameters needs to be performed for the MCAFFSS. This is a very important element in determining the overall feasibility of the concept. Based on the data discussed above, a very general, preliminary design guideline would be to require two units per aircraft. Spacing scenarios should be developed to determine if "standard" spacing can be implemented. This would be desirable in terms of limiting equipment variability (e.g., nozzle height and angle adjustments). The potential variability of aircraft parking locations and different hangar designs/configurations, combined with up-tempo situations (e.g., war time) make it questionable that standard spotting of the units can be realistically accomplished. If this is the situation, personnel will be relied on to position the units as a function of the target hazard. Frequent movement of devices would require assessment in terms of manpower effort and training requirements, in addition to the required published guidance. An example of concepts for implementing MCAFFSS in terms of protection area, acquisition, maintenance and operations is contained in Appendix D.

The concept of targeting selected hazard areas beyond the perimeter of the hangar wall suggests that areas near the hangar will remain unprotected. This is a change from the current ETL design concept, where peripheral areas between aircraft and the hangar structure are protected (essentially the entire floor area). There is anecdotal information that spills occur which cover large areas. Ignition of these spills is rare, but not unheard of. Spotting of the nozzles to protect specific aircraft would have to be addressed in redefined technical requirements. The analysis would involve the following:

- likelihood of a spill, reasonable spill size, and maximum expected spill size;
 - characterization of ignition sources, and likelihood that the ignition source is intimate with the aircraft or aircraft parking area vs. ignition outside the immediate parking area;
 - potential fire spread/growth from the ignition (based on data from this test series and the JP-8 ignition study [15]);
 - probability that fire growth in areas targeted by MCAFFSS are limited to a size which can be controlled and extinguished by the MCAFFSS unit (including effects of obstructions or detection); and
 - potential impact of an uncontrolled fire outside the targeted area damaging aircraft due to thermal radiation (factoring in duration of potential spill fire).
- The methodology used in a recent Fire Hazard Analysis of USAF Hush Houses is amenable for this application [23].

Based on this analysis, design fire scenarios can be selected, and the risk of only using targeted units can be quantified.

RECOMMENDATION - Conduct a complete feasibility analysis of using a portable, targeted MCAFFSS using the parameters described above.

8.2.2.4 MCAFFSS Hardware Design

Although a detailed hardware design was not performed on the COTS MCAFFSS unit, one fundamental design change would be appropriate if the concept was implemented. These tests confirmed the data in the literature, summarized by Scheffey [18], that low level application of non-air aspirated AFFF is highly effective on floor spill fires. The data in these tests show no significant difference in fire extinguishment and reignition performances between the AFFF (non-air aspirated nozzle) and the CAFS nozzle where air is injected to aspirate the foam. This is not surprising since the expansion/drainage ratio was adjusted to optimize reach/throw characteristics for the CAFS nozzle, so that it was similar to the AFFF (non-air aspirated) nozzle. Previous testing of USAF vehicles demonstrated the importance of non-air aspirating foam in providing optimum stream reach and fluidity characteristics [24].

A recent analysis of hangar foam systems confirmed that these systems historically have had a lower reliability compared to water-only suppression systems [25]. Any design change to simplify the system is appropriate. Unit reliability is potentially reduced if foam expansion/drainage characteristics are left field adjustable. The foam may be set at an expansion ratio/drain time that may actually degrade fire extinguishment performance (e.g., by limiting

stream reach). A highly aerated foam might be used for vapor suppression in a unignited spill scenario. This improvement would have to be quantified. There is a question whether foam would be immediately used on the spill since the AFFF would contribute to the clean up process. More likely, personnel would stand by with AFFF handlines in the event of a spill.

Aerating the foam using compressed air is unnecessary from a fire performance standpoint and potentially reduces reliability.

RECOMMENDATION - The air injection feature of the MCAFFSS should be eliminated. The use of a COTS non-air aspirated nozzle is recommended if a portable system is implemented.

Other design features could be modified to improve reliability, e.g., limiting and optimizing the settings on the nozzle height/sweep angle sweep speed. These improvements should be implemented only after the positioning/targeting issues are resolved.

RECOMMENDATION - Modify the breadboard MCAFFSS only after conducting the feasibility study. The performance requirements should then be fully documented so that a independent, third party test agency could approve the device and similar COTS units. Maintenance and operational guidelines would also have to be developed (see Appendix D for an outline of these concepts).

9.0 CONCLUSIONS

9.1 Water Sprinkler System

Results indicate that water sprinklers at the rates tested will not prevent flame spread/fire growth on a thin JP-8 fuel spill on concrete. Water suppression systems at the application rates tested (6.9 and 10.7 Lpm/m², 0.17 and 0.25 gpm/ft²) did not halt fire growth when a JP-8 fuel spill was ignited. Positive effects in limiting fire growth were observed in only one situation, where sprinklers discharging at 10.2 Lpm/m² (0.25 gpm/m²) were activated immediately upon ignition of the spill. In this case, the fire grew to only 40% of the fire size of the spill where there was no suppression. In other situations, sprinklers did not limit fire growth and fires continued to grow to the size established under free burn conditions. In situations where there was a significant delay in sprinkler activation (e.g., greater than 1 minute), reduction in the fire size was attributable to fire burnout, not to suppression effects of the sprinklers.

Flame spread rates on the JP-8 fuel under free burn conditions were less than rates published in the literature. This may be a result of the unevenness in the concrete pad used in testing (i.e., high and low spots) or the inherently thin film thickness of the pool. Flame spread rates after sprinkler actuation were equal to or greater than published flame spread rates for free burning spills. The physical phenomena responsible for this increase in flame spread rate is unclear, but is probably attributable to the fuel substrate thickness and pool cohesiveness before and after sprinkler actuation.

Water suppression system tests conducted using deluge and automatic sprinklers demonstrated that neither type of system could control JP-8 spill fires. There were differences in the heat flux and temperatures measured, but it was not possible to determine to what extent these differences were related to the type of system. The differences between the deluge and closed-head systems tested are most likely the result of differences in the activation times and not indicative of differences in performance. All 36 sprinklers operated in each of the closed-head sprinkler system tests. The activation time for the deluge system had a significant effect on the fire size and the resulting heat flux and temperature measurements. With almost no delay the sprinkler system was able to limit the size of the fire, compared to the other tests. This scenario was considered unrealistic. The longer activation times resulted in fires, which increased in size after sprinkler system activation. The water density had some effect on the fire growth after sprinkler system activation. At the higher density (10.2 Lpm/m² (0.25 gpm/ft²)) the fire size and intensity increased quicker than the lower density (6.9 Lpm/m² (0.17 gpm/ft²)).

The sprinklers in these tests were operated using an optimistic scenario, i.e., rapid activation at a relatively low ceiling height (15 m (48 ft)).

In the planning for these tests, analytical tools developed from previous high bay hangar tests were used to predict sprinkler actuation time. The predicted and actual times were in reasonably good agreement. These tools should be used to predict the potential of closed-head sprinklers or thermal detectors to actuate in high bay situations (15-38 m (50-125 ft)). This analysis should be used to determine the damage potential prior to sprinkler actuation to aircraft not intimately involved in the initial ignition source. This analysis, combined with the probability of ignition of a large spill, should be used to determine if current engineering criteria for ceiling suppression system is reasonable and cost effective. The analysis may indicate that reliance on thermal detection at the ceiling (current criteria) would result in an unacceptably high risk of damage to multiple aircraft.

9.2 MCAFFSS

The breadboard MCAFFSS unit evaluated in these tests would not meet current USAF ETL, MIL Handbook, or NFPA criteria as a one-to-one replacement for fixed hangar fire protection systems. Within the parameters tested, the MCAFFSS can detect and operate to control/extinguish JP-8 fuel spill fires. Obstructions which might be found in a hangar have an impact on performance. It was found that the current USAF fire protection design approach for floor nozzle orientation is the appropriate approach. The best results were obtained when agent was discharged on the floor at the edge of the hazard and the nozzle stream allowed to push the agent below and around obstructions. It was found that a COTS non-air aspirating nozzle was as effective as the CAFS nozzle; air injection for aeration is unnecessary. Obstructions and alignment affected detection time, but the times were within acceptable limits. Placement of the MCAFFSS as currently designed would likely be more dependent on nozzle spray pattern characteristics than on detection range limitations. Recent data from optical detector fire tests with jet fuel spill scenarios could be used to optimize the detection performance characteristics. Placement of the units with respect to fuel spill hazards, ignition sources, spray pattern area and aircraft/maintenance obstructions requires careful consideration if the units are designed to "target" hazards and not provide total floor area coverage.

Significant operational and logistical questions remain regarding the feasibility of fielding the unit. Although intended to replace fixed detection and suppression systems, the level of fire protection which would be provided by the system as currently designed is not equivalent to that established by USAF design guidelines. The system should be assessed in terms of providing a similar level of established protection. Alternately, the technical requirements which have led to the established design criteria should be reassessed to consider changes in the fire hazard, environmental impact of suppression systems, and the acceptable risk posture of management. In terms of the MCAFFSS concept, a significant unknown is related not to its fire performance capability, but operational viability. In other words, can a spotting plan be generalized and standardized to reduce potential performance variability and the need for continuous field movement/adjustment? If not, is it feasible to allow field personnel wide latitude in assessing the hazard, spotting the device, and making control adjustments? This feasibility assessment would be based on manpower requirements, reliability and cost trade-offs (both initial capital and life-cycle costs). Ultimately, it would be part of an overall technical requirements review. Since the feasibility of the MCAFFSS concept is in question, this element of a technical requirements review should be a high priority in any advancement of the concept. Any specific design optimization of MCAFFSS should be held until the feasibility assessment is completed.

Since a number of aspects related to current design requirements have been raised (e.g., impact of JP-8 replacement of JP-4, detector actuation in high-bay spaces, environmental impact of foam, optical detector performance and reliability), a complete reassessment of the hangar technical requirements appears to be warranted. A key element of this assessment would be the quantification of the acceptable level of risk (i.e., damage to aircraft and structure) consistent with the expected performance of the protection system. A fire hazard analysis could be used to quantify the risk and system performance.

10.0 ACKNOWLEDGMENTS

Thanks are extended to the Underwriters Laboratory test team under the direction of Martin Pabich and Daniel Stepan. Thanks are also extended to Steve Wells and Rick Brown for their assistance in evaluating the MCAFFSS units.

11.0 REFERENCES

1. AFCEA Technical Support Directorate, "Aircraft Hangar JP-8 Fire Threat Analysis," U.S. Air Force Civil Engineering Support Agency Briefing Paper, Tyndall AFB, FL, 5 June 1997.
2. Fitzgerald, P.M., "Protection of Aircraft Hangars Against Fuel Spill Fires Part I - Water Deluge Systems Protection," FMRC Serial No. 19370-1, Factory Mutual Research, Norwood, MA, January 6, 1971.
3. Personal communication with Fred Walker, USAF AFCEA, 16 April 1998.

4. Chambers, G.D., "Flight Line Extinguisher Evaluation," DOD-AGFSRS-76-9, DOD Aircraft Ground Fire Suppression and Rescue Systems Office (ASD/SMGF), Wright Patterson AFB, OH, January 1977.
5. Leonard, J.T., Fulper, C.R., Darwin, R., Back, G.G., Burns, R.E., and Ouellette, R., "Fire Hazards of Mixed Fuels on the Flight Deck," NRL Memo Rpt 6180-92-6975, April 28, 1992.
6. Scheffey, J.L., Hill, S.A., Walker, F., Williams, F.W., "USAF Hangar Test Plan," NRL Ltr Rpt Ser 6180/0316, 24 June, 1998.
7. MIL-F-24385F, "Fire Extinguishing Agent, Aqueous Film Forming Foam (AFFF) Liquid Concentrate, for Fresh and Seawater," Military Specification, 7 January, 1992.
8. United States Air Force, "Engineering Technical Letter (ETL) 98-7: Fire Protection Engineering Criteria - New Aircraft Facilities," HQ AFCEA/CES, Tyndall AFB, FL April 1998.
9. Military Handbook 1008C, "Fire Protection for Facilities Engineering, Design, and Construction," Headquarters, Naval Facilities Engineering Command, Alexandria, VA, June 1997.
10. NFPA 412, "Standard for Evaluating Aircraft Rescue and Fire Fighting Foam Equipment," National Fire Protection Association, Quincy, MA, 1998.
11. ASTM E-119 88, "Standard Methods of Fire Tests of Building Construction and Materials," American Society of Testing and Materials, Philadelphia, PA, 1988.
12. Mackinven, R., Hansel, J.G., and Glassman, I., "Influence of Laboratory Parameters on Flame Spread Across Liquid Fuels," *Combustion Science and Technology*, 1, 1970, pp. 293-306.
13. Budnick, E.K., Forssell, E.W., Nelson, H.E., Wong, J.T., "Fire Performance and Suppressibility of Composite Materials Phase II Final Report," HAI Report 92-1071, prepared for U.S. Air Force HQ WL/FIVC, Tyndall AFB, FL, 15 December 1992.
14. NFPA 409, "Aircraft Hangars," National Fire Protection Association, Quincy, MA, 1995.
15. Wells, S.P., Cozart, K.S., Mitchell, M.B., and Dodsworth, R.D., "Aircraft Hangar Fire Threat and Study Analysis," USAF Technical Report WL-TR-97-xx, HQ AFCEA/AQ/CESM, Tyndall AFB, FL, December 1997 (draft).
16. Hughes Associates, Inc., "Technical Requirements for United States Air Force Hush House Fire Protection," HAI Report 98-5500-1 (Rev.1), prepared for Versar, Inc., Springfield, VA, March 25, 1998.

17. Gottuk, D.T., Tatem, P.A., Williams, F.W., Scheffey, J.L., and Gott, J.E., "Optical Fire Detection (OFD) for Military Aircraft Hangars: Test Plan for OFD Performance to Fuel Spill Fires," NRL Ltr Rpt Ser 6180/0194, April 30, 1998.
18. Scheffey, J.L., "Foam Agents and AFFF Design Considerations," *The SFPE Handbook of Fire Protection Engineering*, P.J. DiNenno (Ed.), Second Edition, National Fire Protection Association, Quincy, MA, June 1995.
19. Department of the Navy, Section 555, "General Specifications for Ships of the United States Navy, 1991 Edition," NAVSEA S9AA0-AA-SPN-010/GEN-SPEC, Department of the Navy, Washington, DC, Jan. 2, 1991.
20. Back, G.G., Williams, F.W., Gott, J.E., Parker, A.J., and Scheffey, J.L., "Aircraft Hangar Fire Protection System Evaluation Full Scale Fire Tests," NRL Memorandum Report (in preparation).
21. Geyer, G.B., "Firefighting Effectiveness of Aqueous Film Forming Foam (AFFF) Agents," FAA Technical Report FAA-NA-72-48, prepared for the DOD Aircraft Ground Fire Suppression and Rescue Unit (ASD-TR-73-13), Washington, DC, April 1973.
22. Scheffey, J.L., Wright, J., and Sarkos, C., "Analysis of Test Criteria for Specifying Foam Firefighting Agents for Aircraft Rescue and Firefighting," FAA Technical Report, DOT/FAA/CT-94/04, FAA Technical Center, Atlantic City, NJ, August 1994.
23. Hughes Associates, Inc., "Overview of Fire Hazard Analysis of United States Air Force Hush Houses," HAI Technical Report 98-5500, prepared for Versar, Inc., Springfield, VA, January 6, 1998.
24. Jablonski, E.J., "Comparative Nozzle Study for Applying Aqueous Film-Forming Foam on Large-scale Fires," U.S. Air Force Report, CEEDO-TR-78-22, Tyndall AFB, FL, April 1978.
25. Vincent, B.G., Kung, H.C., Stavrianidis, P., "Fire Protection for U.S. Army Helicopter Hangars," Factory Mutual Research Corporation Technical Report FMRC J.I. 0X0N1.RA, prepared for Diversified Engineering, Inc., Washington, DC, September 1993.

APPENDIX A

Results of JP-8 Background Burns (Tests BB6-BB8)

Test BB6

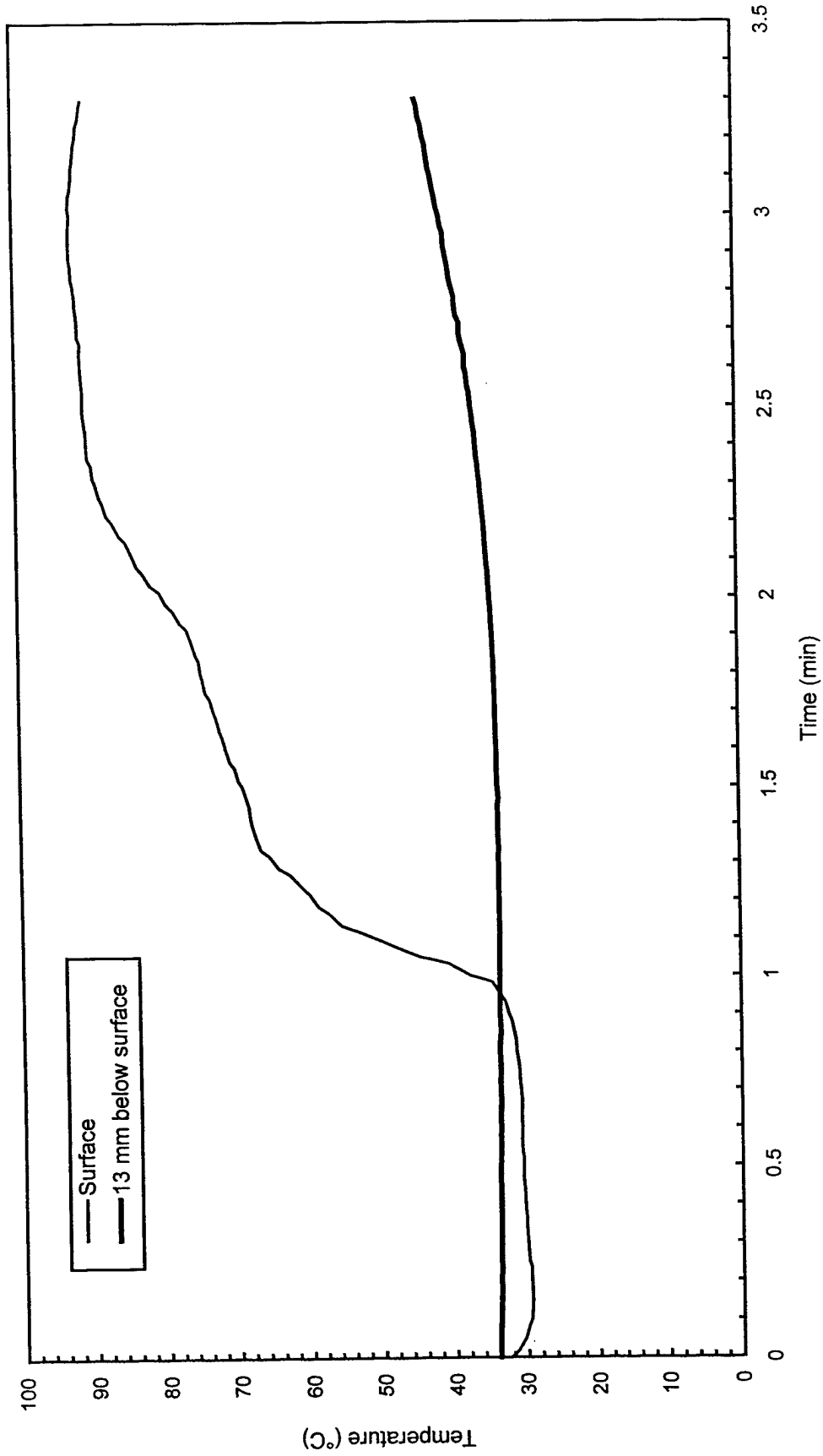


Fig. A1 - Concrete temperatures at center of pad

Test BB6

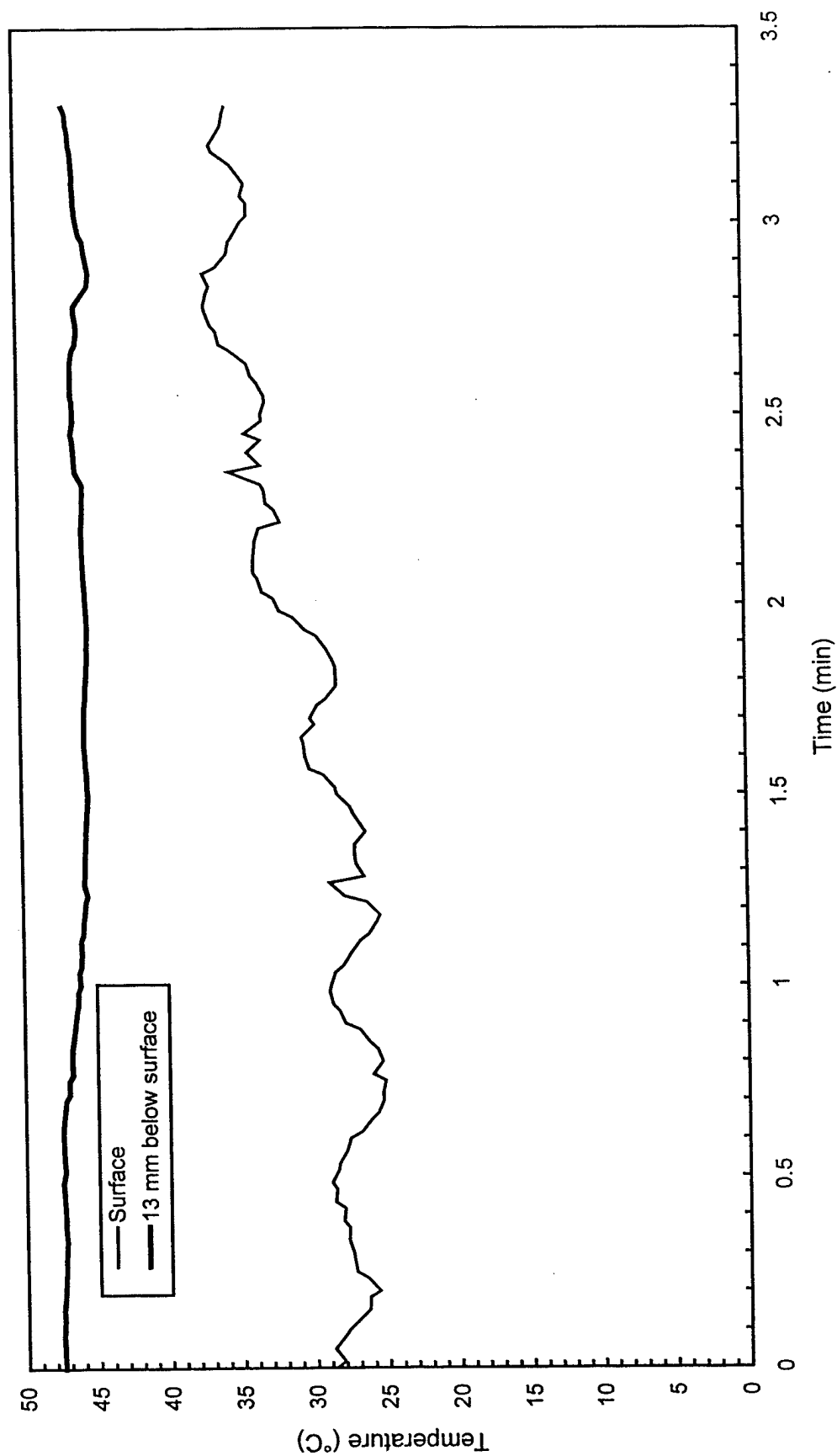


Fig. A2 - Concrete temperatures 3 m (10 ft) East of center of pad

Test BB6

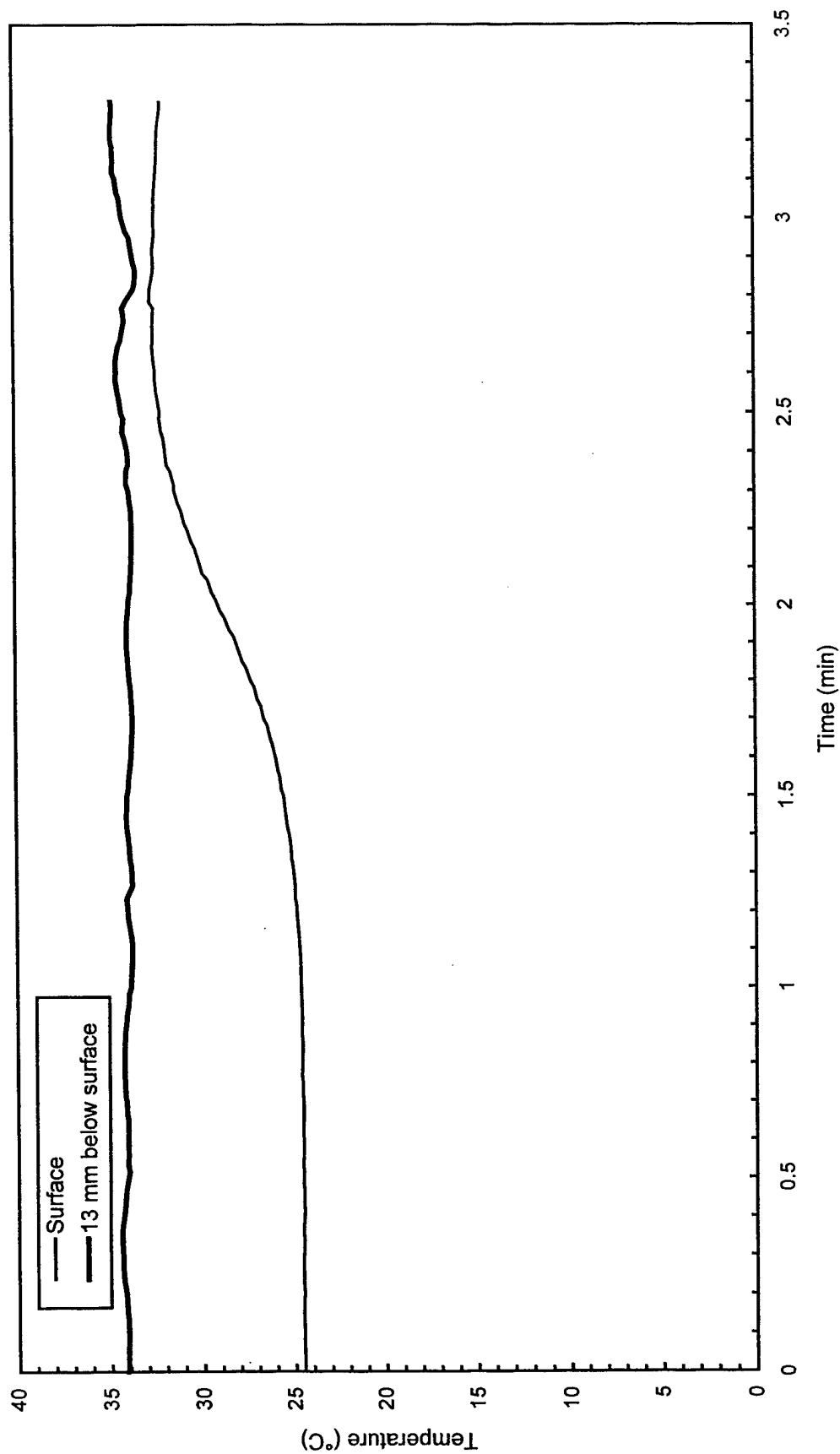


Fig. A3 - Concrete temperatures 3 m (10 ft) West of center of pad

Test BB6

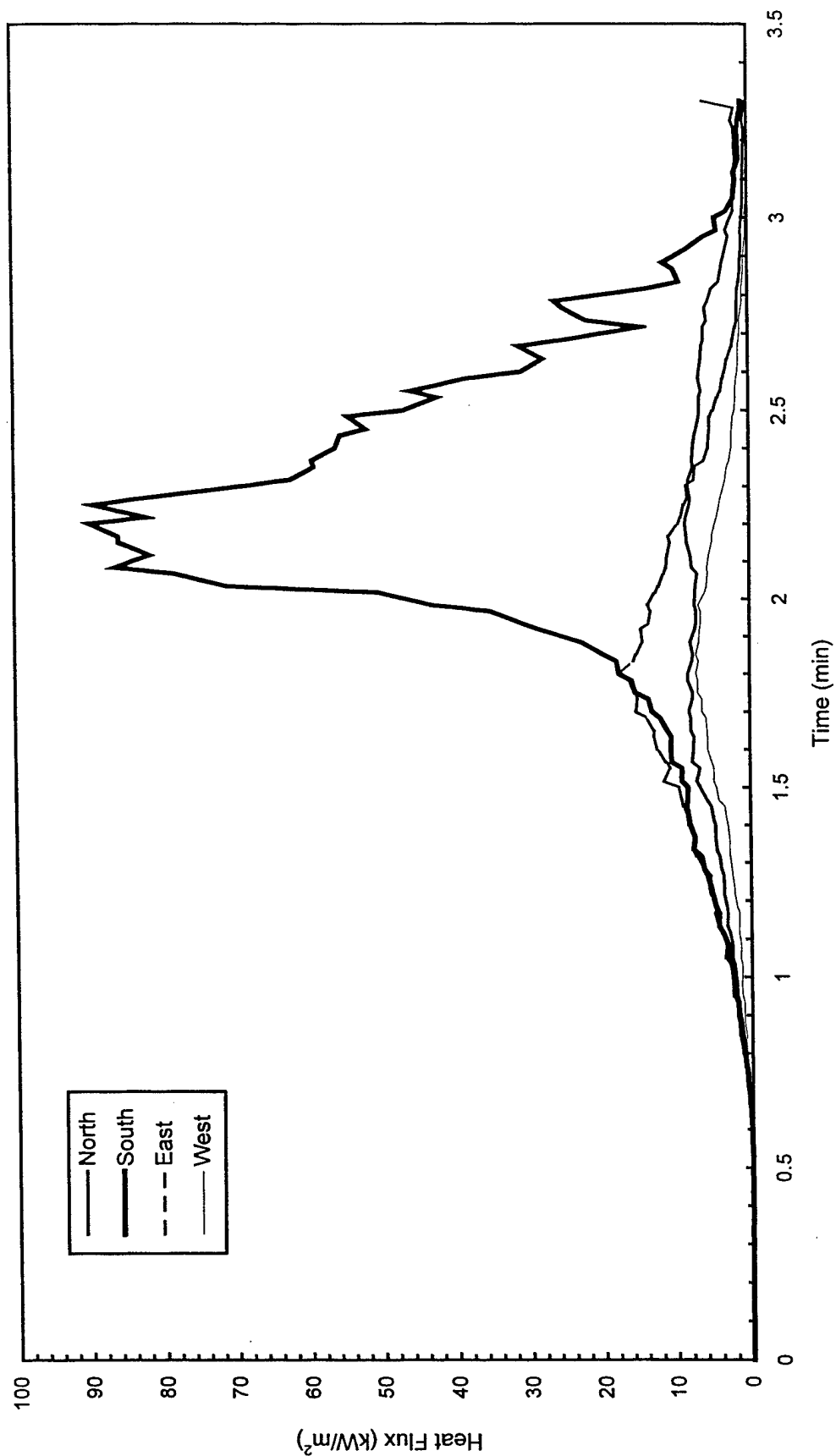


Fig. A4 - Heat flux measured at edge of pad

Test BB6

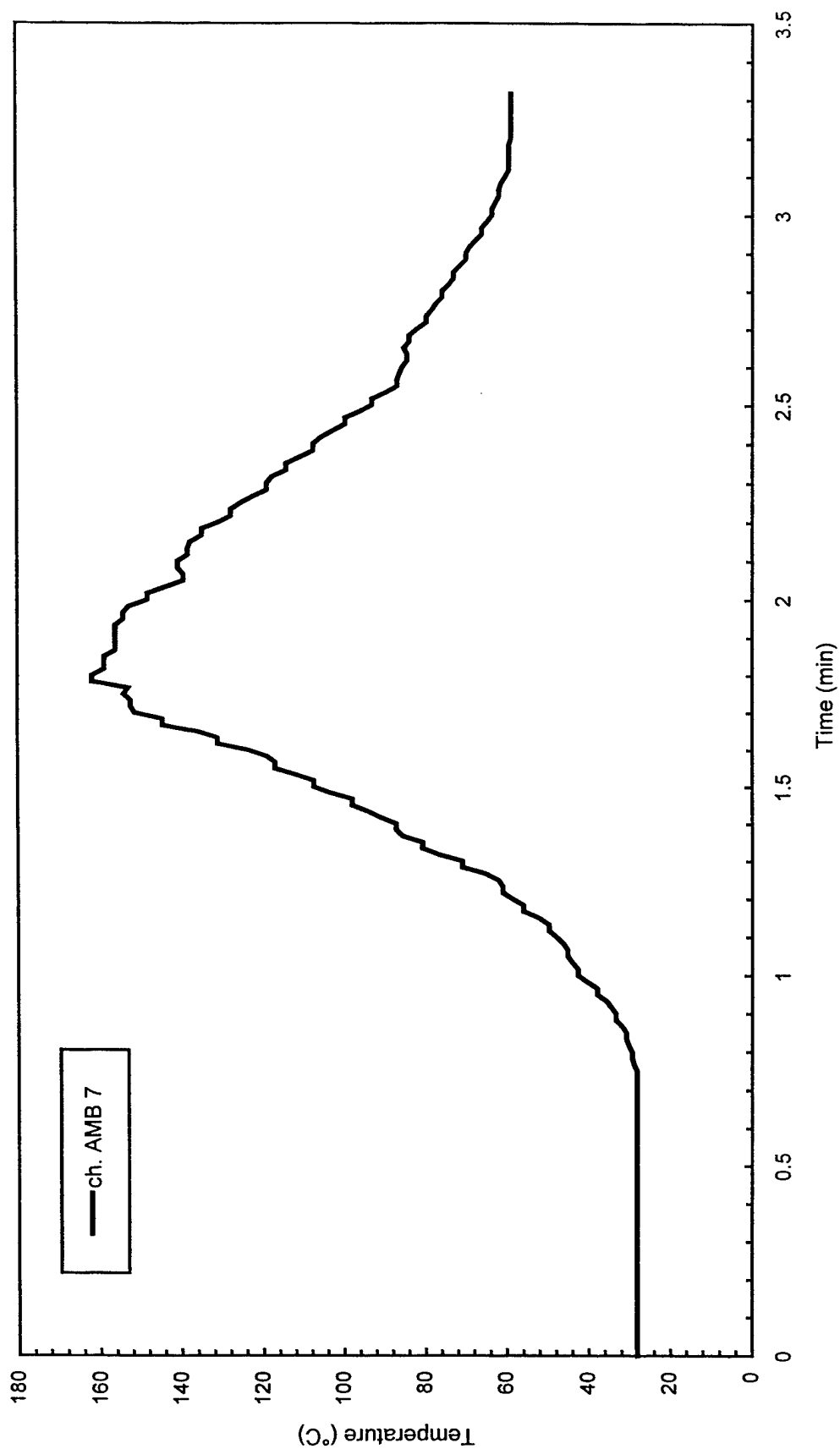


Fig. A5 - Air temperatures over center of pad

Test BB6

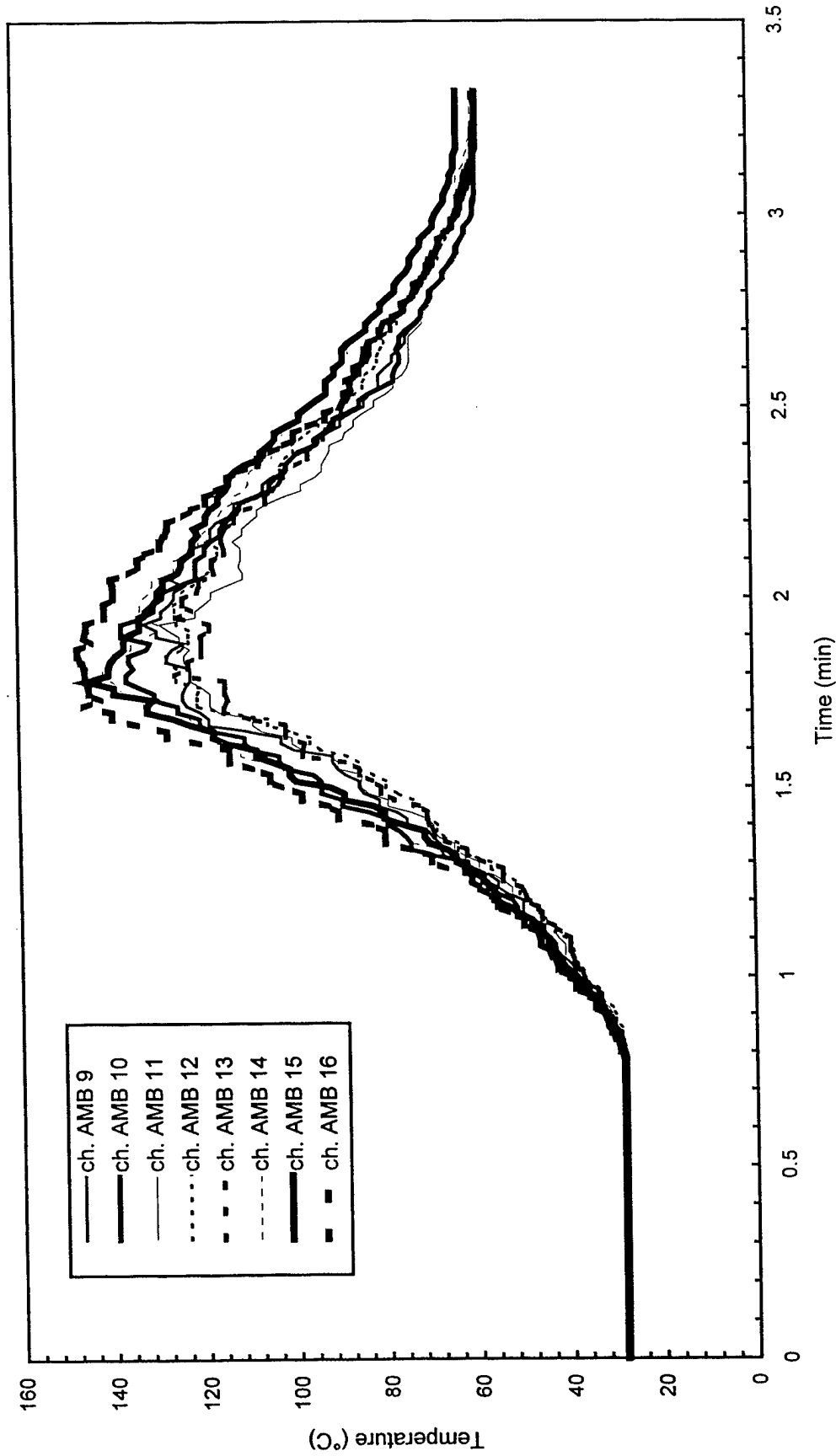


Fig. A6 - Air temperatures around 3 m (10 ft) radius from center of pad

Test BB6

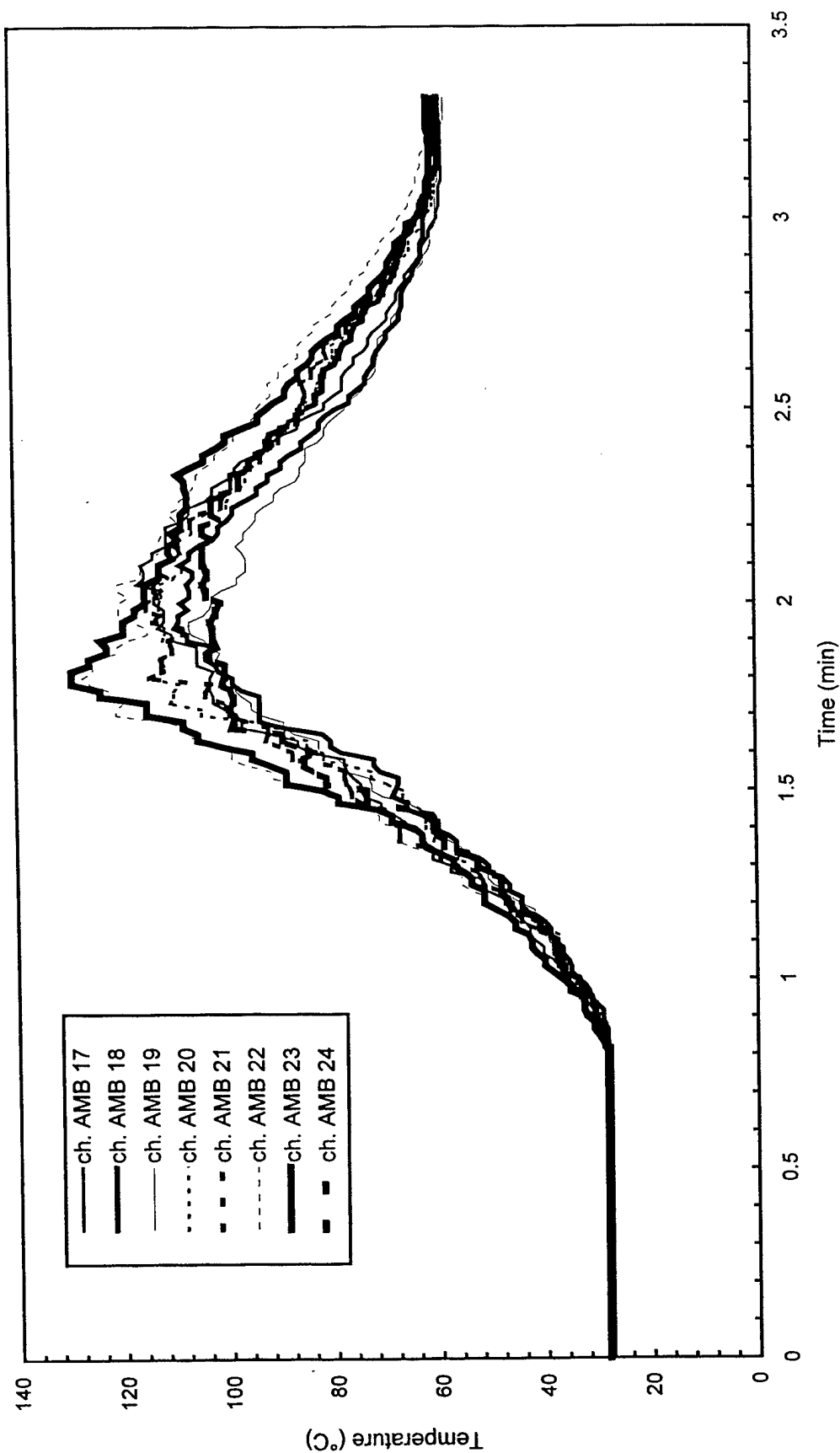


Fig. A7 - Air temperatures around 4.6 m (15 ft) radius from center of pad

Test BB6

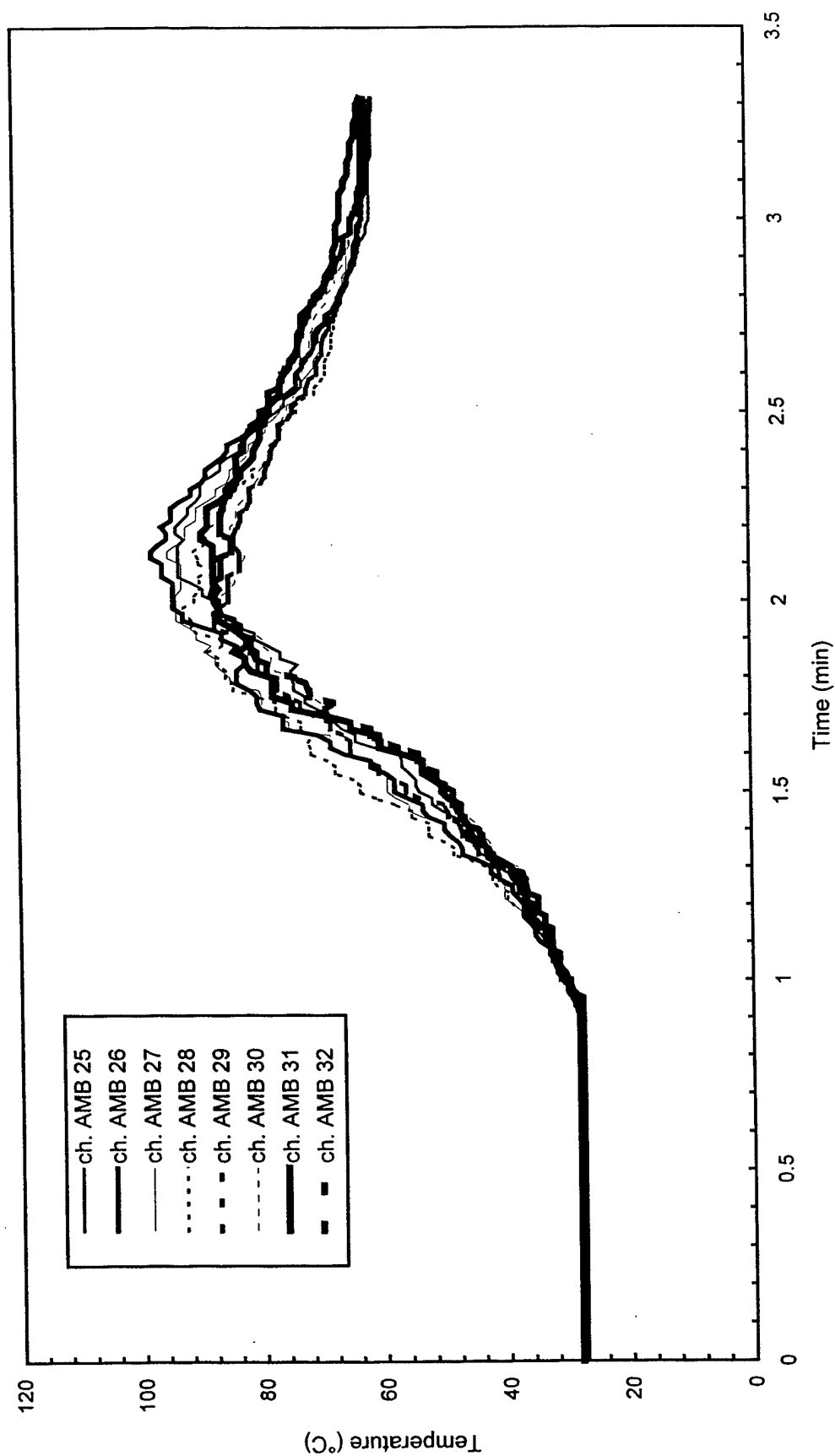


Fig. A8 - Air temperatures around North half of 7.6 m (25 ft) radius from center of pad

Test BB6

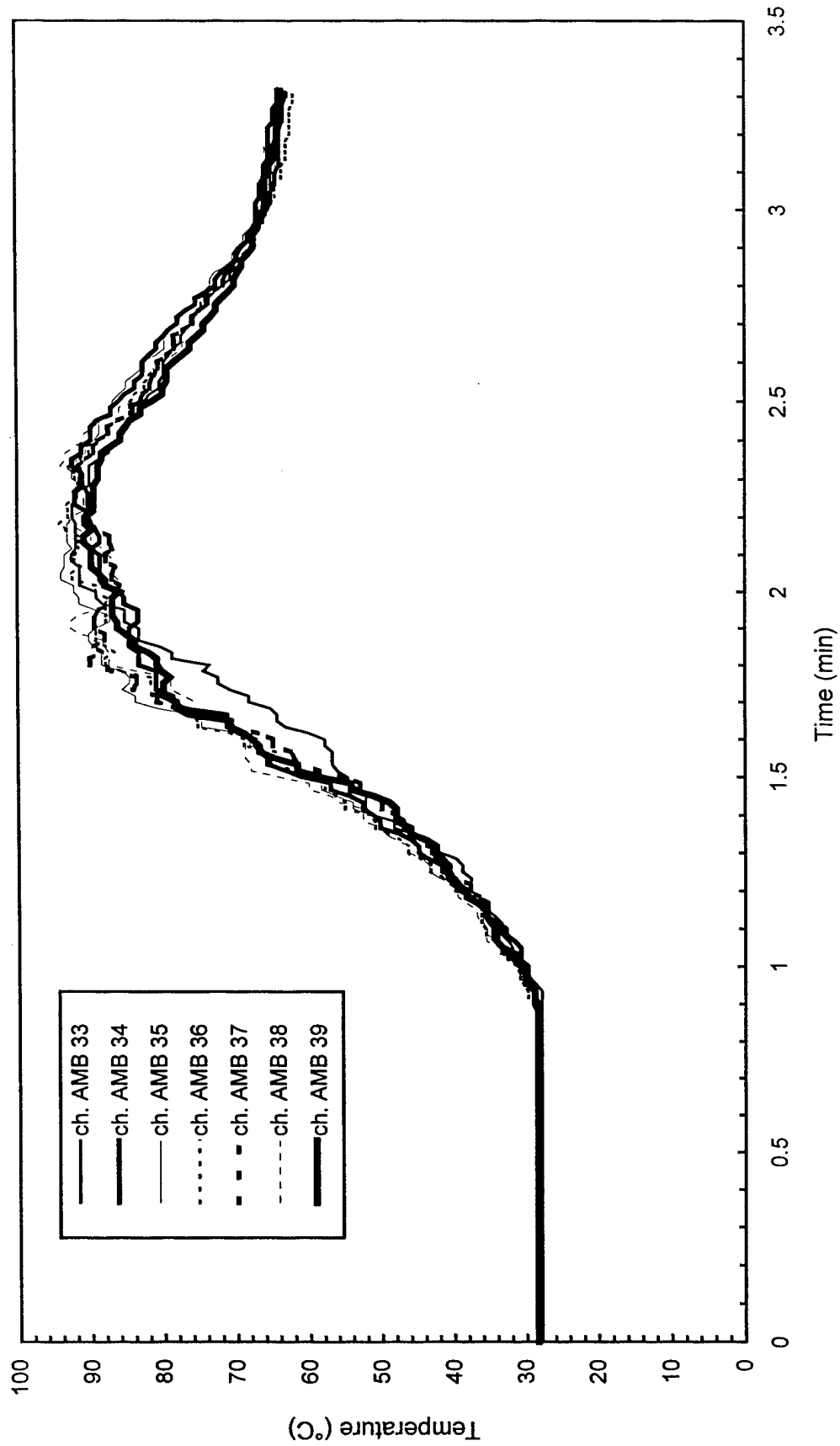


Fig. A9 - Air temperatures around South half of 7.6 m (25 ft) radius from center of pad

Test BB6

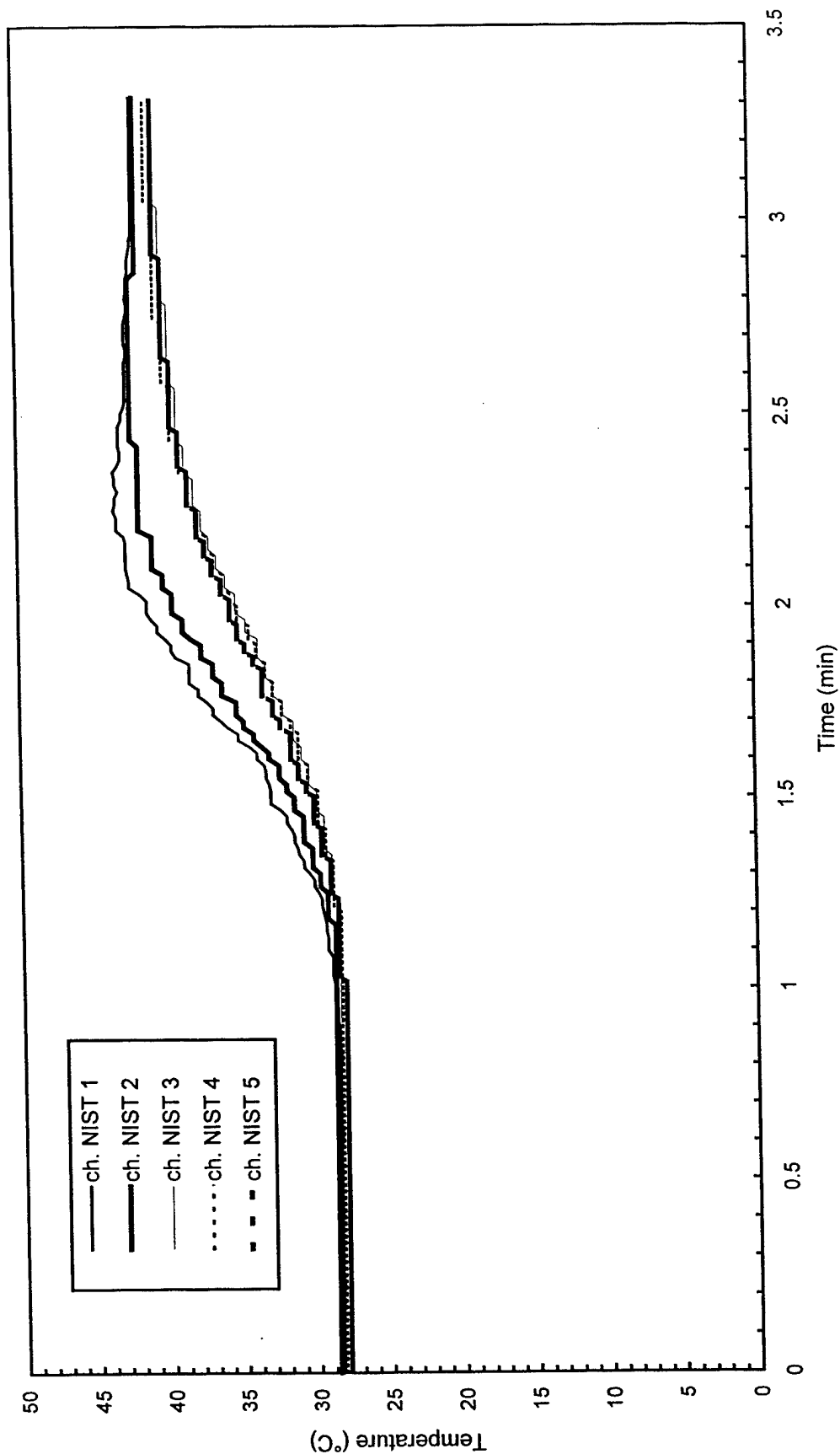


Fig. A10 - Temperature of West steel beam

Test BB6

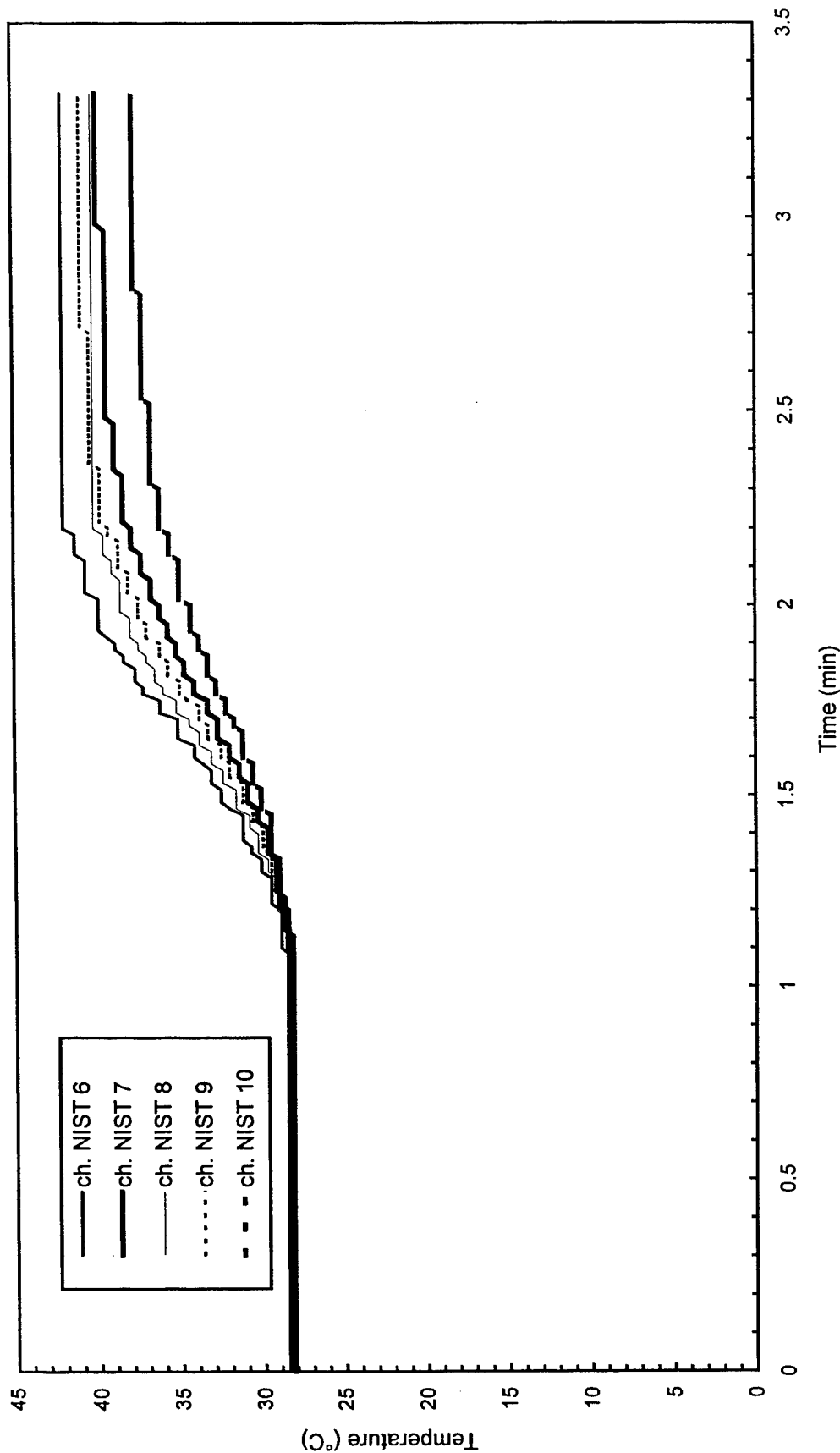


Fig. A11 - Temperature of North steel beam

Test BB6

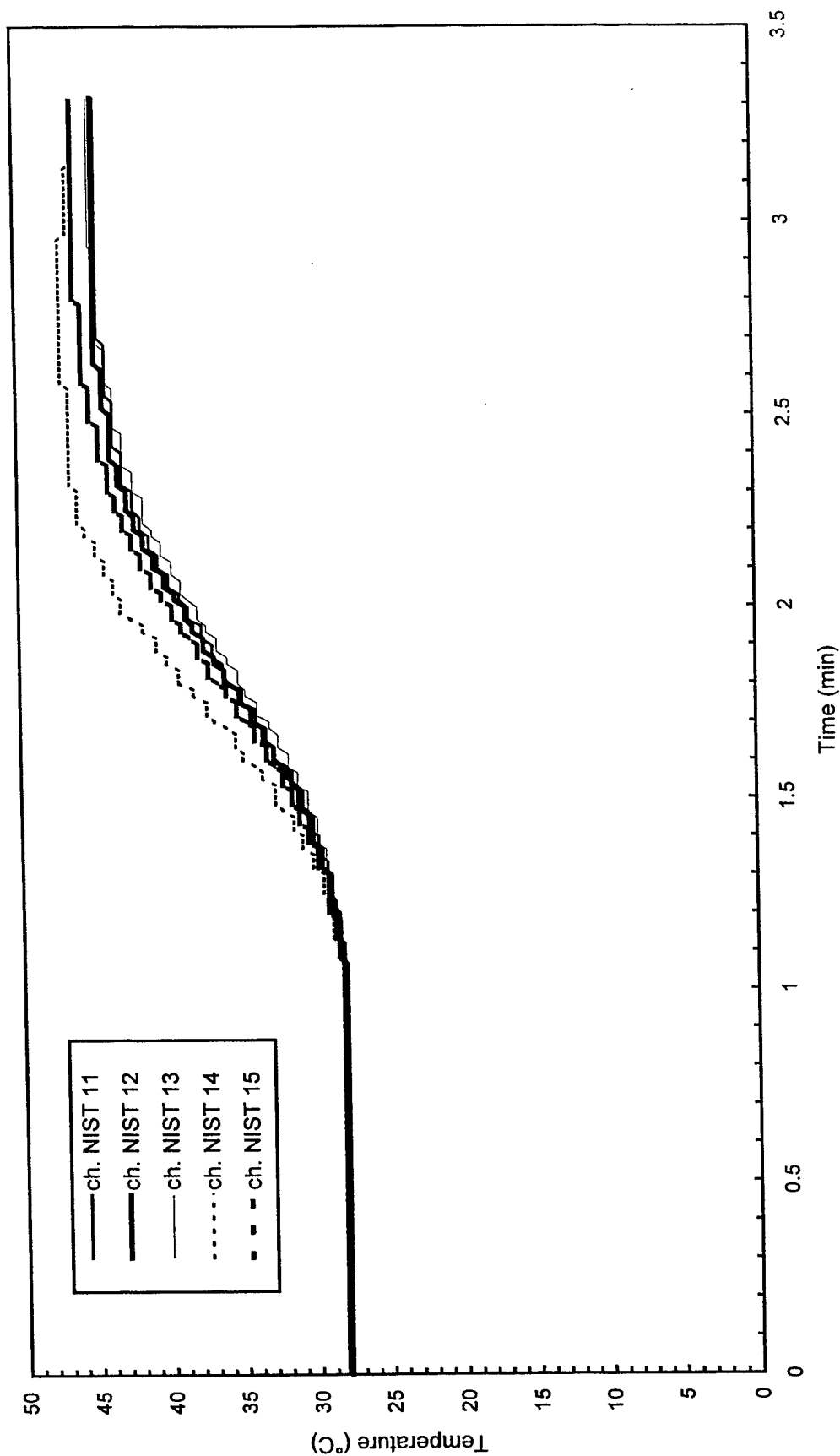


Fig. A12 - Temperature of East steel beam

Test BB6

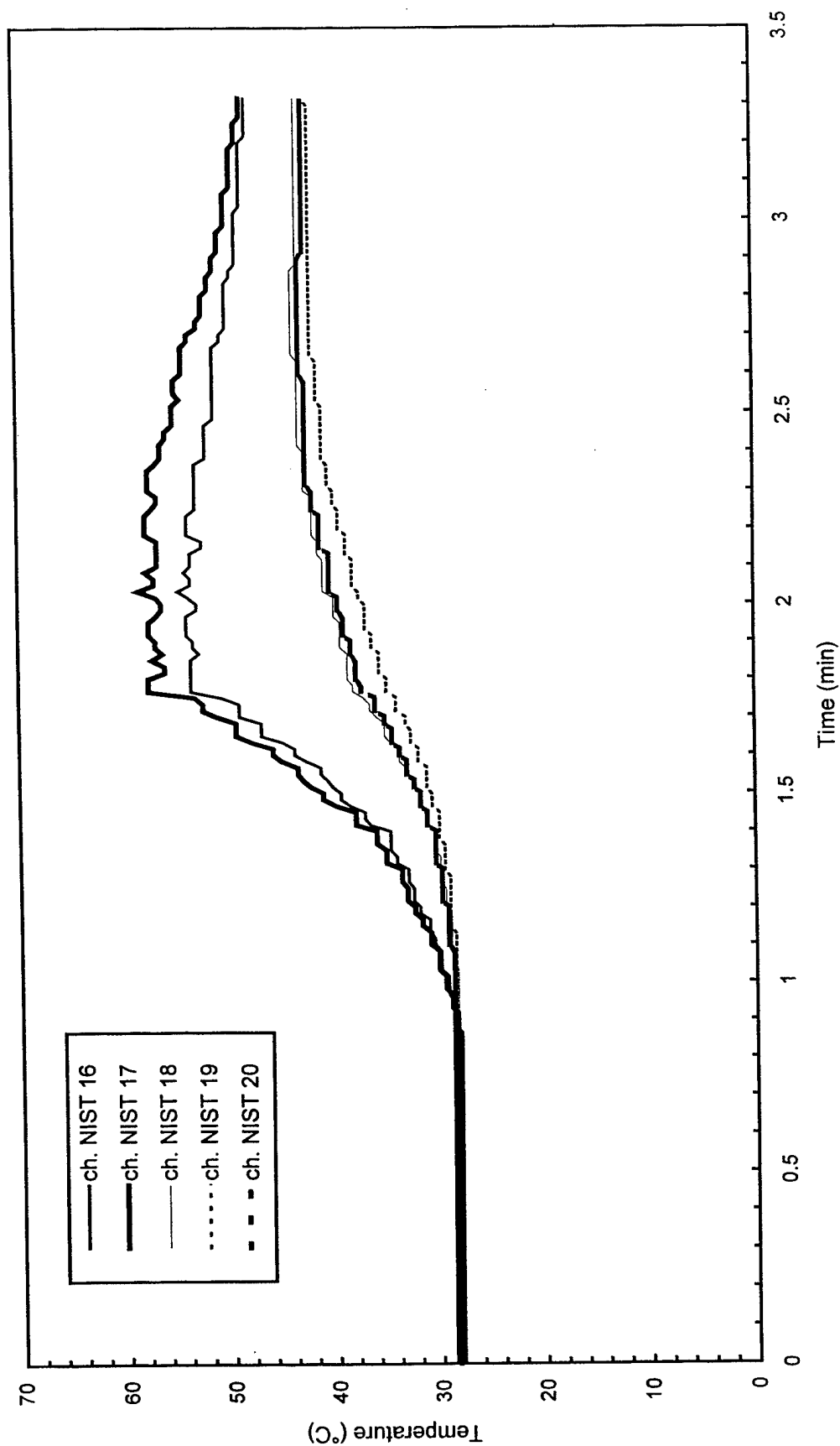


Fig. A13 - Temperature of South steel beam

Test BB6

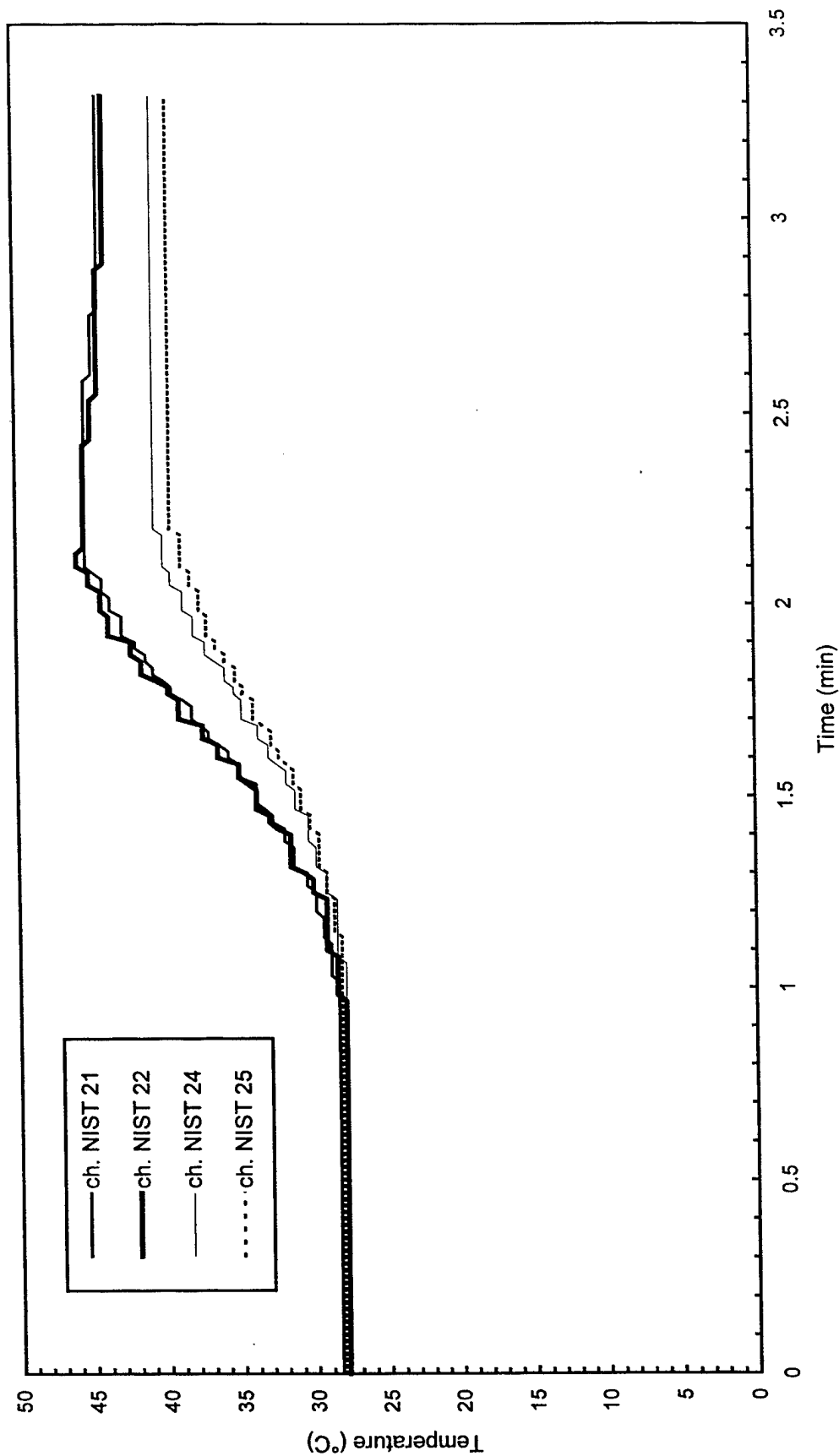


Fig. A14 - Temperature of Northwest steel beam

Test BB6

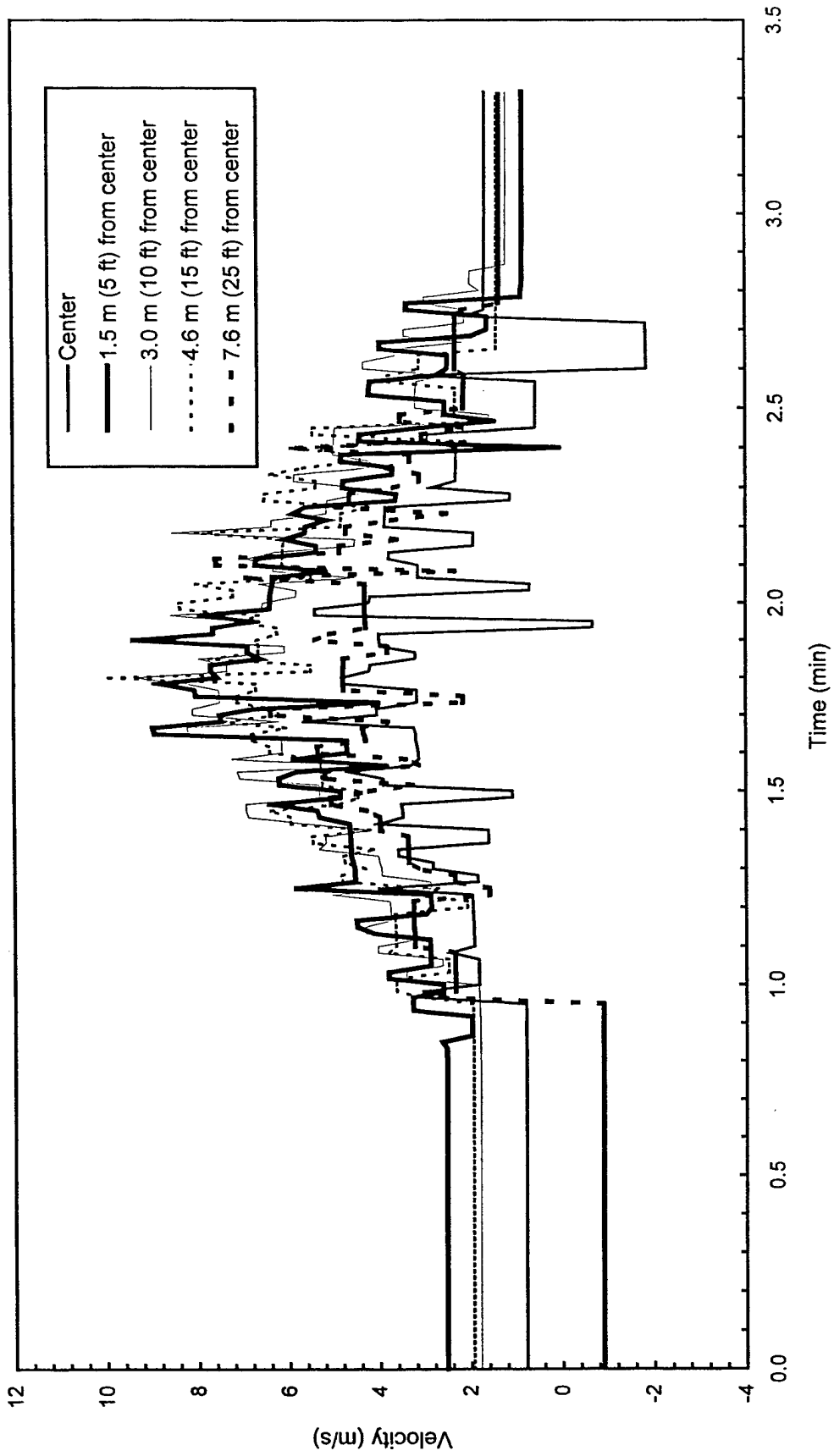


Fig. A15 - Plume and ceiling jet velocities

Test BB7

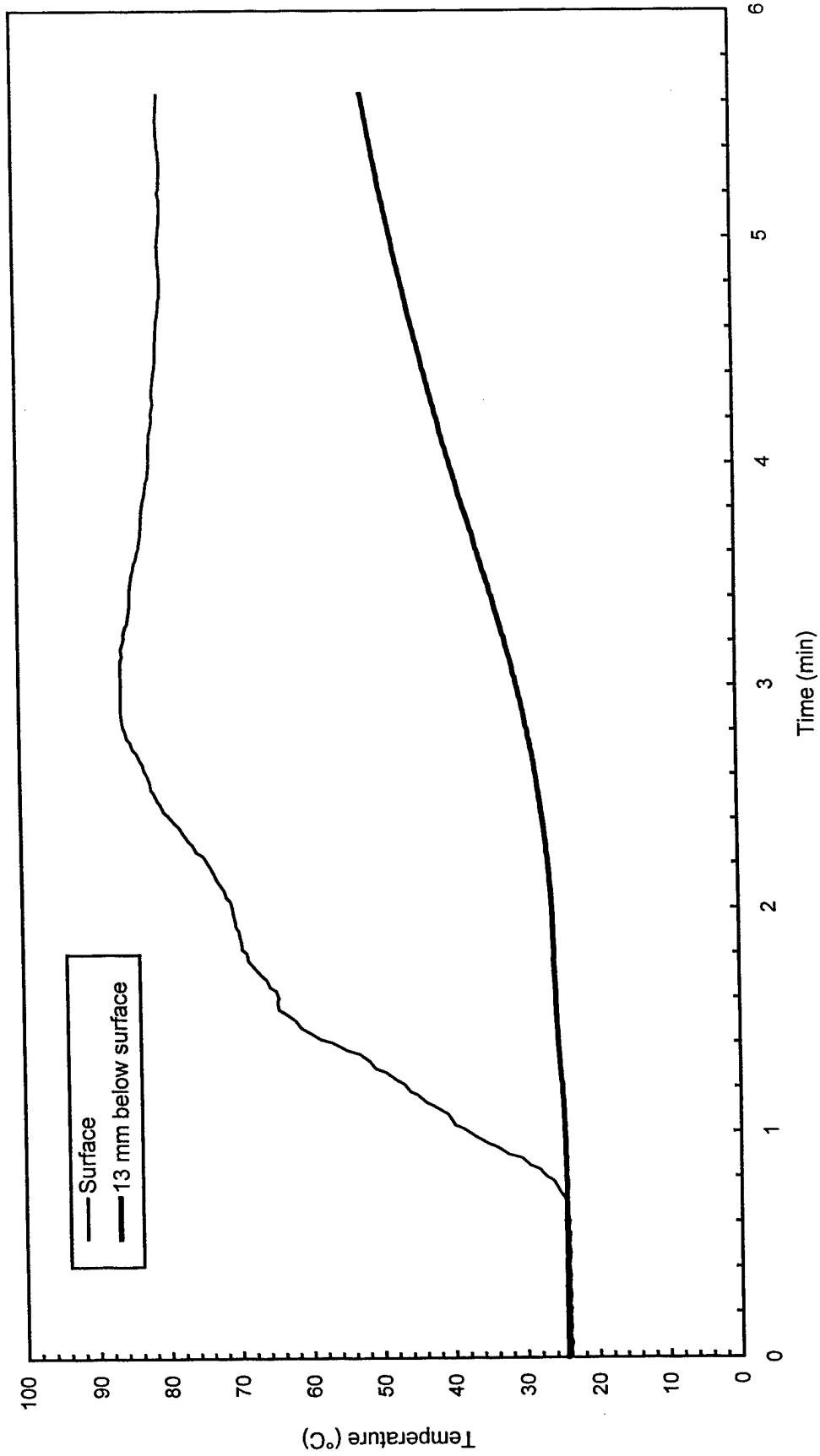


Fig. A16 - Concrete temperatures at center of pad

Test BB7

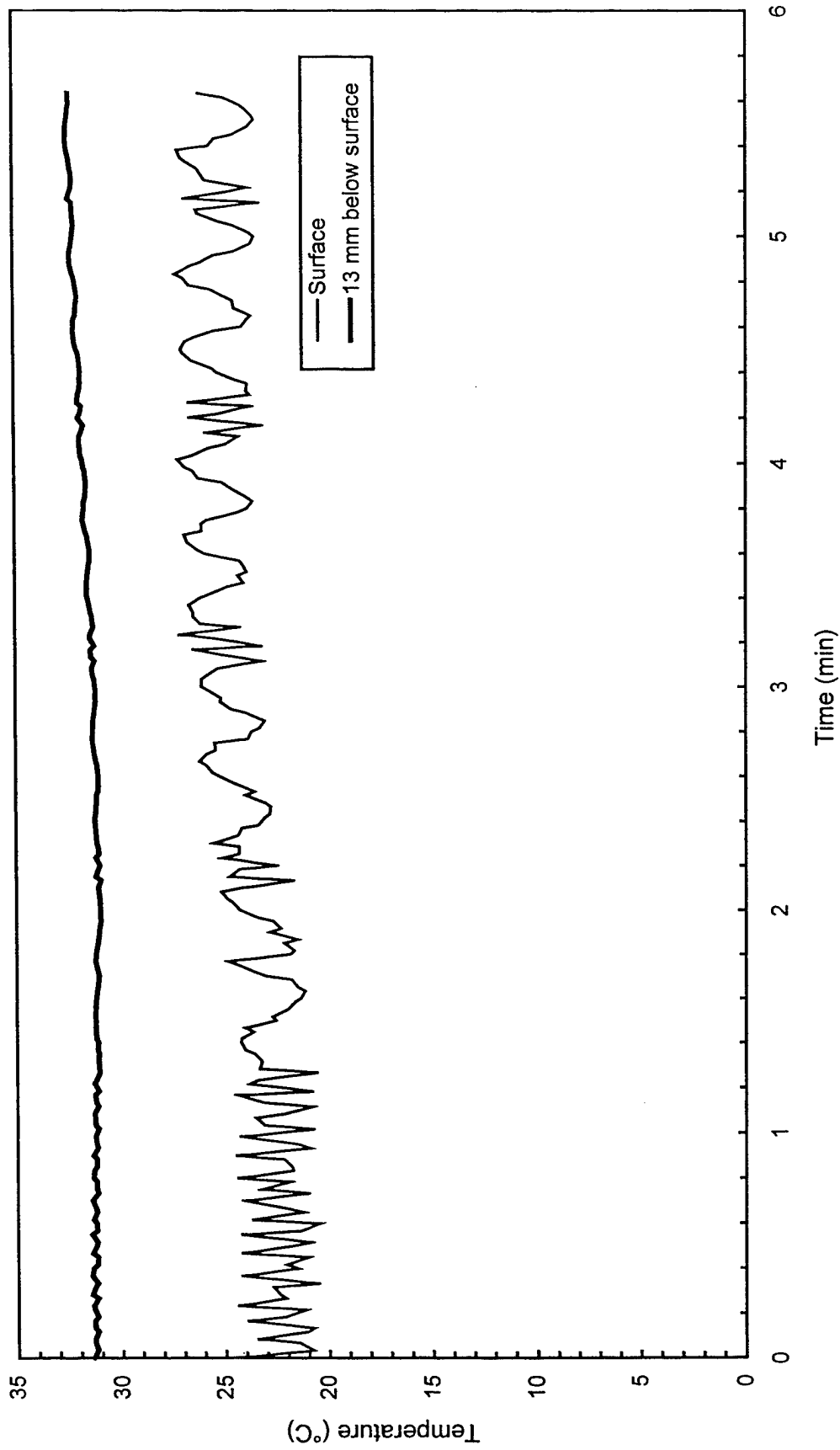


Fig. A17 - Concrete temperatures 3 m (10 ft) East of center of pad

Test BB7

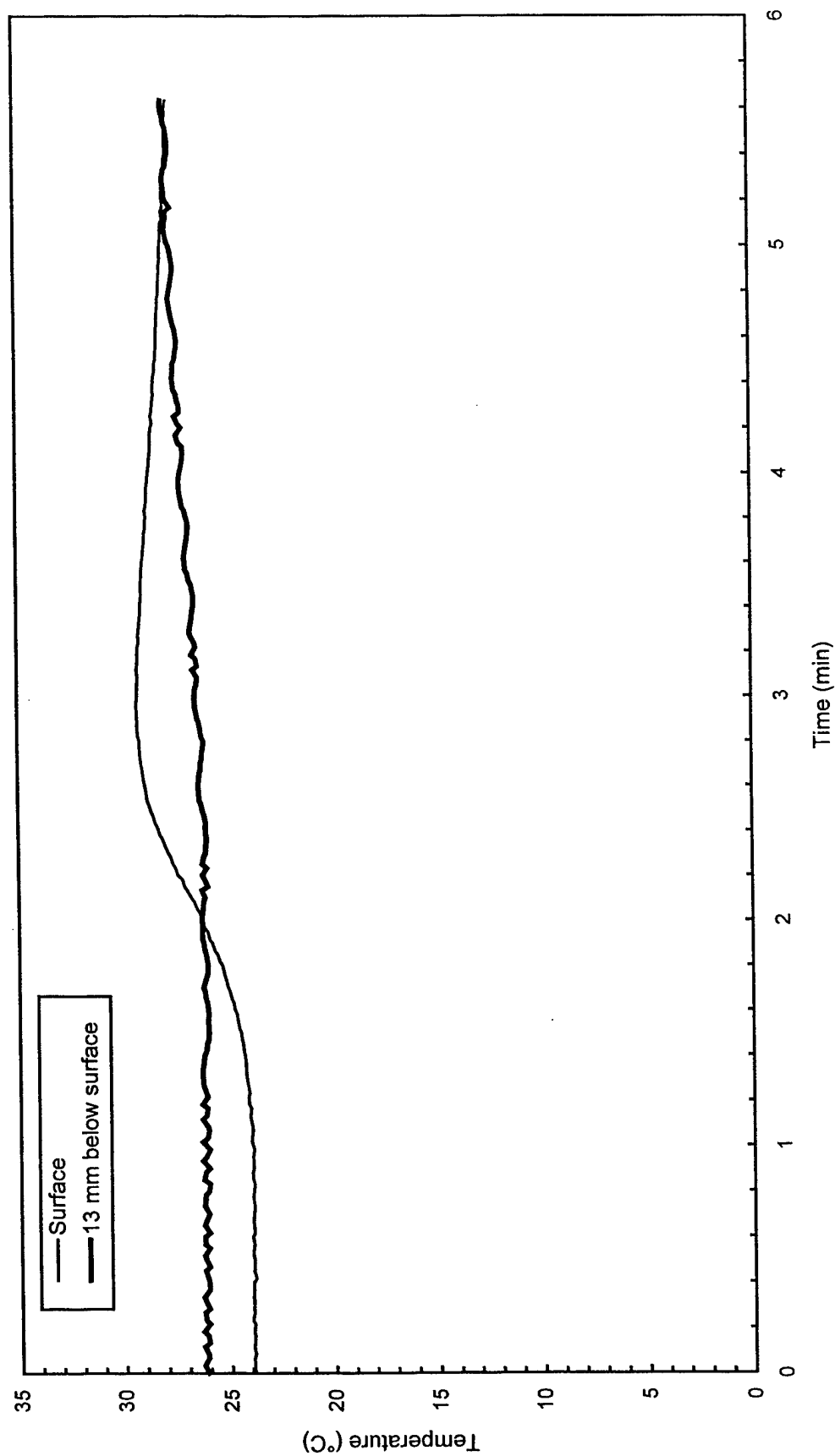


Fig. A18 - Concrete temperatures 3 m (10 ft) West of center of pad

Test BB7

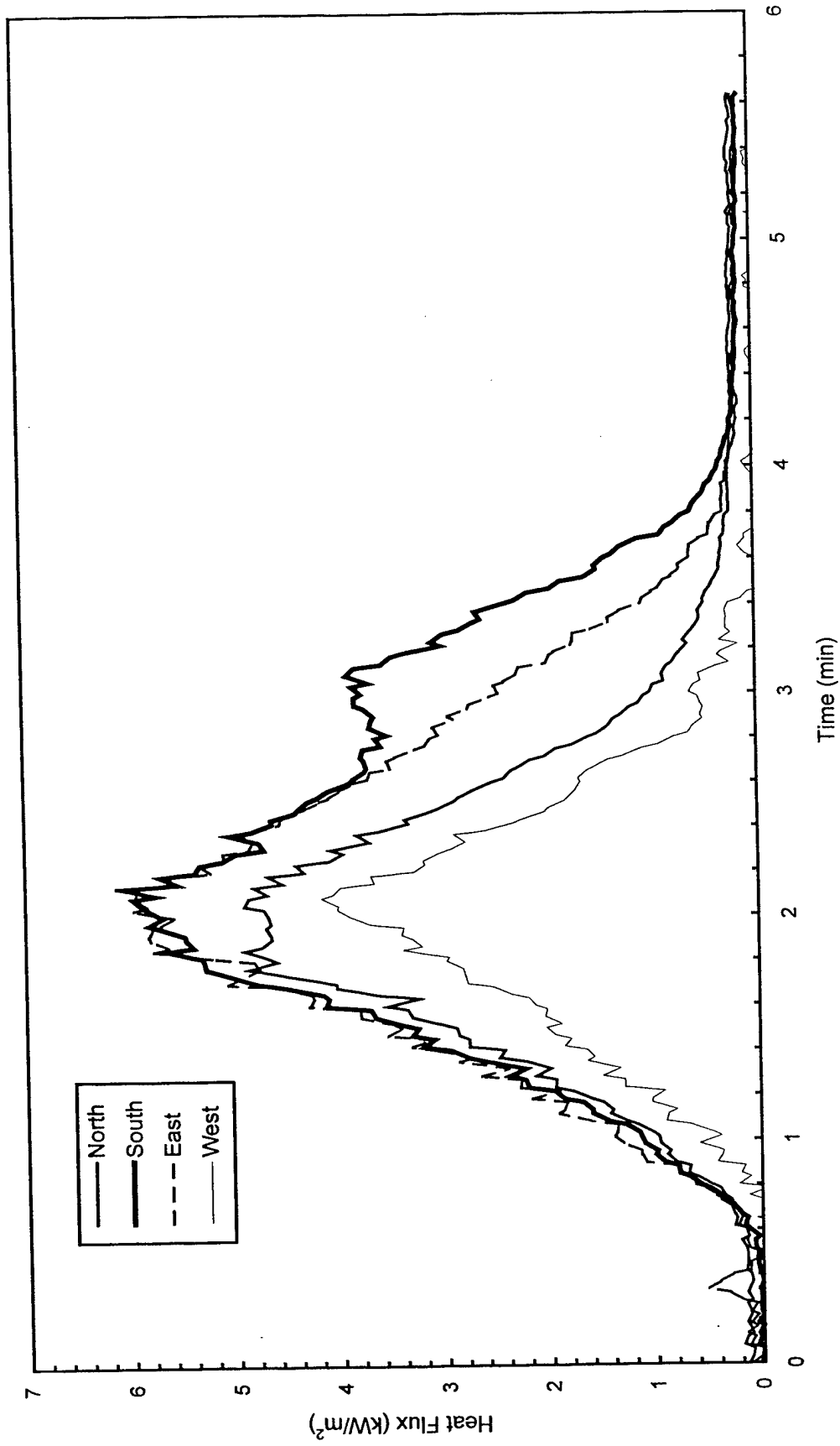


Fig. A19 - Heat flux measured at edge of pad

Test BB7

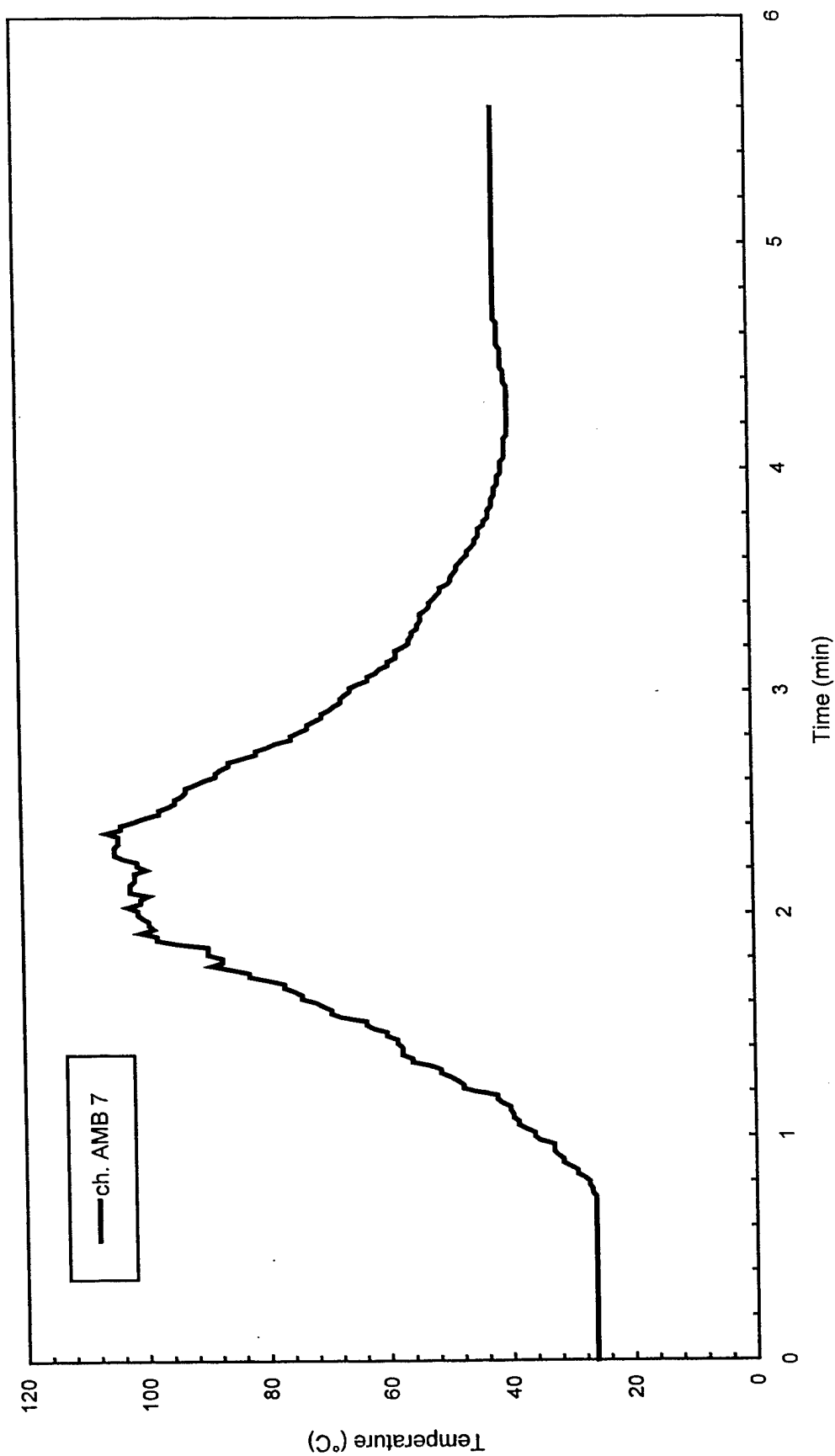


Fig. A20 - Air temperatures over center of pad

Test BB7

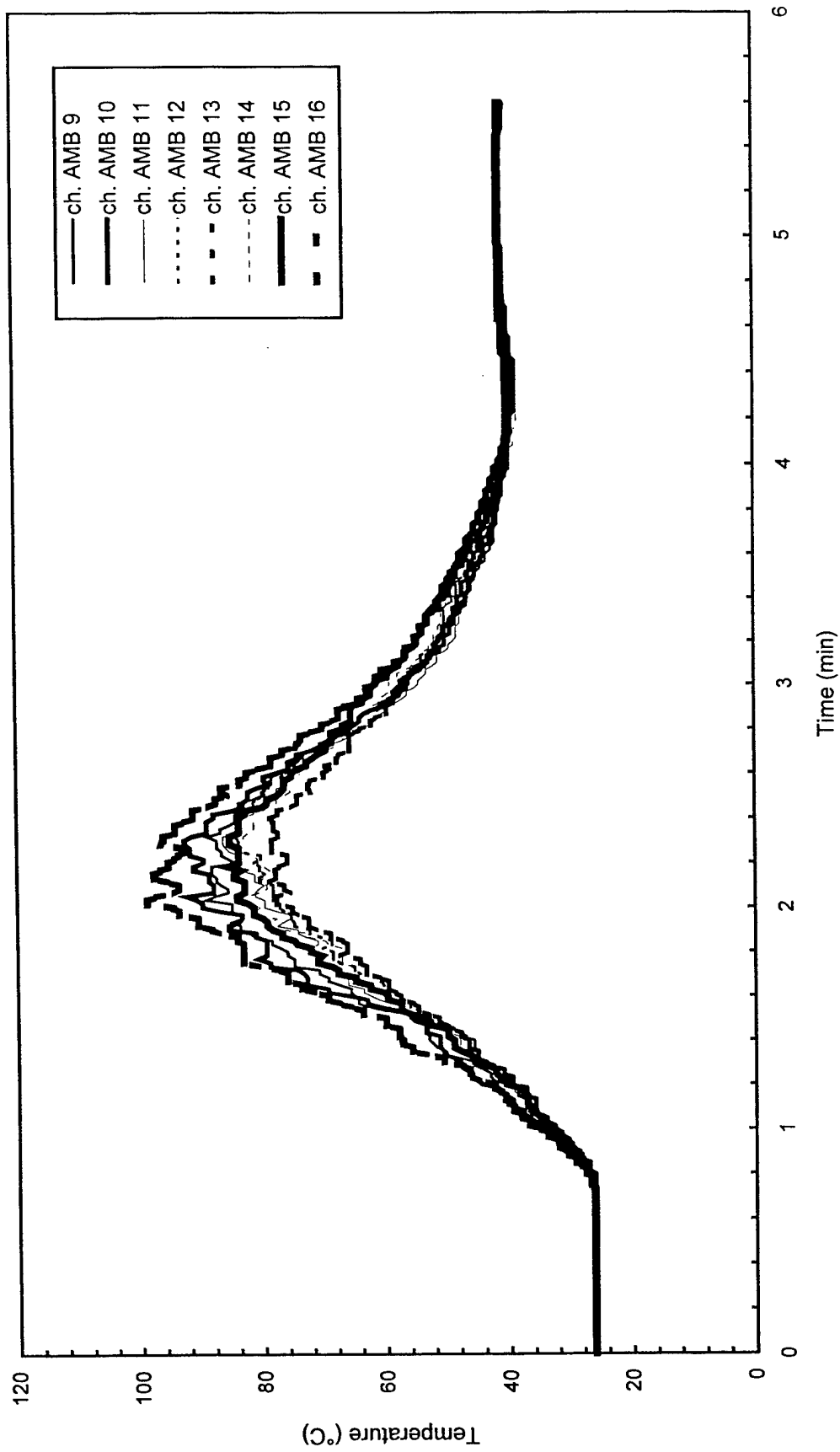


Fig. A21 - Air temperatures around 3 m (10 ft) radius from center of pad

Test BB7

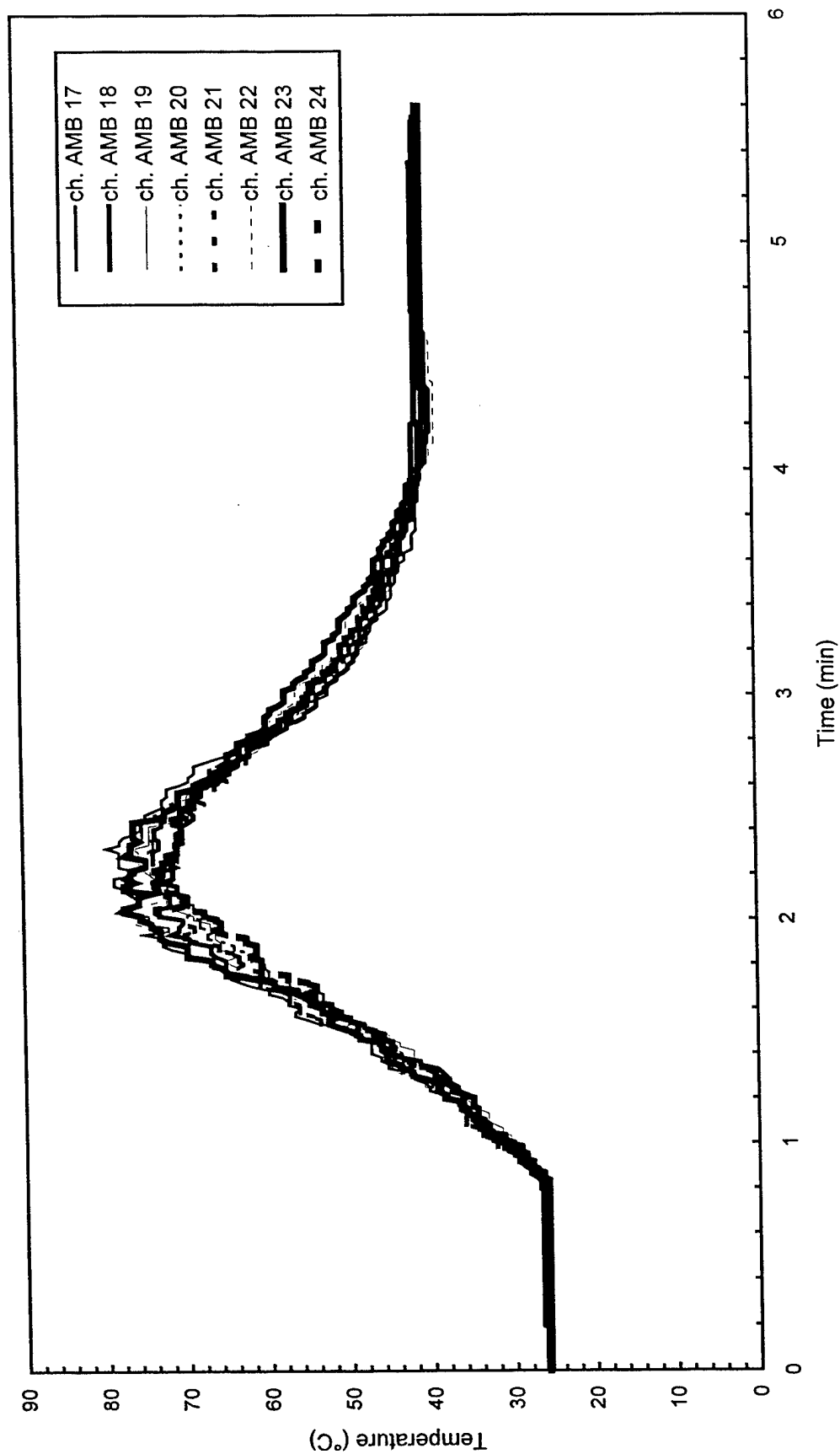


Fig. A22 - Air temperatures around 4.6 m (15 ft) radius from center of pad

Test BB7

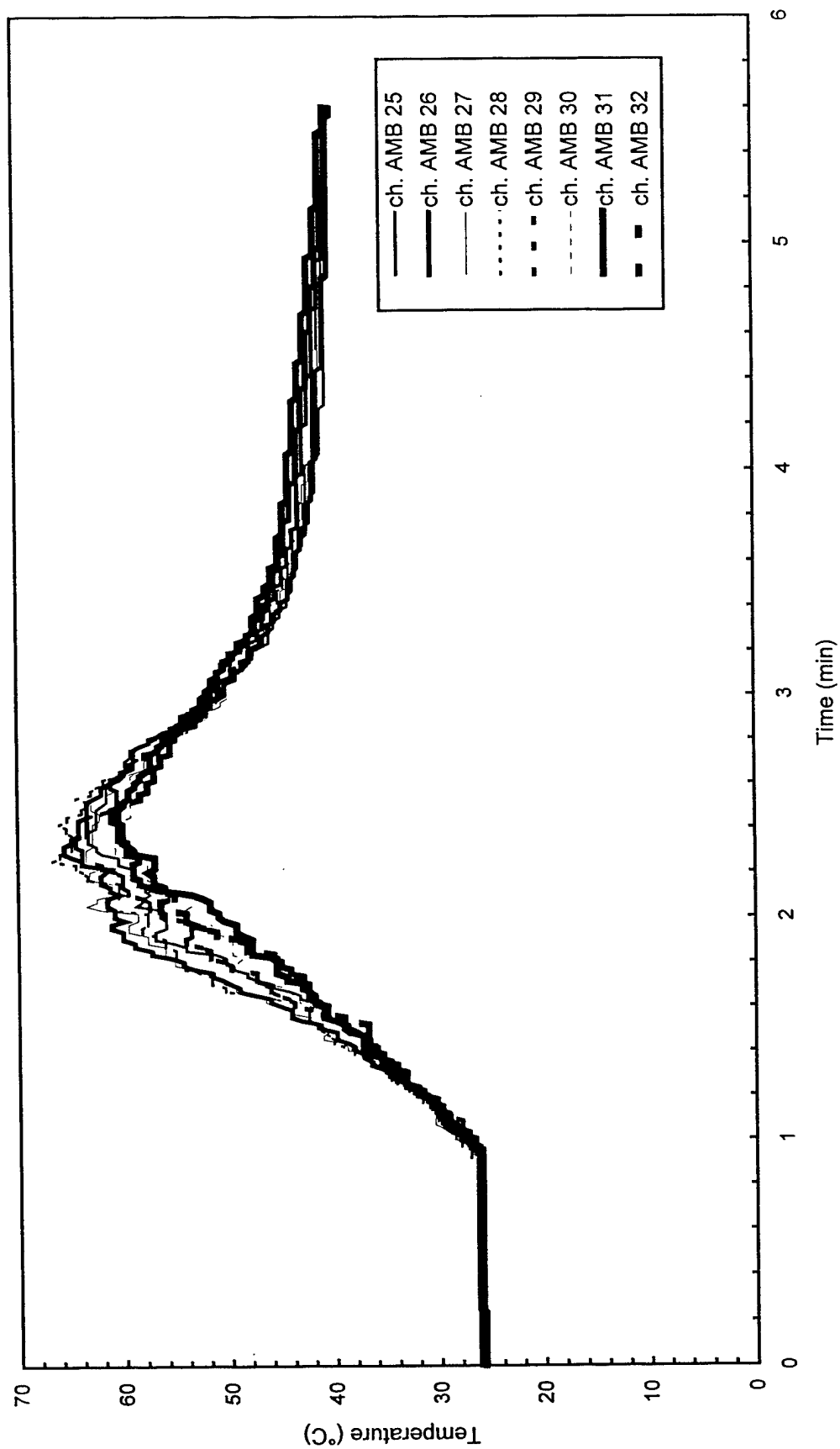


Fig. A23 - Air temperatures around North half of 7.6 m (25 ft) radius from center of pad

Test BB7

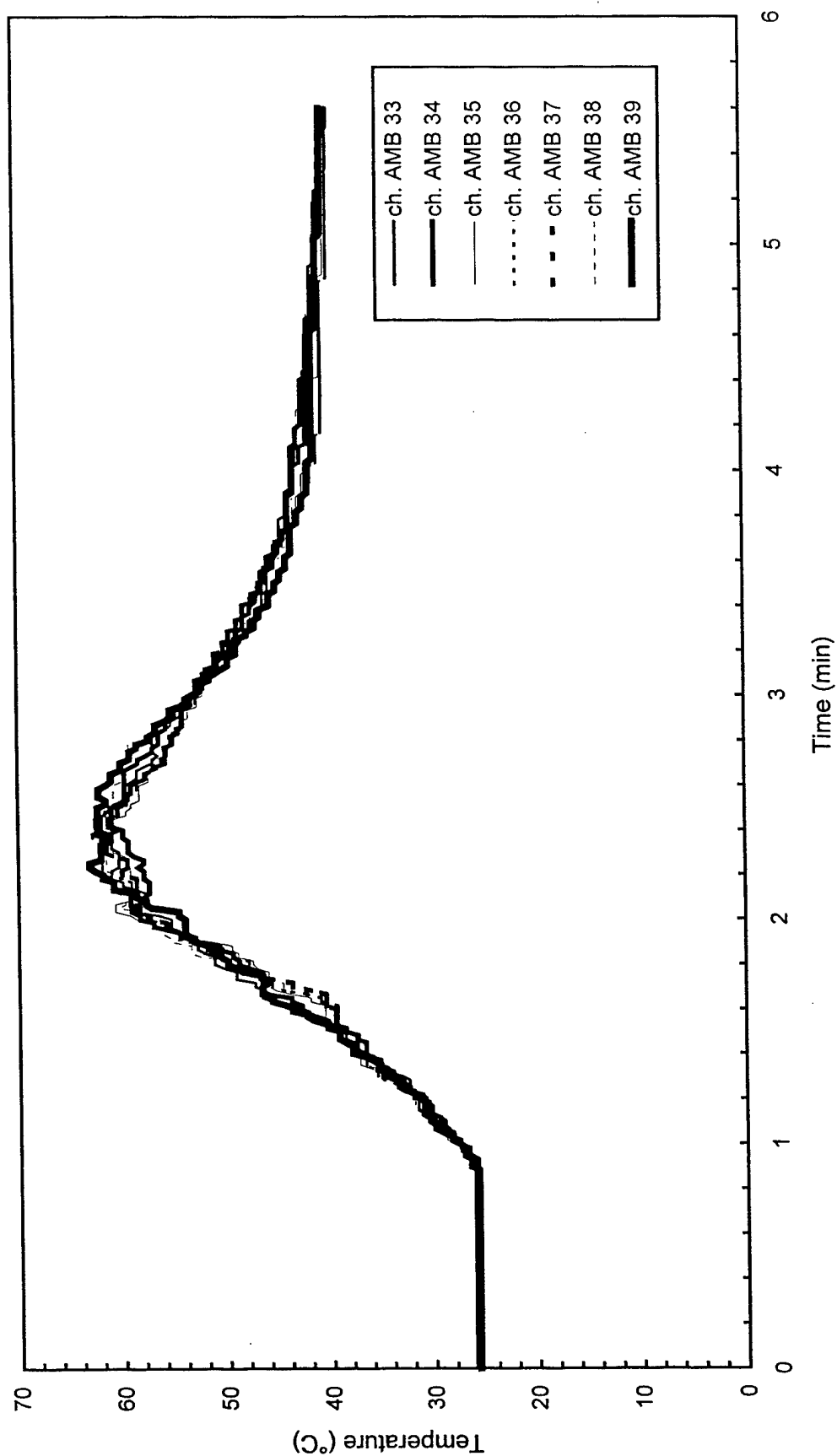


Fig. A24 - Air temperatures around South half of 7.6 m (25 ft) radius from center of pad

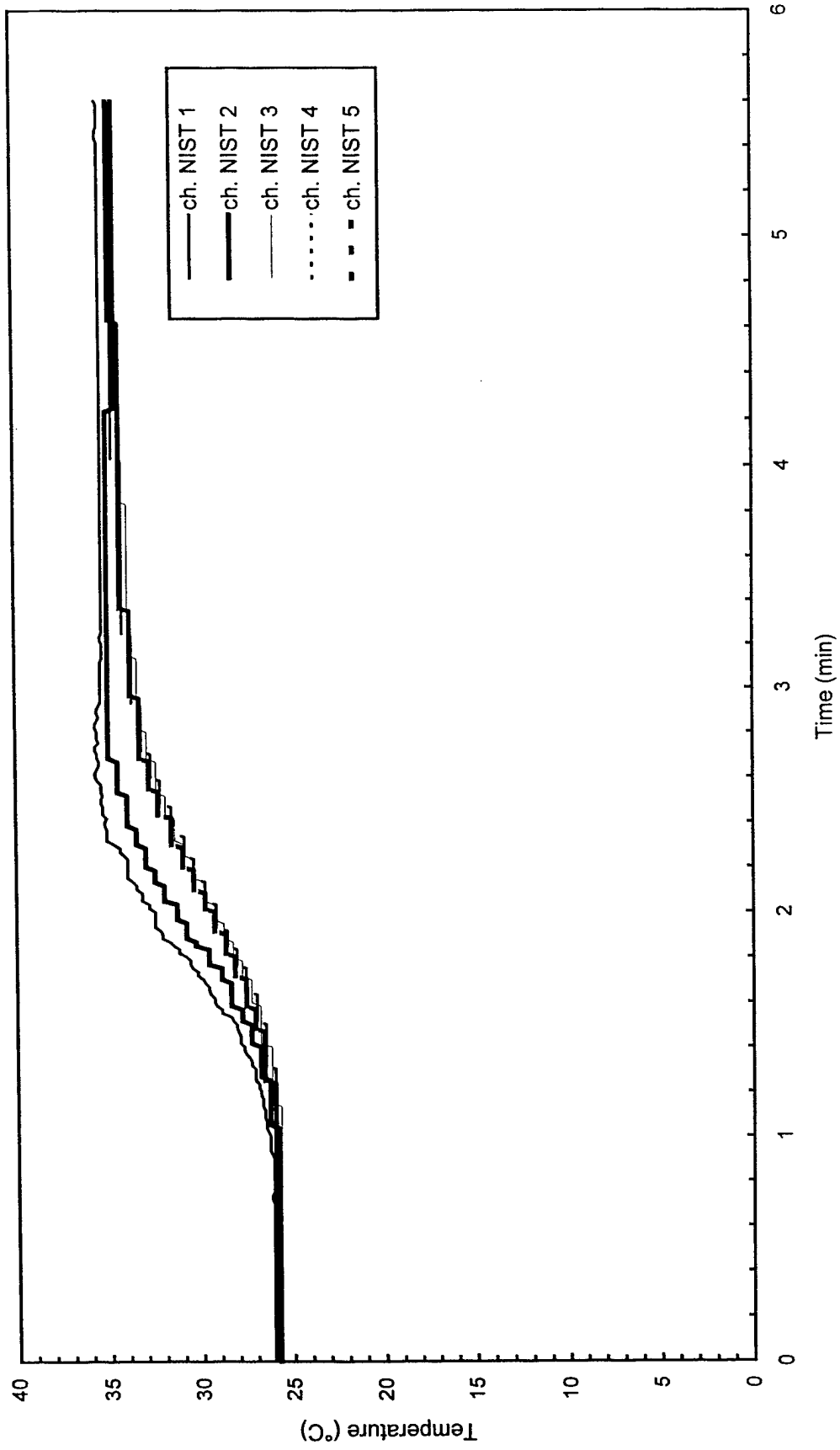


Fig. A25 - Temperature of West steel beam

Test BB7

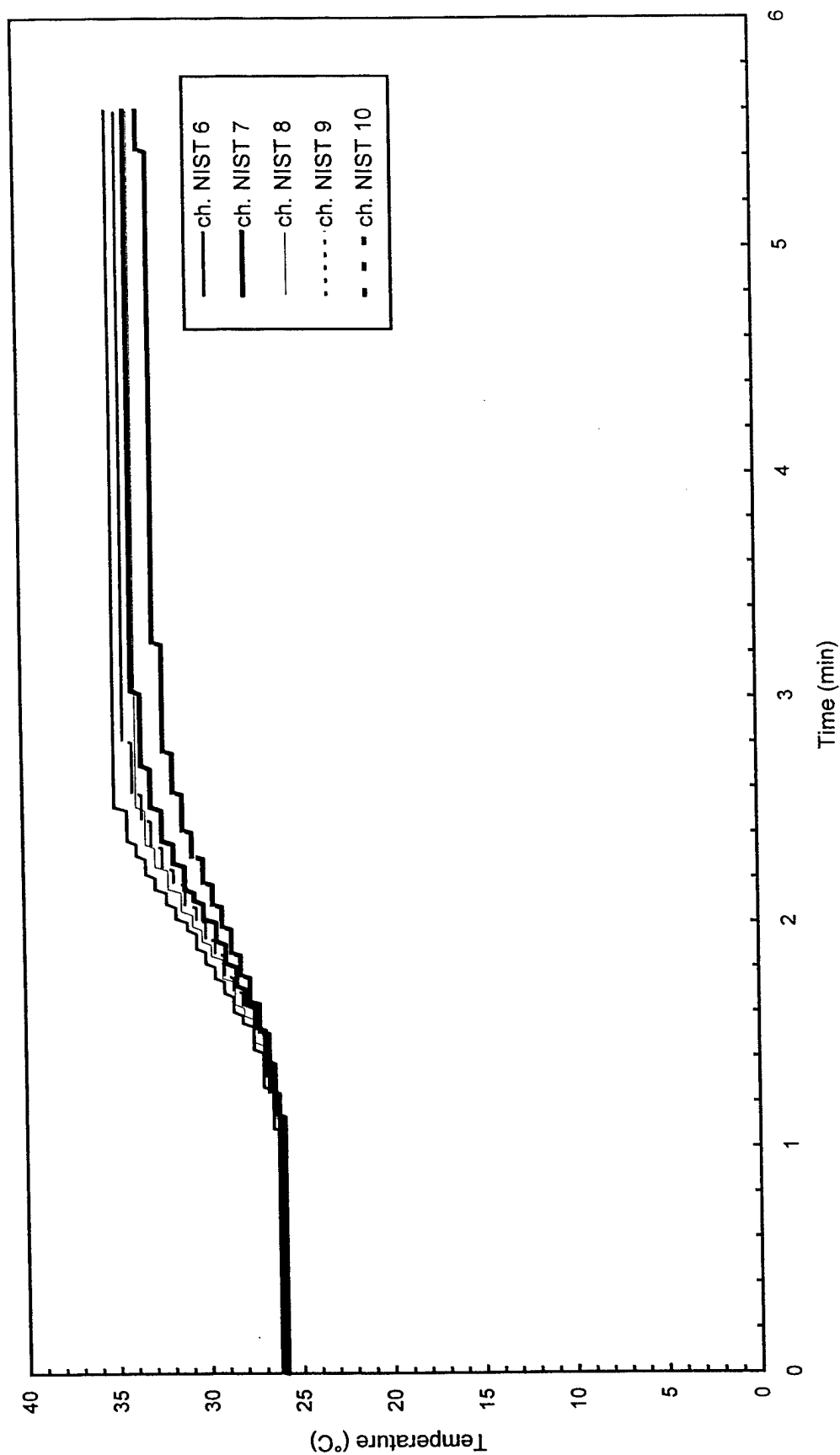


Fig. A26 - Temperature of North steel beam

Test BB7

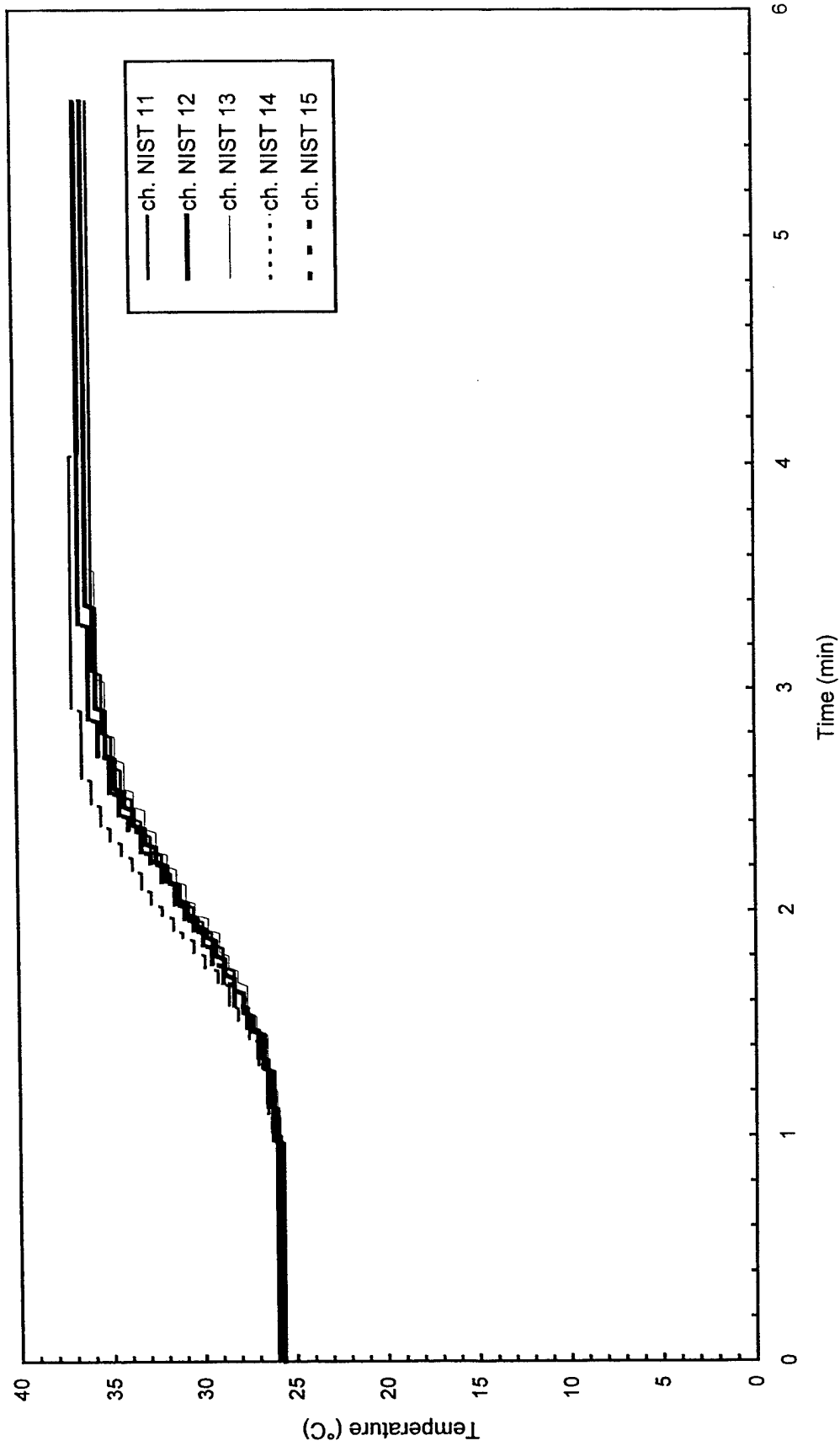


Fig. A27 - Temperature of East steel beam

Test BB7

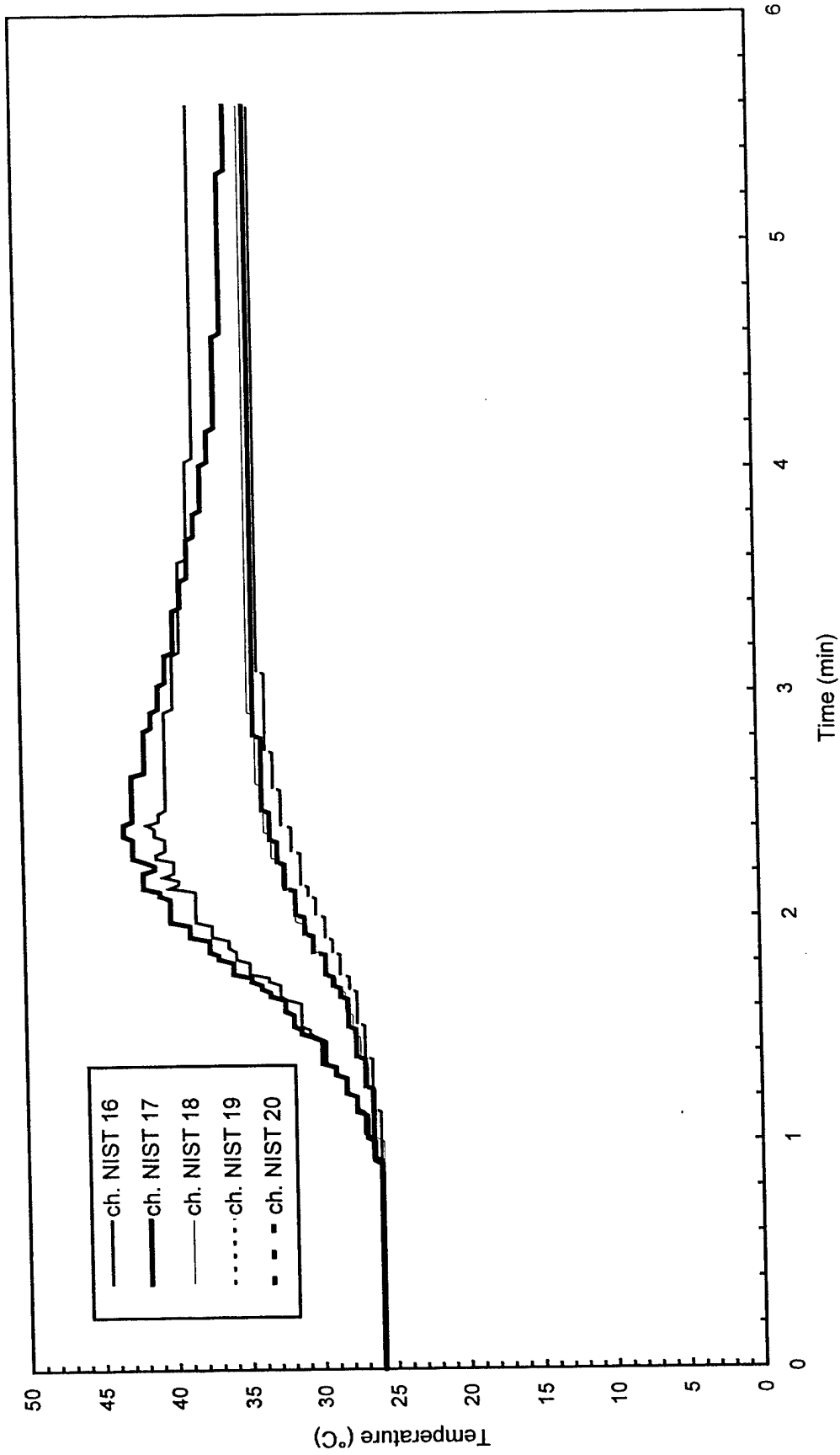


Fig. A28 - Temperature of South steel beam

Test BB7

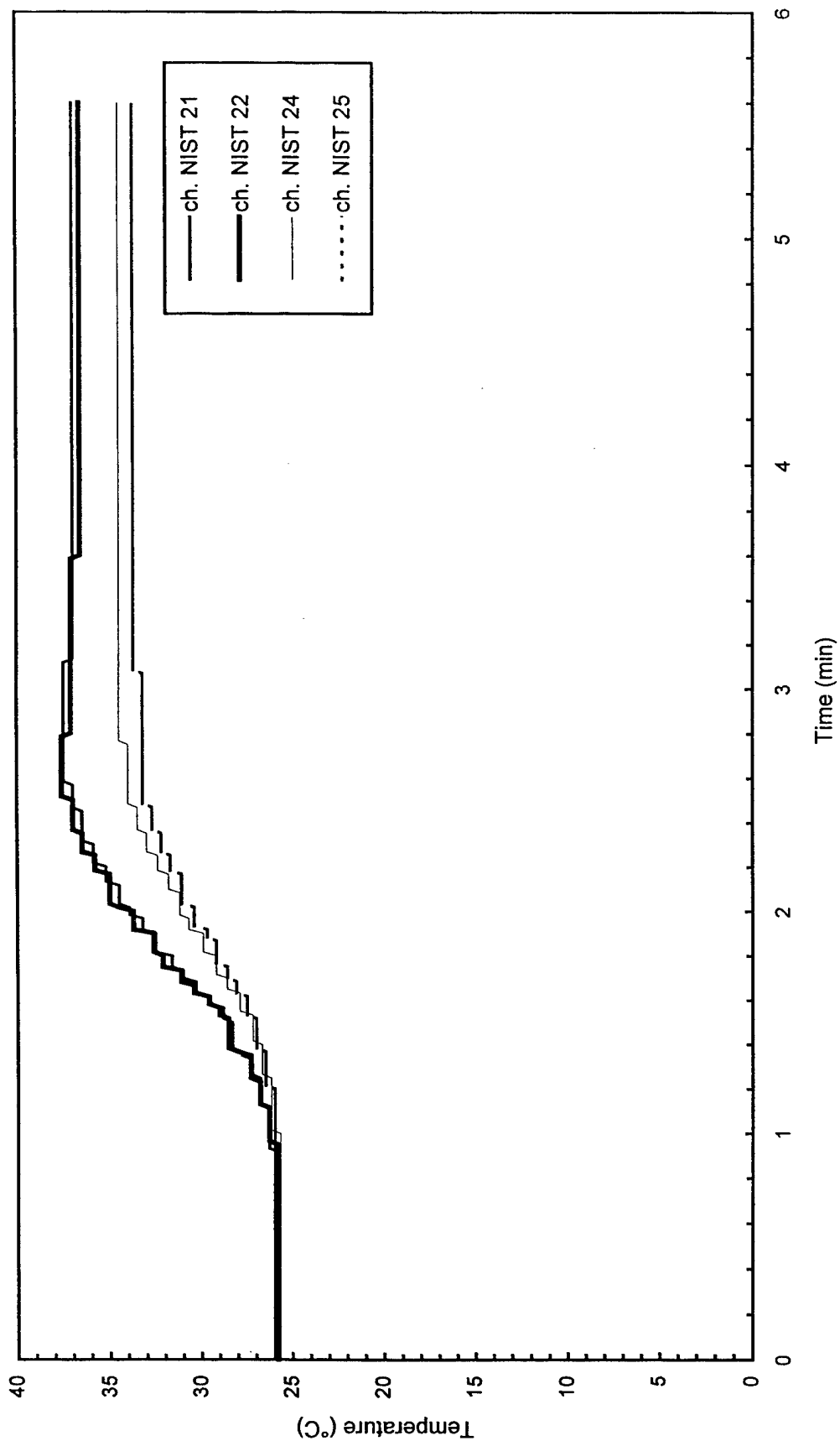


Fig. A29 - Temperature of Northwest steel beam

Test BB7

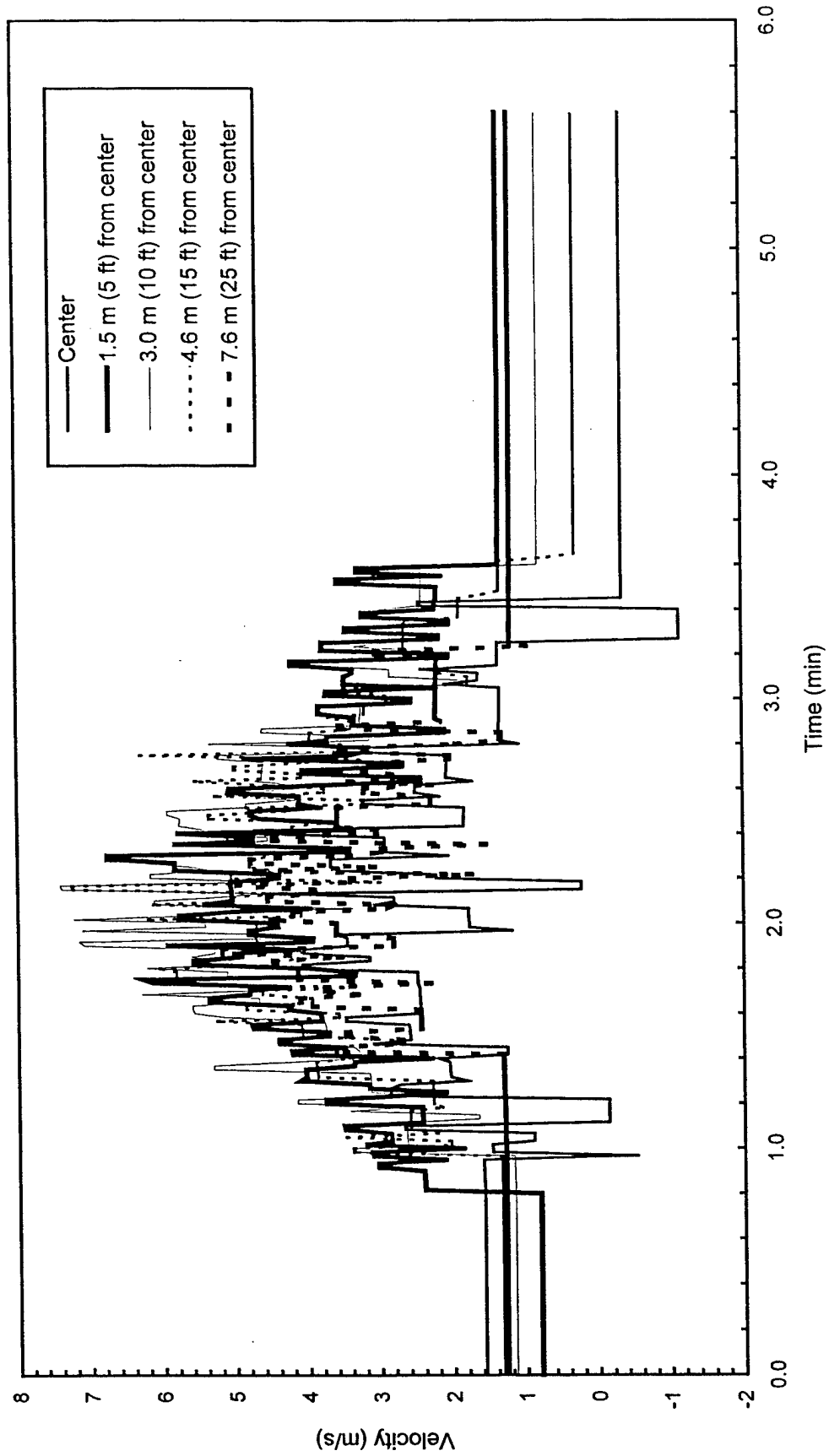


Fig. A30 - Plume and ceiling jet velocities

Test BB8

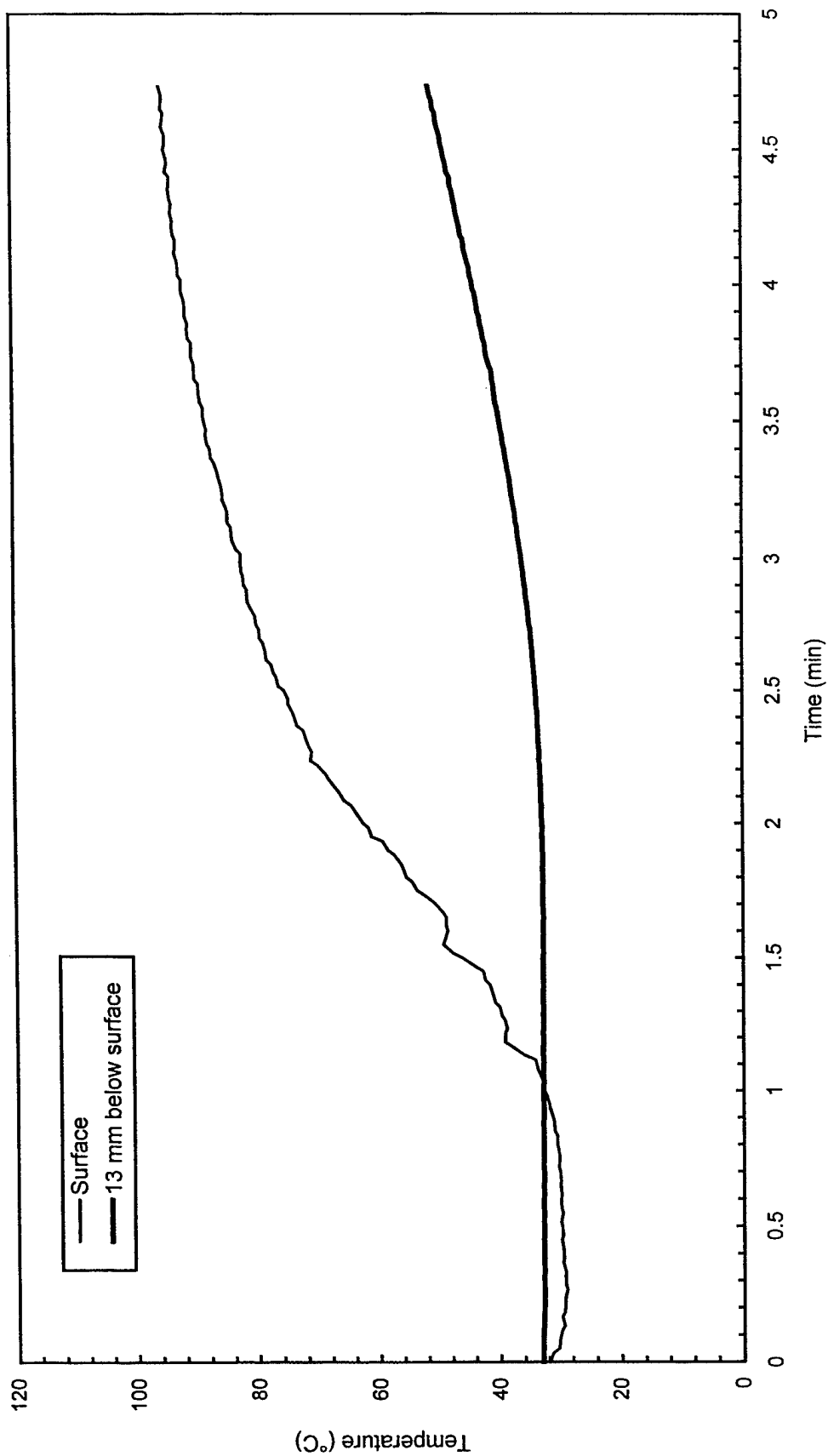


Fig. A31 - Concrete temperatures at center of pad

Test BB8

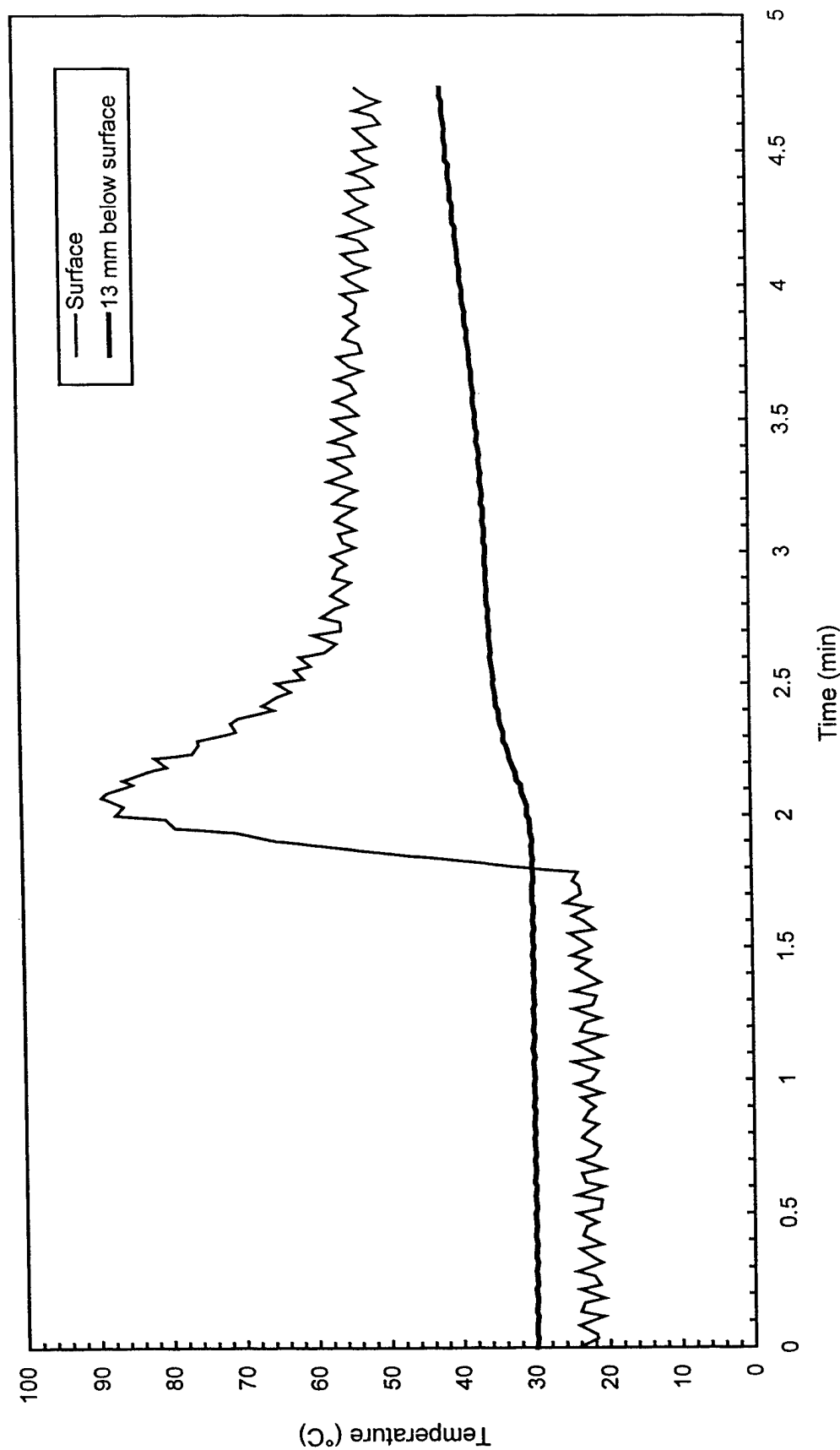


Fig. A32 - Concrete temperatures 3 m (10 ft) East of center of pad

Test BB8

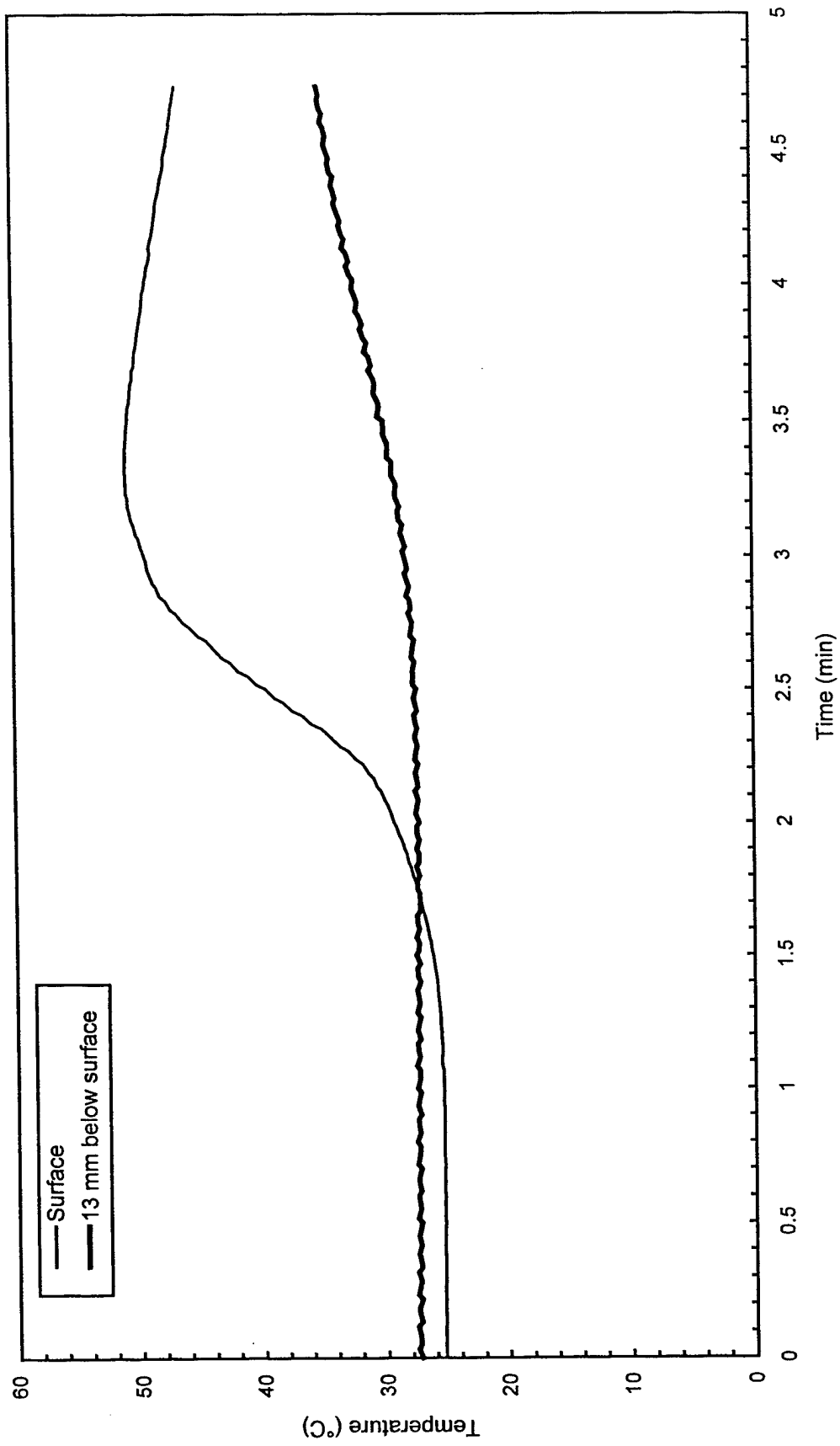


Fig. A33 - Concrete temperatures 3 m (10 ft) West of center of pad

Test BB8

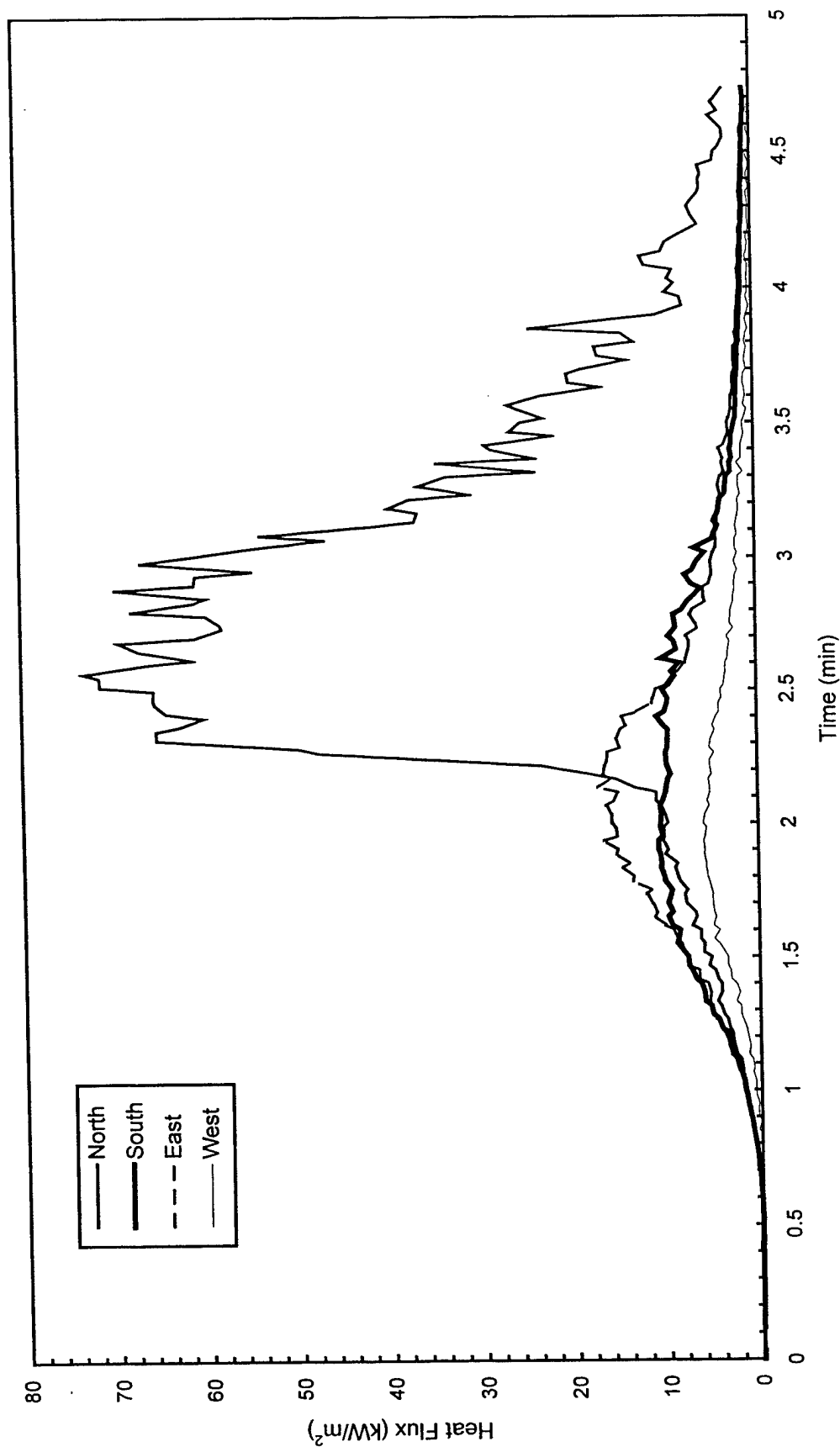


Fig. A34 - Heat flux measured at edge of pad

Test BB8

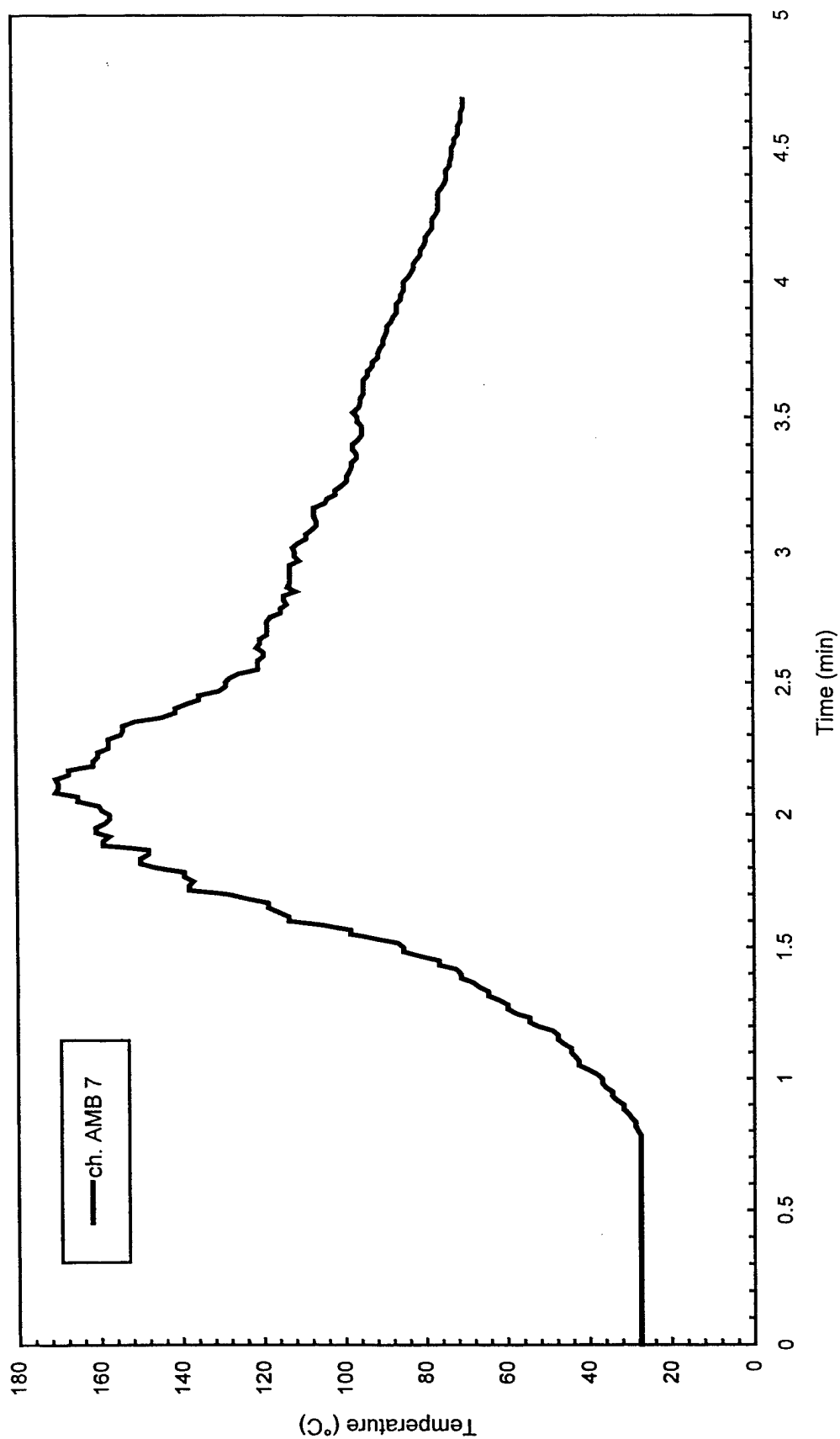


Fig. A35 - Air temperatures over center of pad

Test BB8

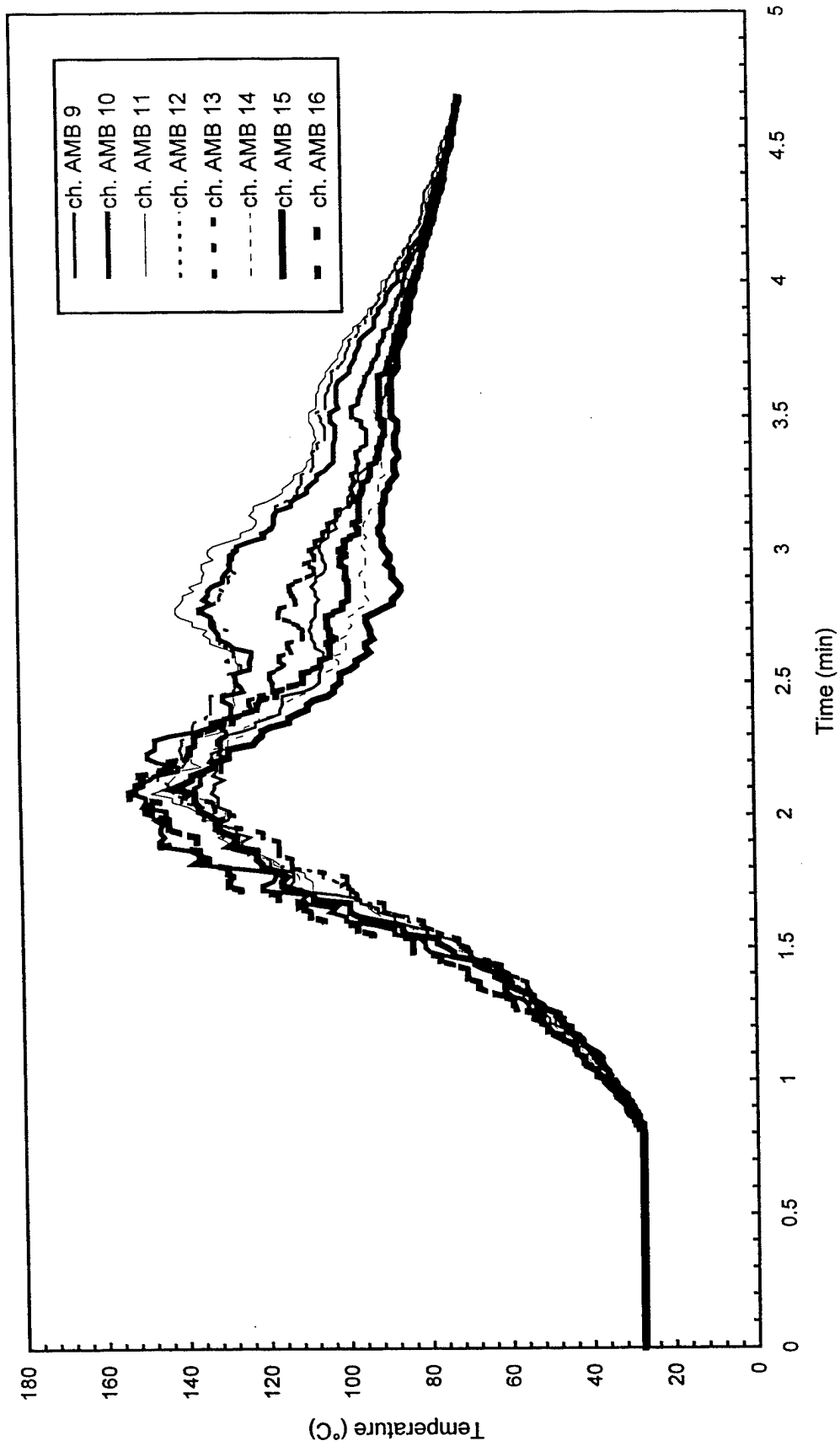


Fig. A36 - Air temperatures around 3 m (10 ft) radius from center of pad

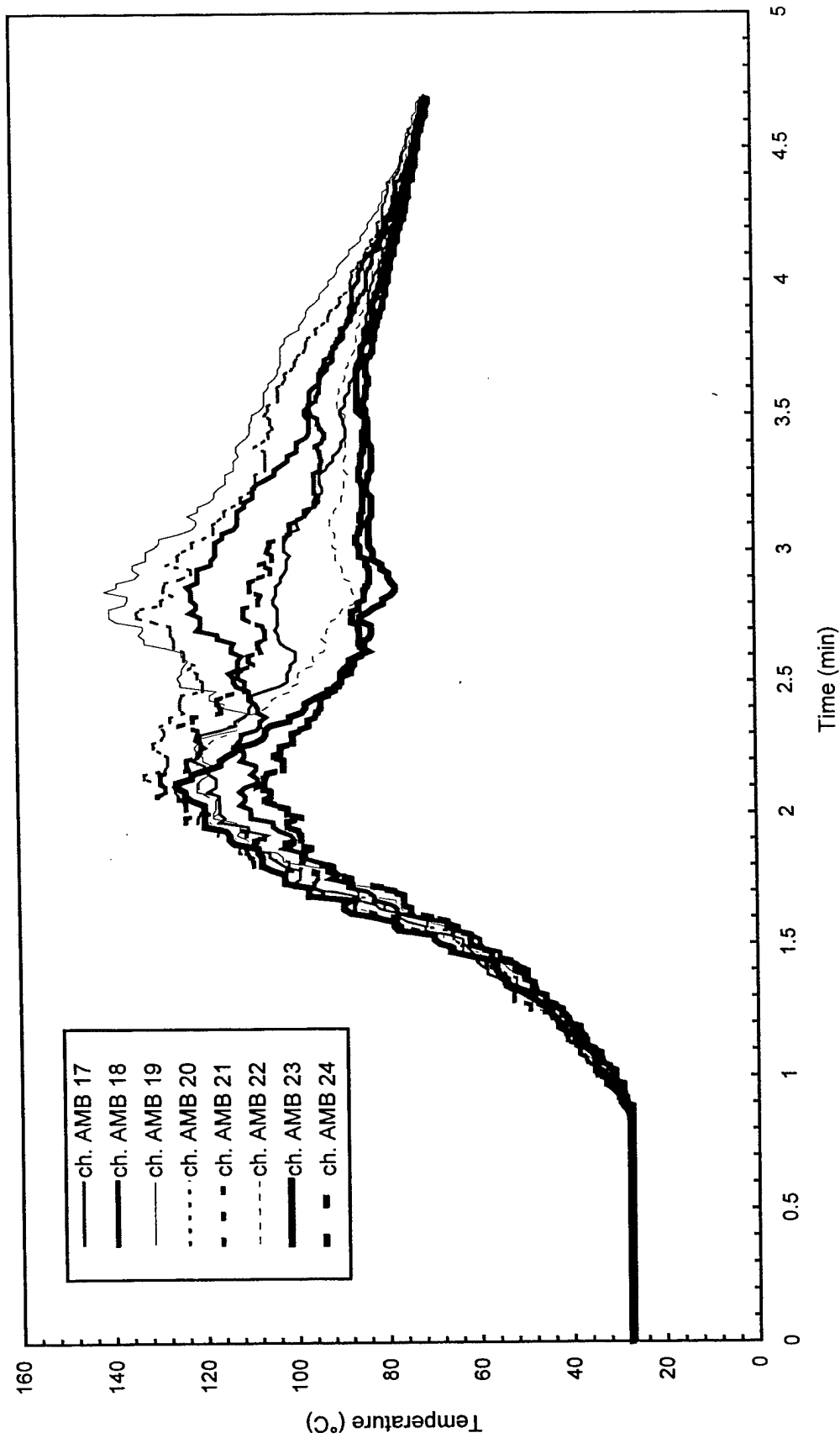


Fig. A37 - Air temperatures around 4.6 m (15 ft) radius from center of pad

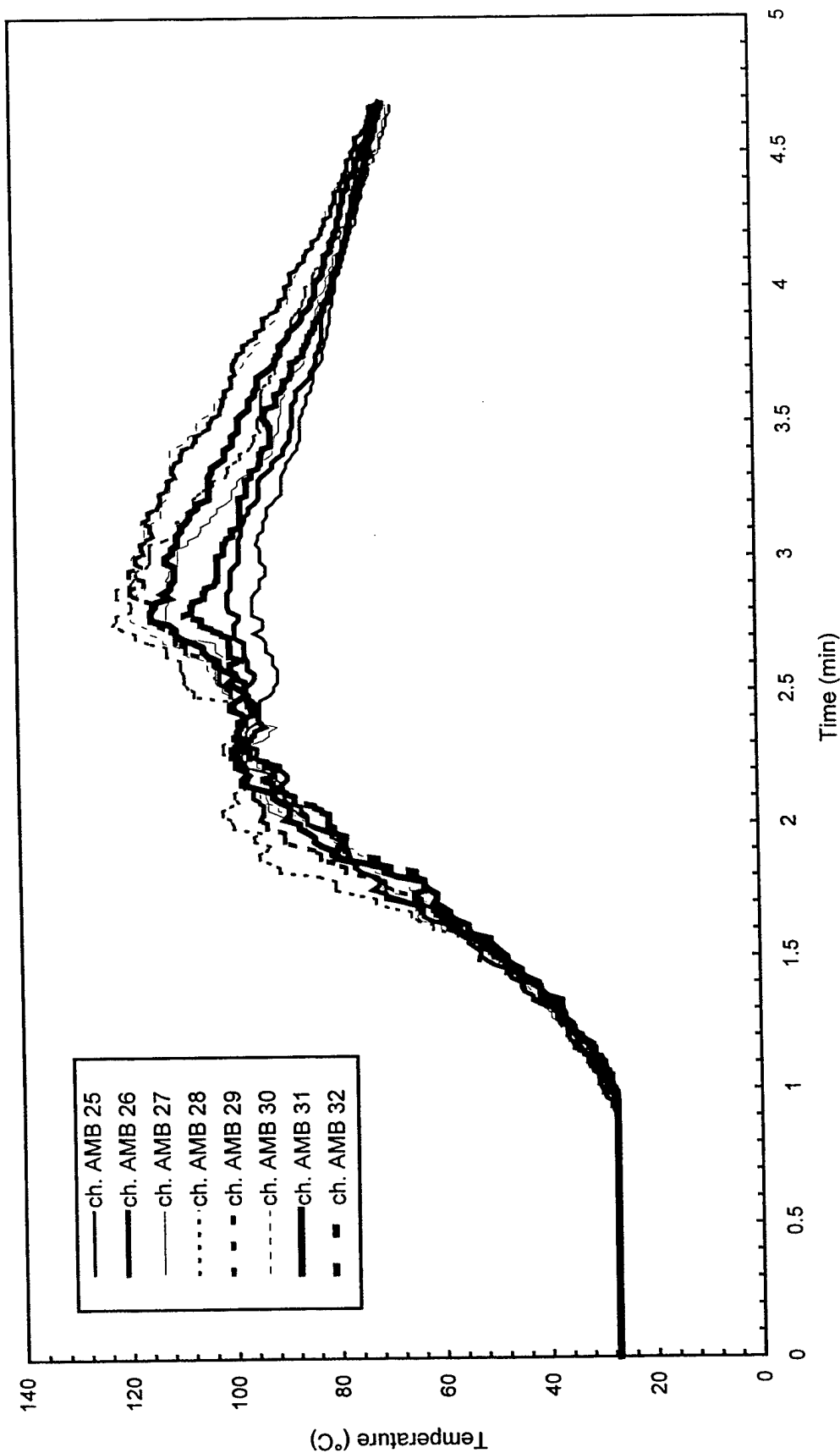


Fig. A38 - Air temperatures around North half of 7.6 m (25 ft) radius from center of pad

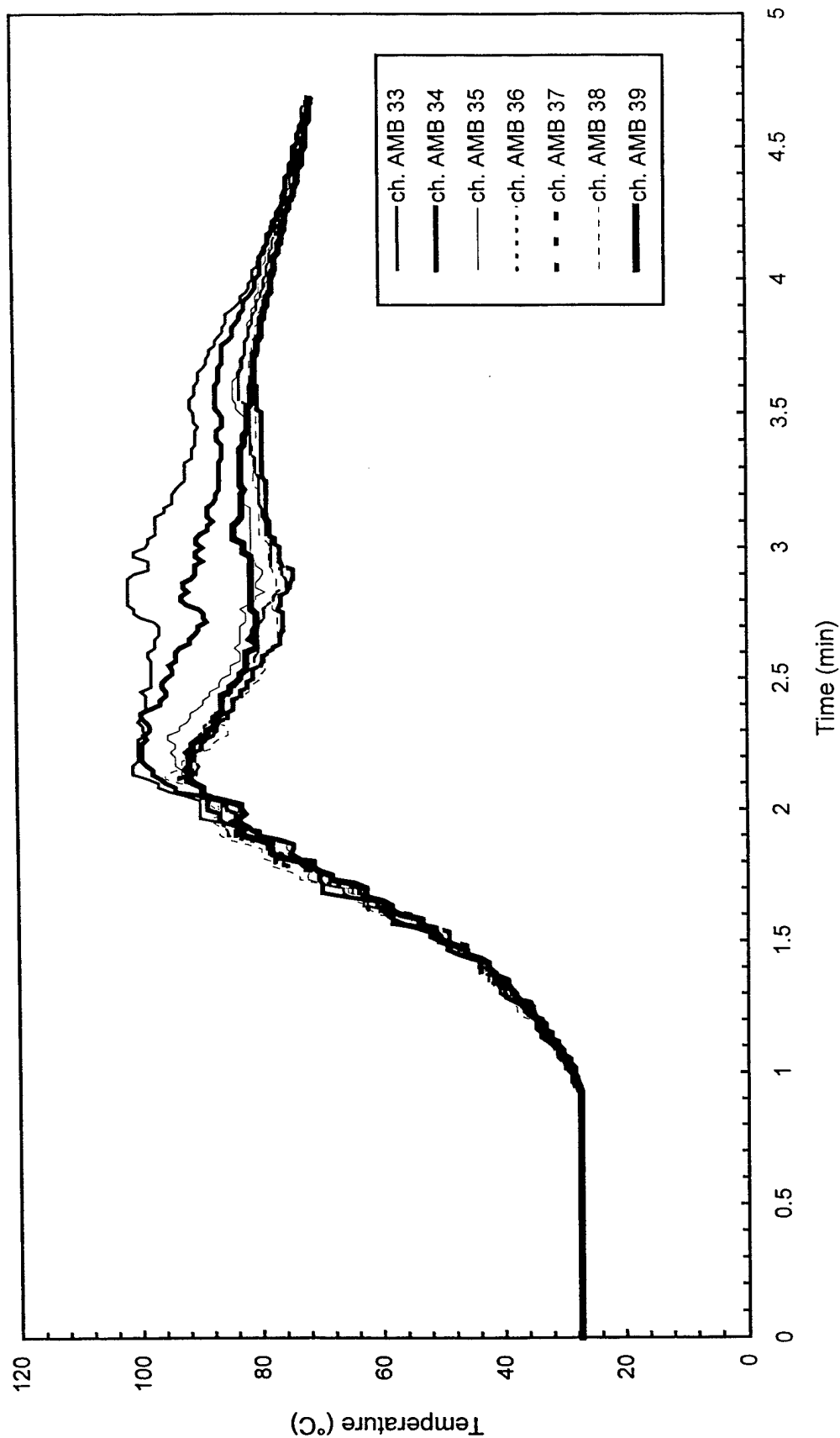


Fig. A39 - Air temperatures around South half of 7.6 m (25 ft) radius from center of pad

Test BB8

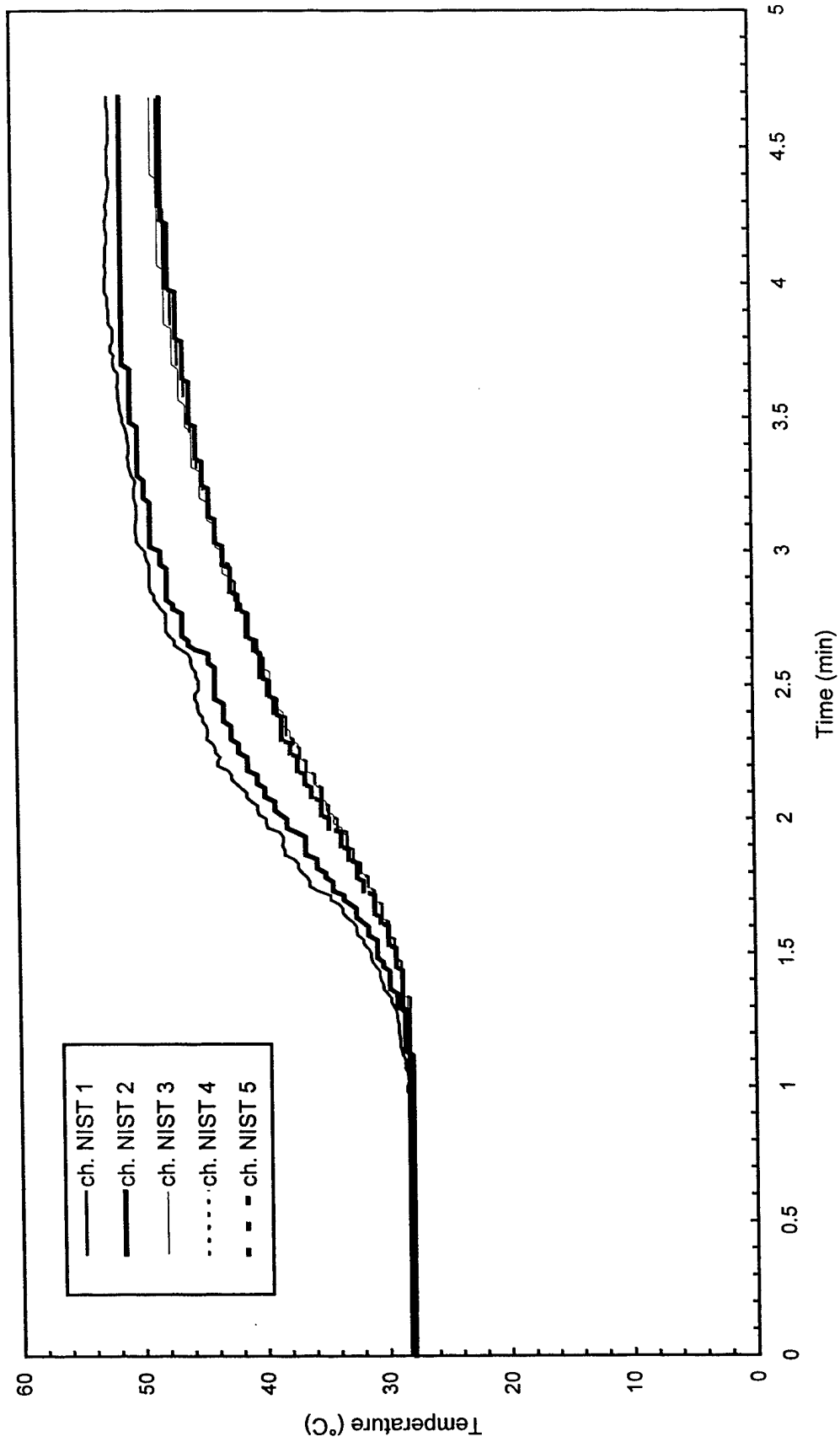


Fig. A40 - Temperature of West steel beam

Test BB8

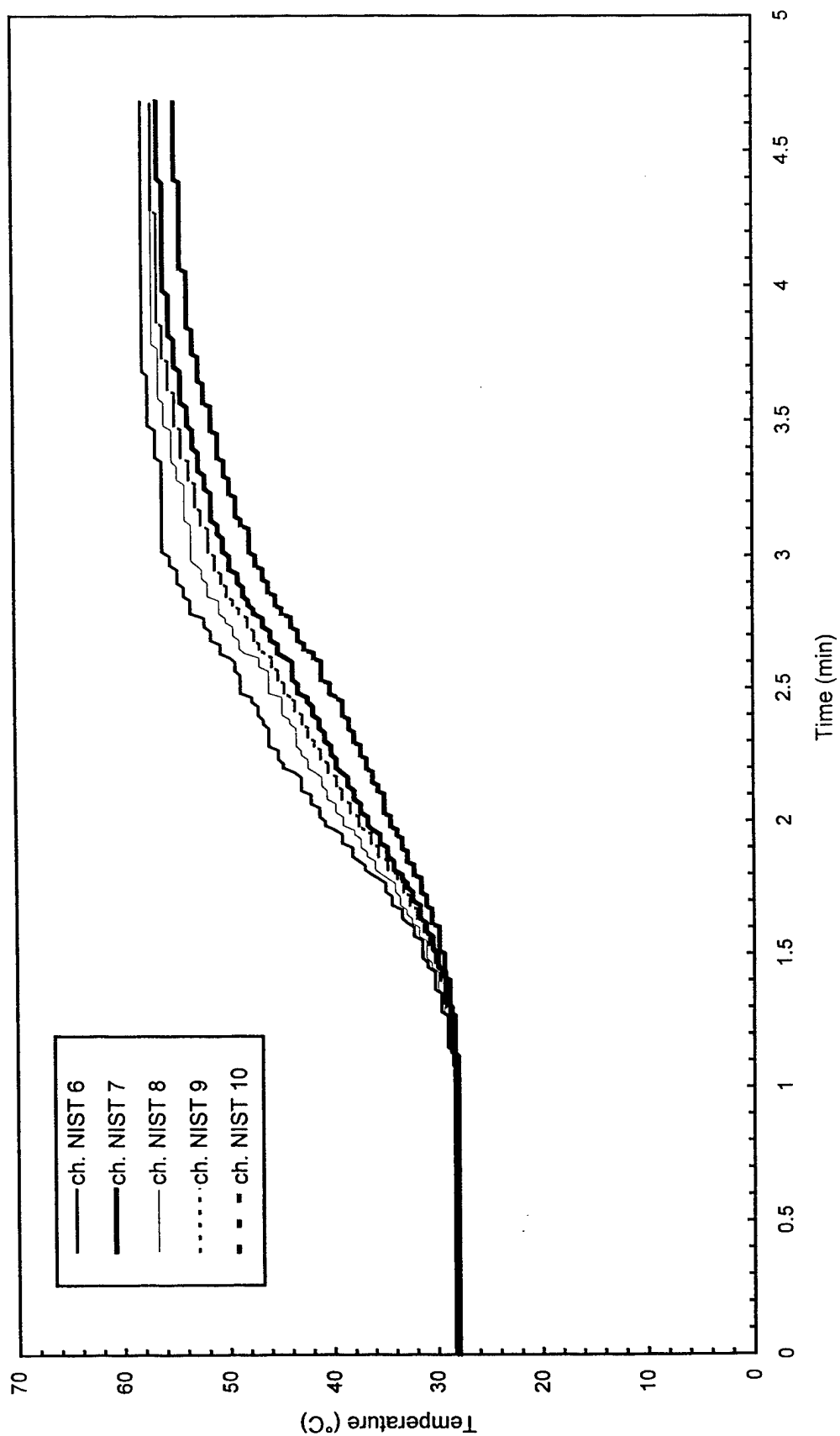


Fig. A41 - Temperature of North steel beam

Test BB8

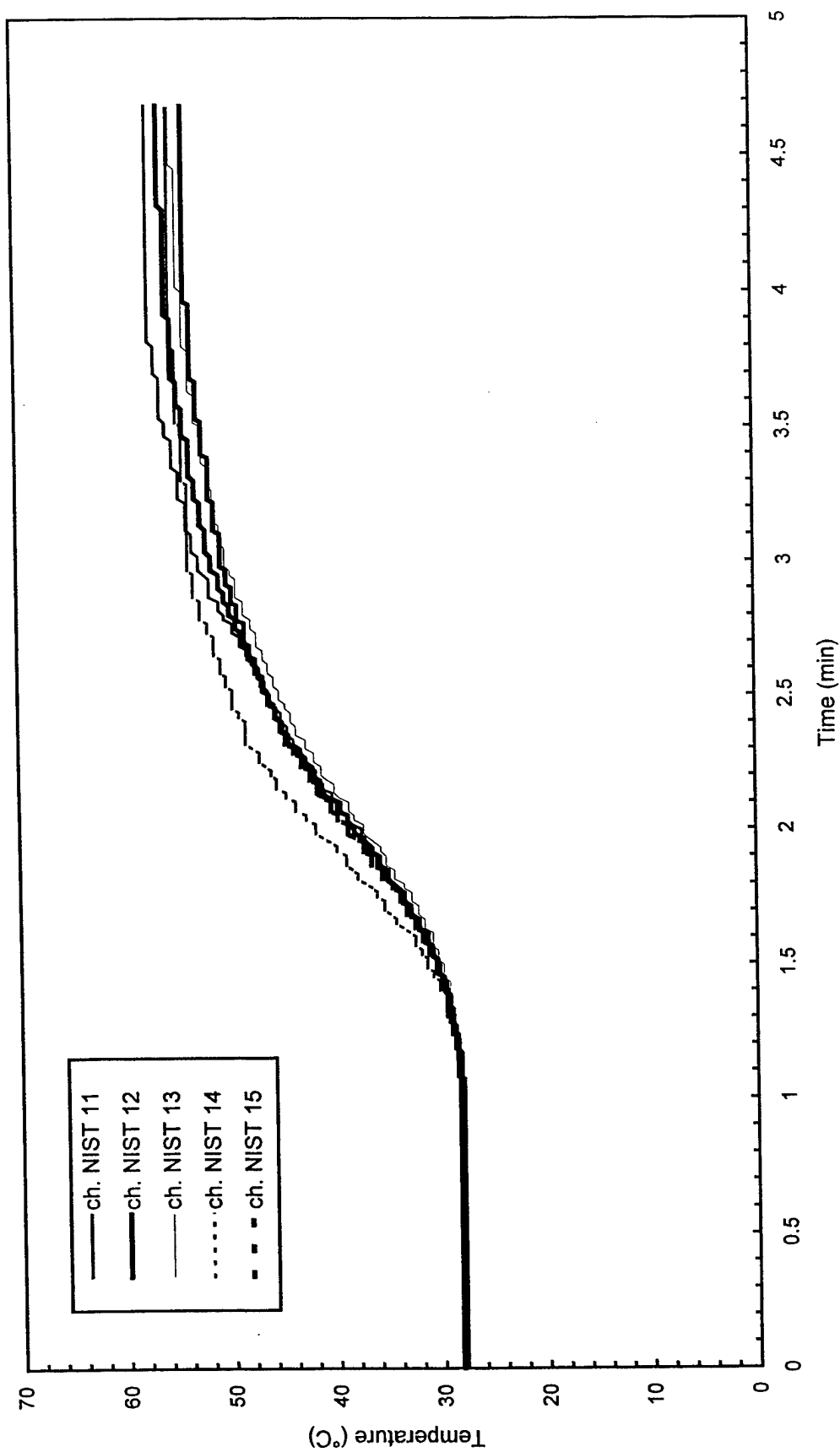


Fig. A42 - Temperature of East steel beam

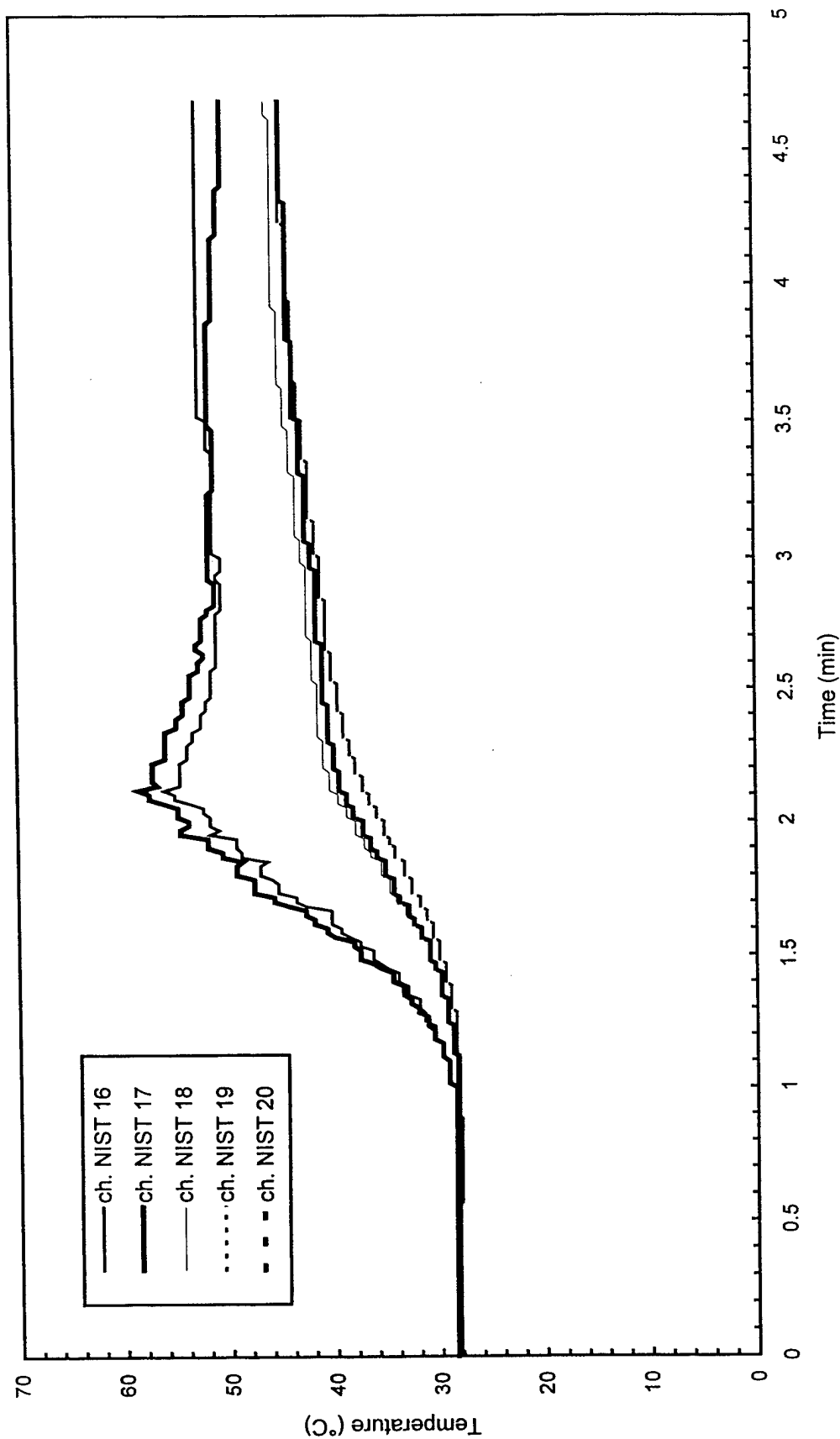


Fig. A43 - Temperature of South steel beam

Test BB8

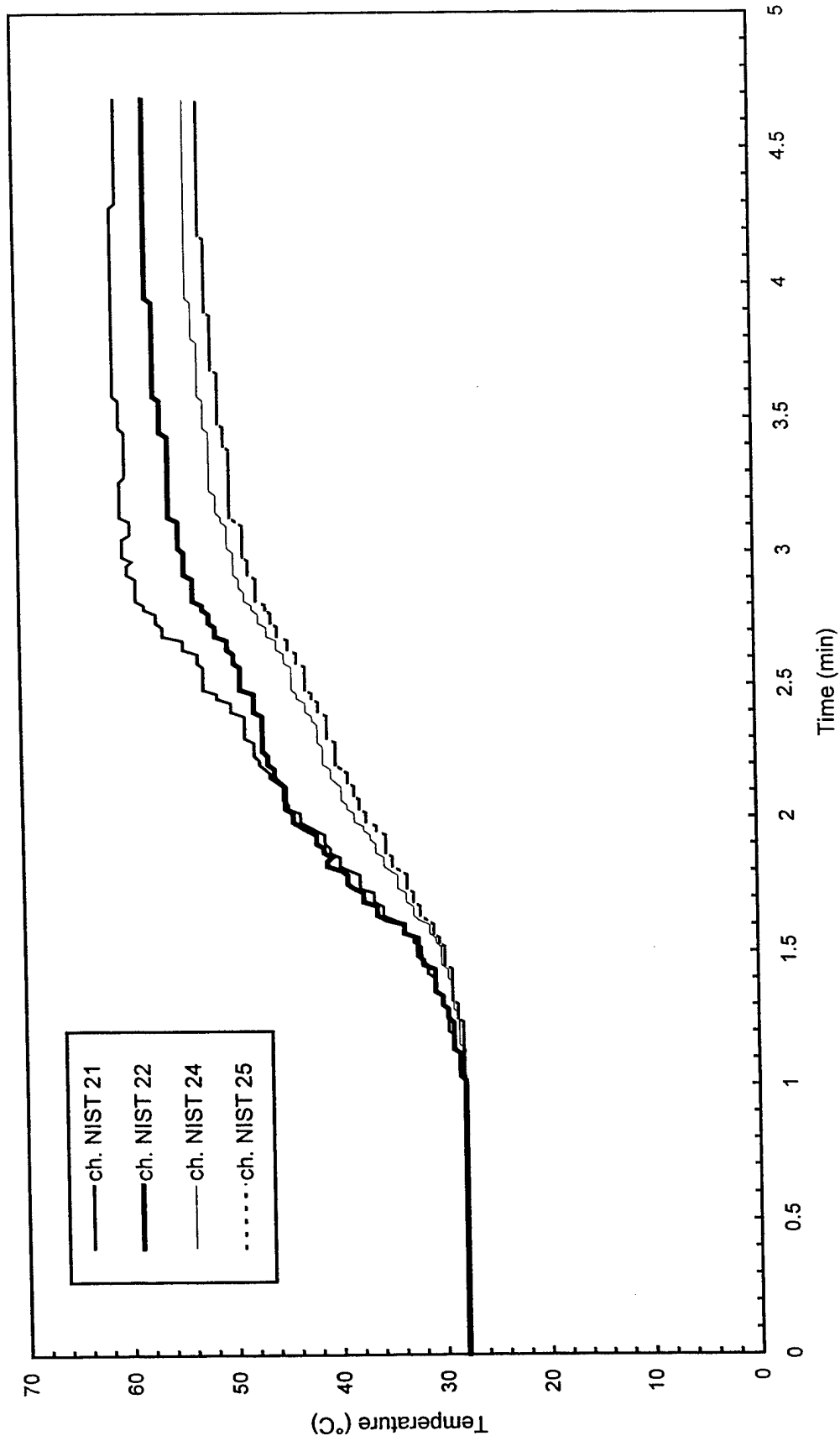


Fig. A44 - Temperature of Northwest steel beam

Test BB8

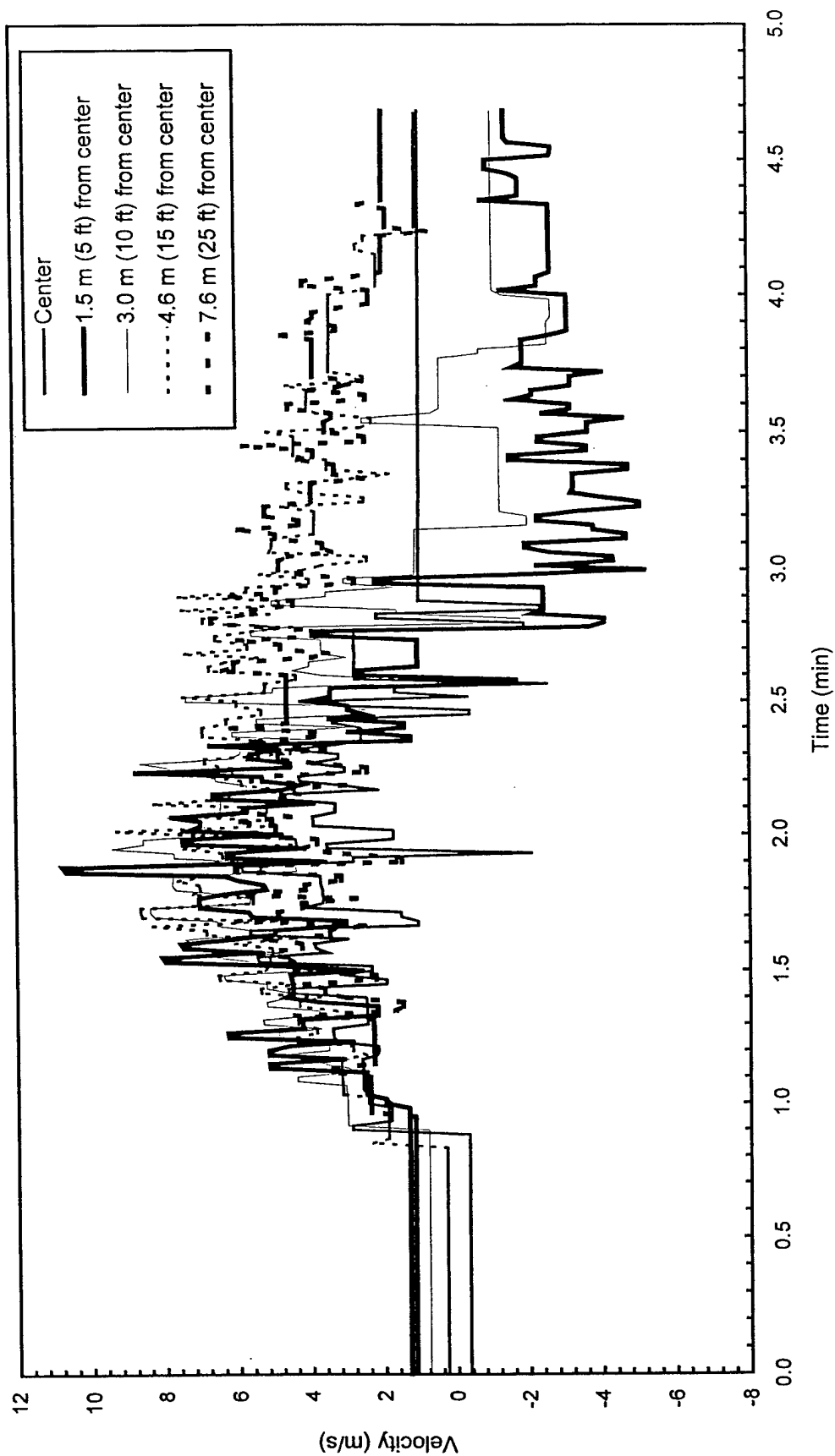


Fig. A45 - Plume and ceiling jet velocities

APPENDIX B
Overhead Sprinkler System Test Data

Test S1

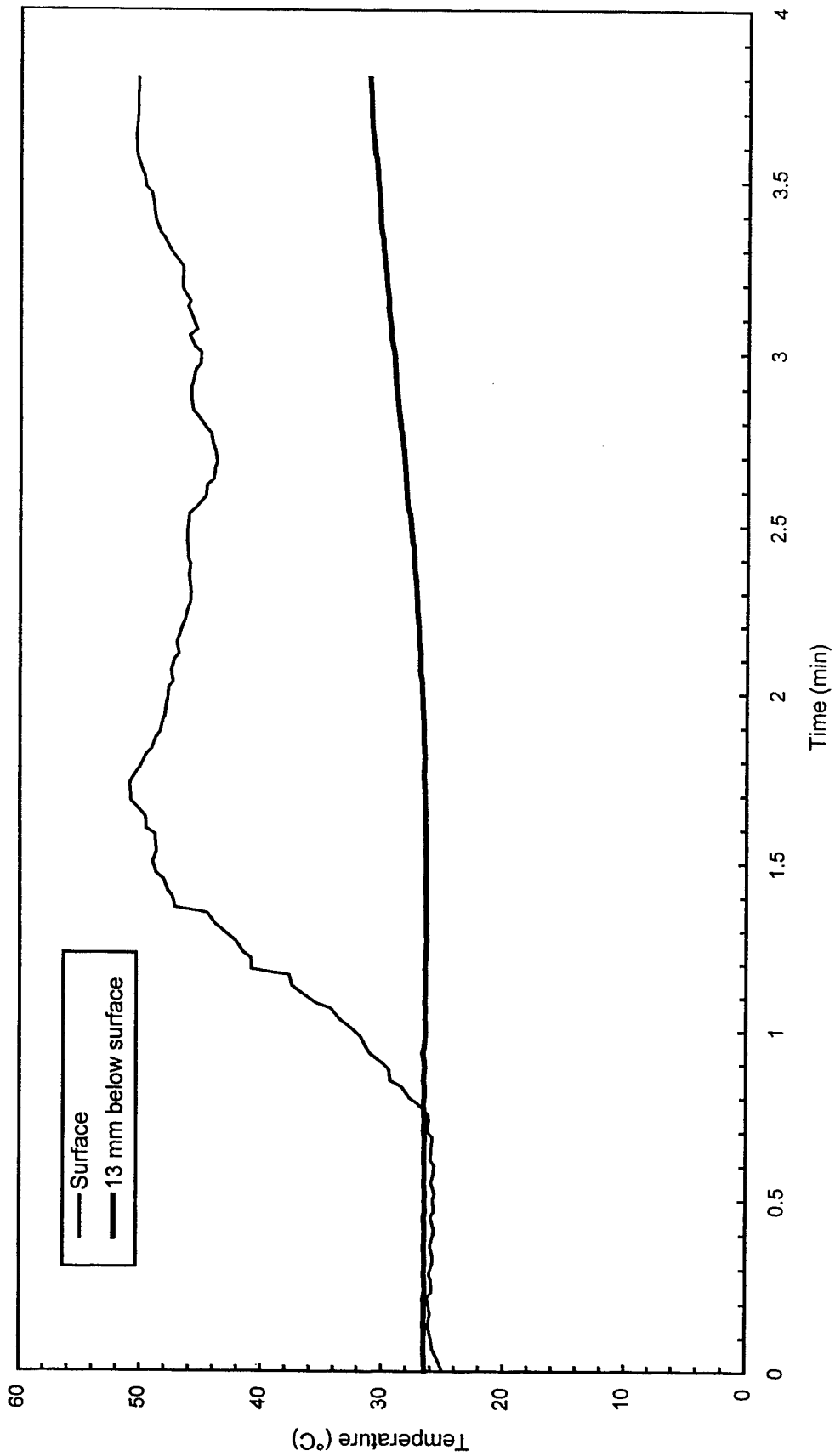


Fig. B1 - Concrete temperatures at center of pad

Test S1

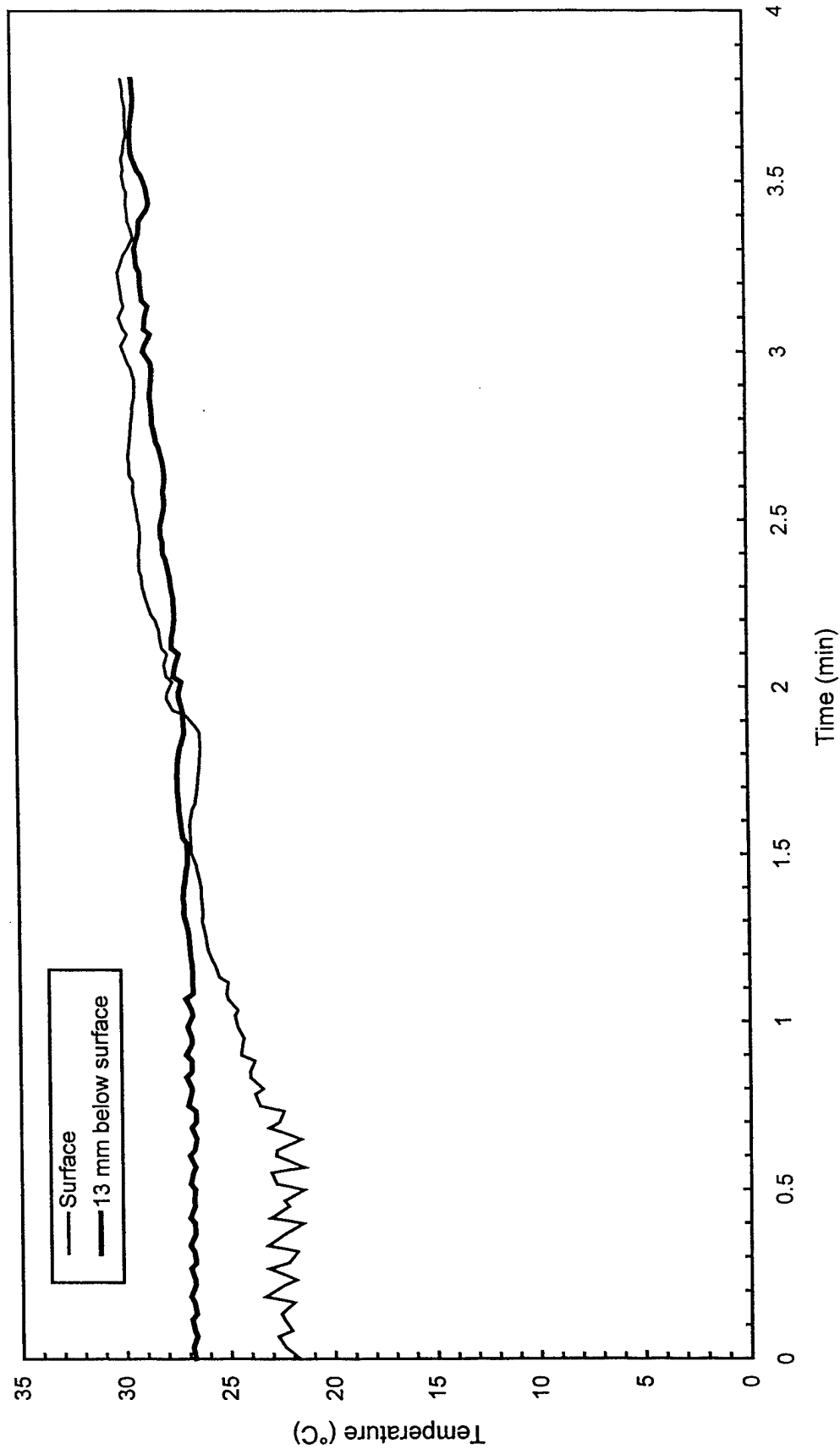


Fig. B2 - Concrete temperatures 3 m (10 ft) East of center of pad

Test S1

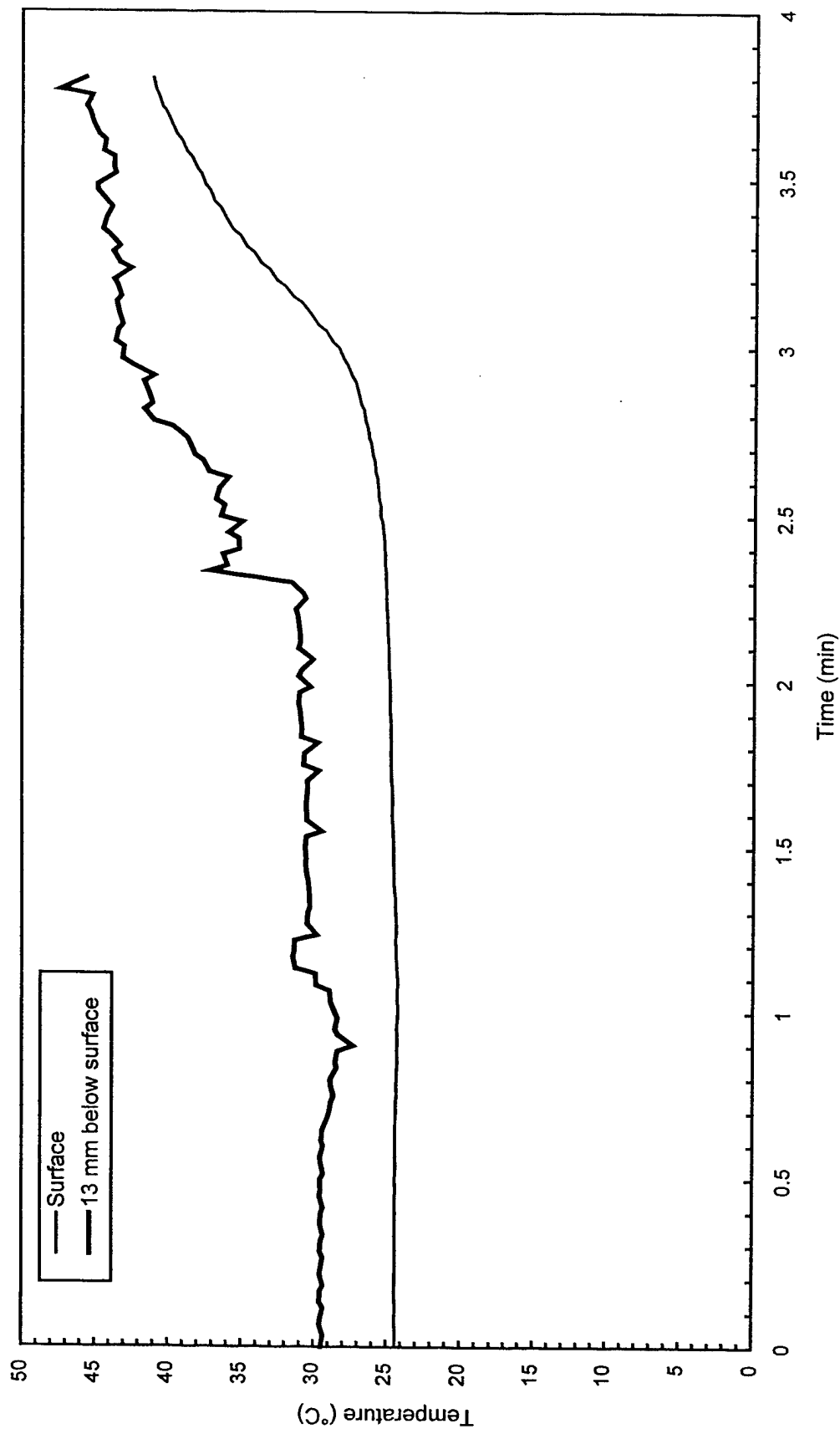


Fig. B3 - Concrete temperatures 3 m (10 ft) West of center of pad

Test S1

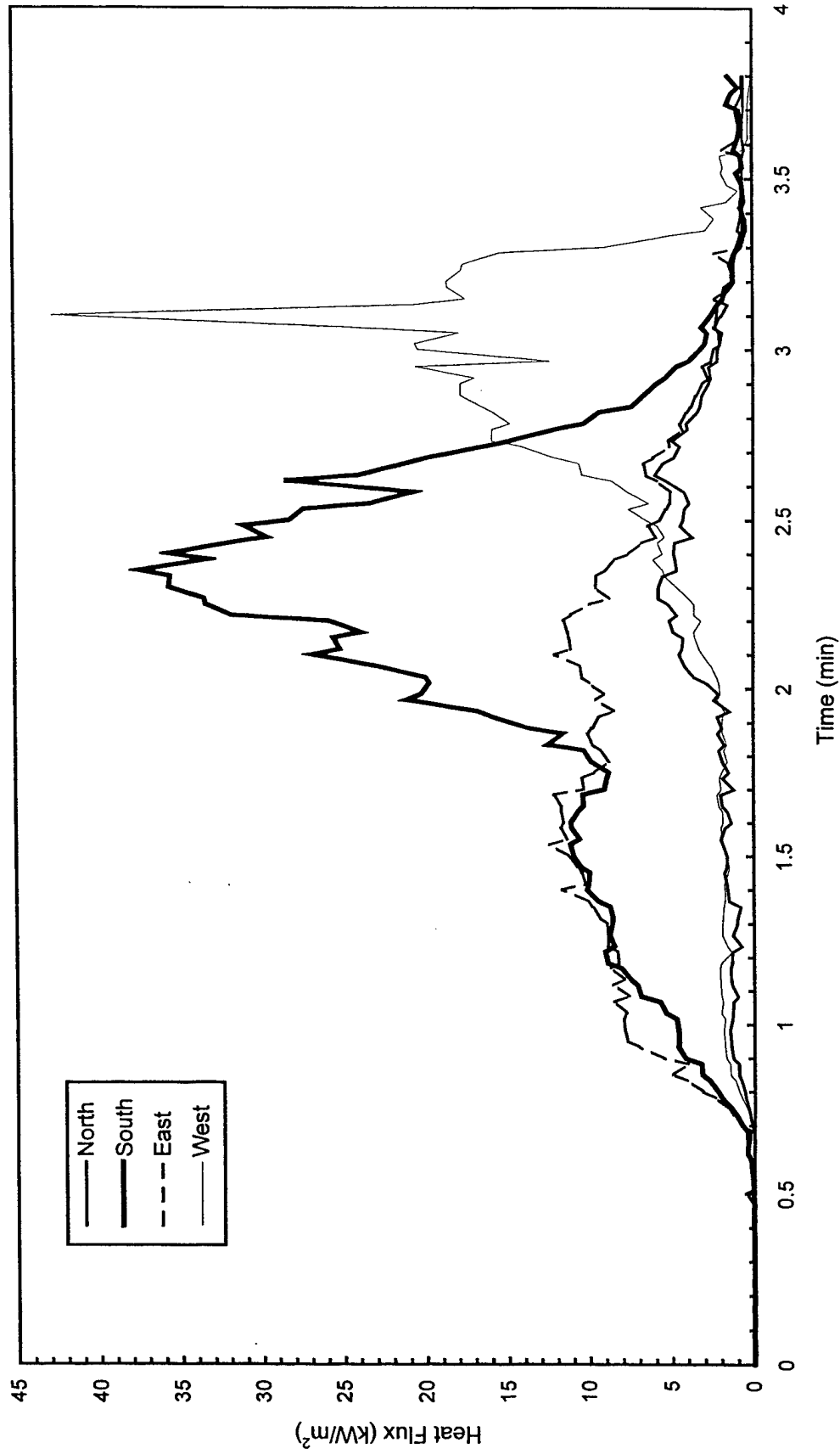


Fig. B4 - Heat flux measured at edge of pad

Test S1

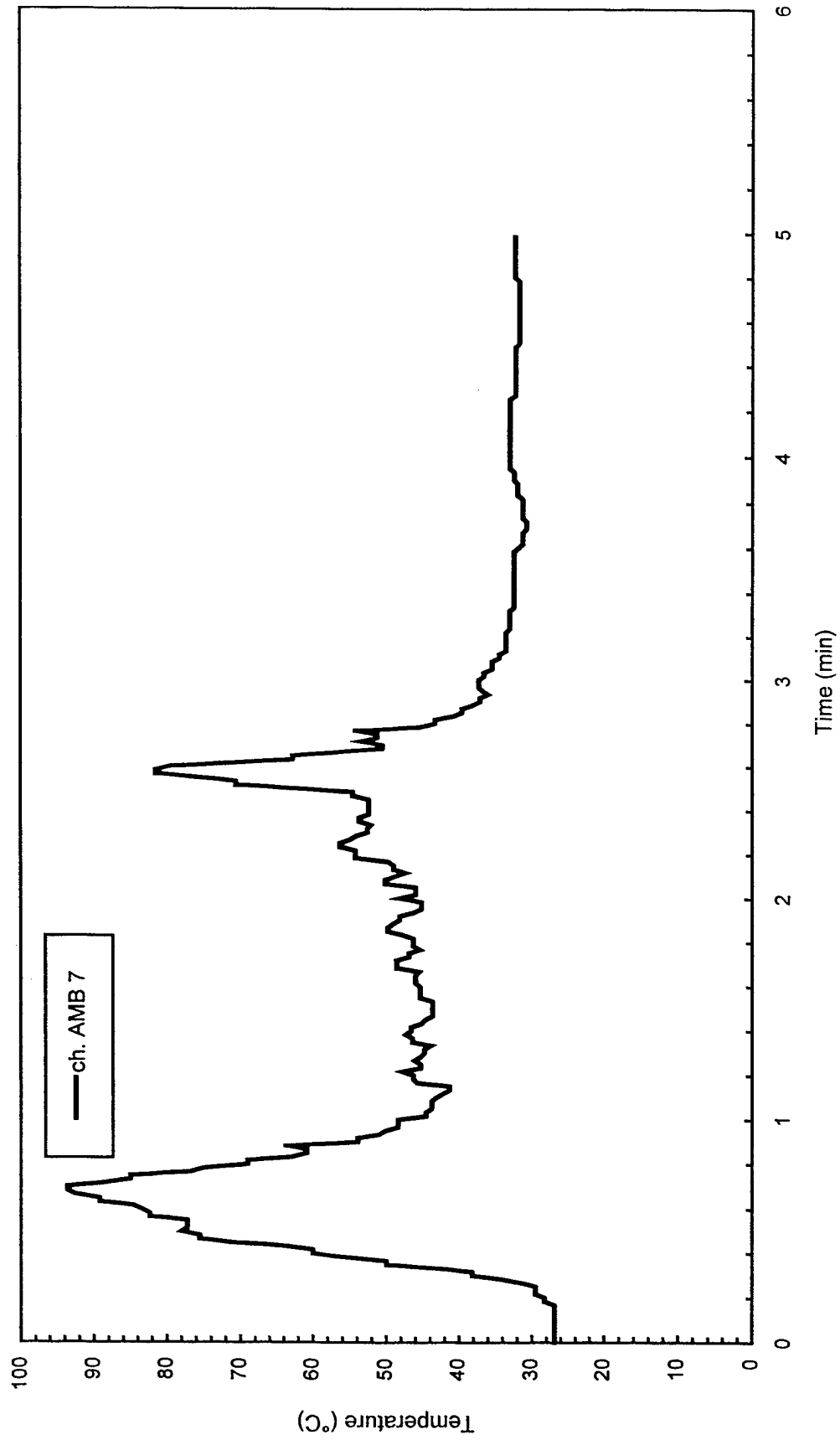


Fig. B5 - Air temperatures over center of pad

Test S1

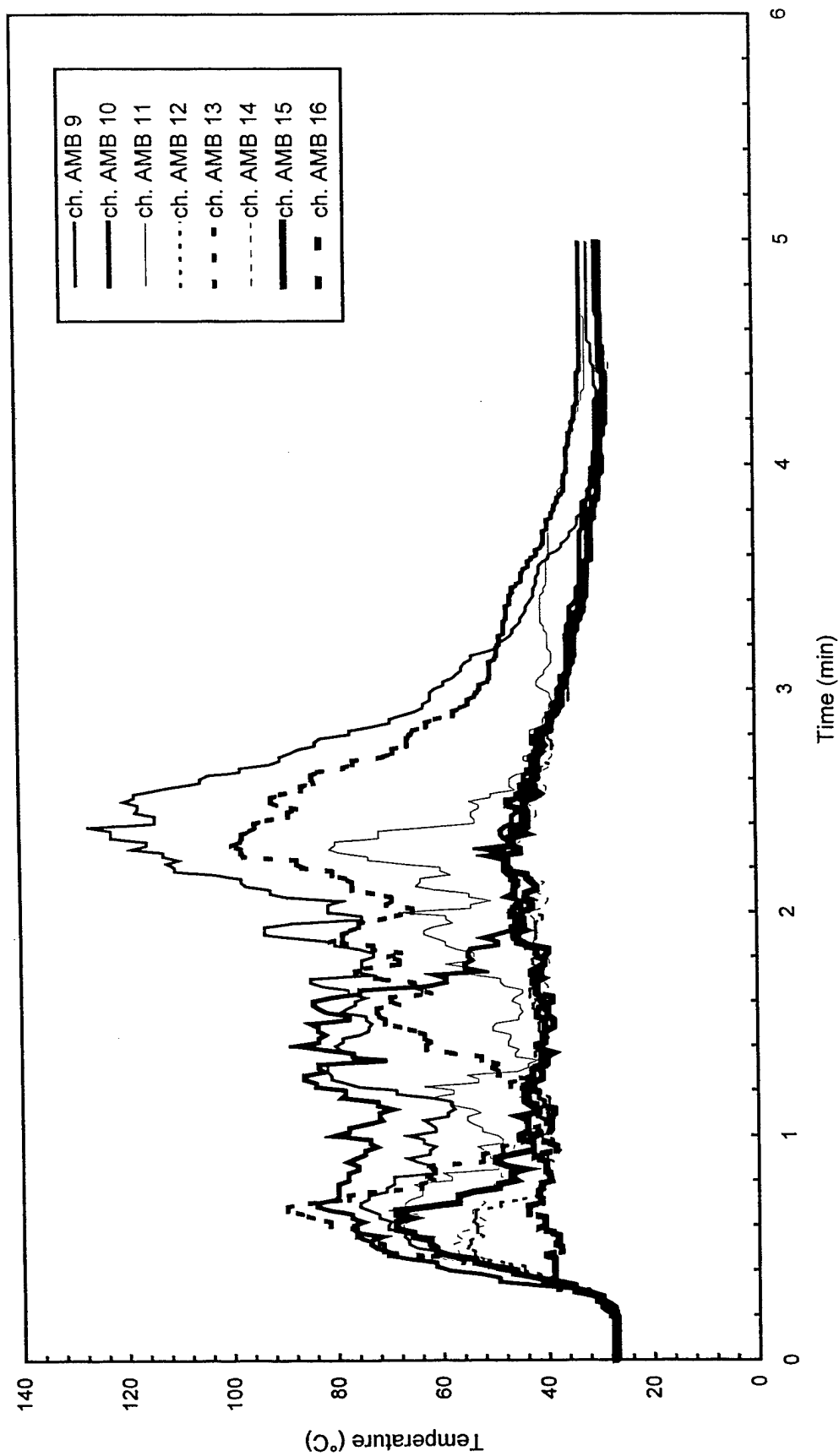


Fig. B6 - Air temperatures around 3 m (10 ft) radius from center of pad

Test S1

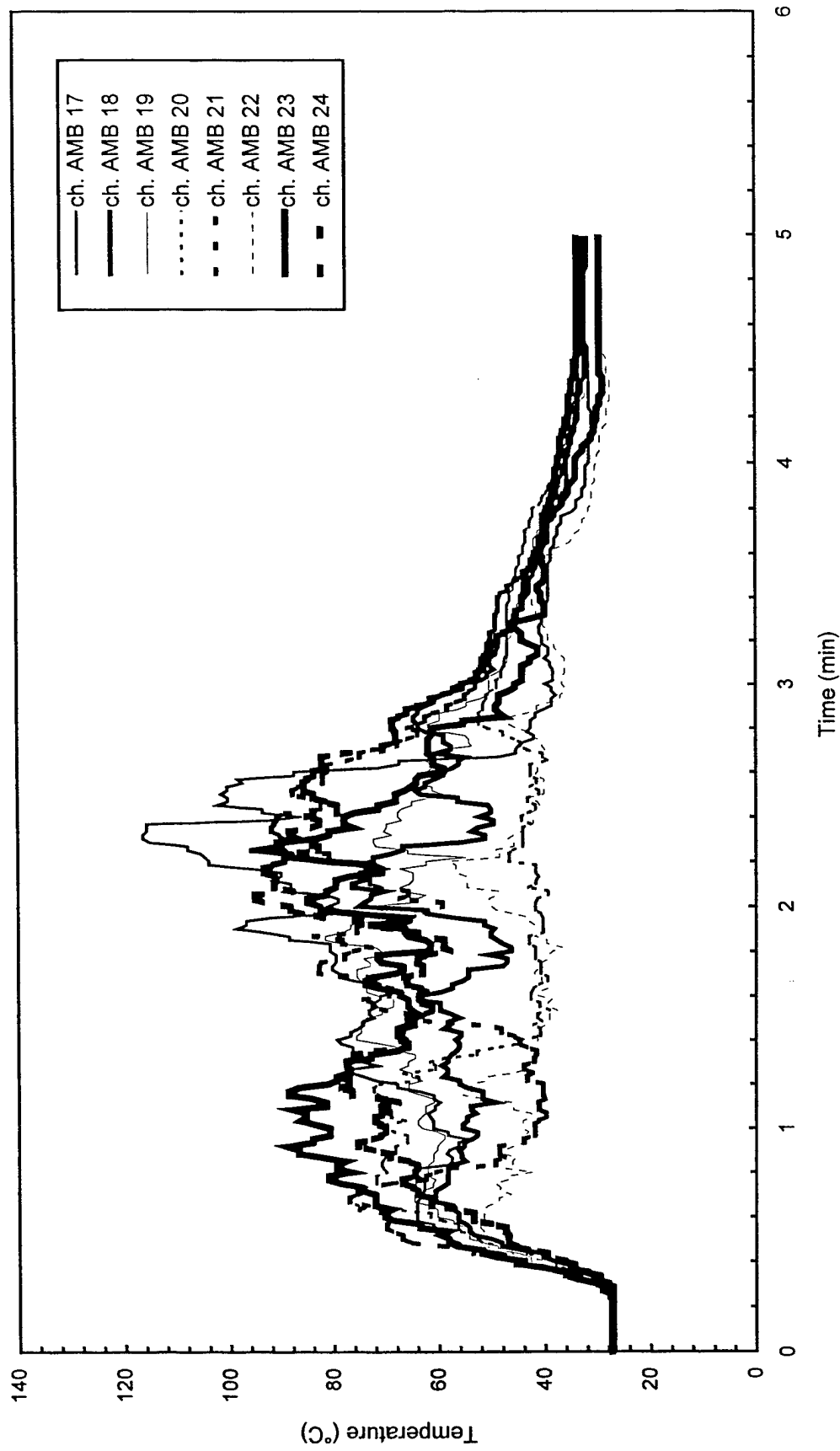


Fig. B7 - Air temperatures around 4.6 m (15 ft) radius from center of pad

Test S1

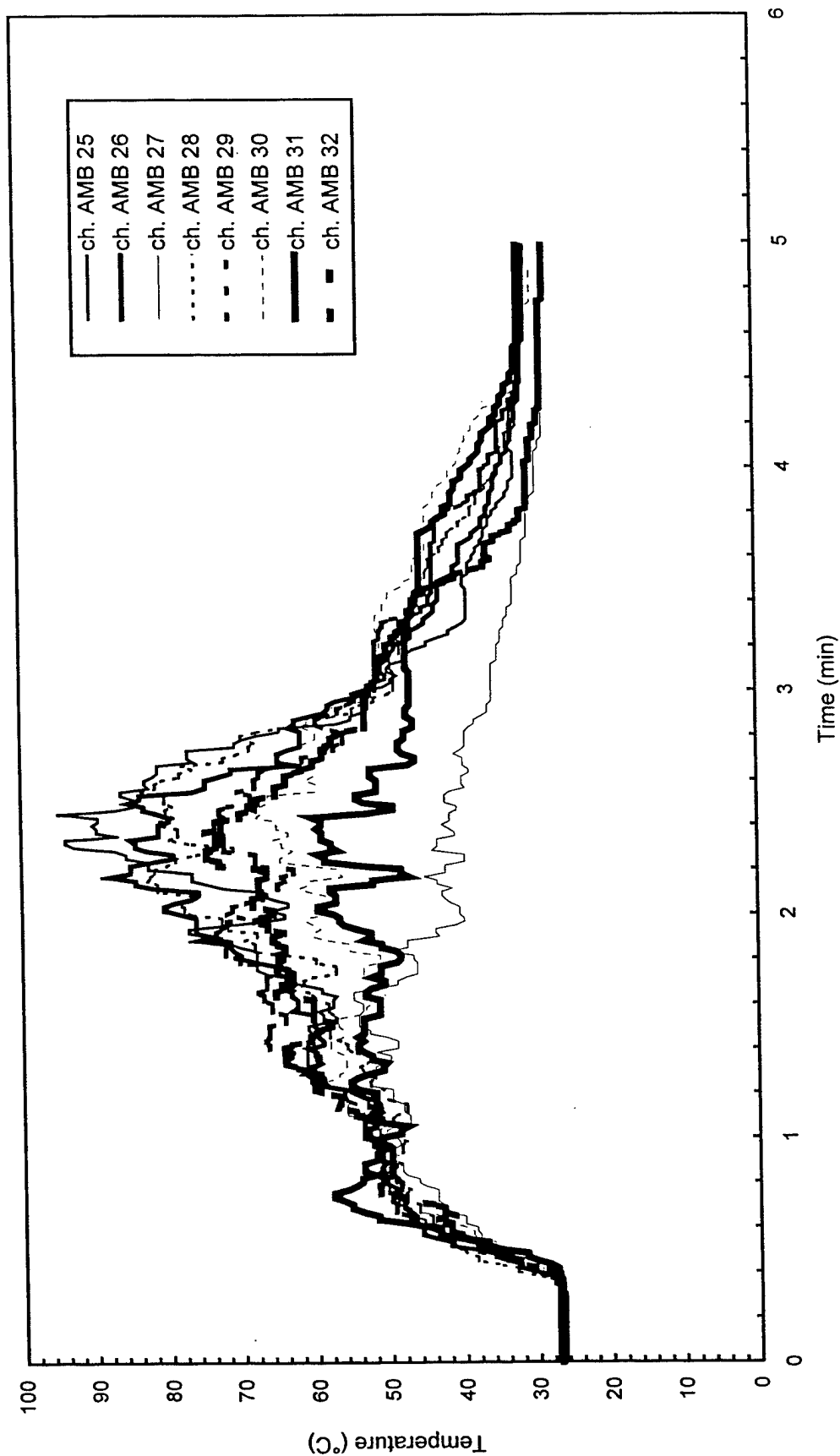


Fig. B8 - Air temperatures around North half of 7.6 m (25 ft) radius from center of pad

Test S1

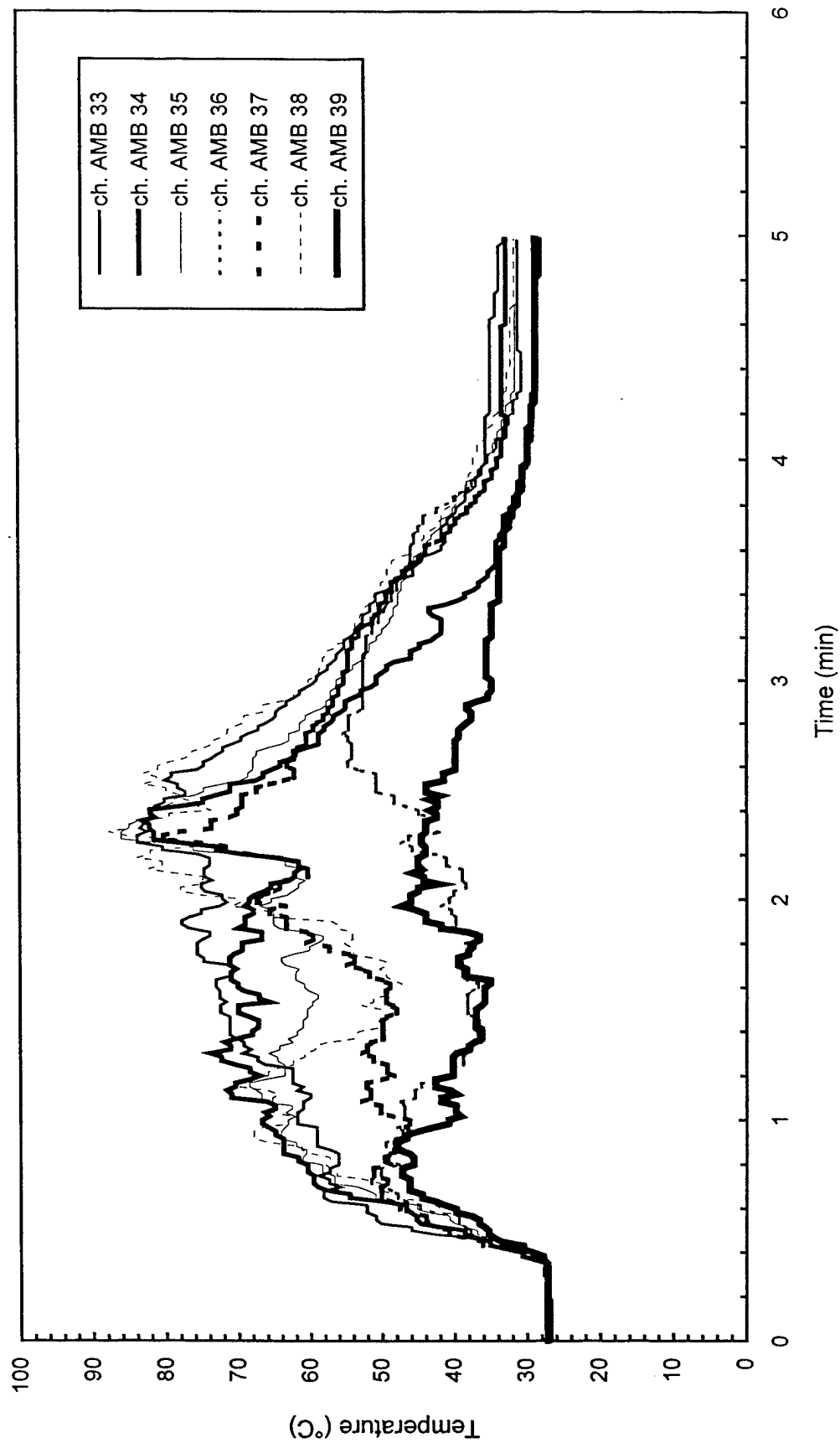


Fig. B9 - Air temperatures around South half of 7.6 m (25 ft) radius from center of pad

Test S1

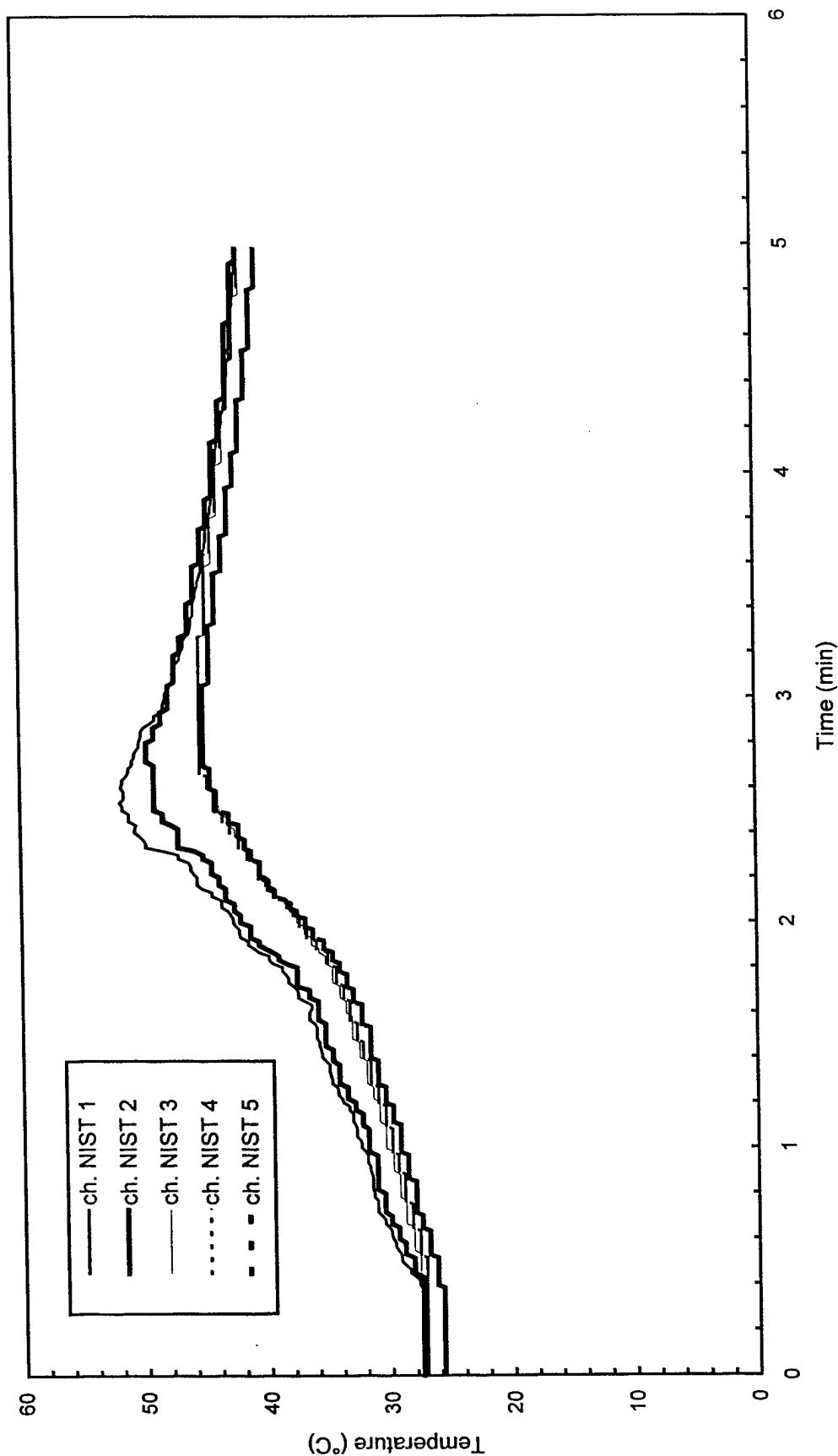


Fig. B10 - Temperature of West steel beam

Test S1

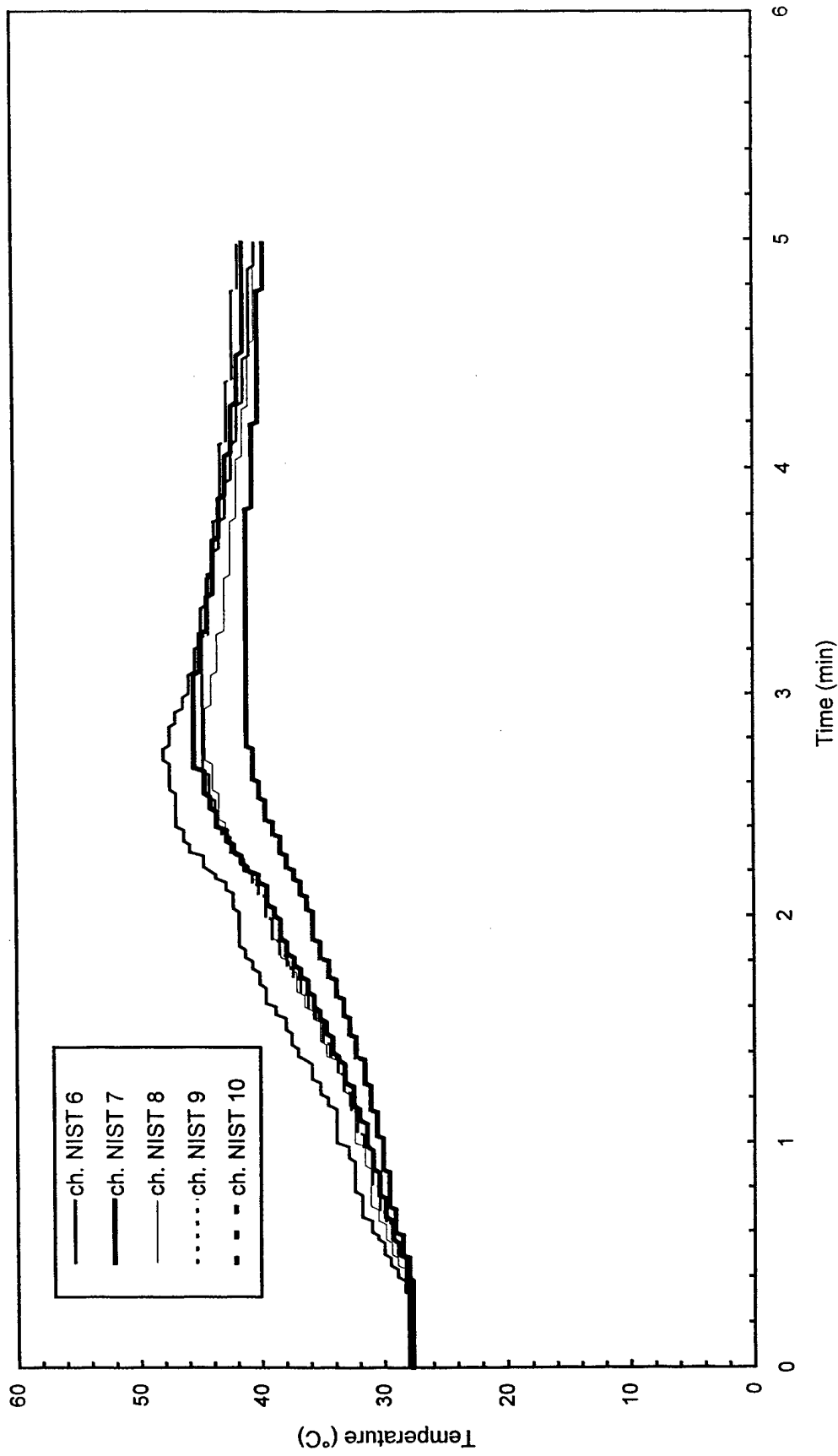


Fig. B11 - Temperature of North steel beam

Test S1

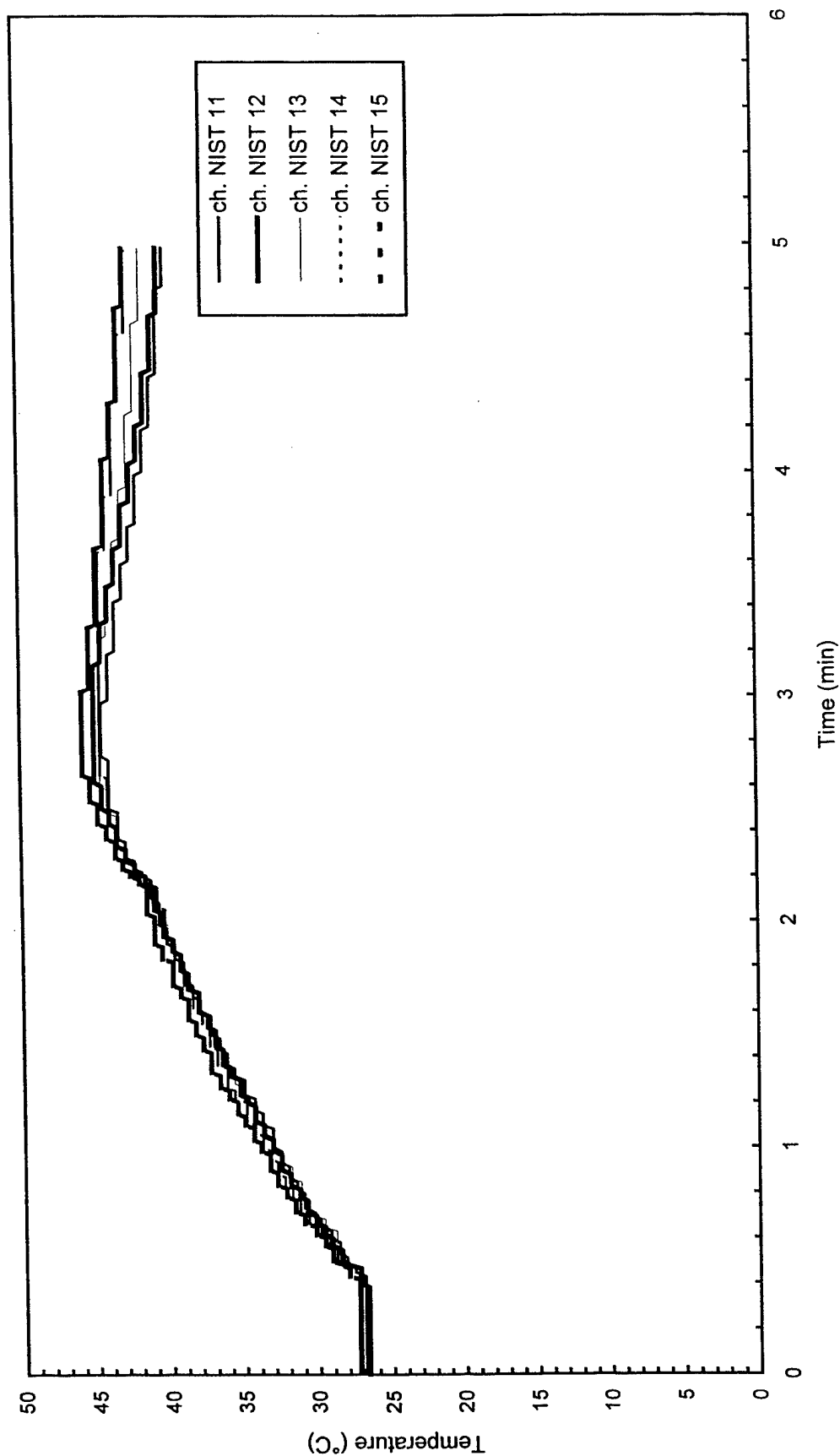


Fig. B12 - Temperature of East steel beam

Test S1

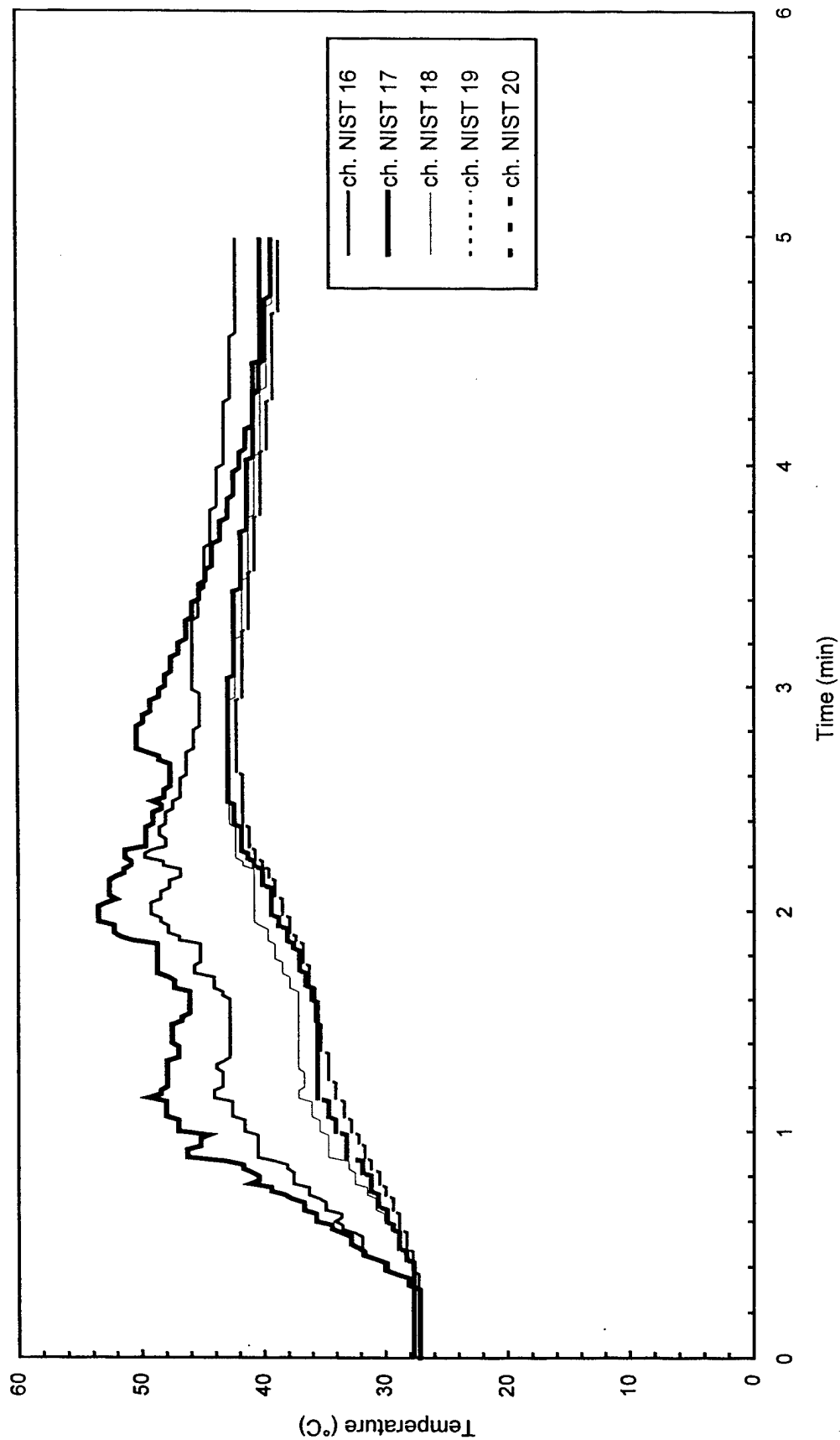


Fig. B13 - Temperature of South steel beam

Test S1

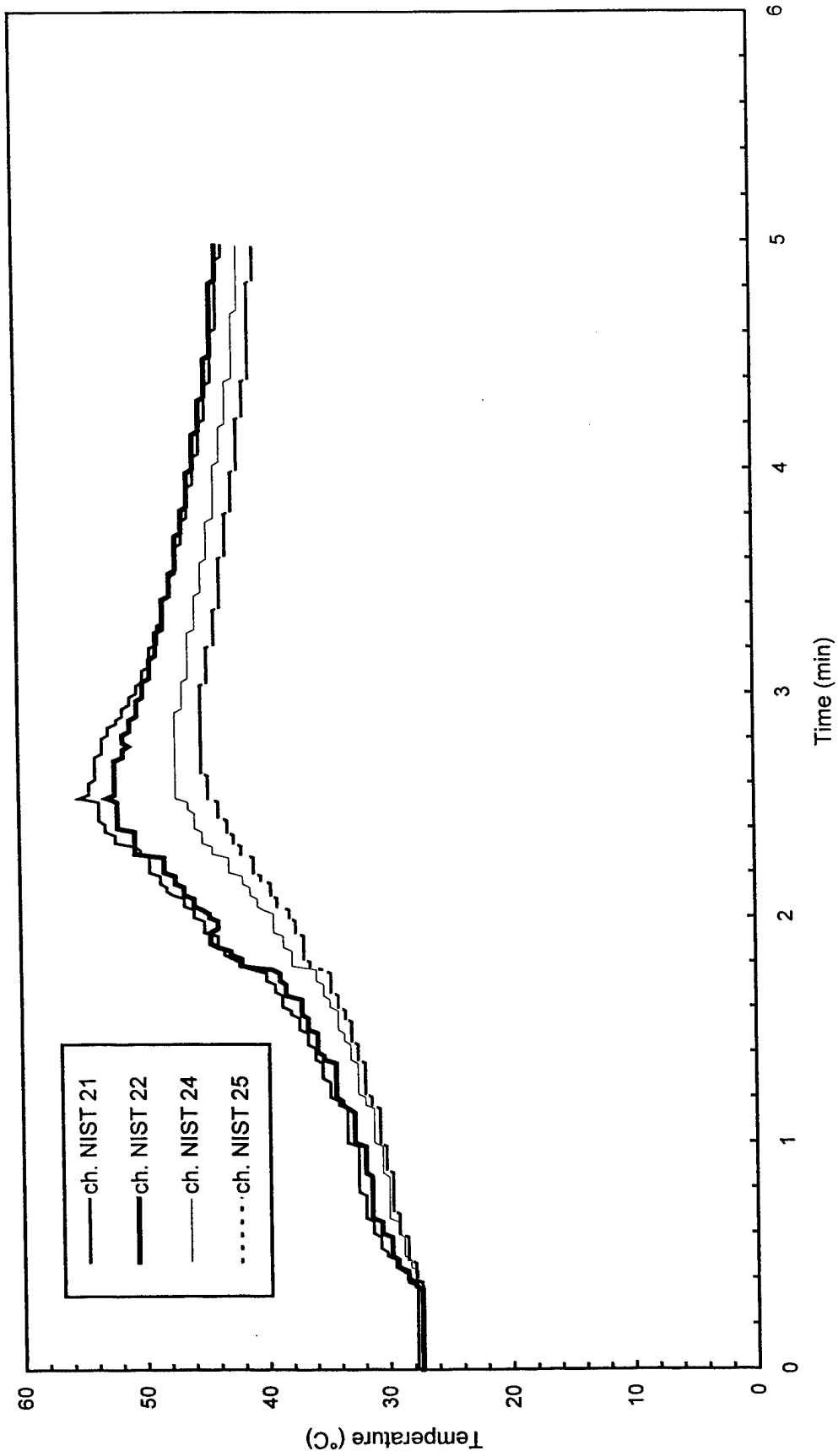


Fig. B14 - Temperature of Northwest steel beam

Test S1

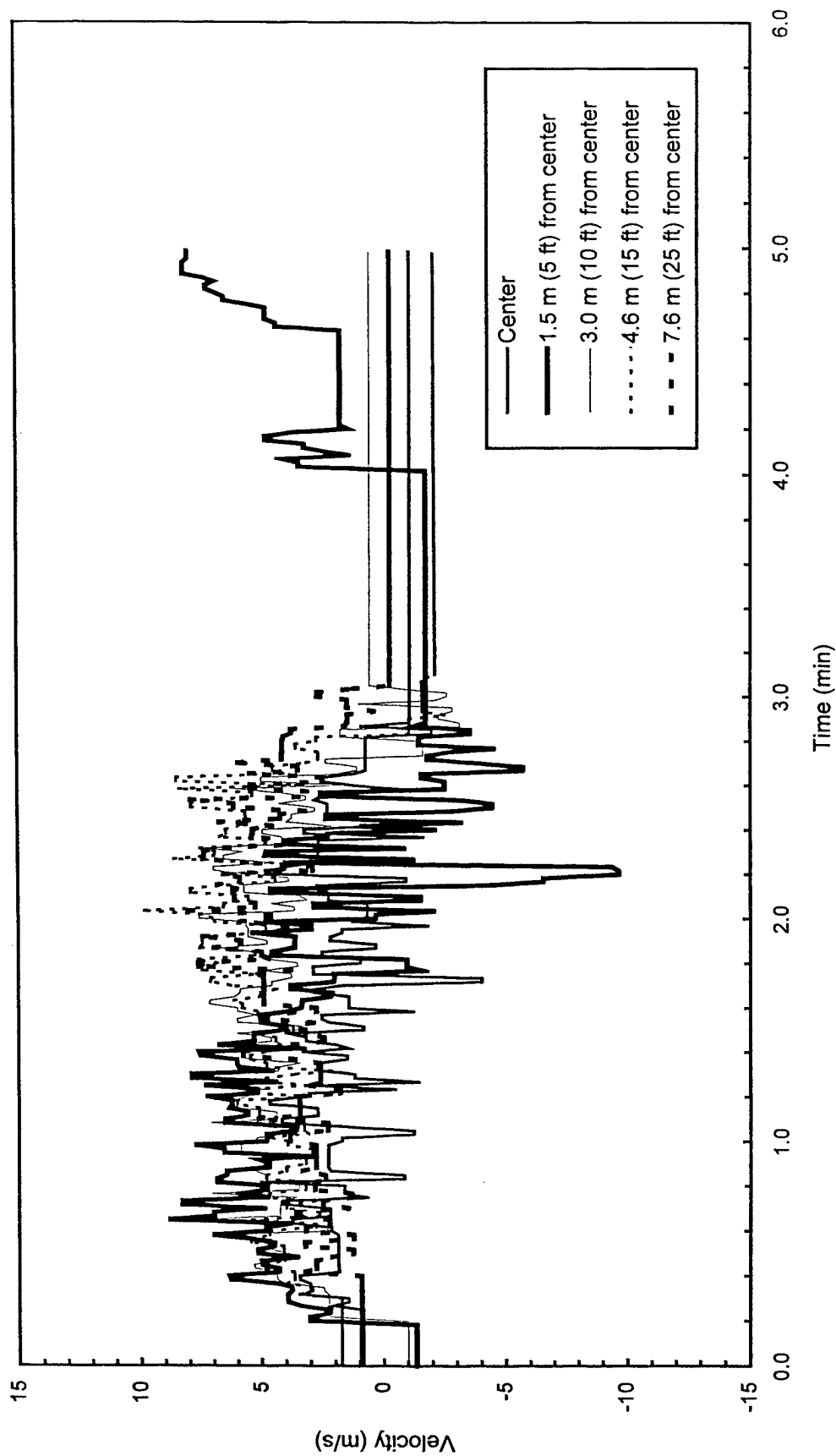


Fig. B15 - Plume and ceiling jet velocities

Test S1

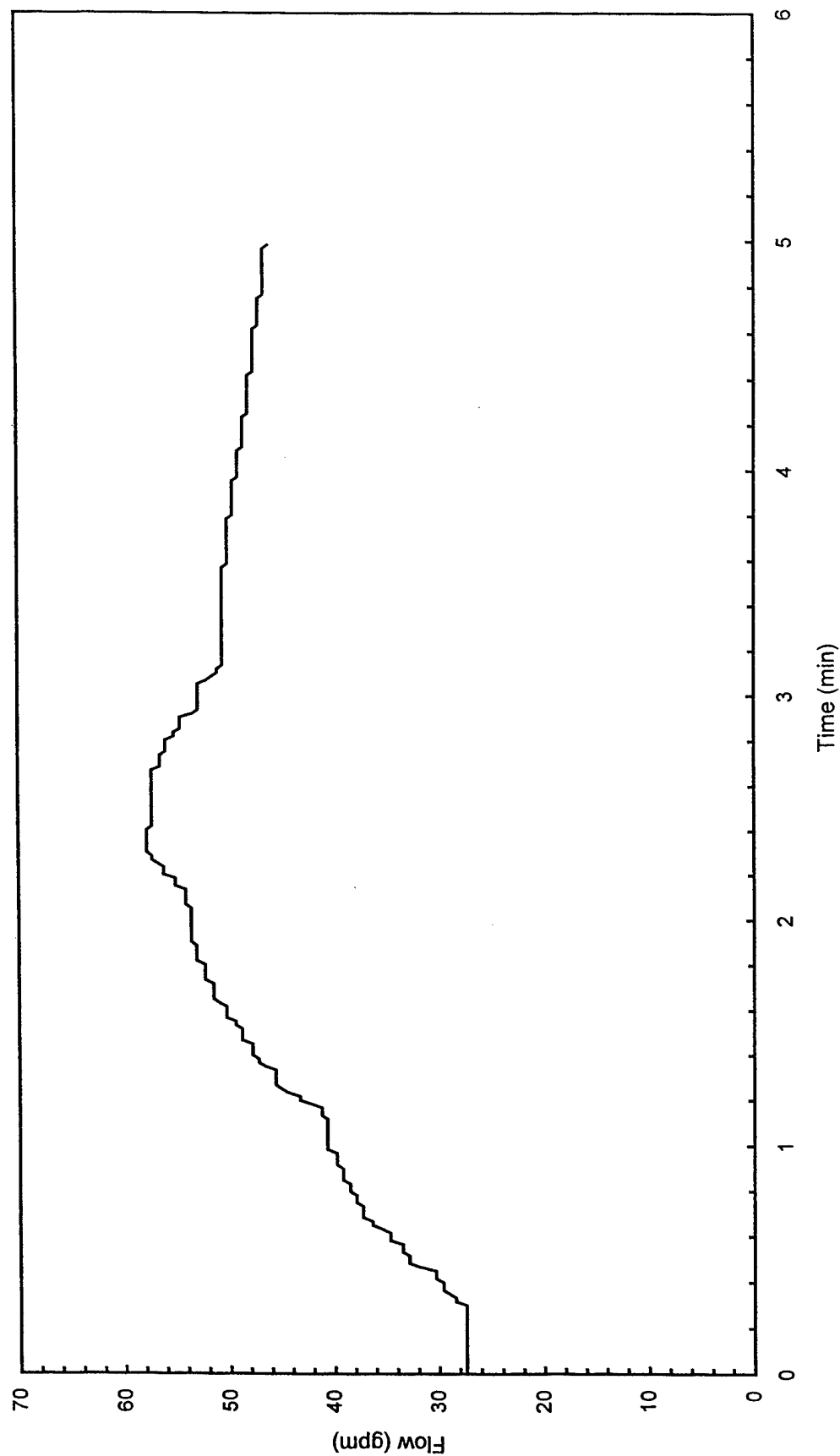


Fig. B16 - Sprinkler system flowrate

Test S1

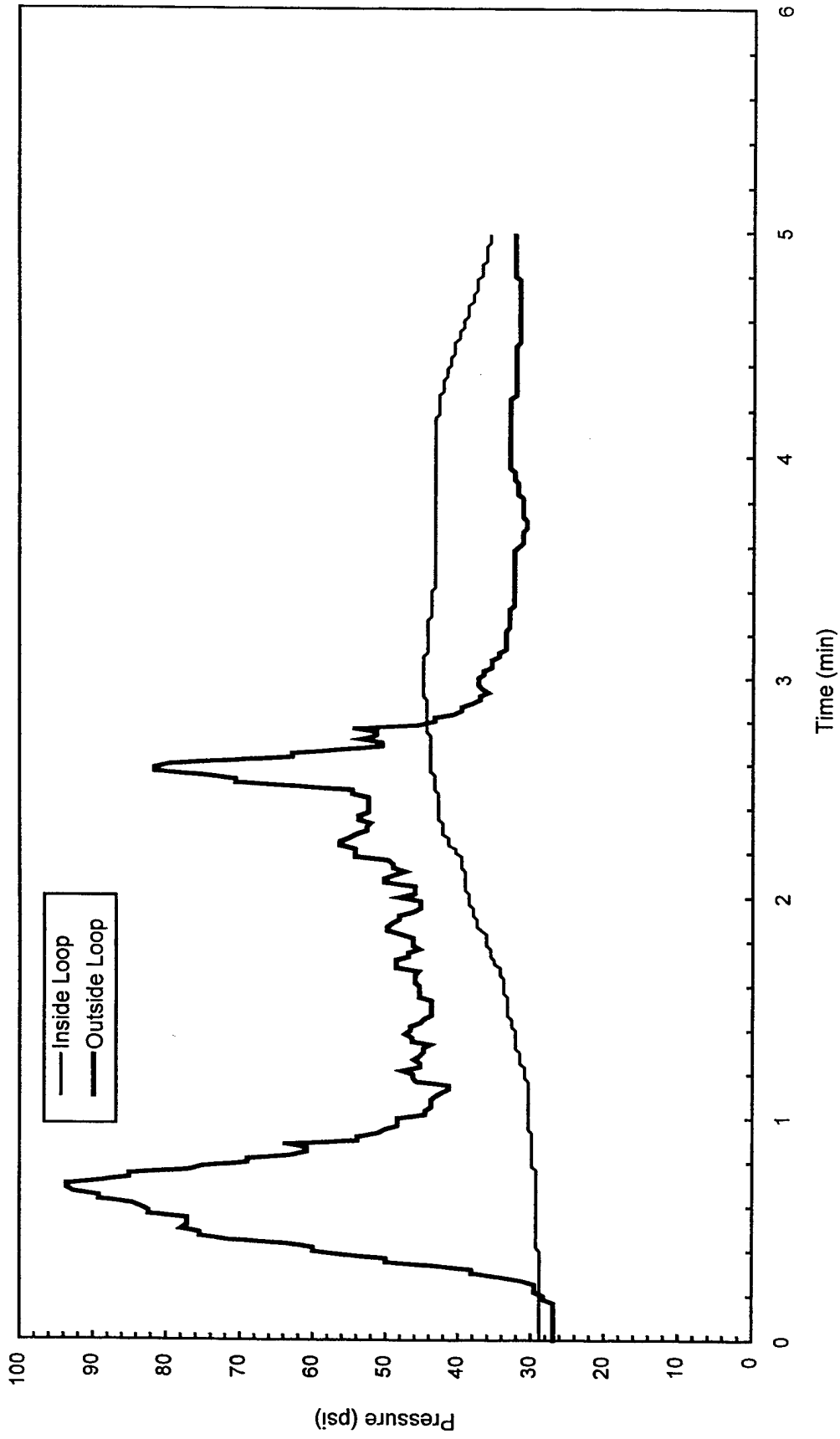


Fig. B17 - Sprinkler system pressure

Test S2

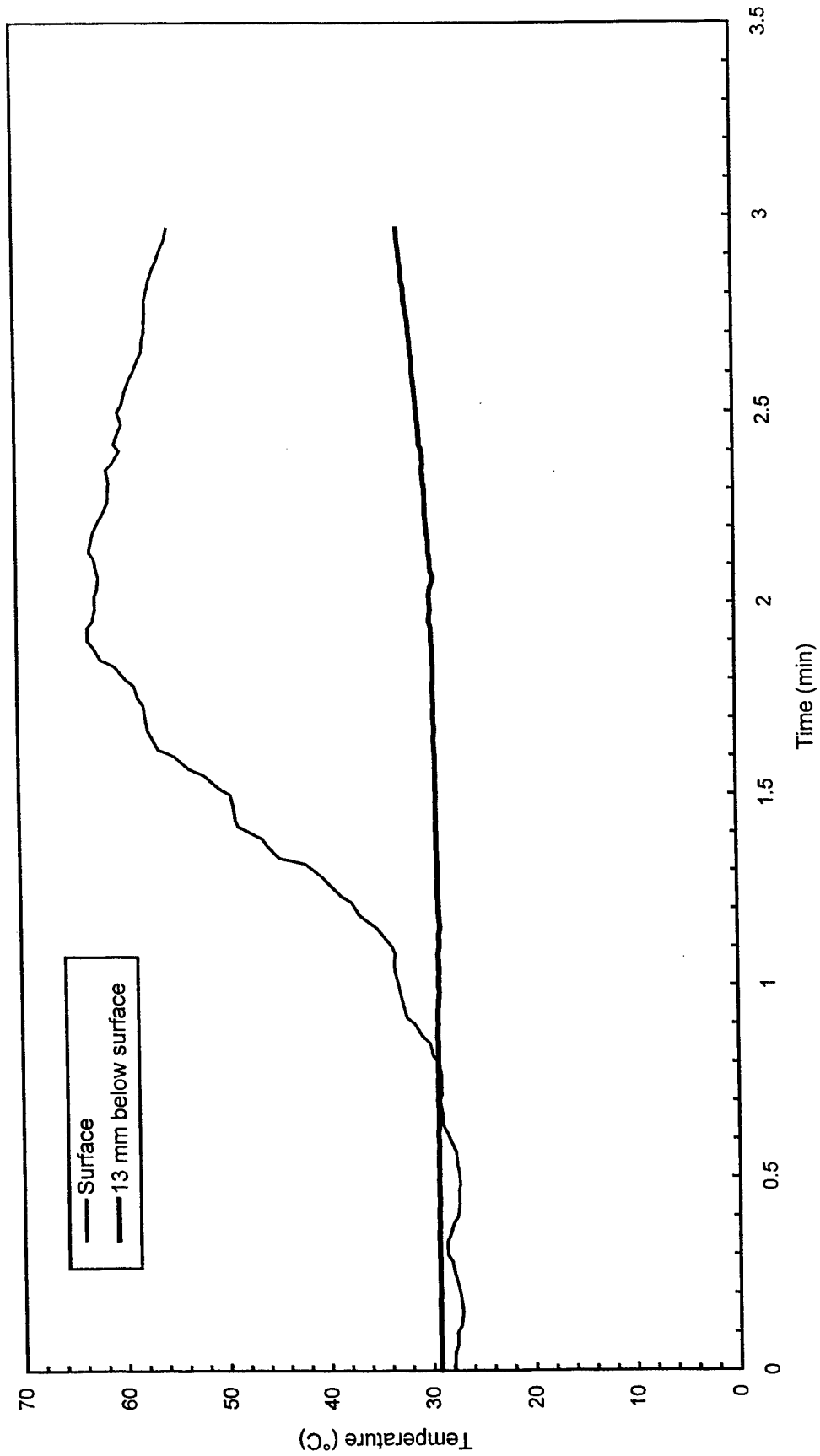


Fig. B18 - Concrete temperatures at center of pad

Test S2

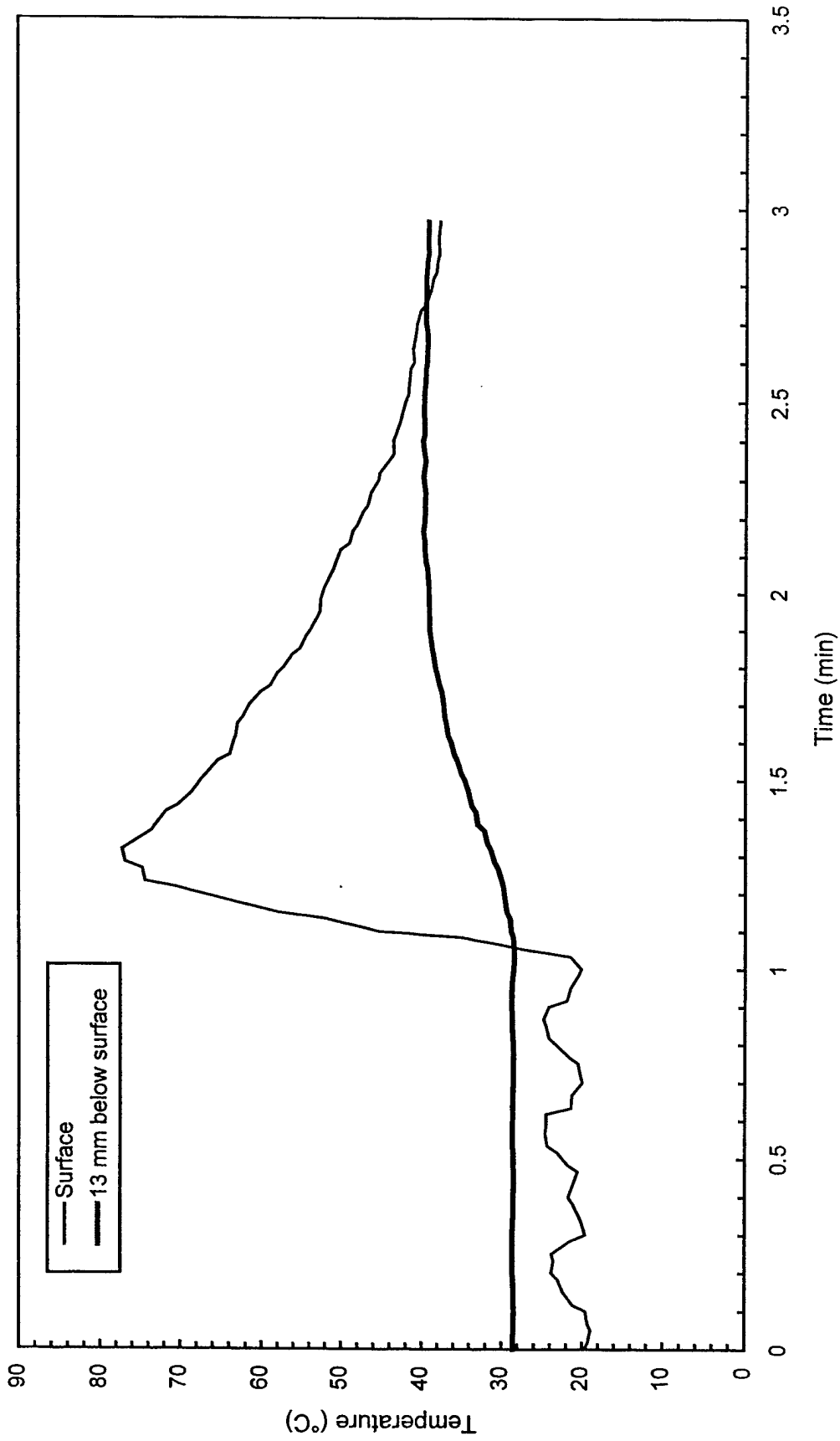


Fig. B19 - Concrete temperatures 3 m (10 ft) East of center of pad

Test S2

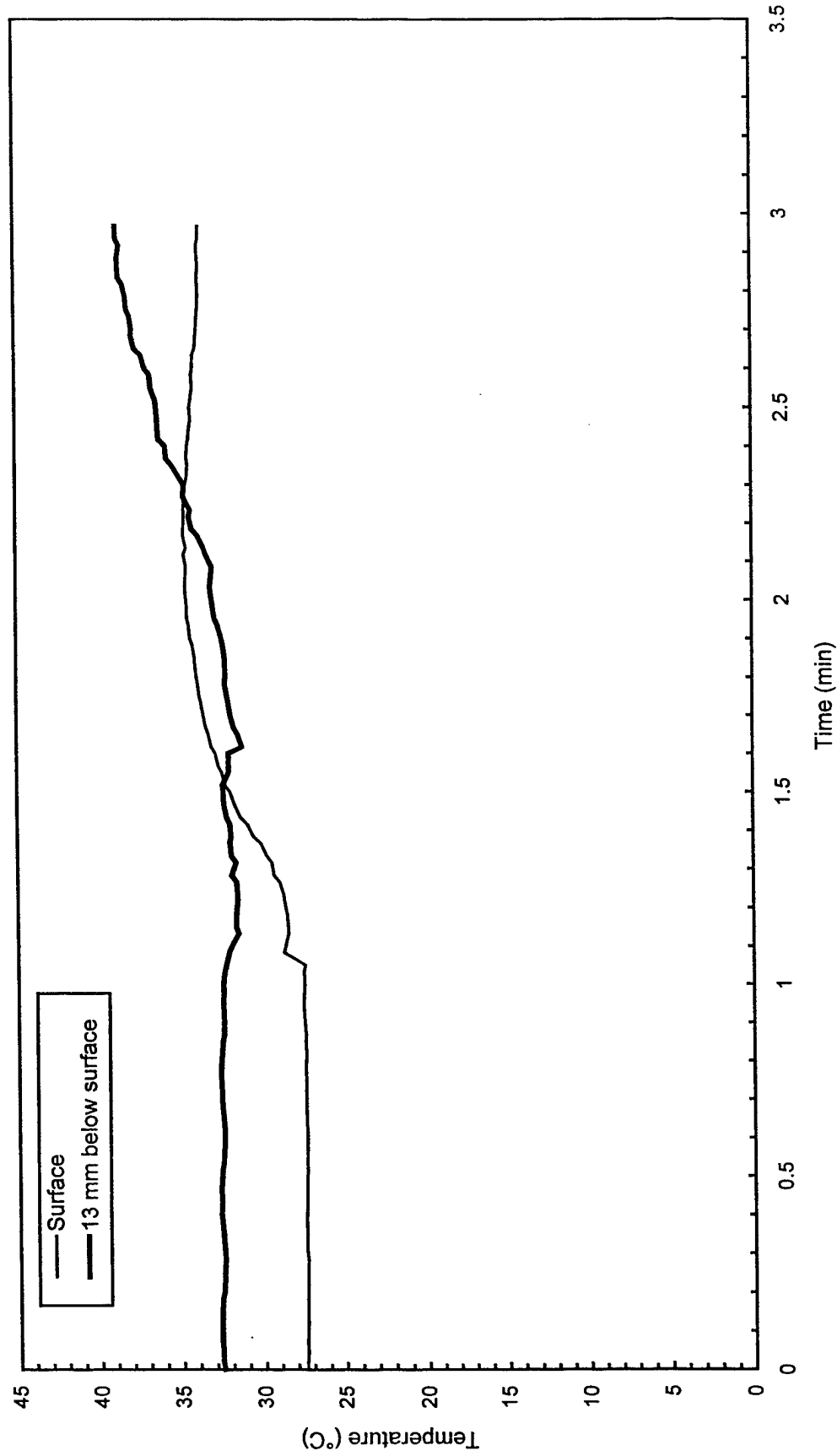


Fig. B20 - Concrete temperatures 3 m (10 ft) West of center of pad

Test S2

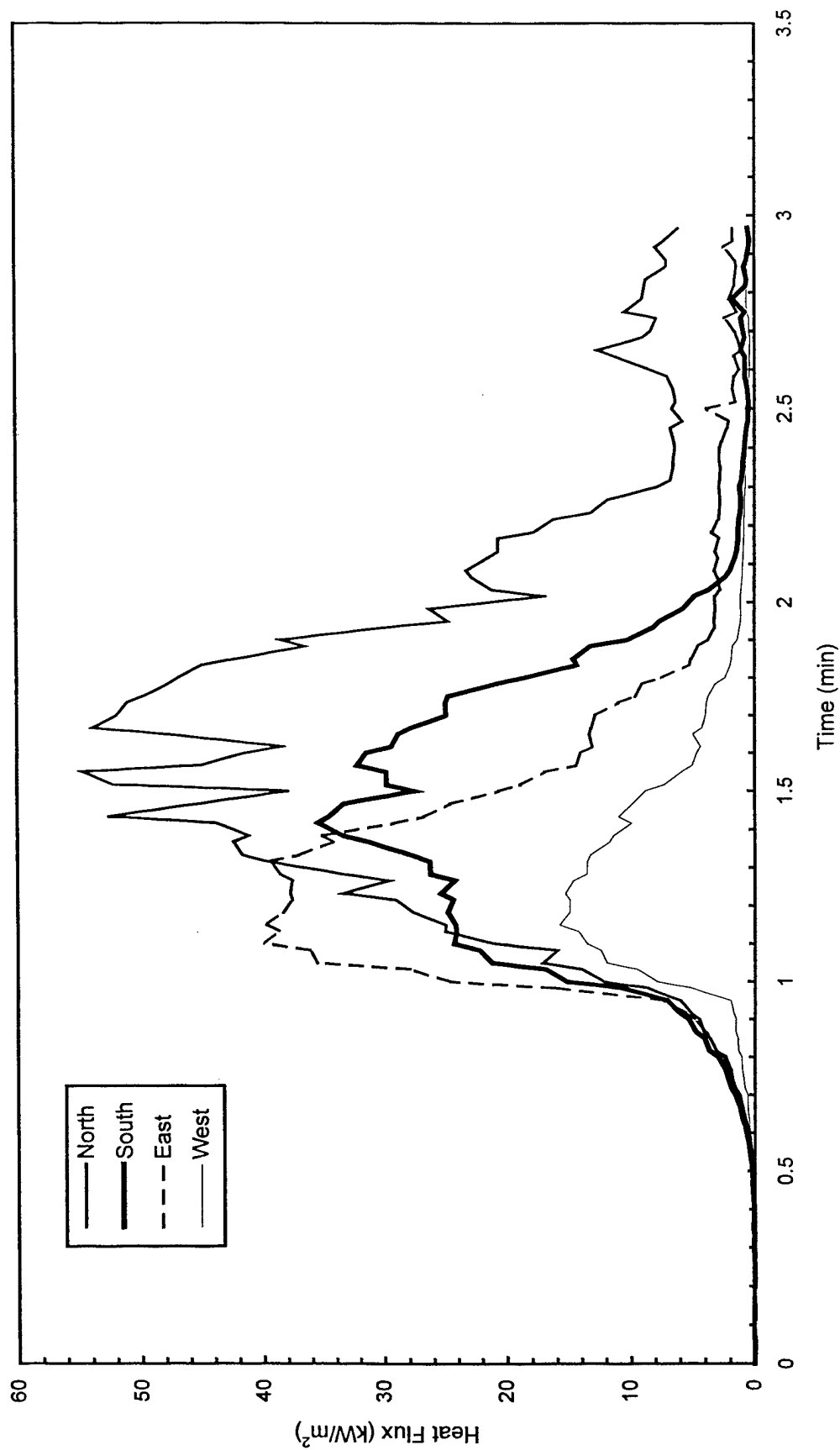


Fig. B21 - Heat flux measured at edge of pad

Test S2

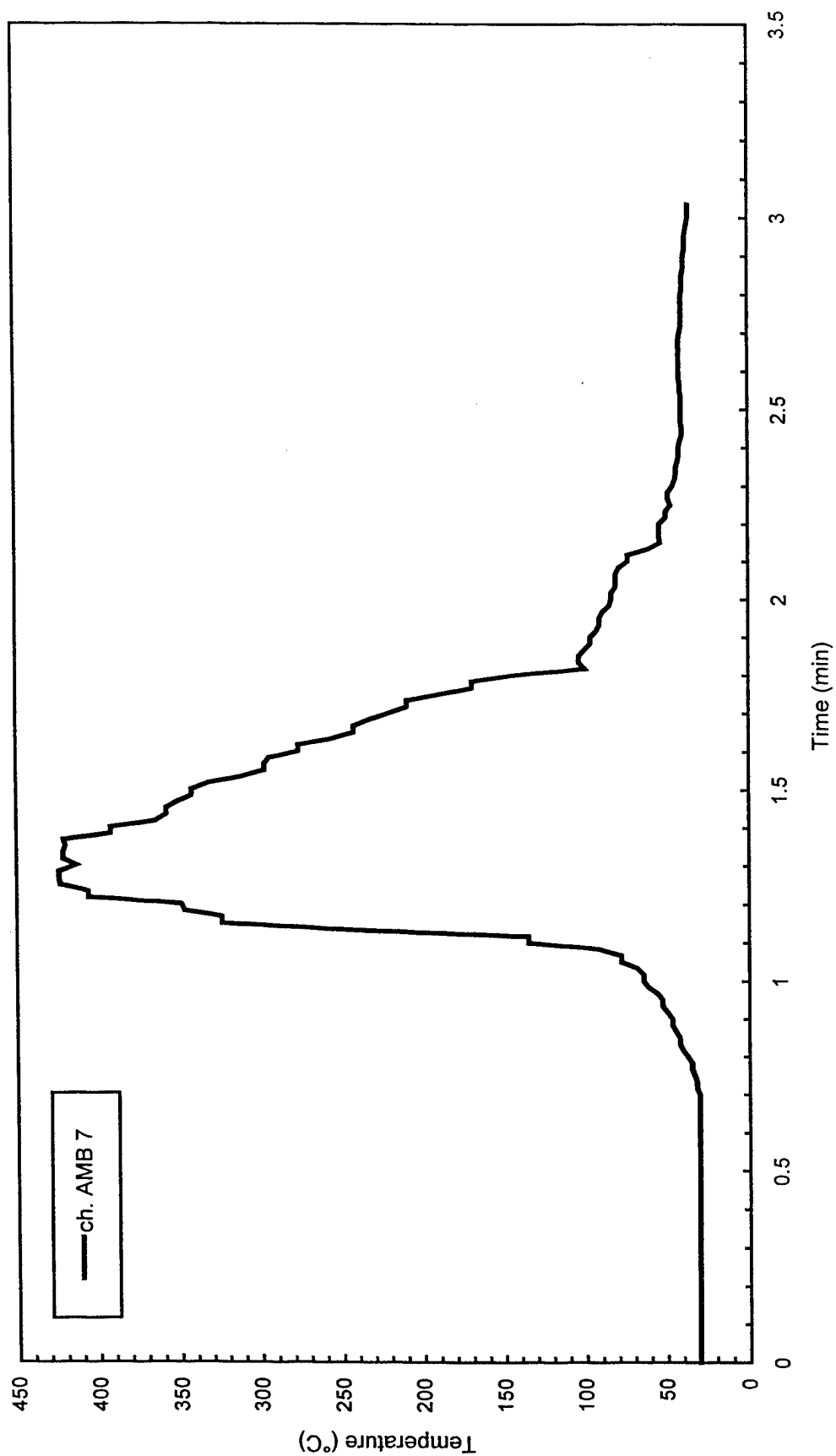


Fig. B22 - Air temperatures over center of pad

Test S2

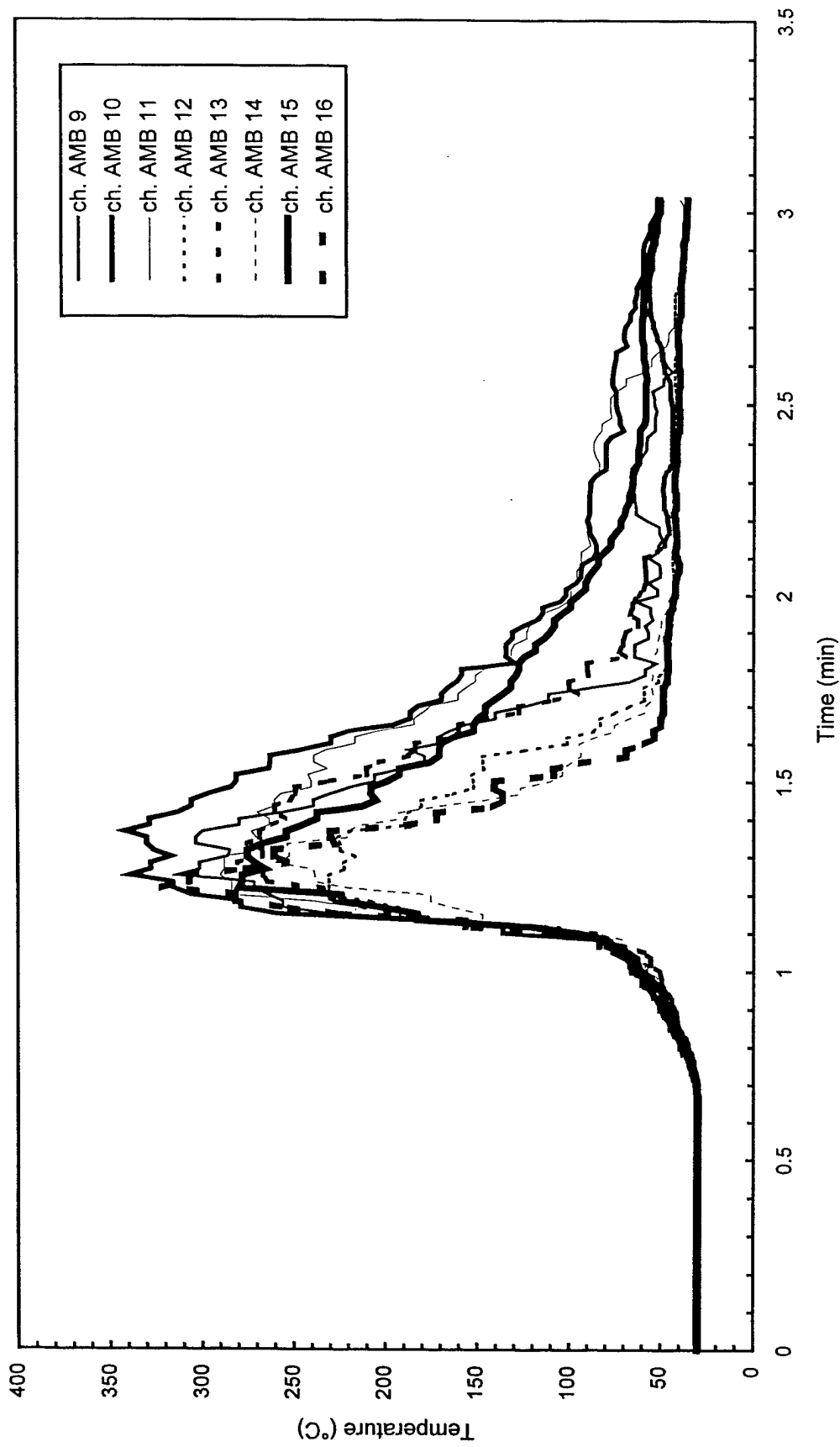


Fig. B23 - Air temperatures around 3 m (10 ft) radius from center of pad

Test S2

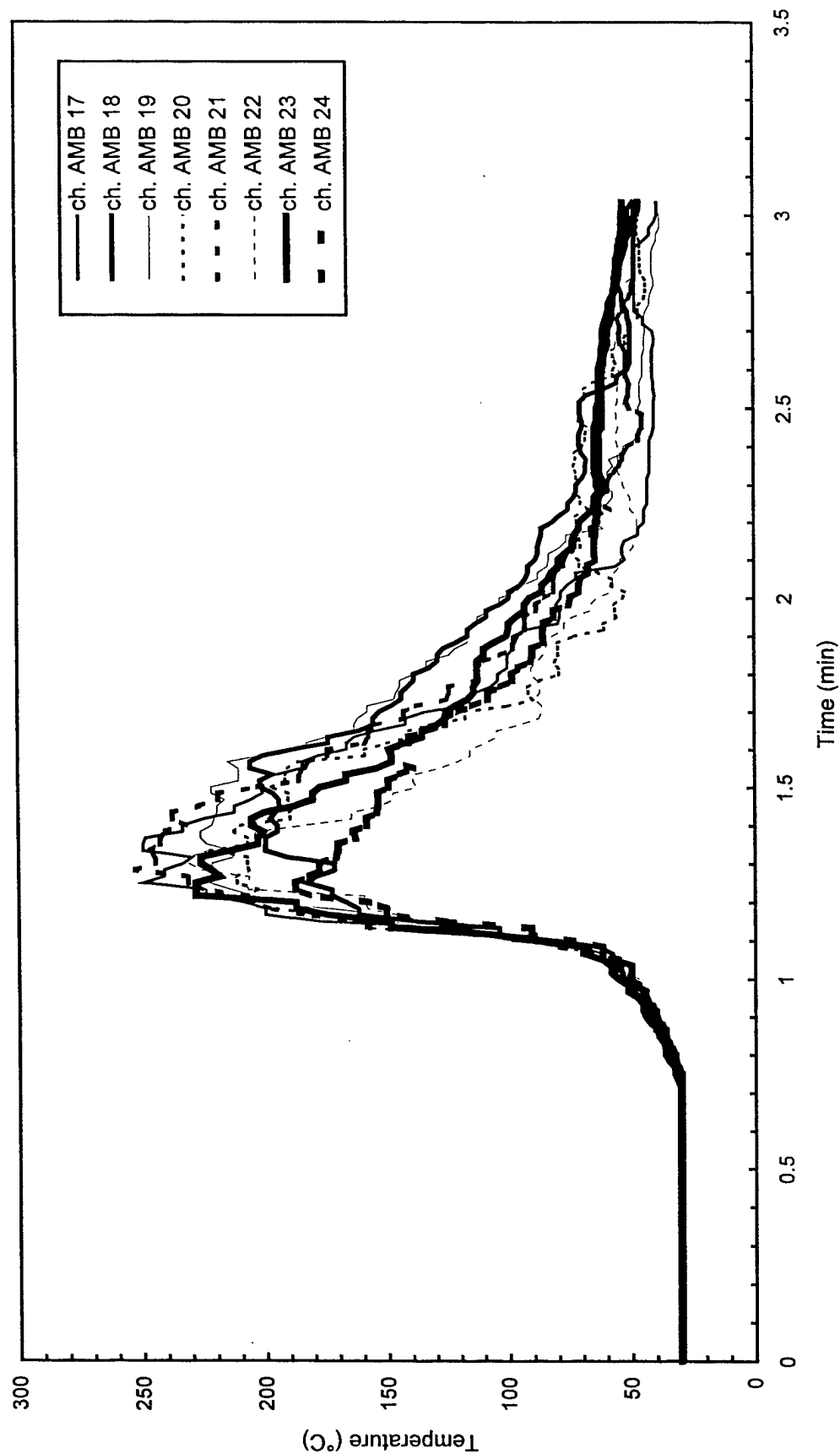


Fig. B24 - Air temperatures around 4.6 m (15 ft) radius from center of pad

Test S2

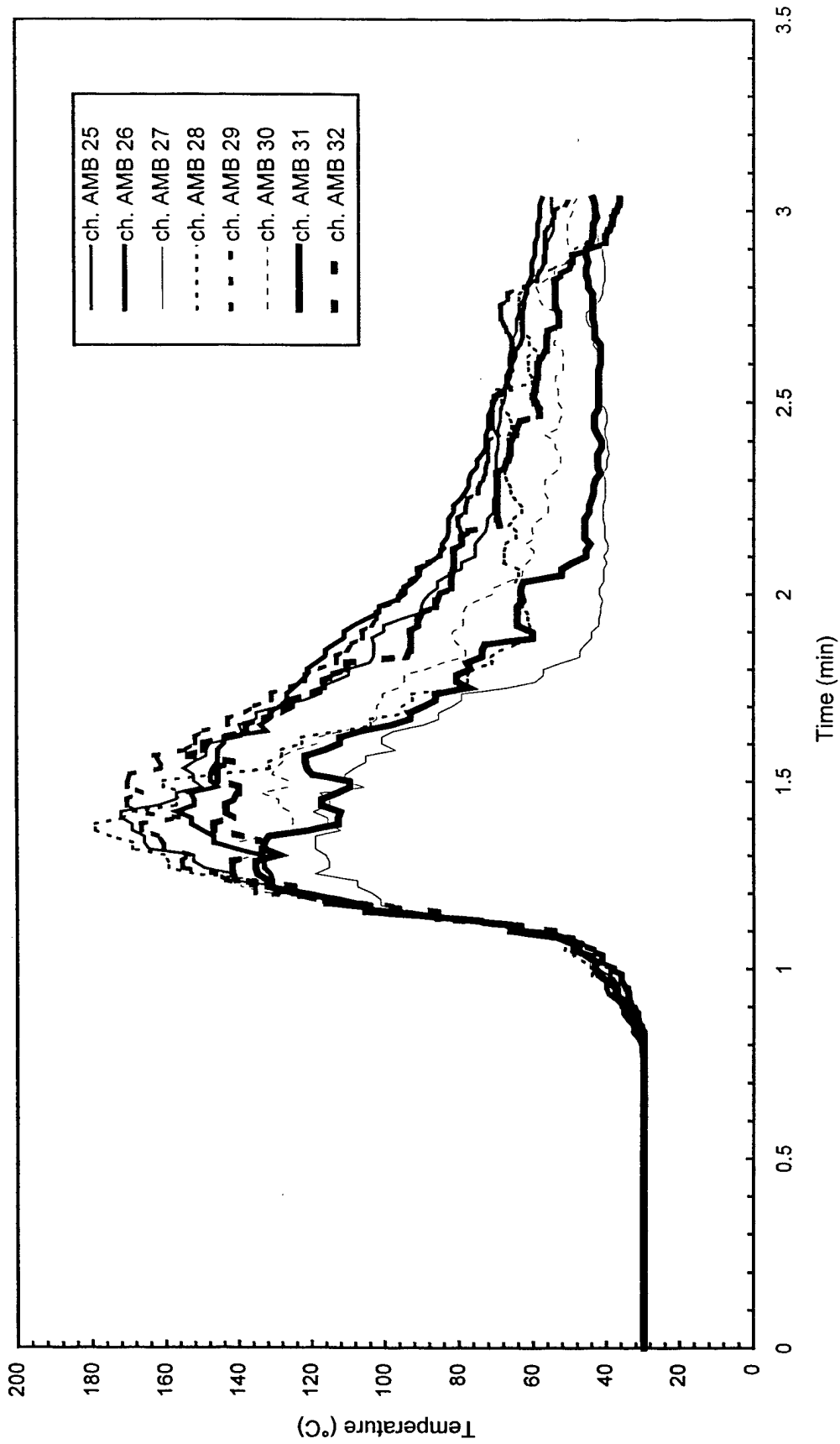


Fig. B25 - Air temperatures around North half of 7.6 m (25 ft) radius from center of pad

Test S2

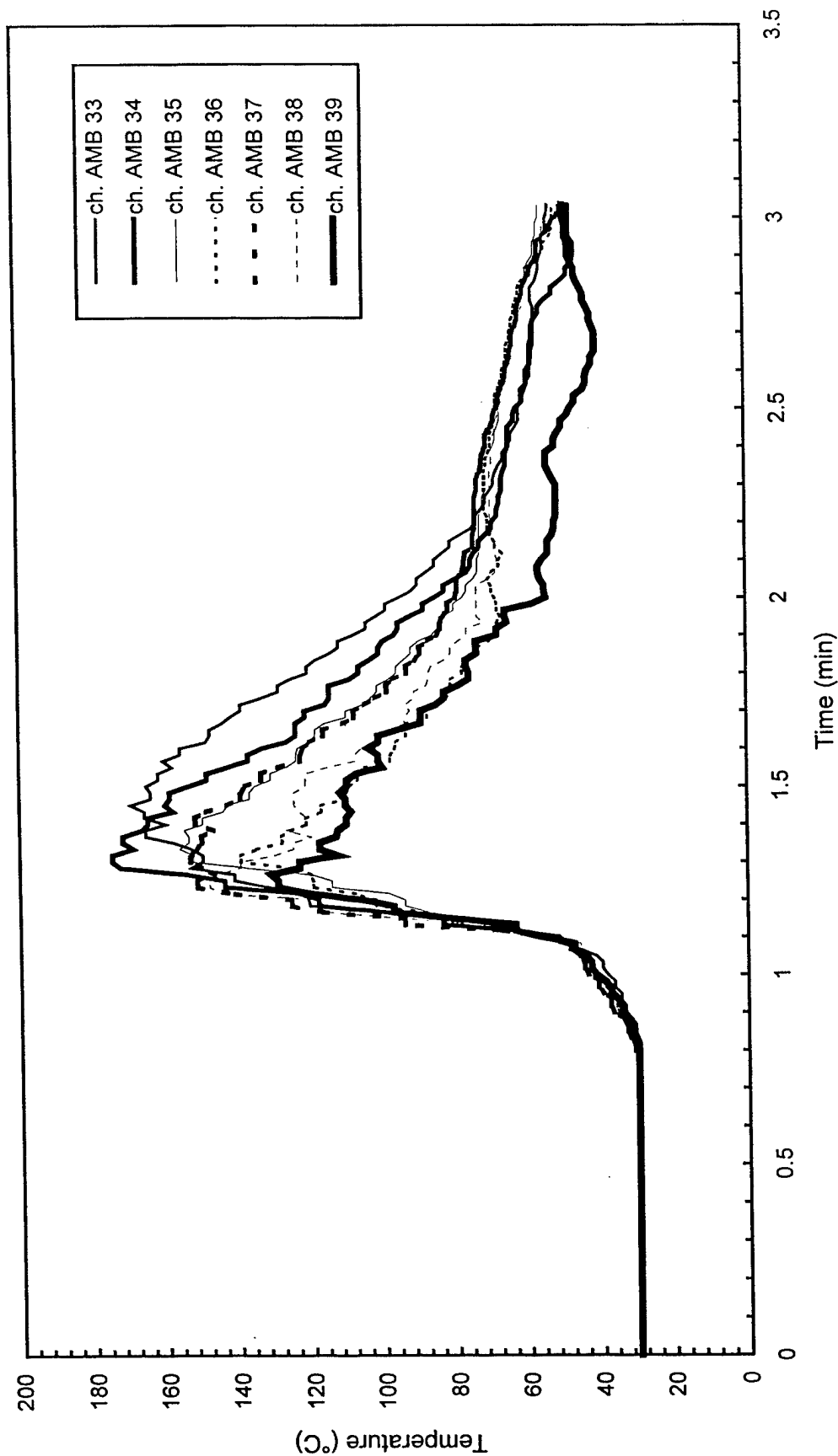


Fig. B26 - Air temperatures around South half of 7.6 m (25 ft) radius from center of pad

Test S2

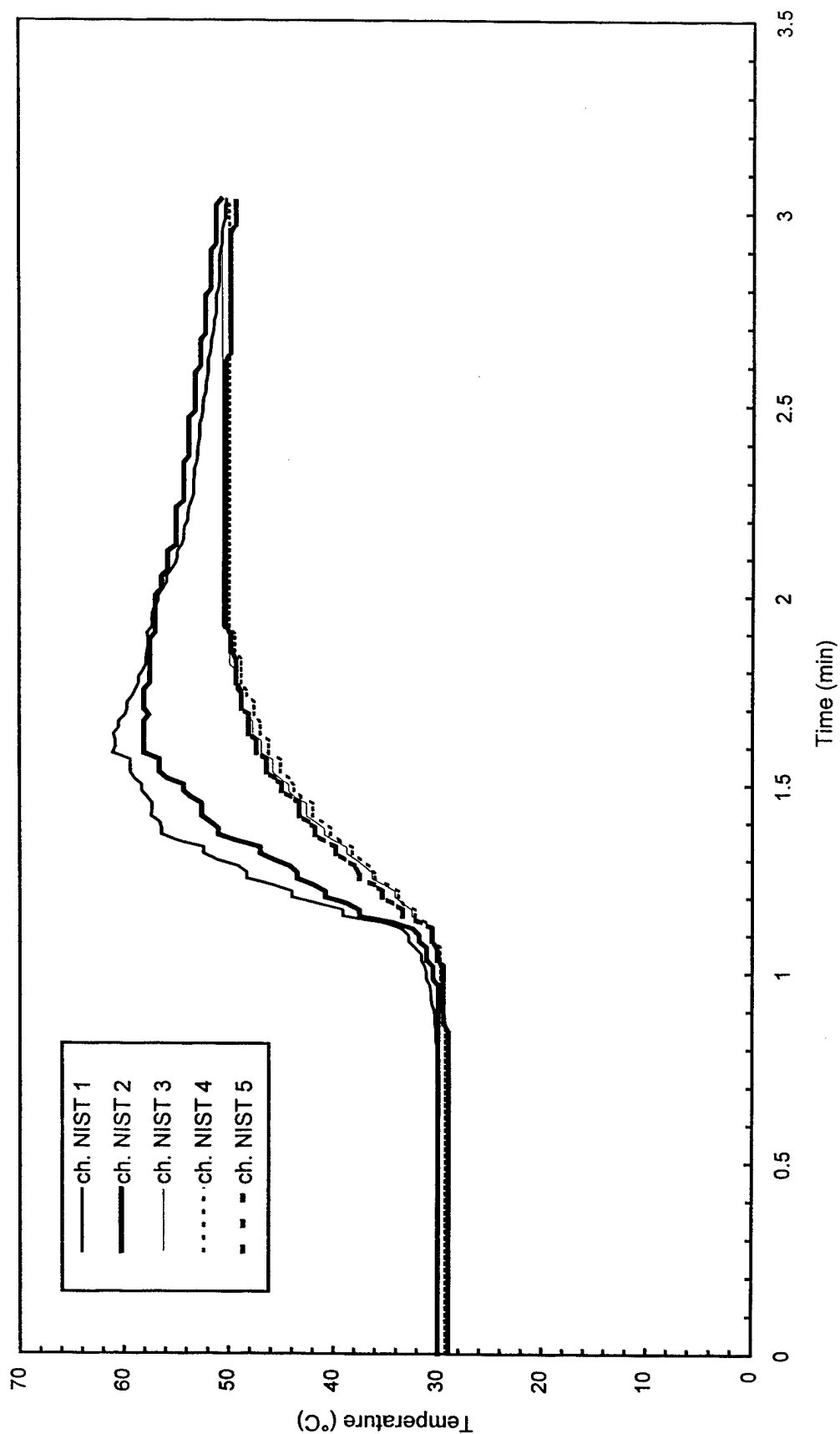


Fig. B27 - Temperature of West steel beam

Test S2

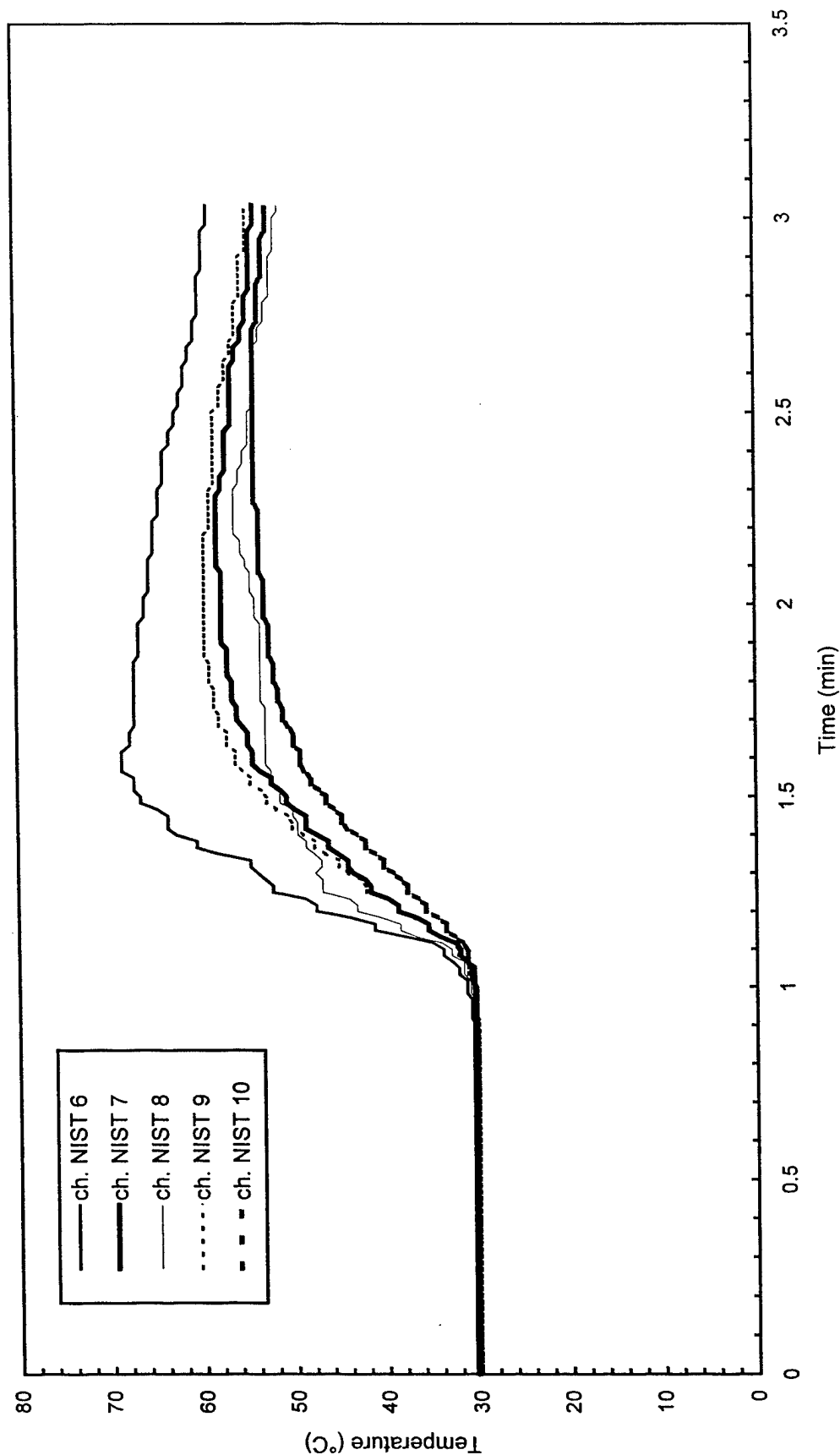


Fig. B28 - Temperature of North steel beam

Test S2

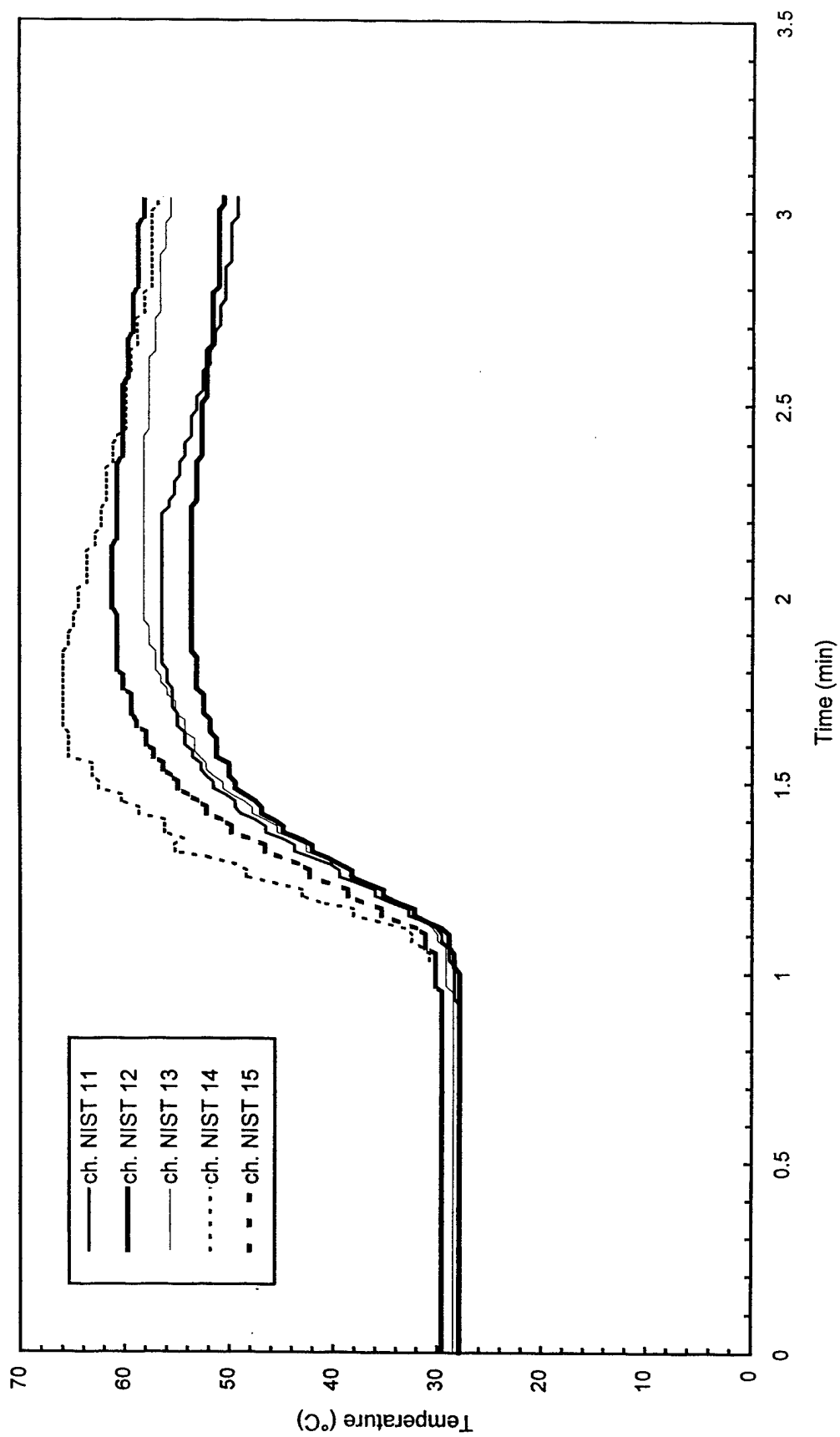


Fig. B29 - Temperature of East steel beam

Test S2

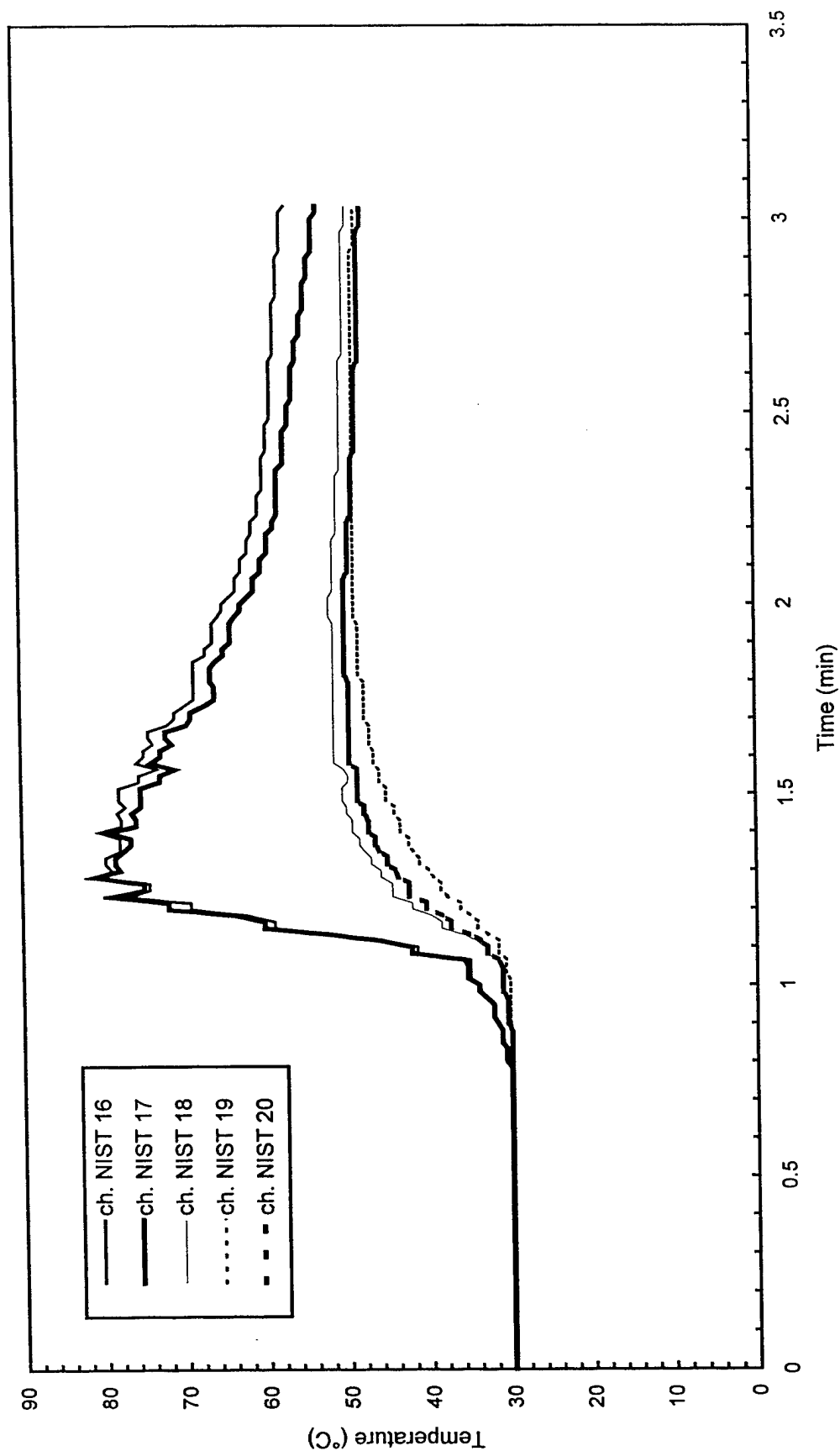


Fig. B30 - Temperature of South steel beam

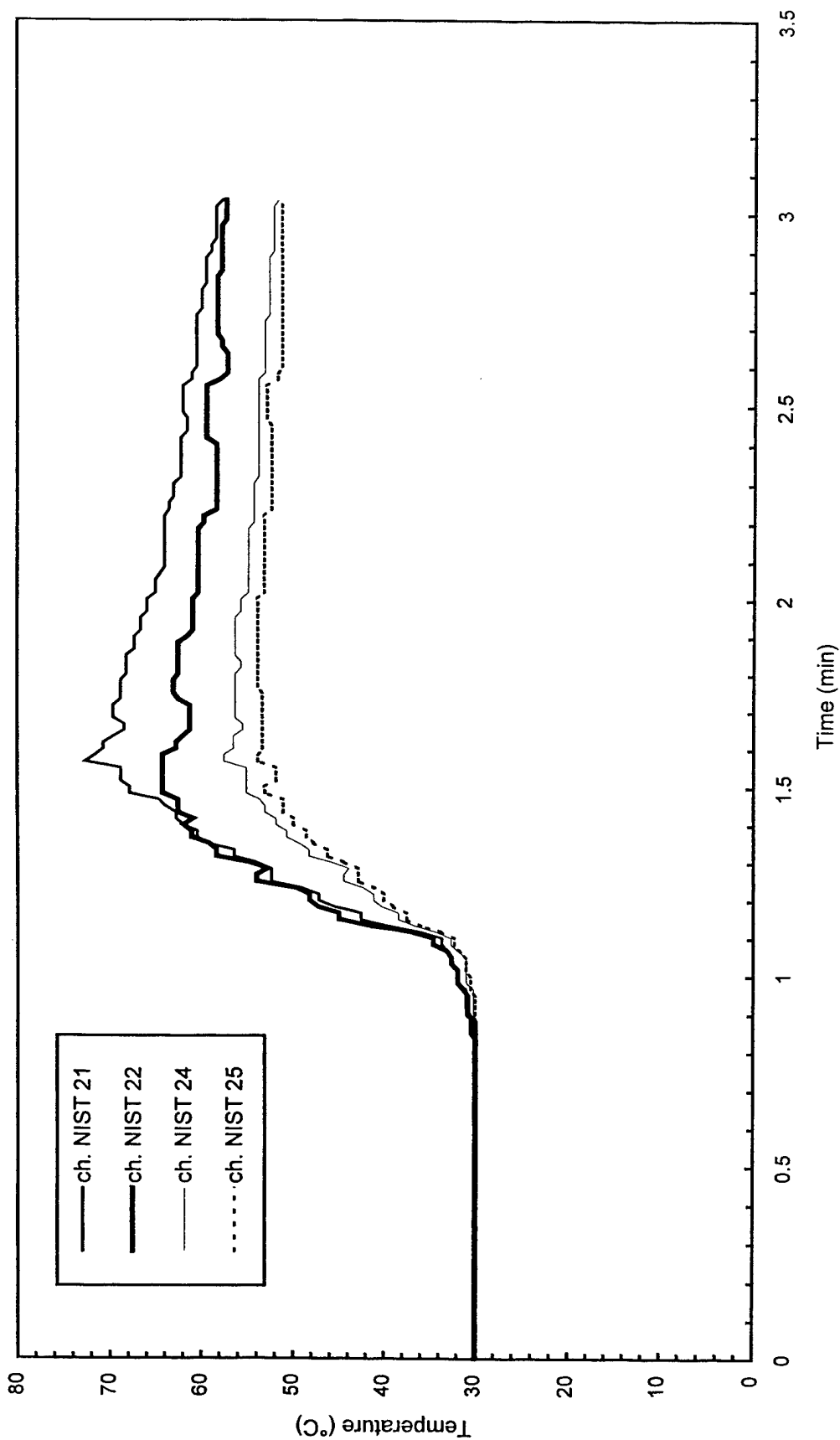


Fig. B31 - Temperature of Northwest steel beam

Test S2

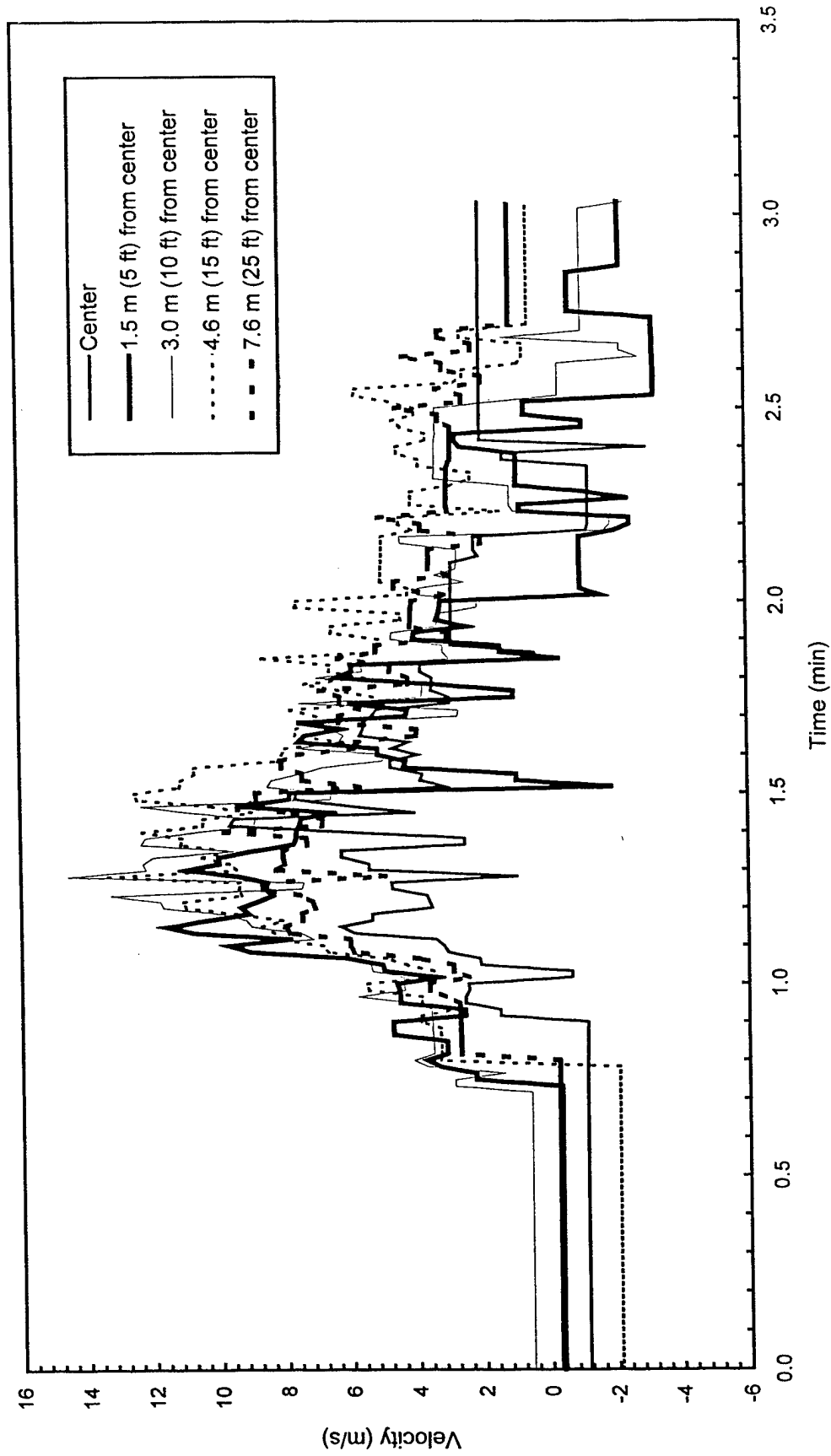


Fig. B32 - Plume and ceiling jet velocities

Test S2

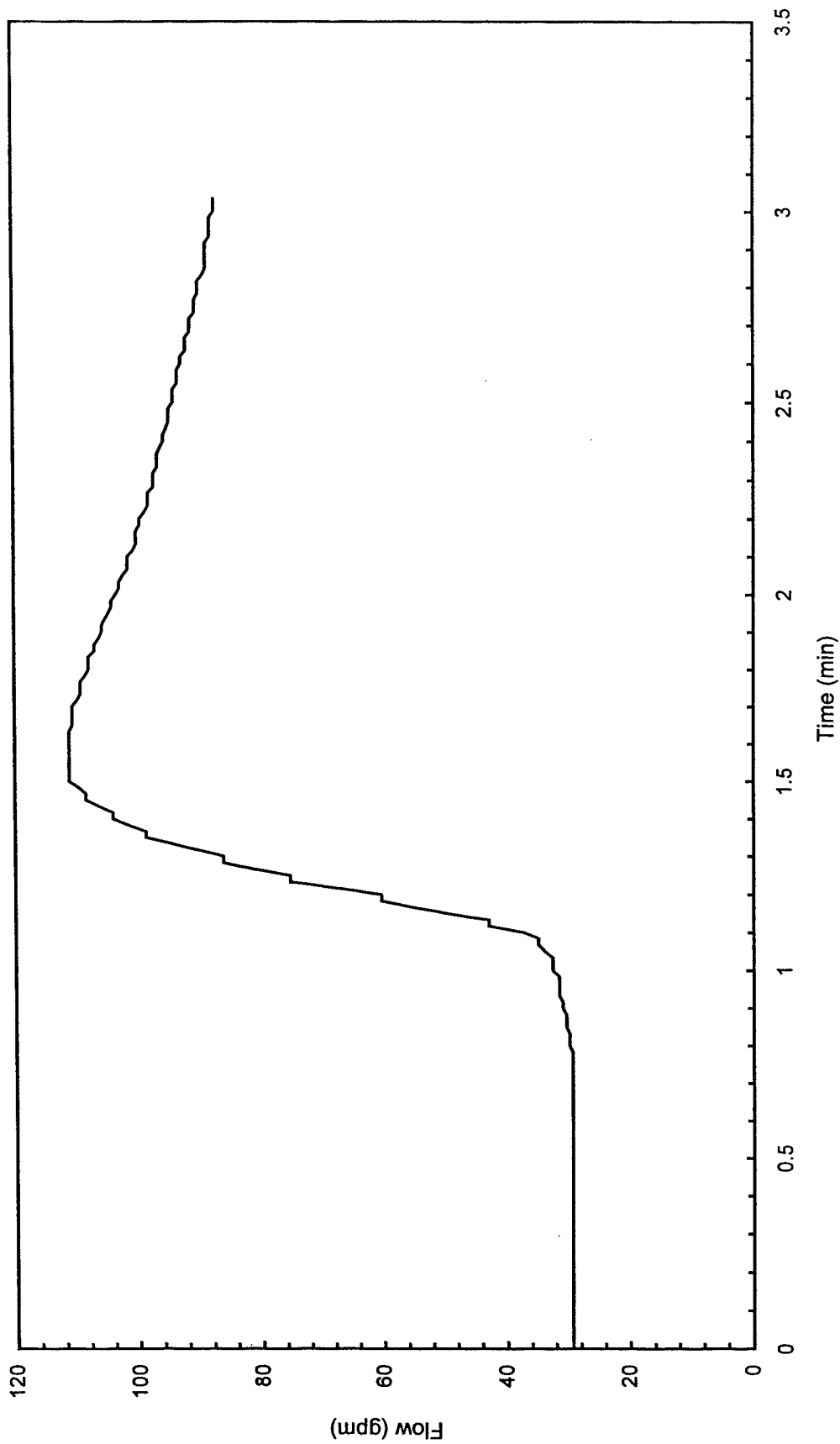


Fig. B33 - Sprinkler system flowrate

Test S2

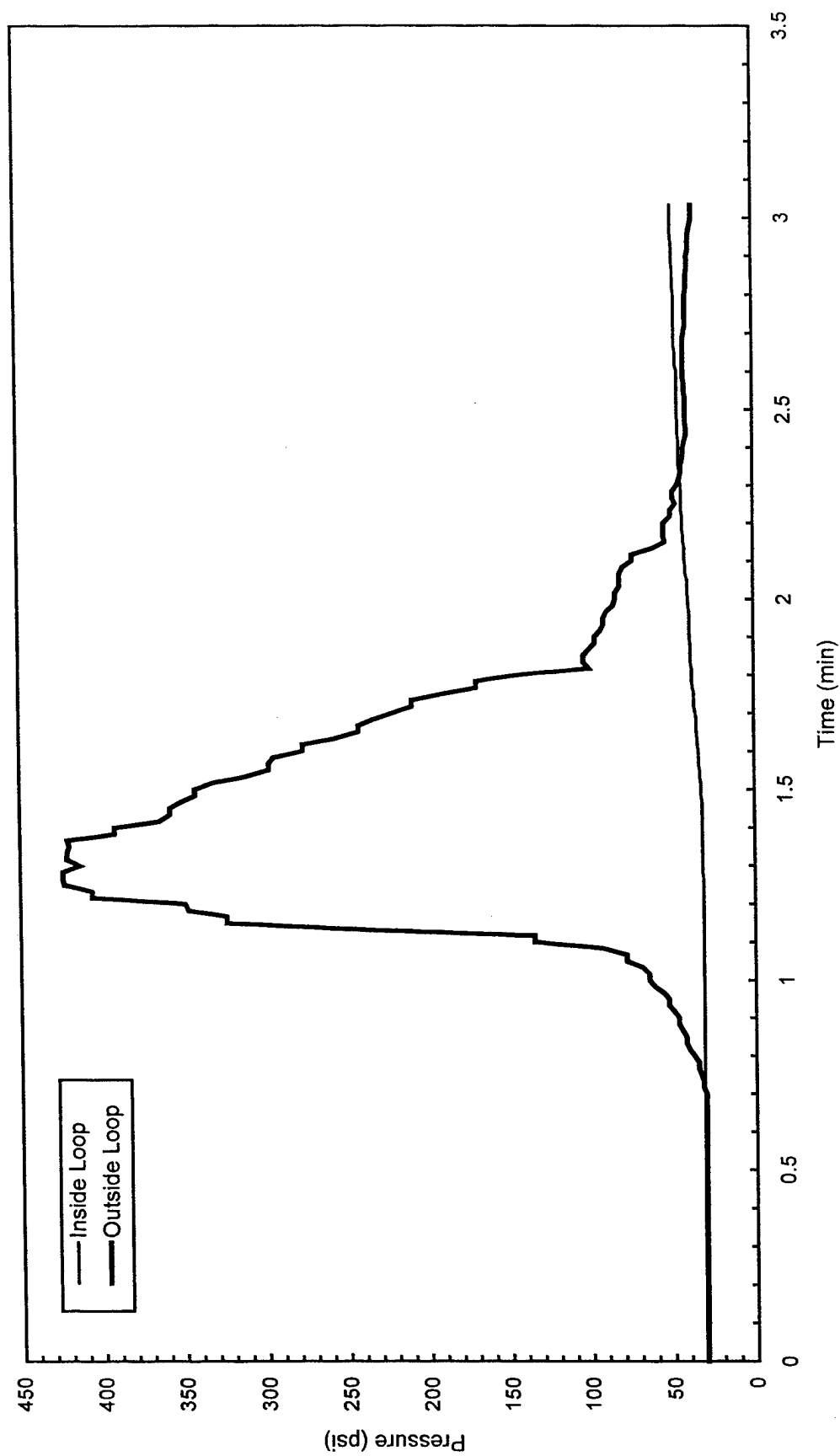


Fig. B34 - Sprinkler system pressure

Test S3

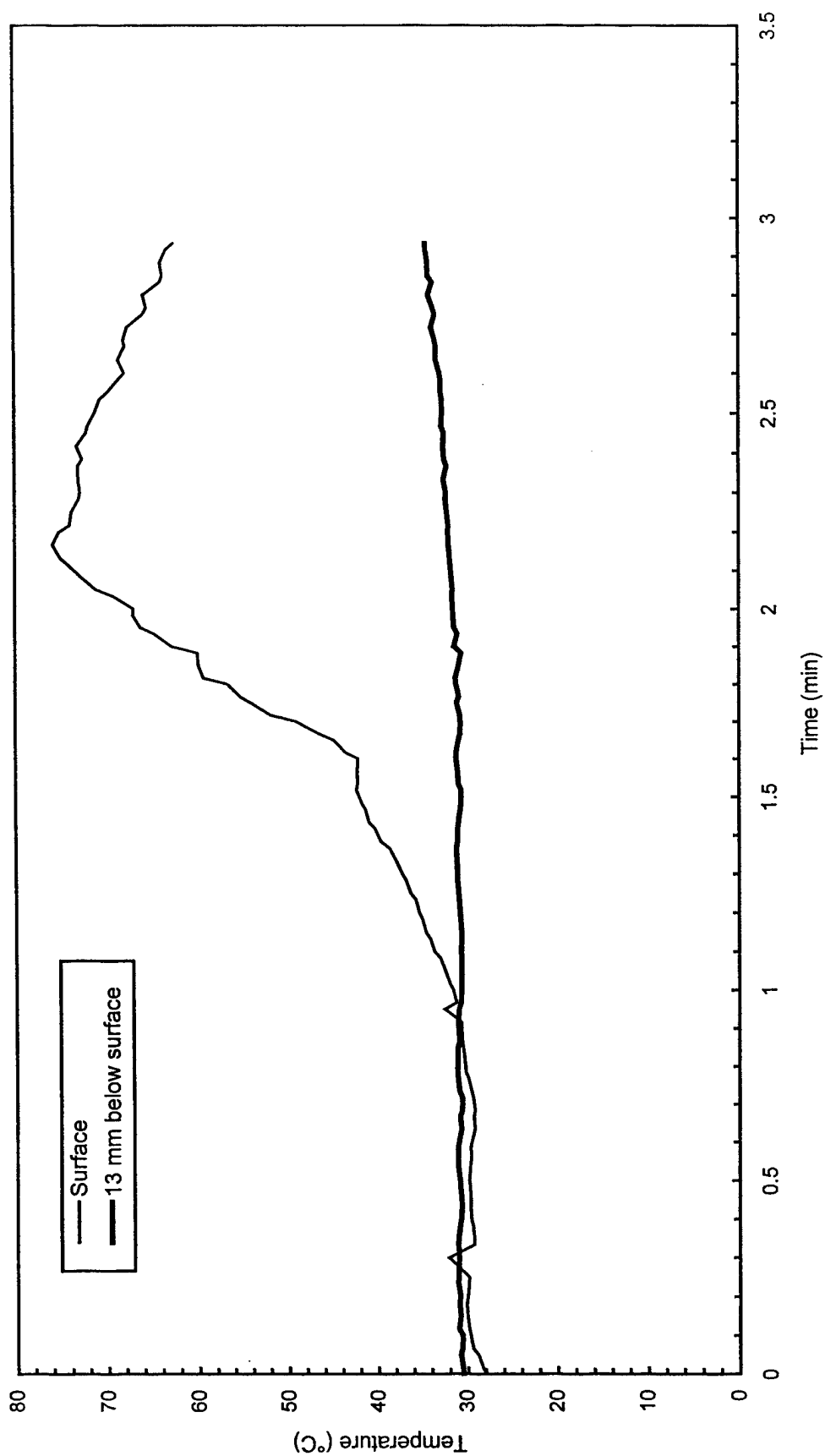


Fig. B35 - Concrete temperatures at center of pad

Test S3

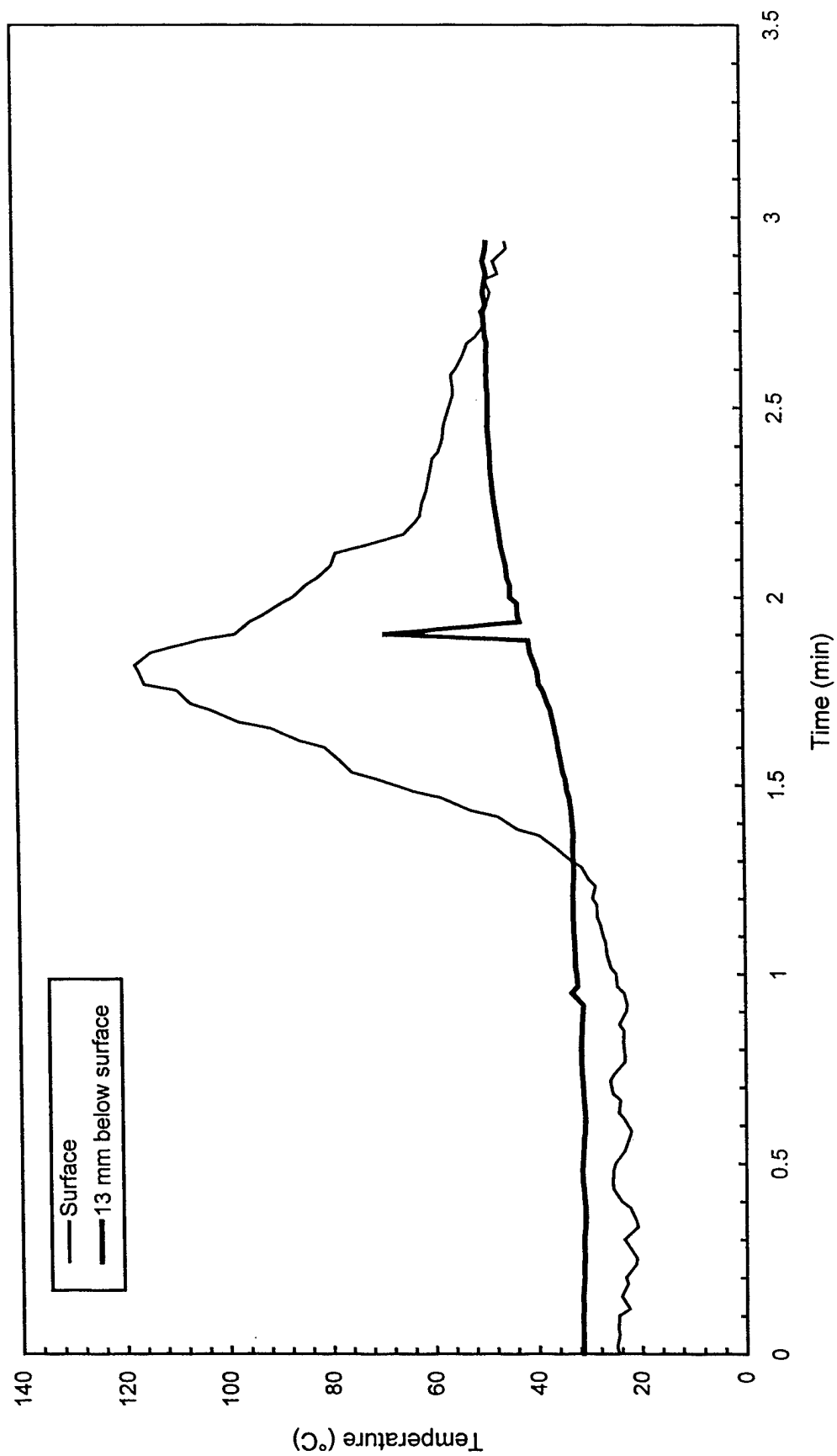


Fig. B36 - Concrete temperatures 3 m (10 ft) East of center of pad

Test S3

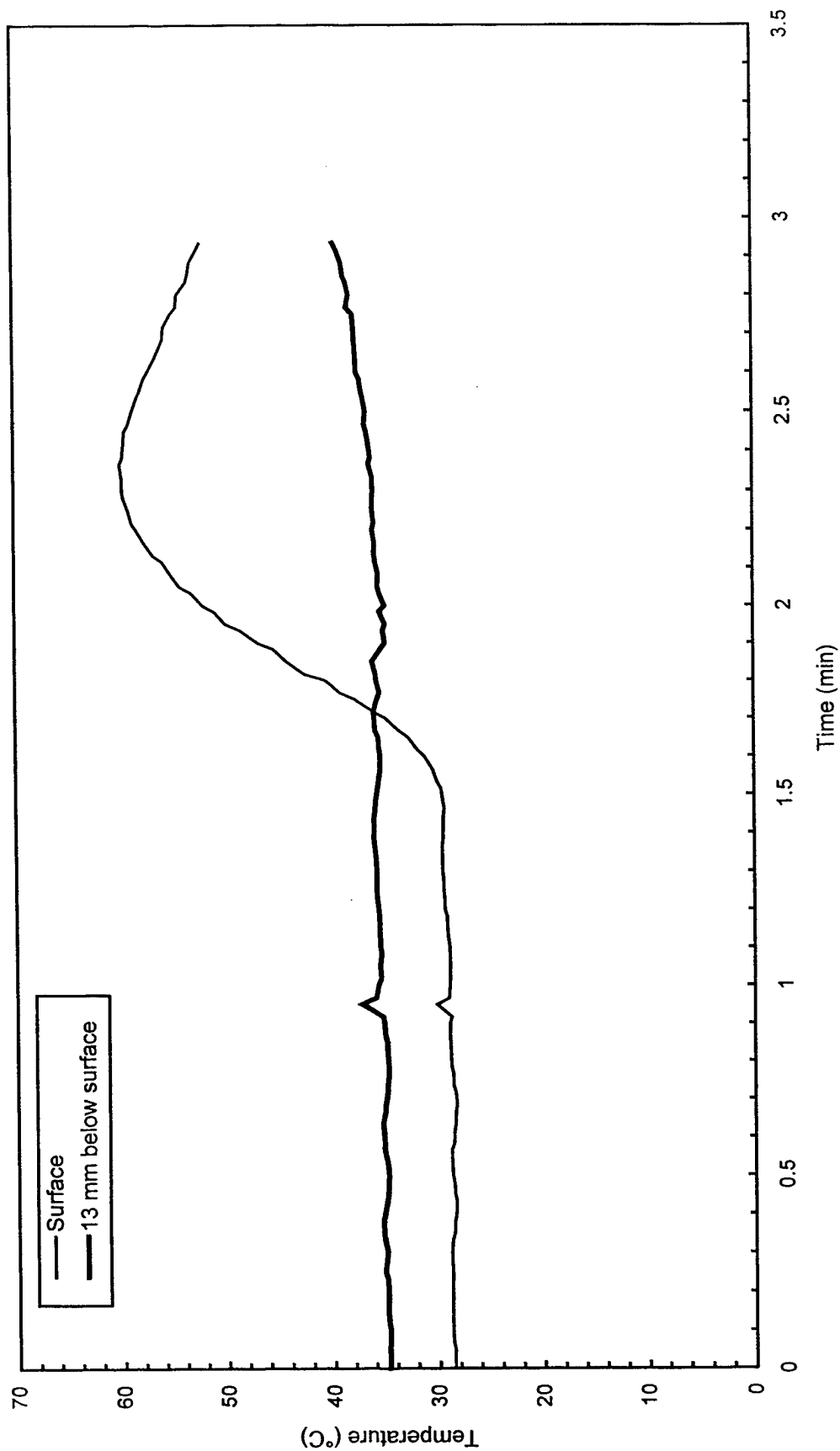


Fig. B37 - Concrete temperatures 3 m (10 ft) West of center of pad

Test S3

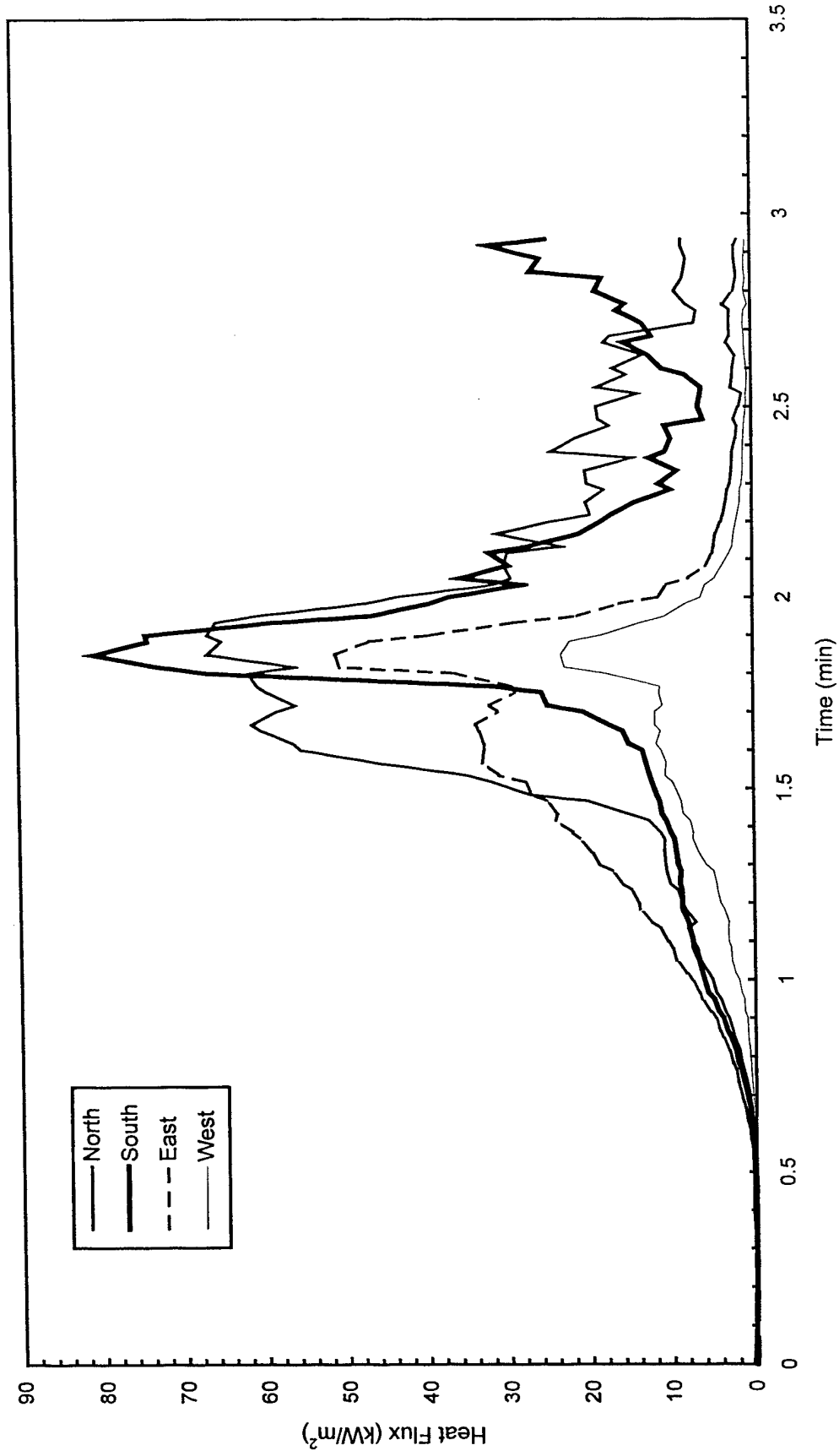


Fig. B38 - Heat flux measured at edge of pad

Test S3

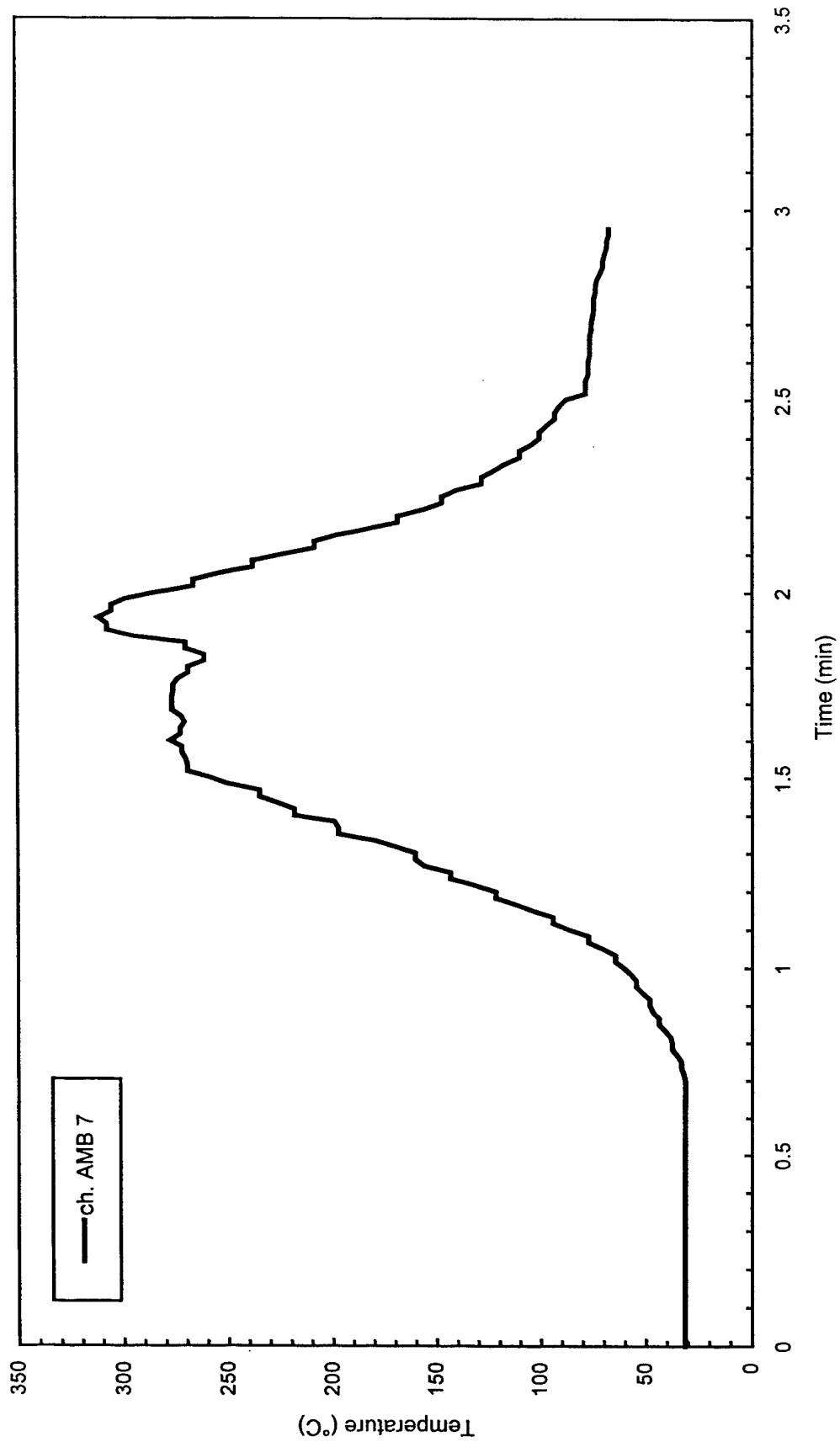


Fig. B39 - Air temperatures over center of pad

Test S3

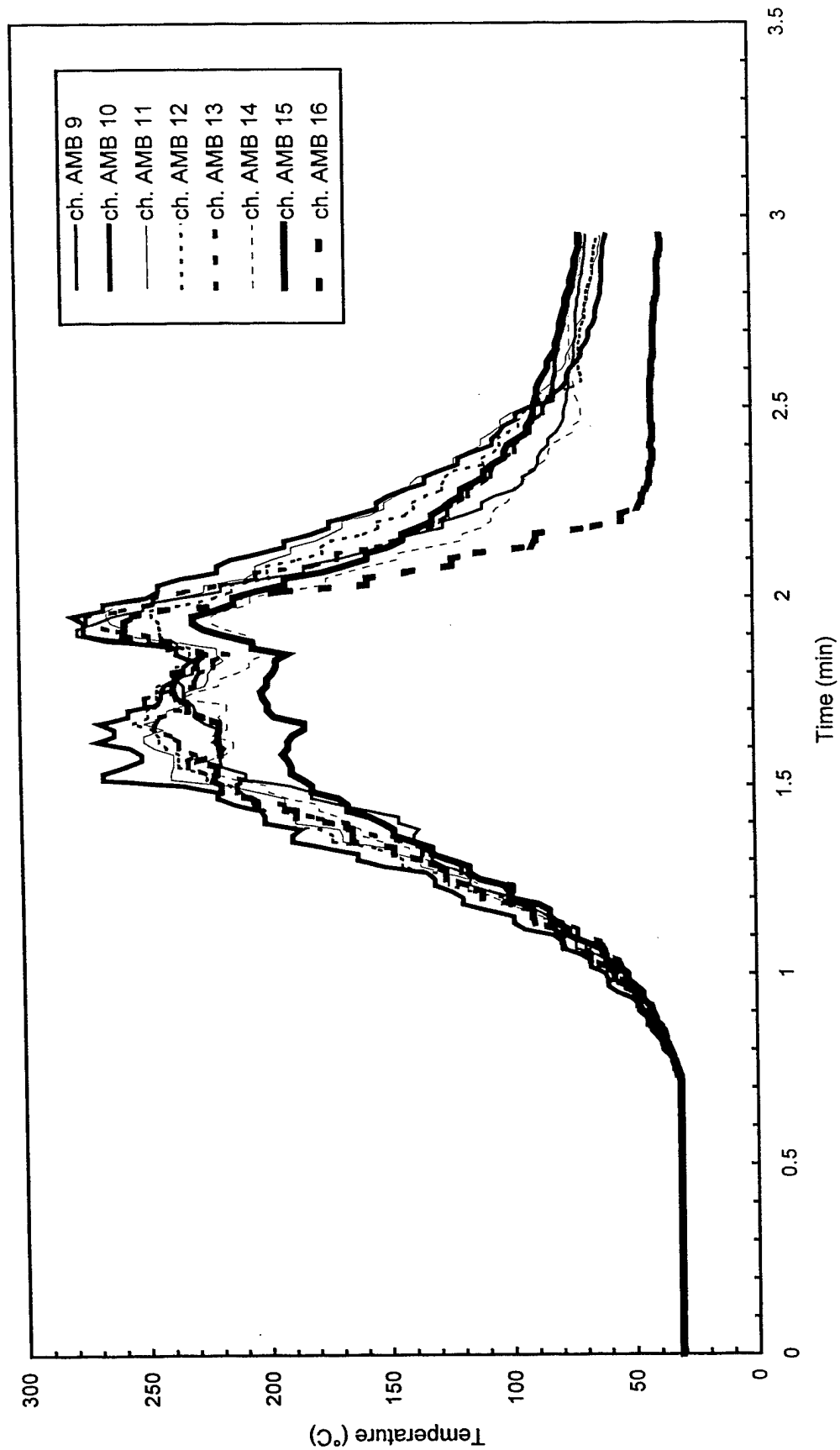


Fig. B40 - Air temperatures around 3 m (10 ft) radius from center of pad

Test S3

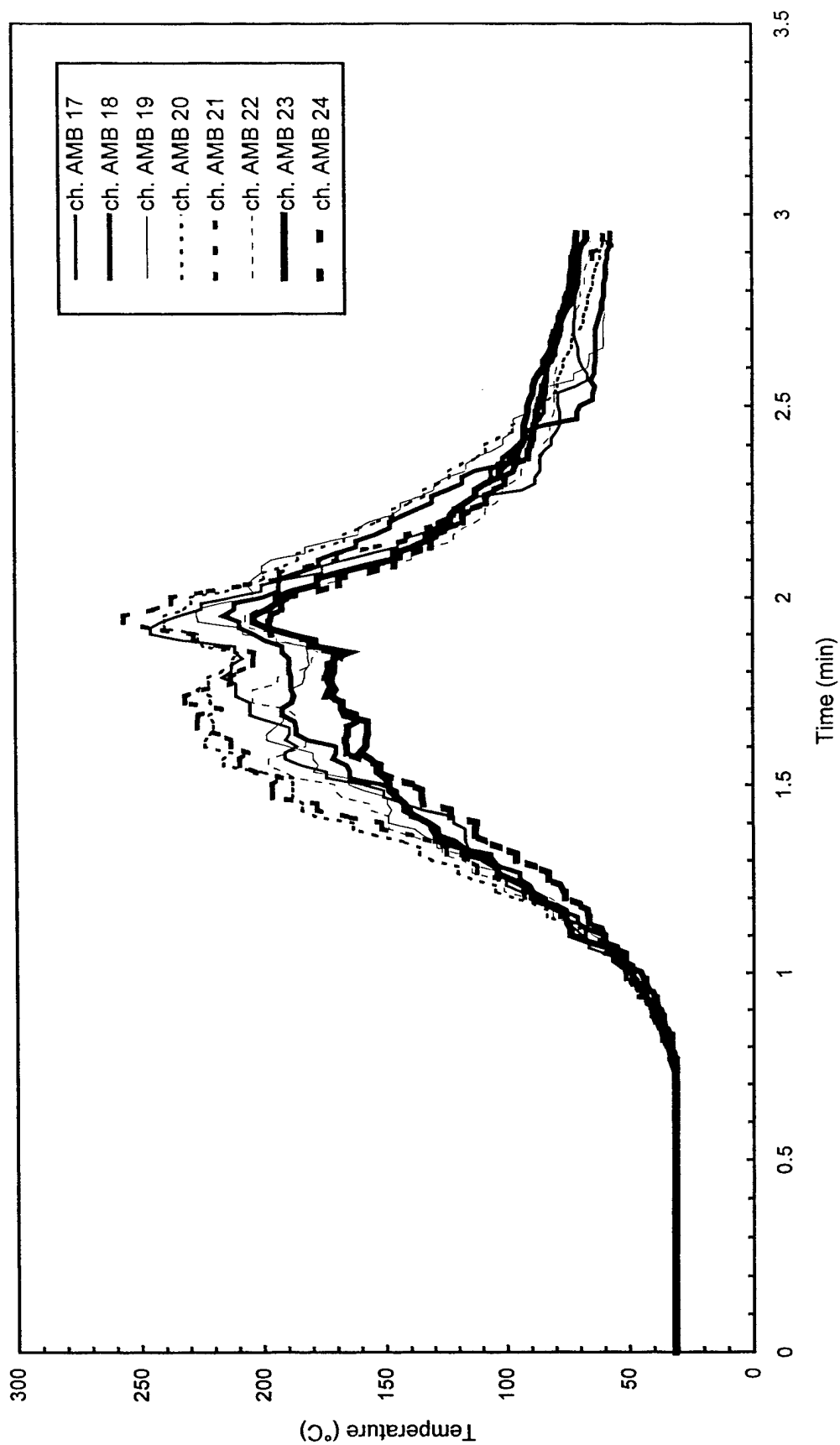


Fig. B41 - Air temperatures around 4.6 m (15 ft) radius from center of pad

Test S3

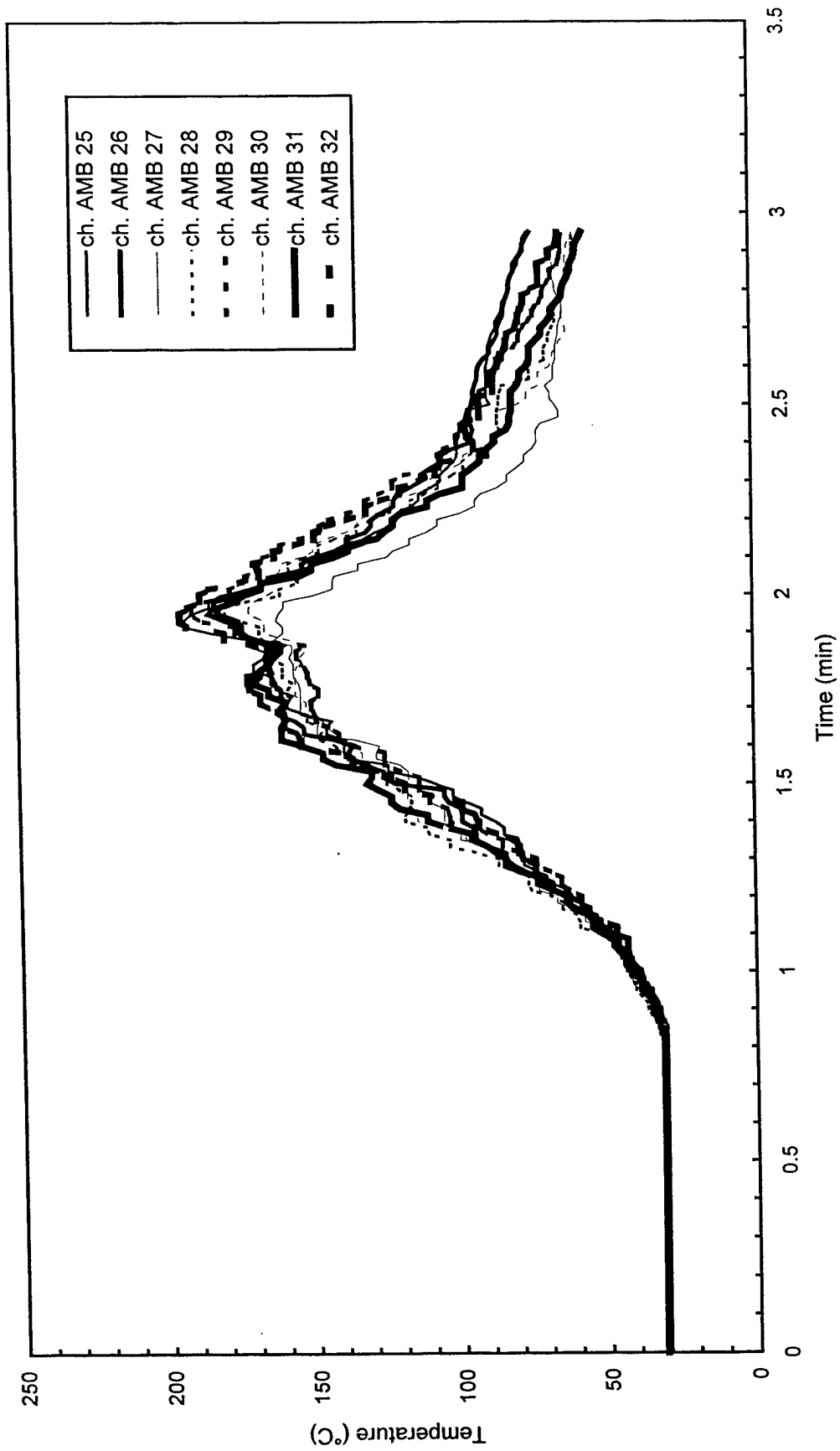


Fig. B42 - Air temperatures around North half of 7.6 m (25 ft) radius from center of pad

Test S3

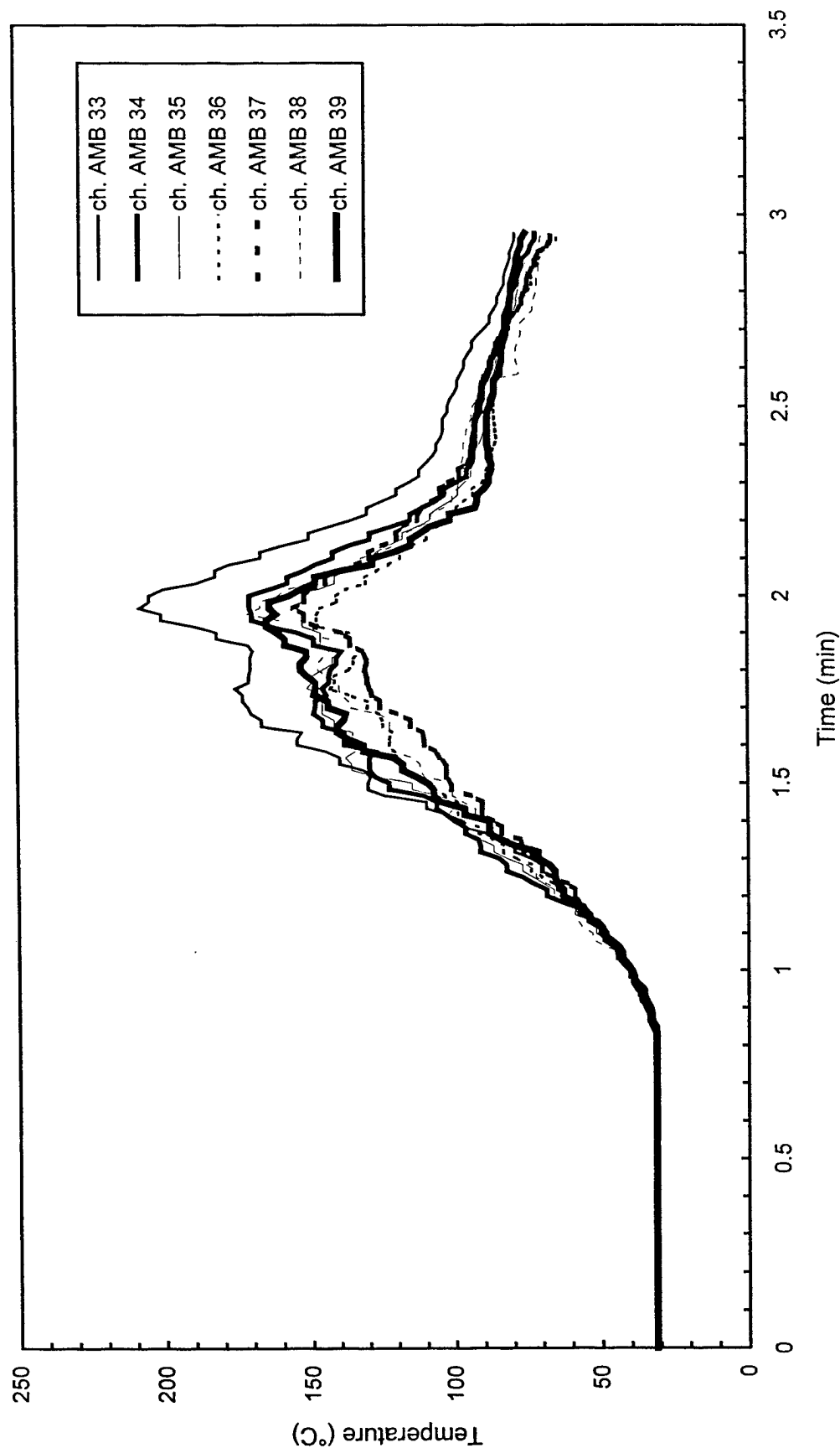


Fig. B43 - Air temperatures around South half of 7.6 m (25 ft) radius from center of pad

Test S3

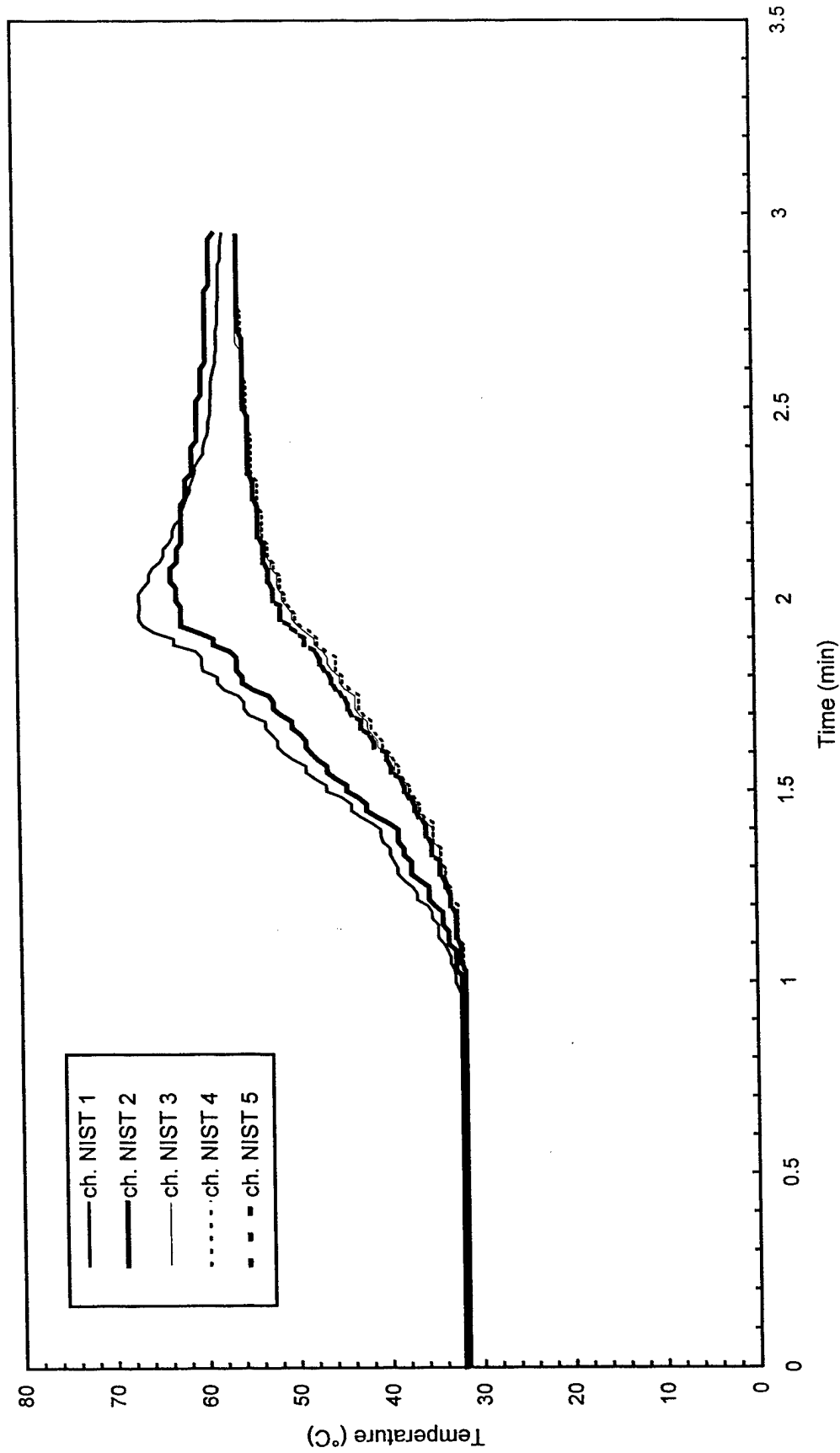


Fig. B44 - Temperature of West steel beam

Test S3

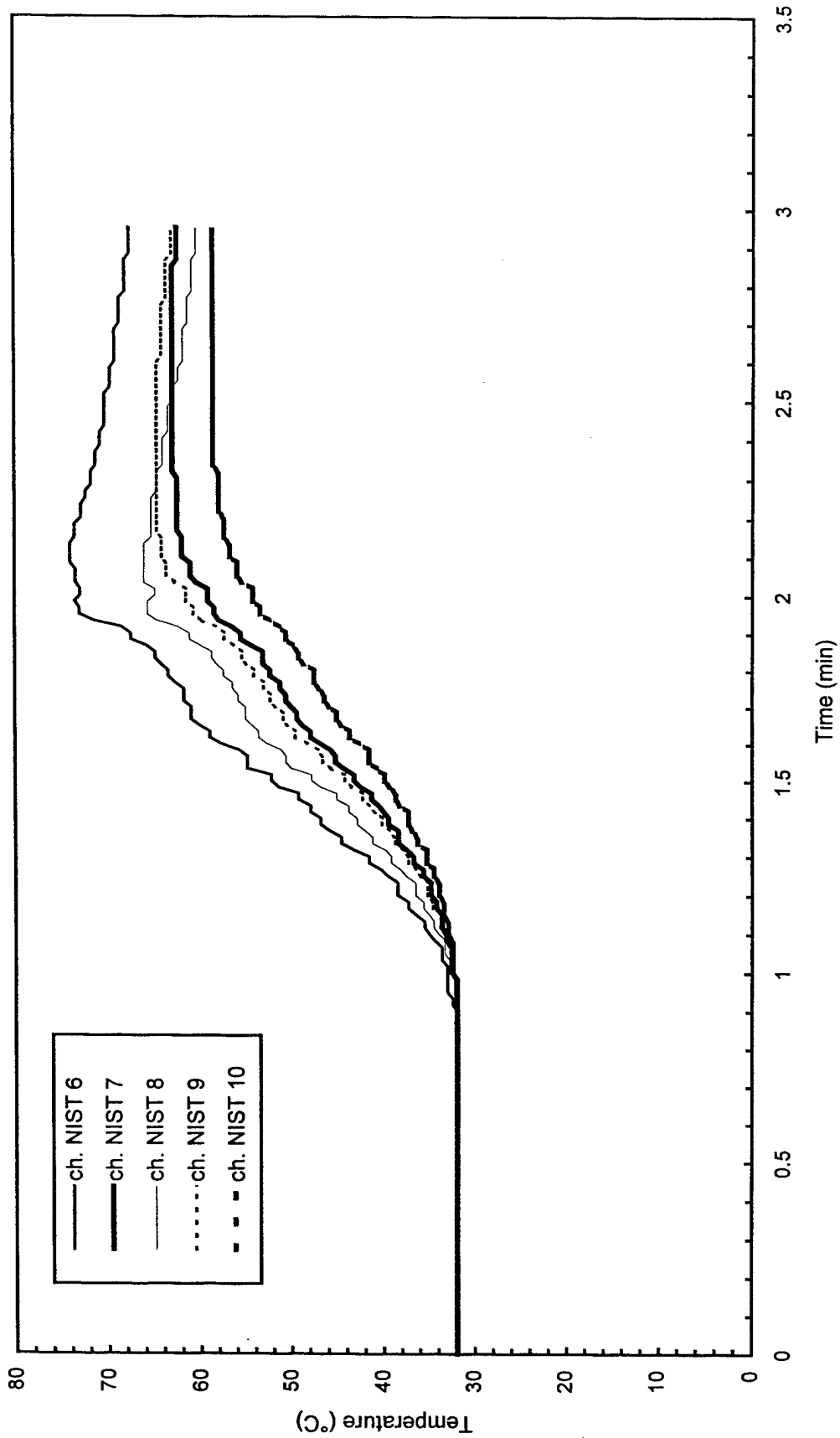


Fig. B45 - Temperature of North steel beam

Test S3

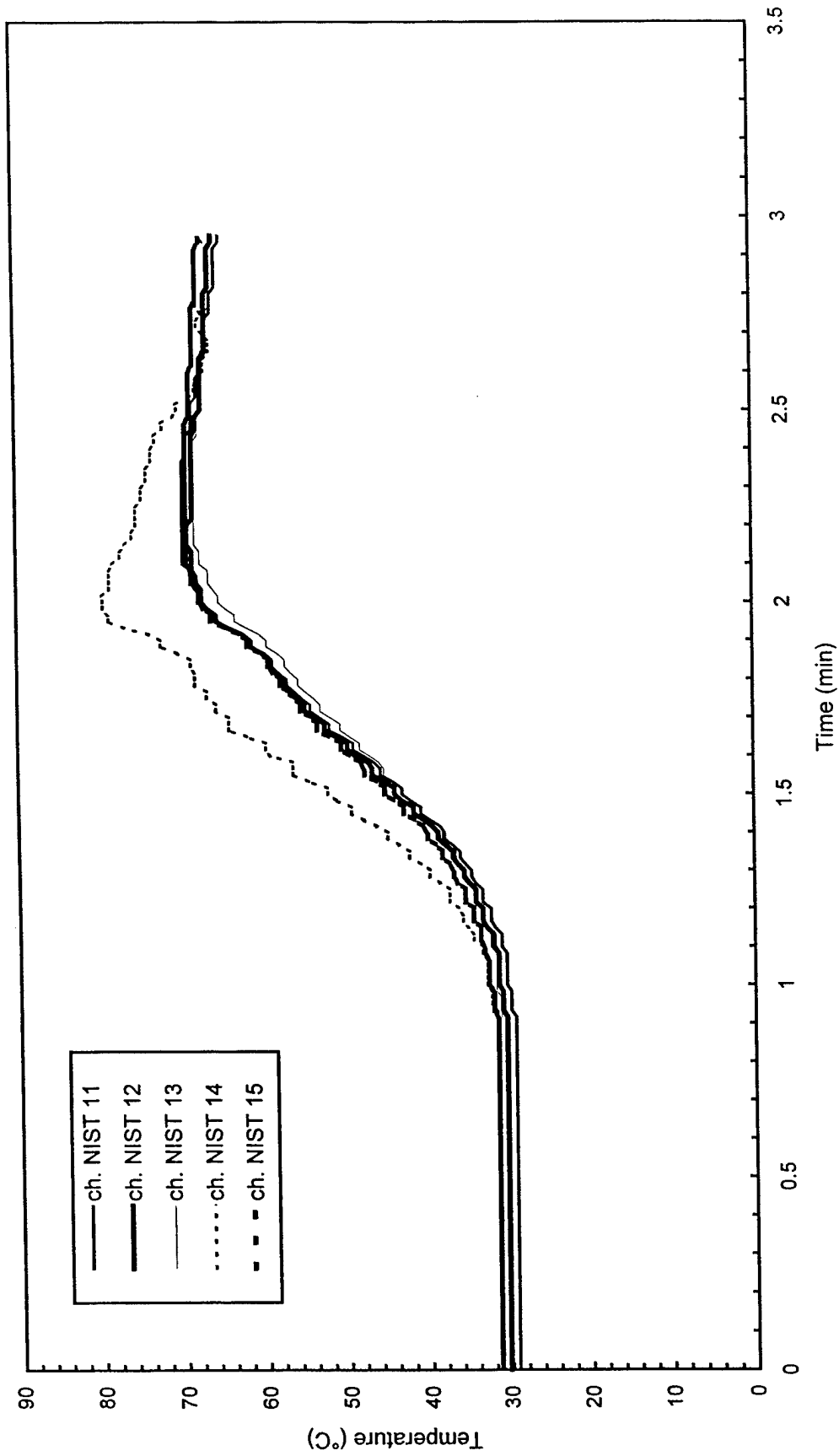


Fig. B46 - Temperature of East steel beam

Test S3

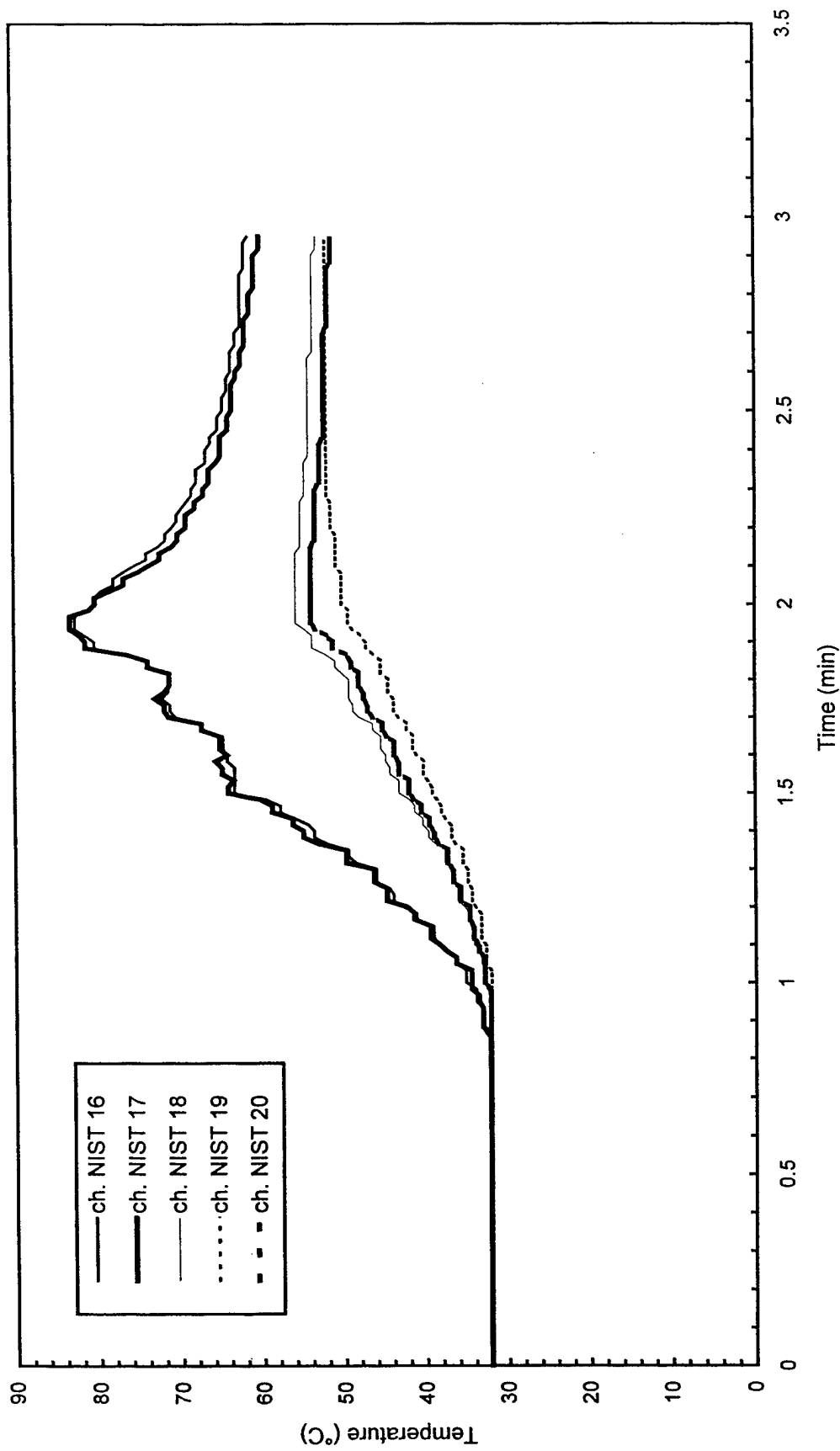


Fig. B47 - Temperature of South steel beam

Test S3

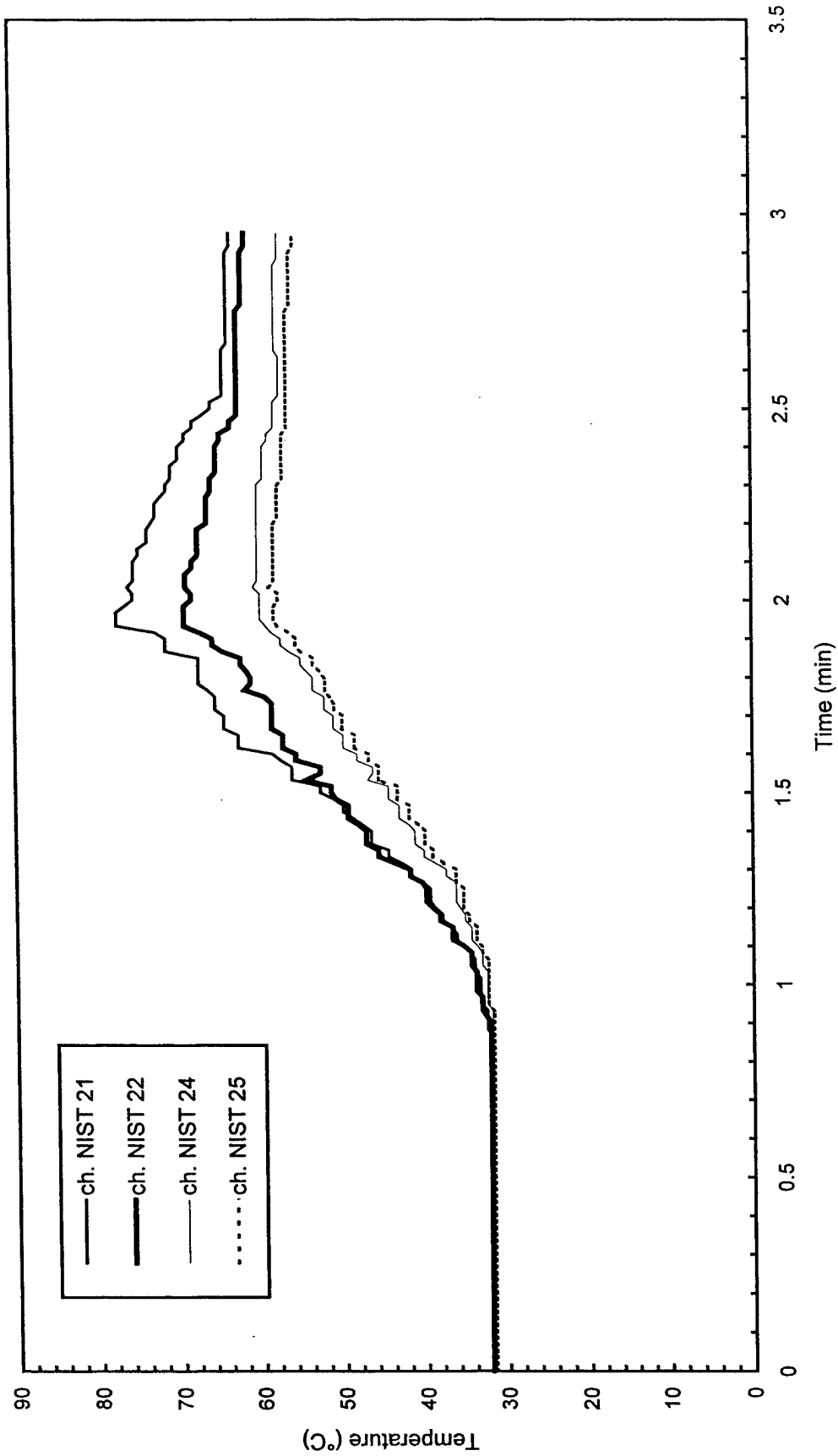


Fig. B48 - Temperature of Northwest steel beam

Test S3

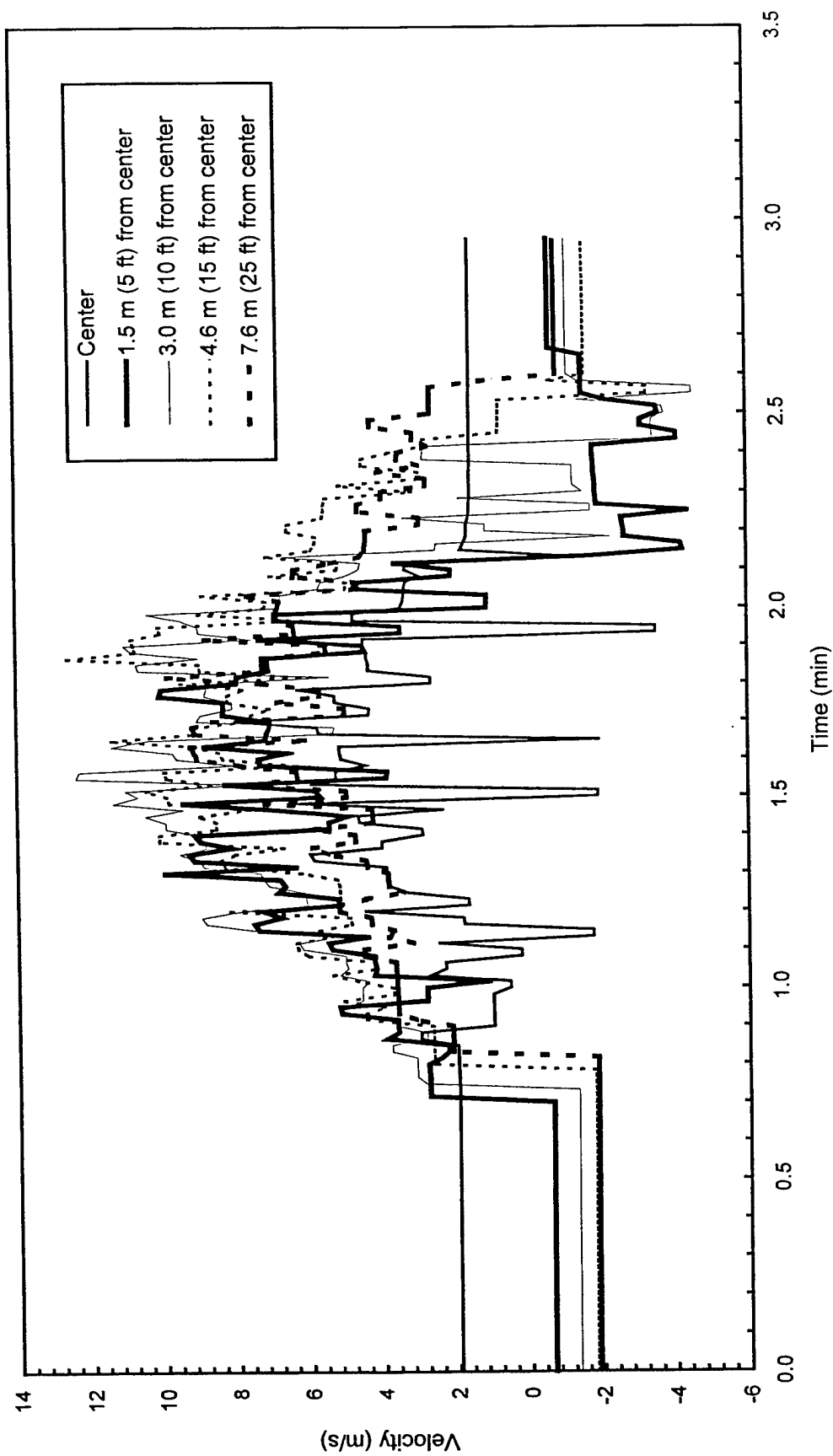


Fig. B49 - Plume and ceiling jet velocities

Test S3

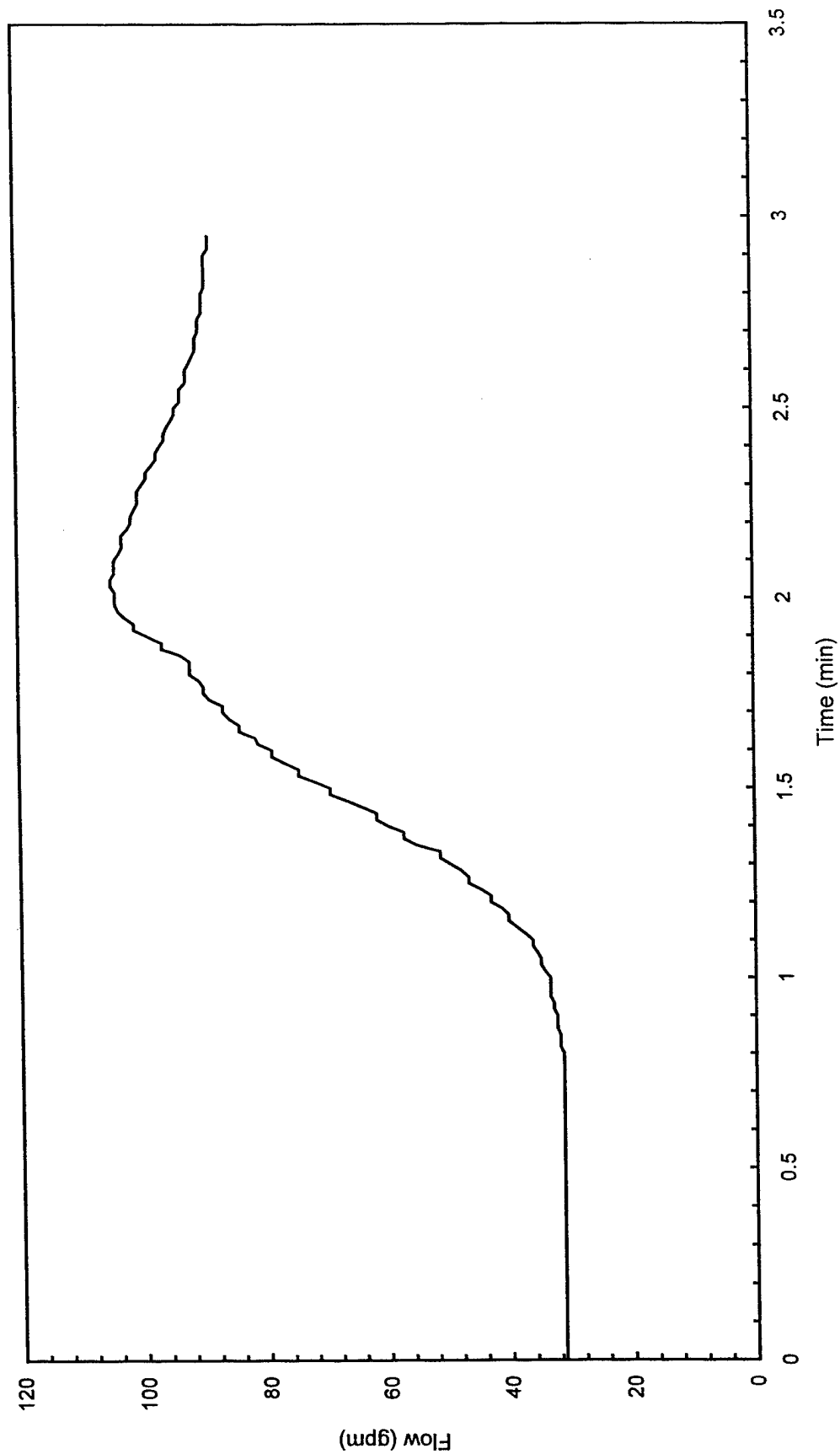


Fig. B50 - Sprinkler system flowrate

Test S3

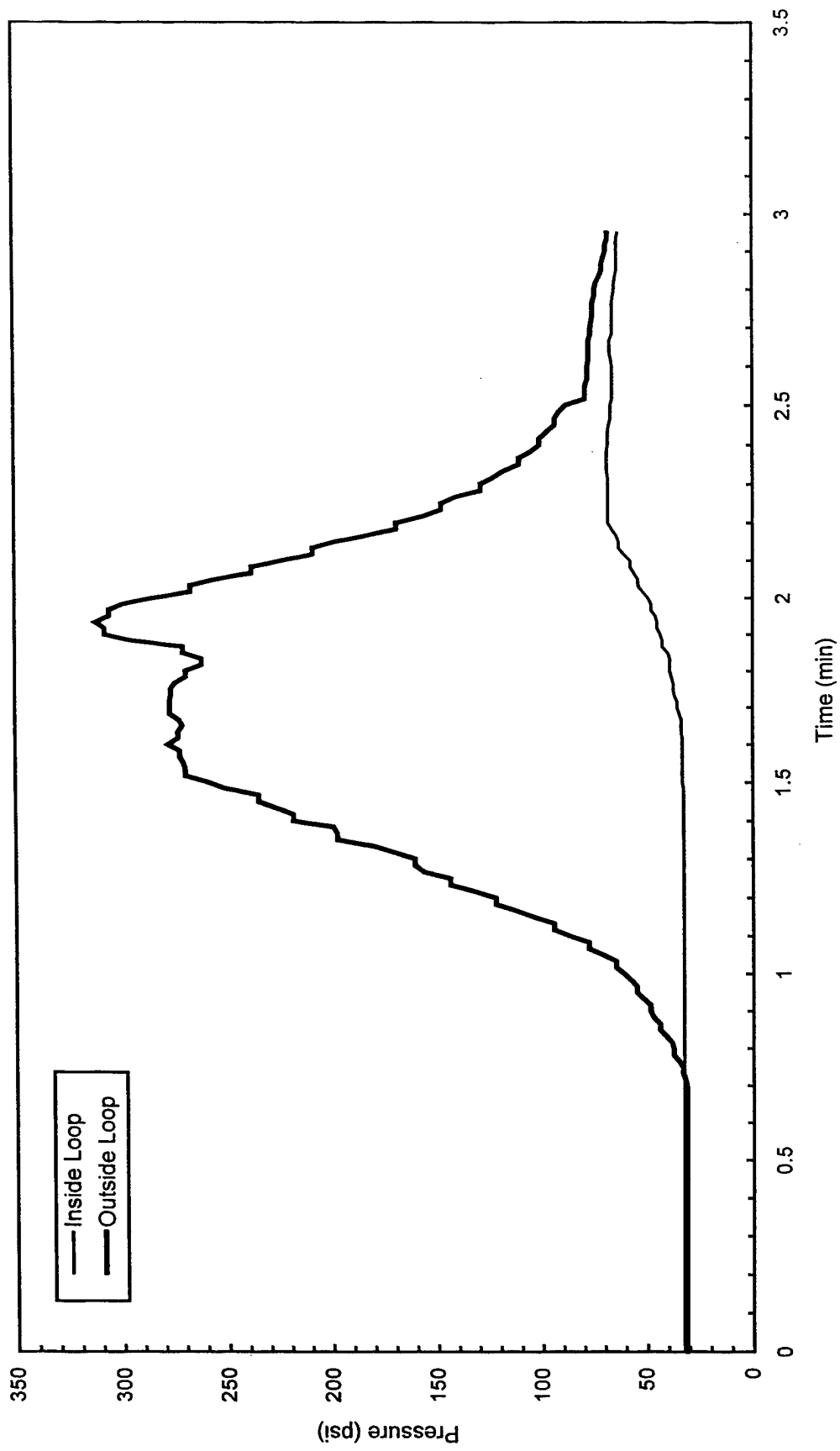


Fig. B51 - Sprinkler system pressure

Test S4

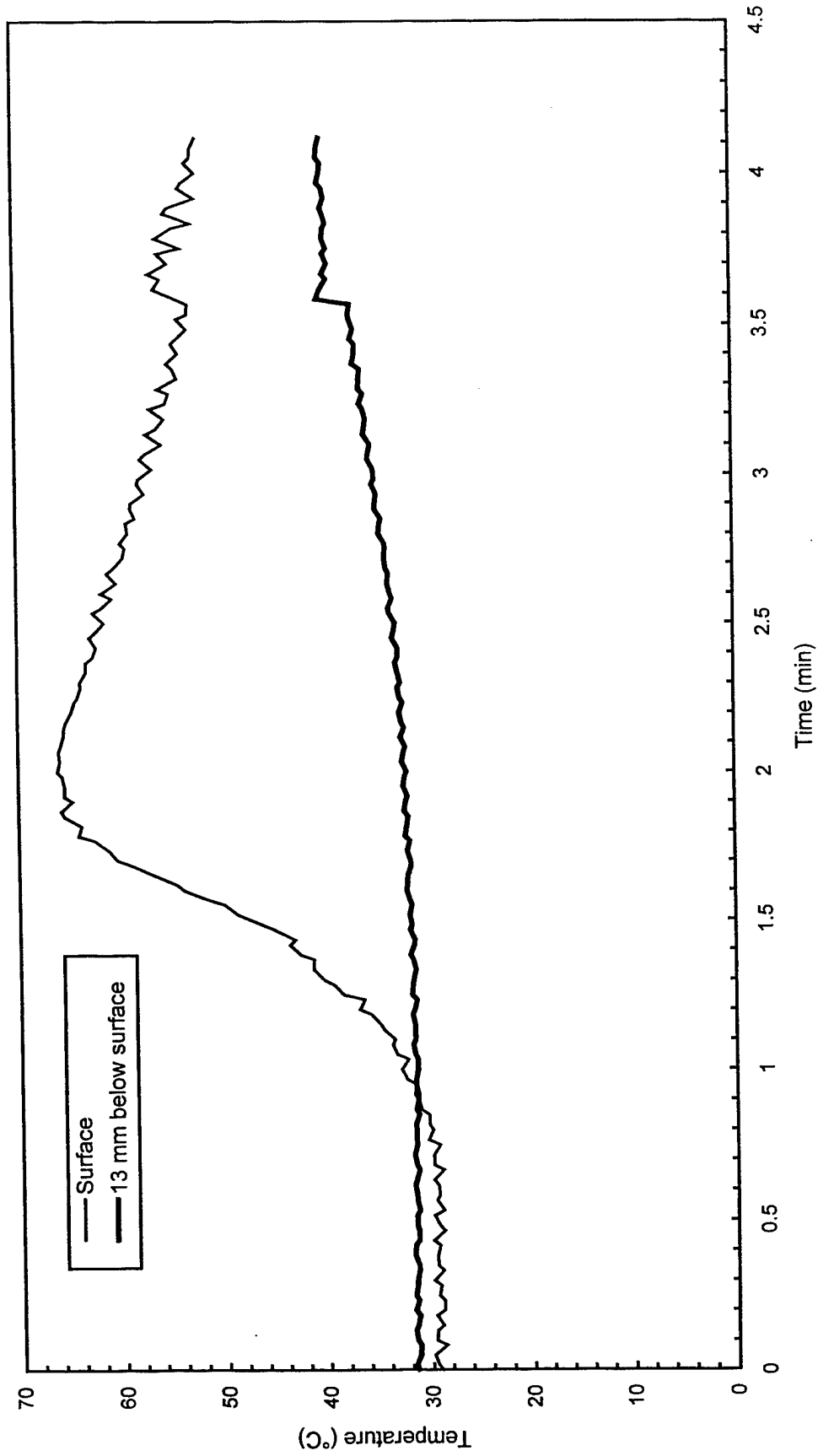


Fig. B52 - Concrete temperatures at center of pad

Test S4

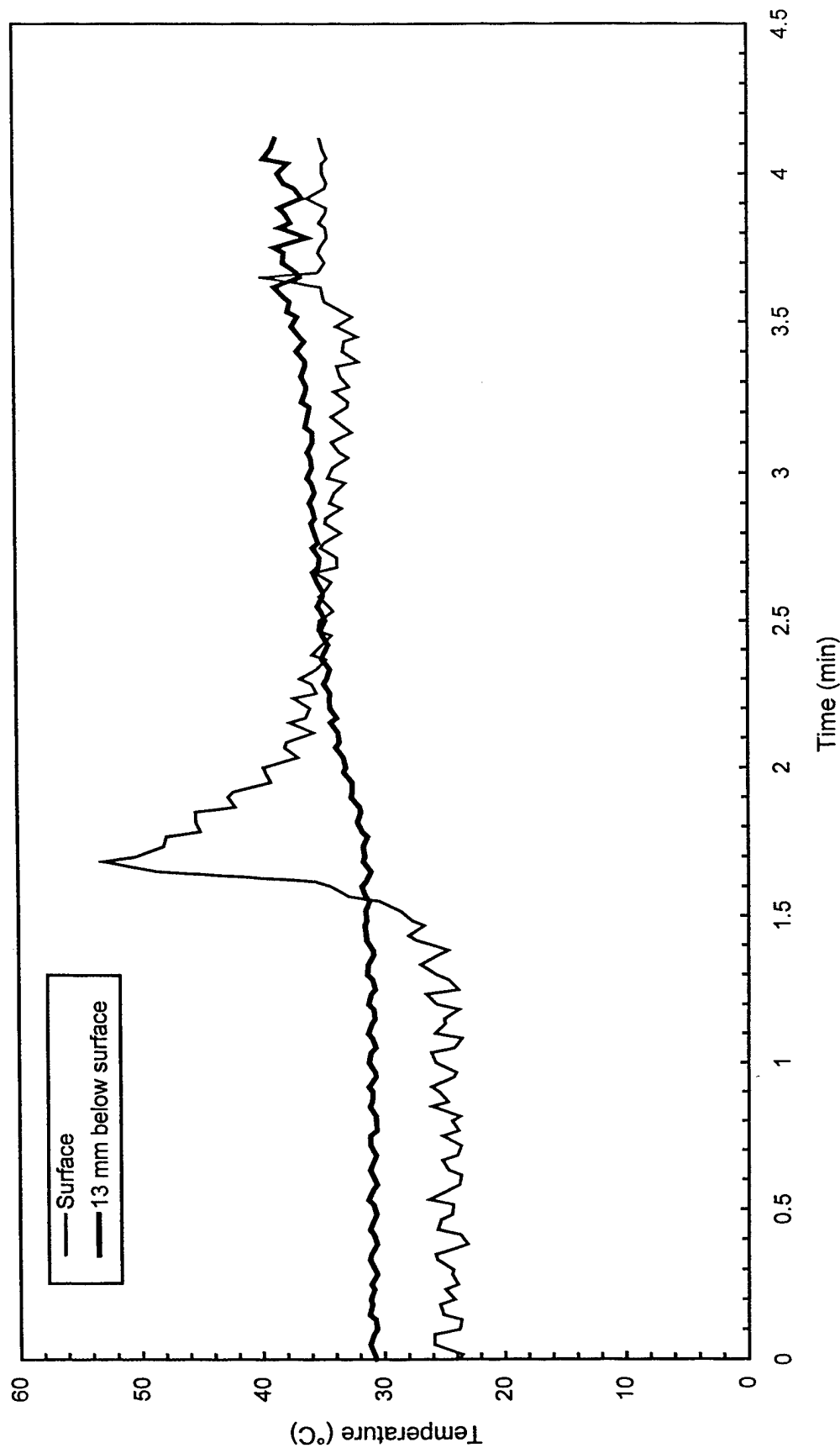


Fig. B53 - Concrete temperatures 3 m (10 ft) East of center of pad

Test S4

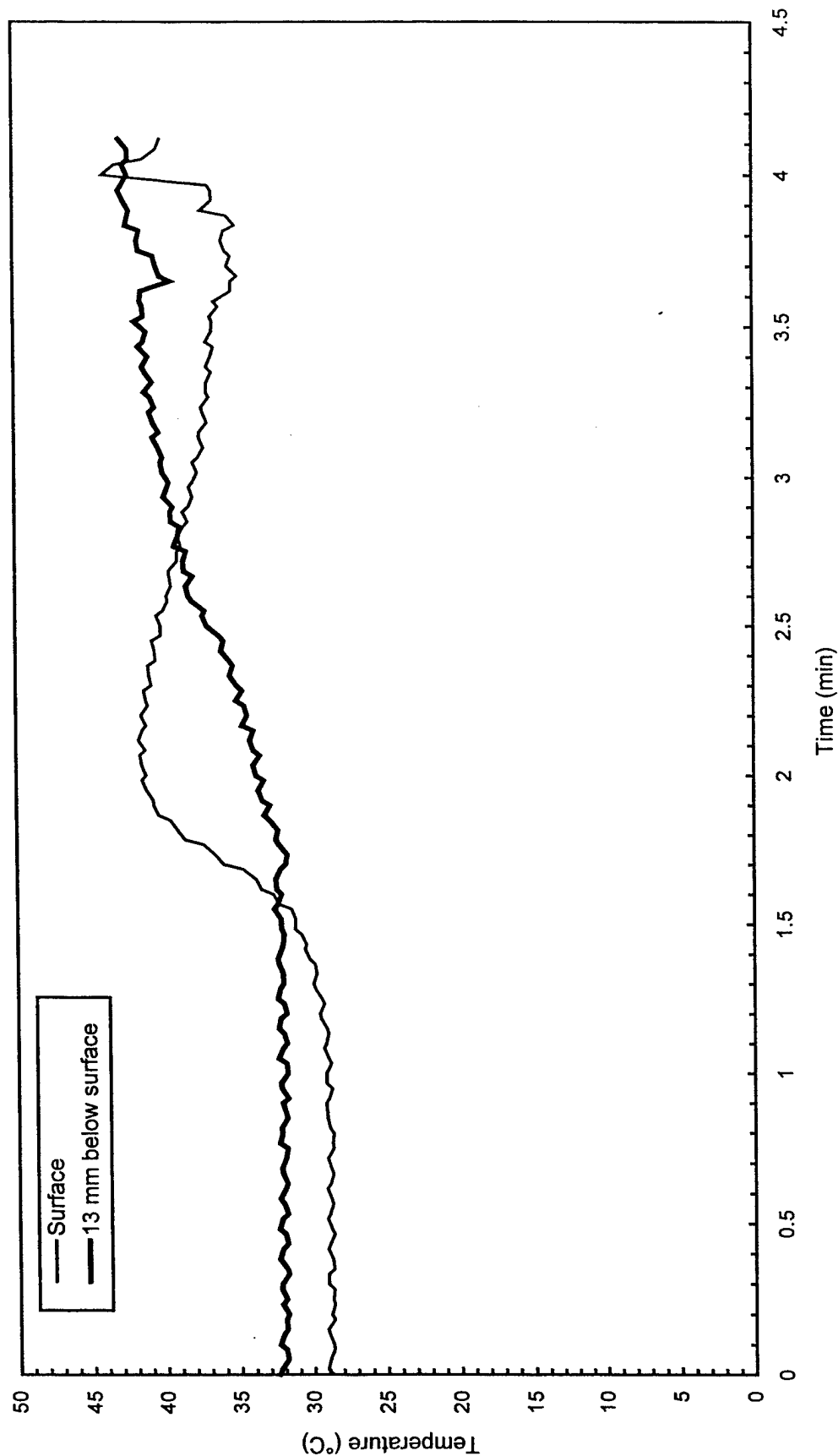


Fig. B54 - Concrete temperatures 3 m (10 ft) West of center of pad

Test S4

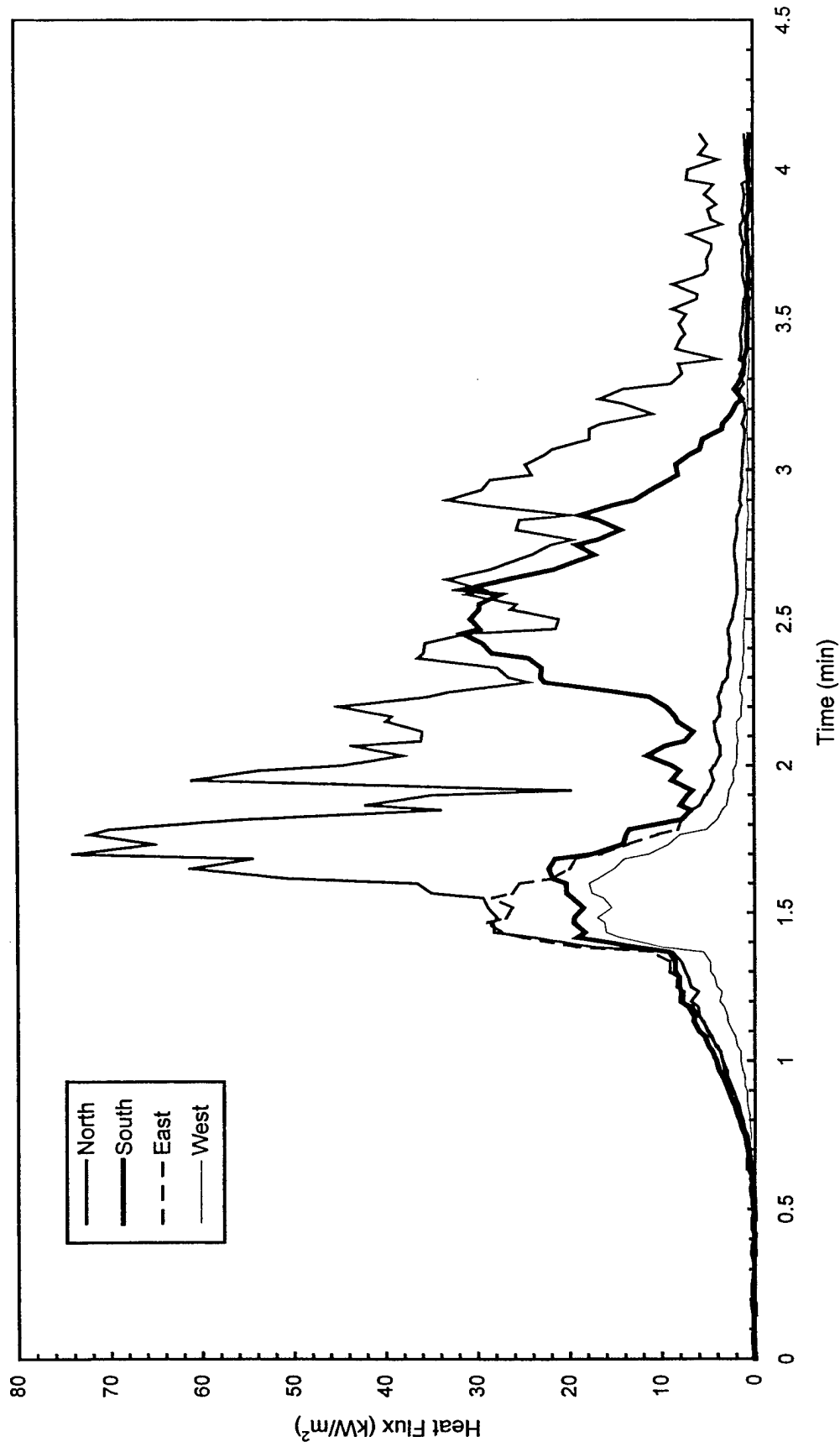


Fig. B55 - Heat flux measured at edge of pad

Test S4

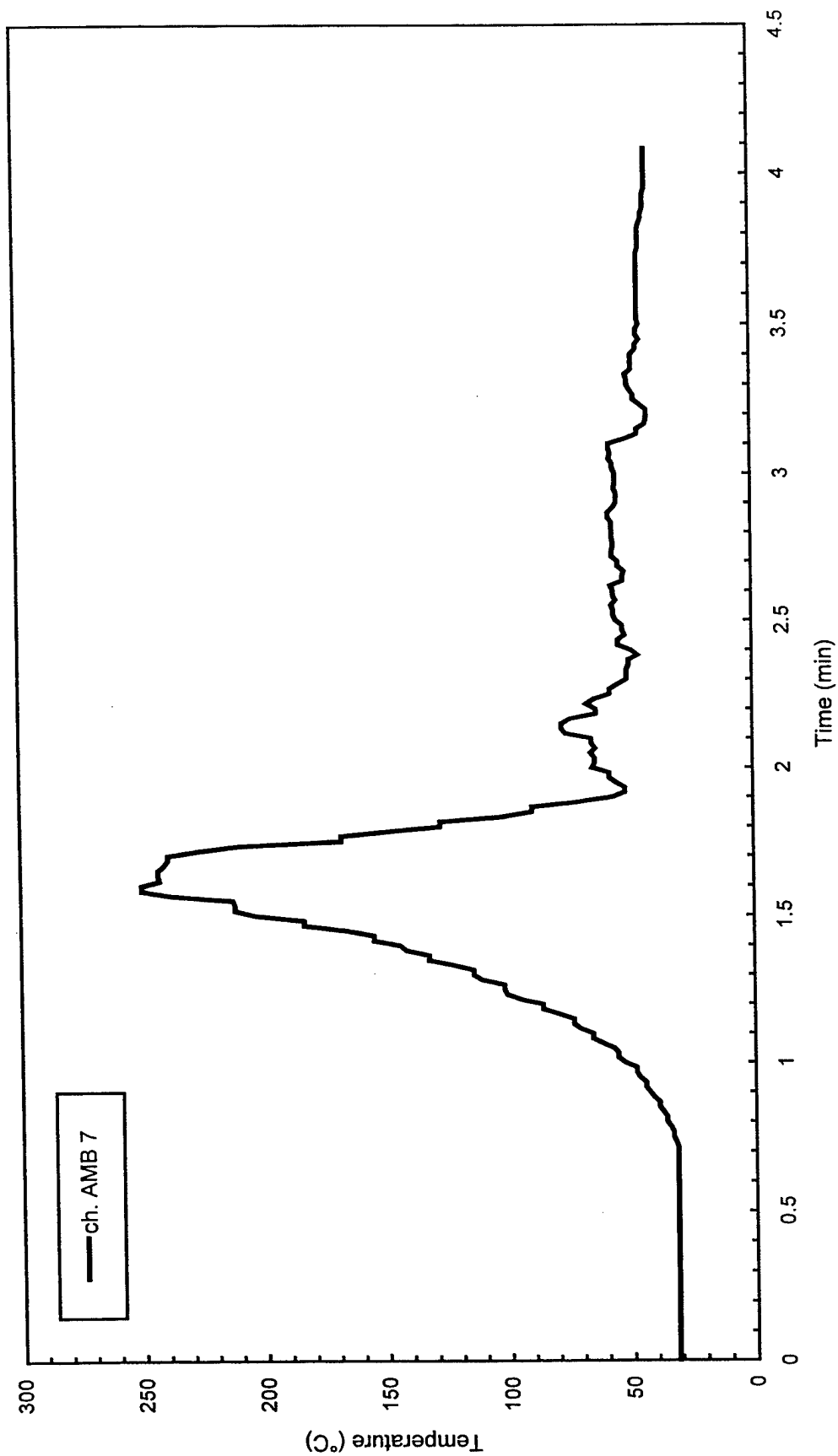


Fig. B56 - Air temperatures over center of pad

Test S4

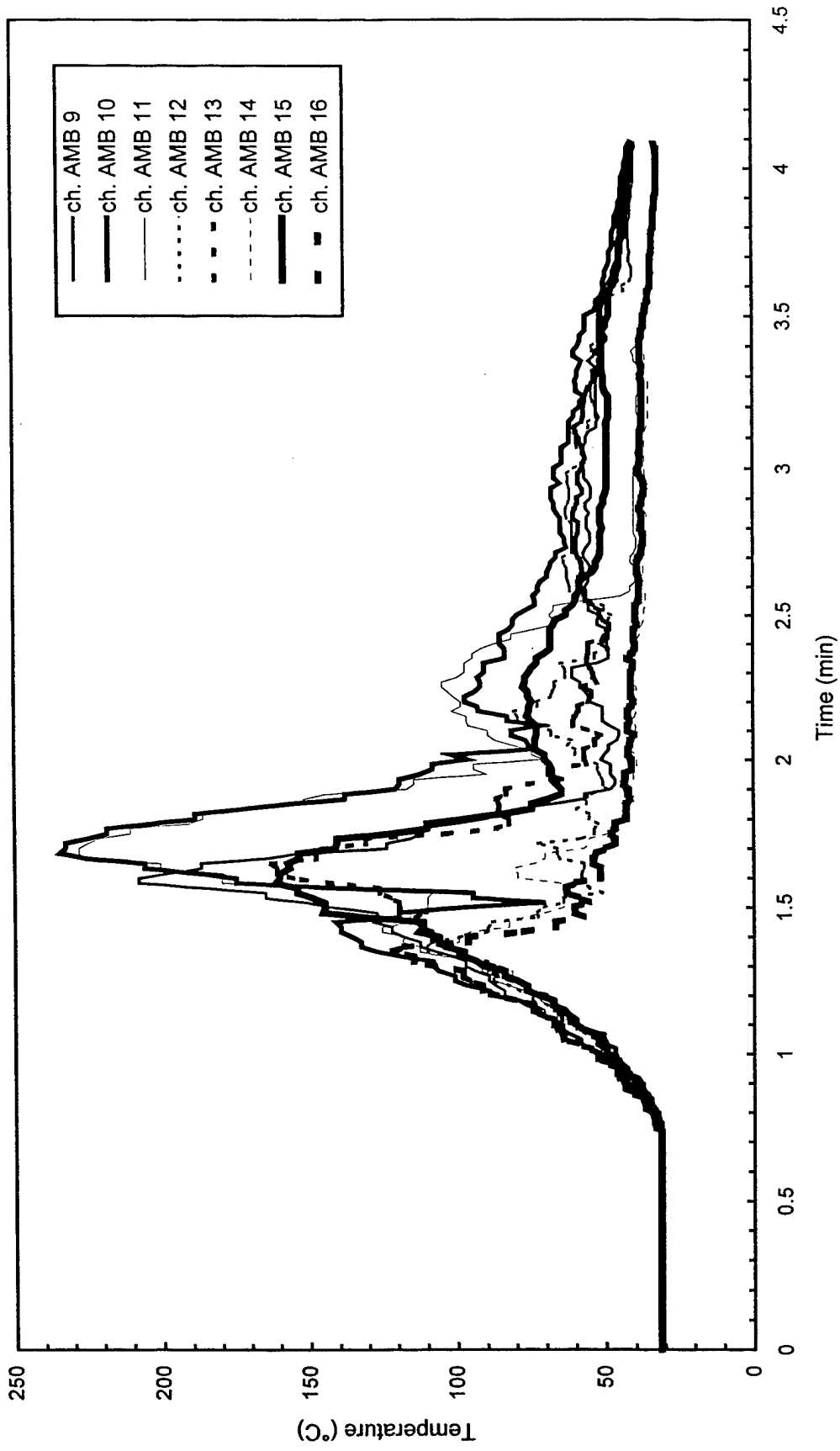


Fig. B57 - Air temperatures around 3 m (10 ft) radius from center of pad

Test S4

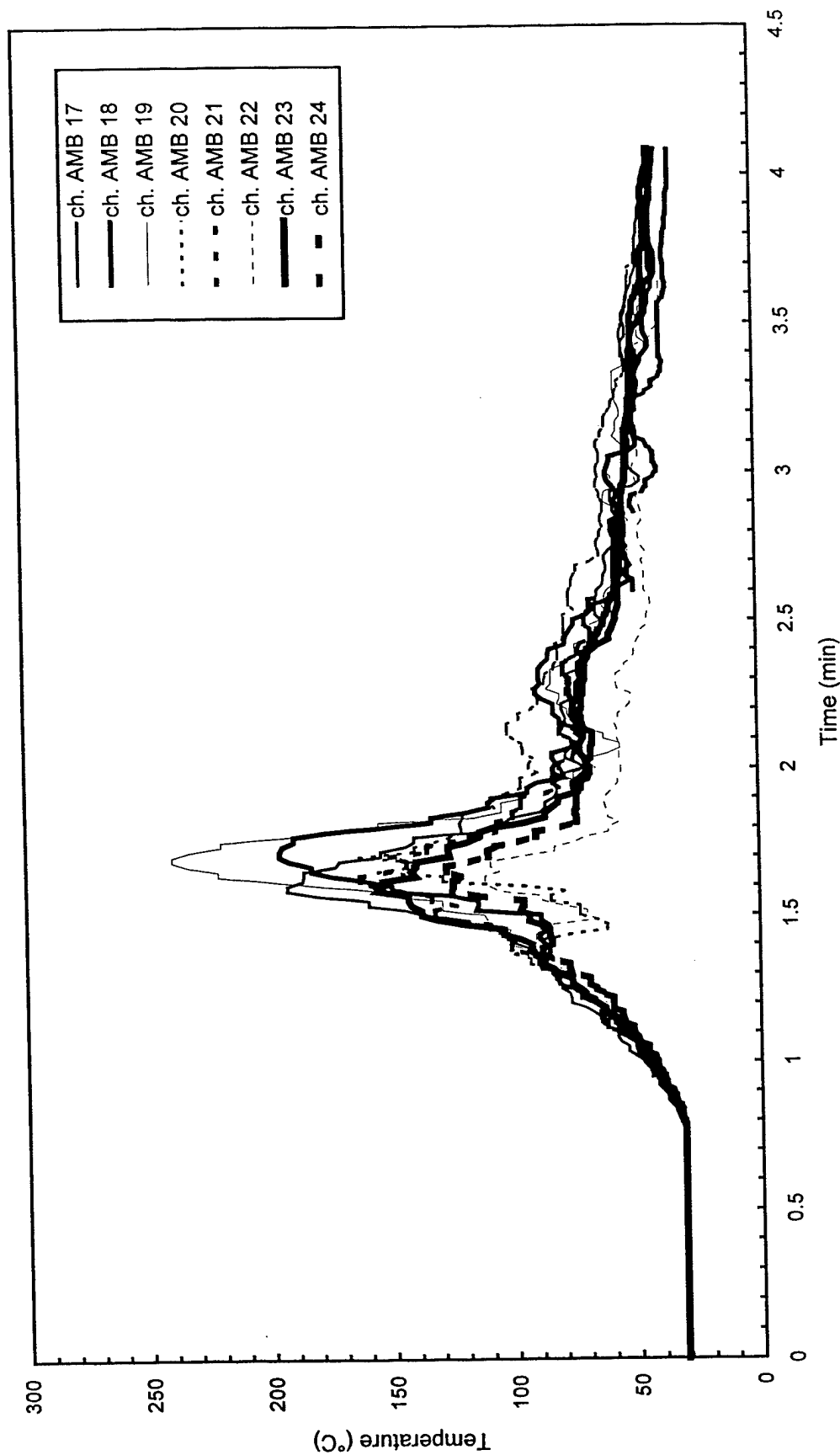


Fig. B58 - Air temperatures around 4.6 m (15 ft) radius from center of pad

Test S4

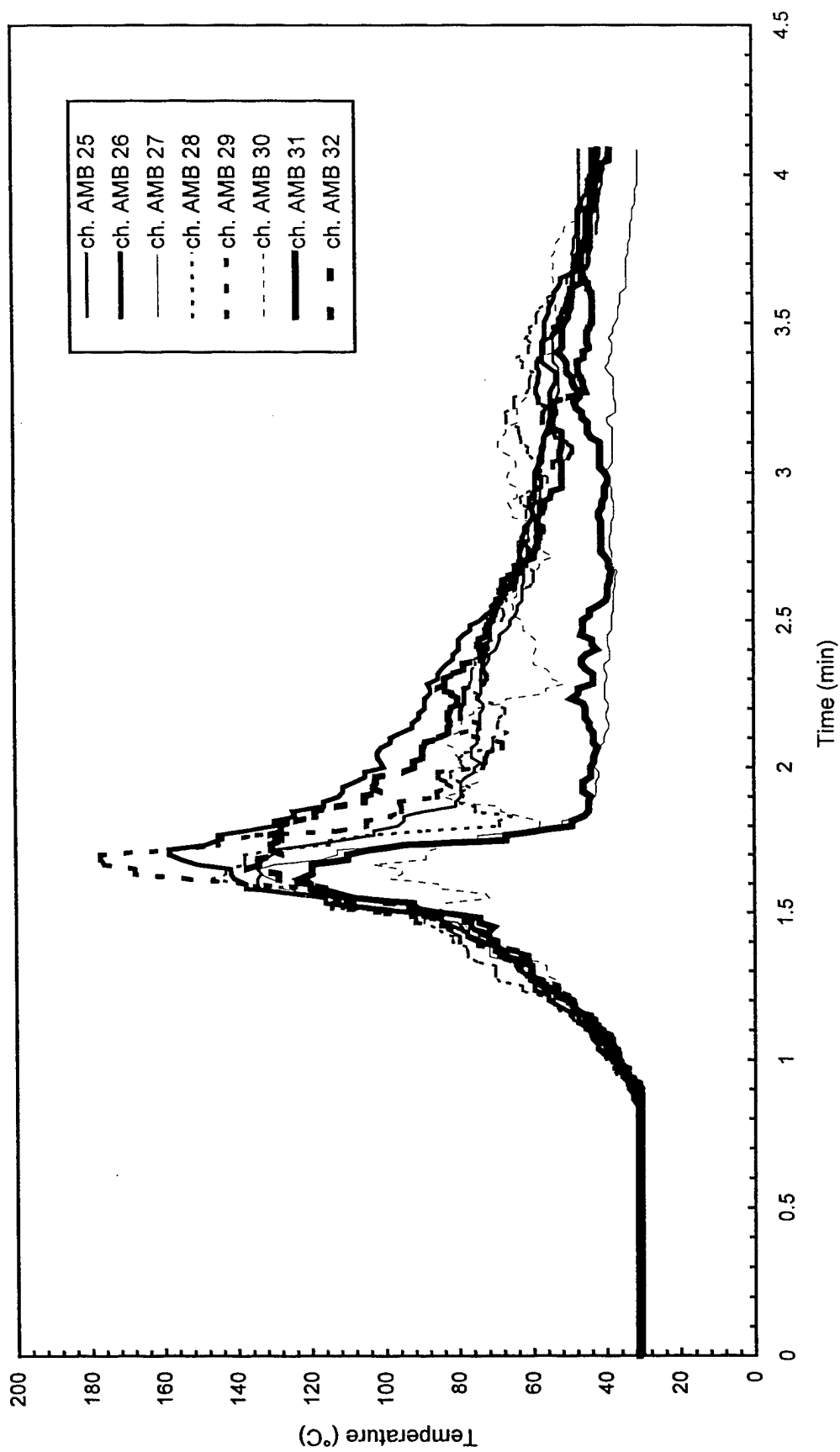


Fig. B59 - Air temperatures around North half of 7.6 m (25 ft) radius from center of pad

Test S4

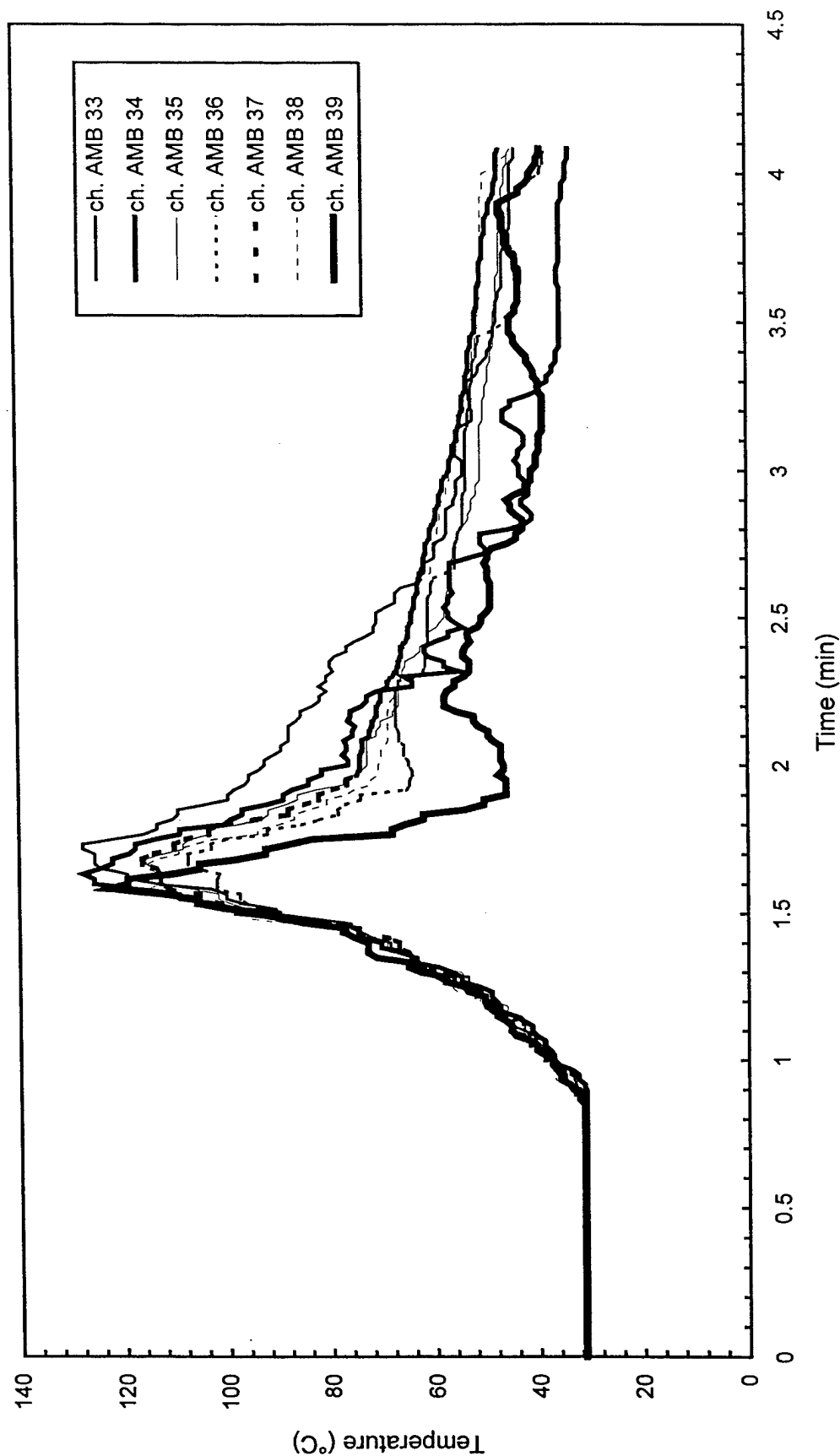


Fig. B60 - Air temperatures around South half of 7.6 m (25 ft) radius from center of pad

Test S4

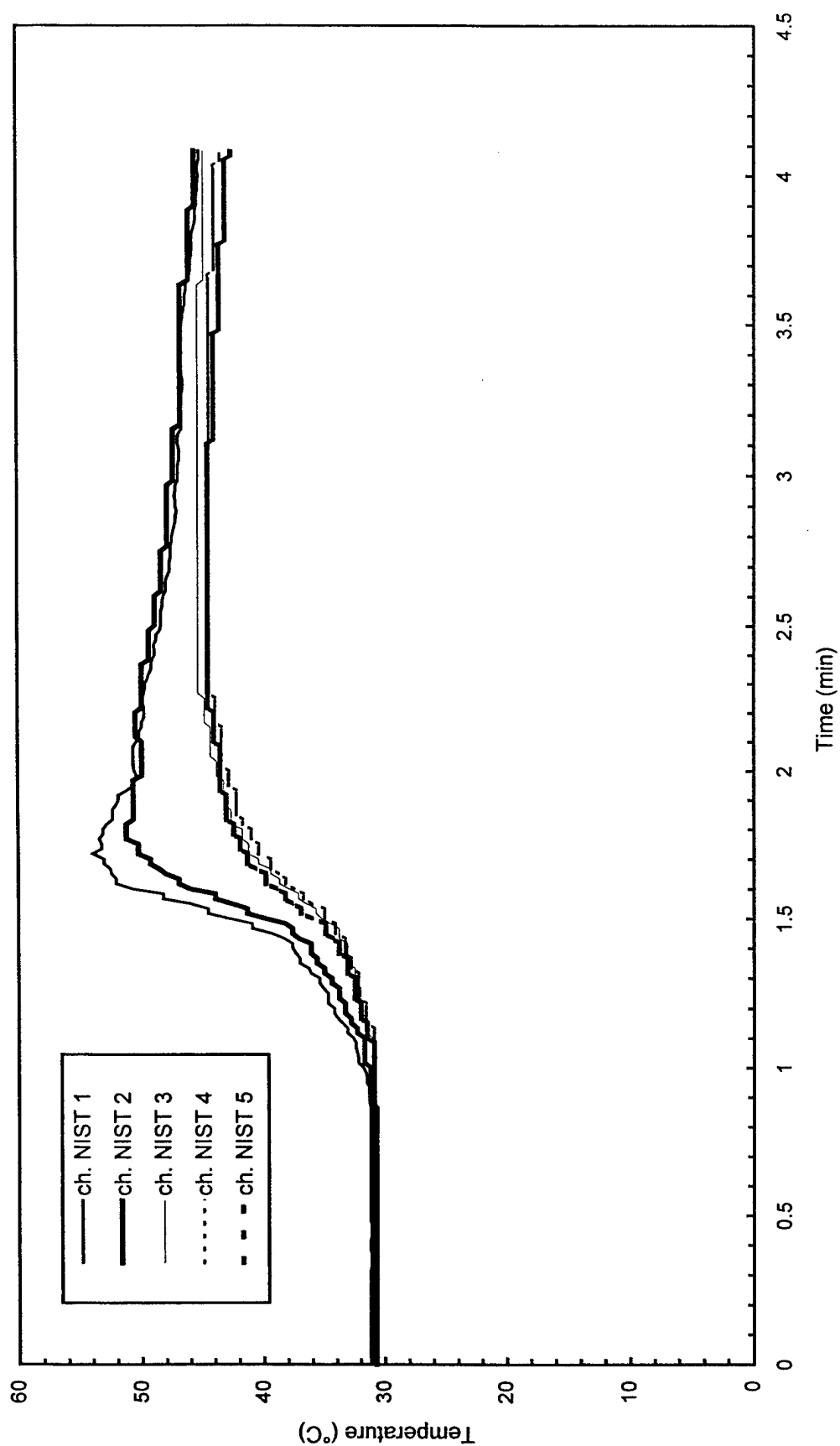


Fig. B61 - Temperature of West steel beam

Test S4

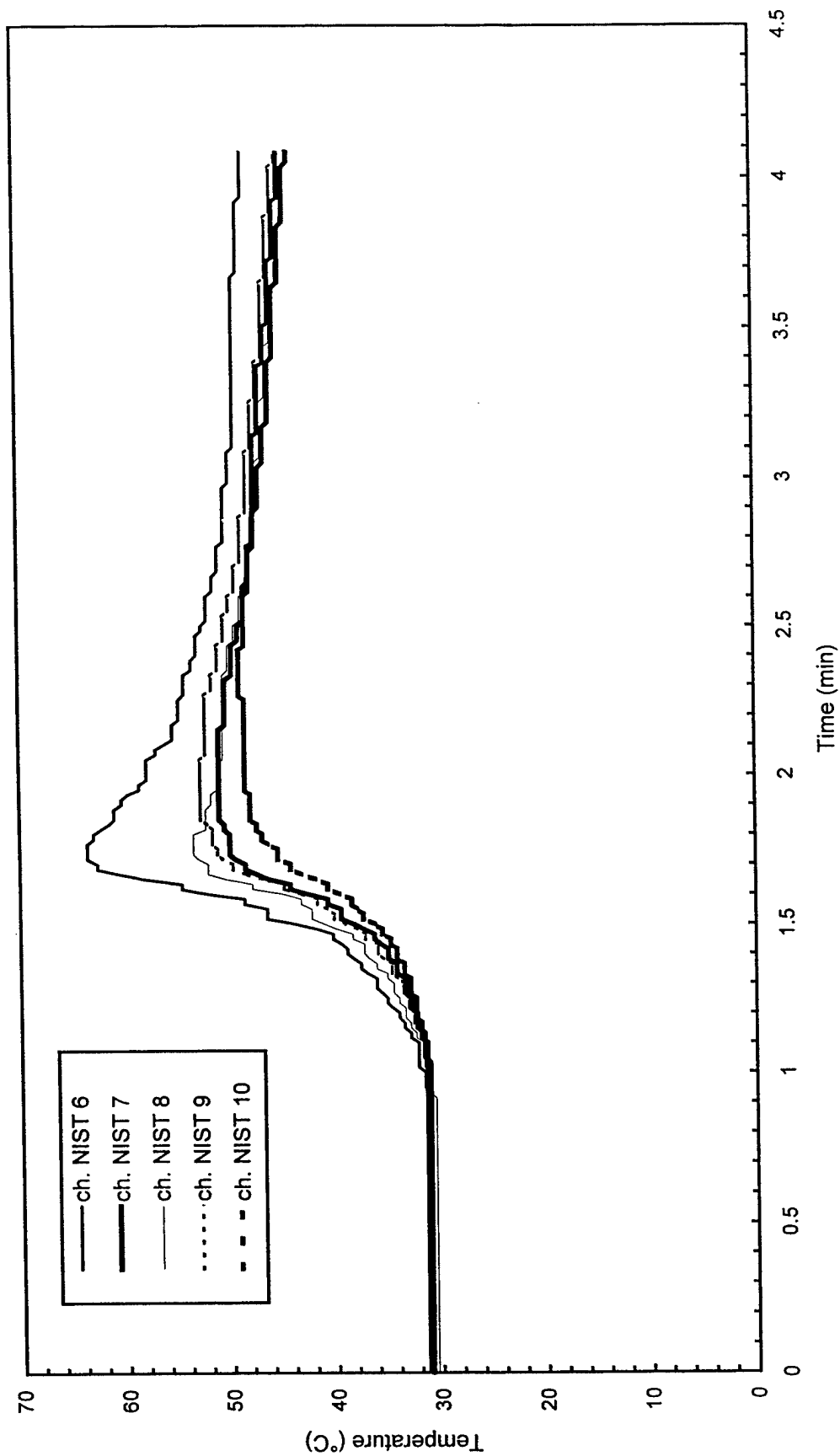


Fig. B62 - Temperature of North steel beam

Test S4

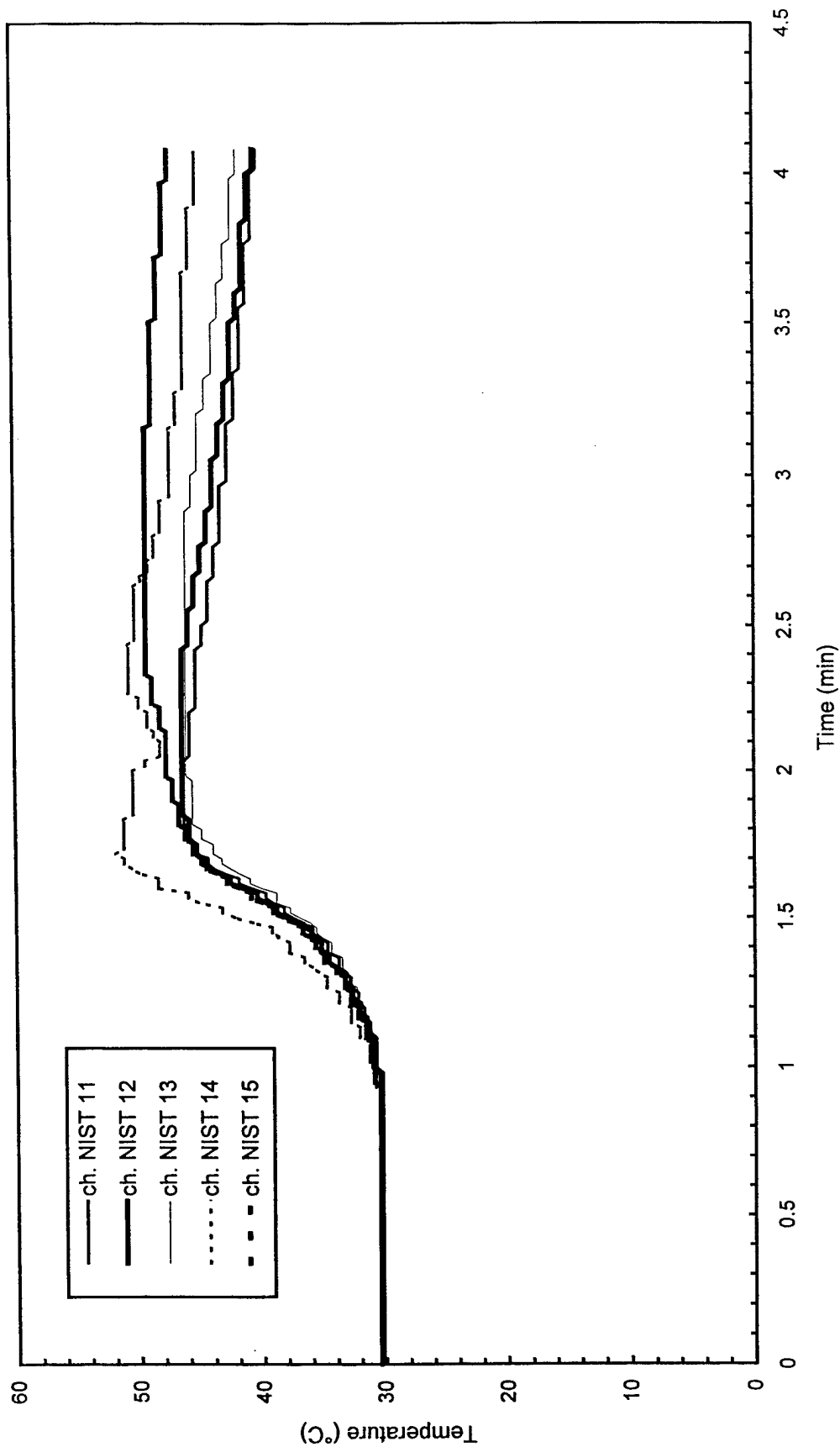


Fig. B63 - Temperature of East steel beam

Test S4

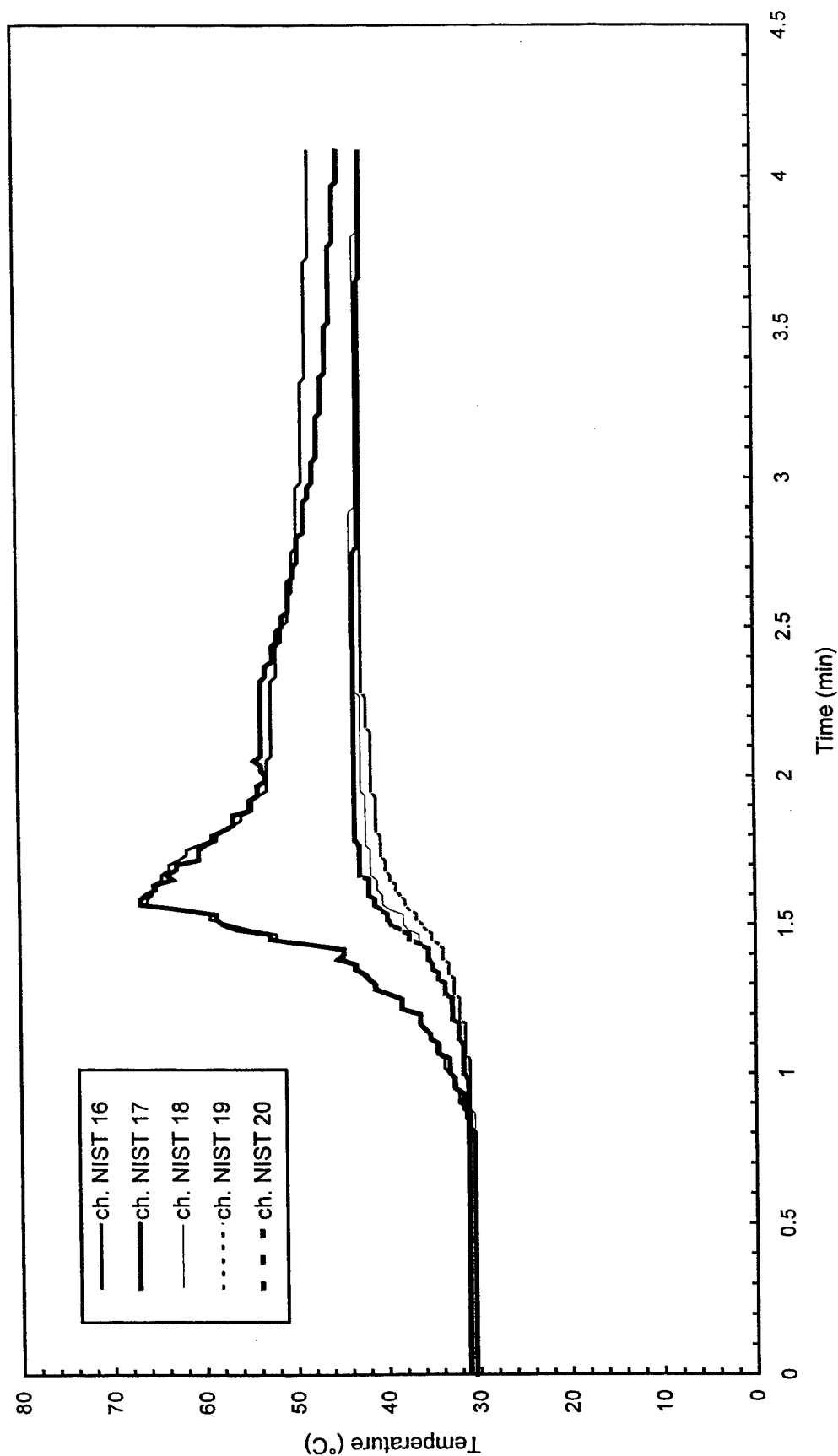


Fig. B64 - Temperature of South steel beam

Test S4

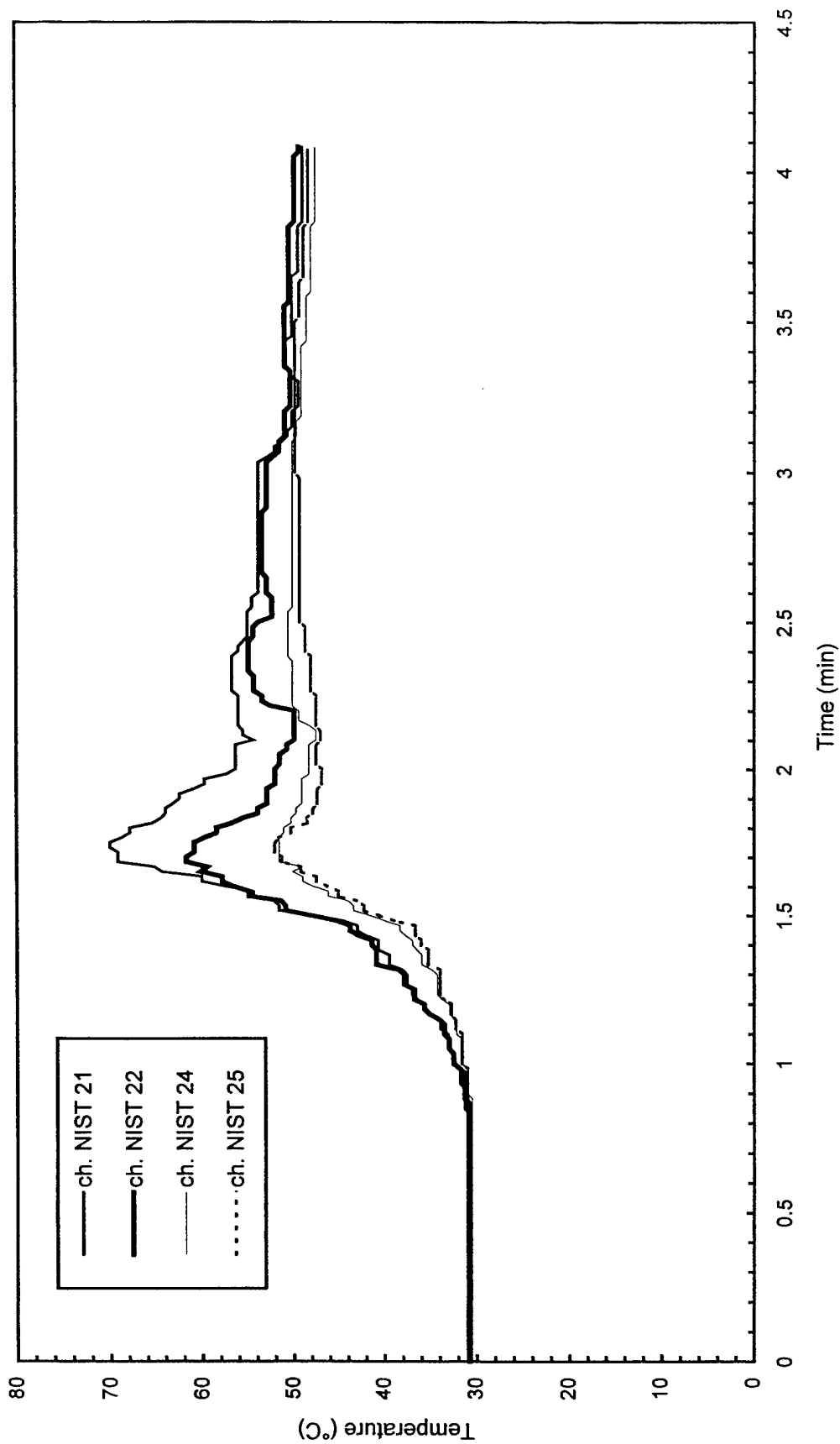


Fig. B65 - Temperature of Northwest steel beam

Test S4

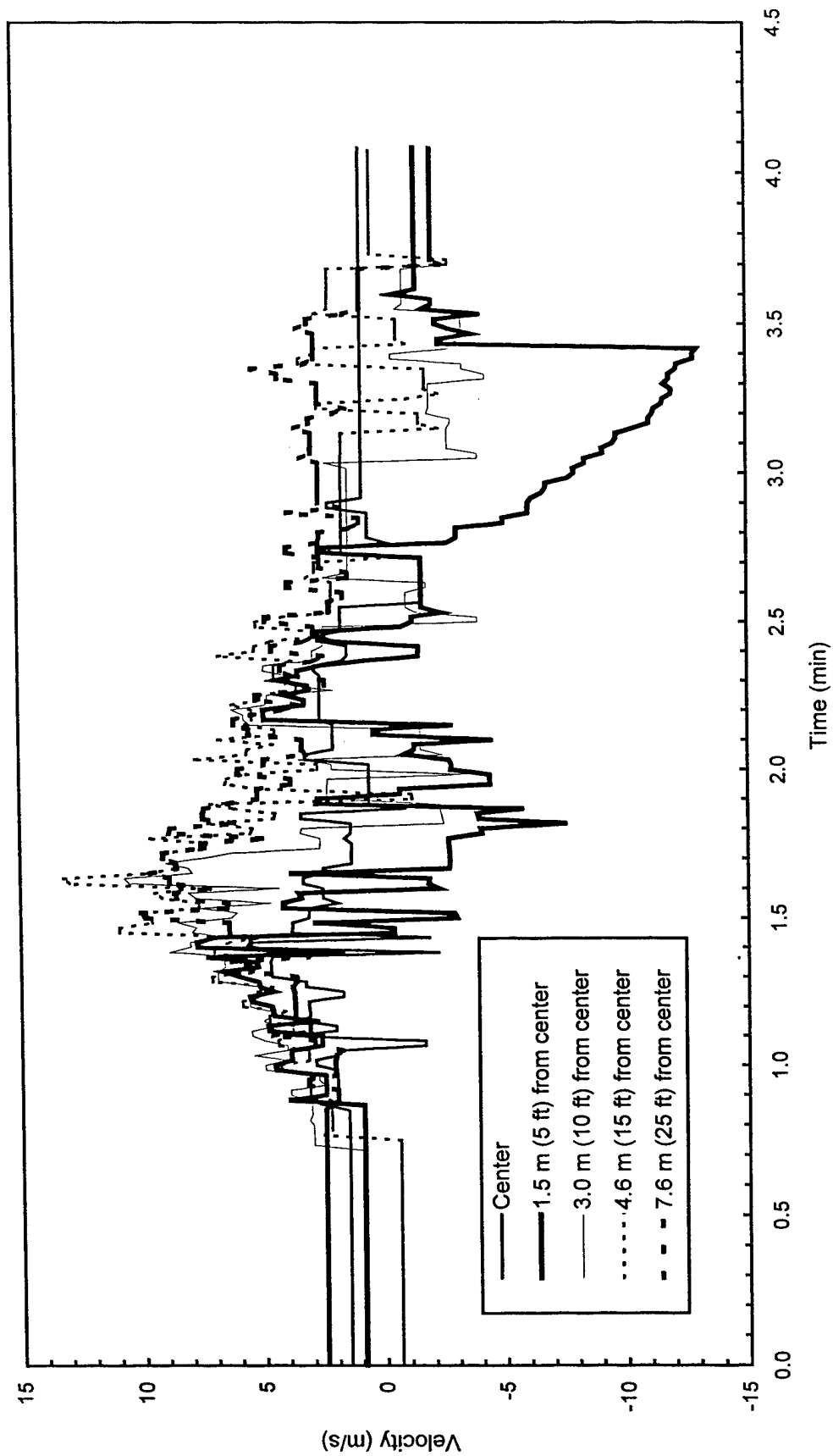


Fig. B66 - Plume and ceiling jet velocities

Test S4

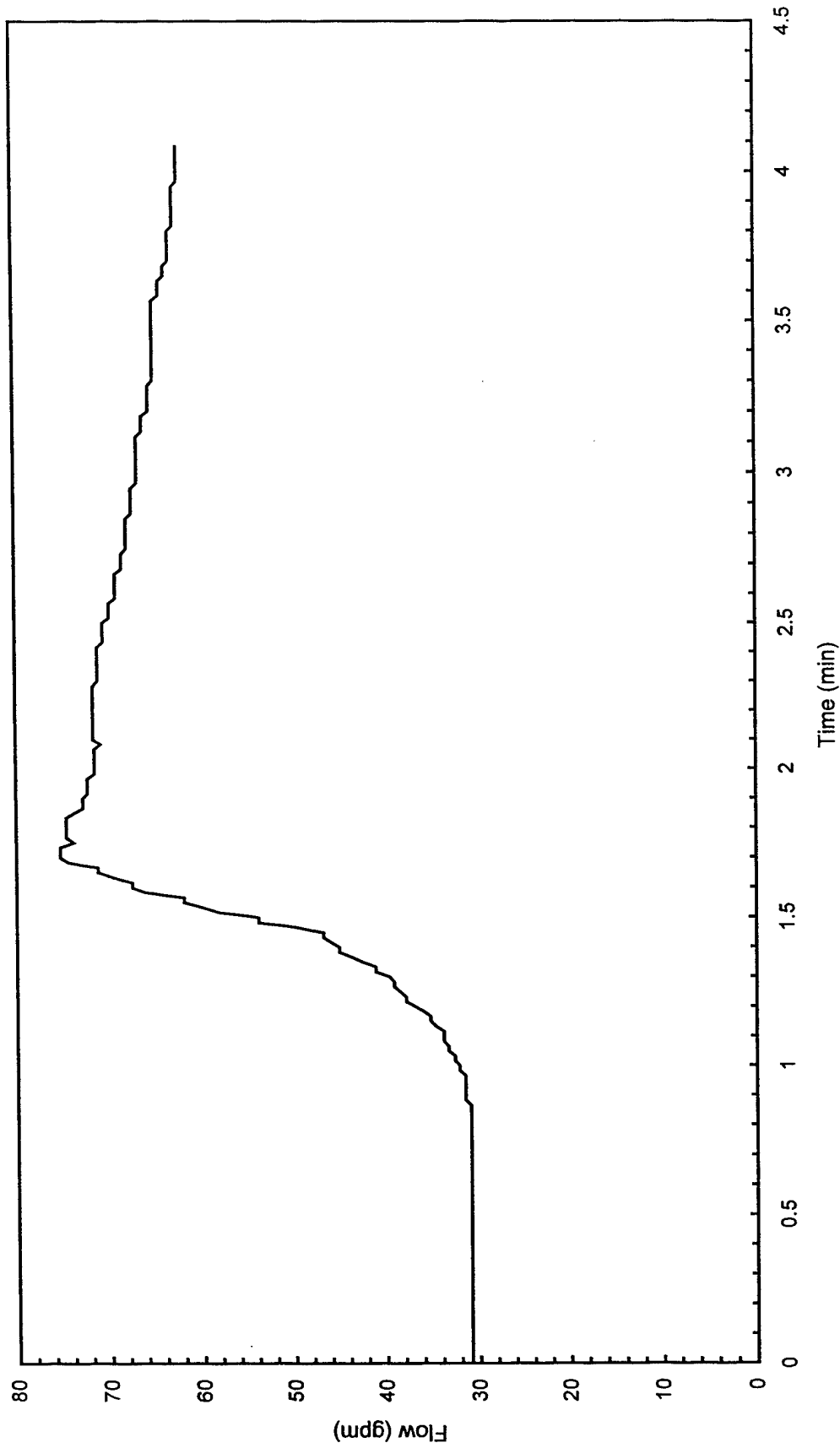


Fig. B67 - Sprinkler system flowrate

Test S4

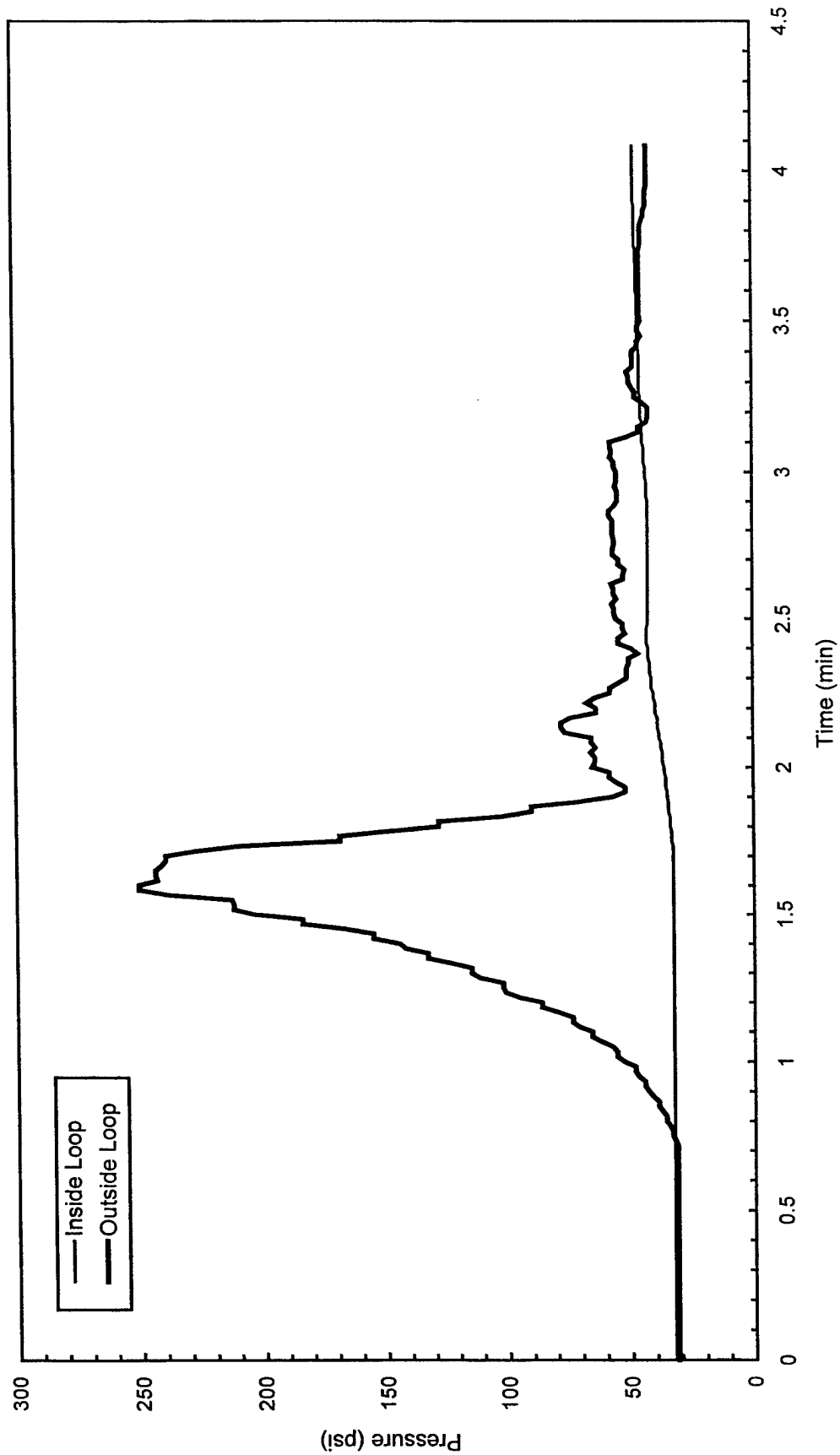


Fig. B68 - Sprinkler system pressure

Test S5

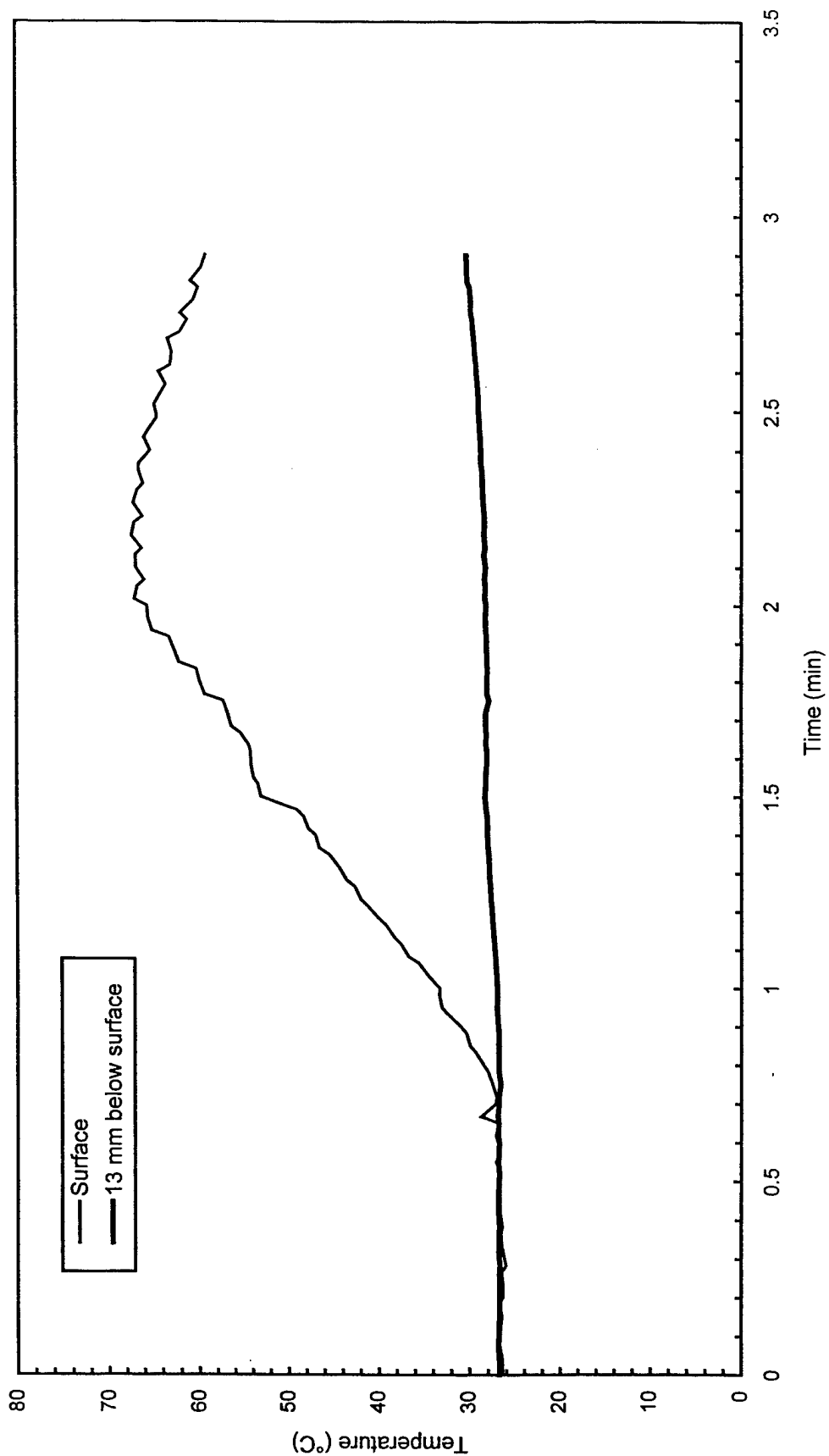


Fig. B69 - Concrete temperatures at center of pad

Test S5

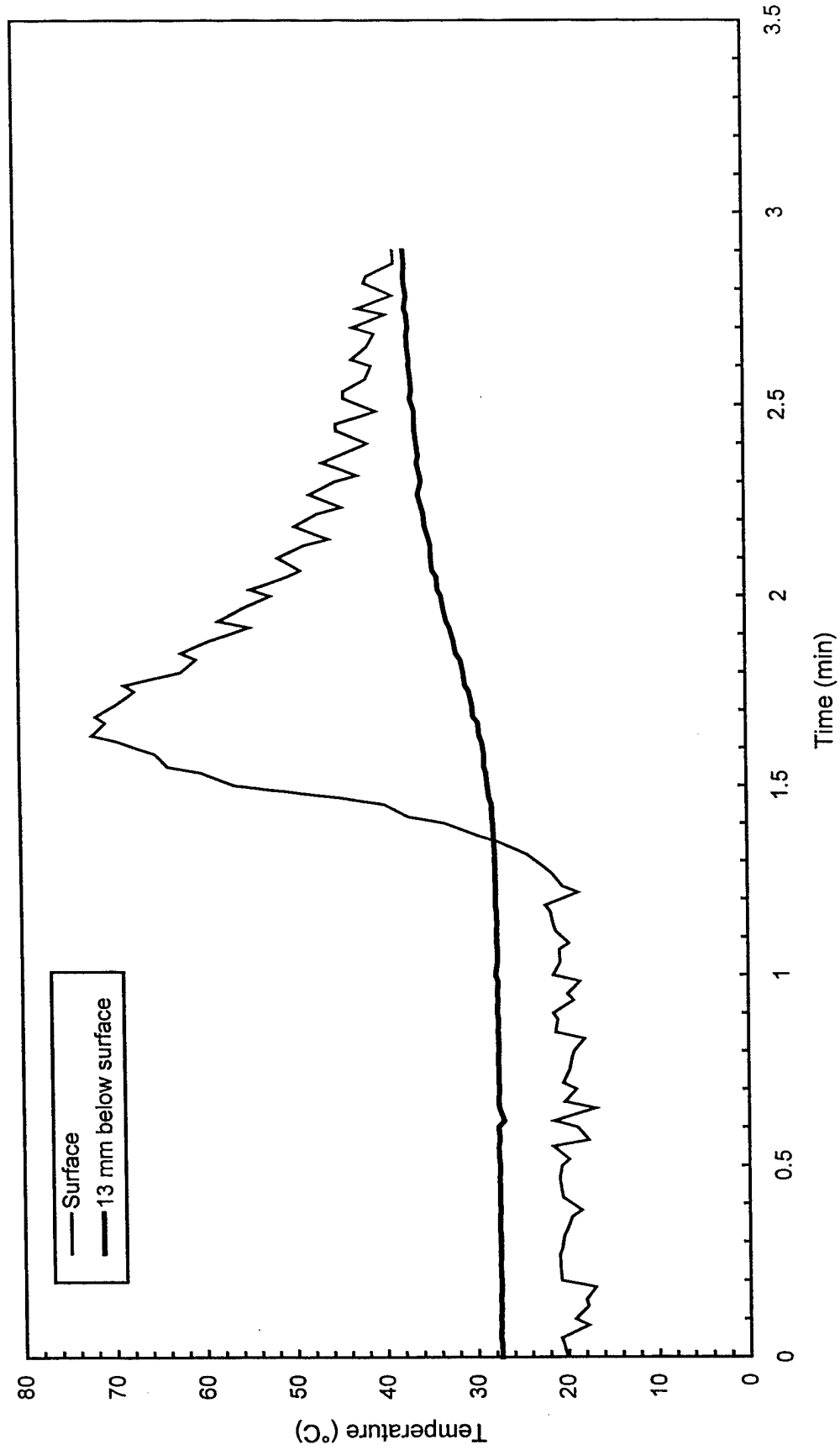


Fig. B70 - Concrete temperatures 3 m (10 ft) East of center of pad

Test S5

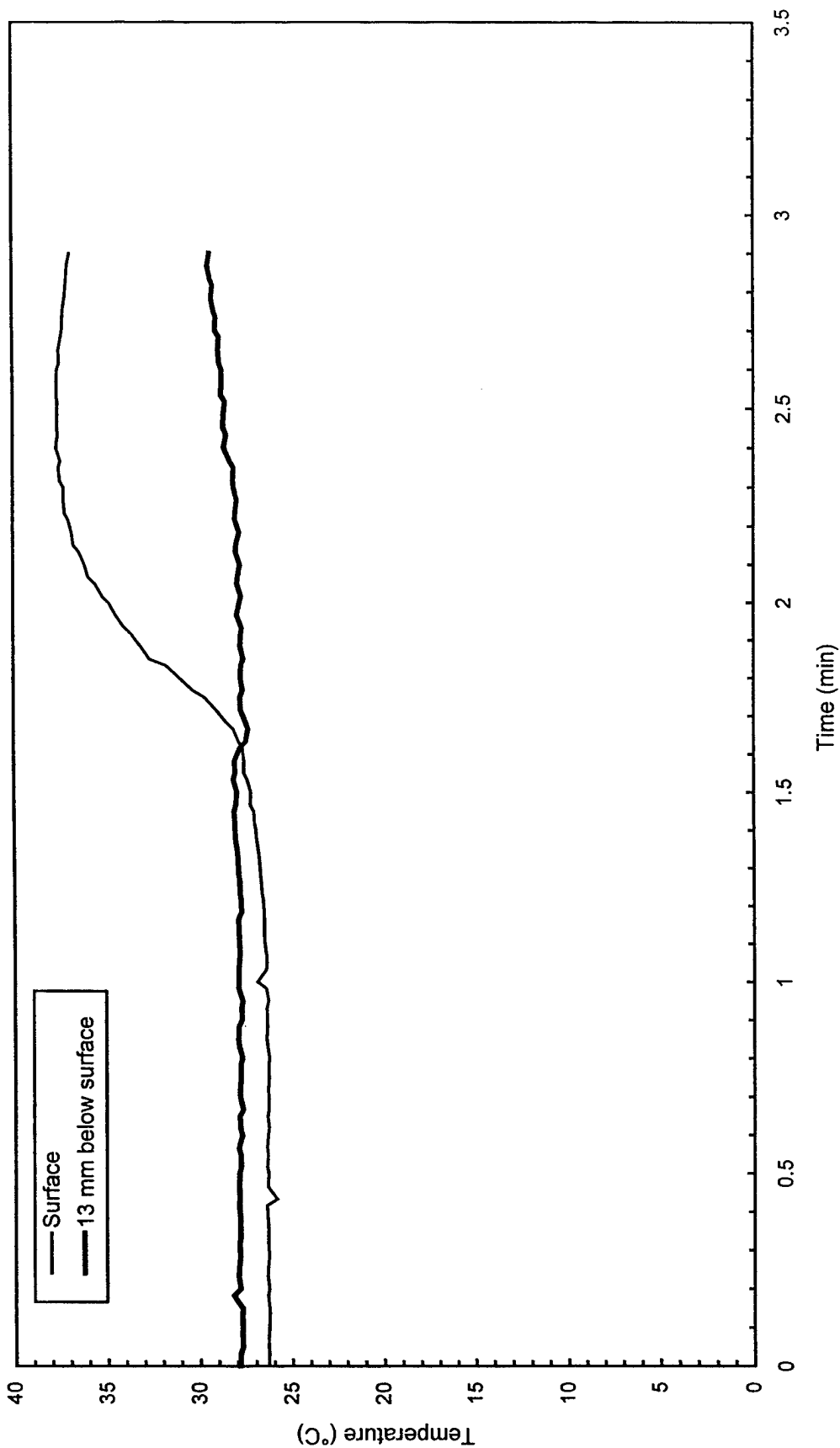


Fig. B71 - Concrete temperatures 3 m (10 ft) West of center of pad

Test S5

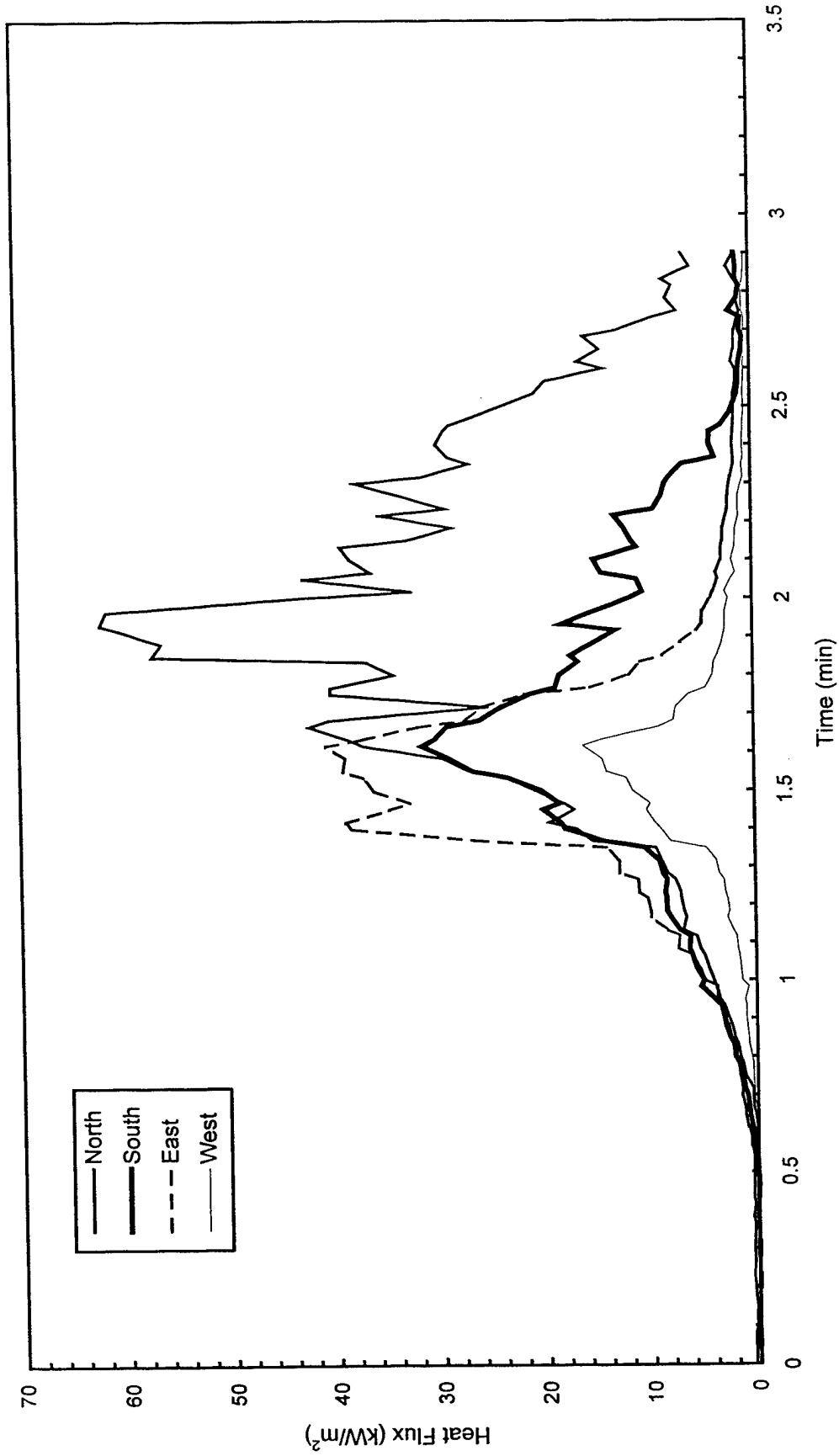


Fig. B72 - Heat flux measured at edge of pad

Test S5

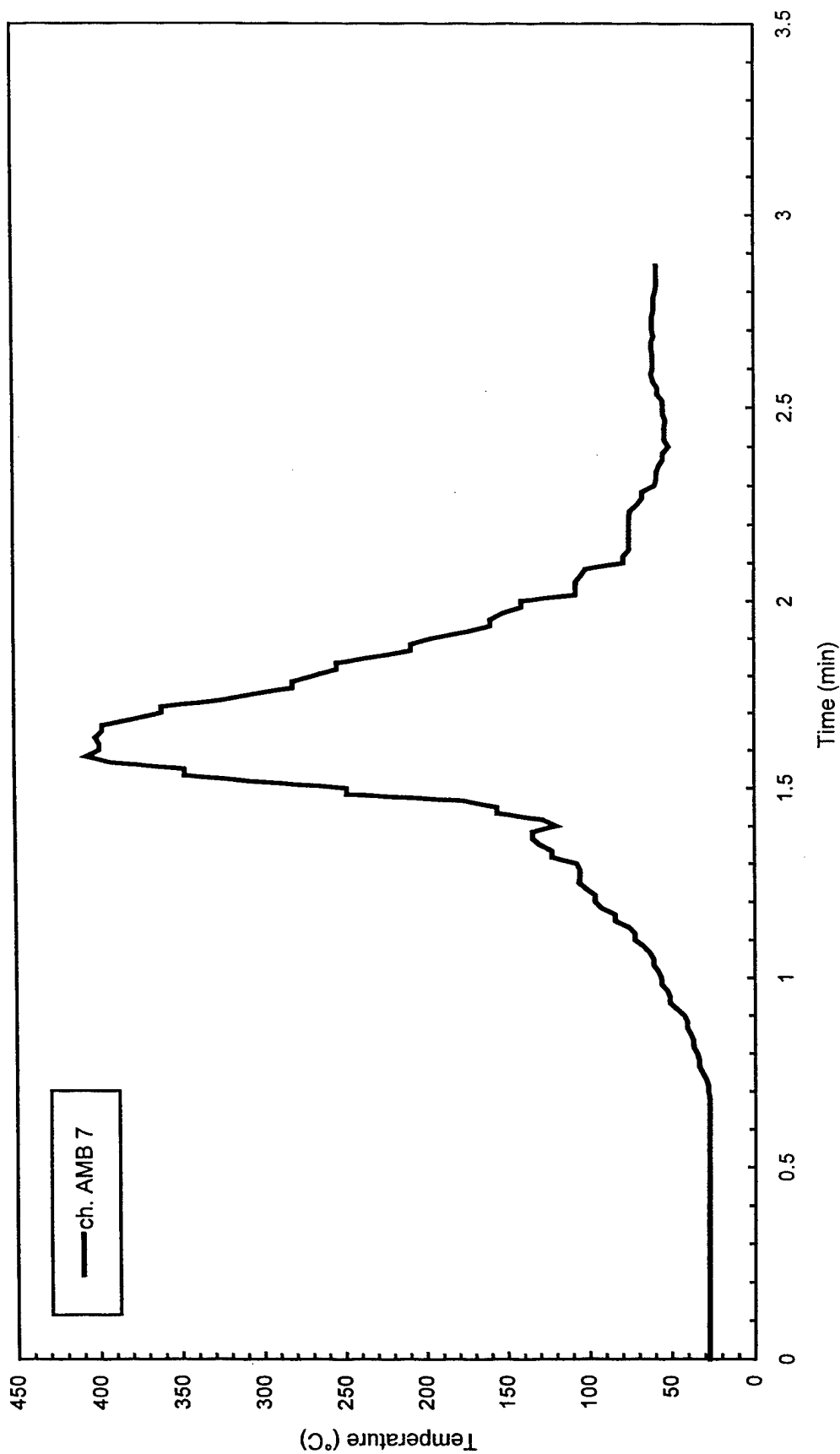


Fig. B73 - Air temperatures over center of pad

Test S5

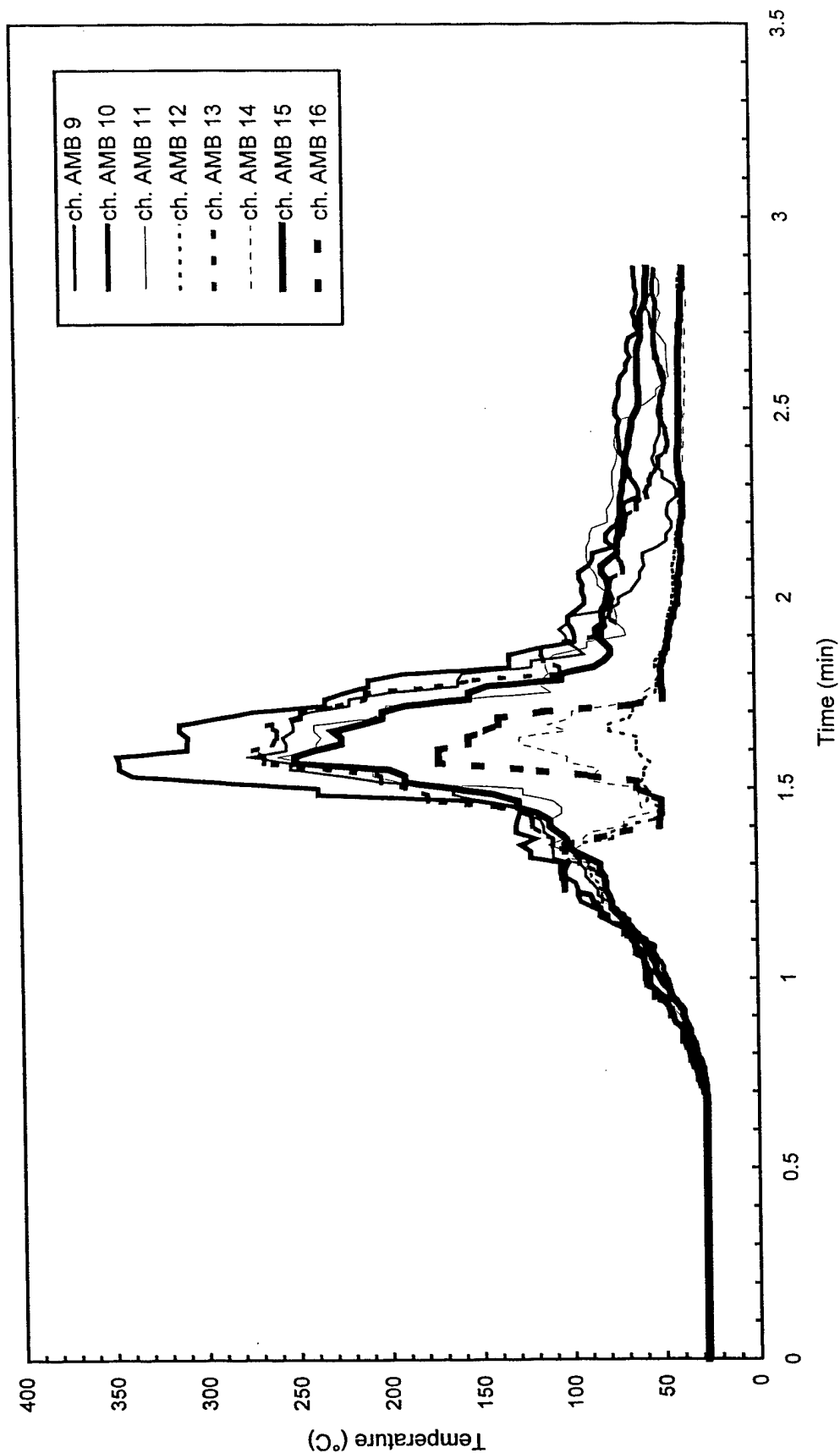


Fig. B74 - Air temperatures around 3 m (10 ft) radius from center of pad

Test S5

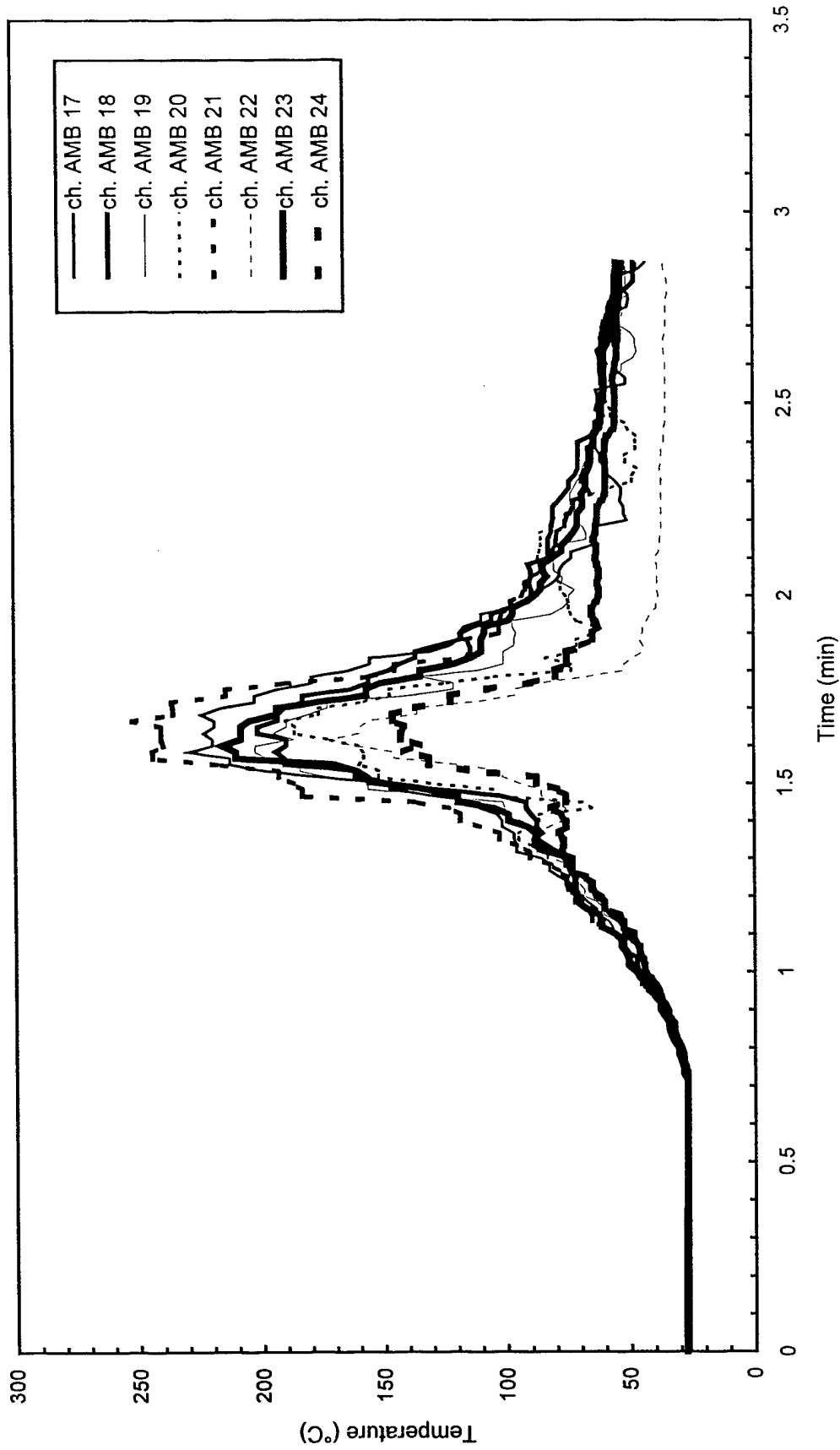


Fig. B75 - Air temperatures around 4.6 m (15 ft) radius from center of pad

Test S5

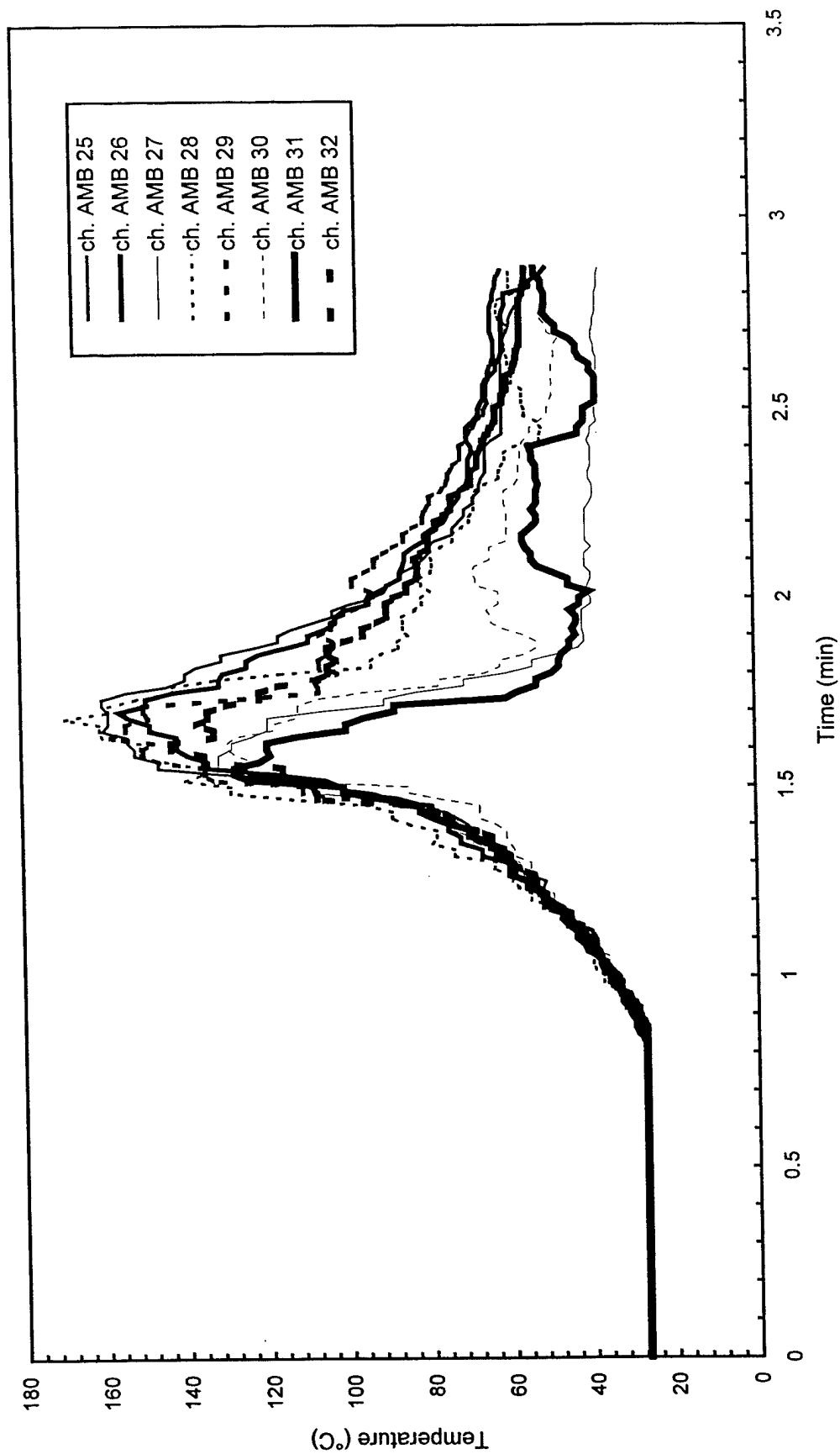


Fig. B76 - Air temperatures around North half of 7.6 m (25 ft) radius from center of pad

Test S5

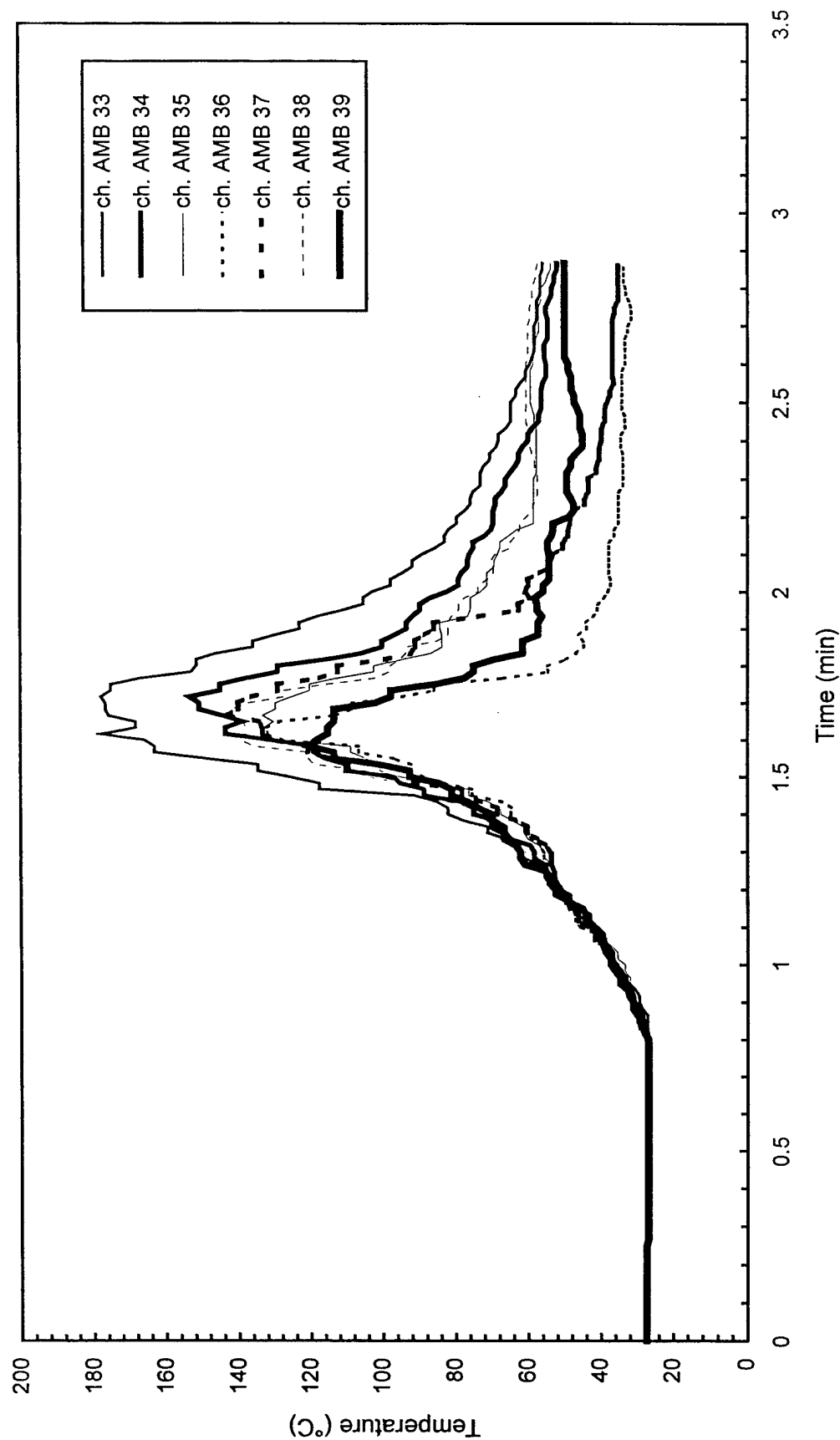


Fig. B77 - Air temperatures around South half of 7.6 m (25 ft) radius from center of pad

Test S5

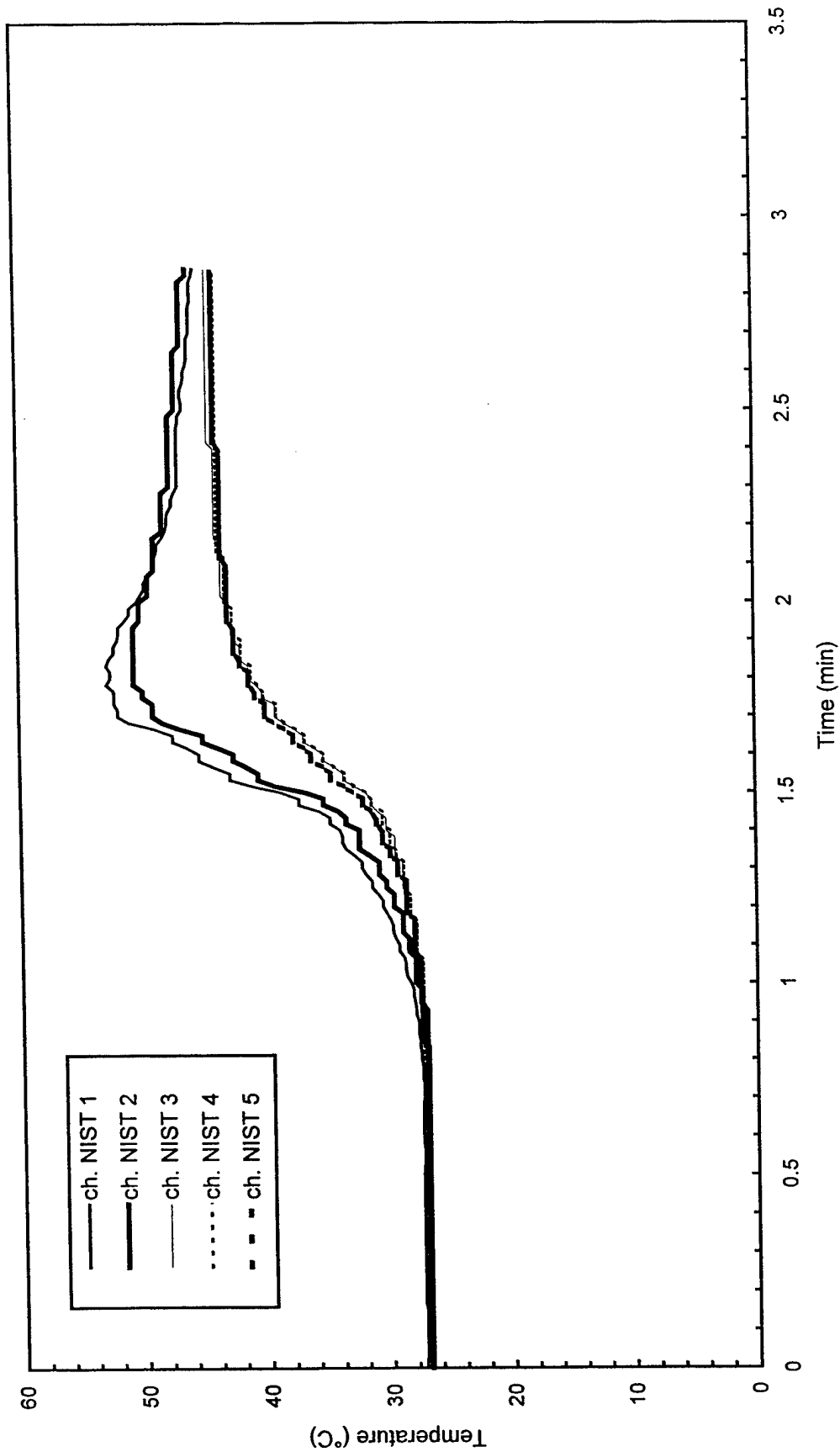


Fig. B78 - Temperature of West steel beam

Test S5

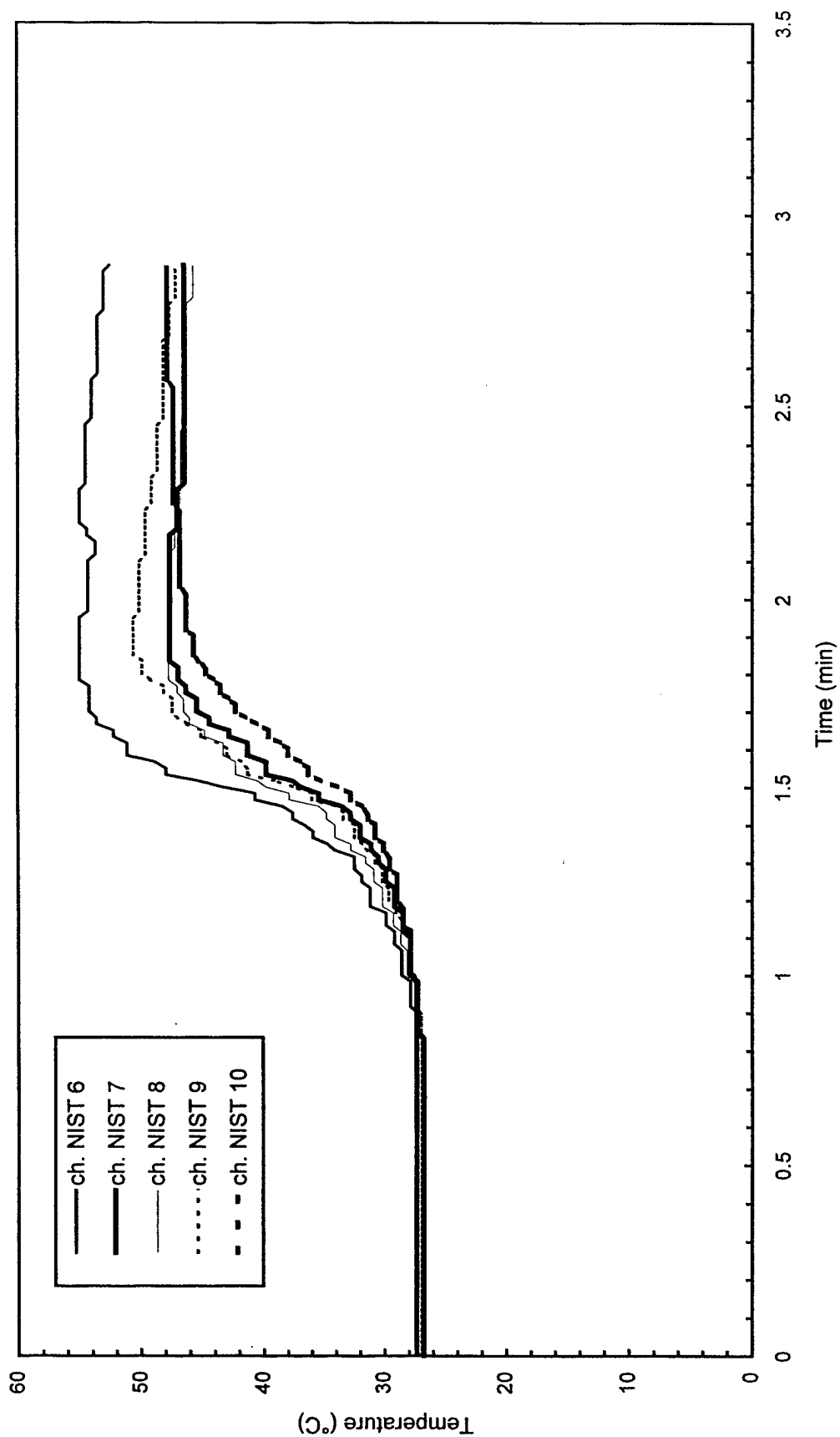


Fig. B79 - Temperature of North steel beam

Test S5

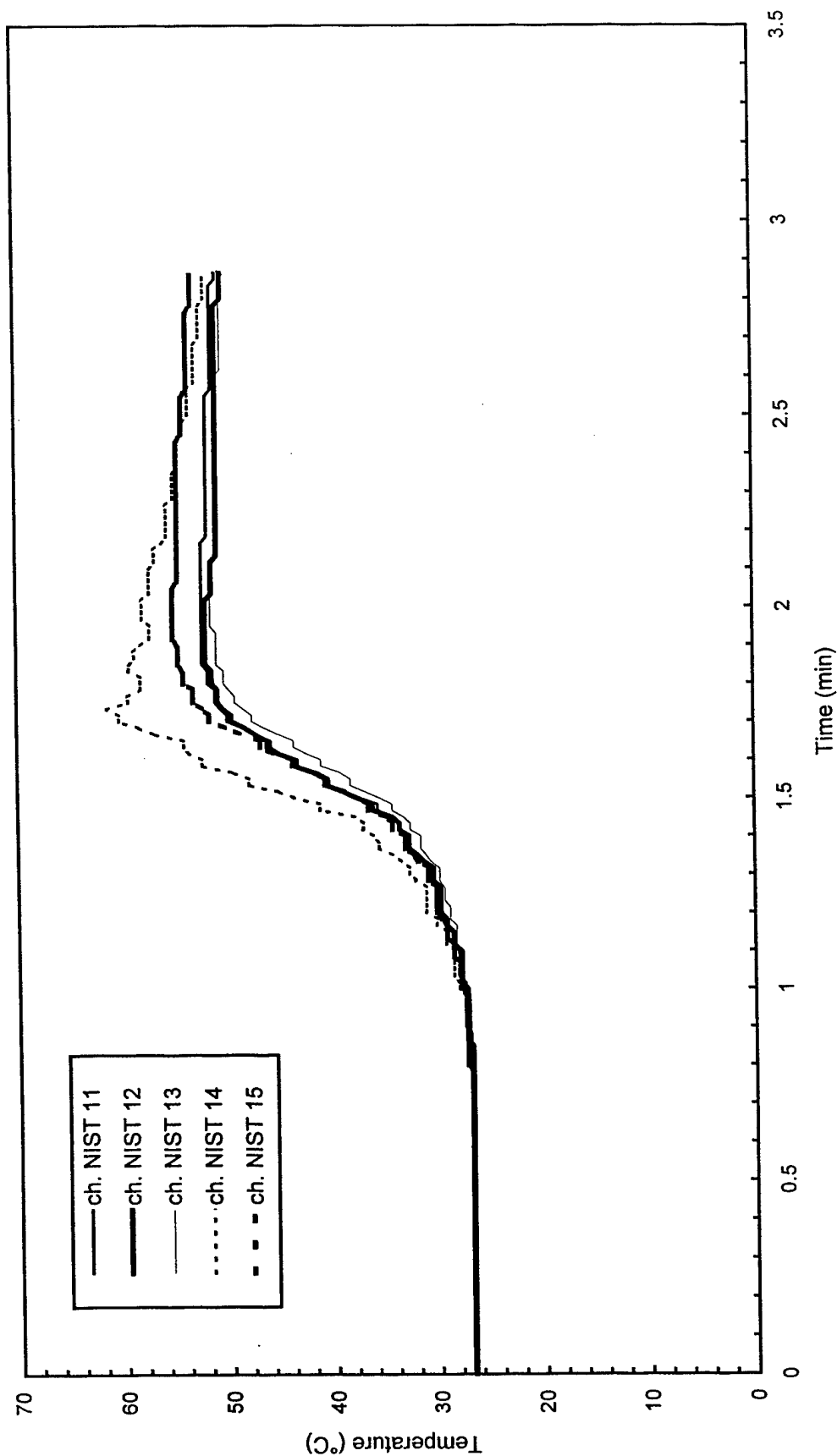


Fig. B80 - Temperature of East steel beam

Test S5

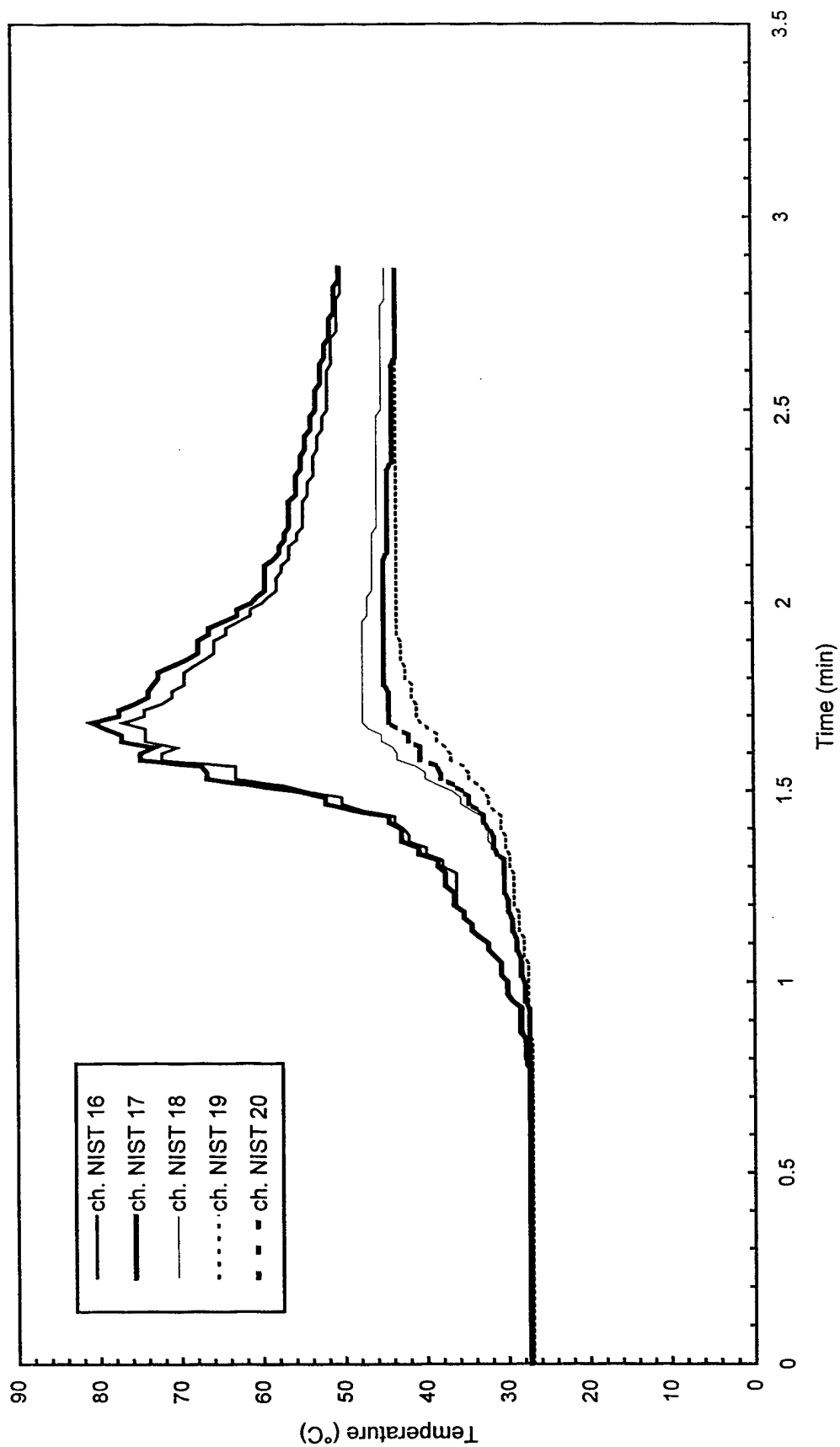


Fig. B81 - Temperature of South steel beam

Test S5

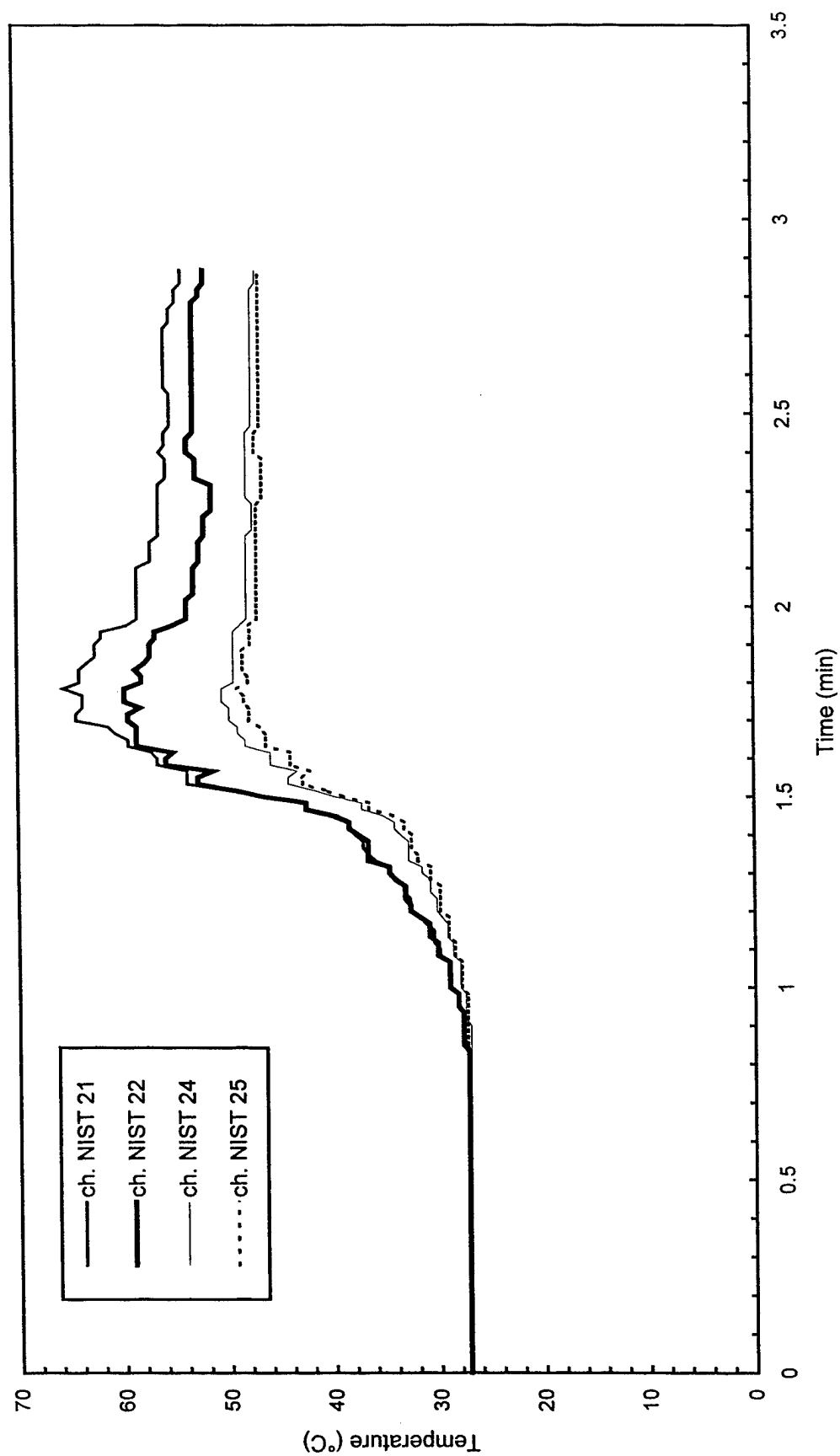


Fig. B82 - Temperature of Northwest steel beam

Test S5

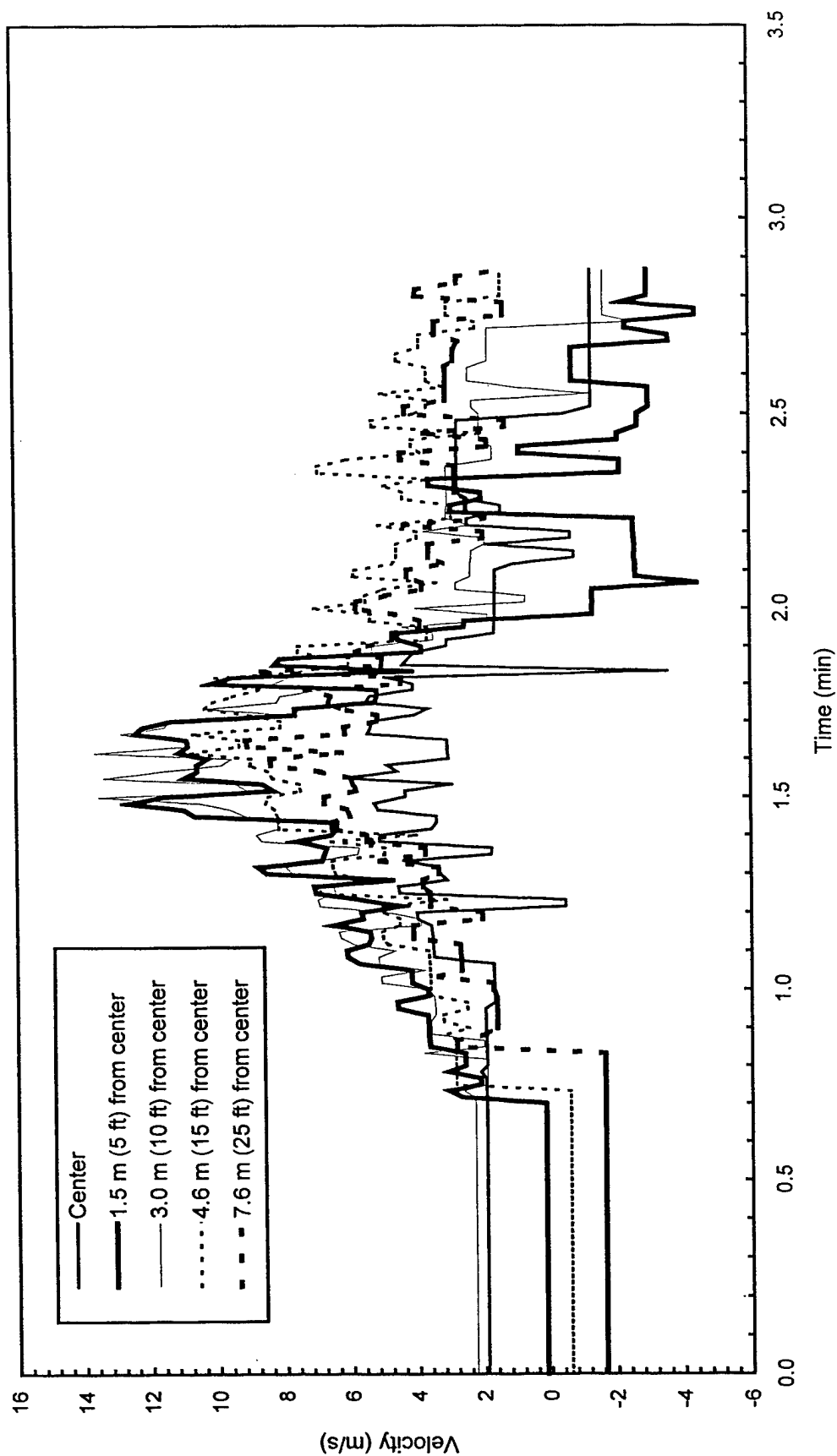


Fig. B83 - Plume and ceiling jet velocities

Test S5

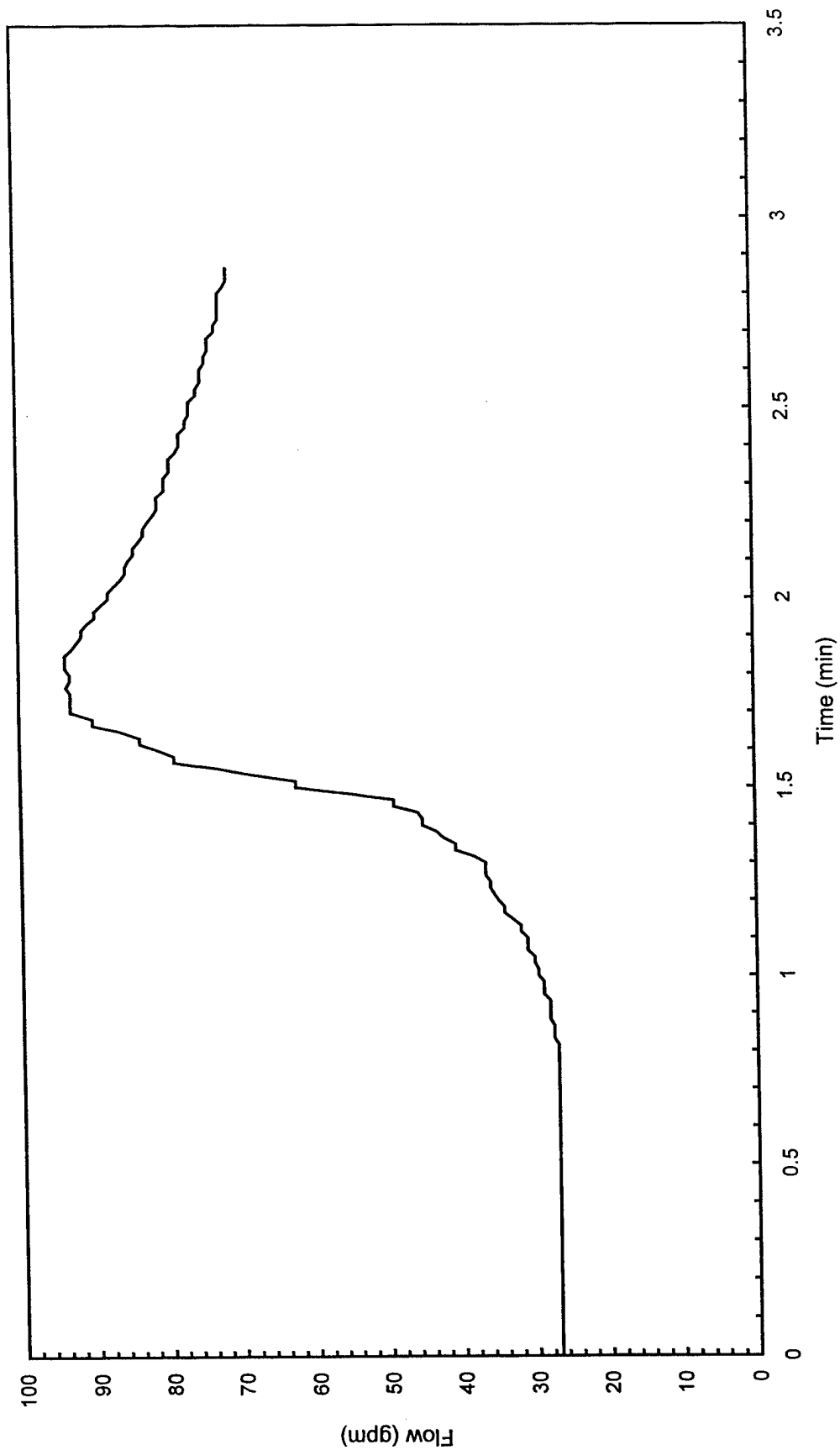


Fig. B84 - Sprinkler system flowrate

Test S5

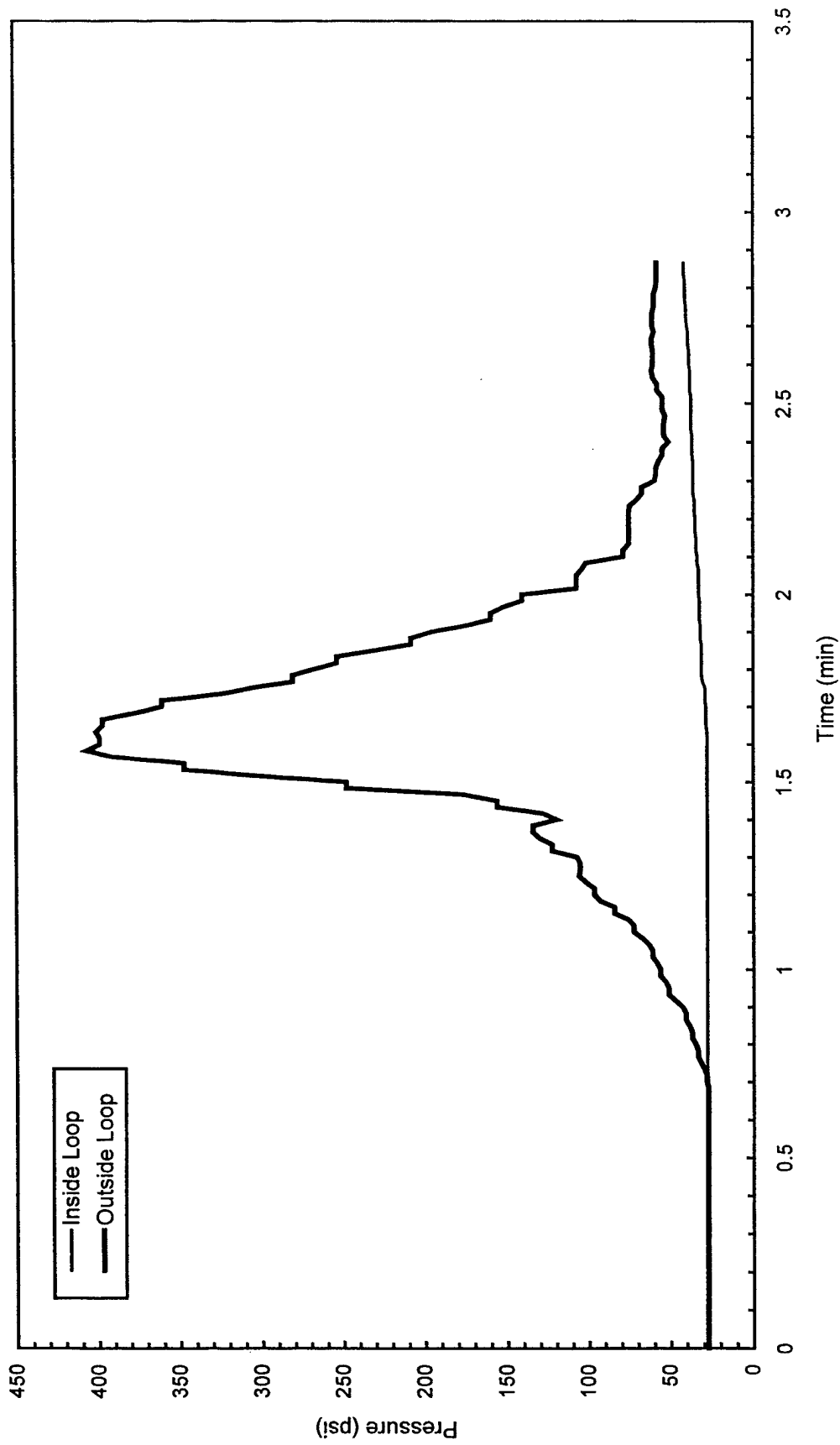


Fig. B85 - Sprinkler system pressure

Test S6

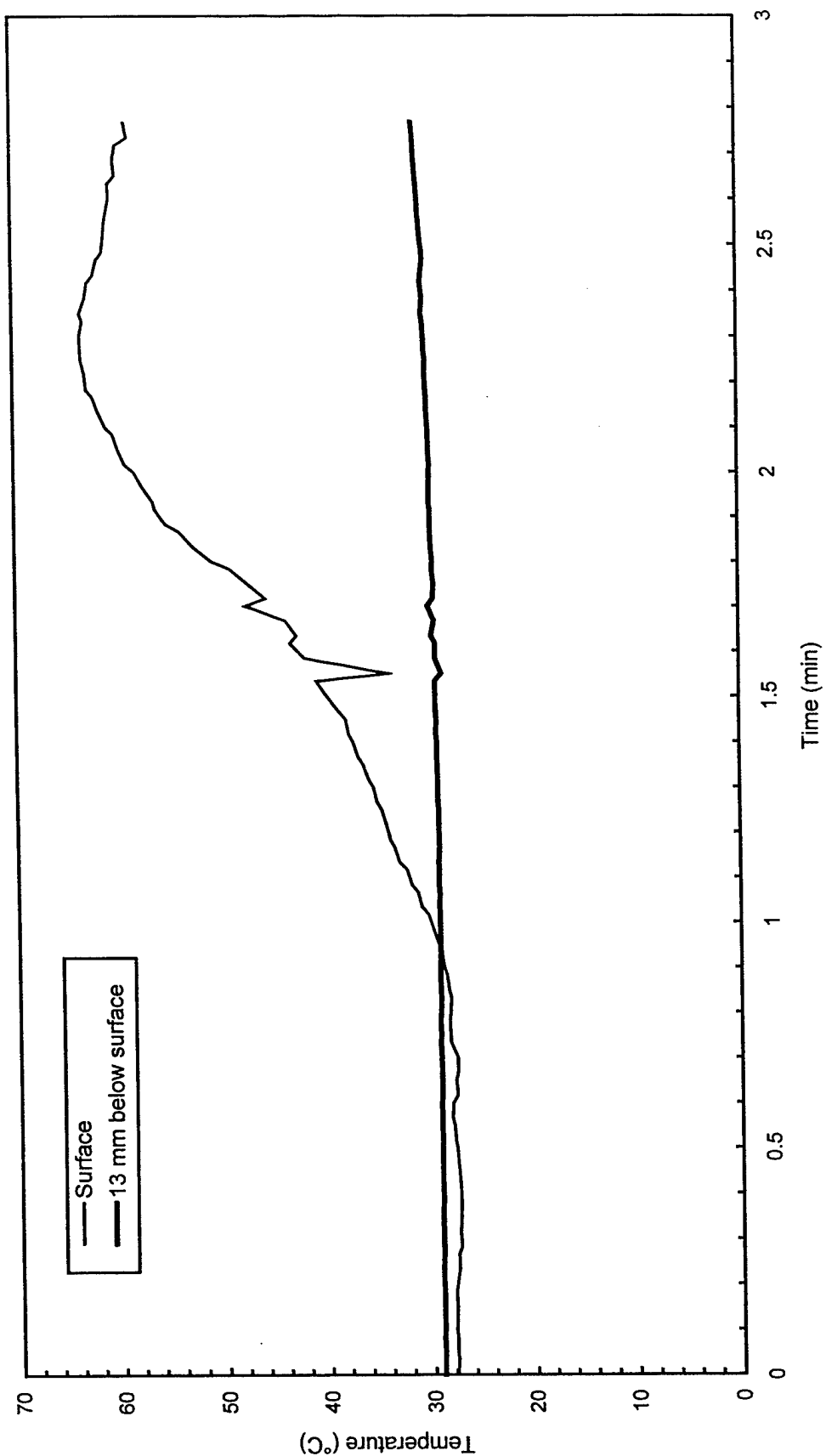


Fig. B86 - Concrete temperatures at center of pad

Test S6

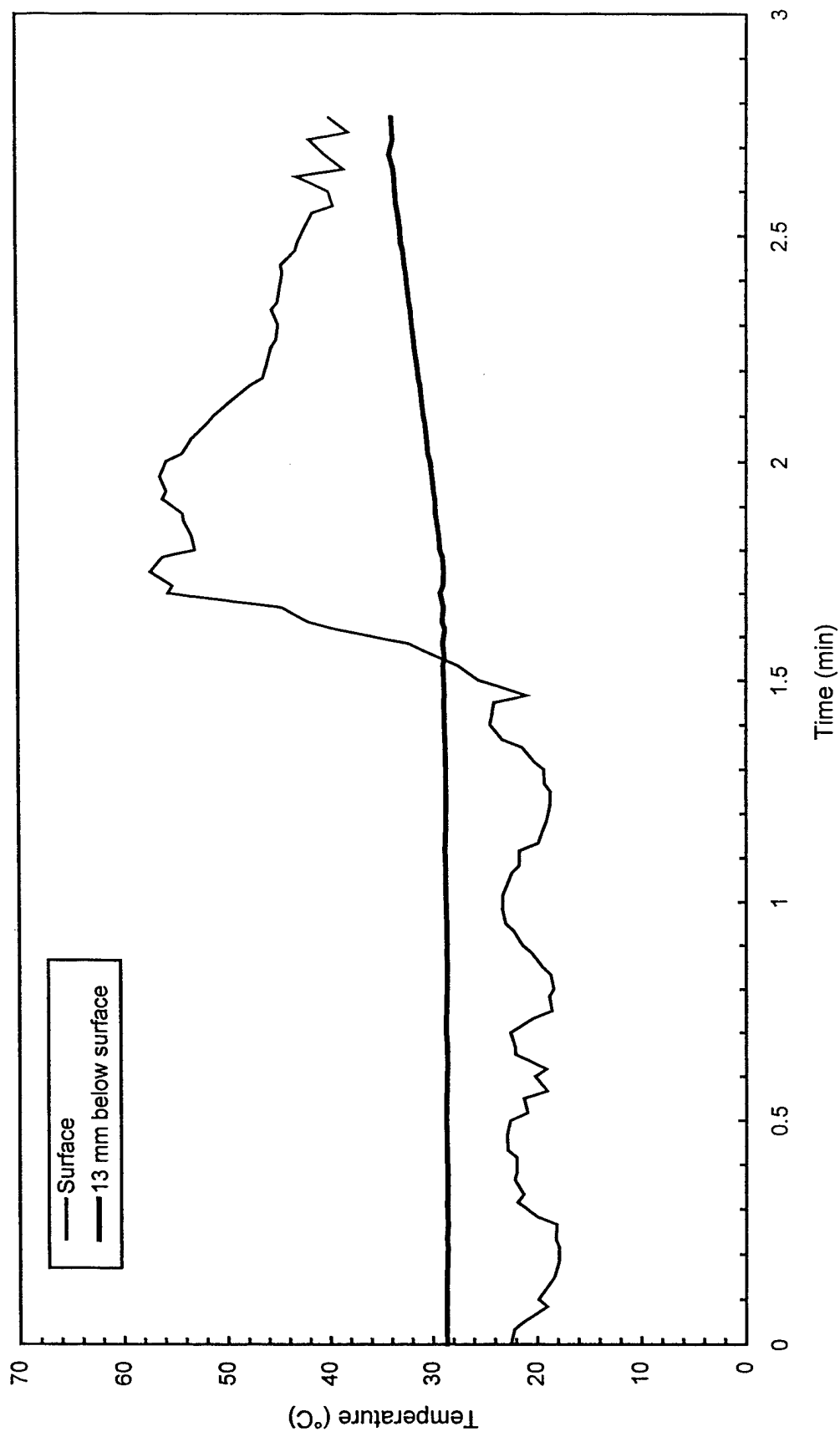


Fig. B87 - Concrete temperatures 3 m (10 ft) East of center of pad

Test S6

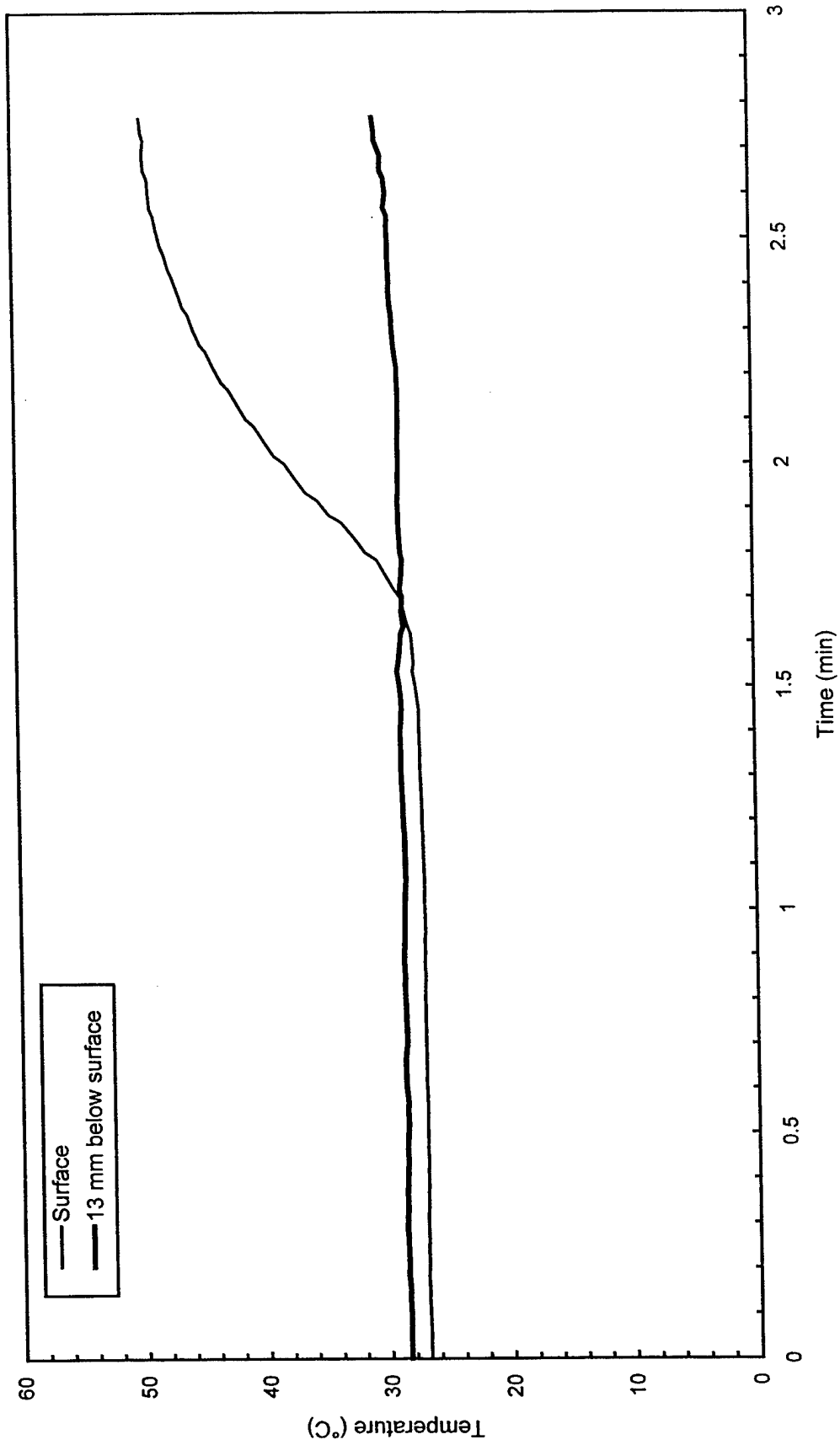


Fig. B88 - Concrete temperatures 3 m (10 ft) West of center of pad

Test S6

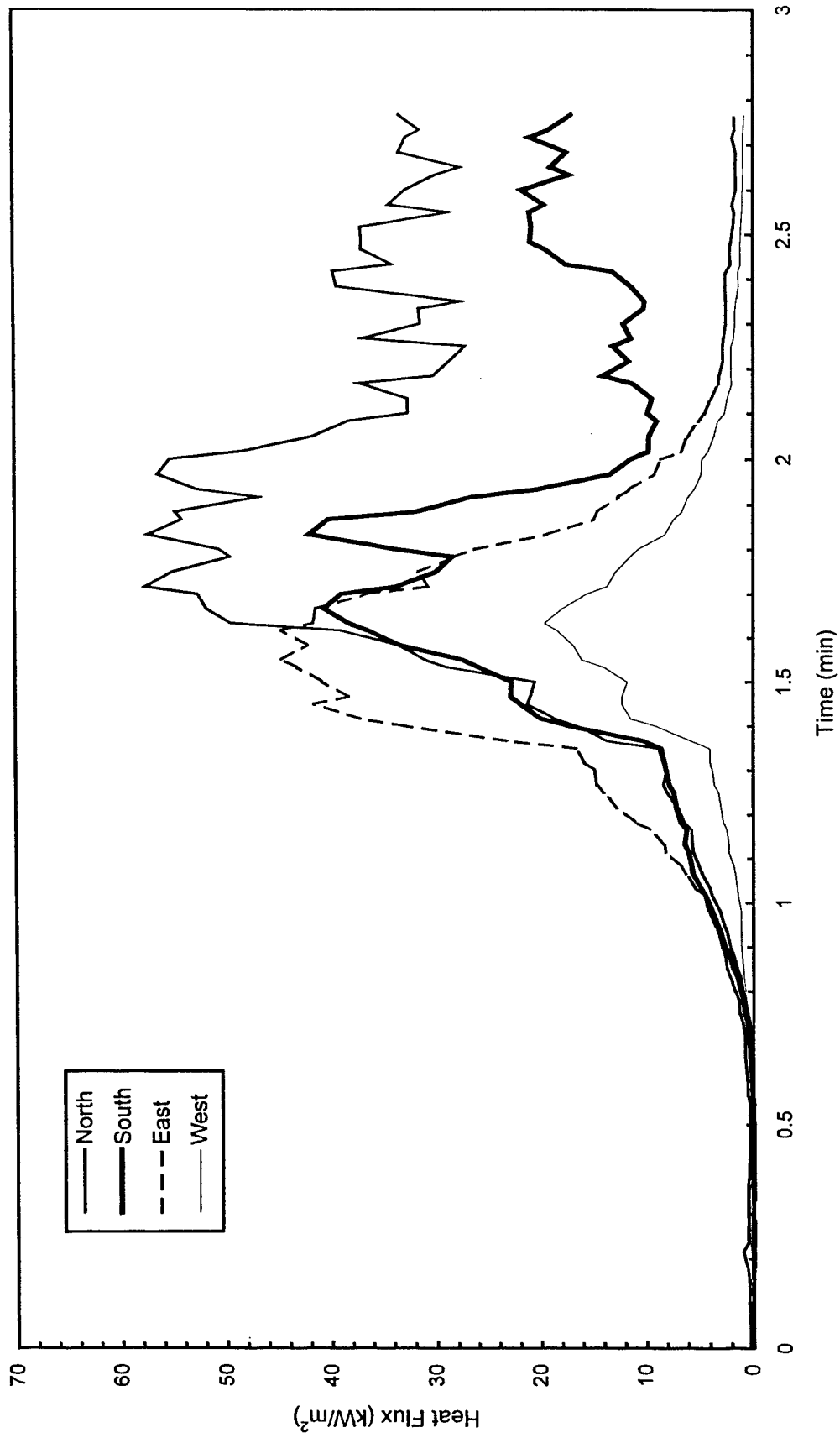


Fig. B89 - Heat flux measured at edge of pad

Test S6

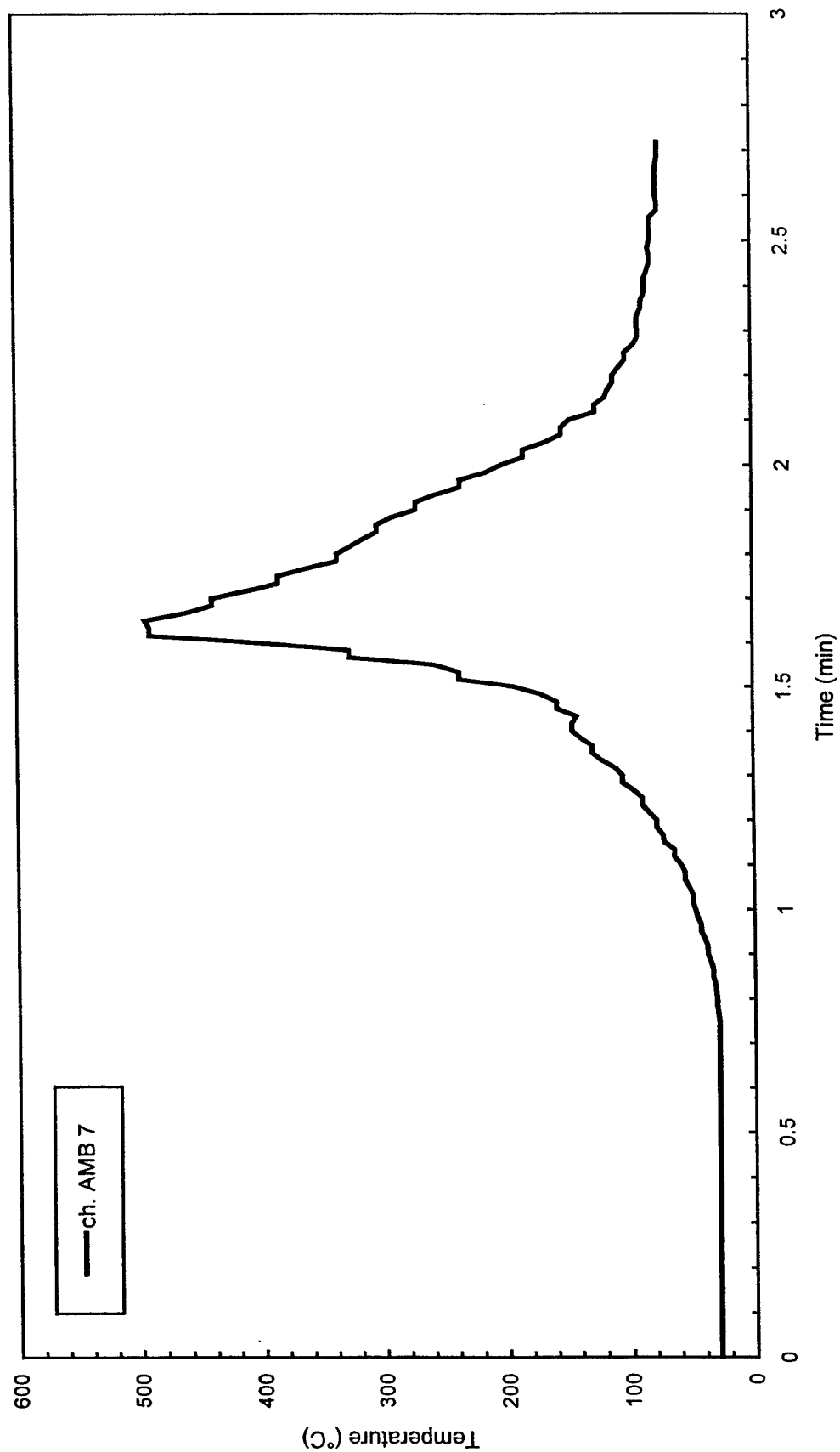


Fig. B90 - Air temperatures over center of pad

Test S6

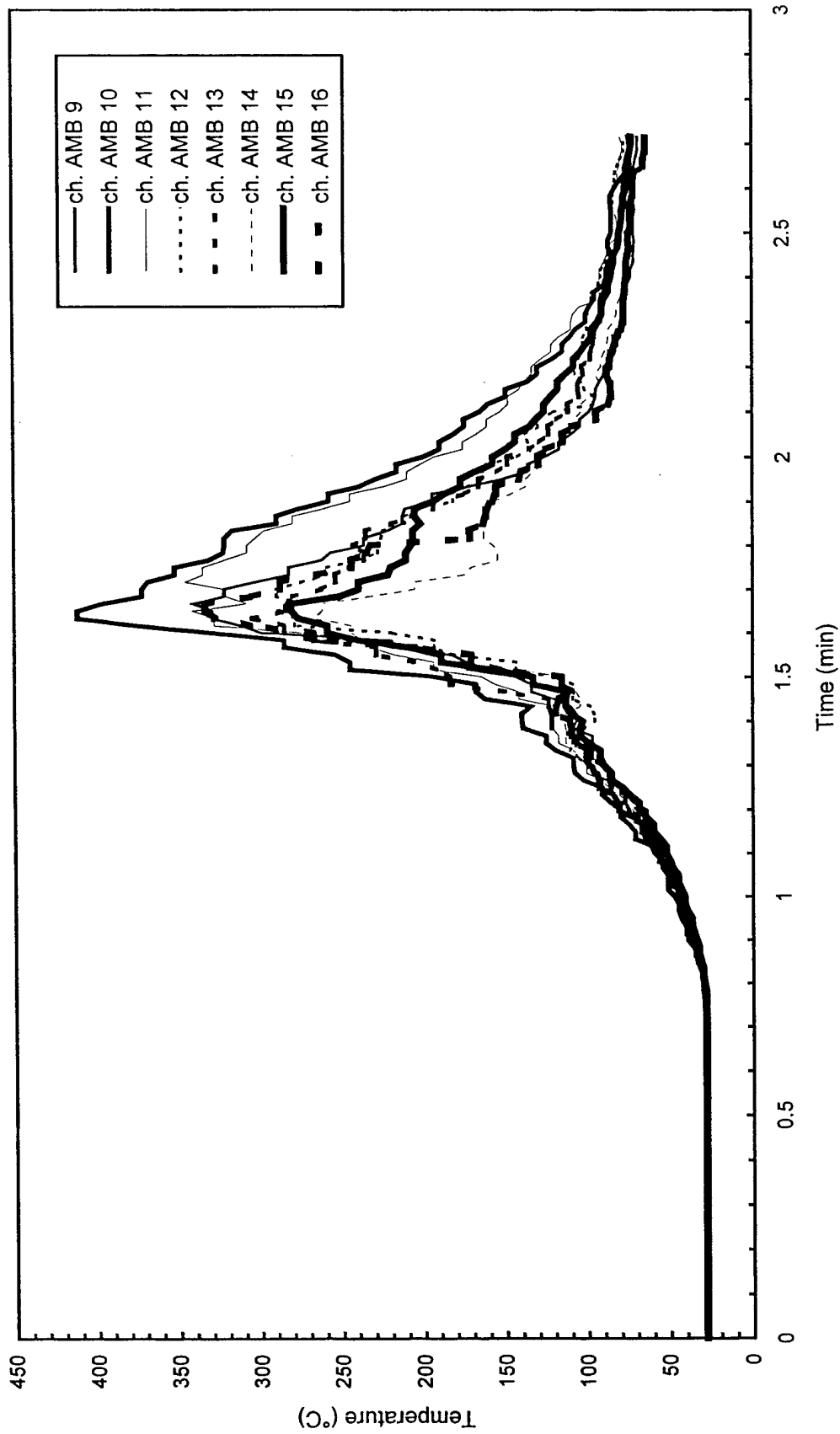


Fig. B91 - Air temperatures around 3 m (10 ft) radius from center of pad

Test S6

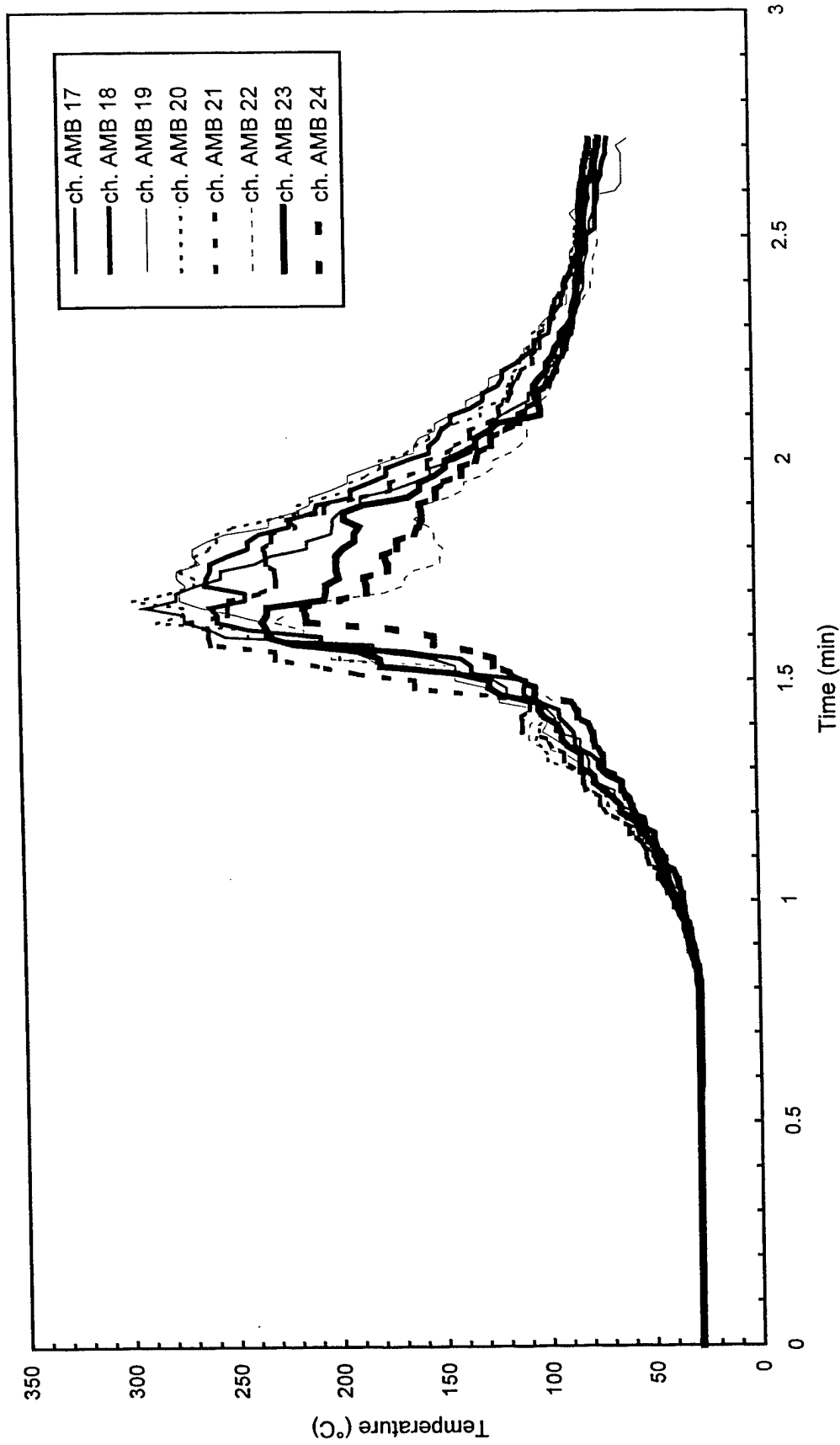


Fig. B92 - Air temperatures around 4.6 m (15 ft) radius from center of pad

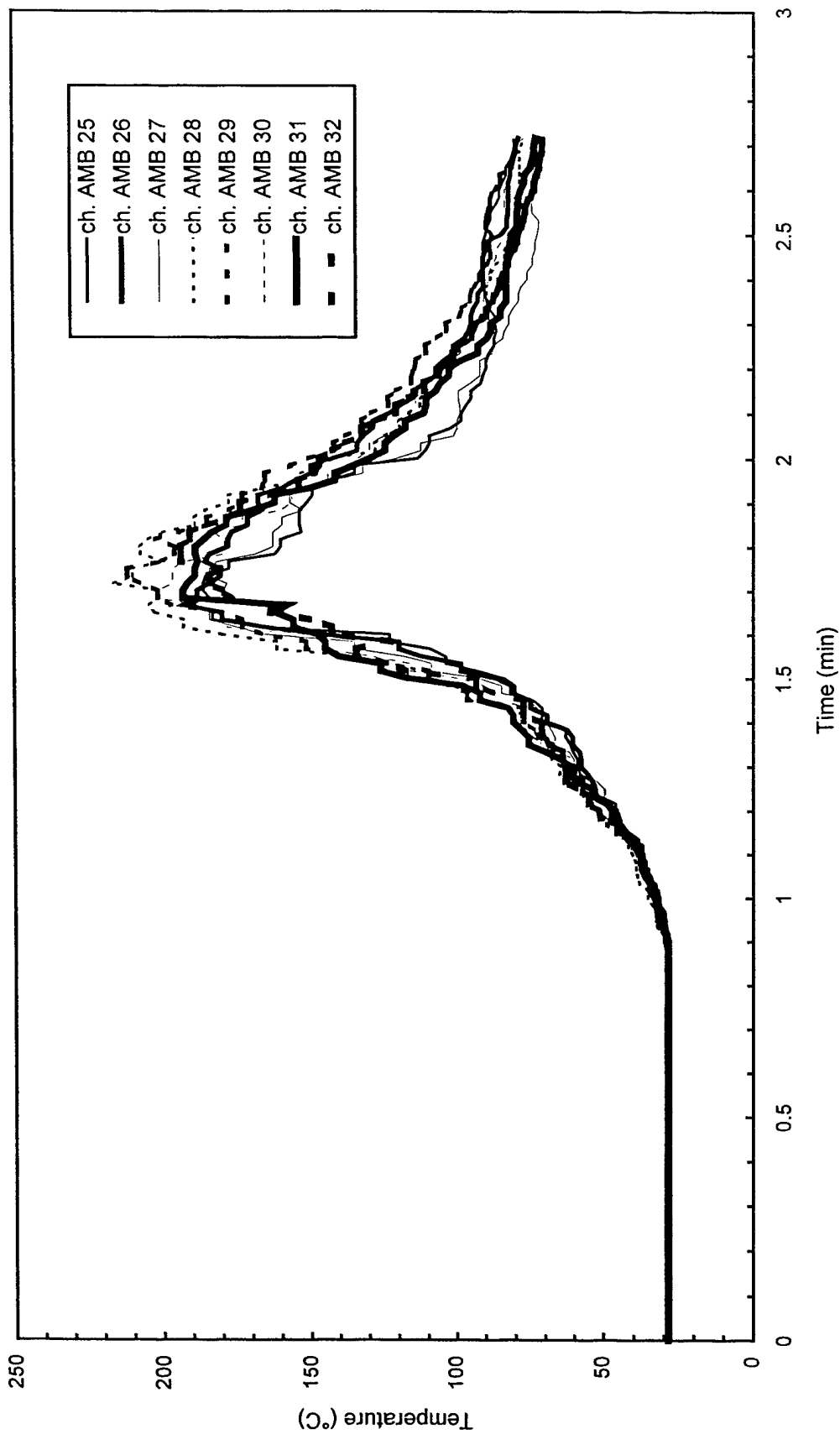


Fig. B93 - Air temperatures around North half of 7.6 m (25 ft) radius from center of pad

Test S6

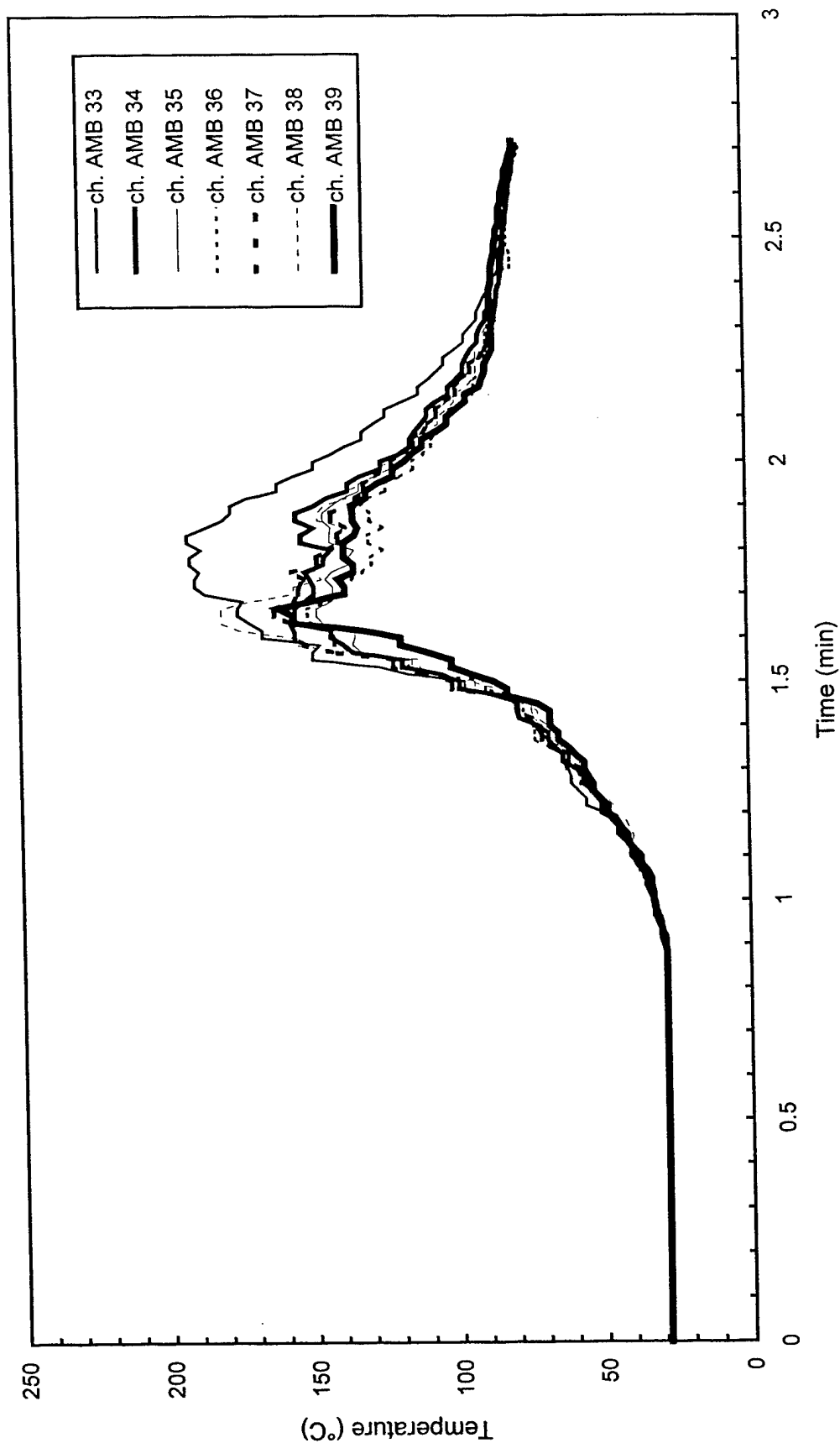


Fig. B94 - Air temperatures around South half of 7.6 m (25 ft) radius from center of pad

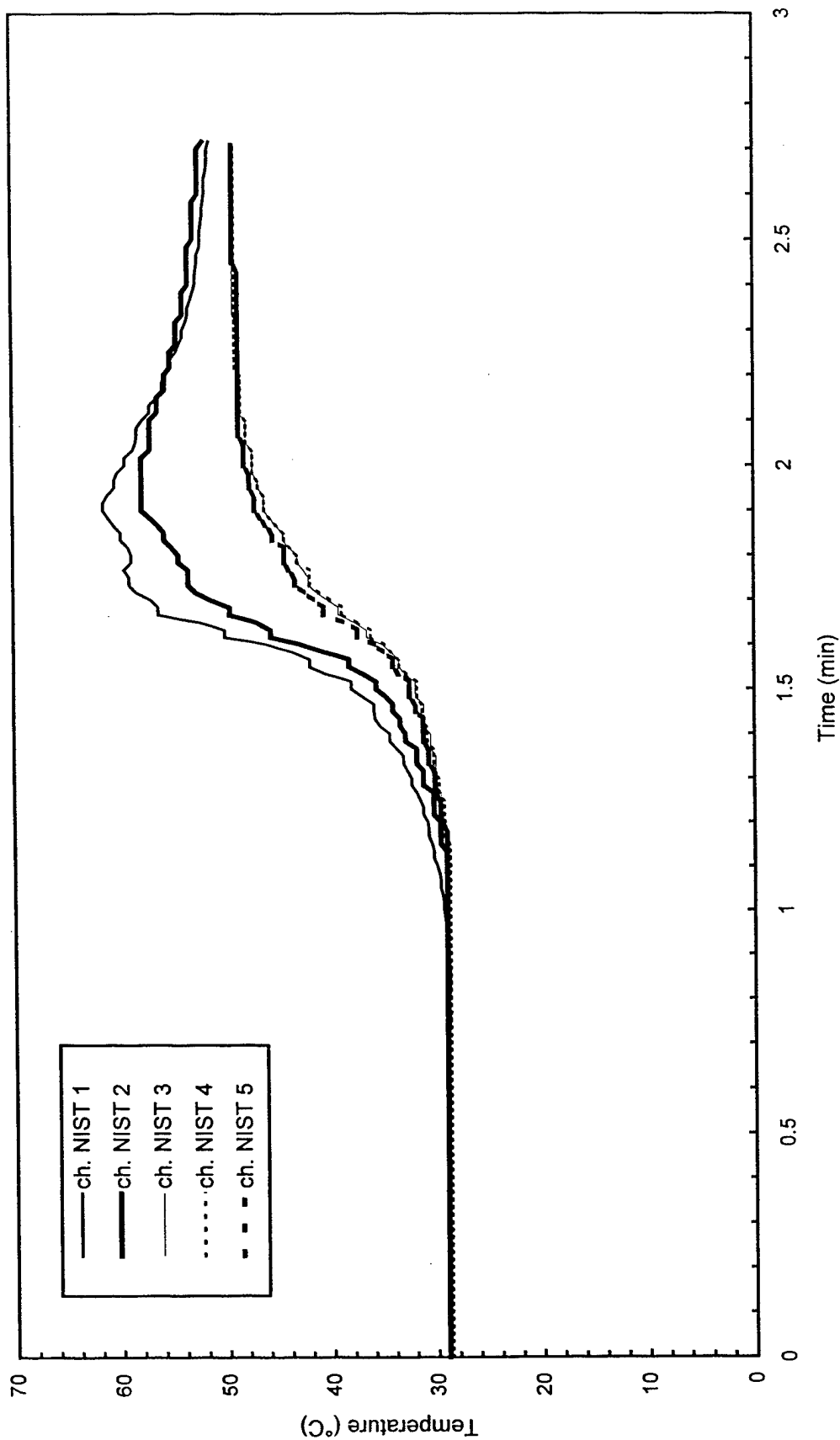


Fig. B95 - Temperature of West steel beam

Test S6

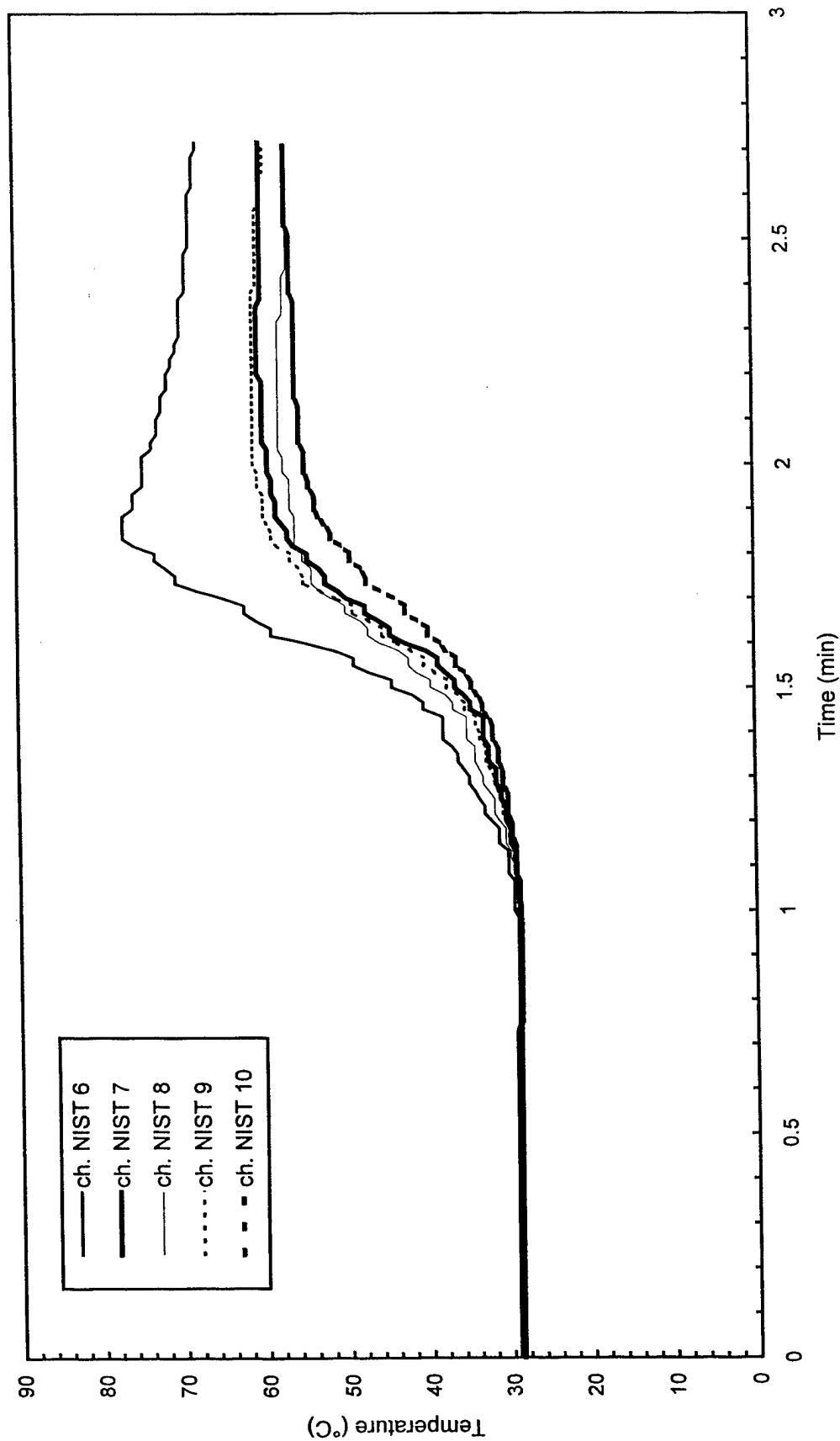


Fig. B96 - Temperature of North steel beam

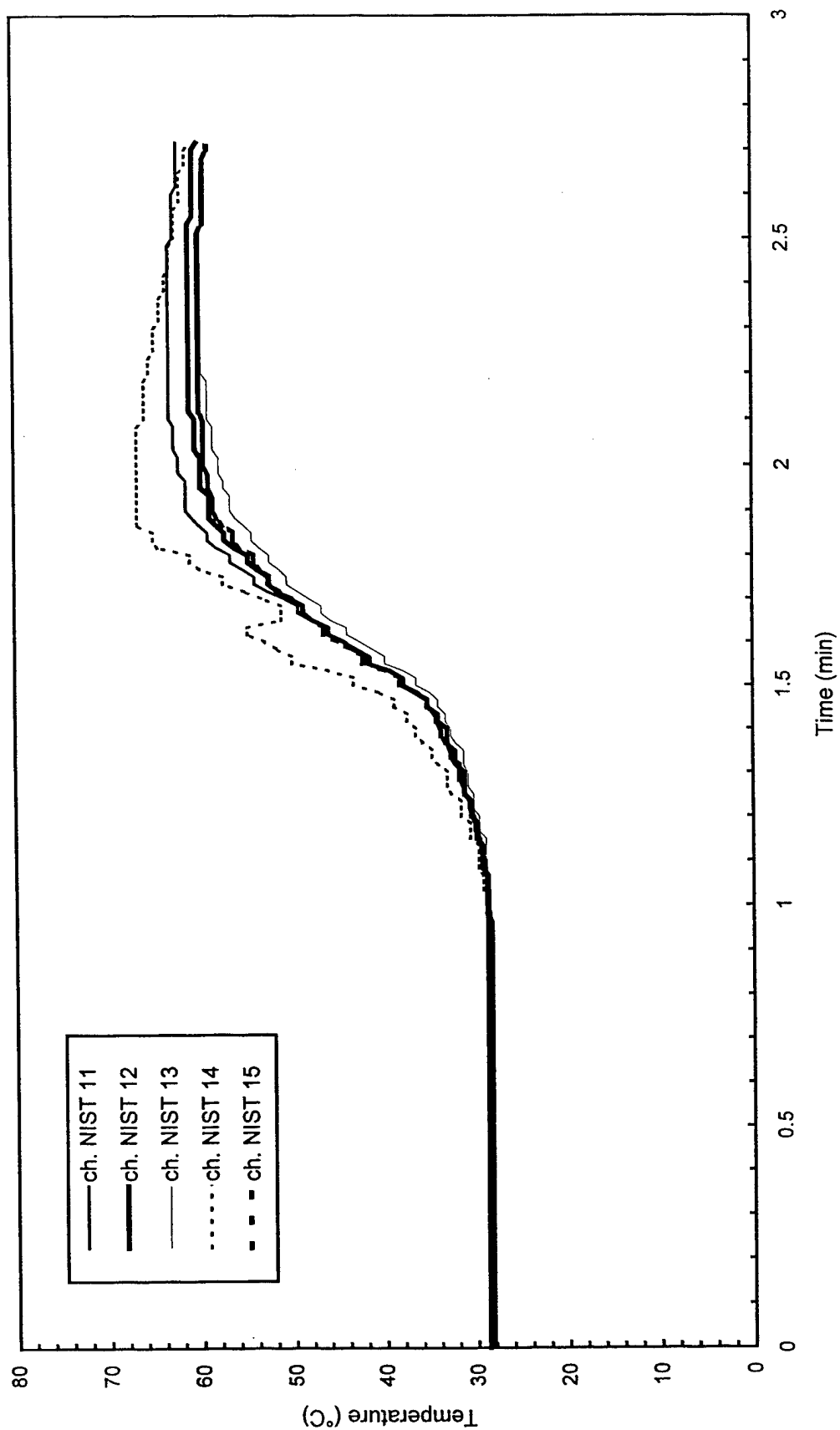


Fig. B97 - Temperature of East steel beam

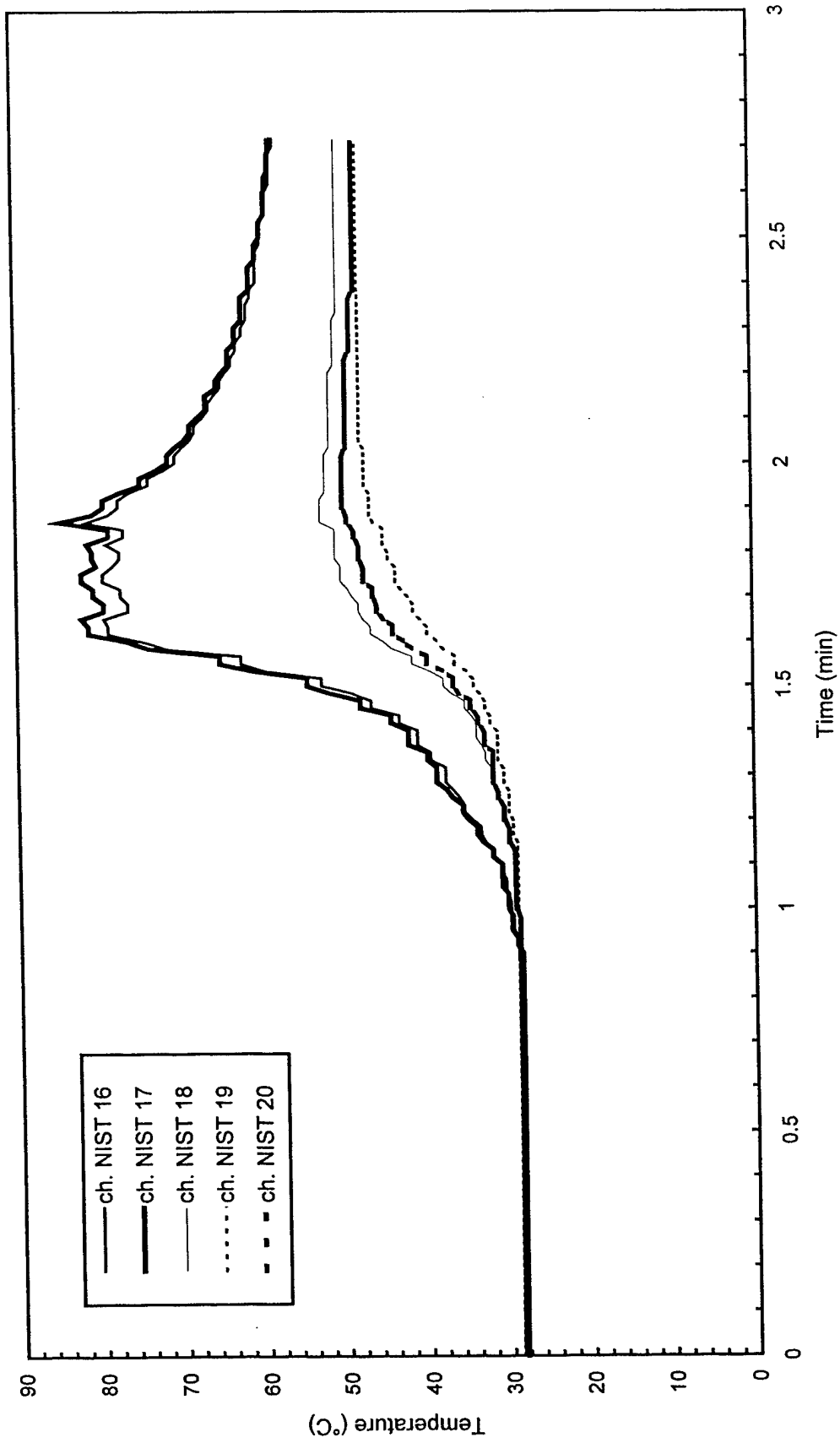


Fig. B98 - Temperature of South steel beam

Test S6

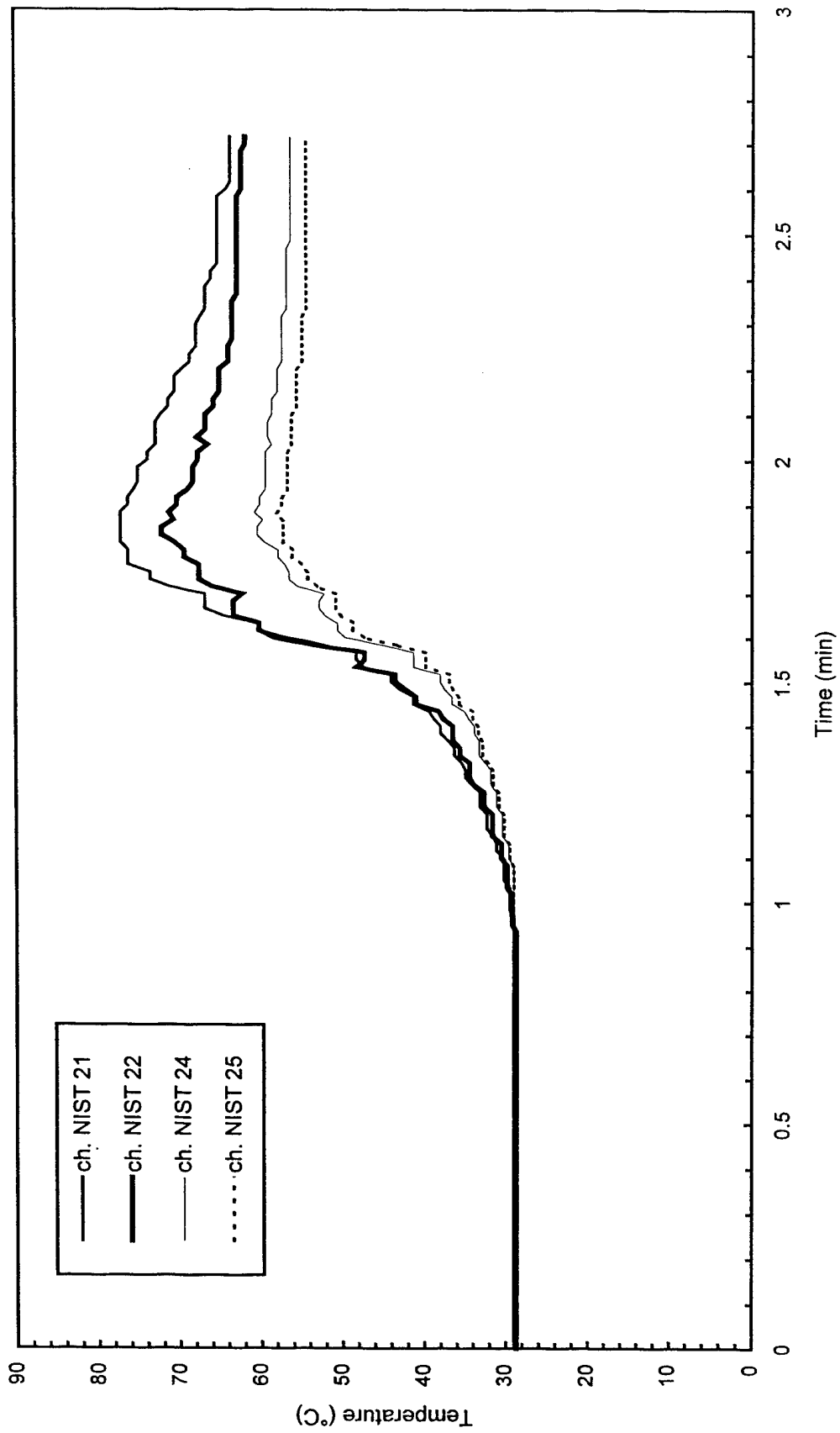


Fig. B99 - Temperature of Northwest steel beam

Test S6

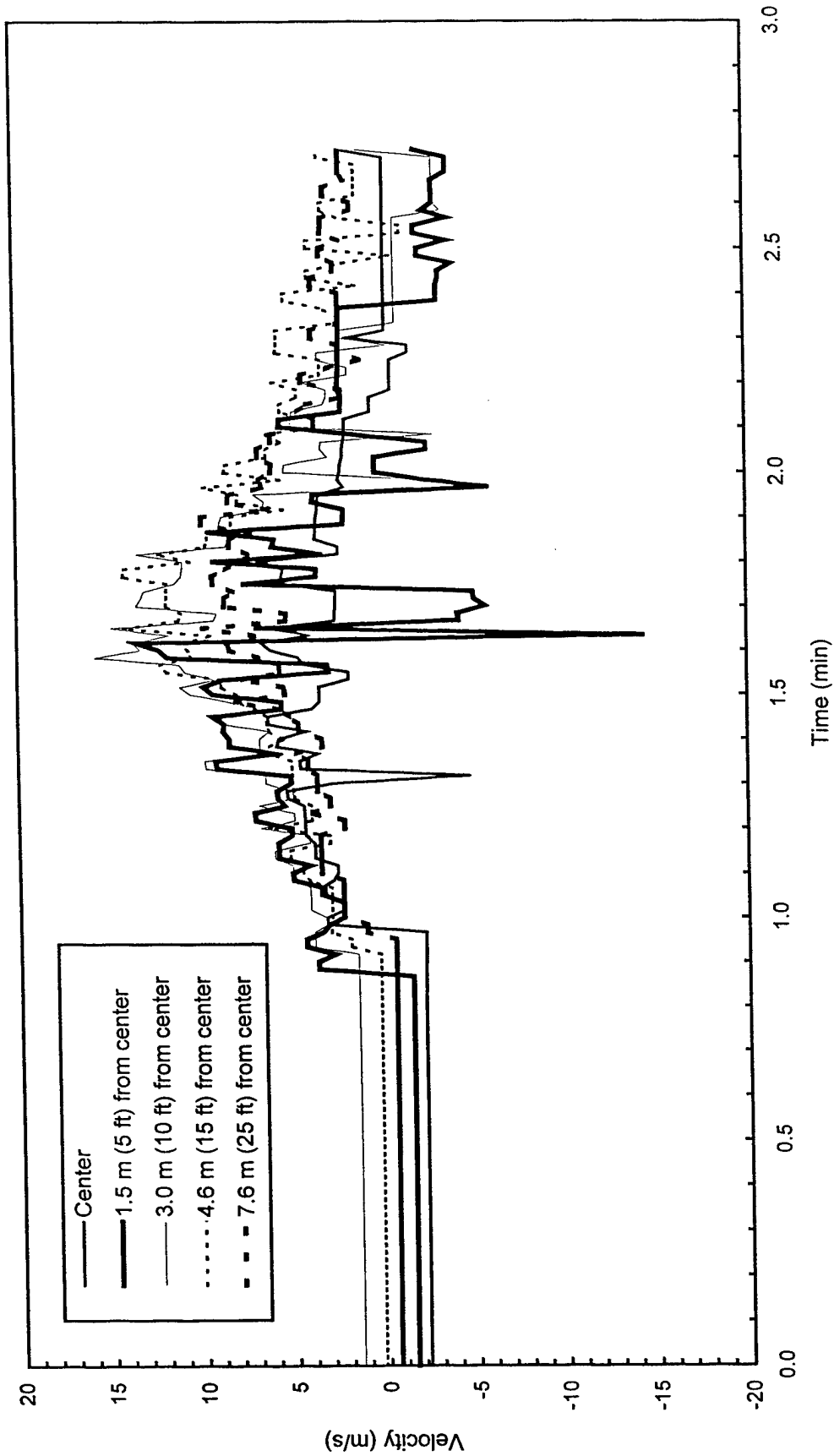


Fig. B100 - Plume and ceiling jet velocities

Test S6

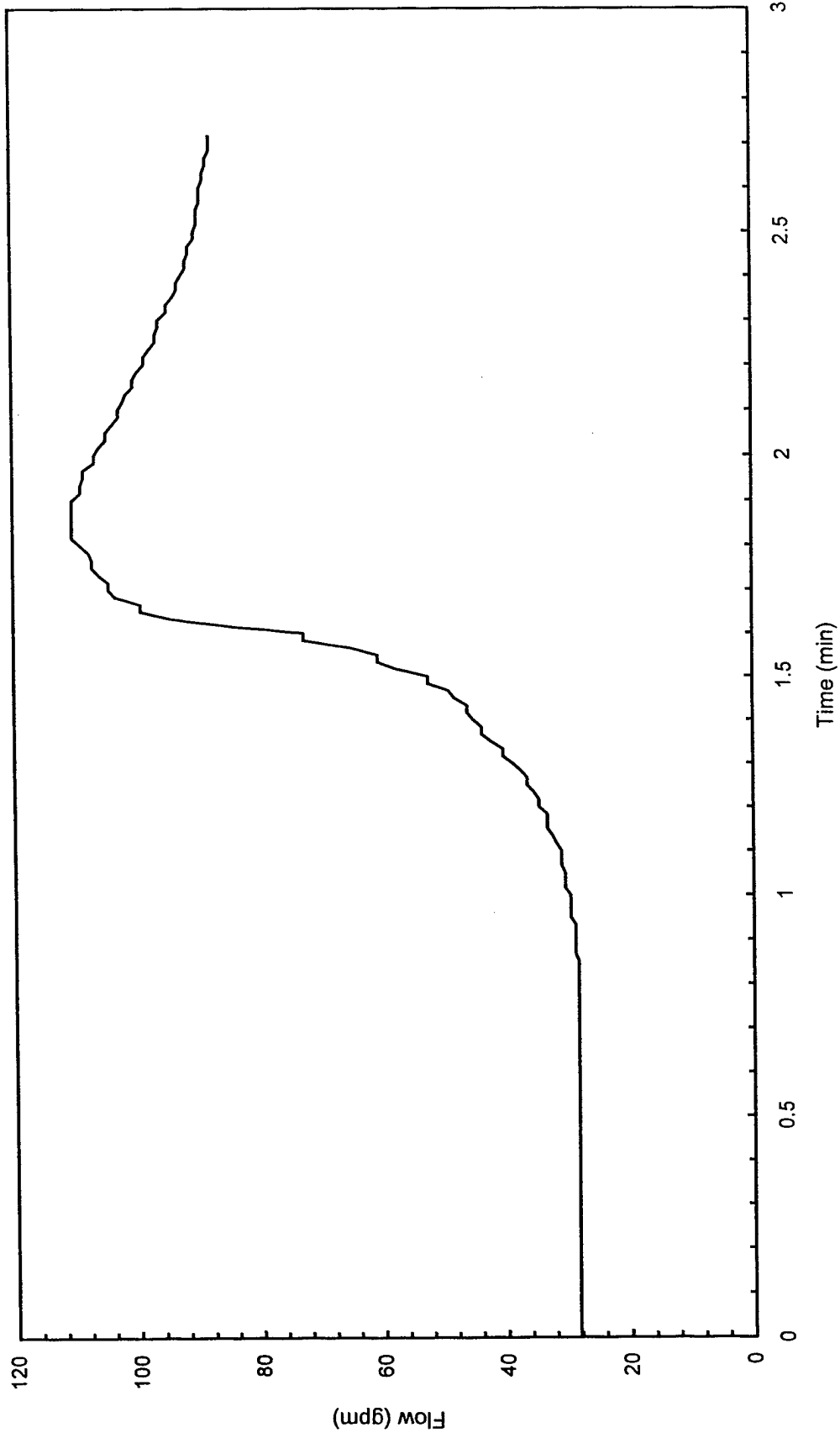


Fig. B101 - Sprinkler system flowrate

Test S6

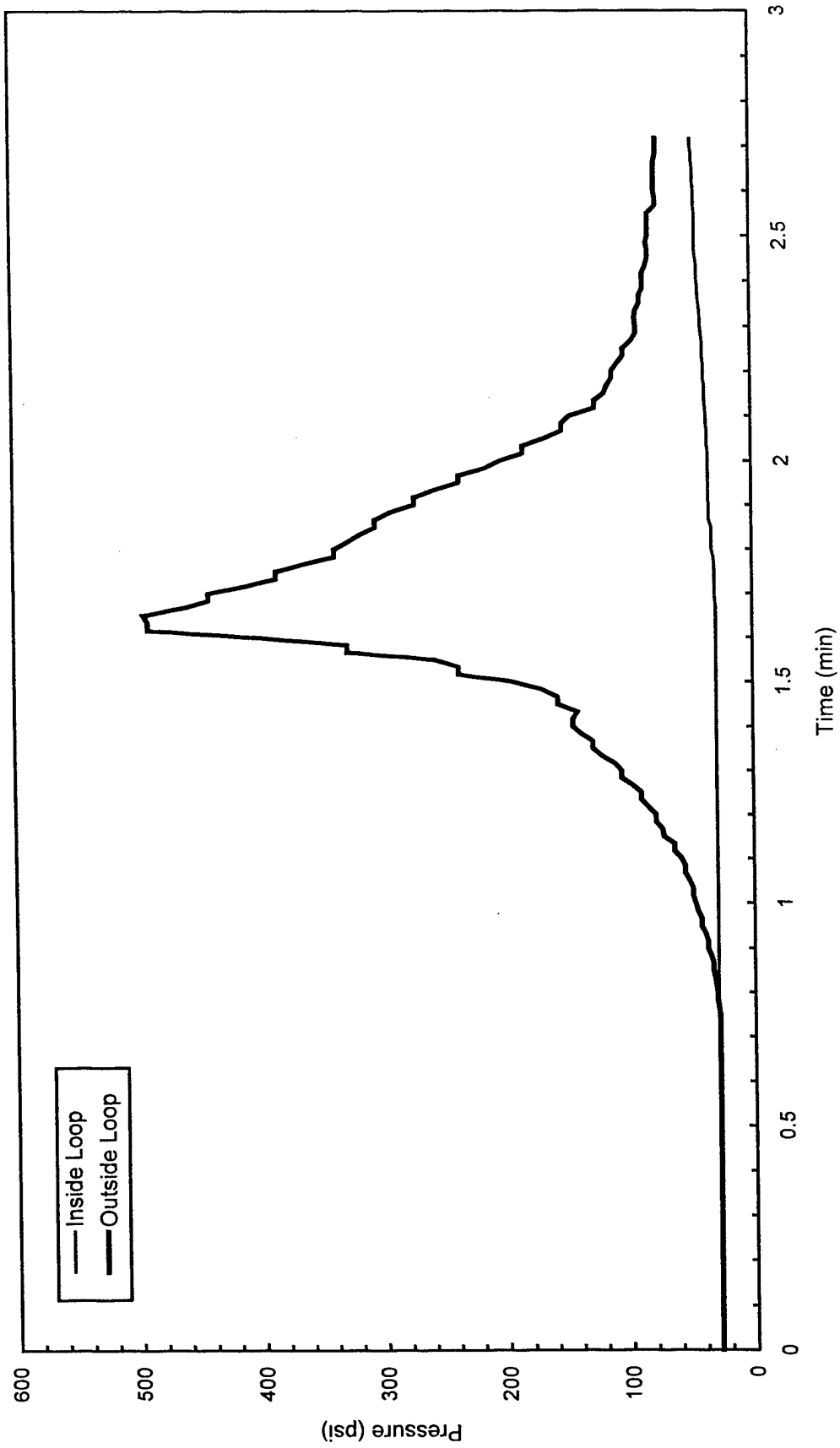


Fig. B102 - Sprinkler system pressure

Test S7

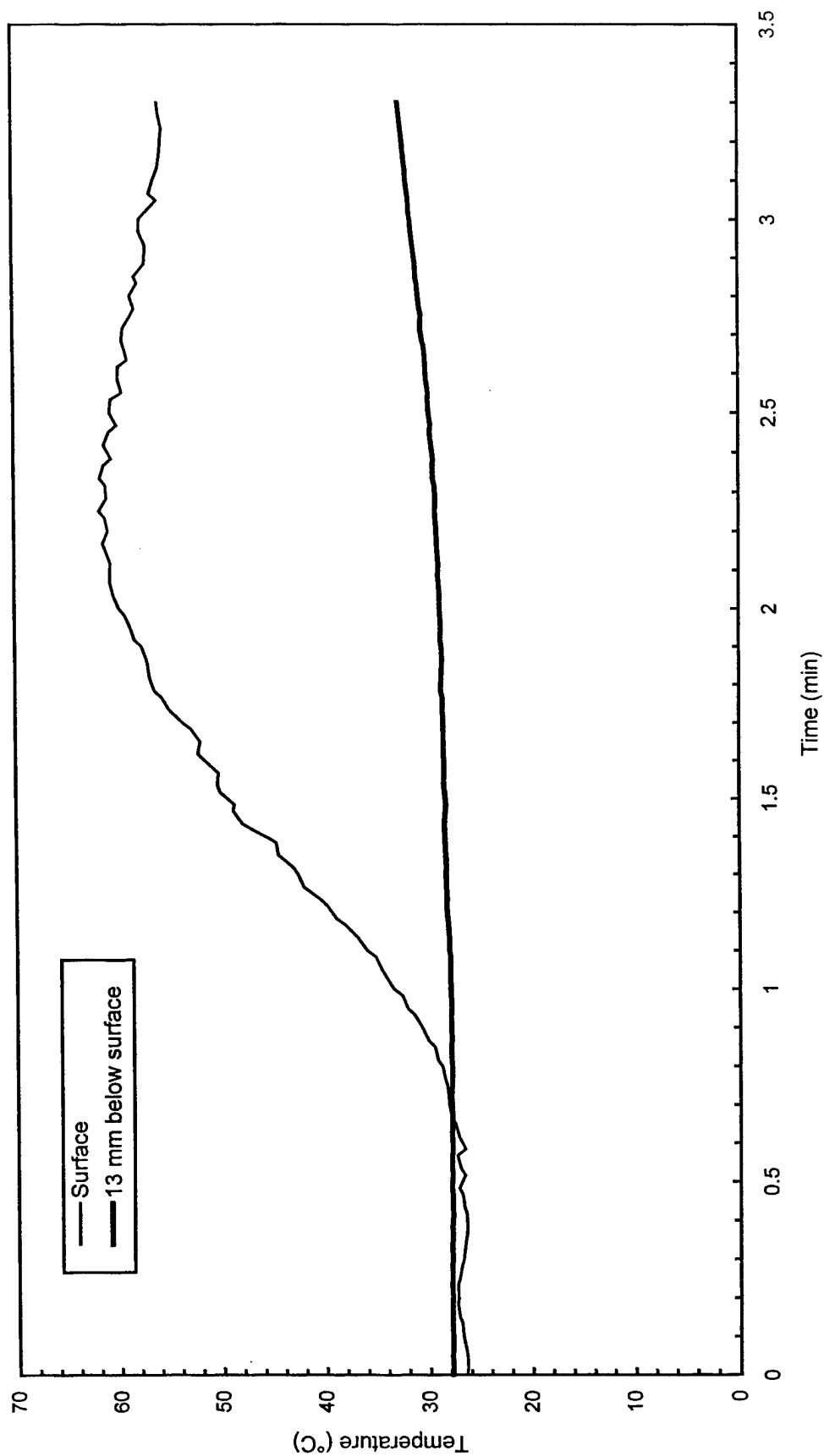


Fig. B103 - Concrete temperatures at center of pad

Test S7

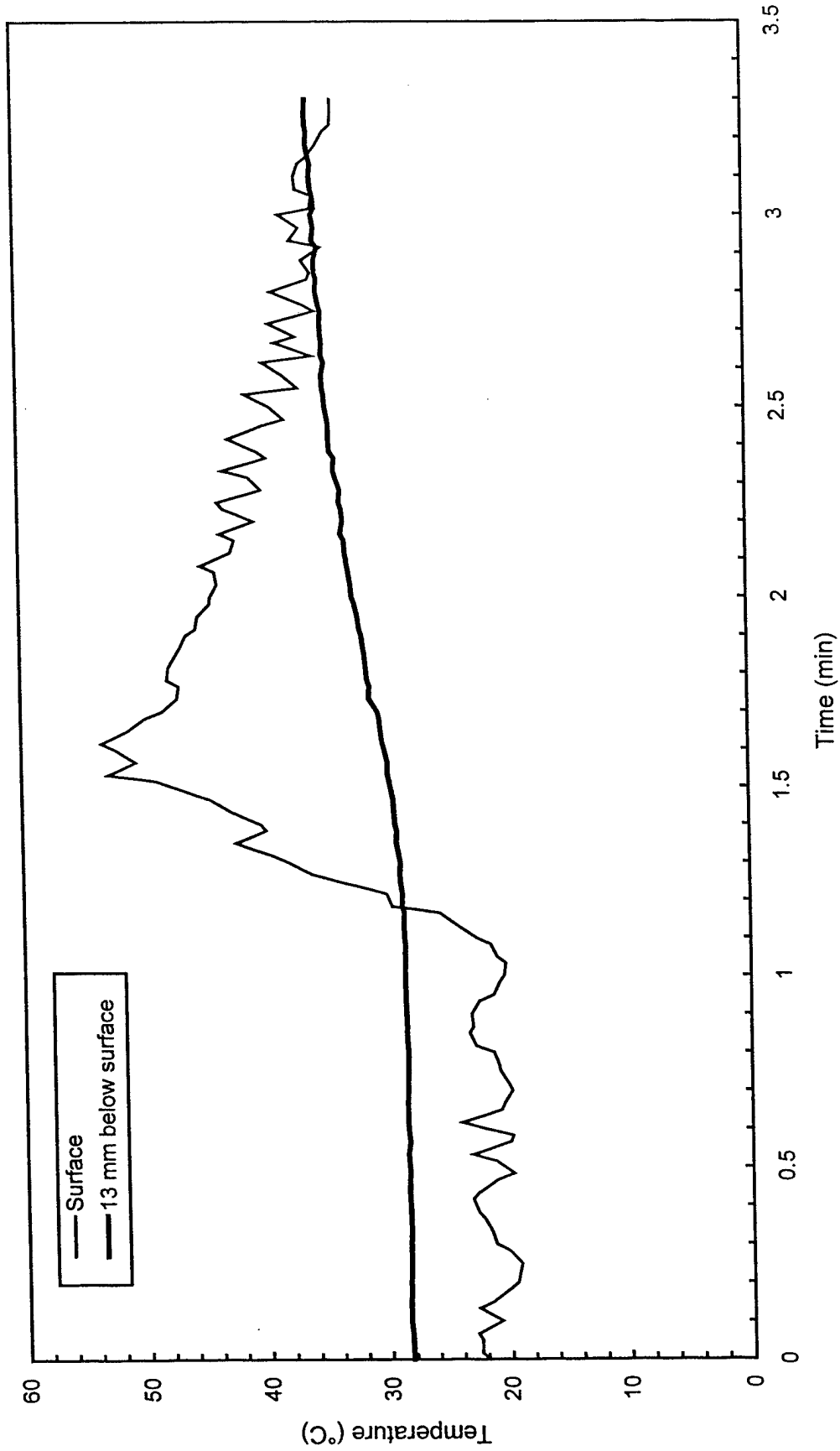


Fig. B104 - Concrete temperatures 3 m (10 ft) East of center of pad

Test S7

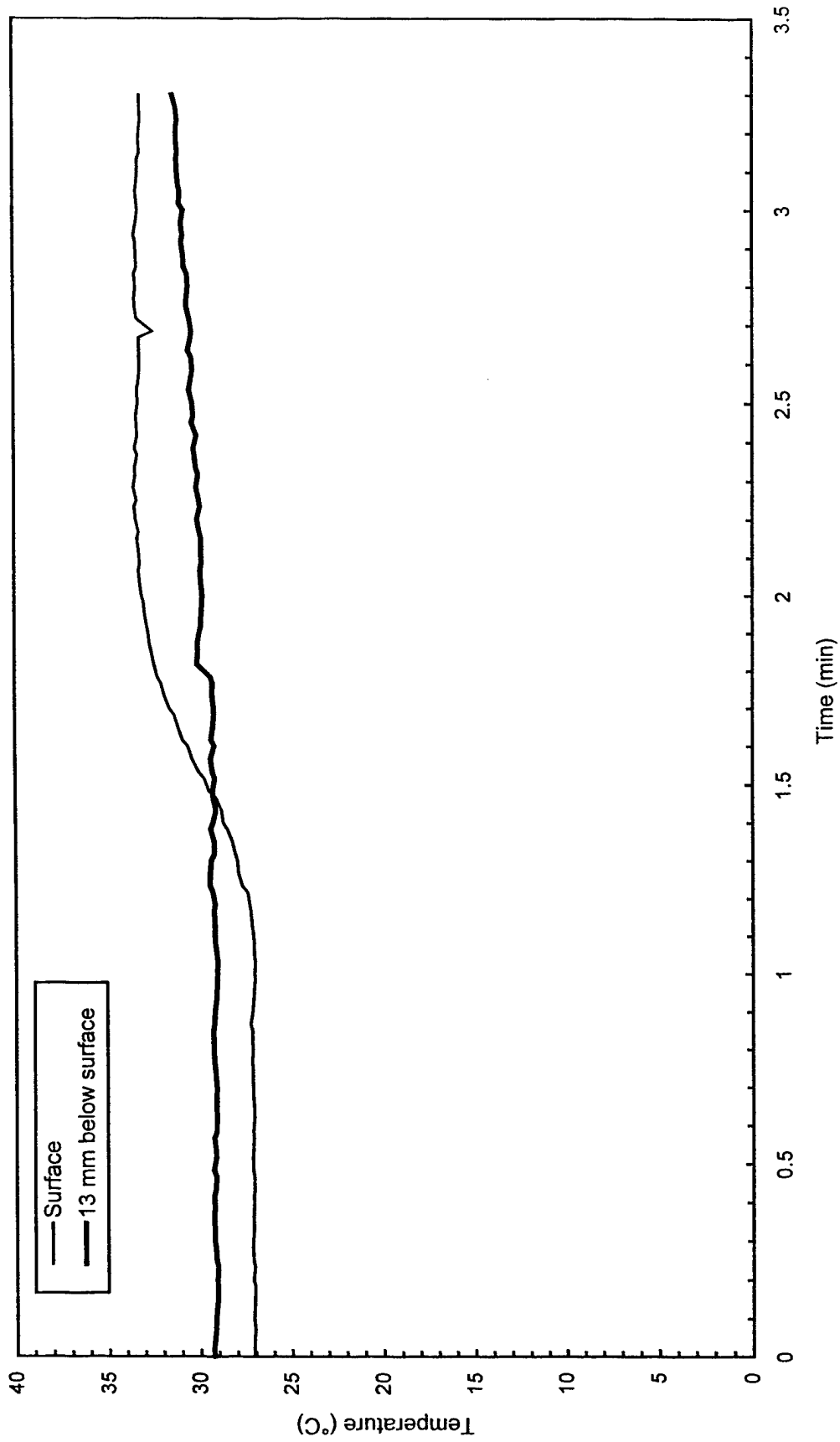


Fig. B105 - Concrete temperatures 3 m (10 ft) West of center of pad

Test S7

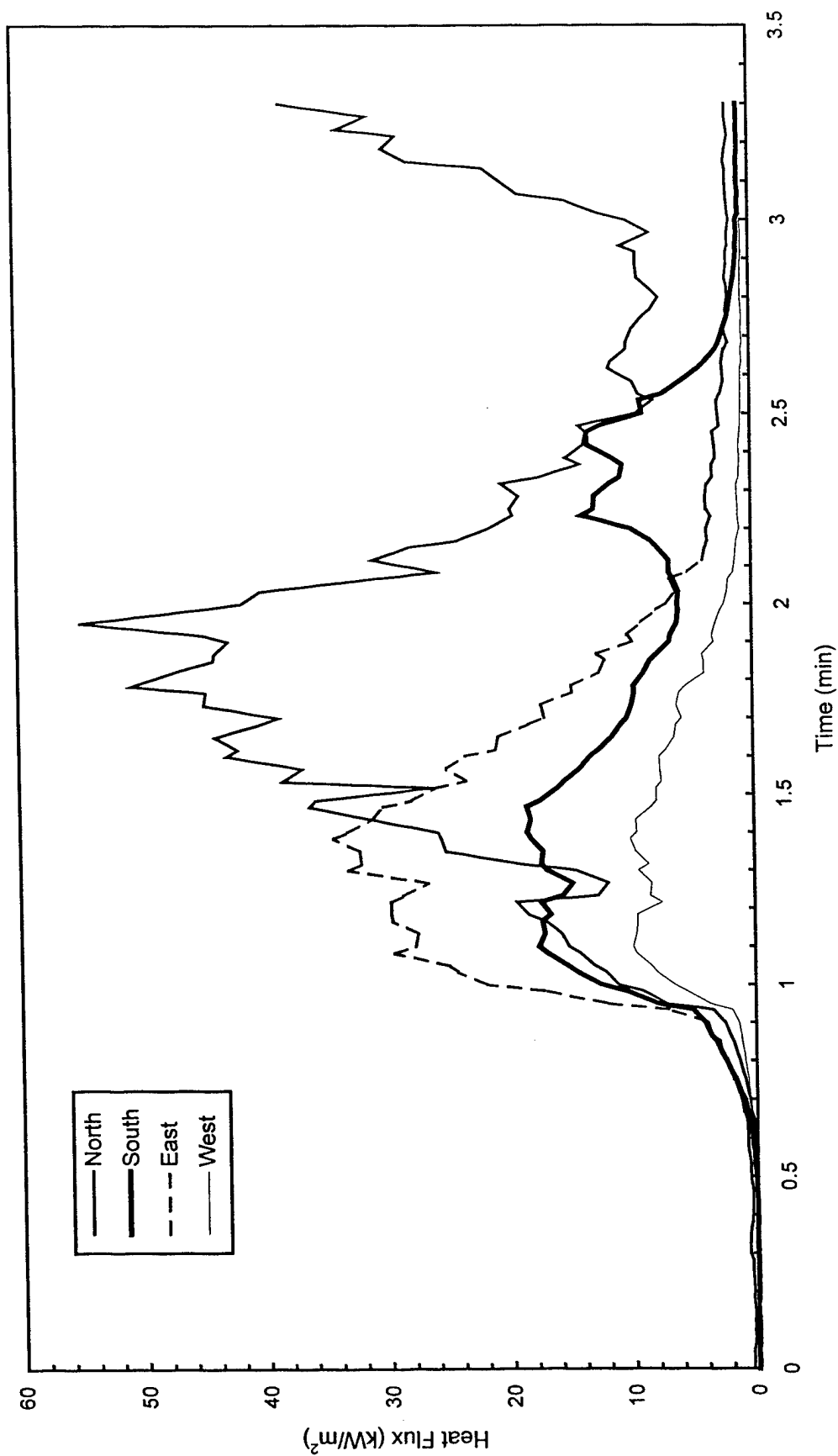


Fig. B106 - Heat flux measured at edge of pad

Test S7

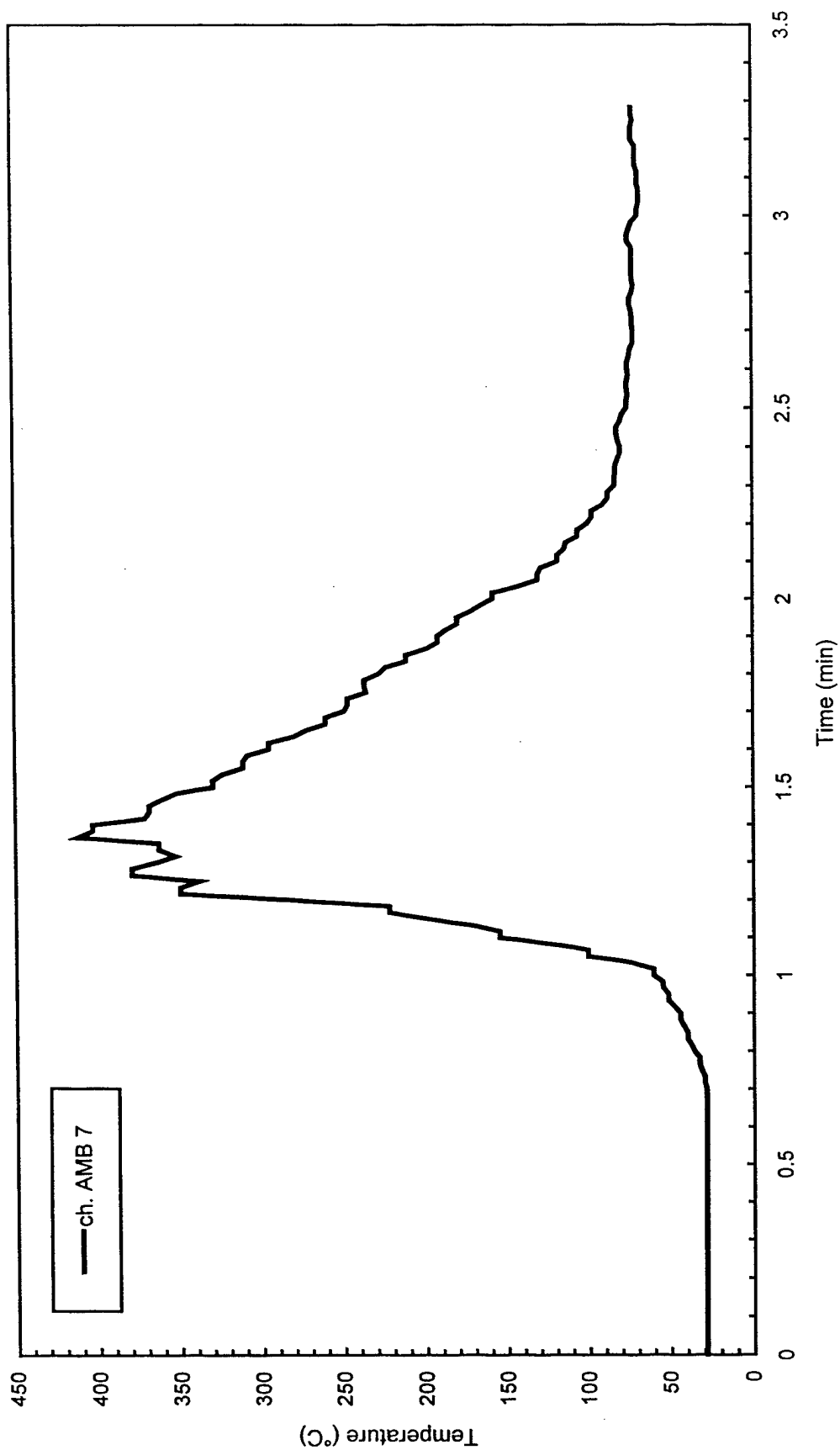


Fig. B107 - Air temperatures over center of pad

Test S7

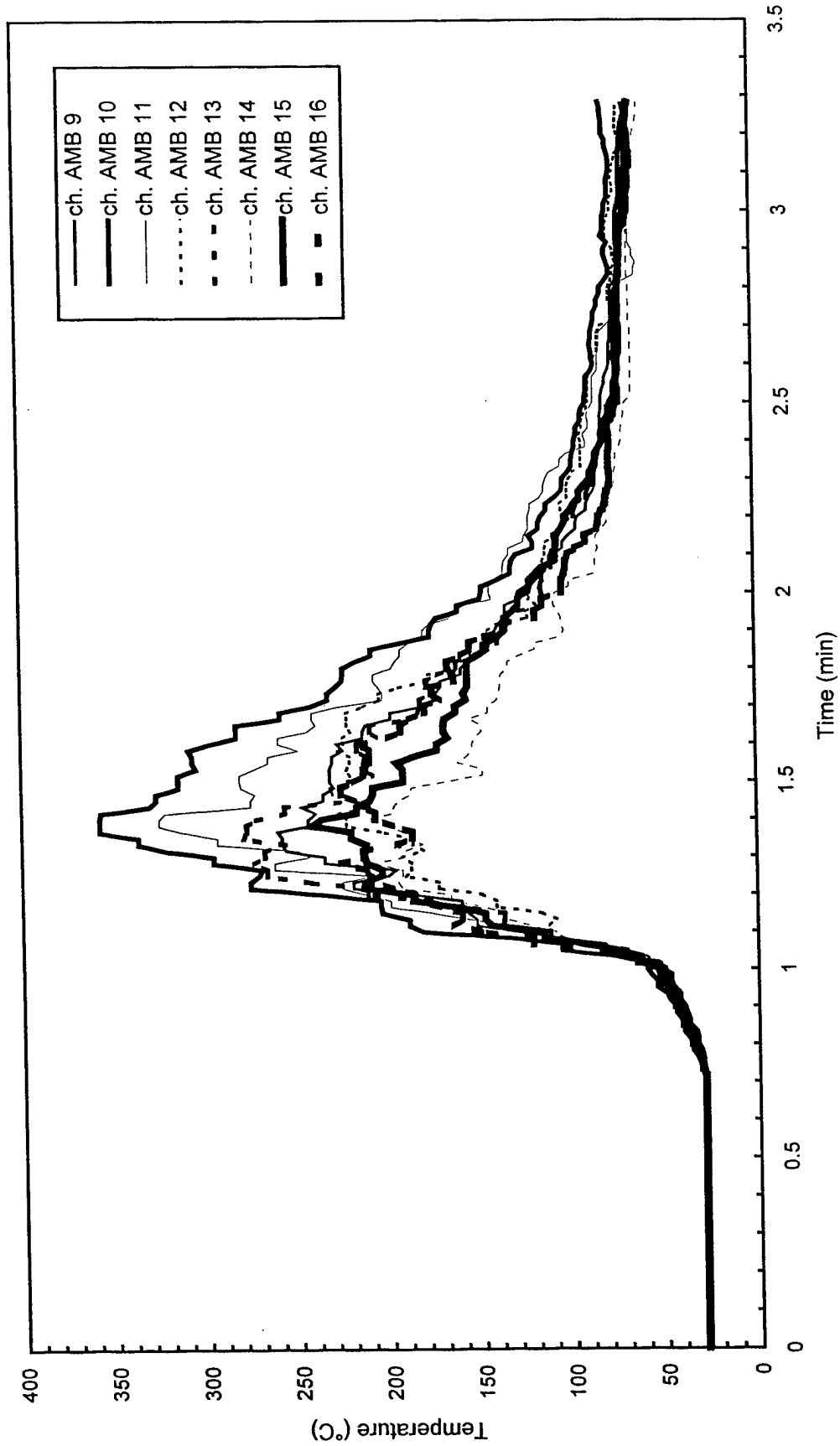


Fig. B108 - Air temperatures around 3 m (10 ft) radius from center of pad

Test S7

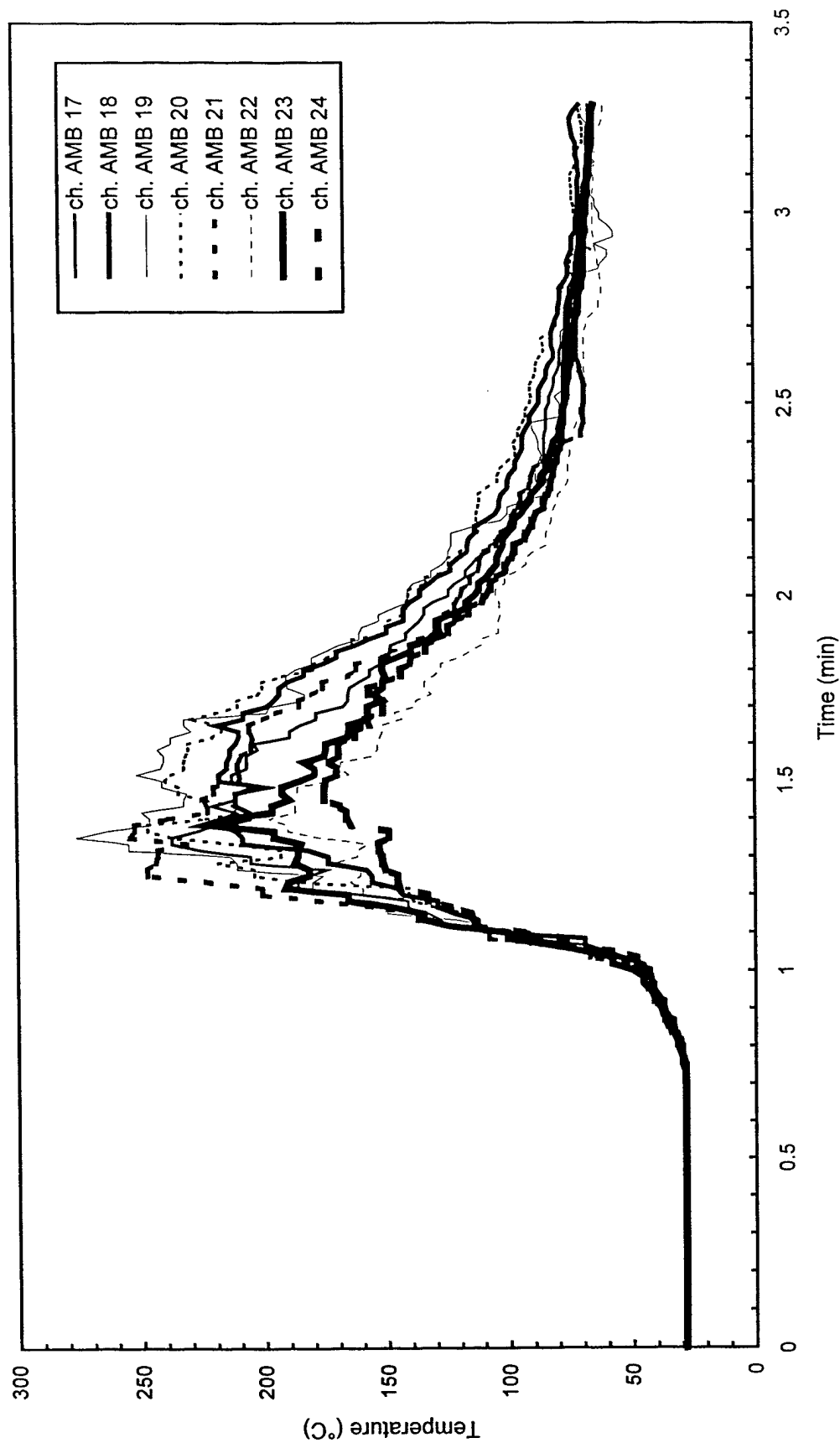


Fig. B109 - Air temperatures around 4.6 m (15 ft) radius from center of pad

Test S7

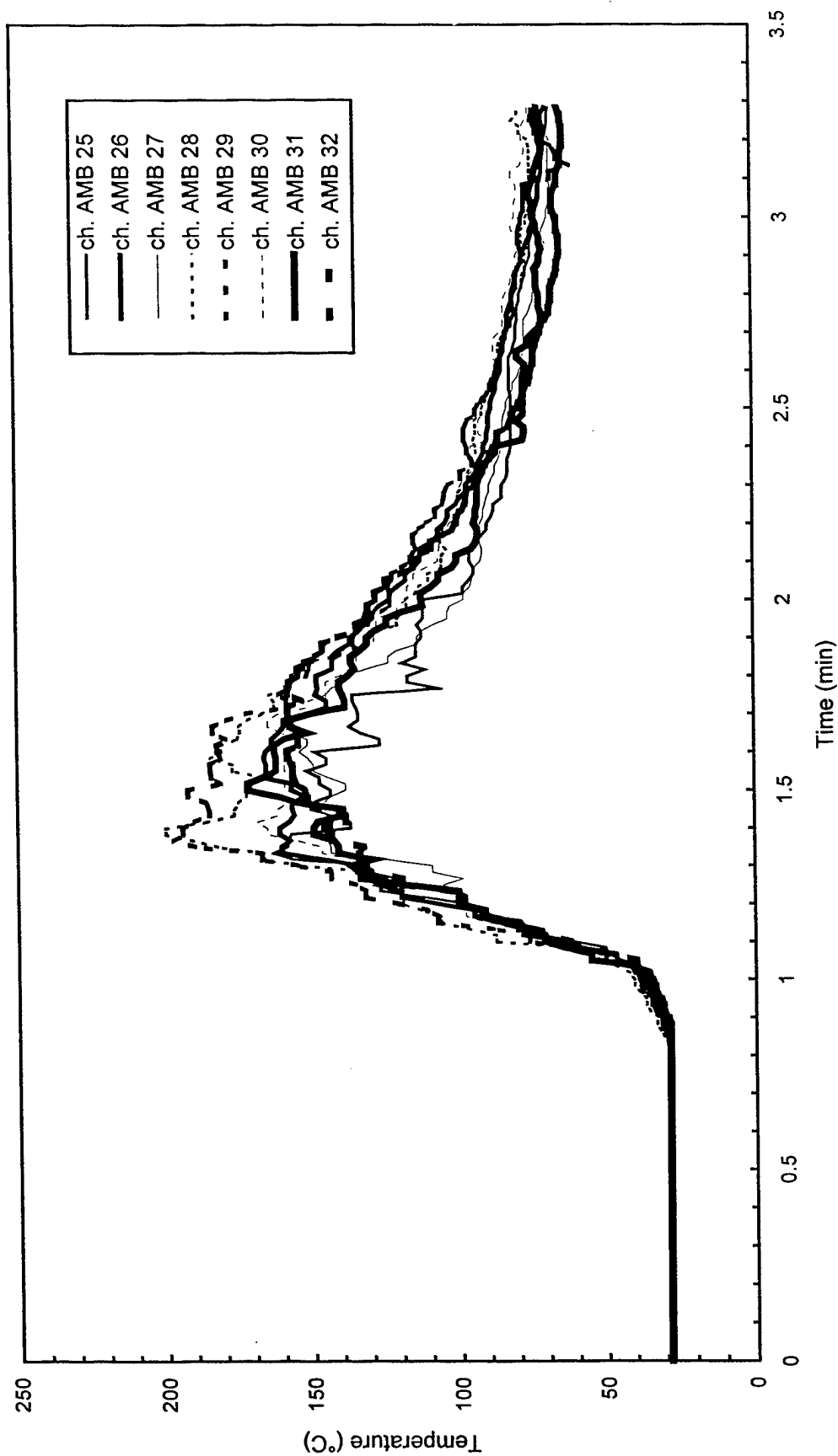


Fig. B110 - Air temperatures around North half of 7.6 m (25 ft) radius from center of pad

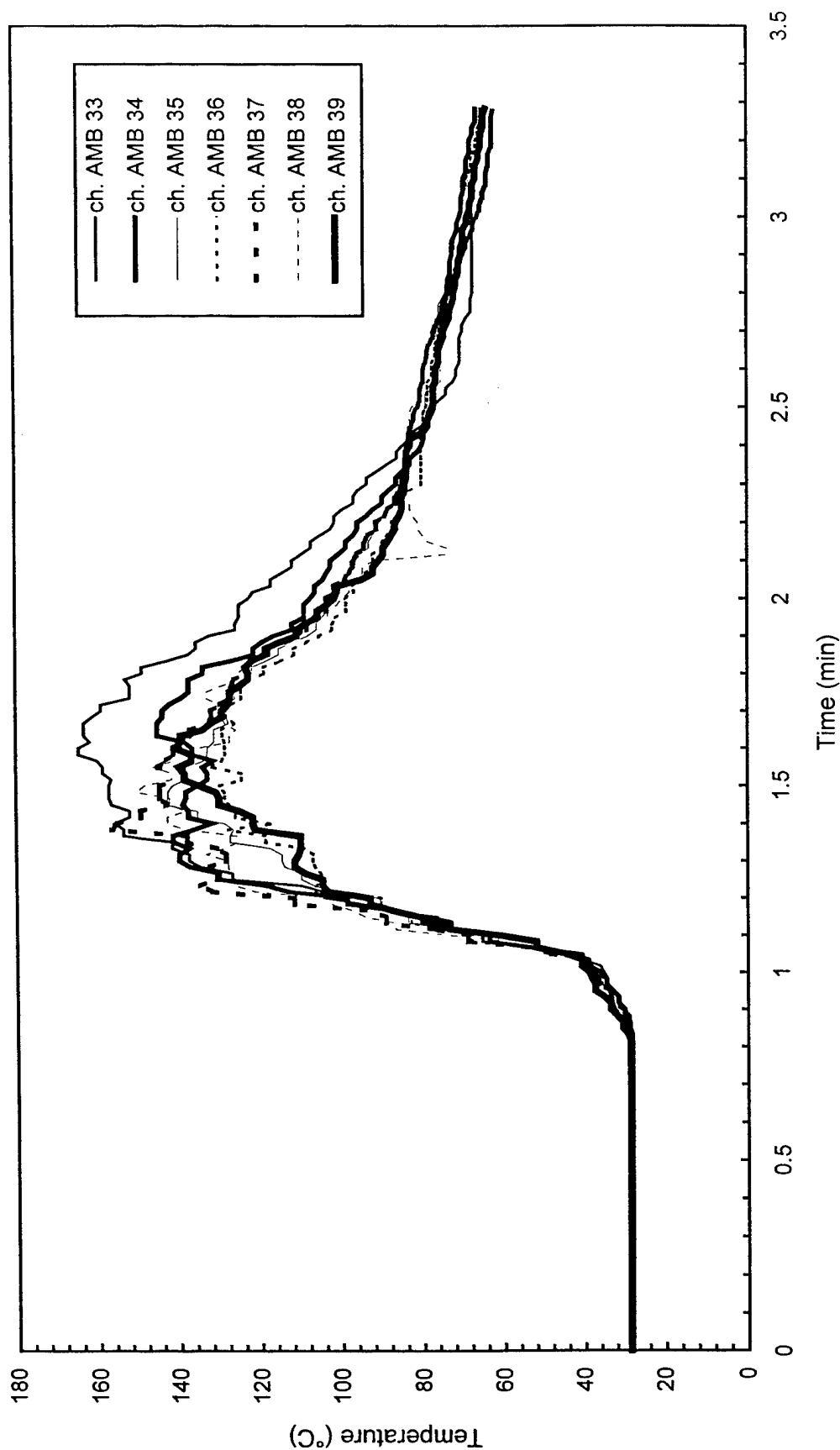


Fig. B111 - Air temperatures around South half of 7.6 m (25 ft) radius from center of pad

Test S7

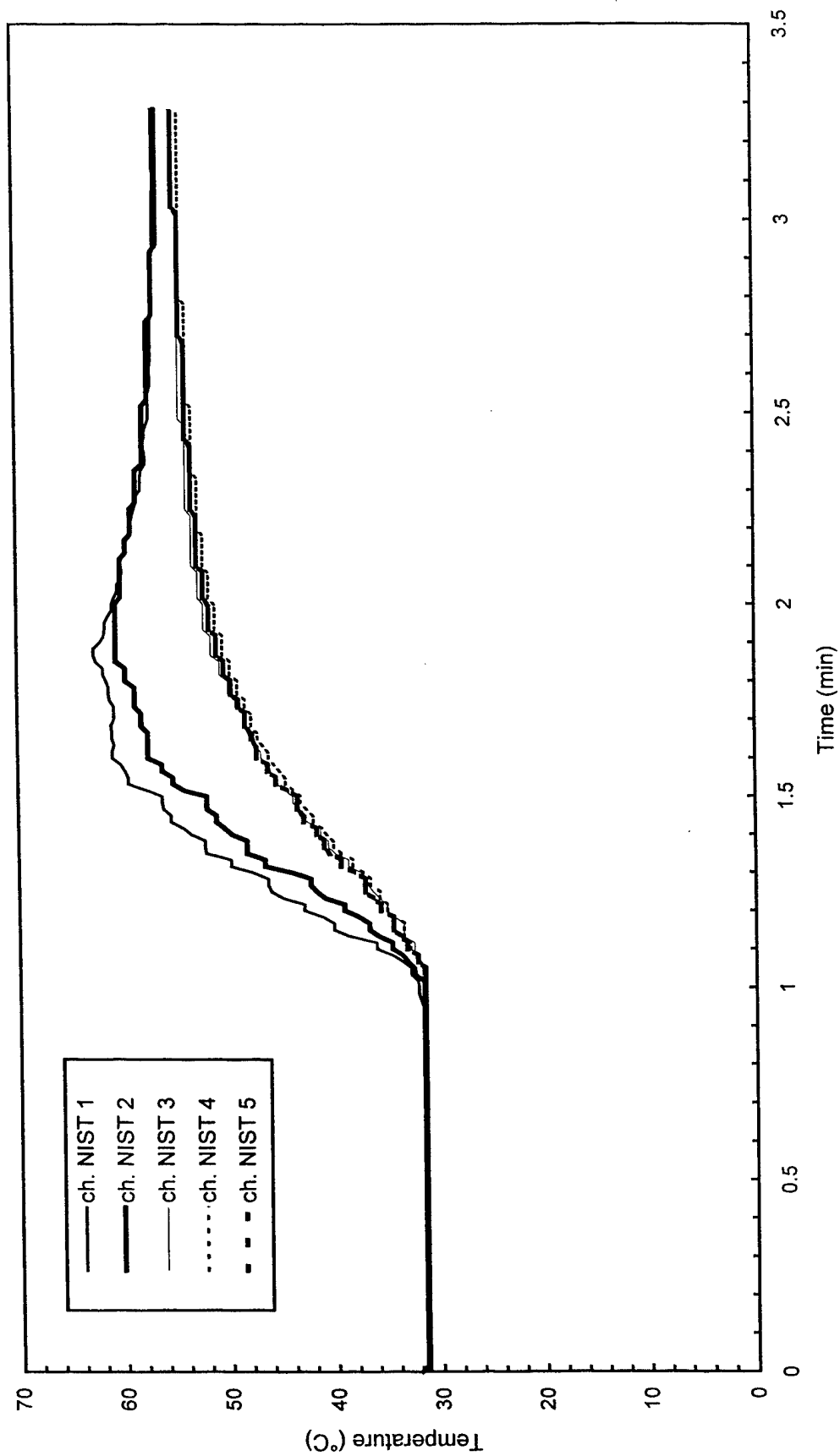


Fig. B112 - Temperature of West steel beam

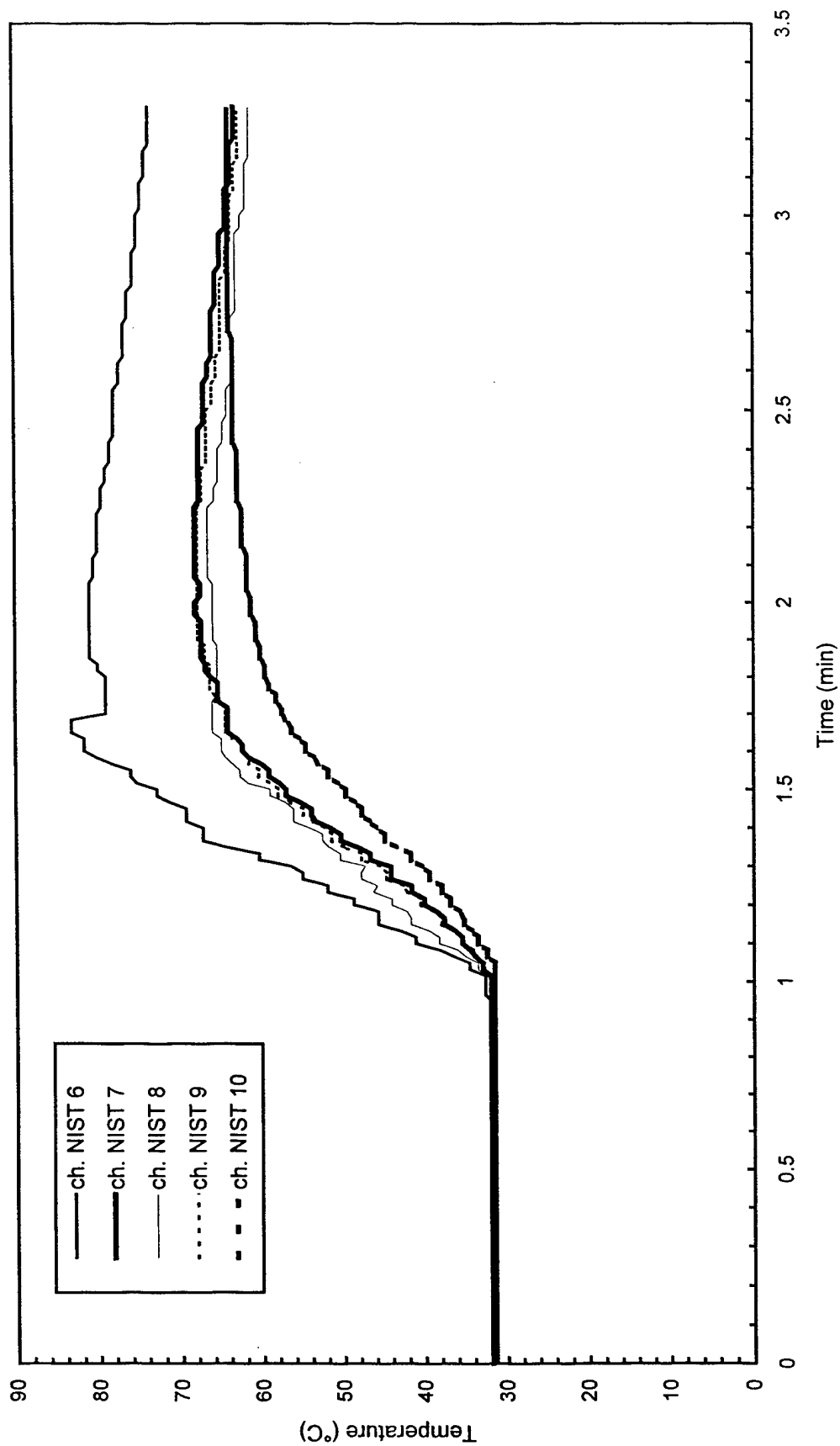


Fig. B113 - Temperature of North steel beam

Test S7

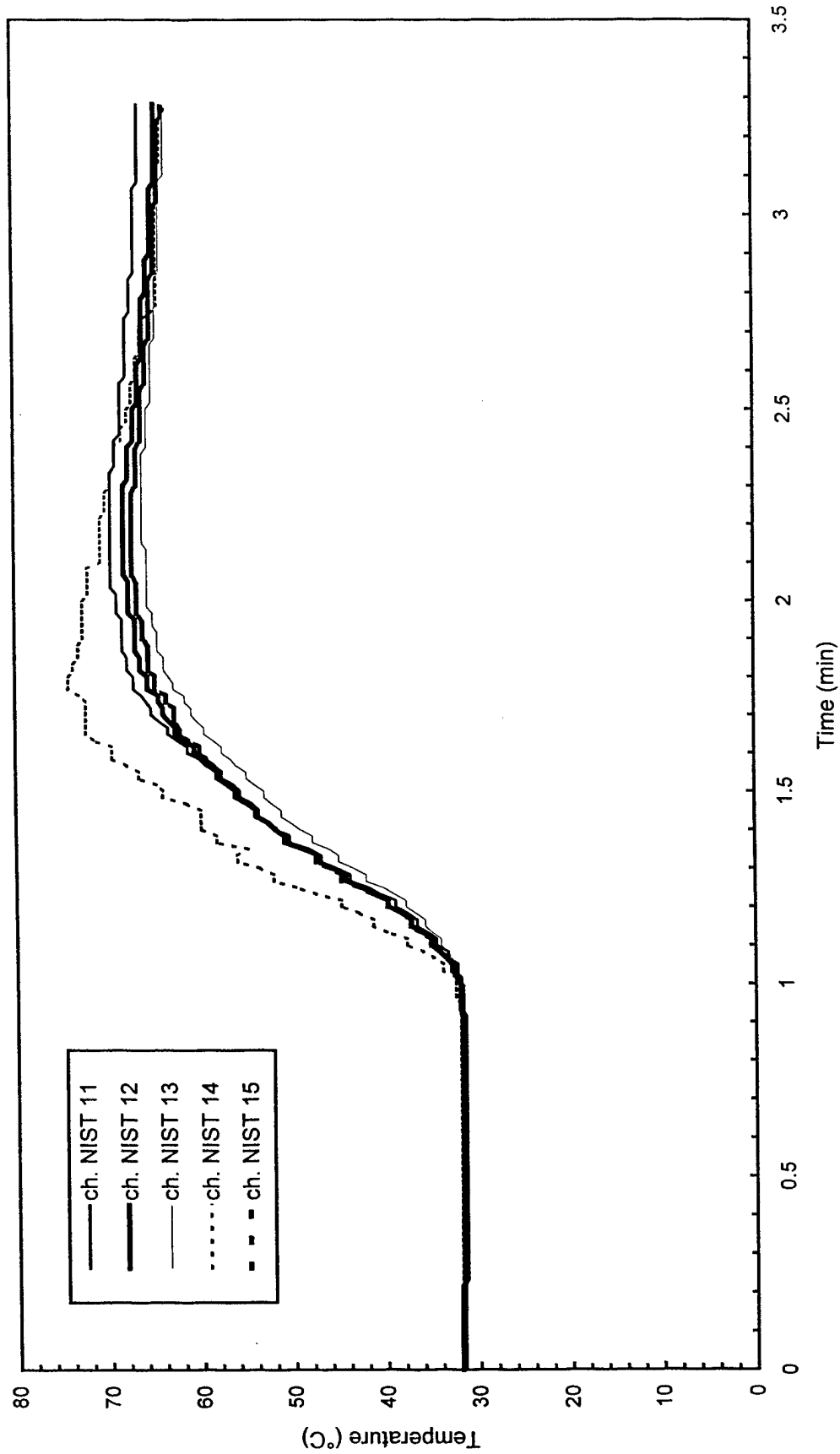


Fig. B114 - Temperature of East steel beam

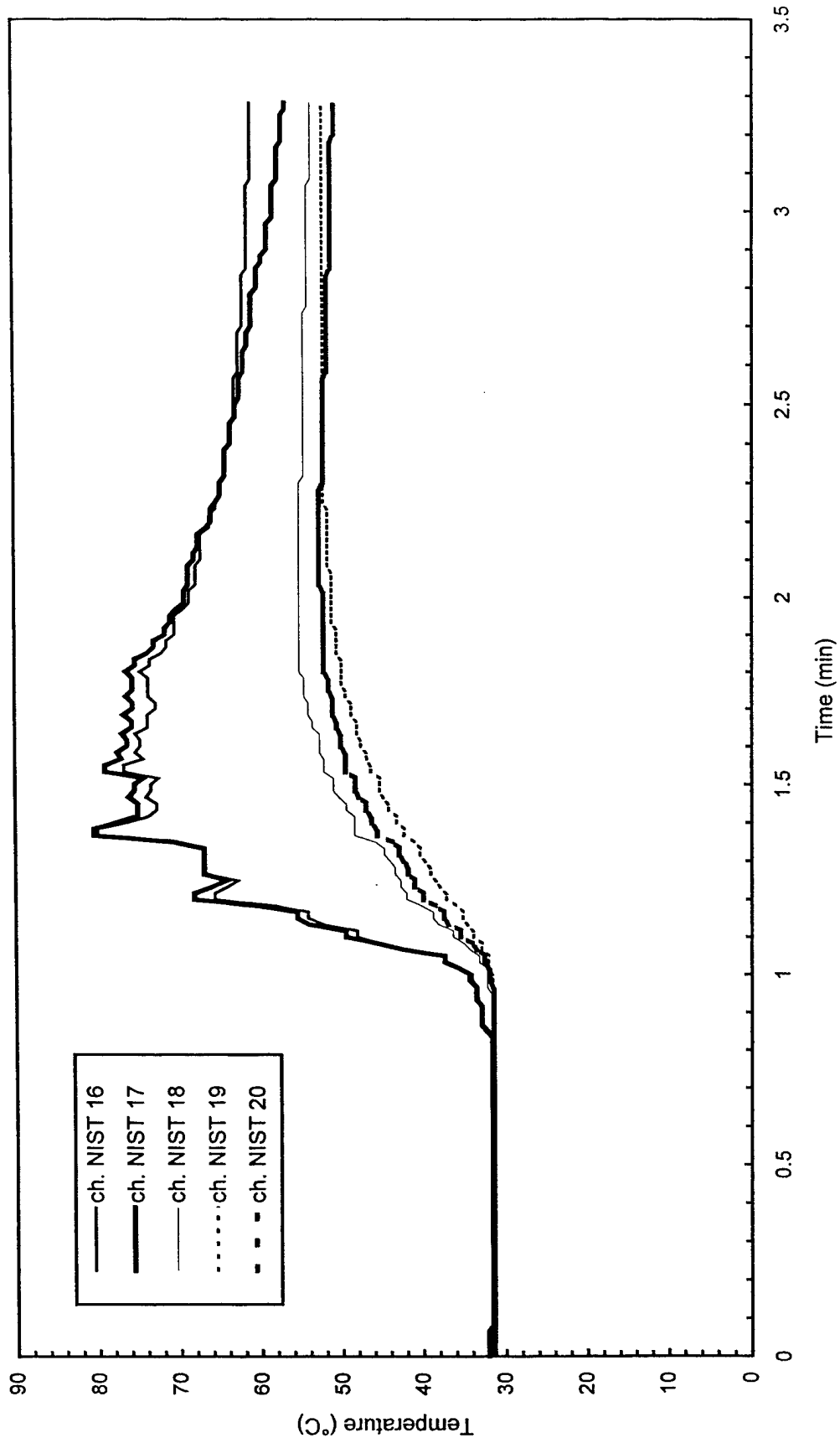


Fig. B115 - Temperature of South steel beam

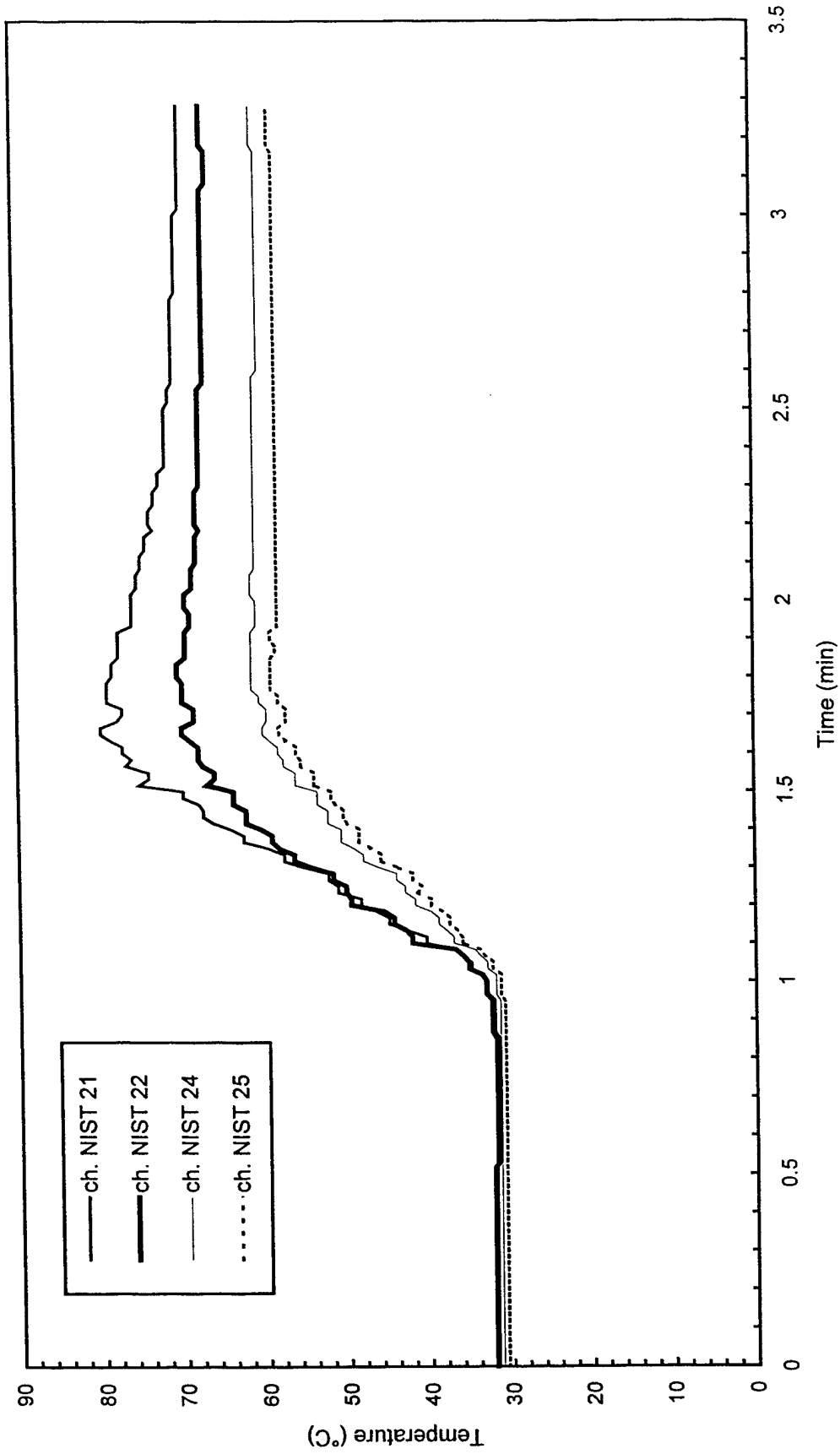


Fig. B116 - Temperature of Northwest steel beam

Test S7

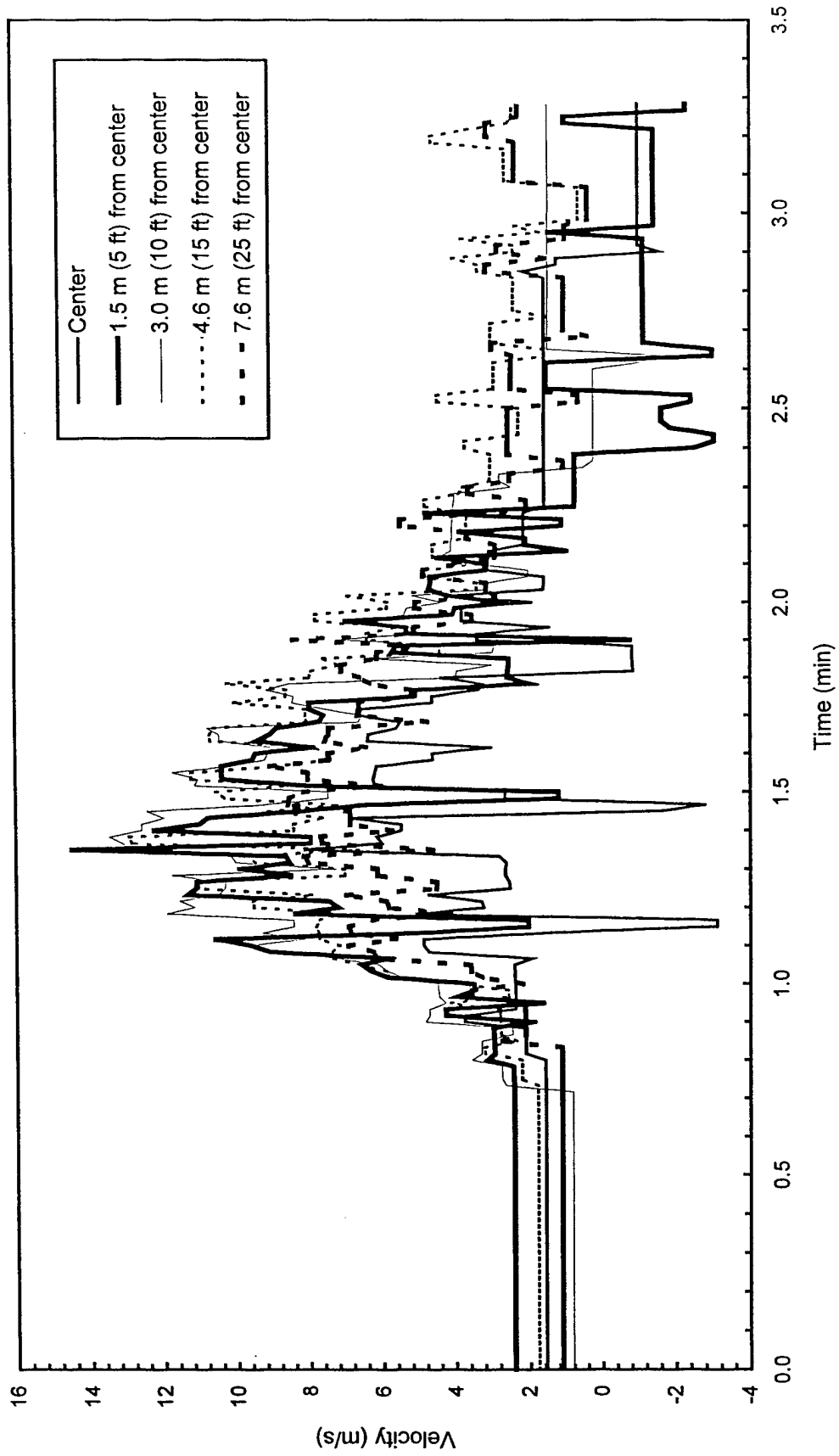


Fig. B117 - Plume and ceiling jet velocities

Test S7

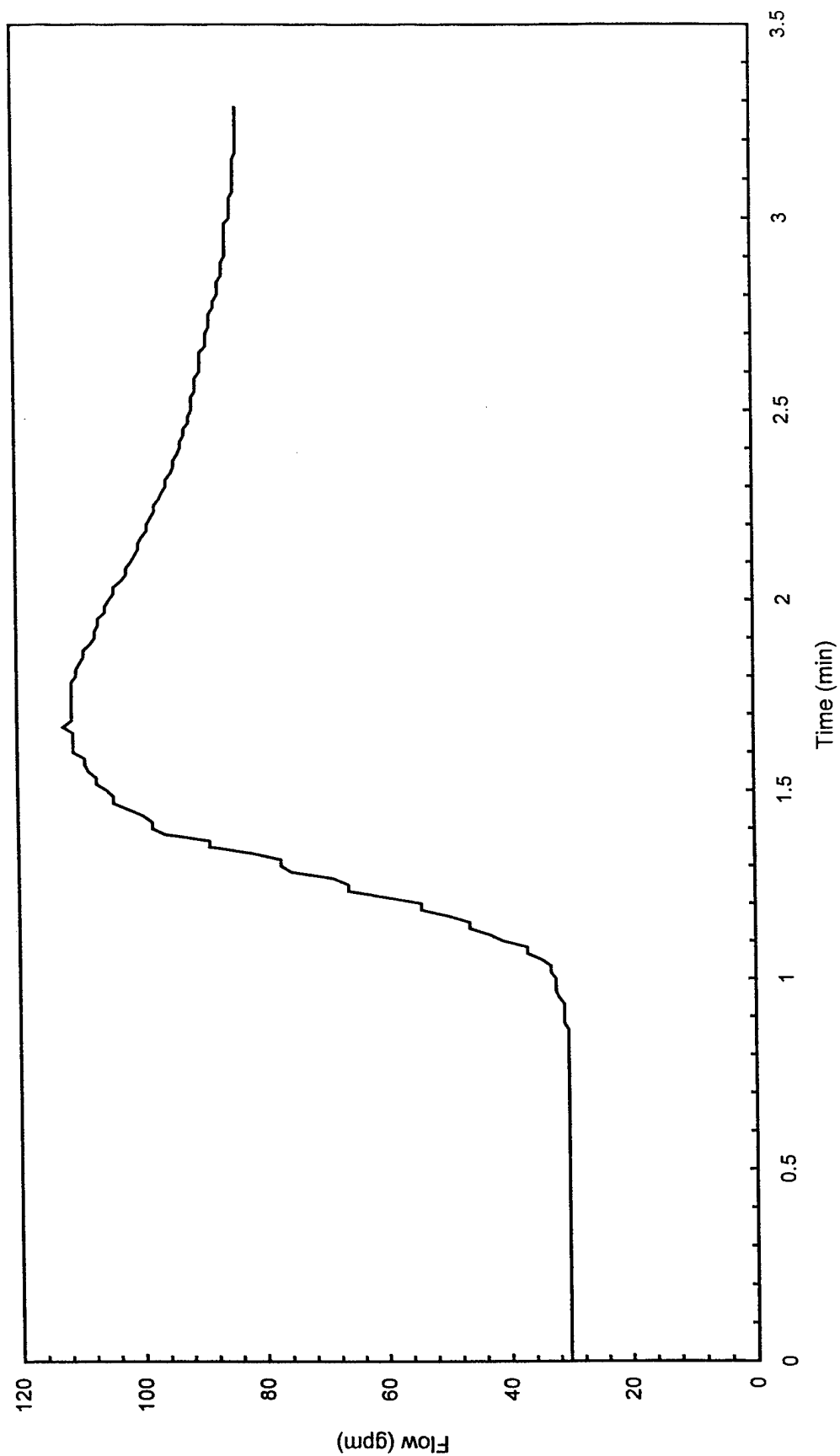


Fig. B118 - Sprinkler system flowrate

Test S7

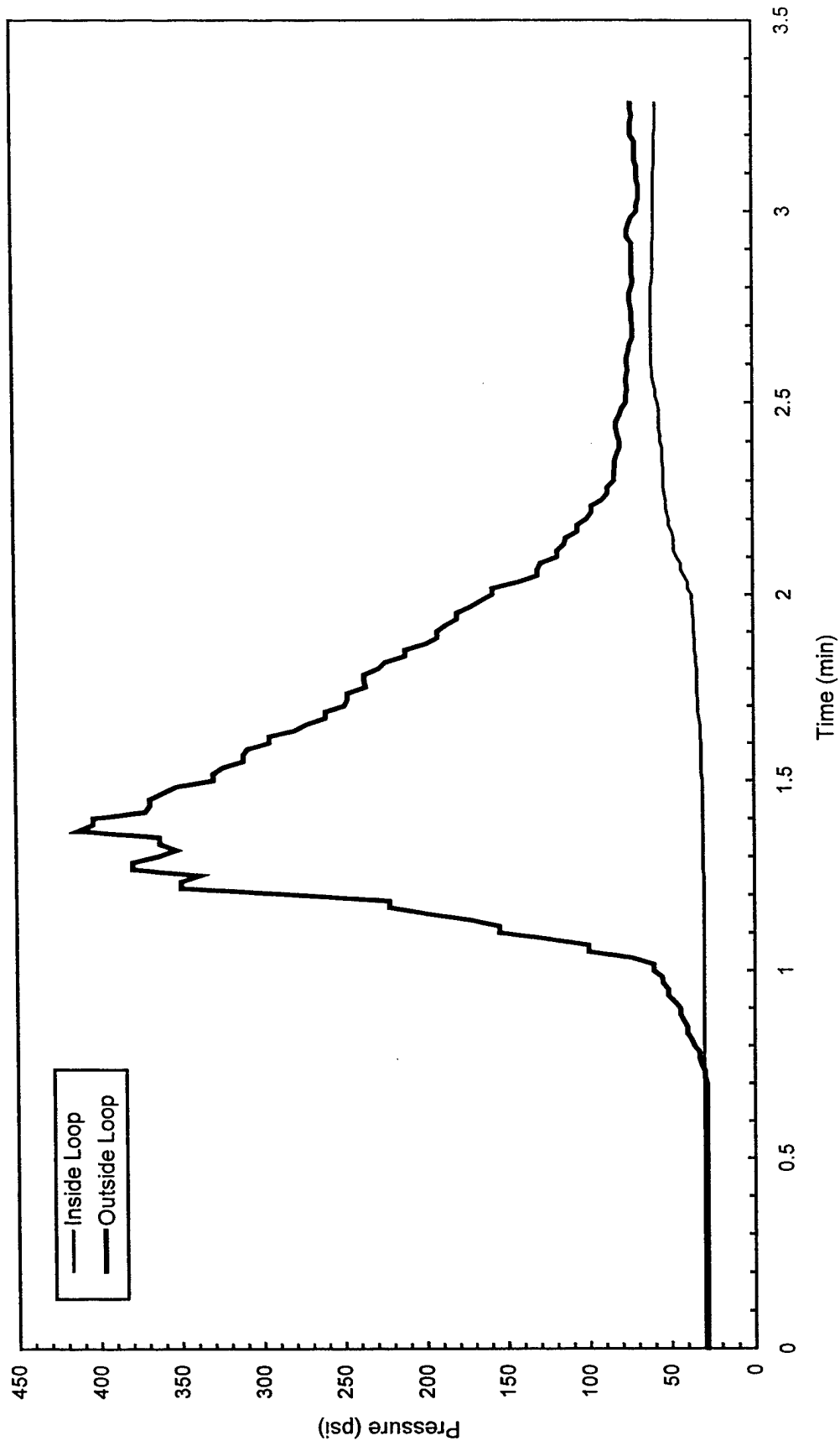


Fig. B119 - Sprinkler system pressure

APPENDIX C
MCAFFSS Test Data

Test F1

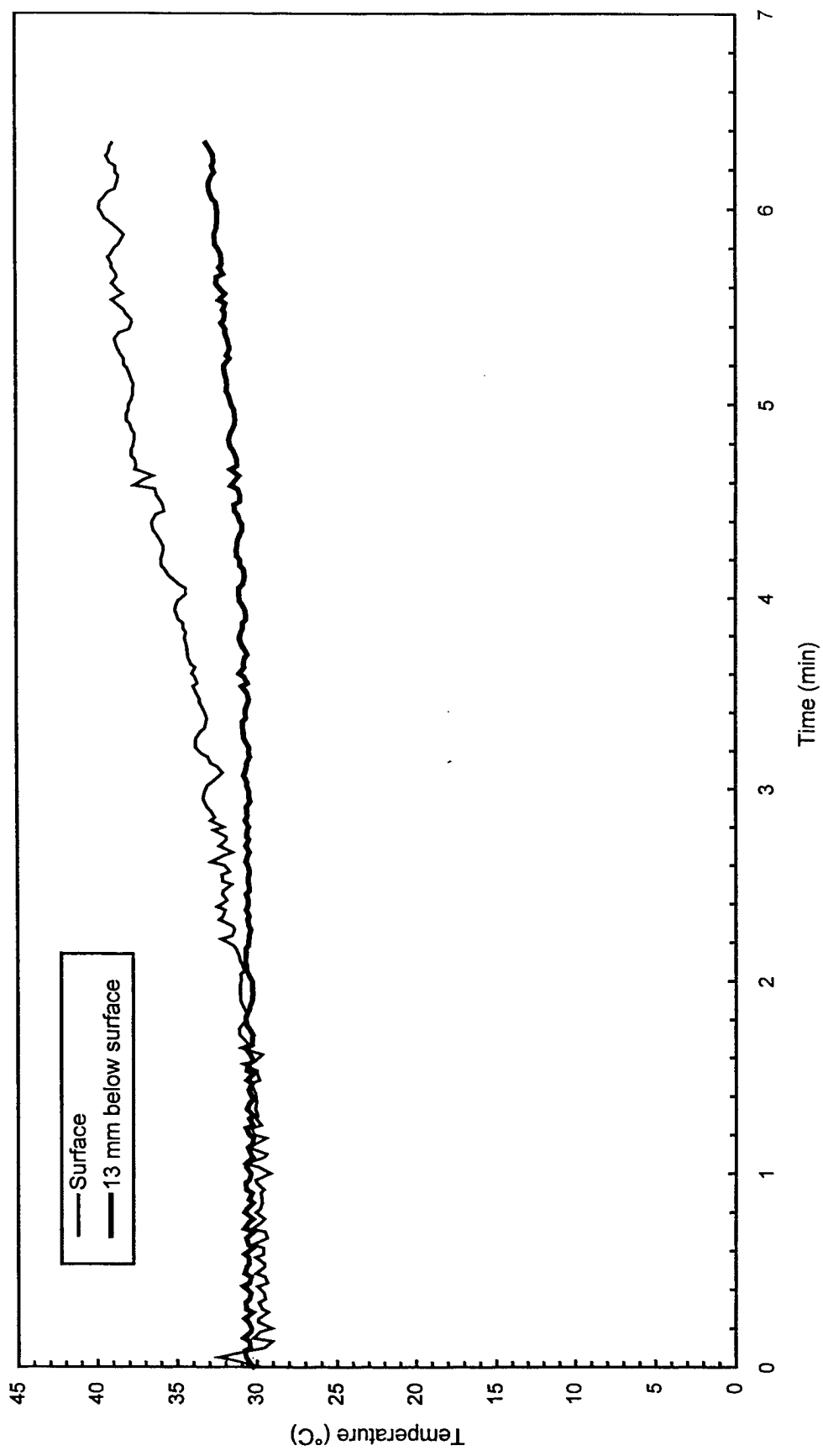


Fig. C1 - Concrete temperatures at center of pad

Test F1

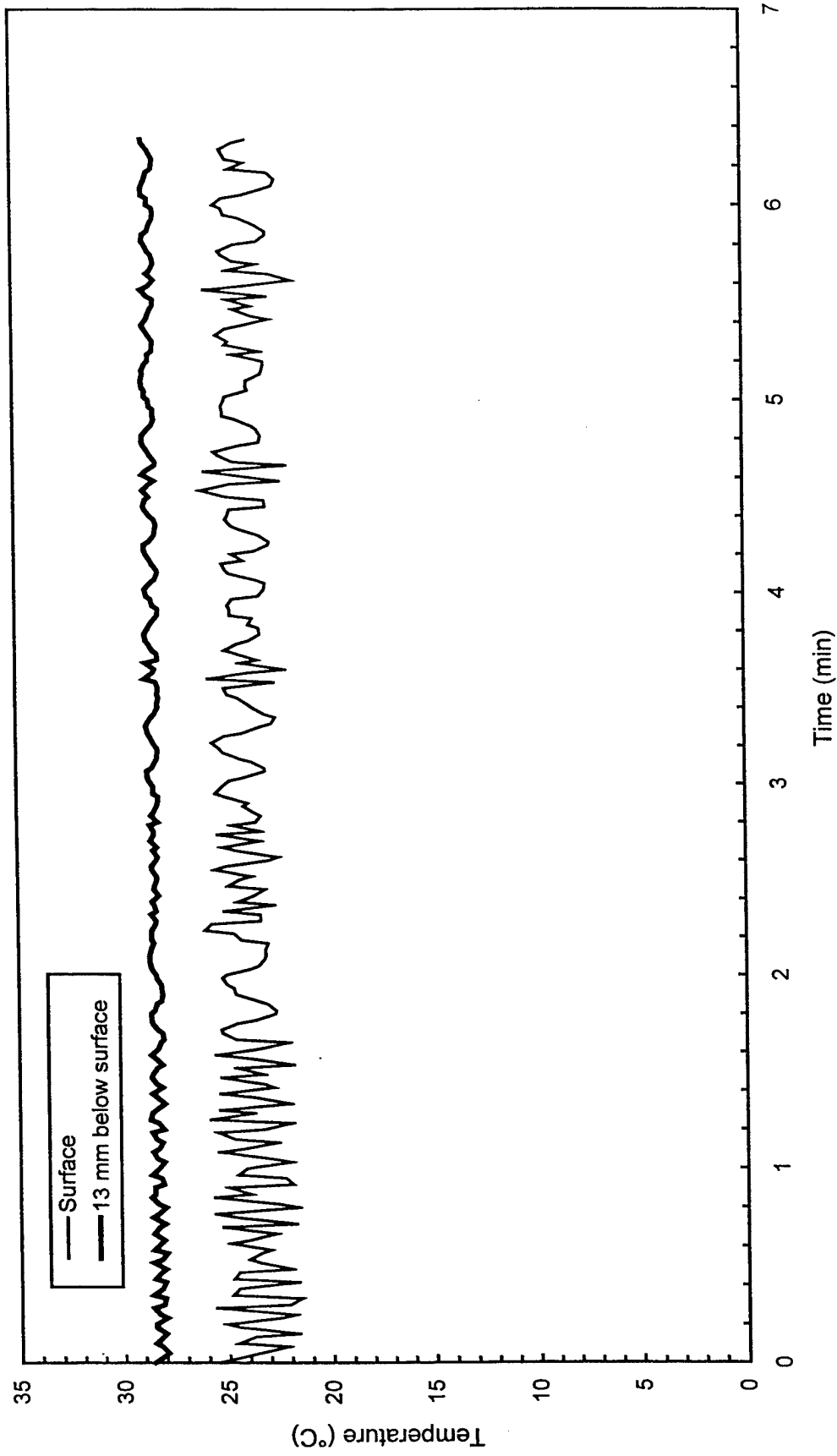


Fig. C2 - Concrete temperatures 3 m (10 ft) East of center of pad

Test F1

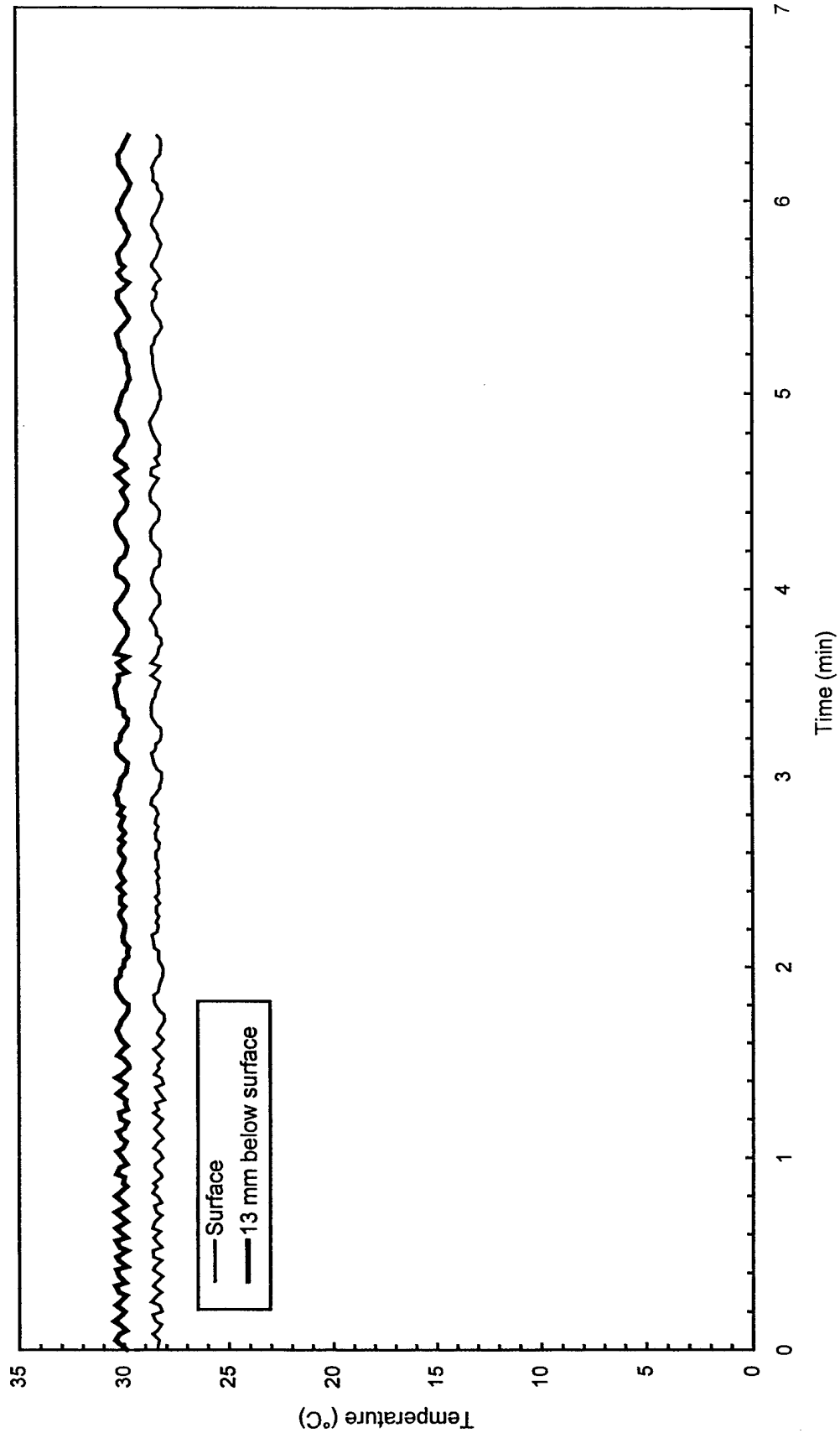


Fig. C3 - Concrete temperatures 3 m (10 ft) West of center of pad

Test F1

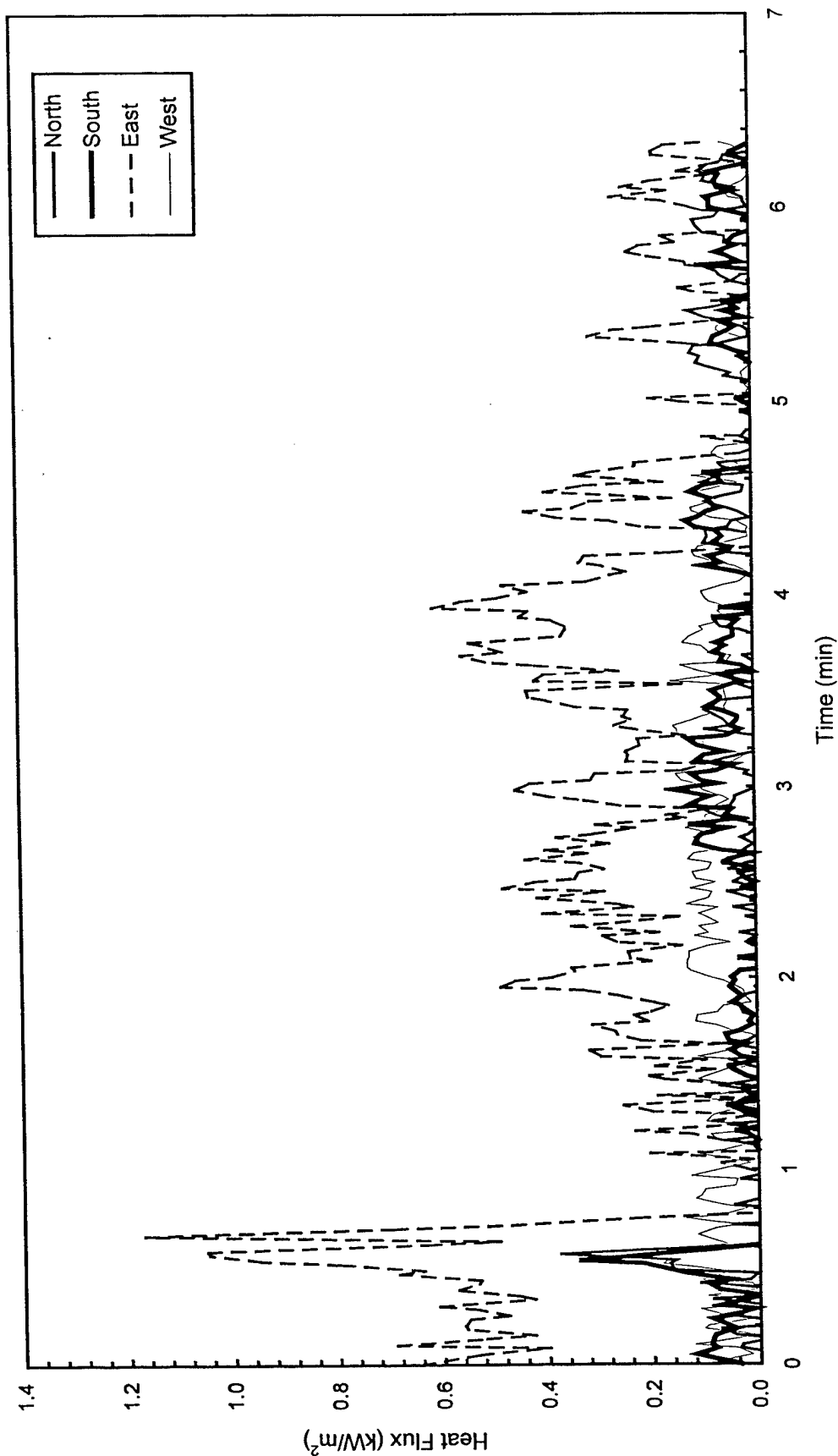


Fig. C4 - Heat flux measured at edge of pad

Test F1

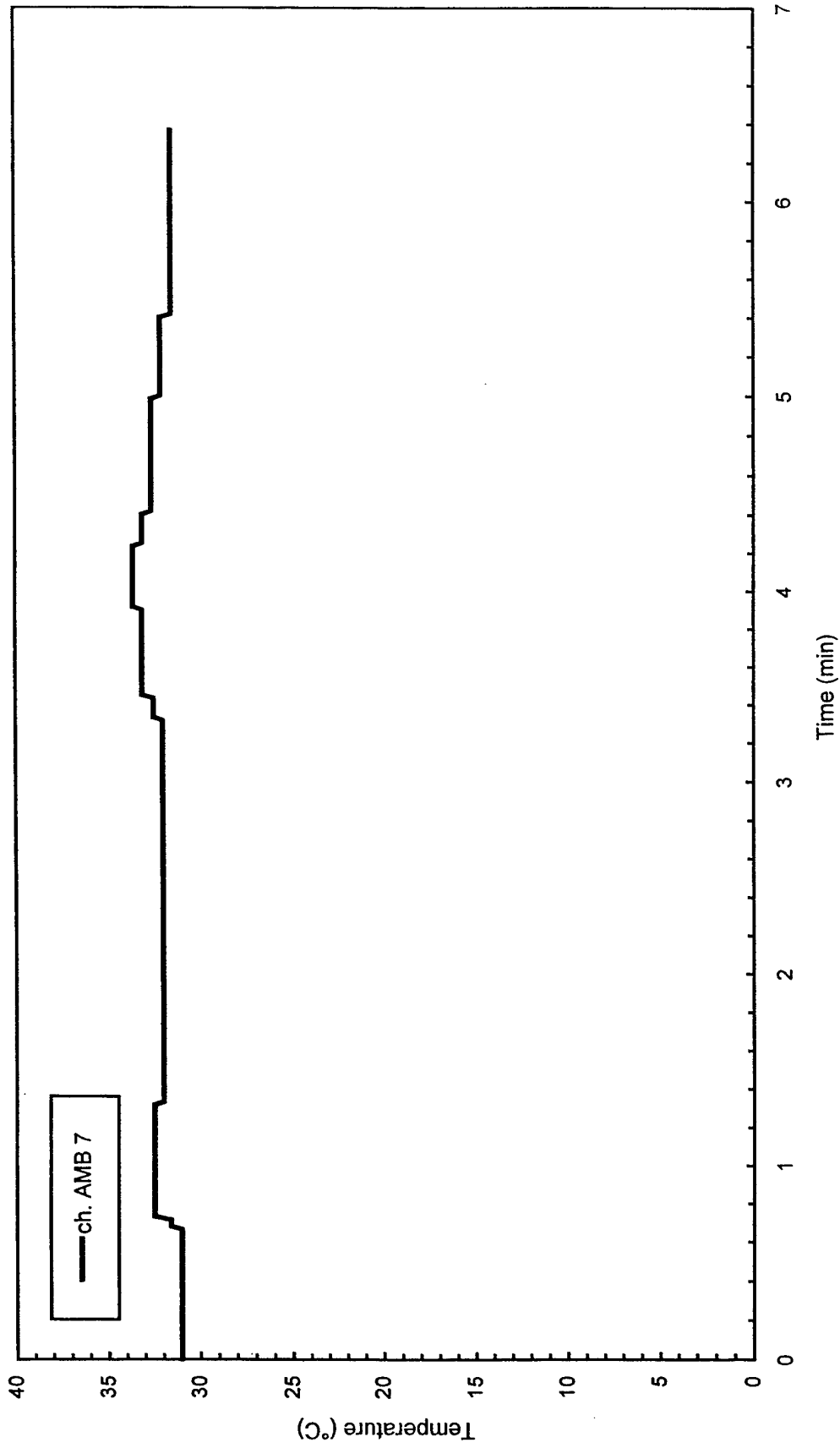


Fig. C5 - Air temperatures over center of pad

Test F1

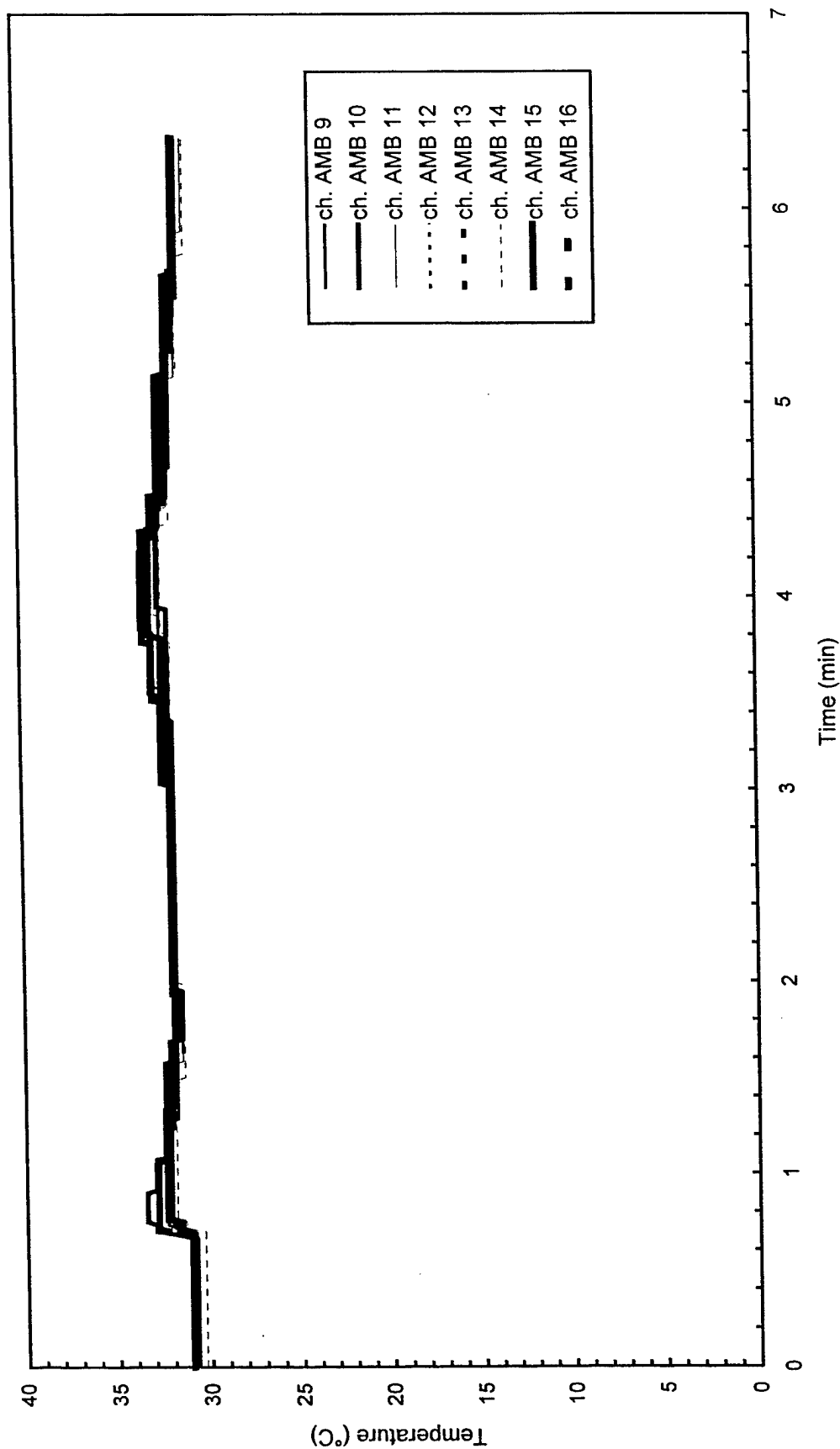


Fig. C6 - Air temperatures around 3 m (10 ft) radius from center of pad

Test F1

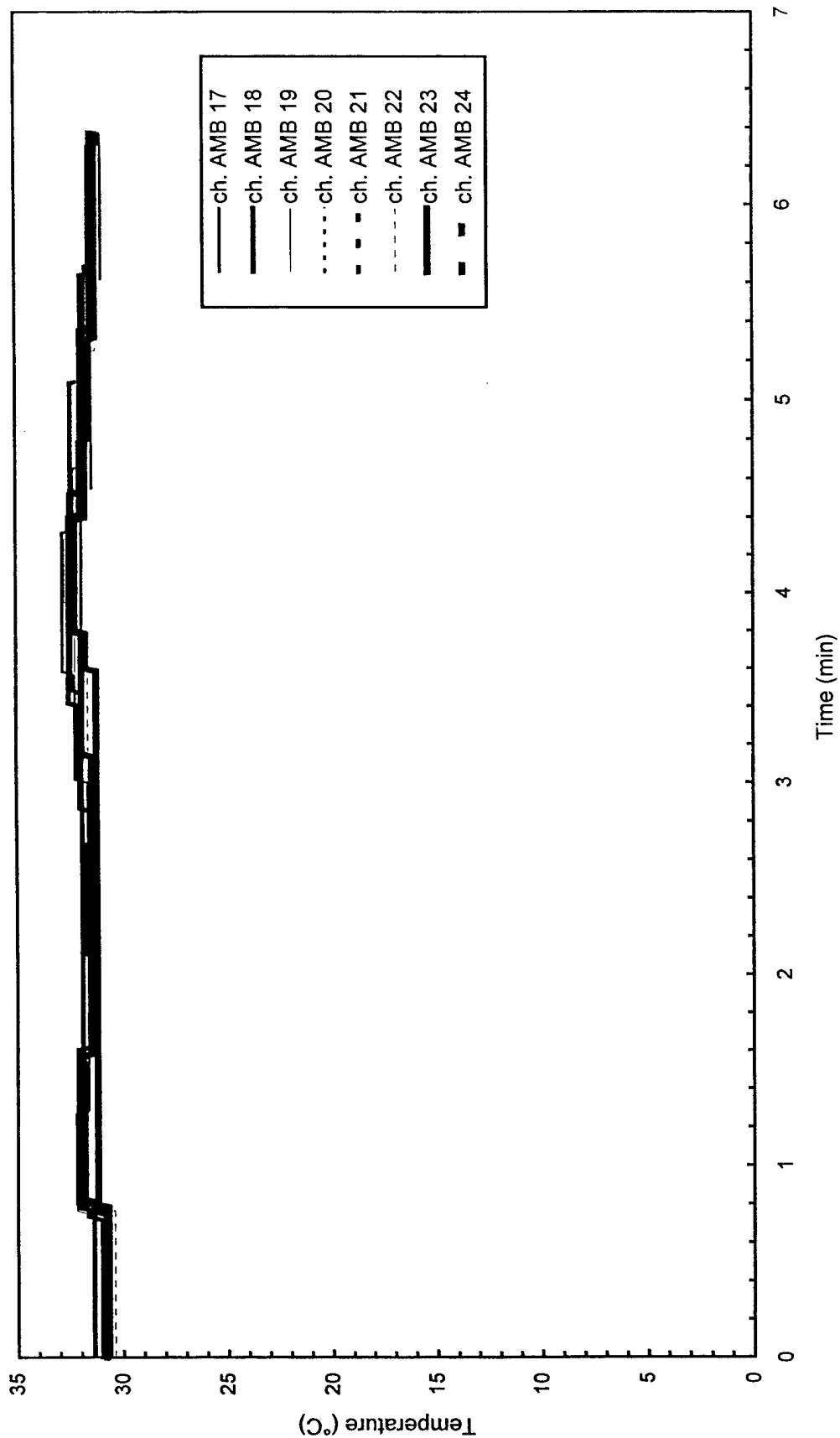


Fig. C7 - Air temperatures around 4.6 m (15 ft) radius from center of pad

Test F1

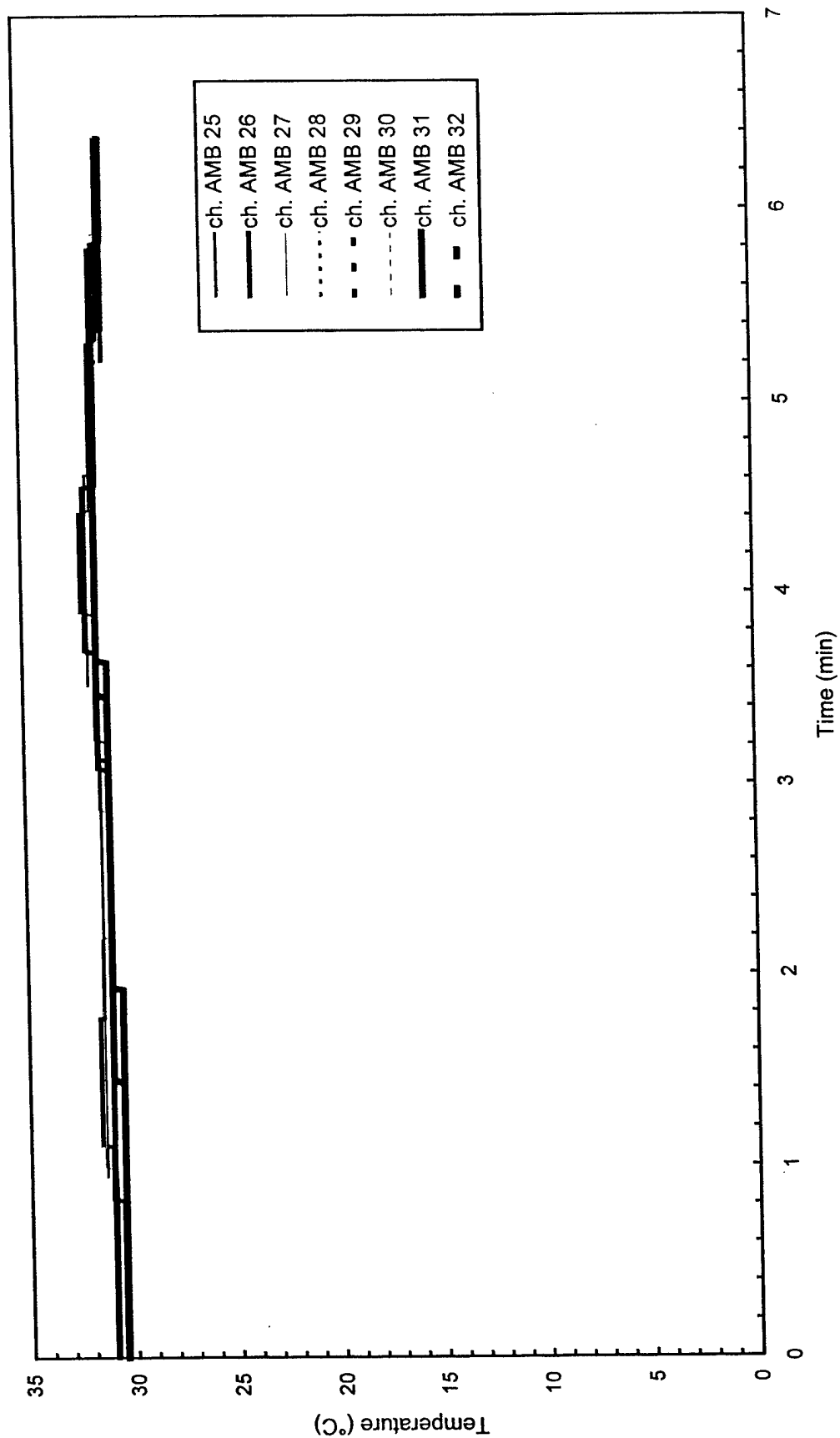


Fig. C8 - Air temperatures around North half of 7.6 m (25 ft) radius from center of pad

Test F1

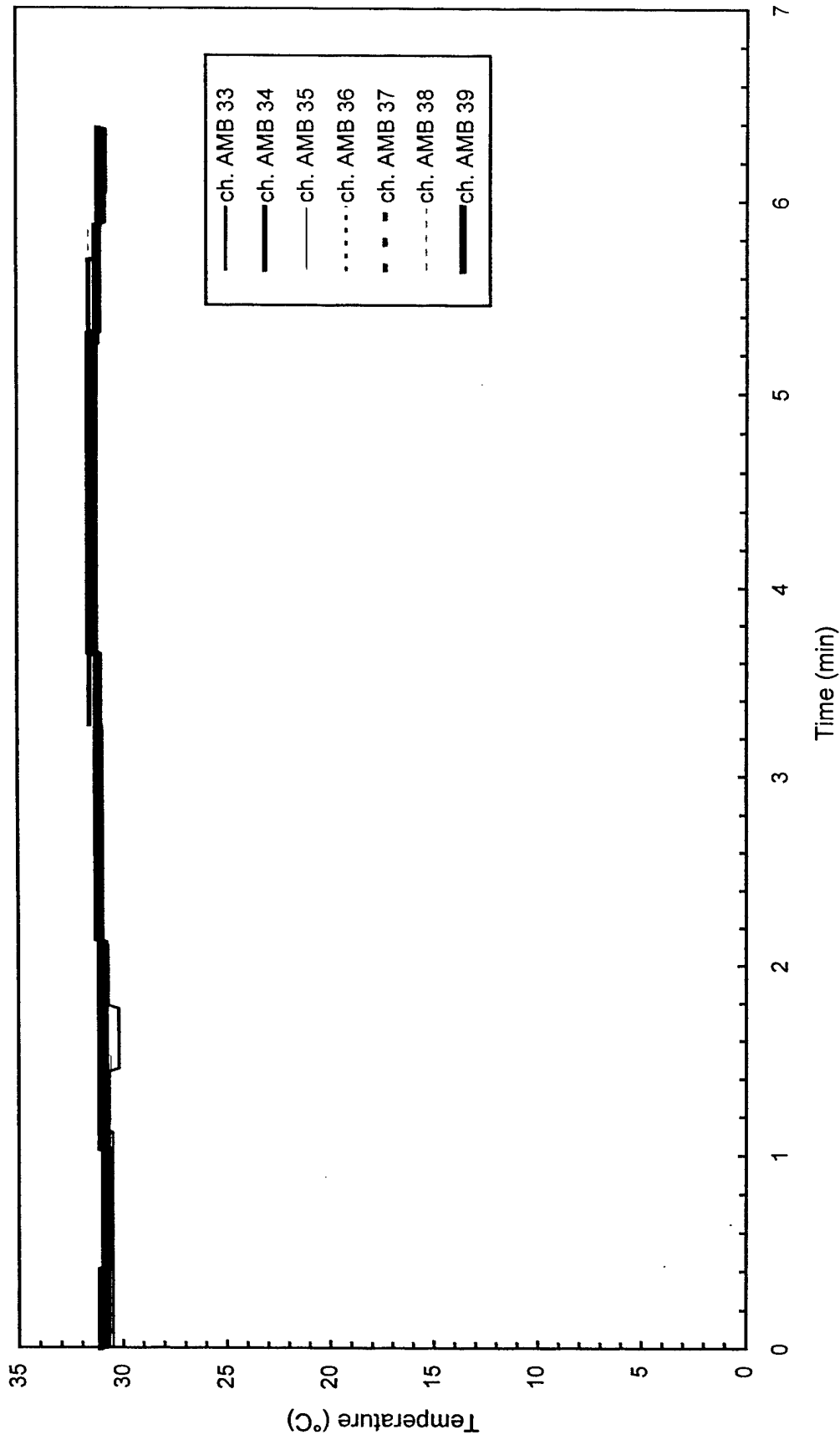


Fig. C9 - Air temperatures around South half of 7.6 m (25 ft) radius from center of pad

Test F1

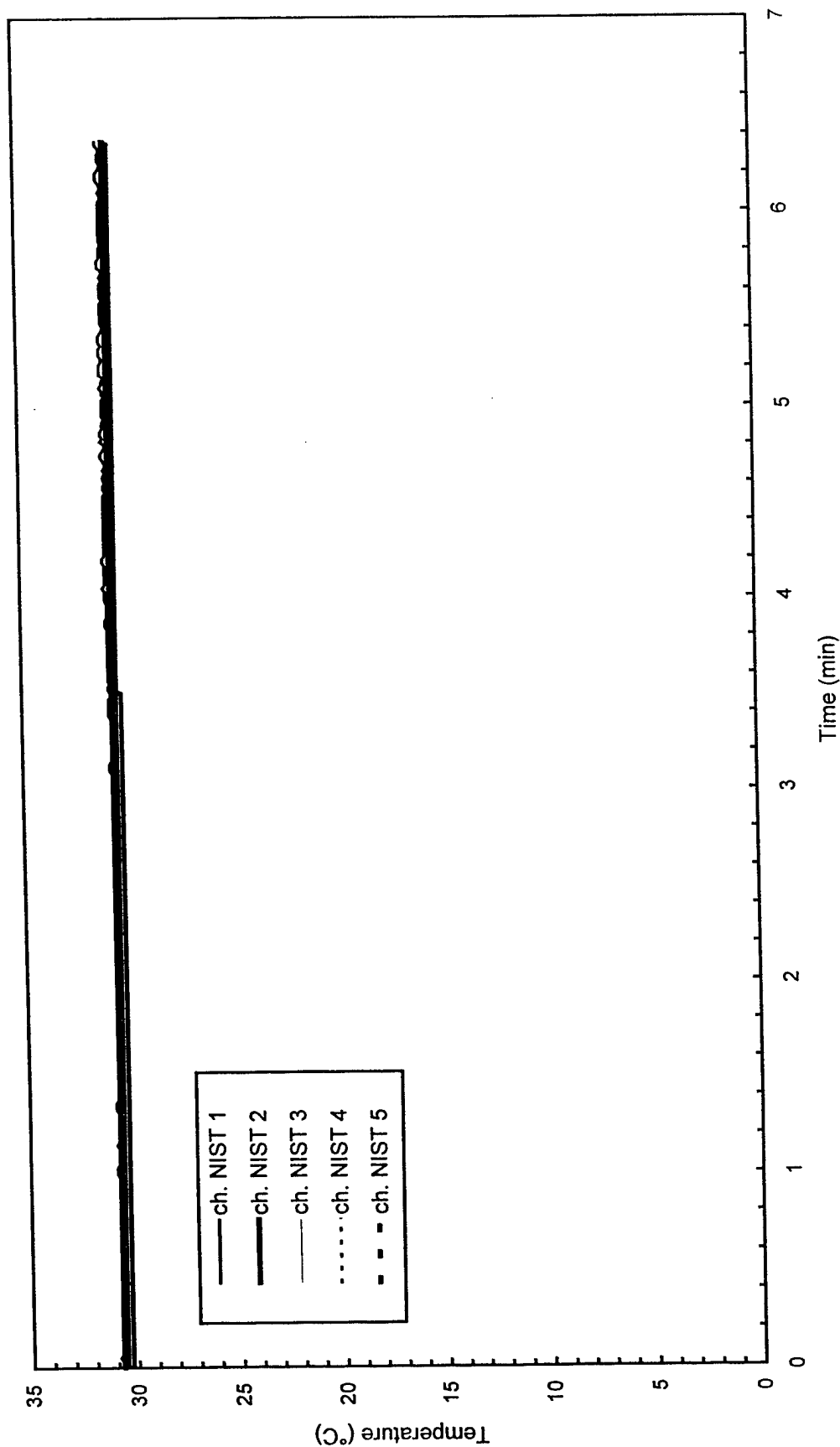


Fig. C10 - Temperature of West steel beam

Test F1

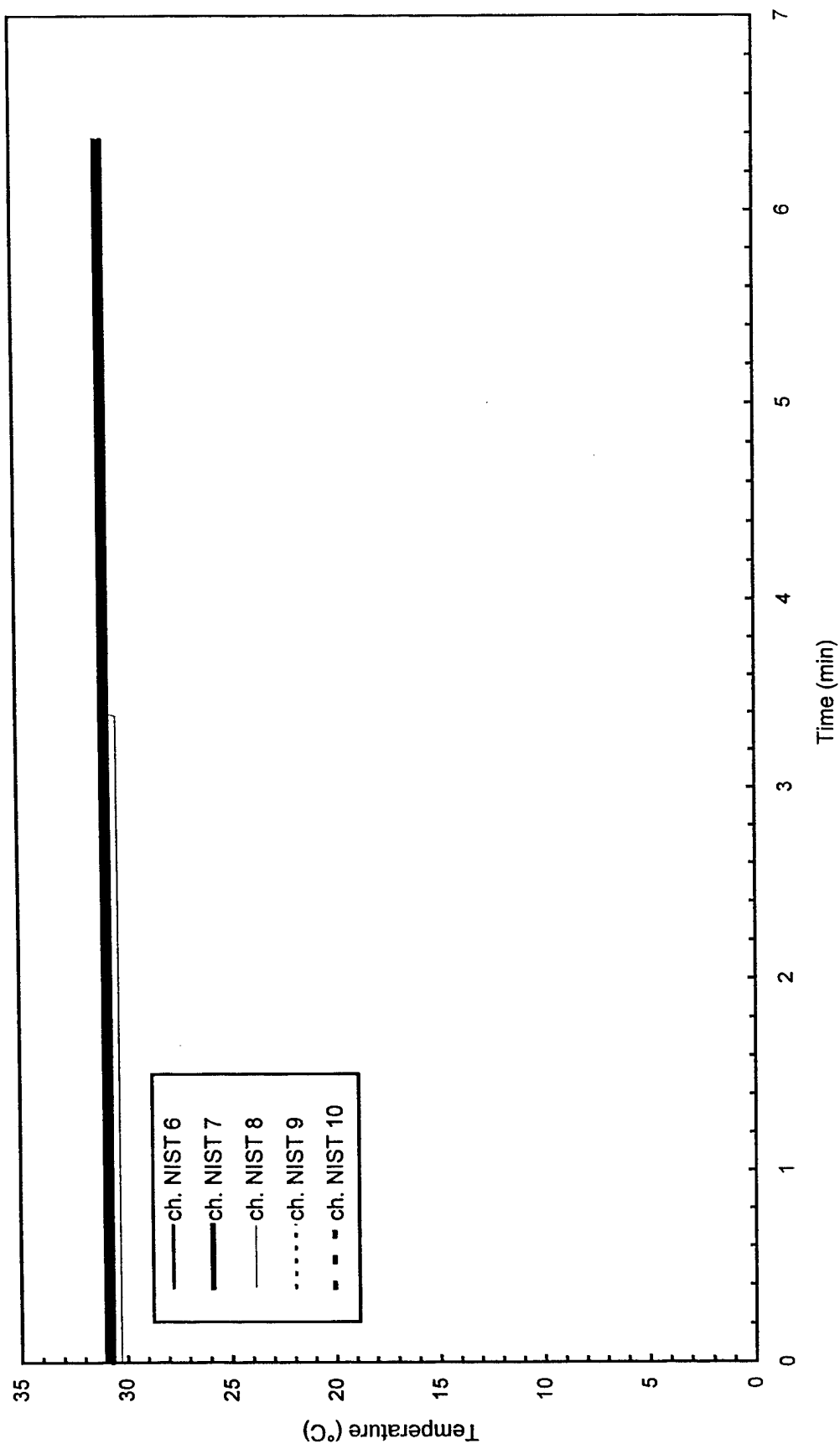


Fig. C11 - Temperature of North steel beam

Test F1

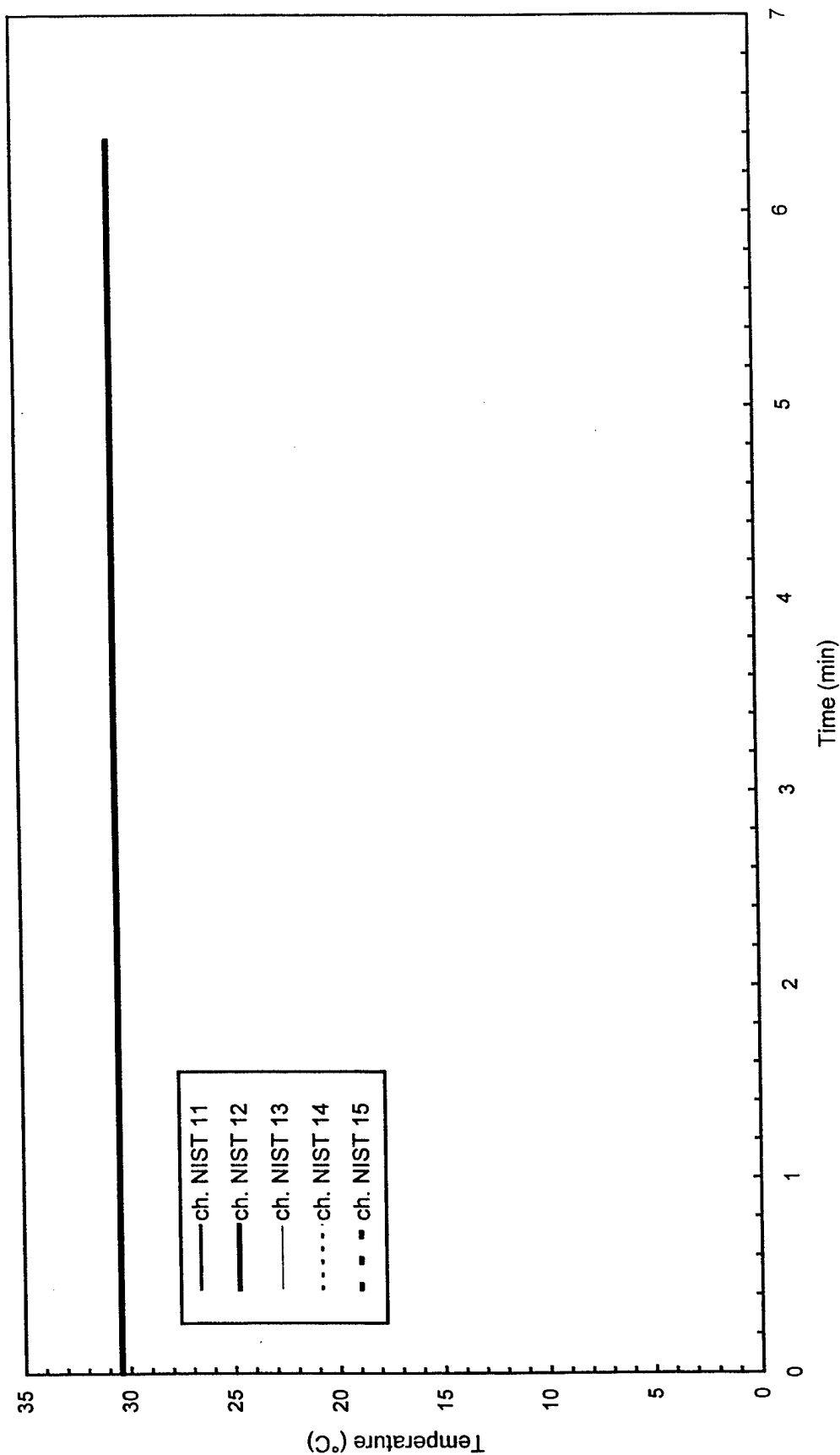


Fig. C12 - Temperature of East steel beam

Test F1

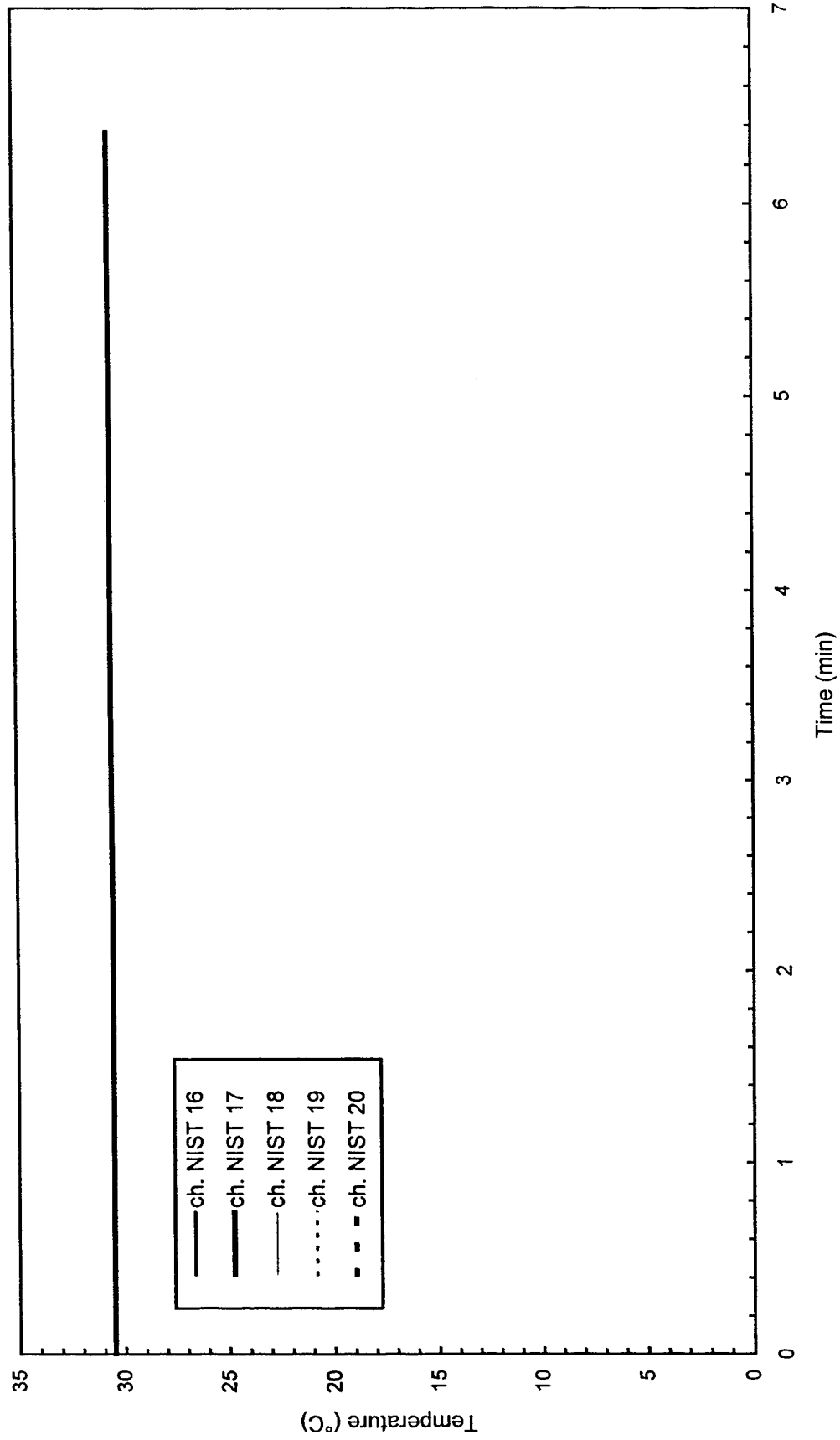


Fig. C13 - Temperature of South steel beam

Test F1

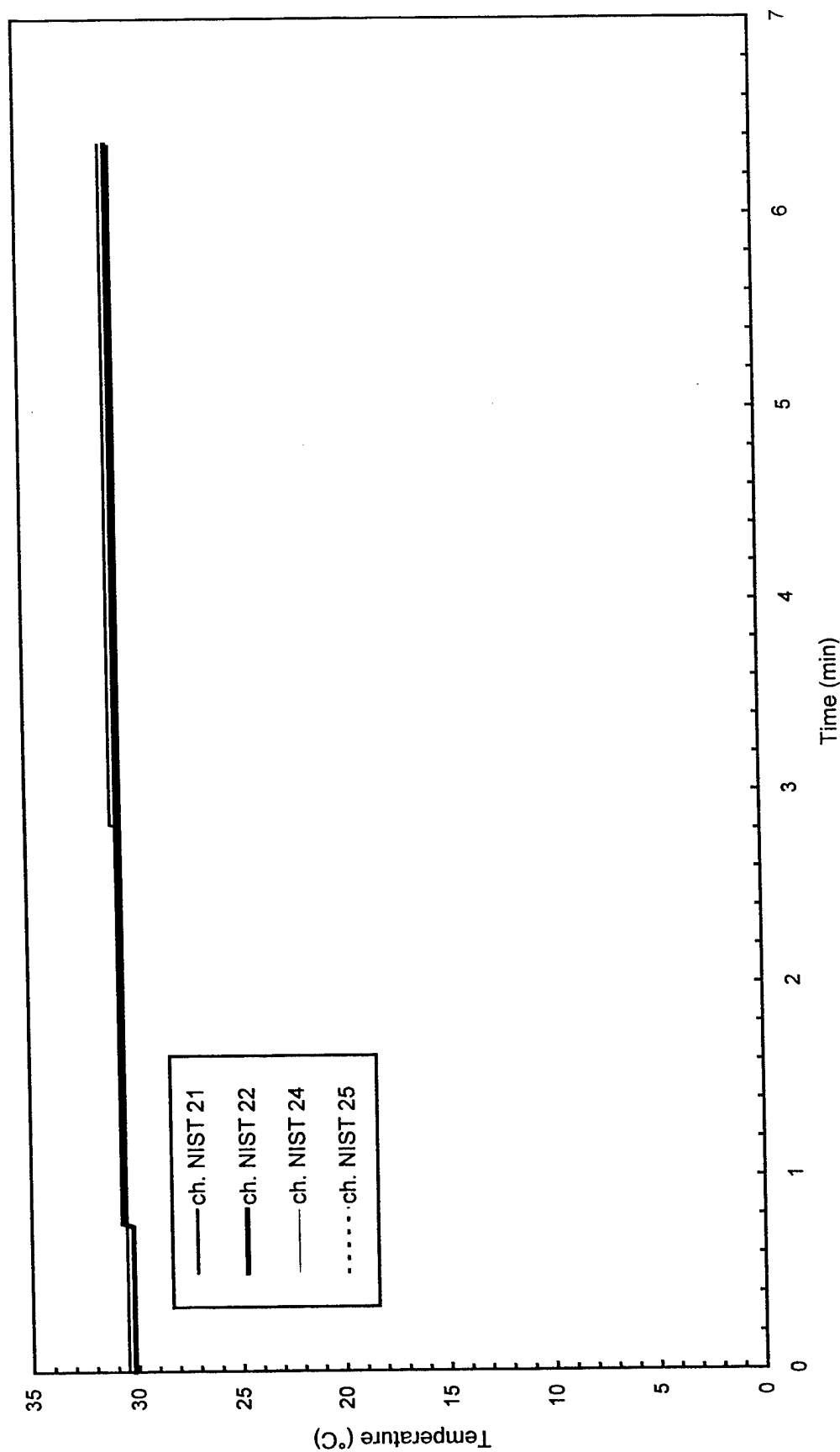


Fig. C14 - Temperature of Northwest steel beam

Test F1

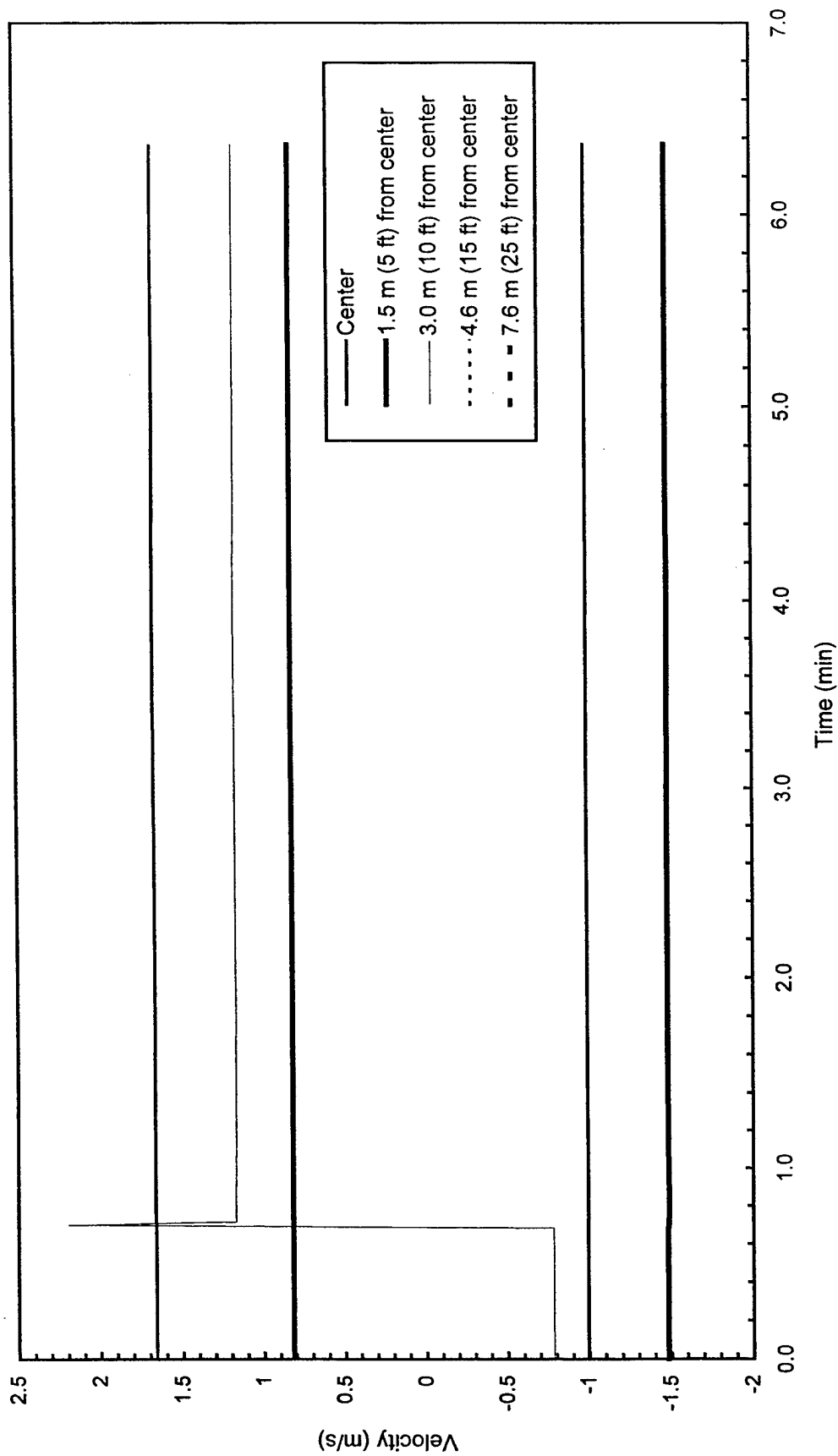


Fig. C15 - Plume and ceiling jet velocities

Test F2

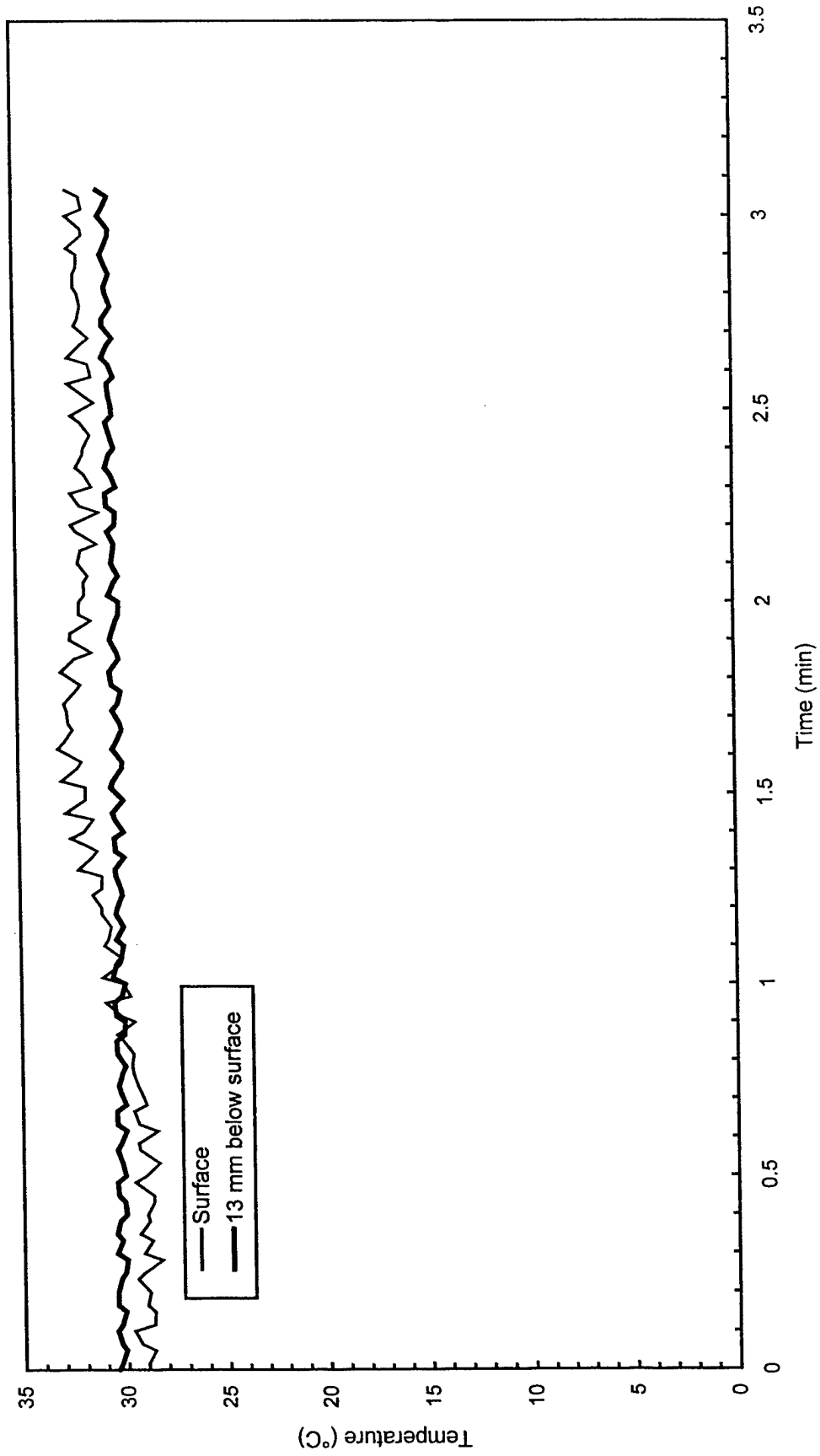


Fig. C16 - Concrete temperatures at center of pad

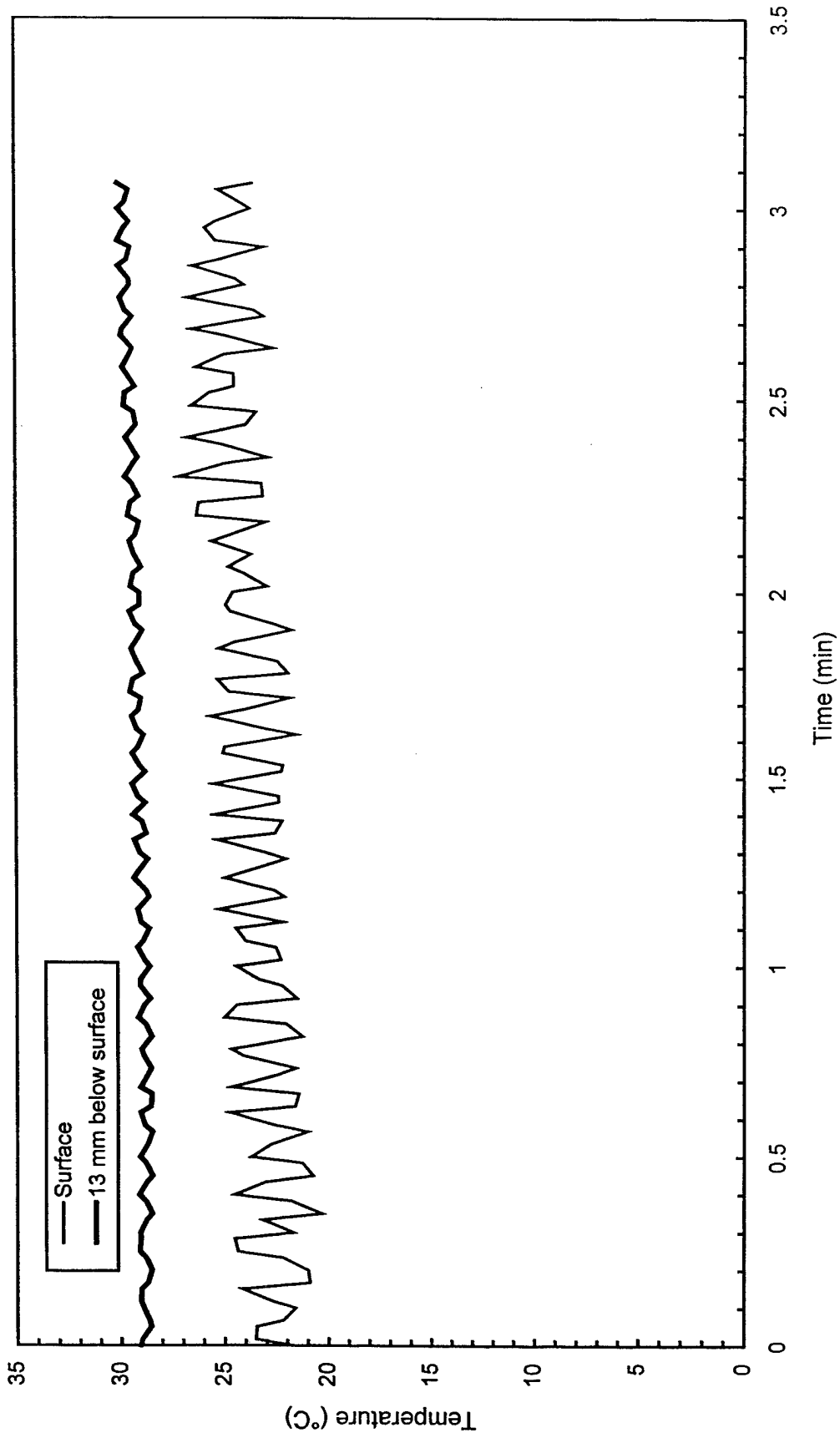


Fig. C17 - Concrete temperatures 3 m (10 ft) East of center of pad

Test F2

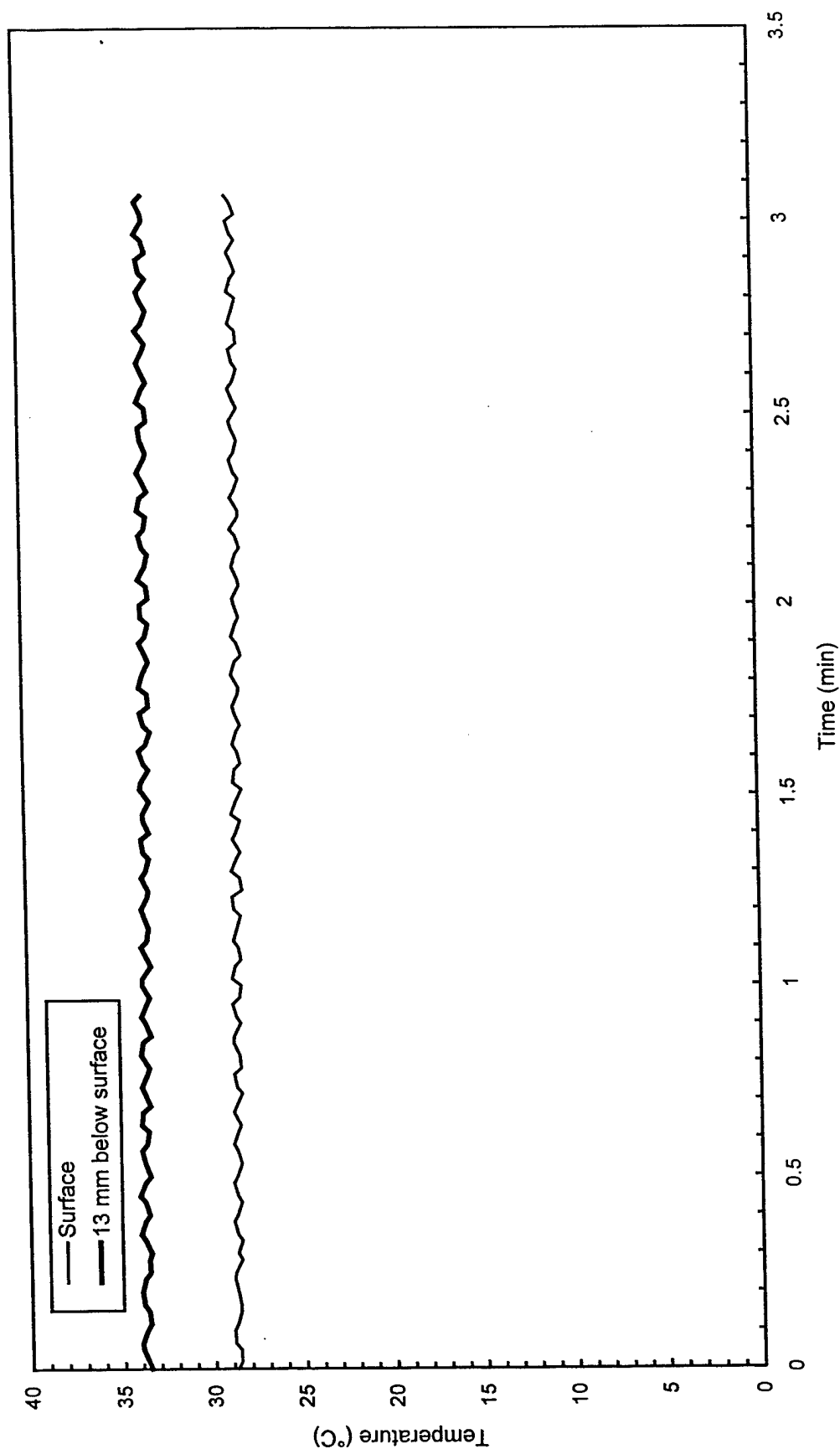


Fig. C18 - Concrete temperatures 3 m (10 ft) West of center of pad

Test F2

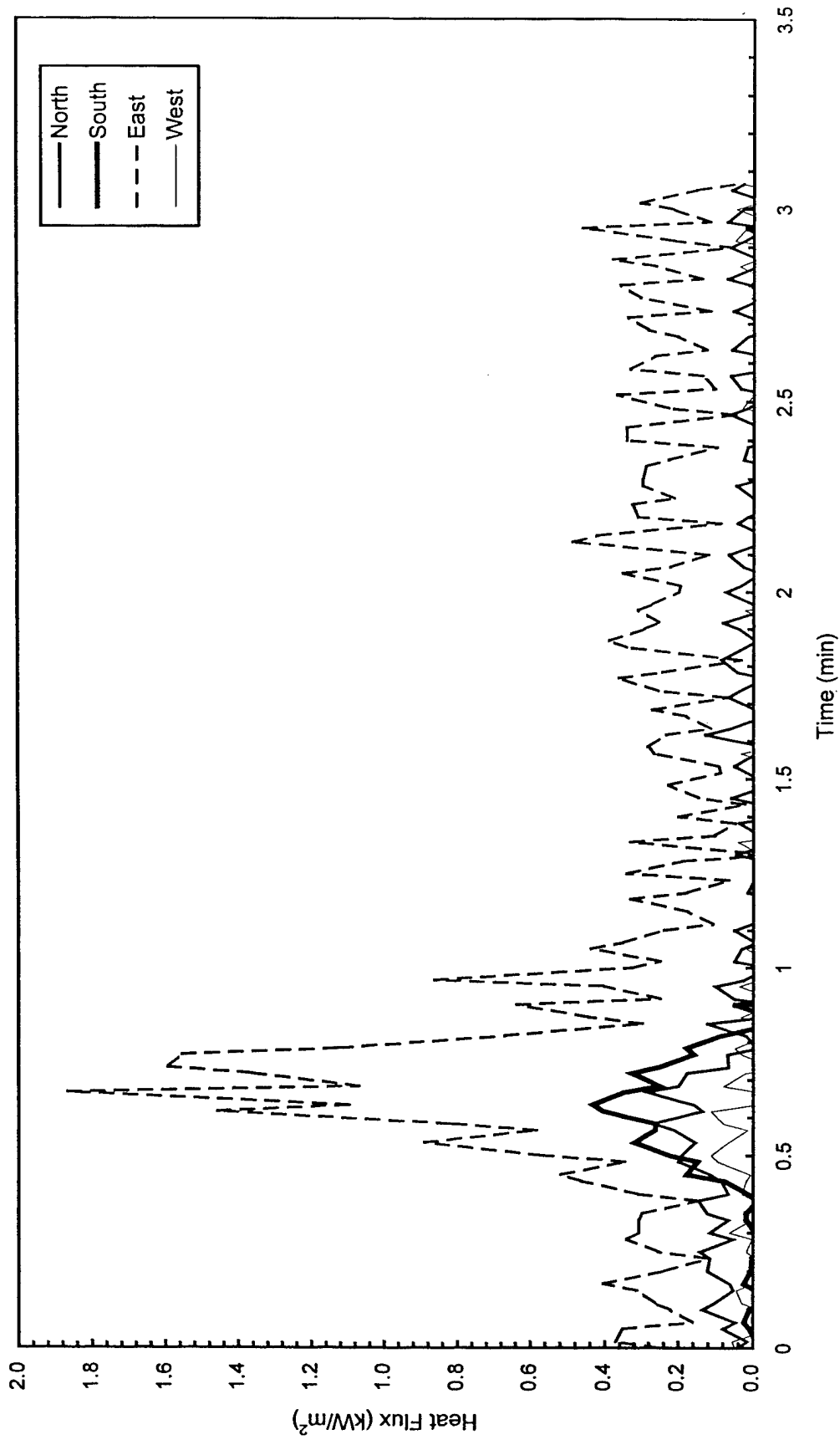


Fig. C19 - Heat flux measured at edge of pad

Test F2

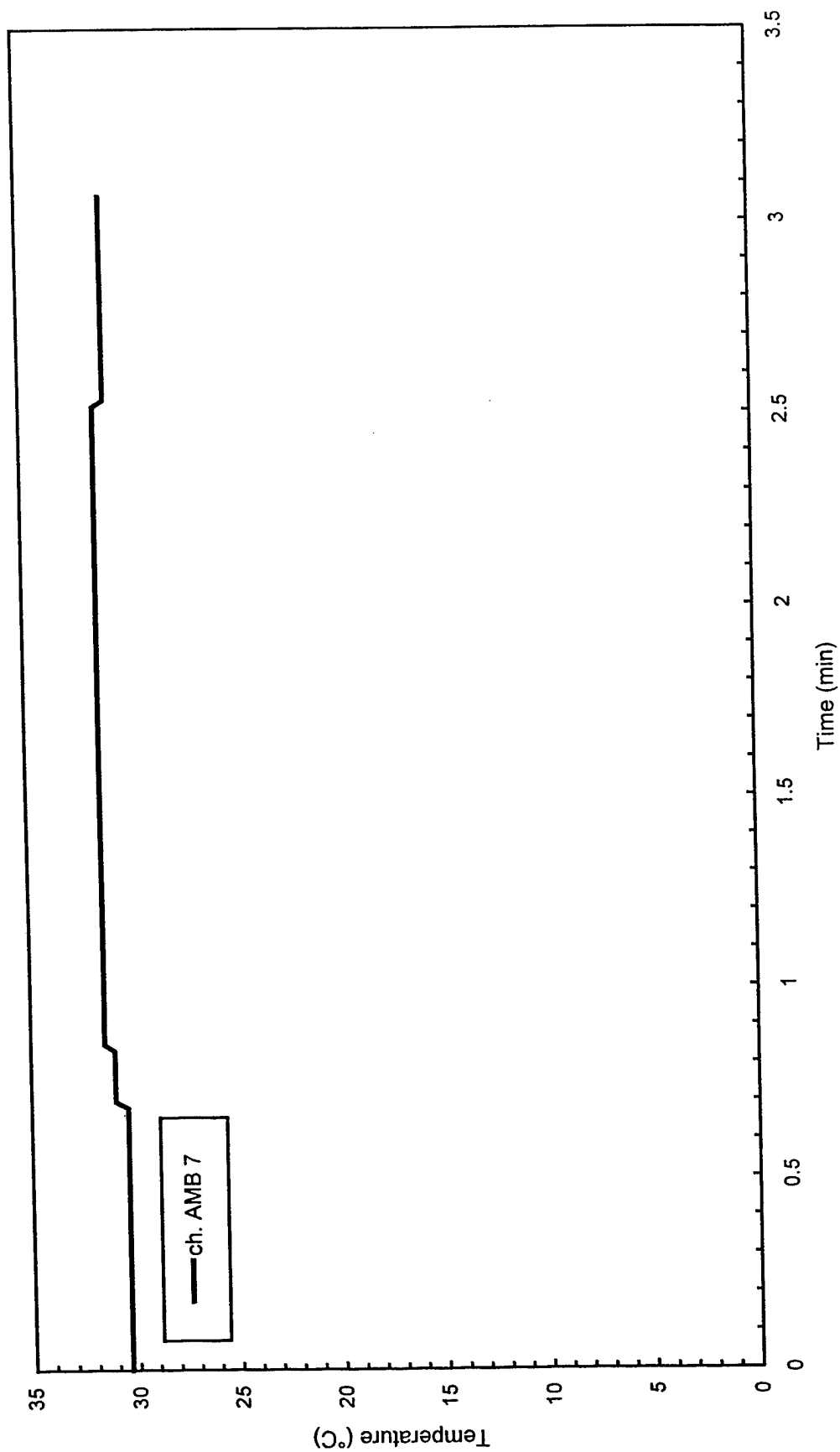


Fig. C20 - Air temperatures over center of pad

Test F2

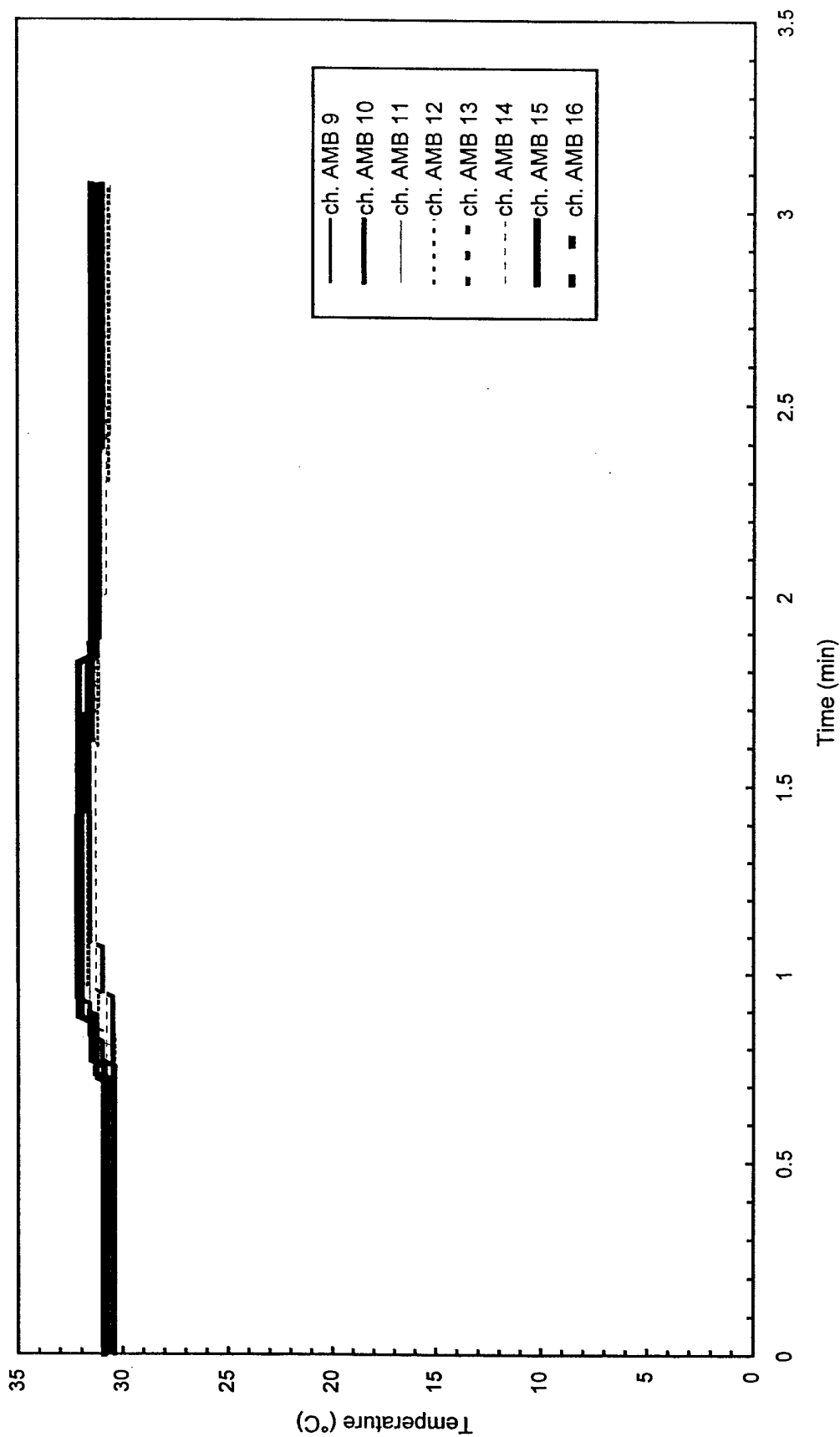


Fig. C21 - Air temperatures around 3 m (10 ft) radius from center of pad

Test F2

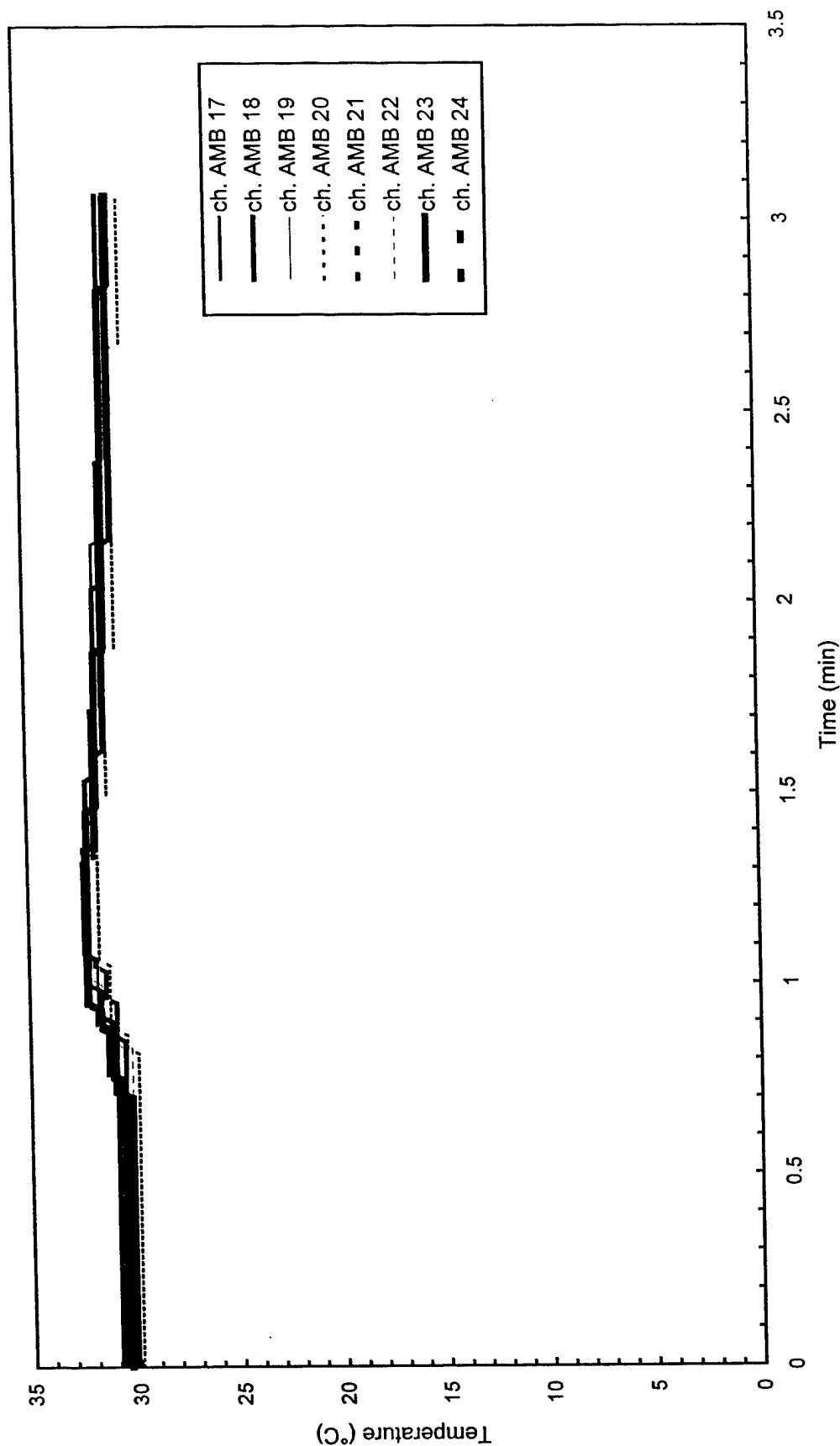


Fig. C22 - Air temperatures around 4.6 m (15 ft) radius from center of pad

Test F2

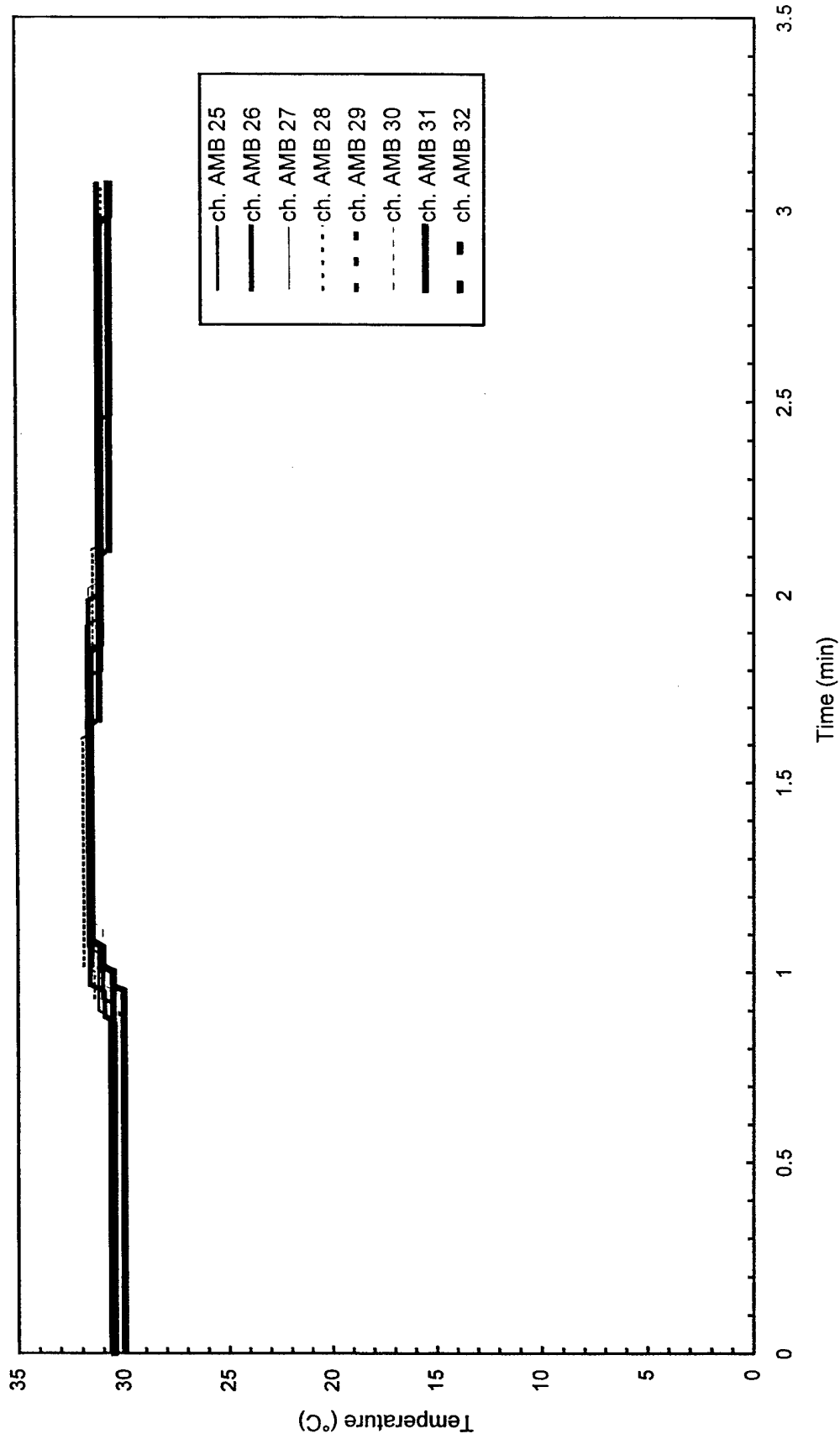


Fig. C23 - Air temperatures around North half of 7.6 m (25 ft) radius from center of pad

Test F2

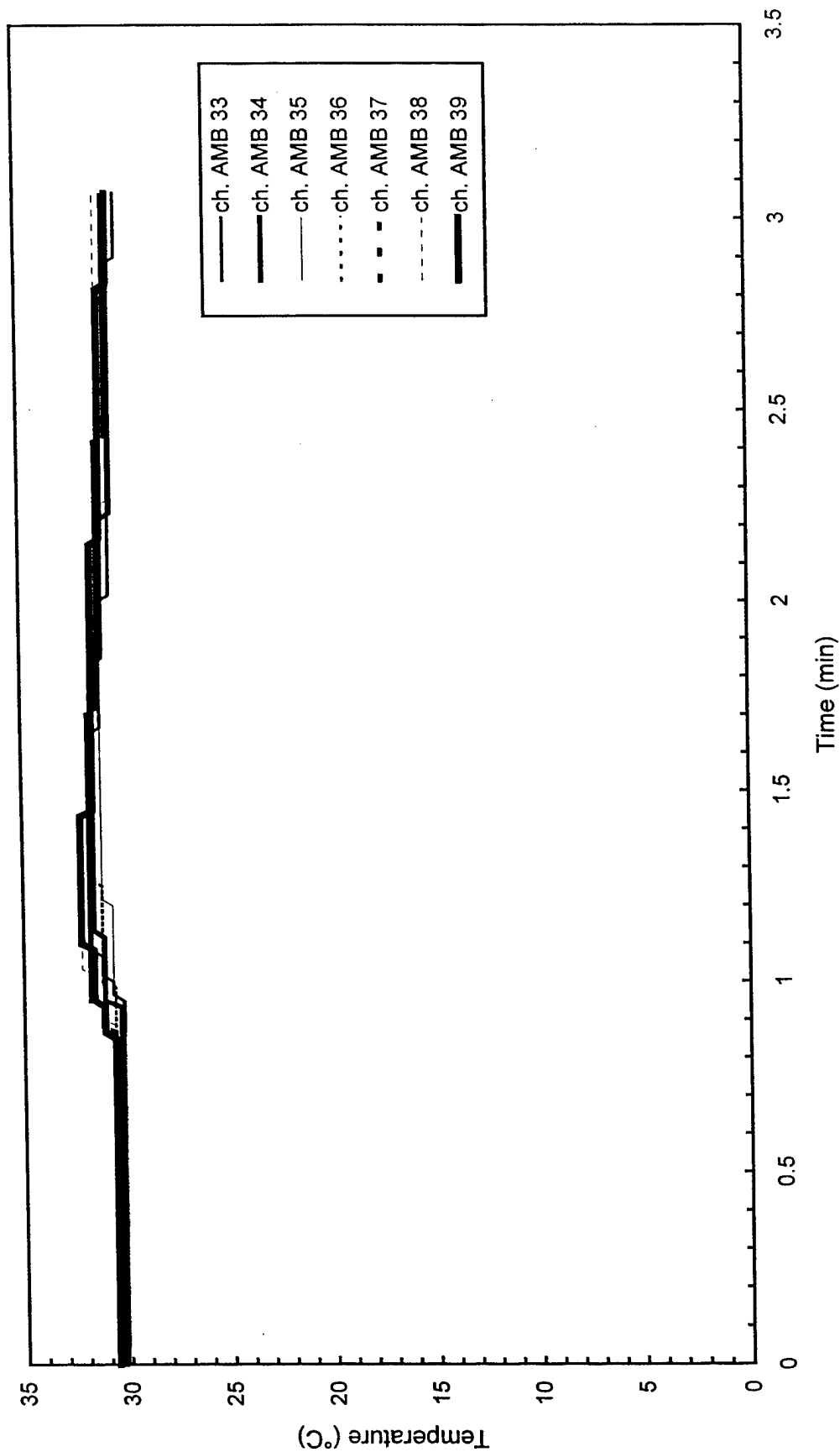


Fig. C24 - Air temperatures around South half of 7.6 m (25 ft) radius from center of pad

Test F2

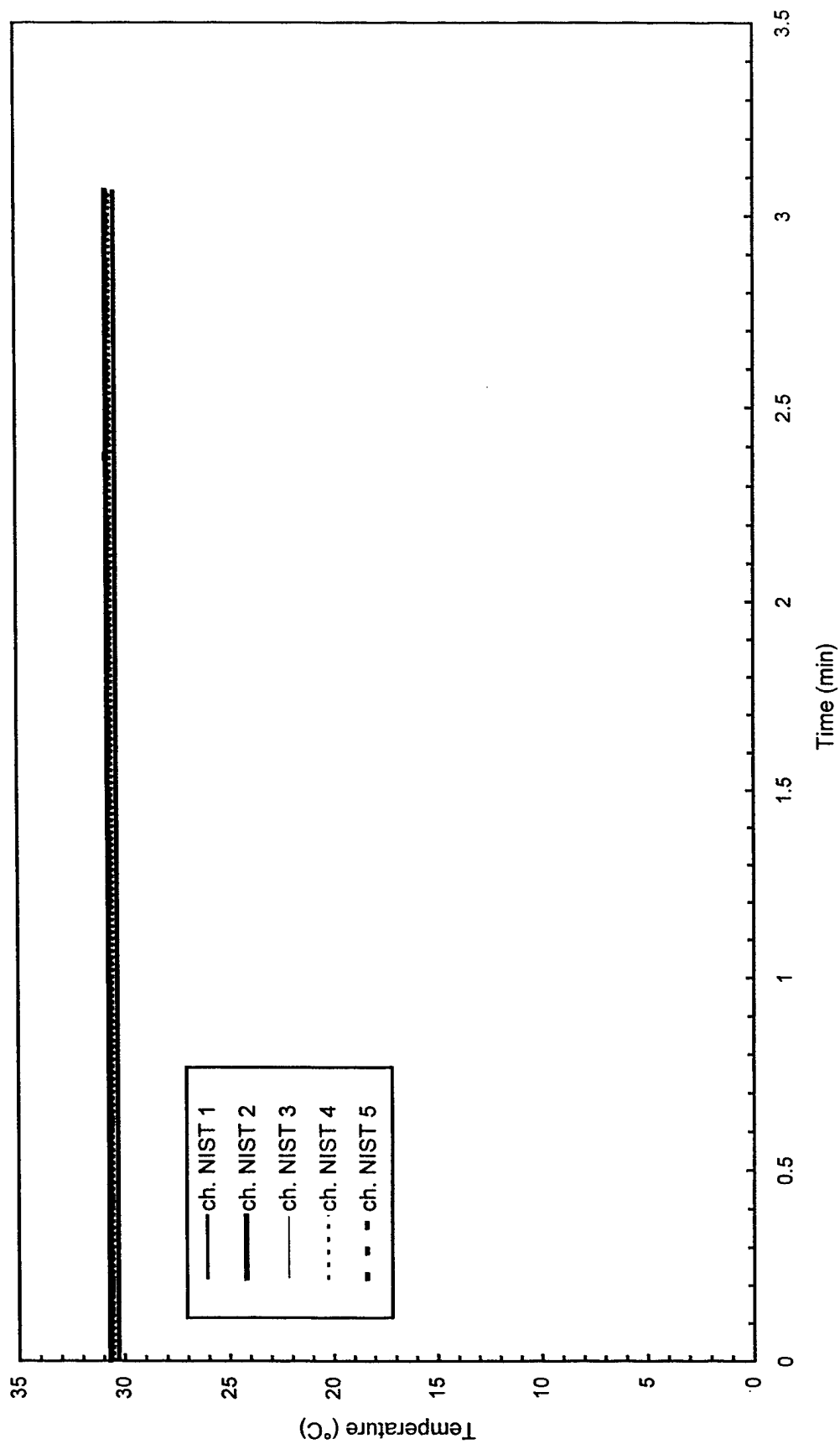


Fig. C25 - Temperature of West steel beam

Test F2

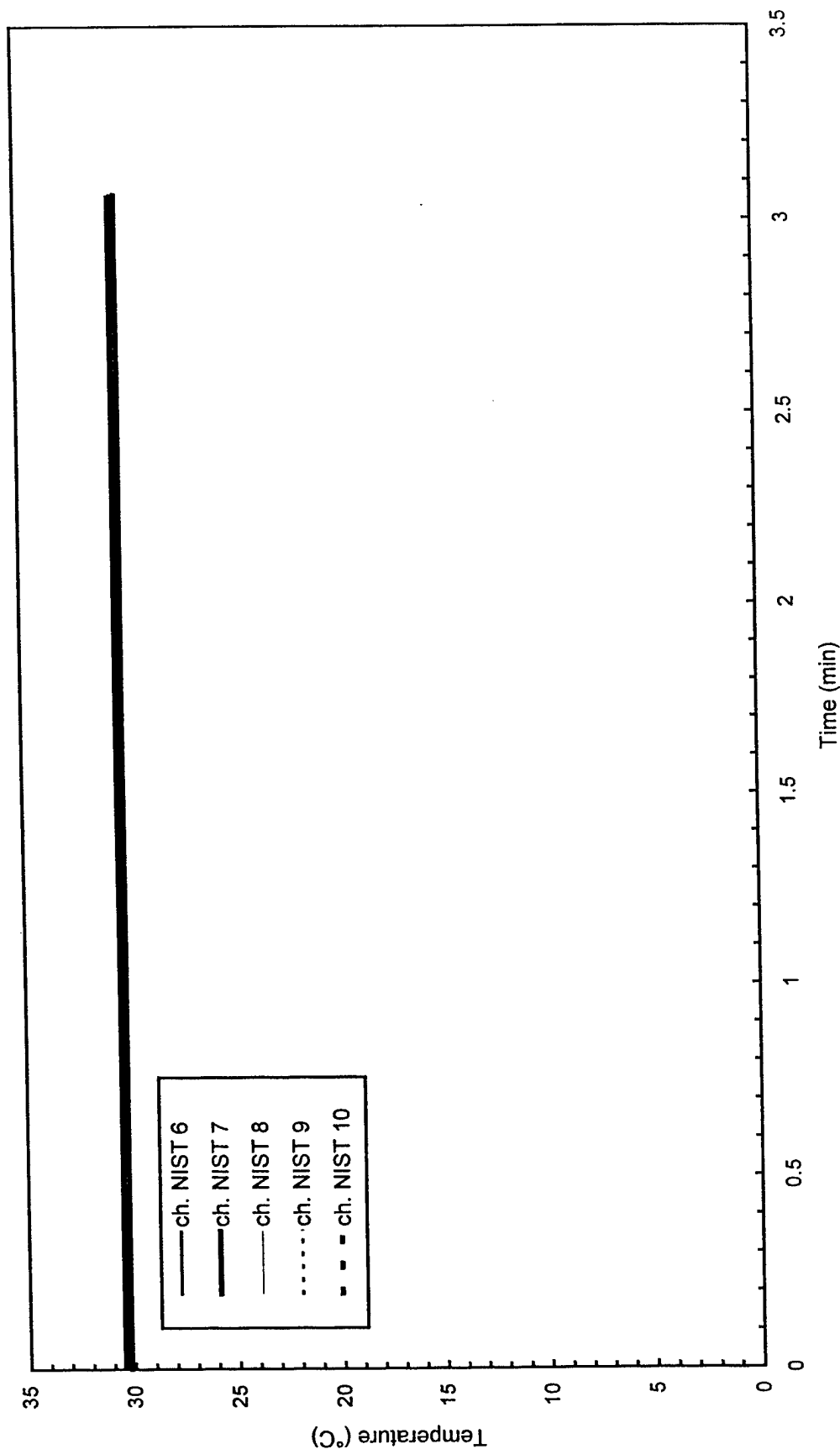


Fig. C26 - Temperature of North steel beam

Test F2

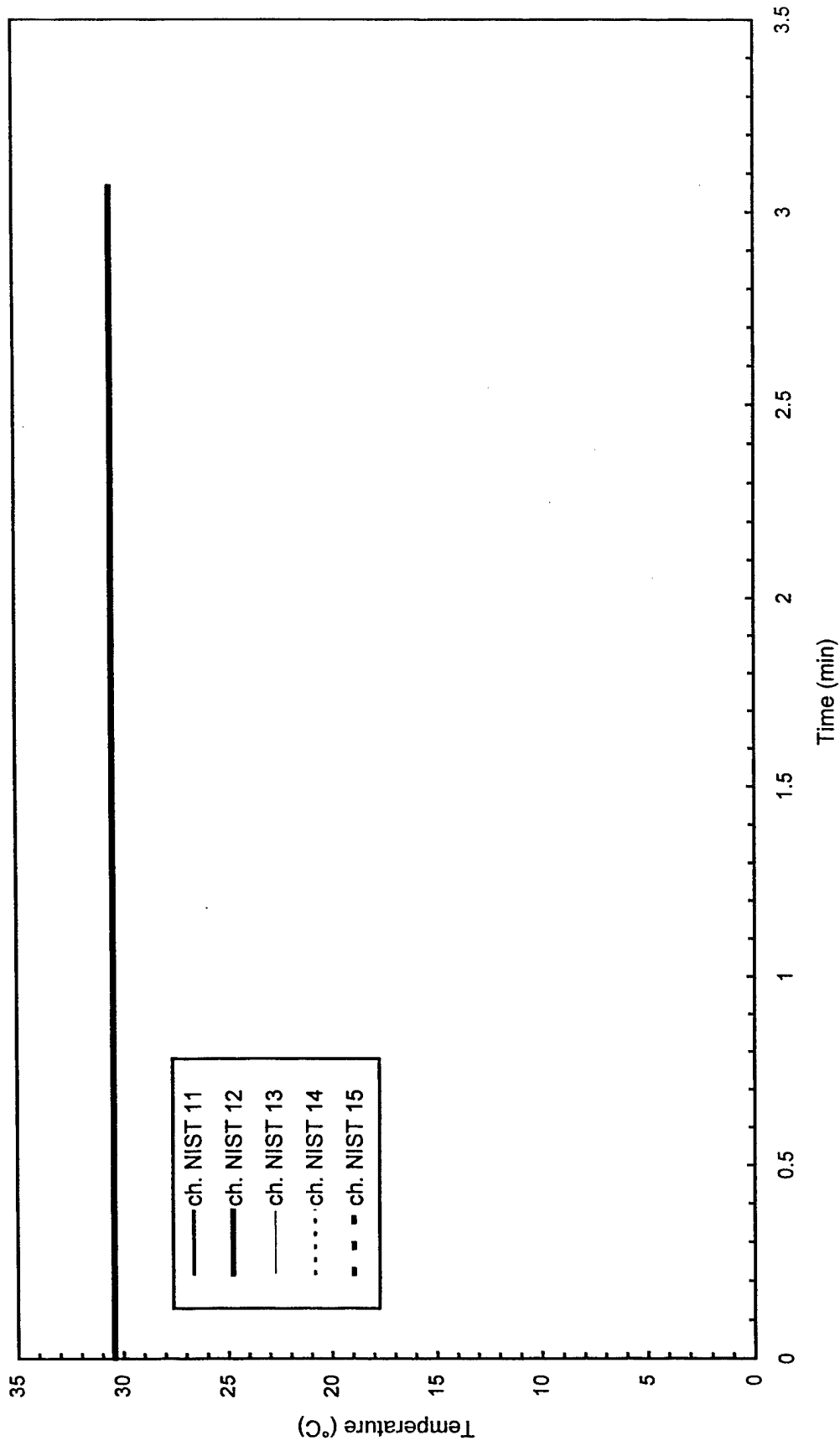


Fig. C27 - Temperature of East steel beam

Test F2

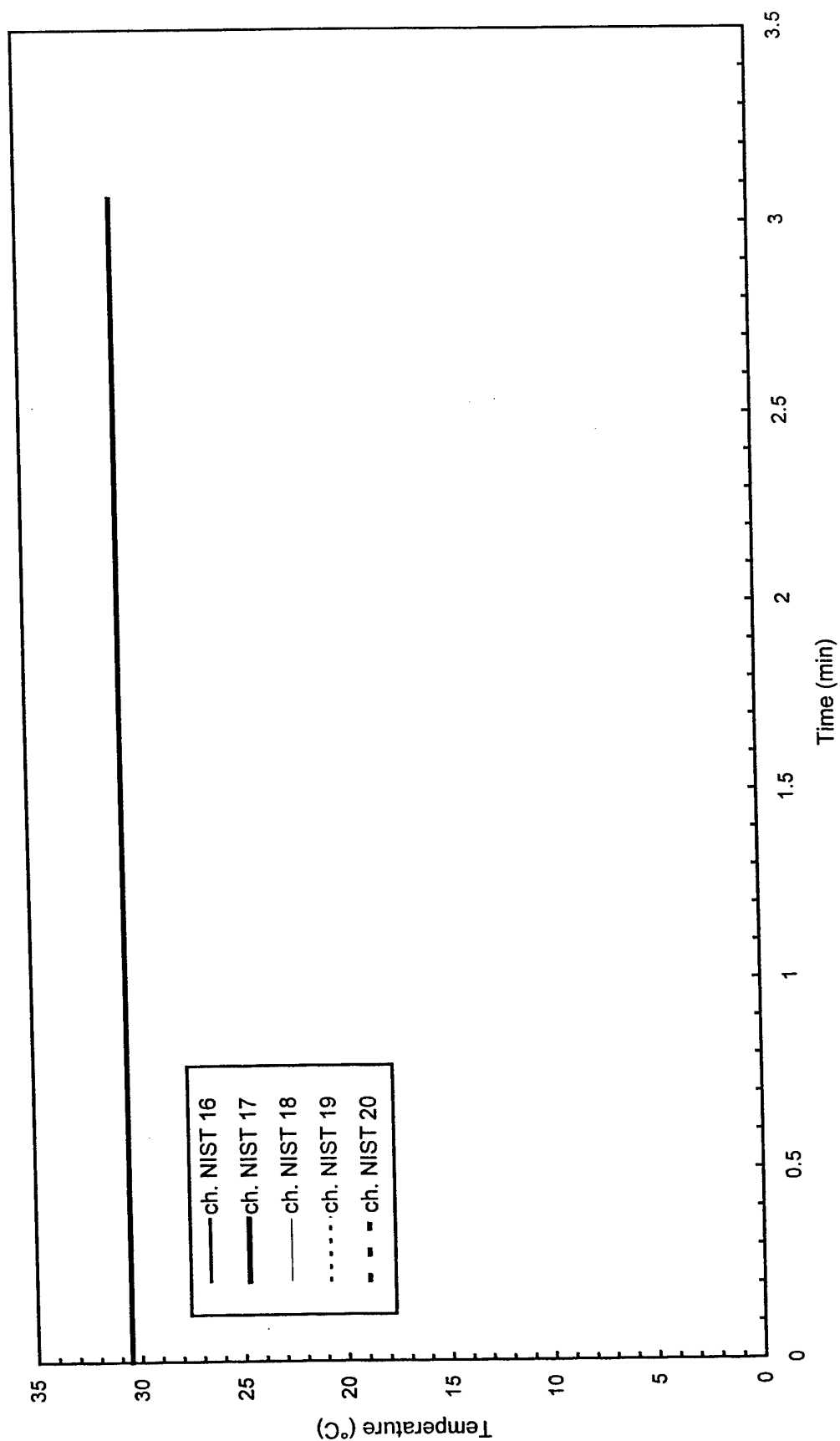


Fig. C28 - Temperature of South steel beam

Test F2

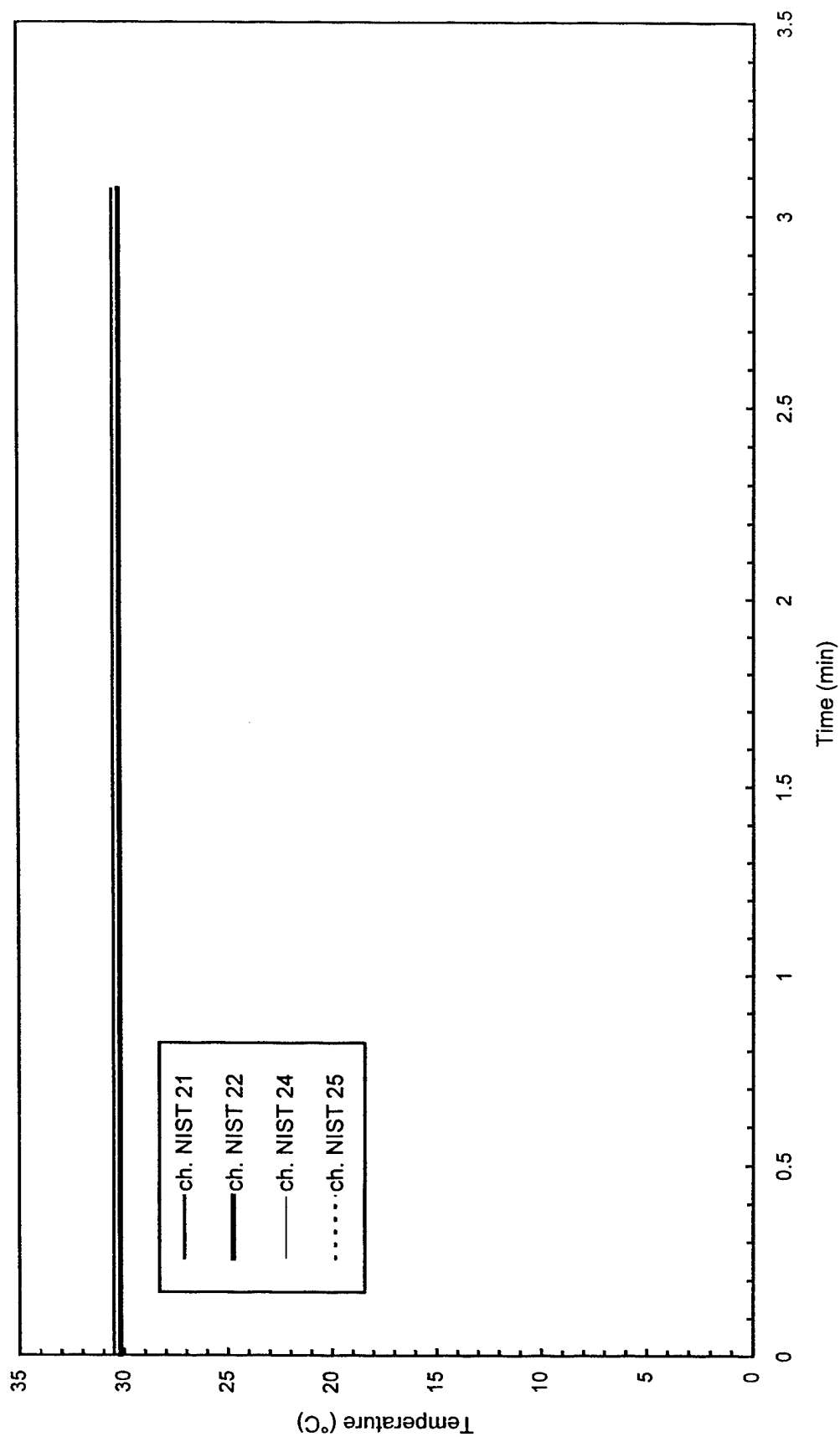


Fig. C29 - Temperature of Northwest steel beam

Test F2

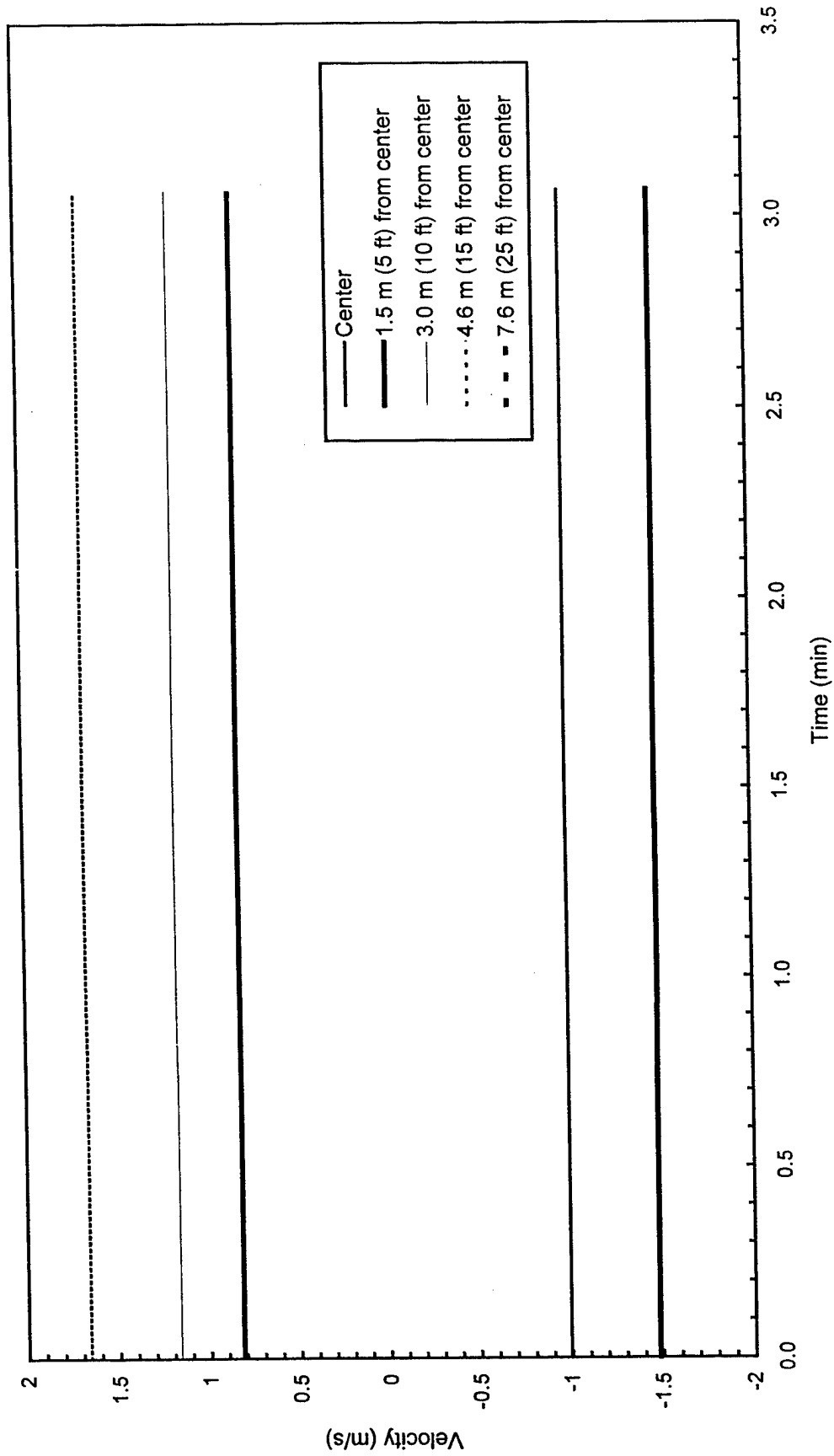


Fig. C30 - Plume and ceiling jet velocities

Test F3

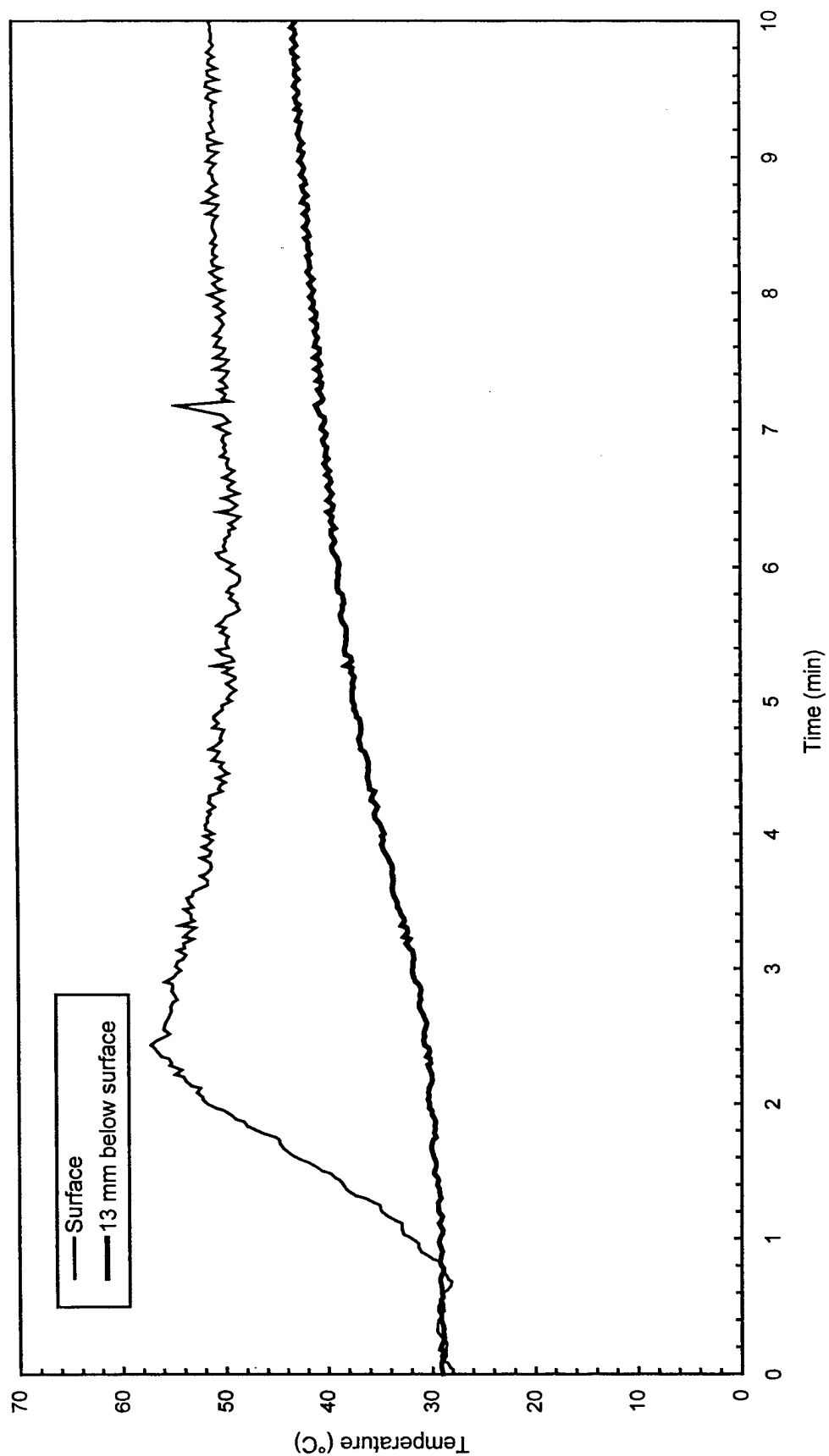


Fig. C31 - Concrete temperatures at center of pad

Test F3

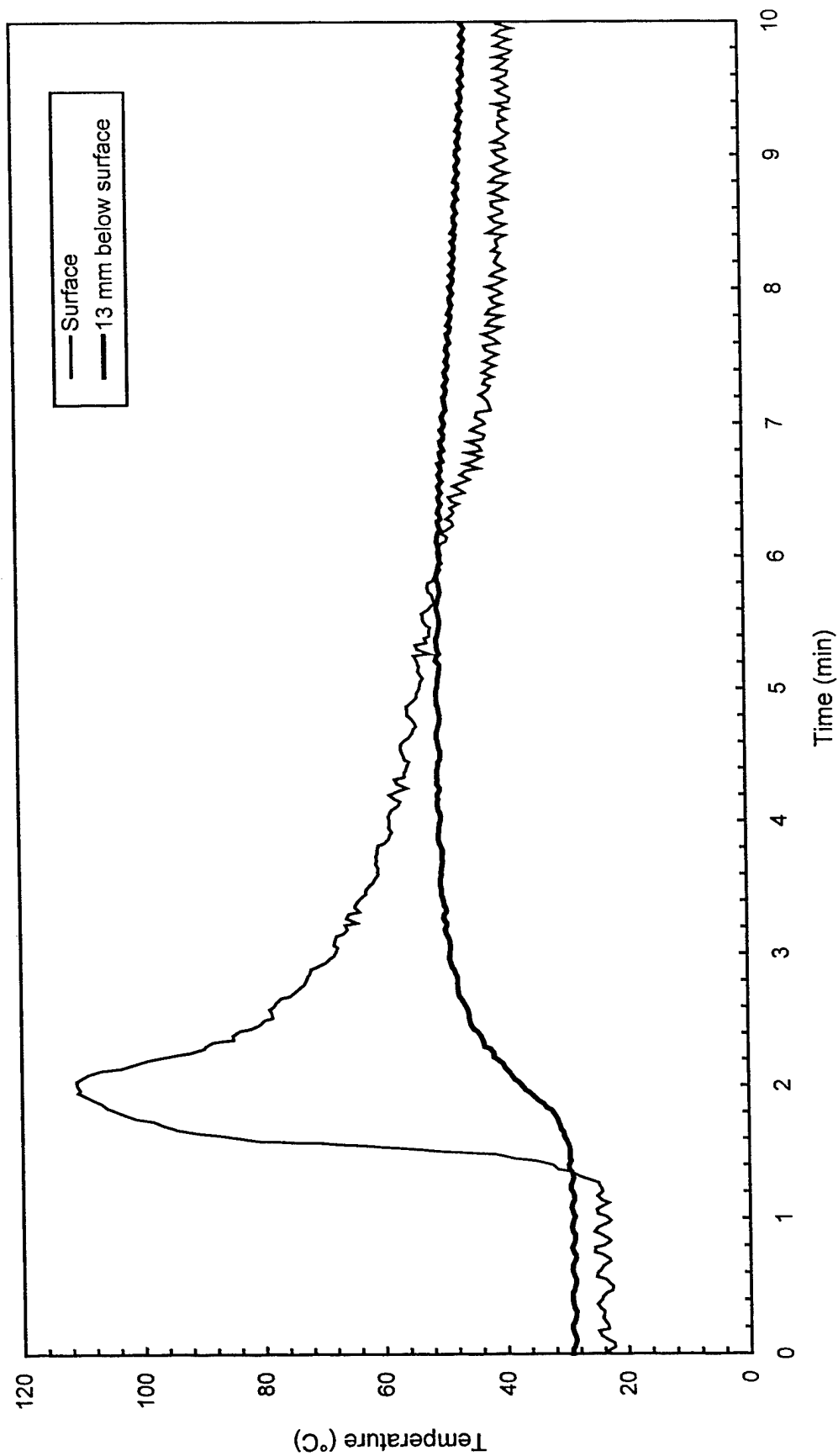


Fig. C32 - Concrete temperatures 3 m (10 ft) East of center of pad

Test F3

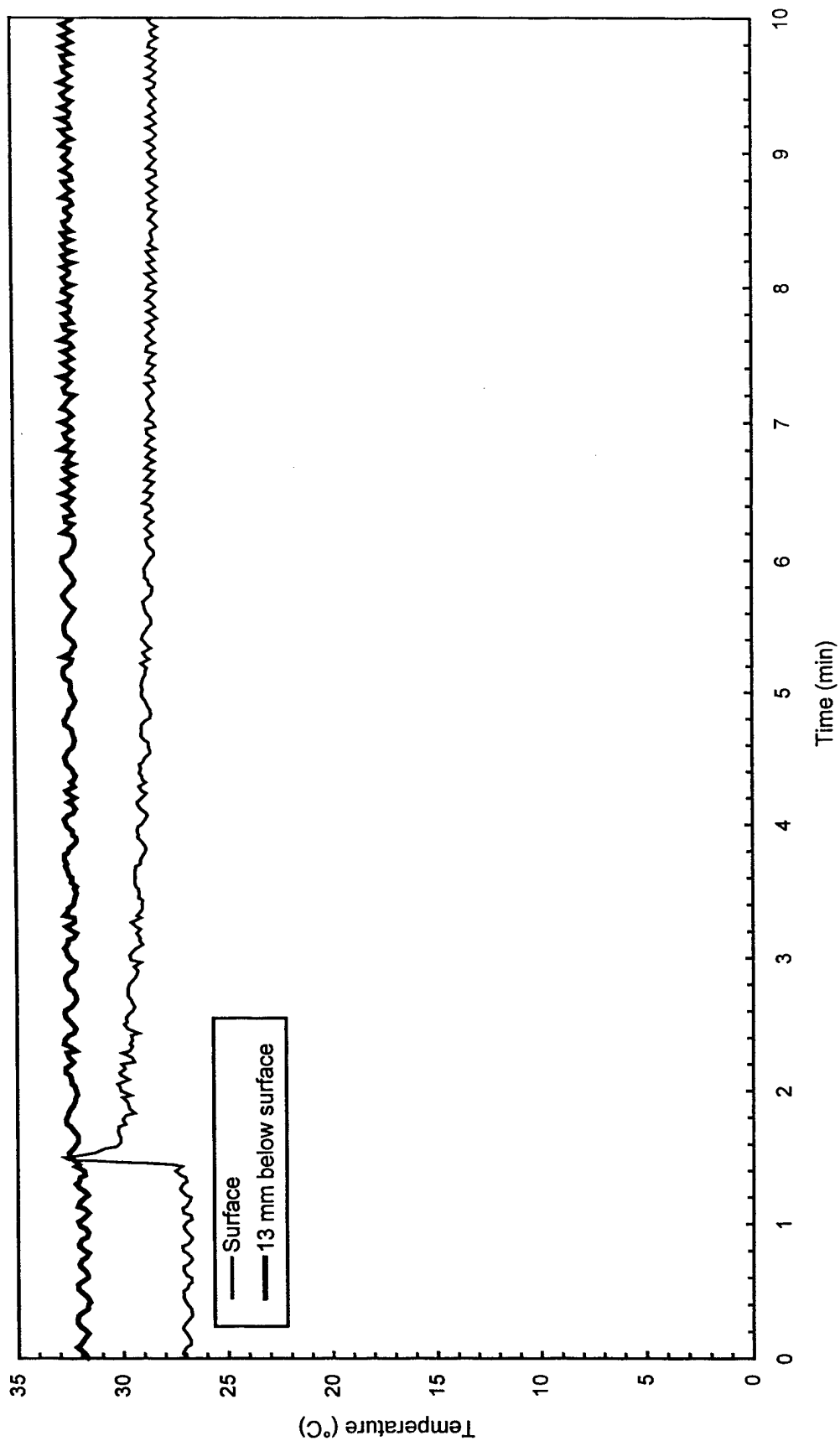


Fig. C33 - Concrete temperatures 3 m (10 ft) West of center of pad

Test F3

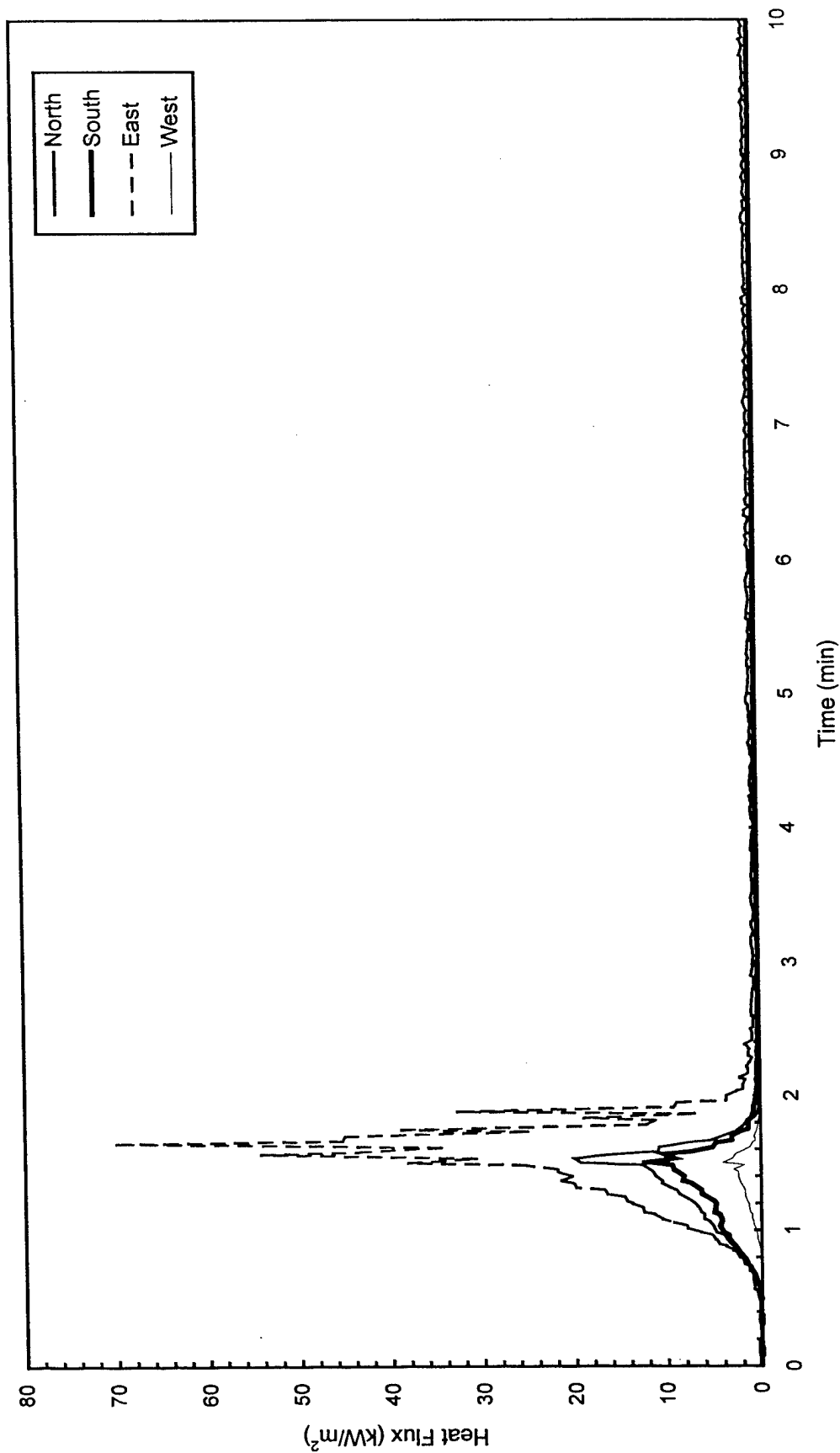


Fig. C34 - Heat flux measured at edge of pad

Test F3

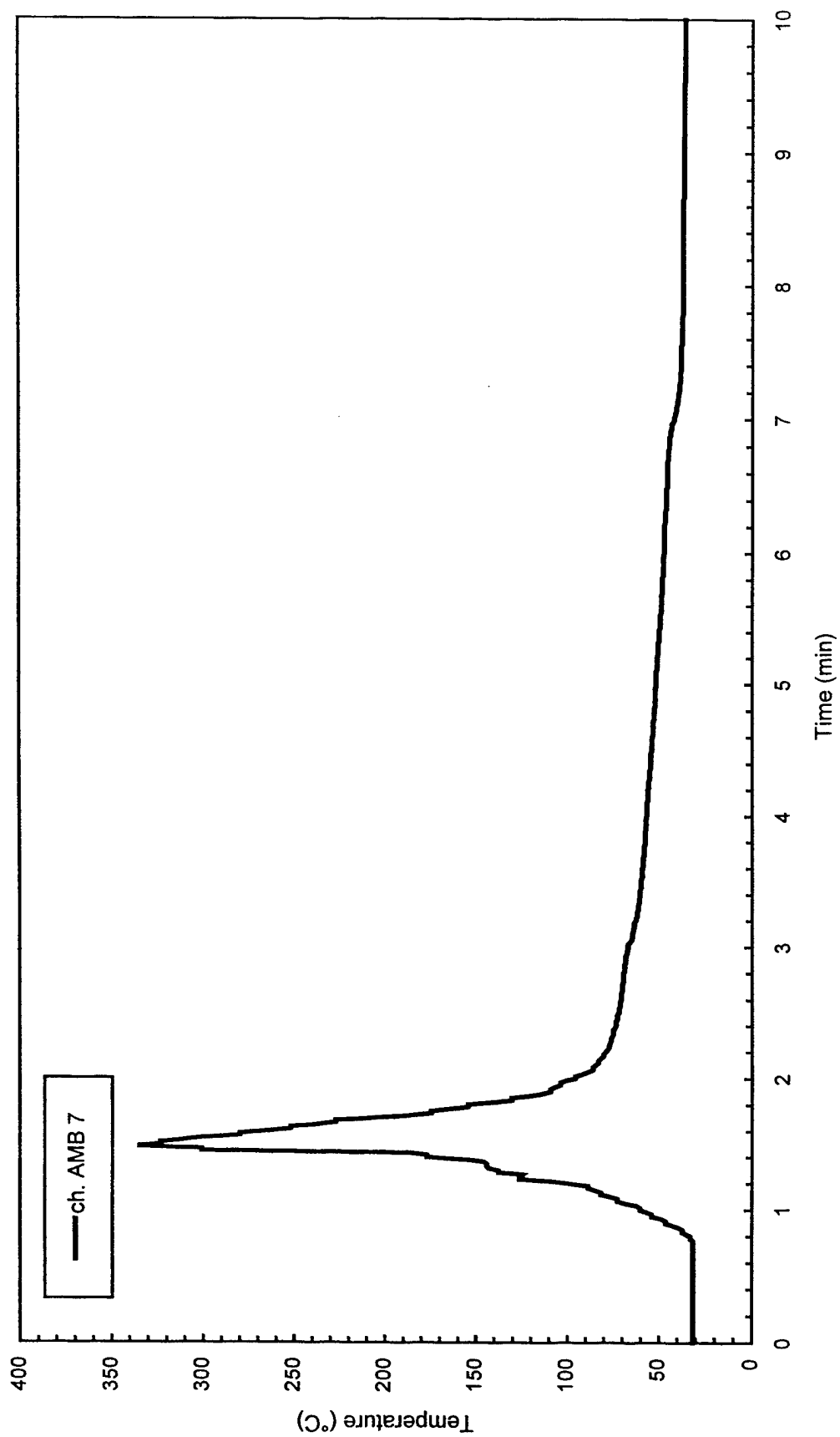


Fig. C35 - Air temperatures over center of pad

Test F3

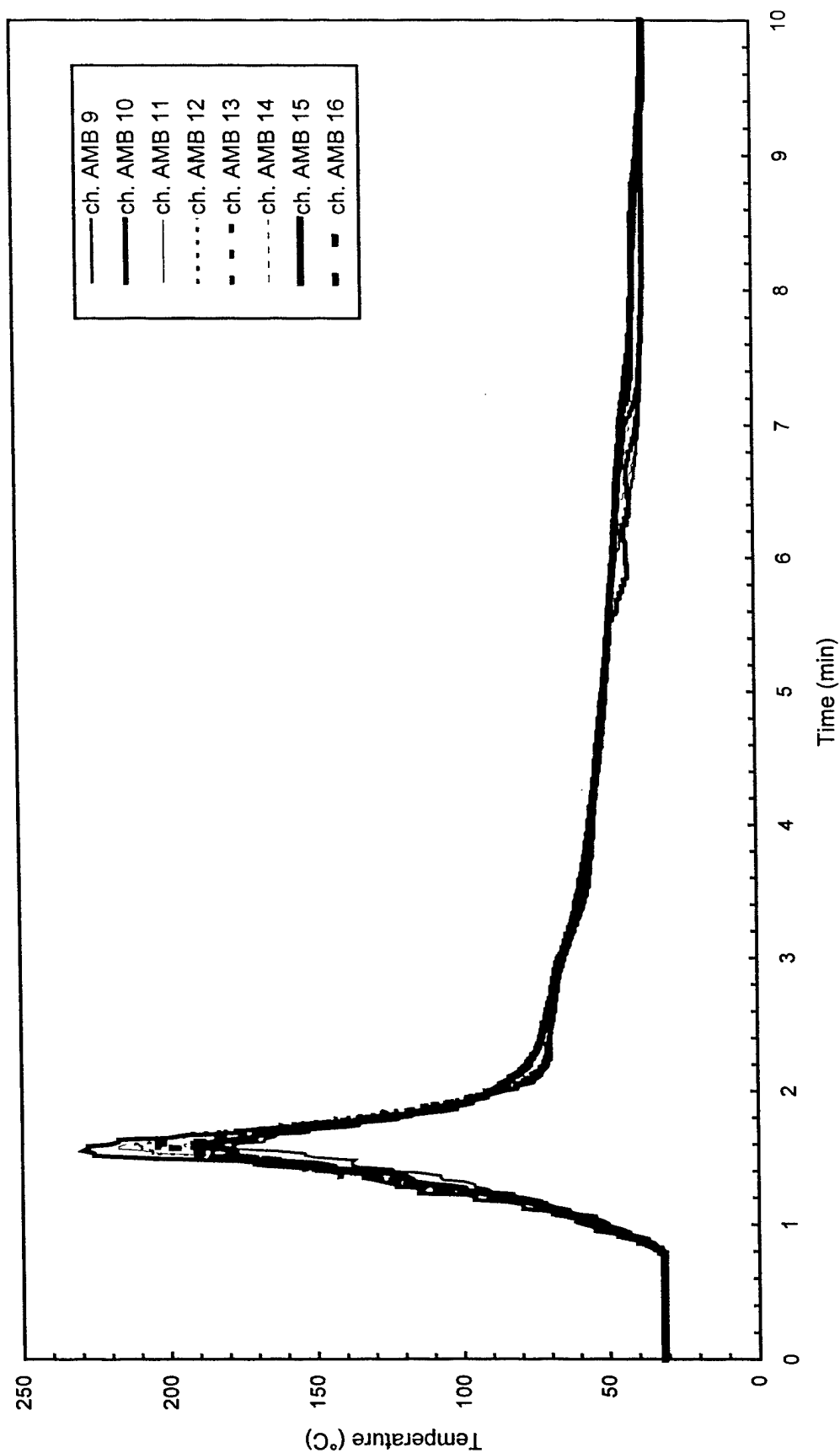


Fig. C36 - Air temperatures around 3 m (10 ft) radius from center of pad

Test F3

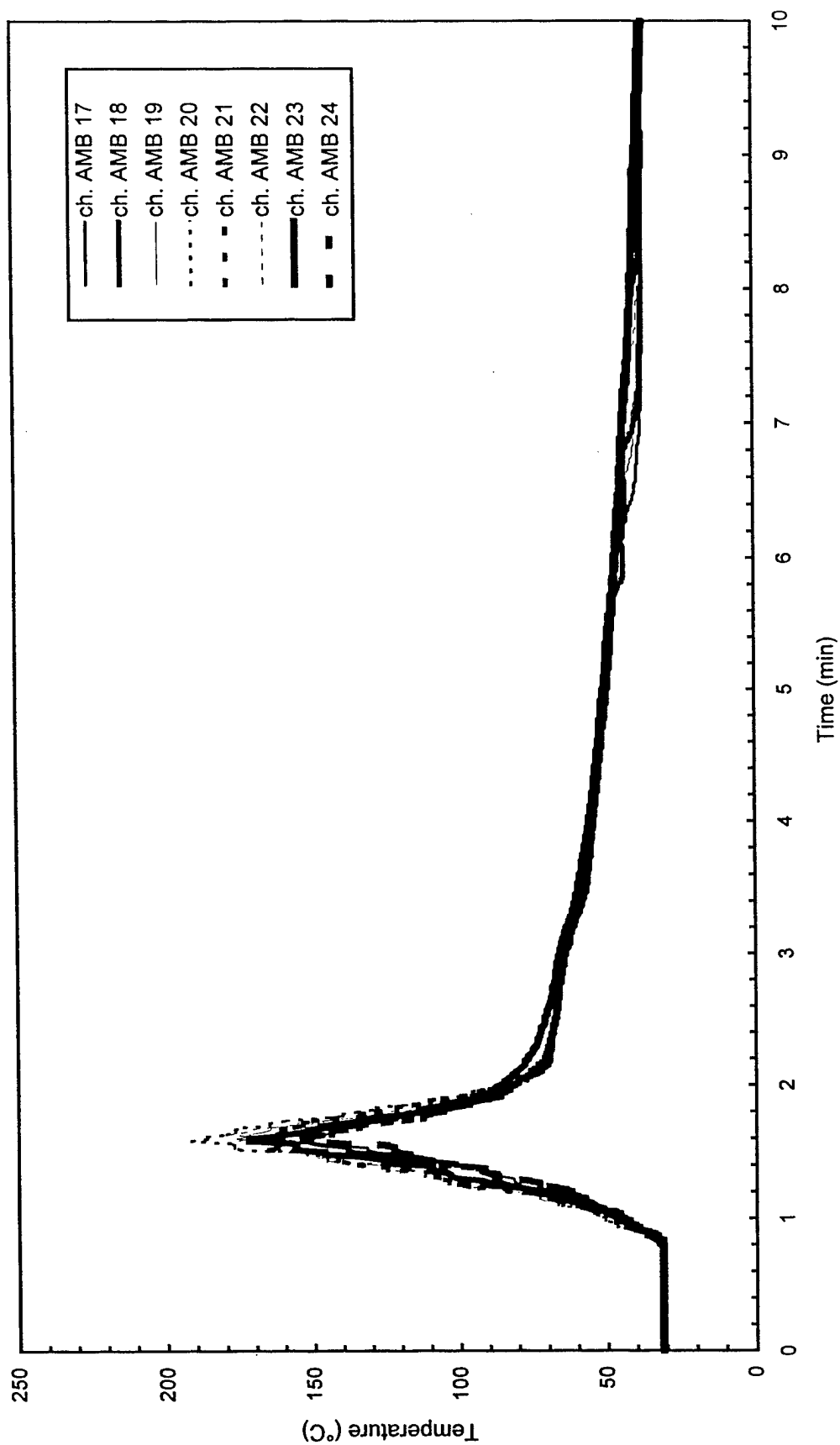


Fig. C37 - Air temperatures around 4.6 m (15 ft) radius from center of pad

Test F3

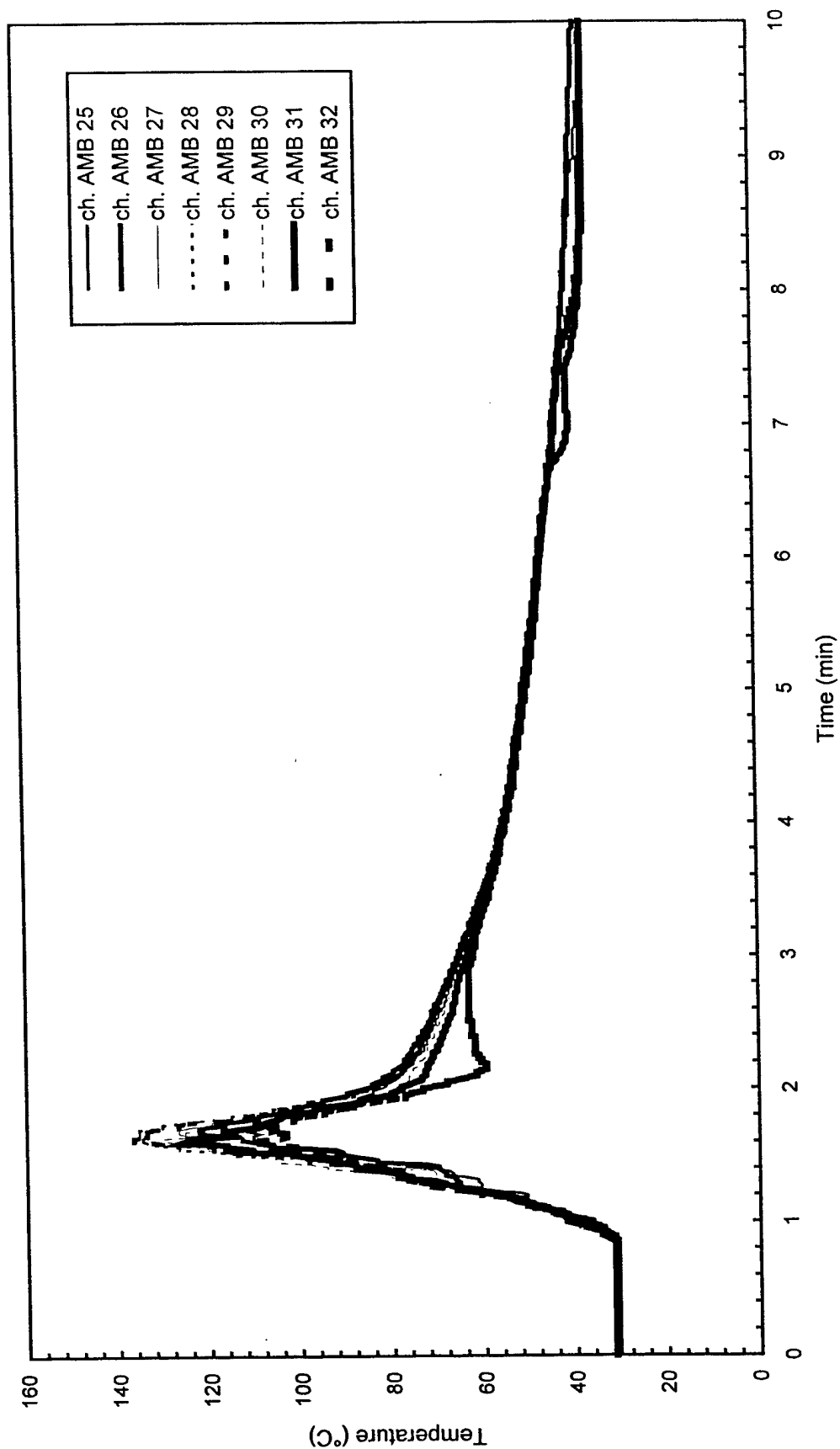


Fig. C38 - Air temperatures around North half of 7.6 m (25 ft) radius from center of pad

Test F3

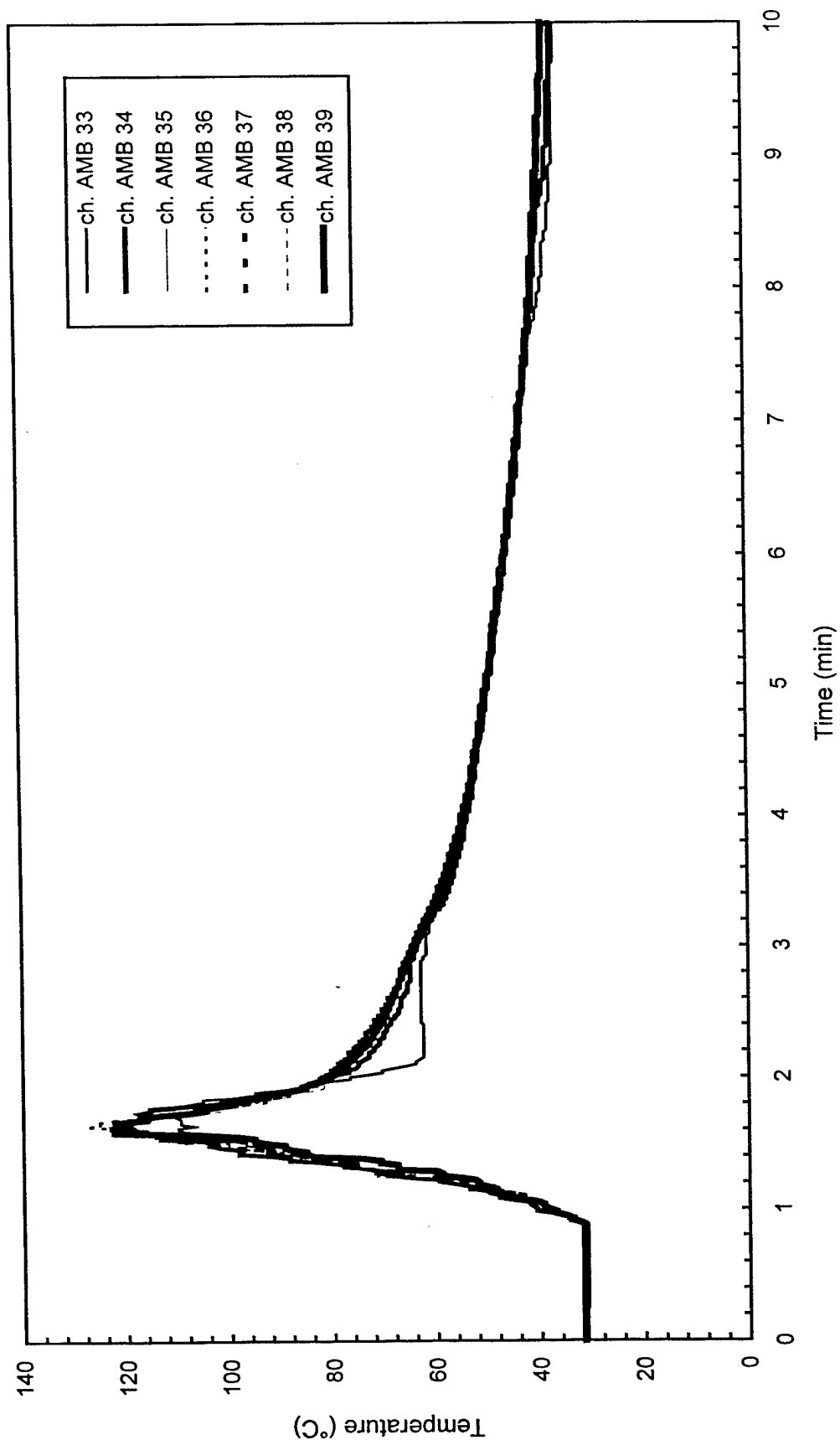


Fig. C39 - Air temperatures around South half of 7.6 m (25 ft) radius from center of pad

Test F3

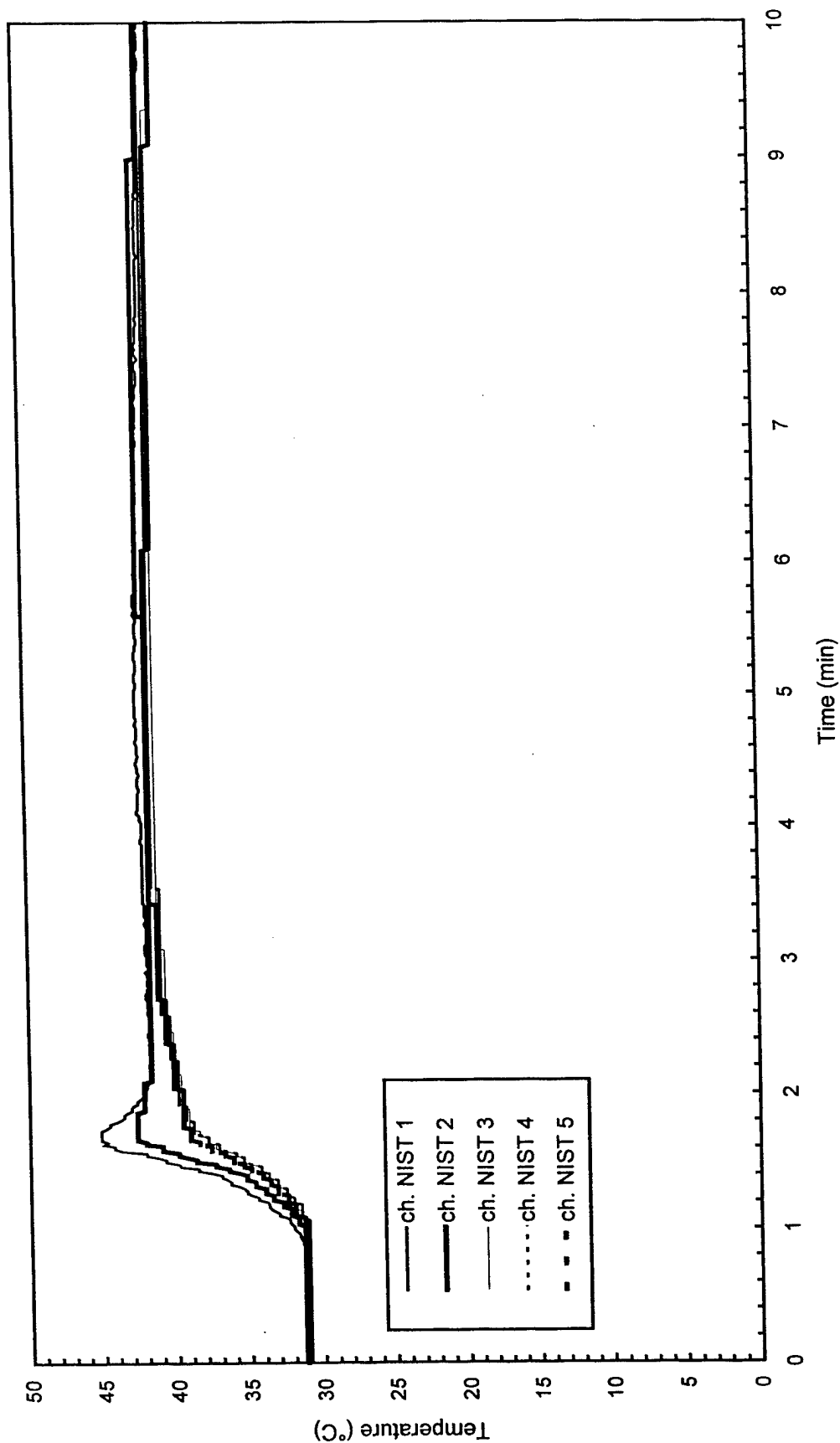


Fig. C40 - Temperature of West steel beam

Test F3

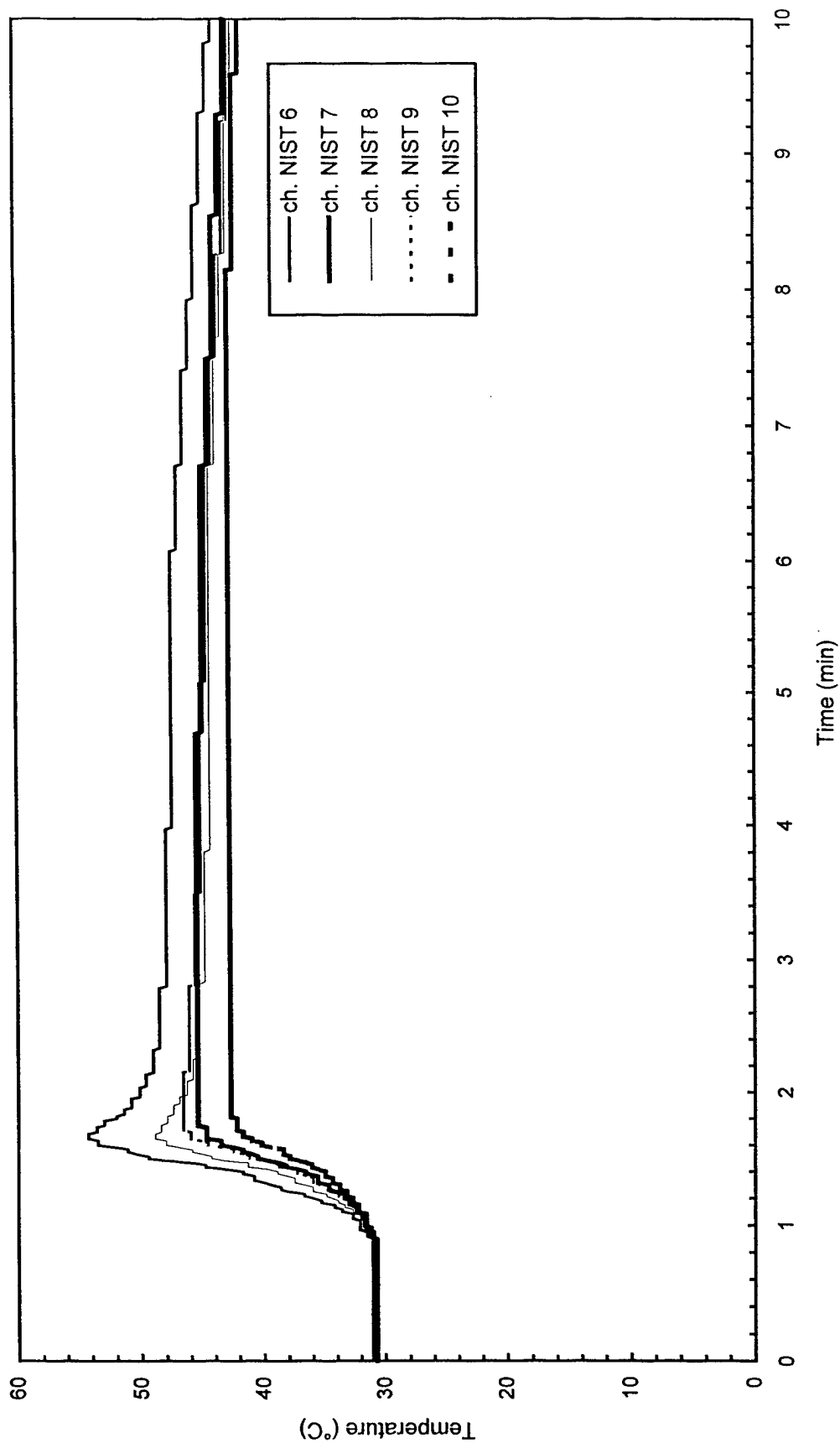


Fig. C41 - Temperature of North steel beam

Test F3

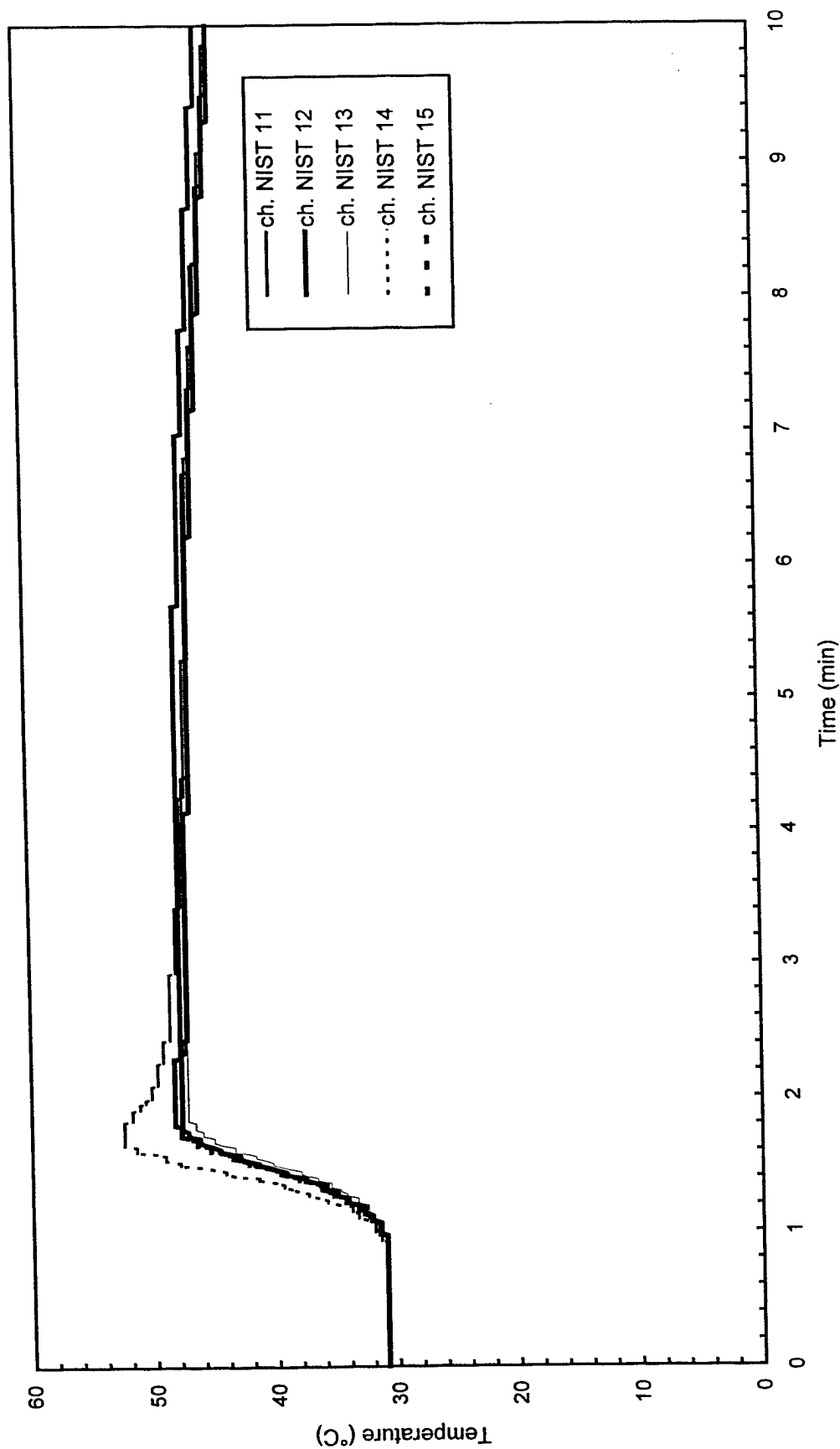


Fig. C42 - Temperature of East steel beam

Test F3

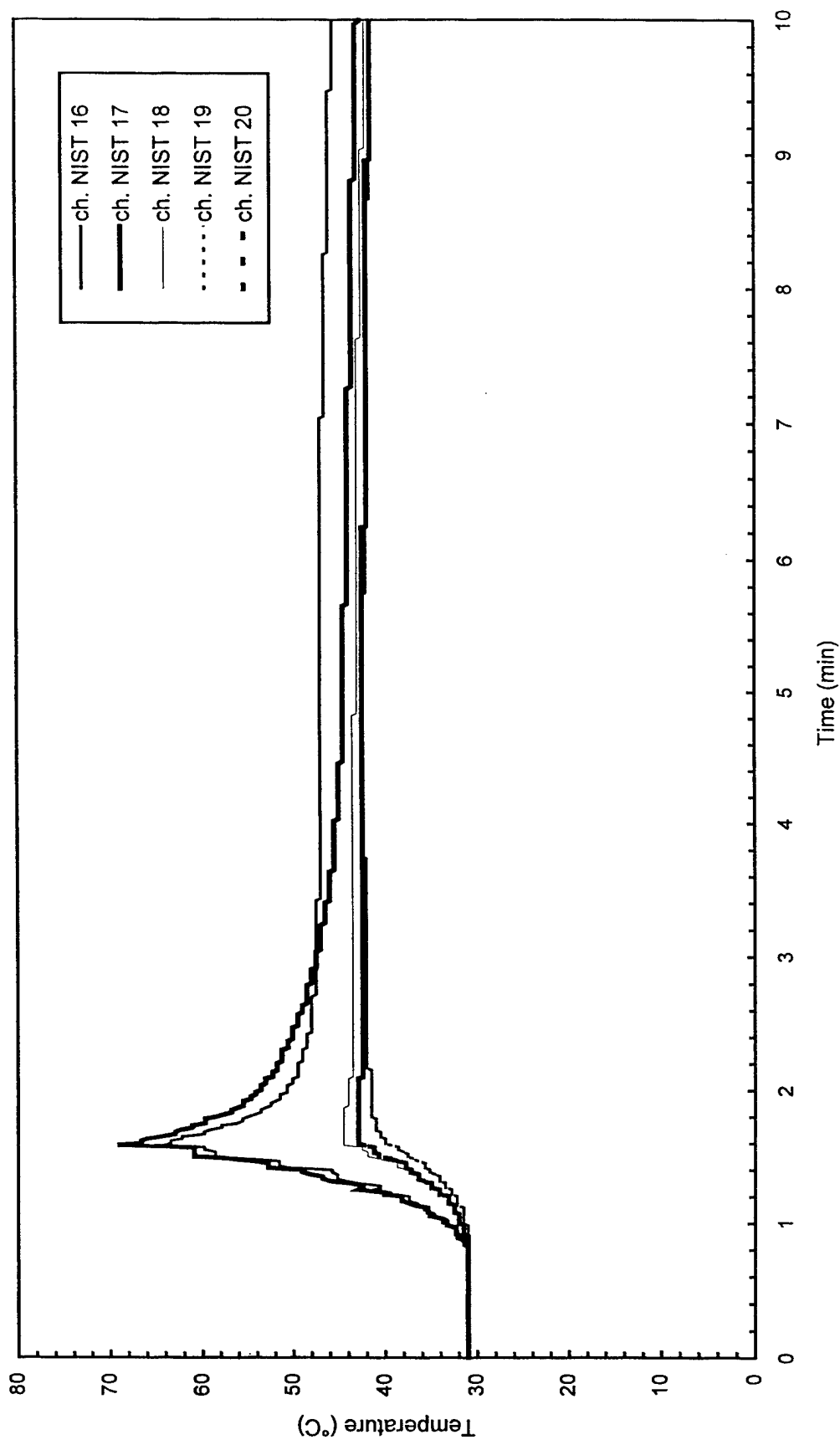


Fig. C43 - Temperature of South steel beam

Test F3

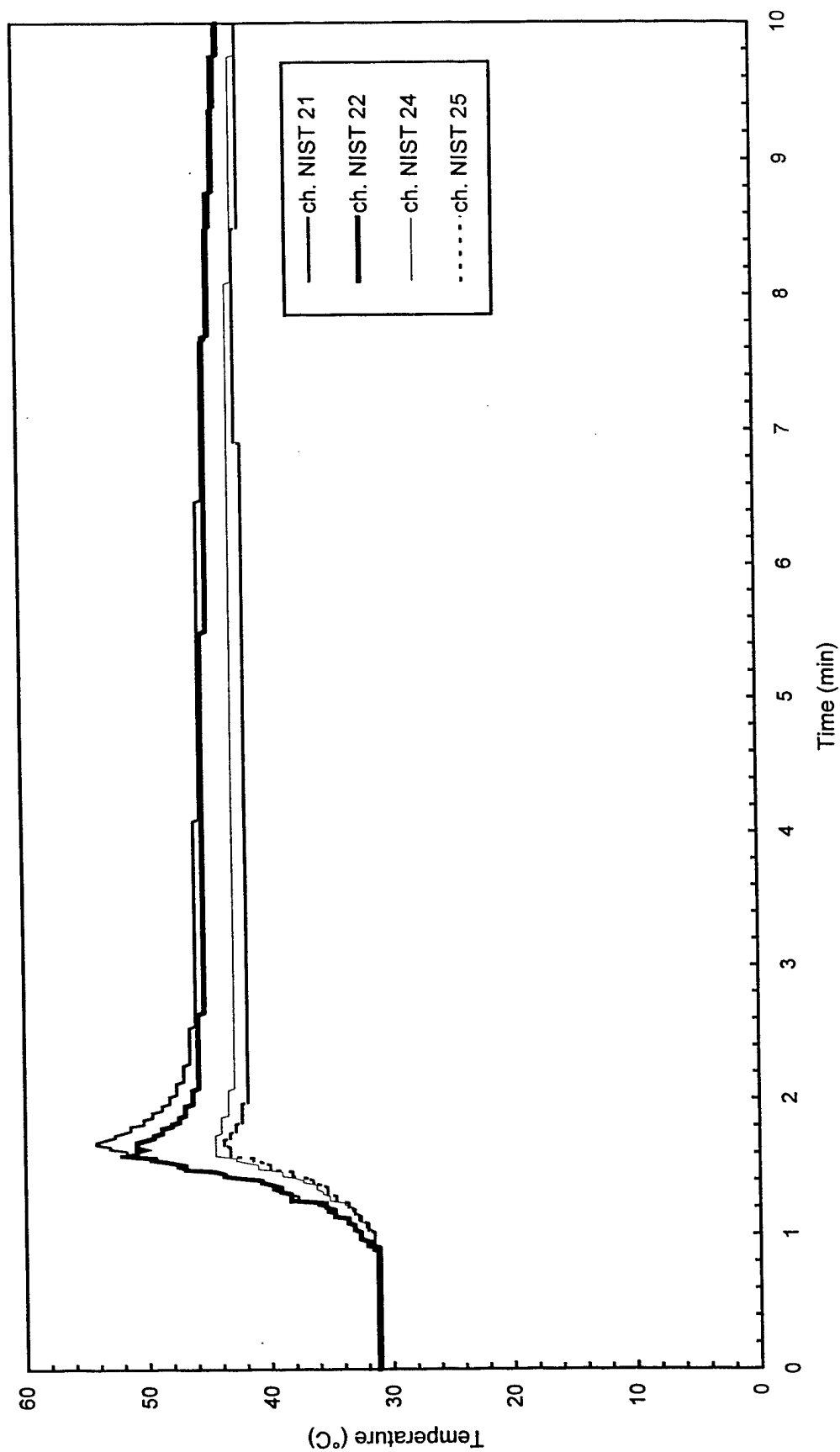


Fig. C44 - Temperature of Northwest steel beam

Test F3

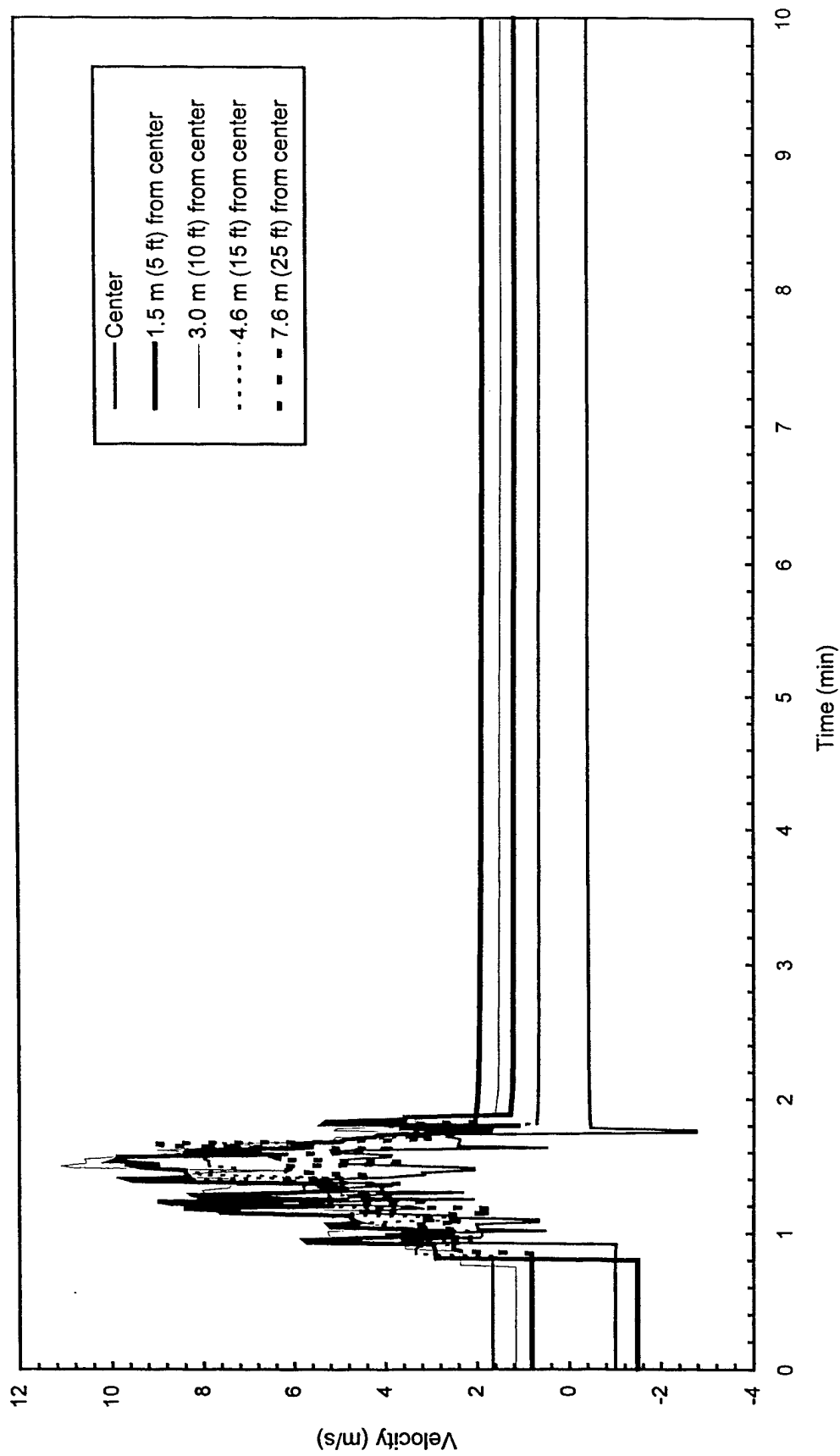


Fig. C45 - Plume and ceiling jet velocities

Test F4

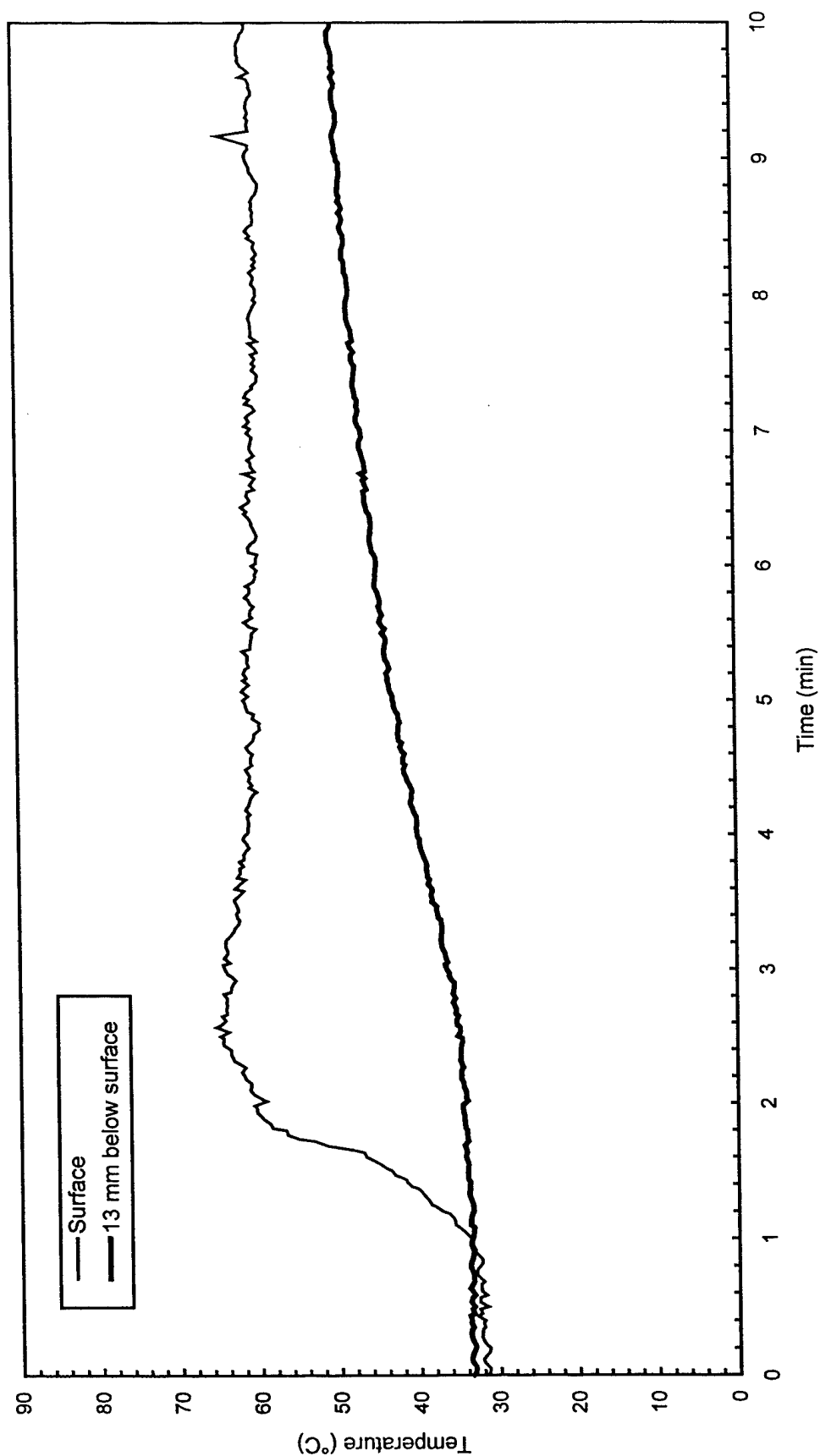


Fig. C46 - Concrete temperatures at center of pad

Test F4

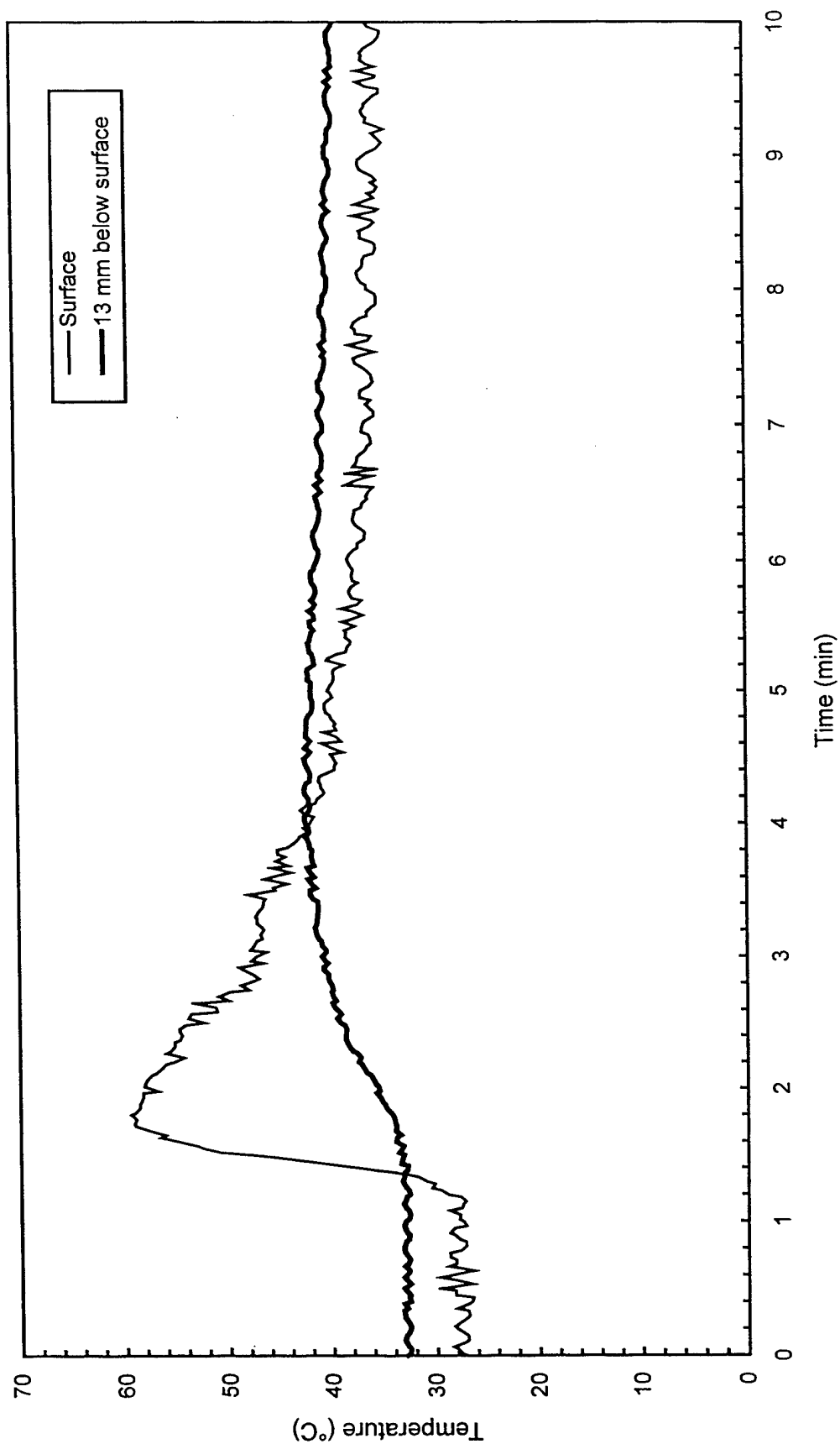


Fig. C47 - Concrete temperatures 3 m (10 ft) East of center of pad

Test F4

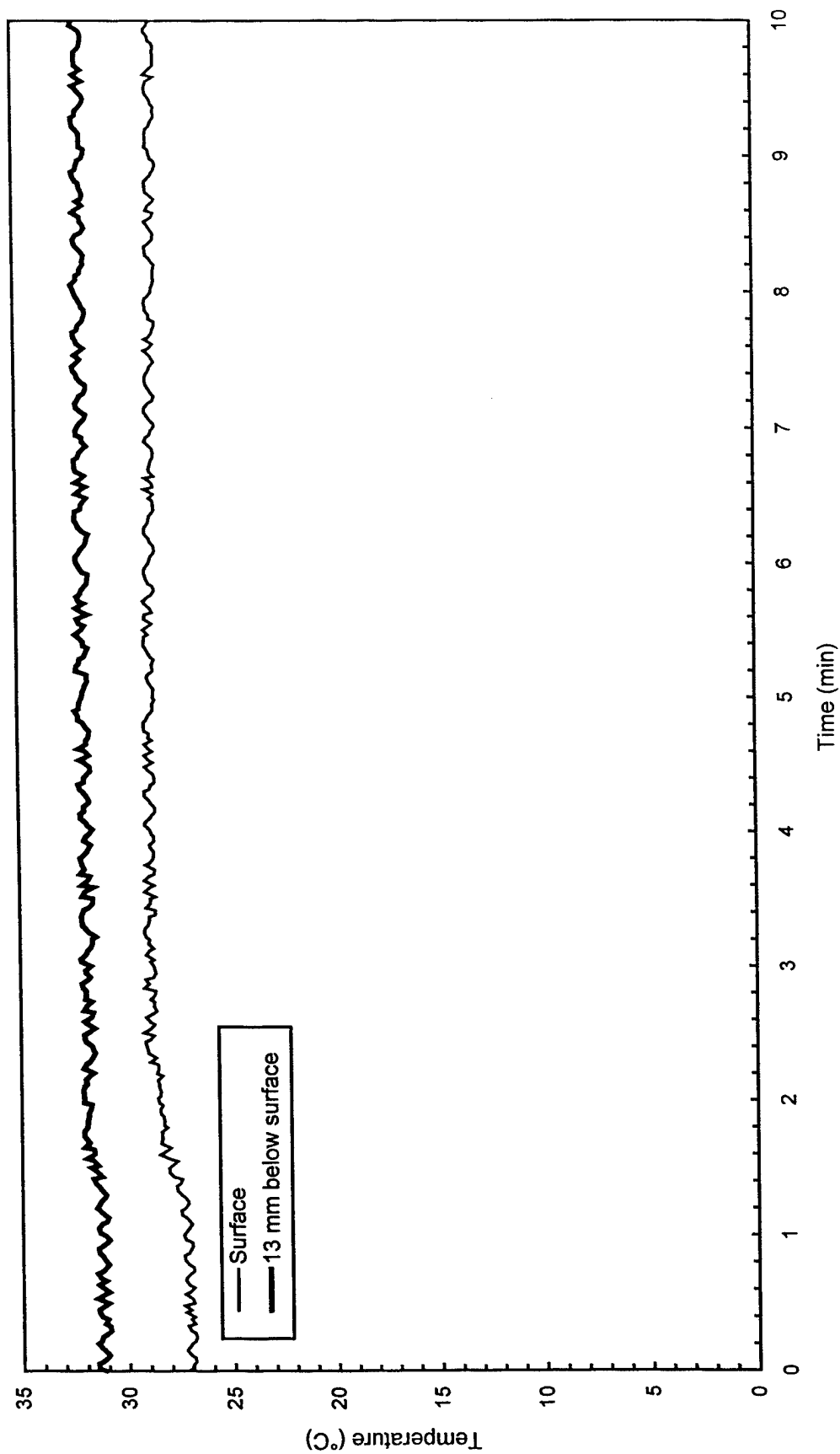


Fig. C48 - Concrete temperatures 3 m (10 ft) West of center of pad

Test F4

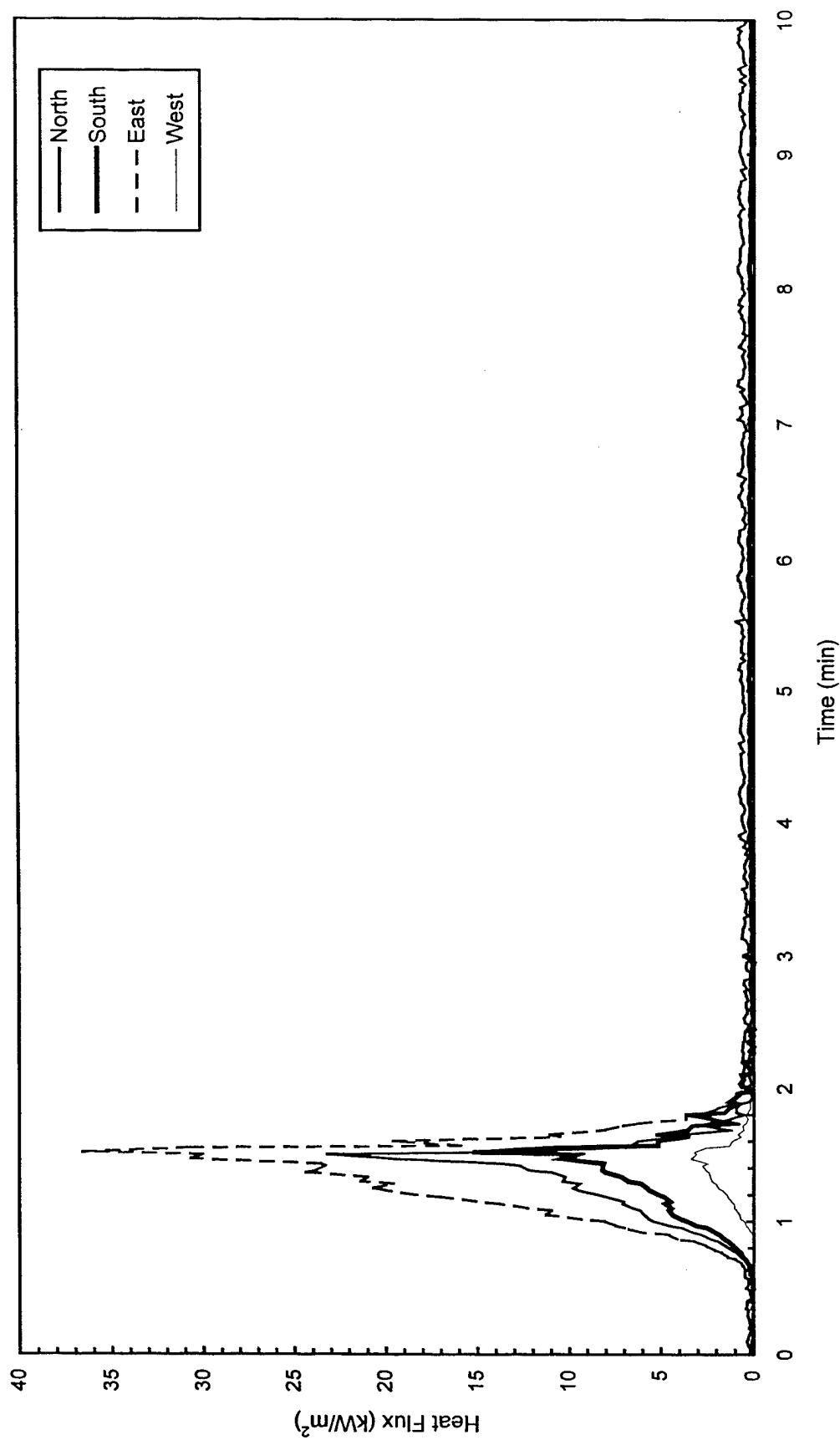


Fig. C49 - Heat flux measured at edge of pad

Test F4

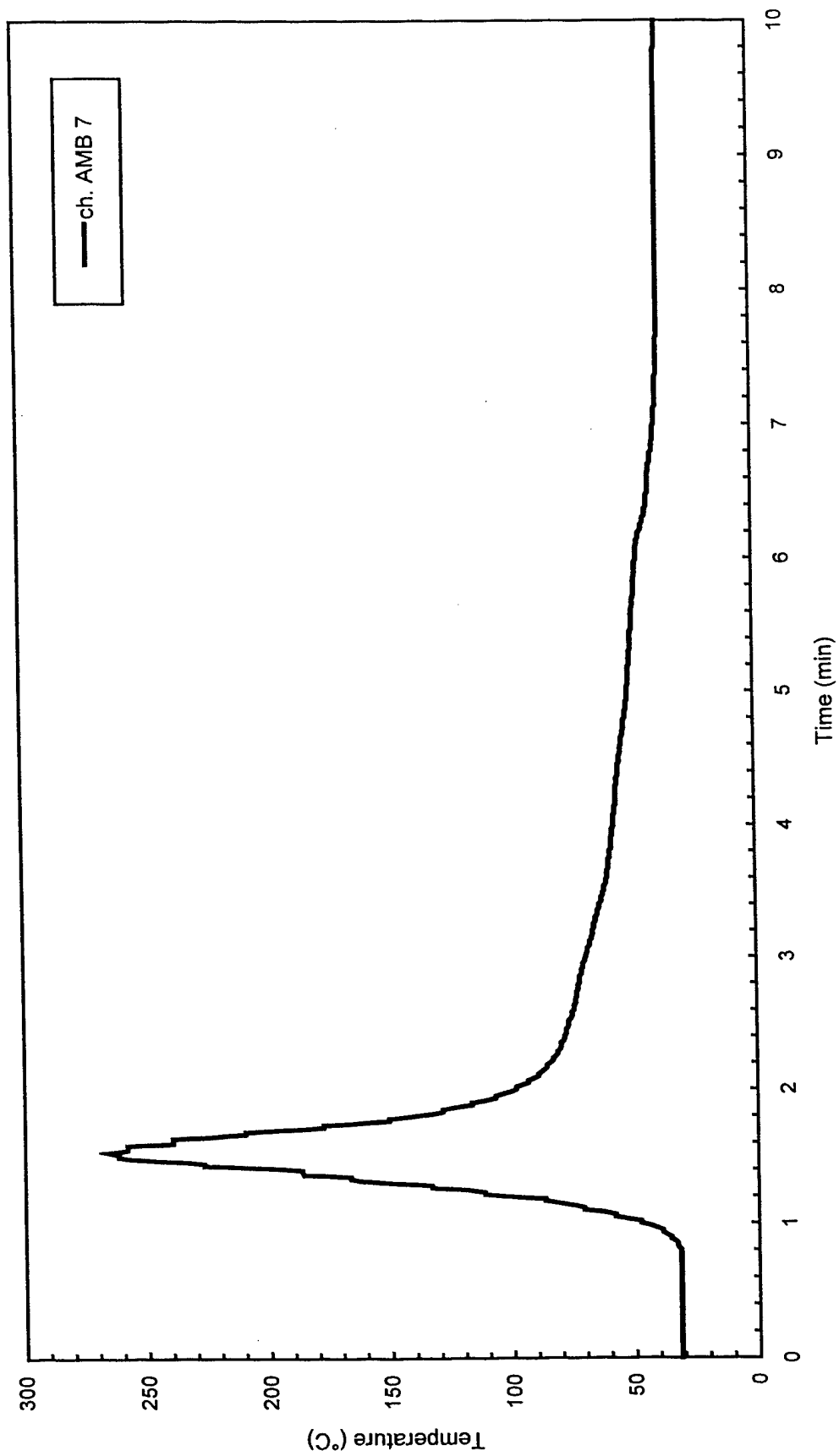


Fig. C50 - Air temperatures over center of pad

Test F4

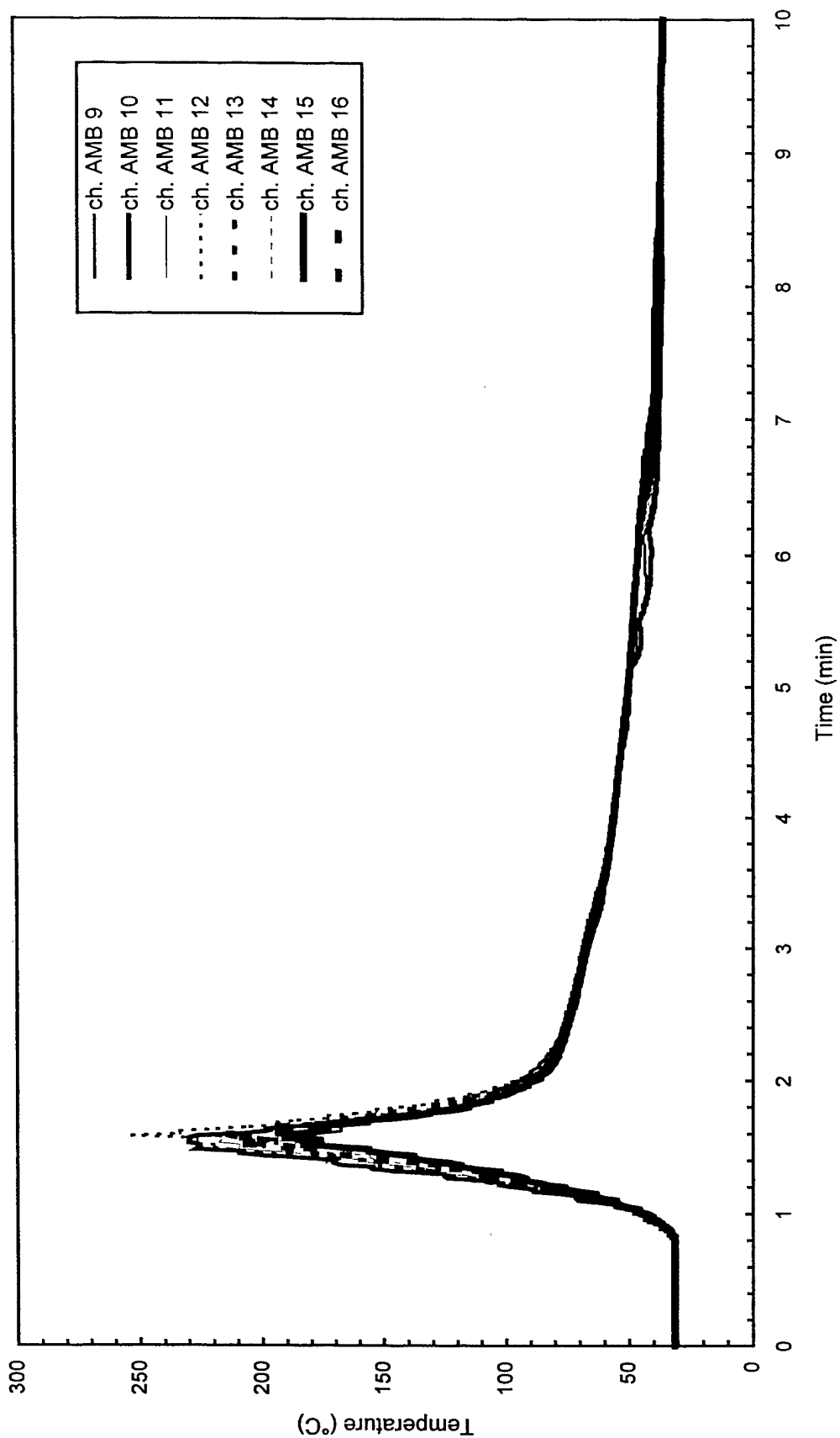


Fig. C51 - Air temperatures around 3 m (10 ft) radius from center of pad

Test F4

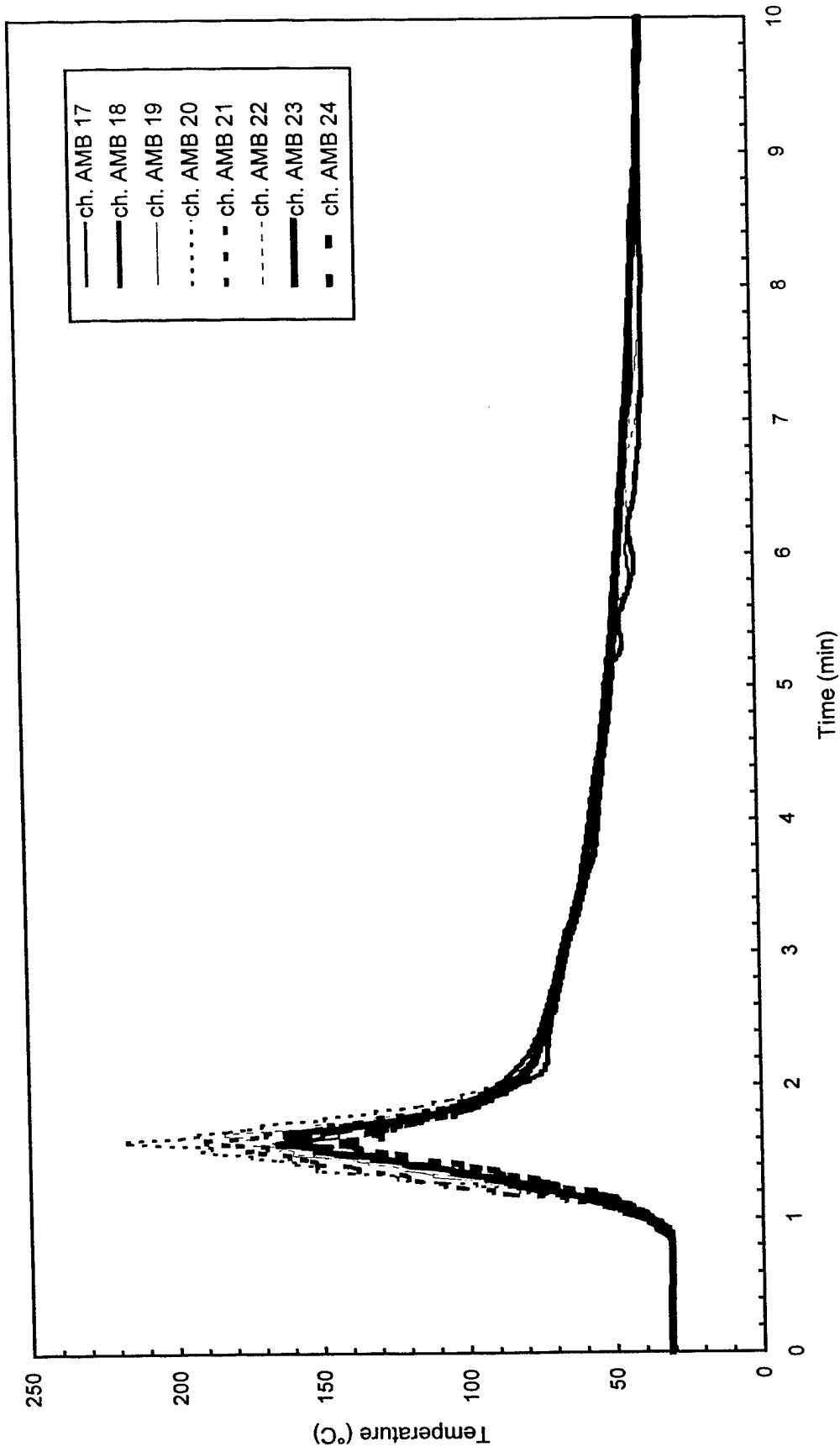


Fig. C52 - Air temperatures around 4.6 m (15 ft) radius from center of pad

Test F4

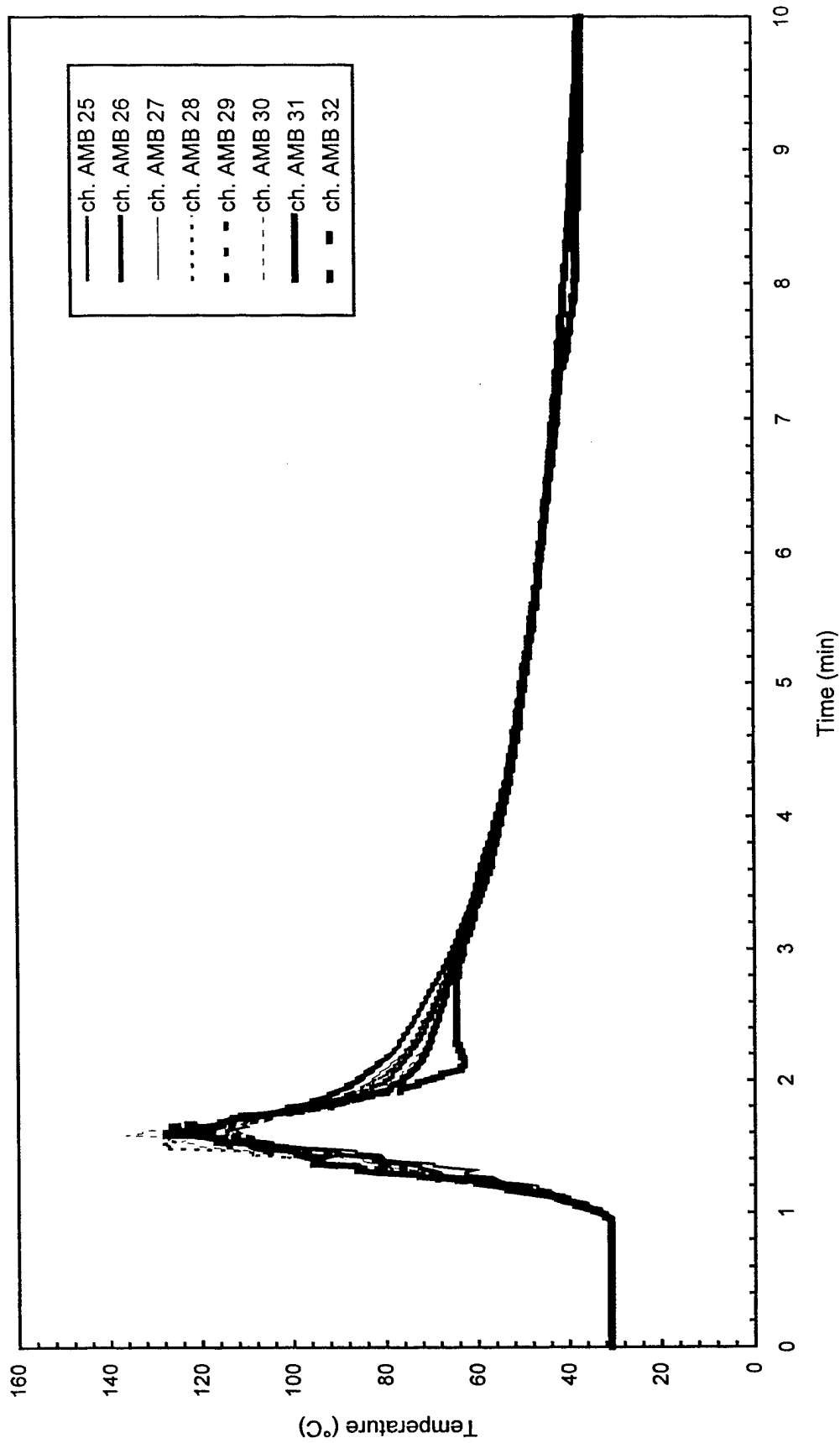


Fig. C53 - Air temperatures around North half of 7.6 m (25 ft) radius from center of pad

Test F4

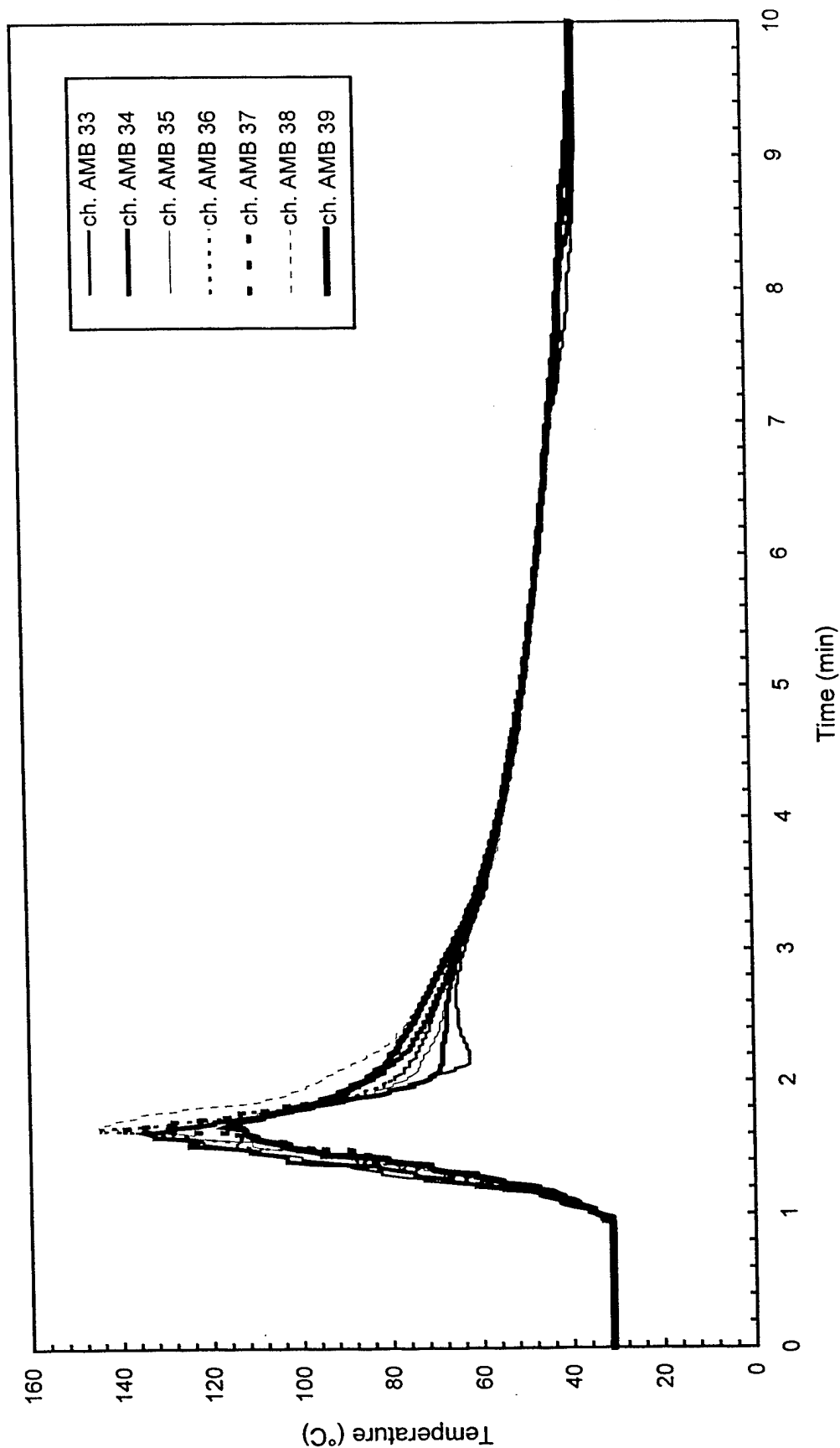


Fig. C54 - Air temperatures around South half of 7.6 m (25 ft) radius from center of pad

Test F4

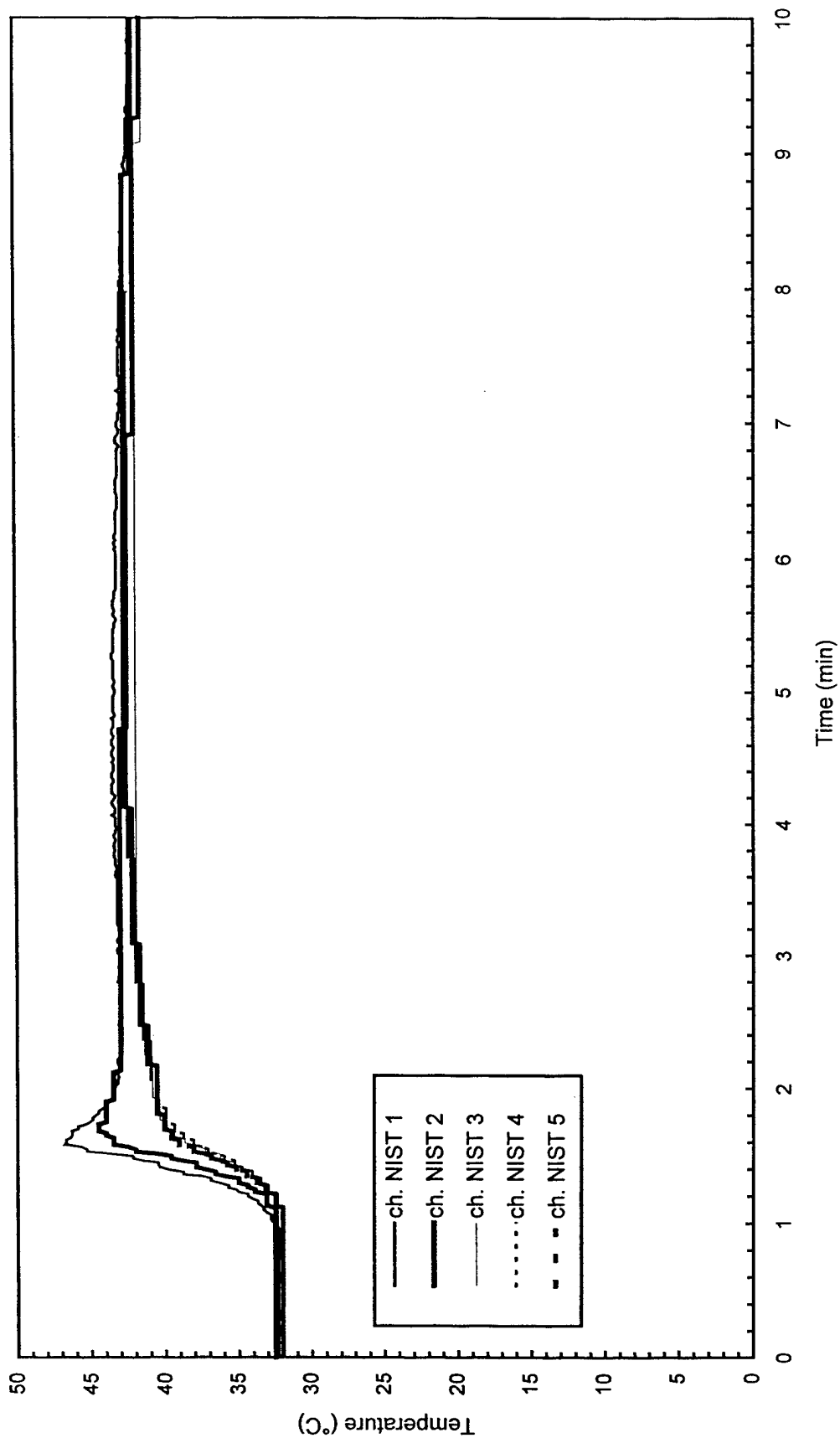


Fig. C55 - Temperature of West steel beam

Test F4

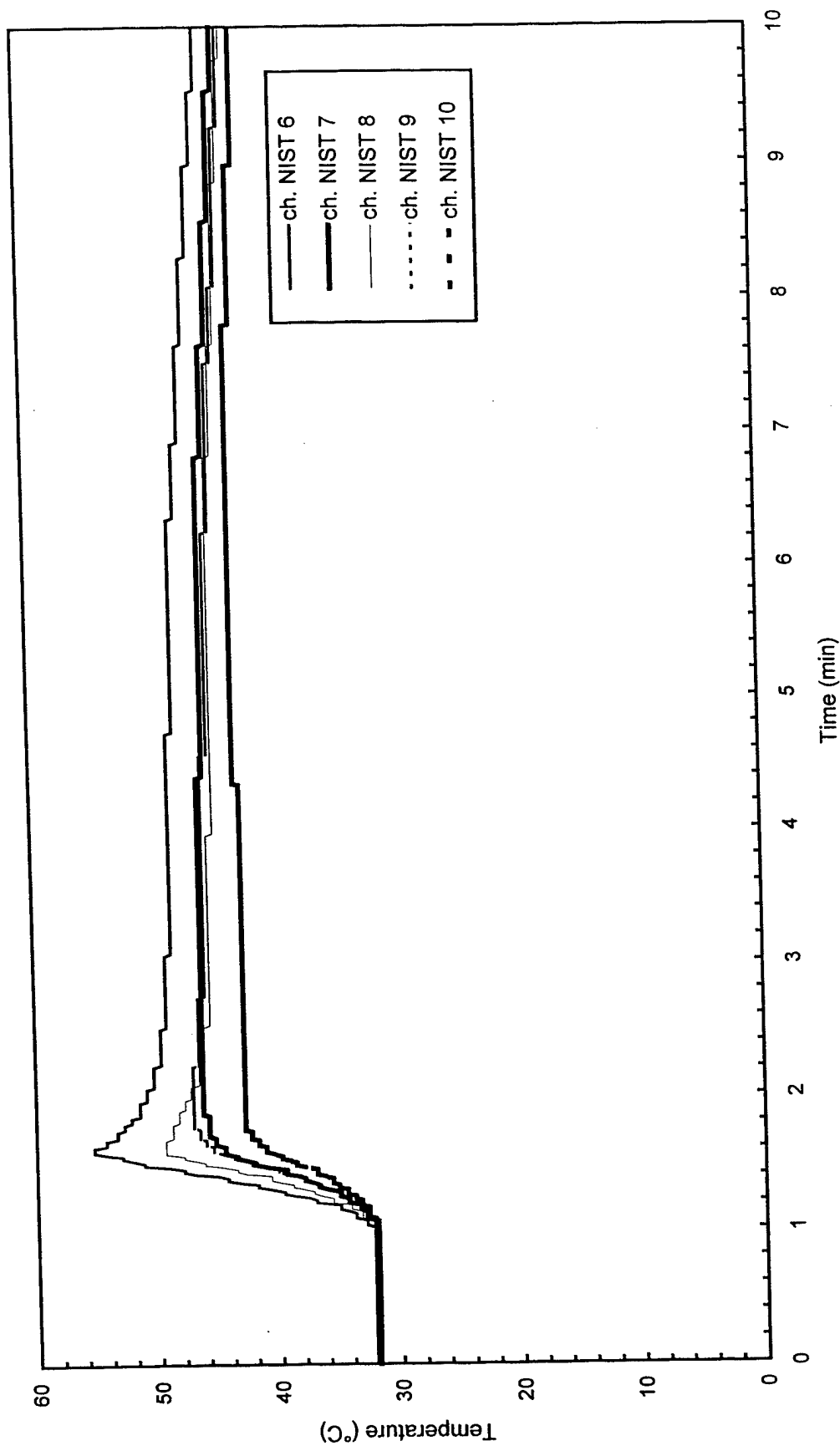


Fig. C56 - Temperature of North steel beam

Test F4

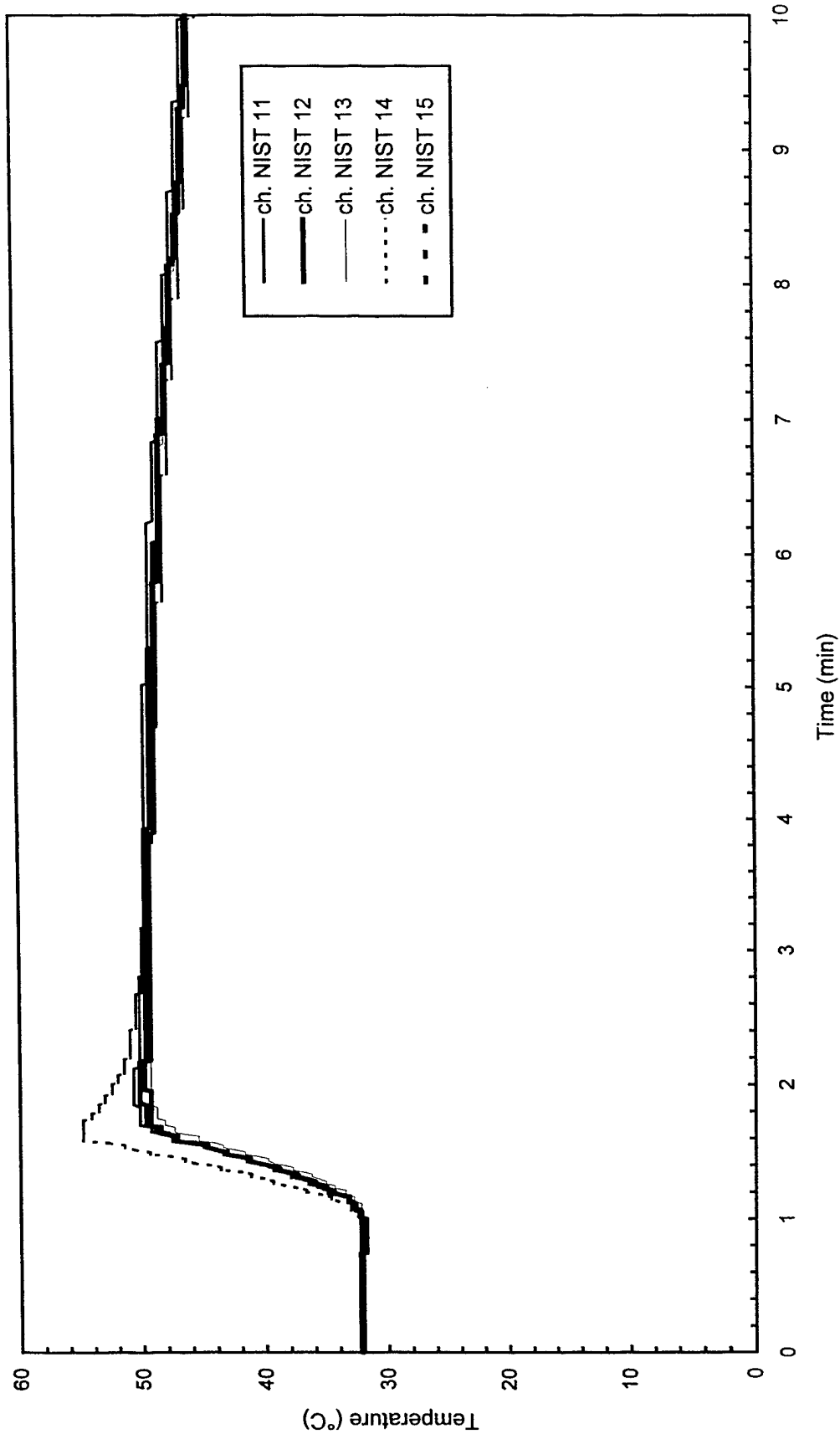


Fig. C57 - Temperature of East steel beam

Test F4

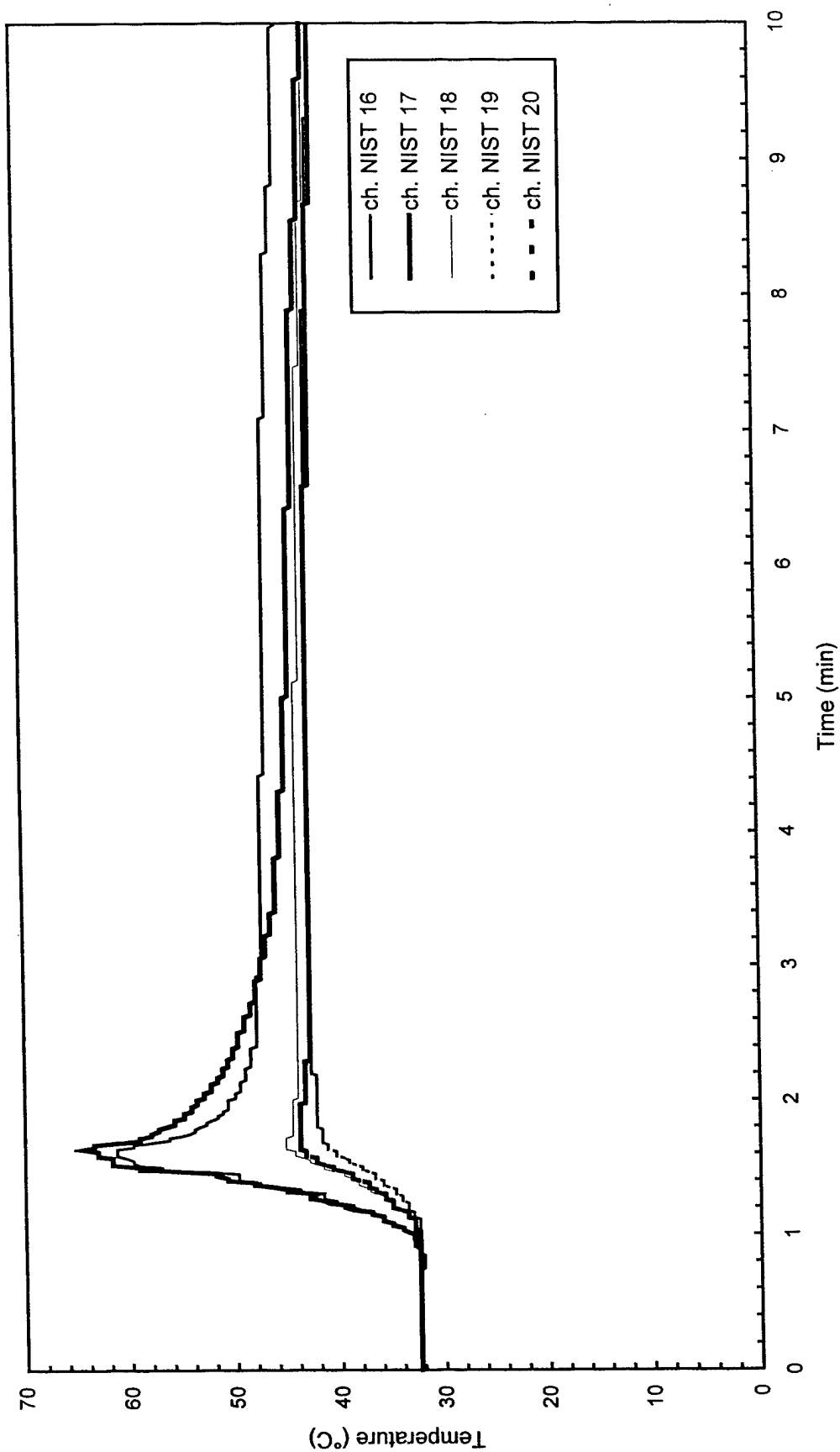


Fig. C58 - Temperature of South steel beam

Test F4

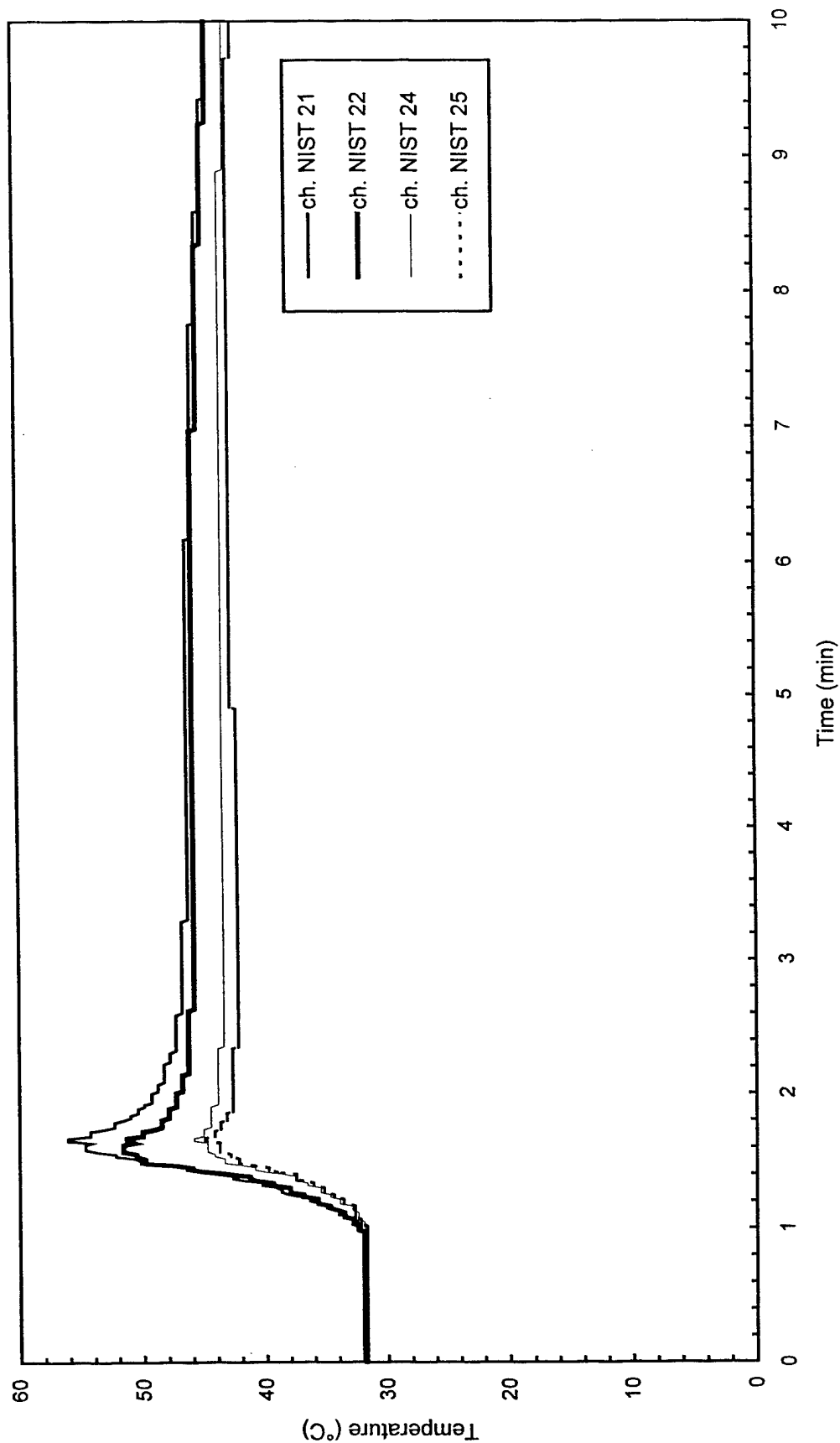


Fig. C59 - Temperature of Northwest steel beam

Test F4

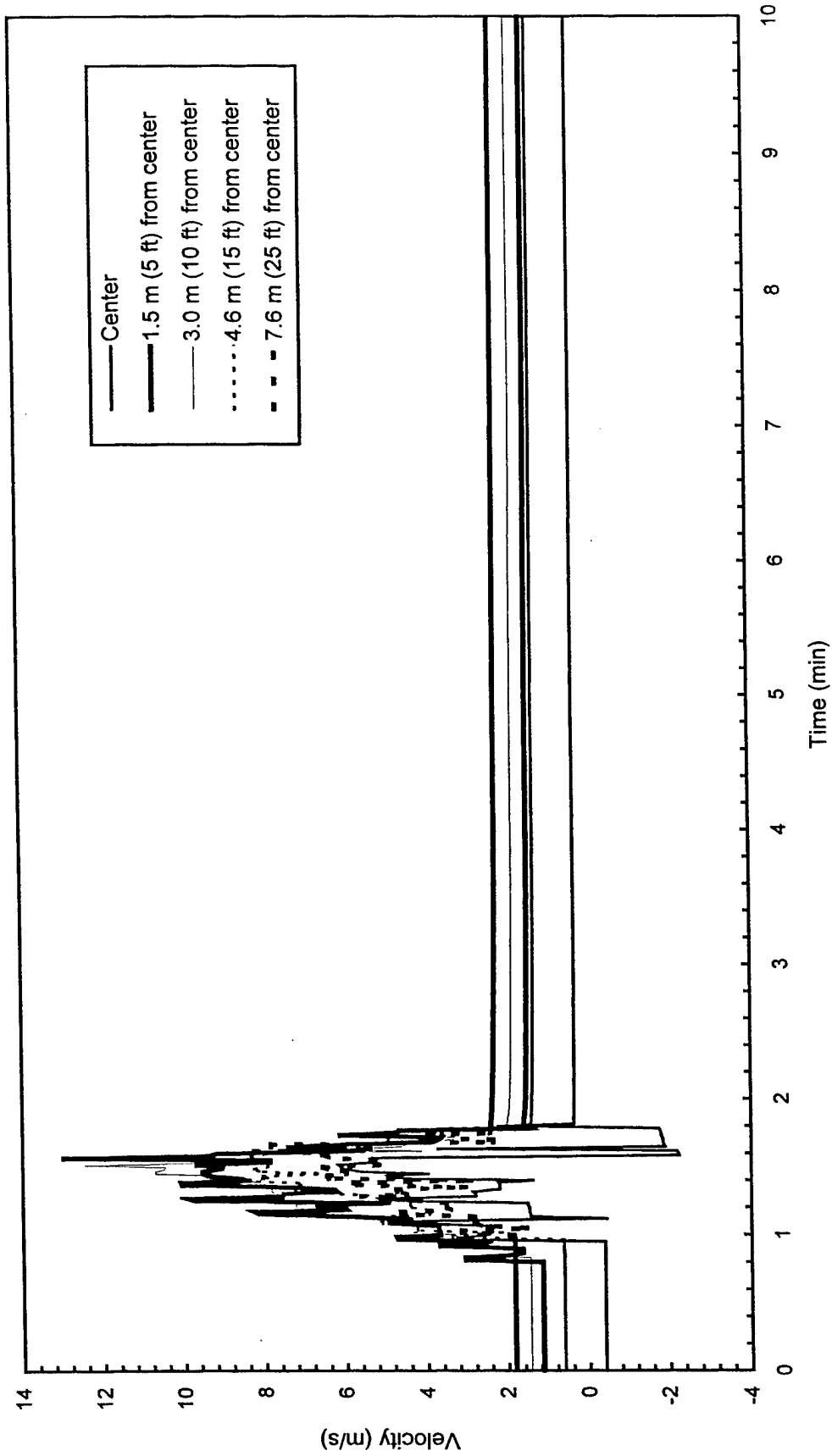


Fig. C60 - Plume and ceiling jet velocities

Test F5

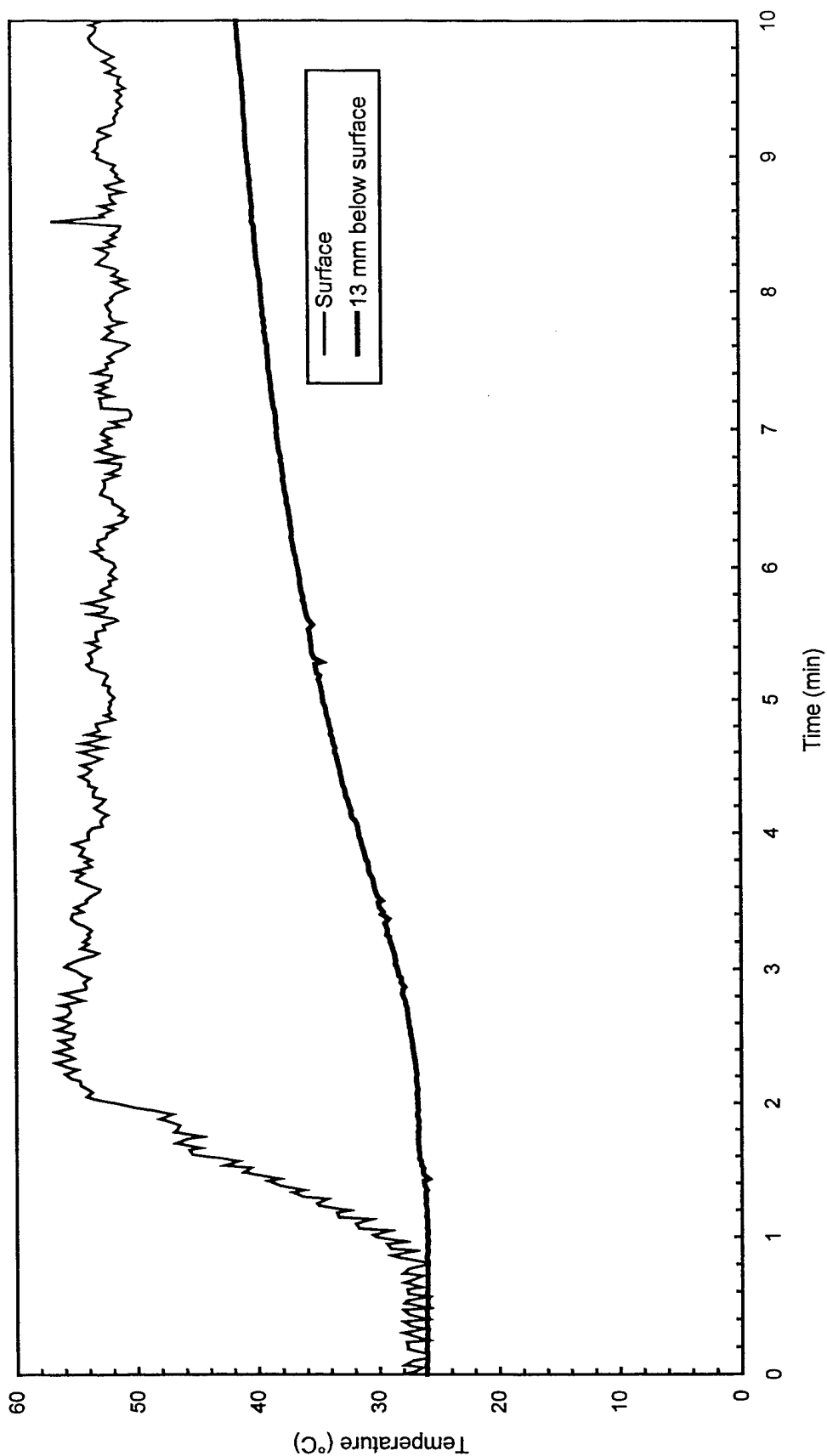


Fig. C61 - Concrete temperatures at center of pad

Test F5

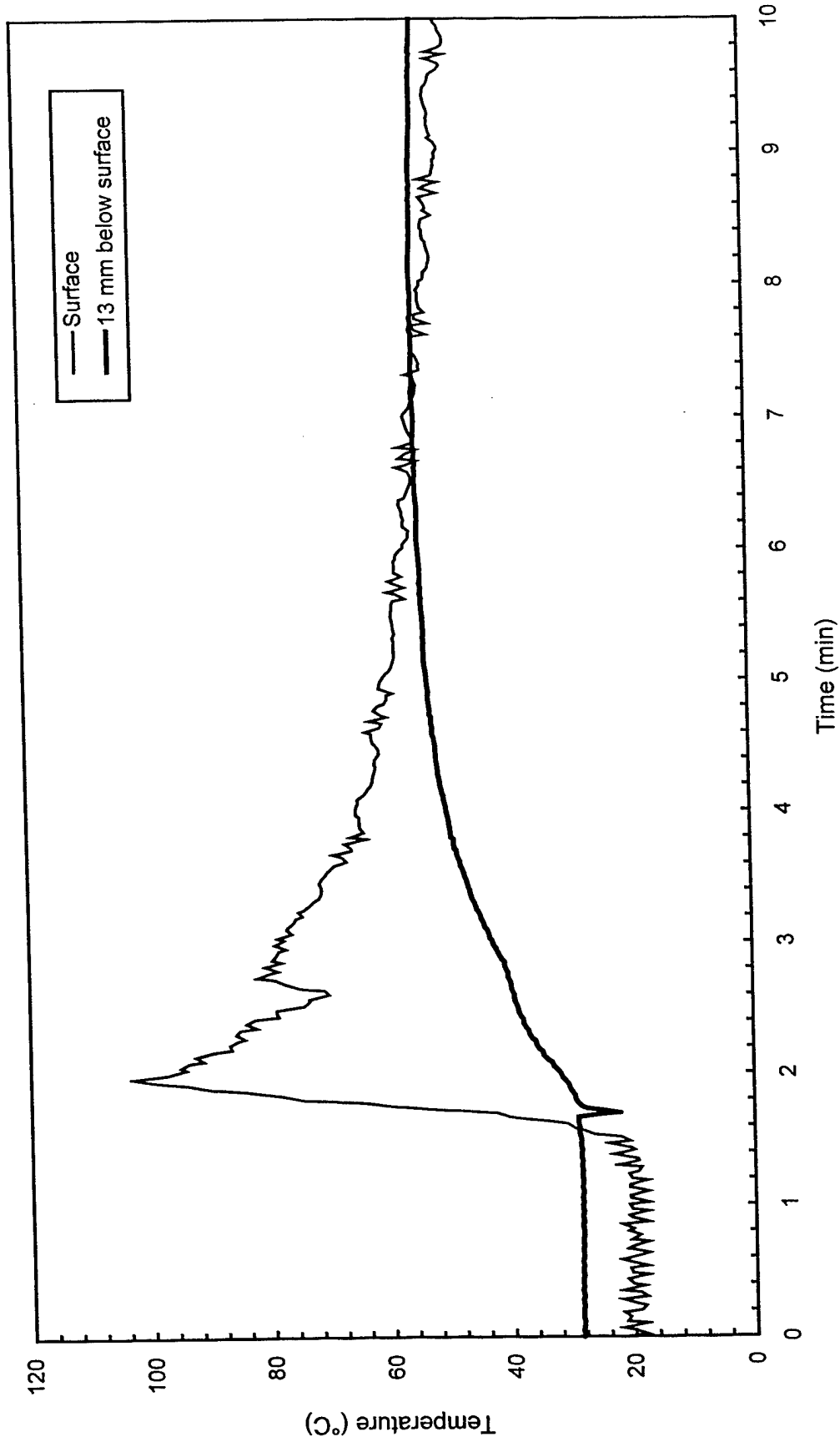


Fig. C62 - Concrete temperatures 3 m (10 ft) East of center of pad

Test F5

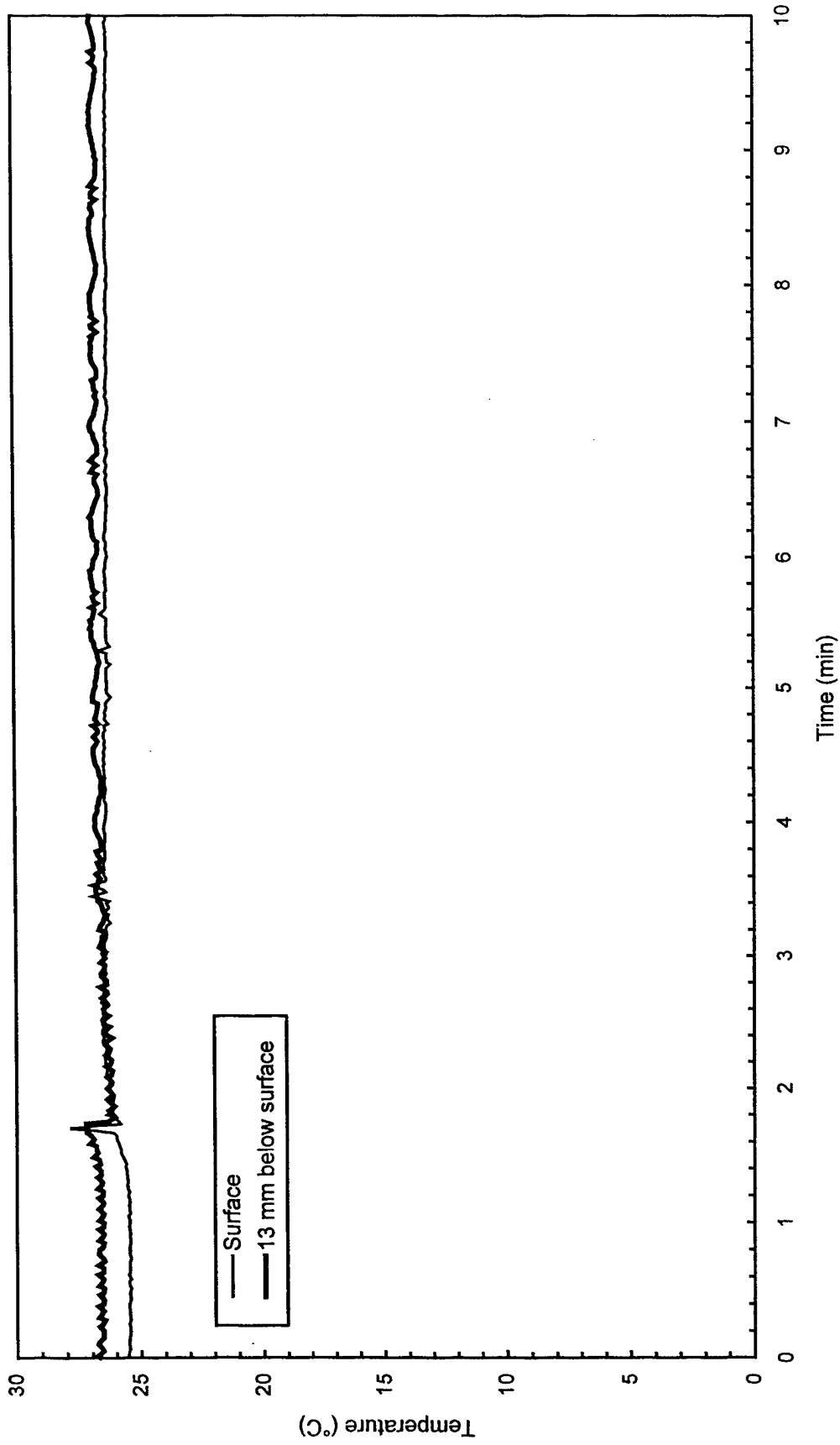


Fig. C63 - Concrete temperatures 3 m (10 ft) West of center of pad

Test F5

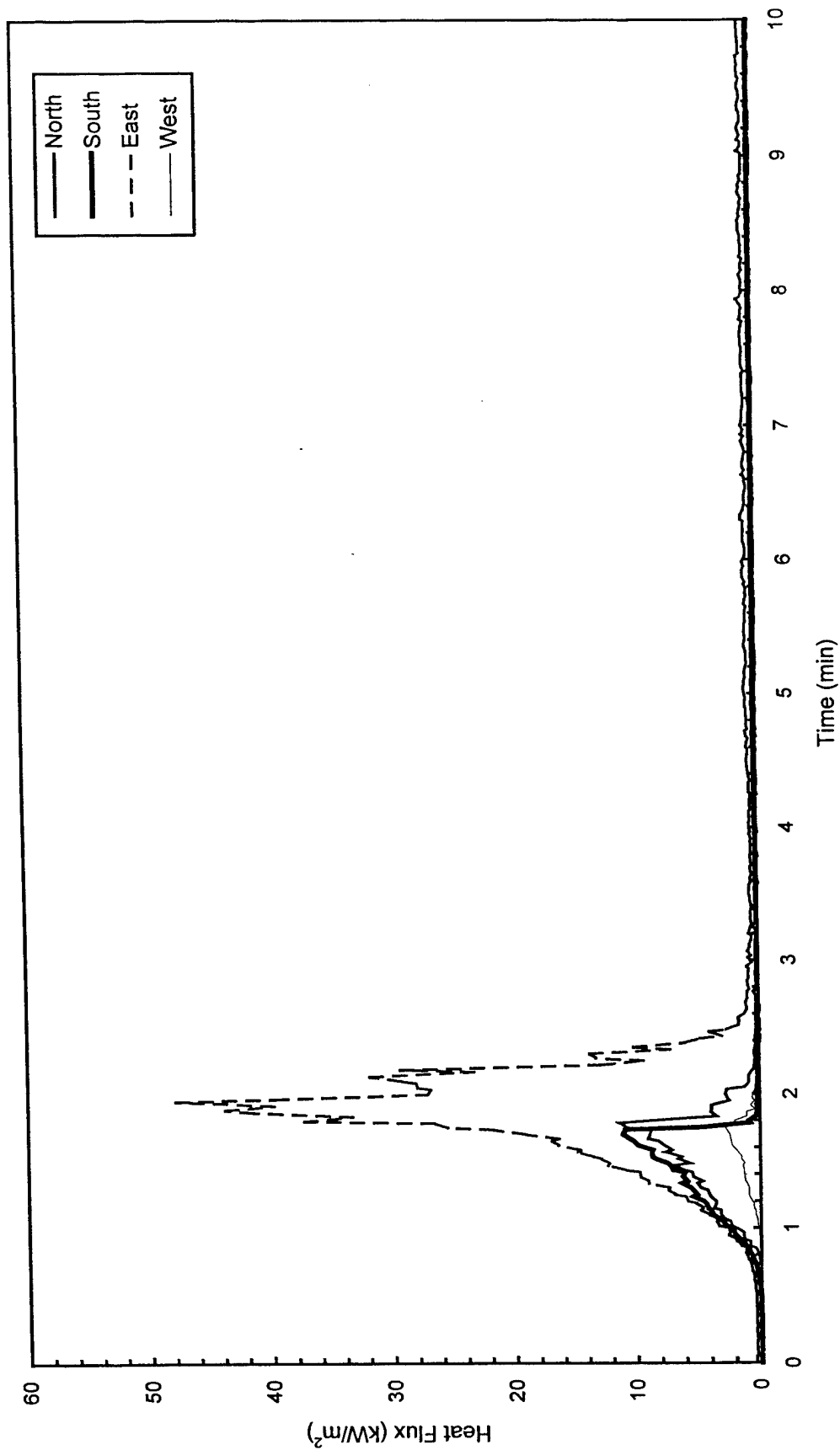


Fig. C64 - Heat flux measured at edge of pad

Test F5

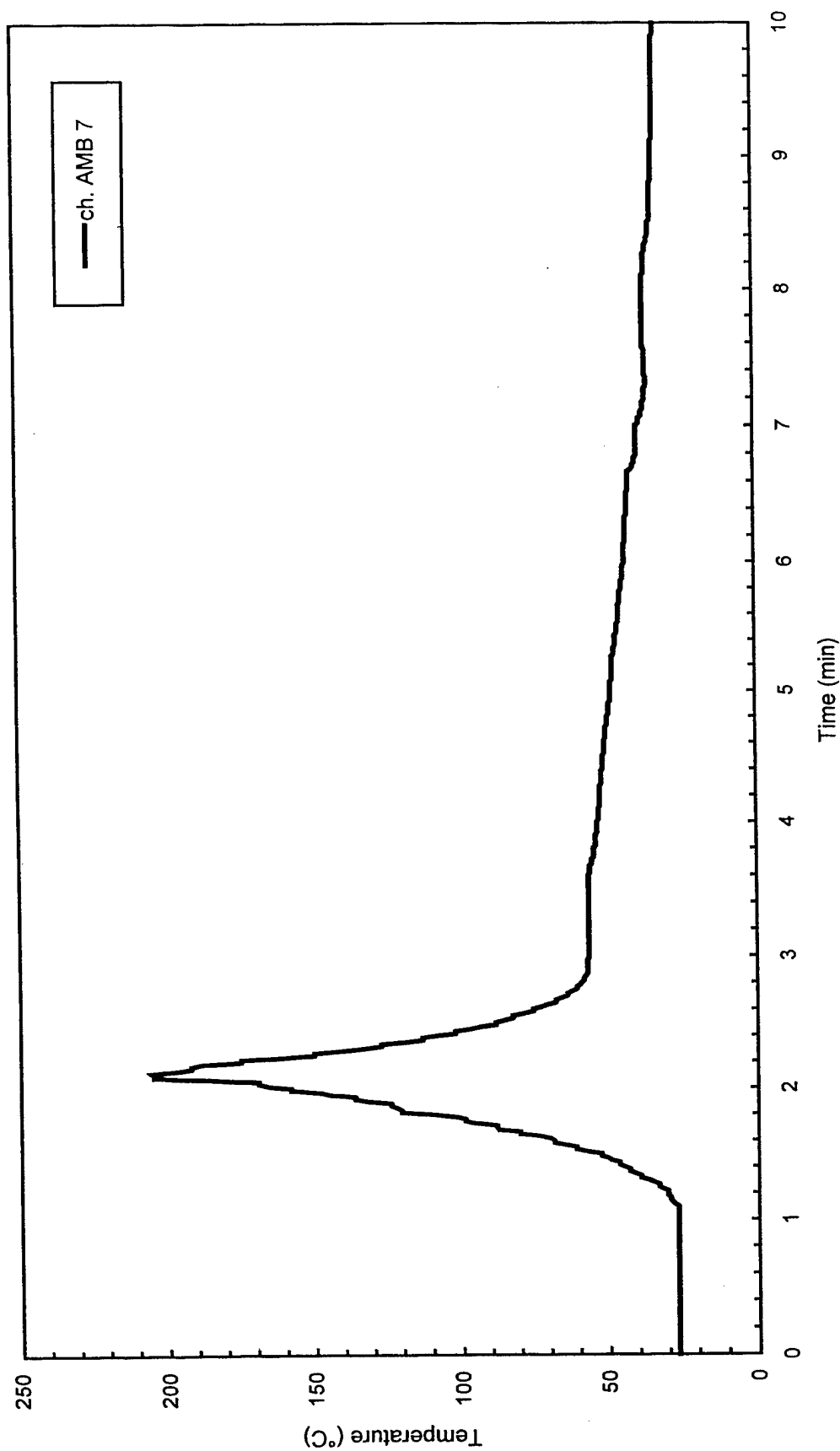


Fig. C65 - Air temperatures over center of pad

Test F5

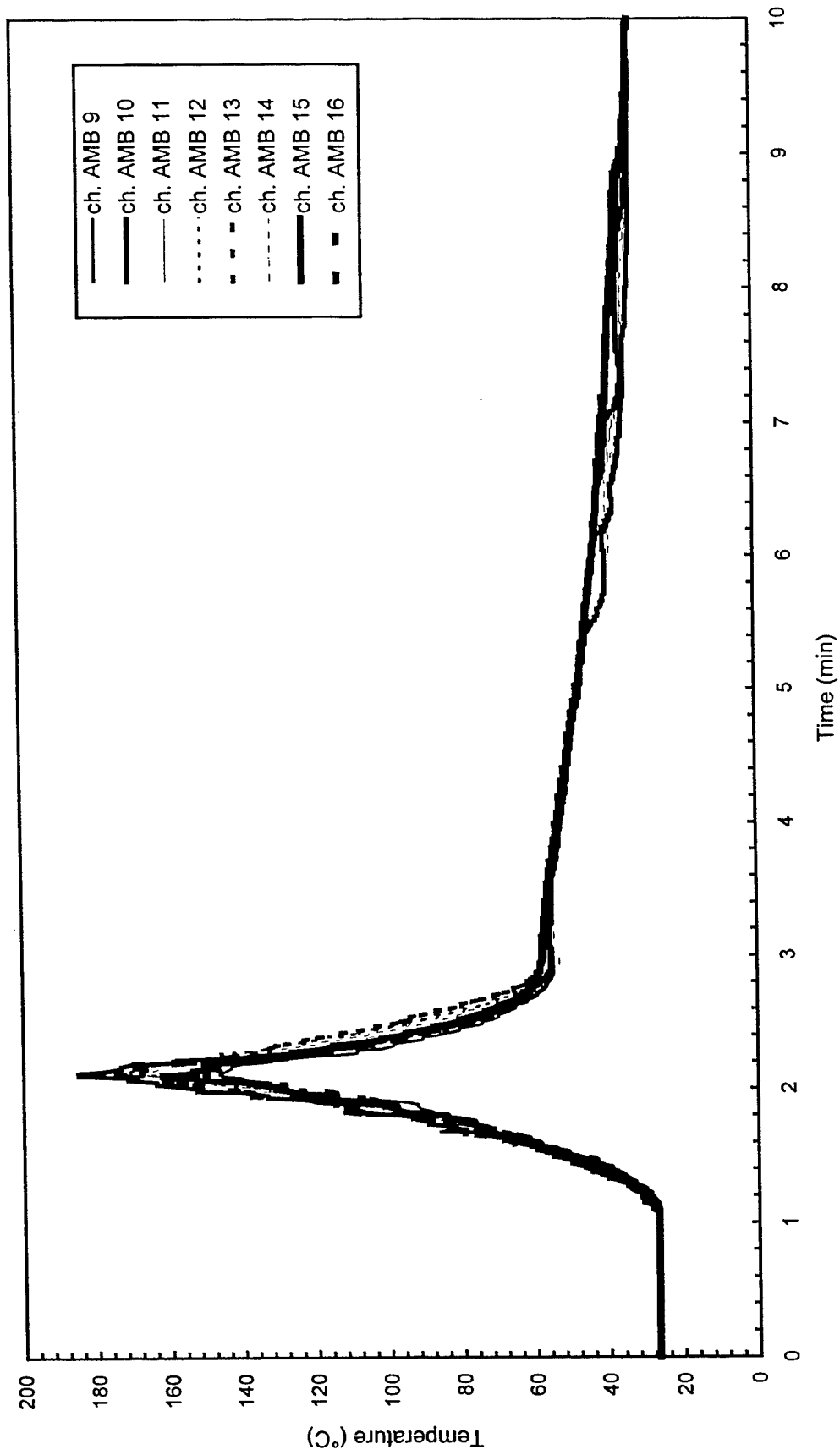


Fig. C66 - Air temperatures around 3 m (10 ft) radius from center of pad

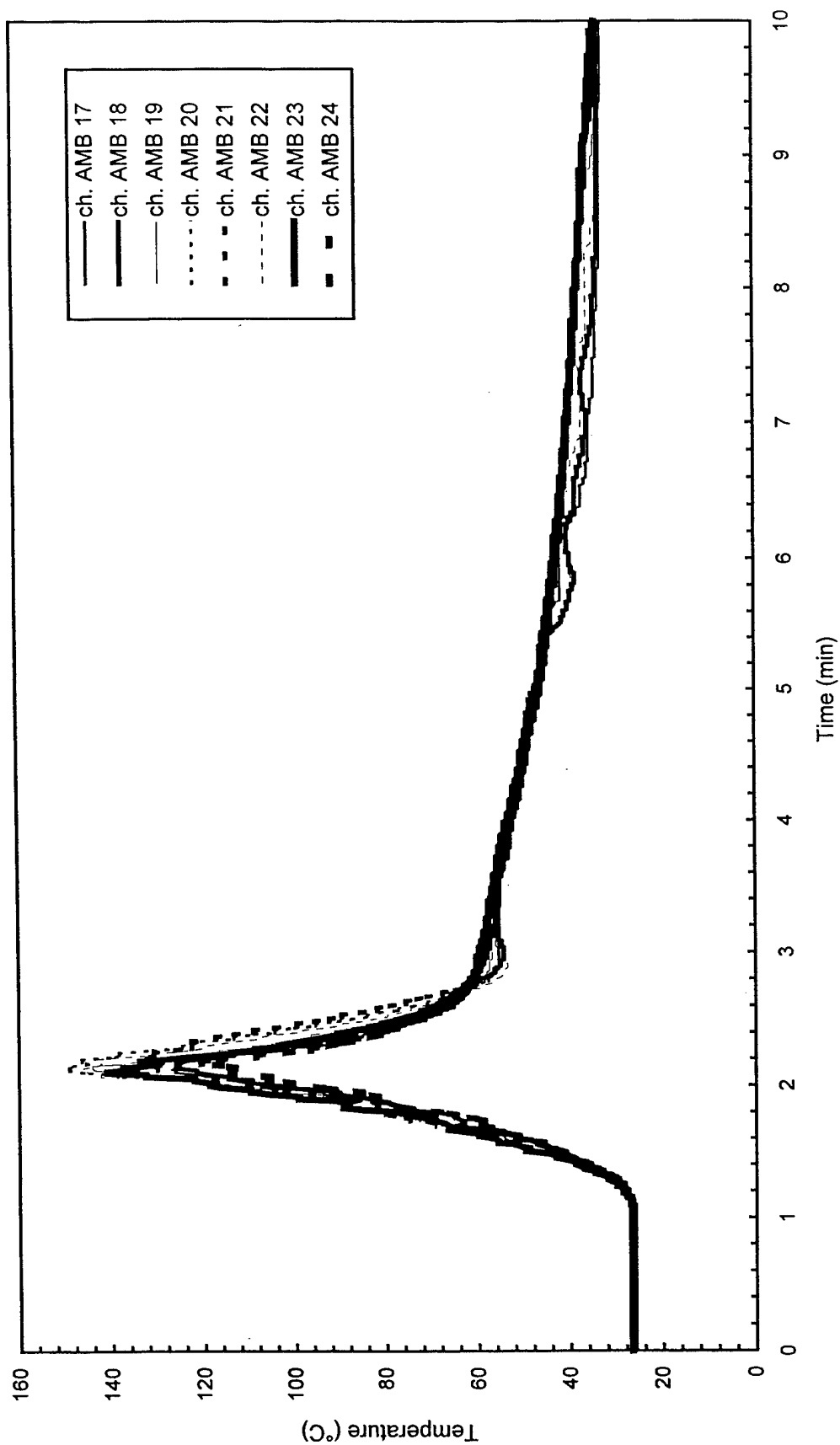


Fig. C67 - Air temperatures around 4.6 m (15 ft) radius from center of pad

Test F5

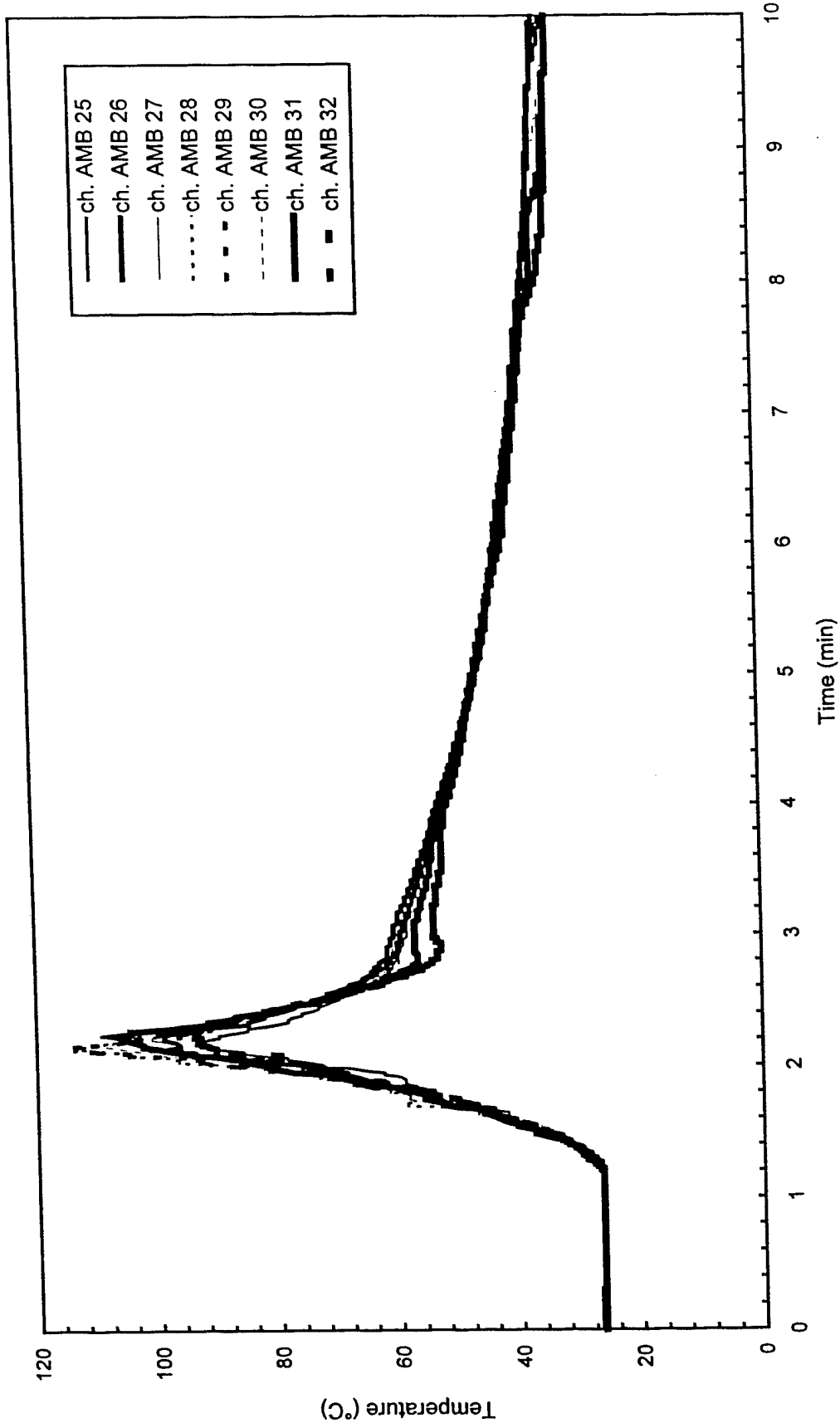


Fig. C68 - Air temperatures around North half of 7.6 m (25 ft) radius from center of pad

Test F5

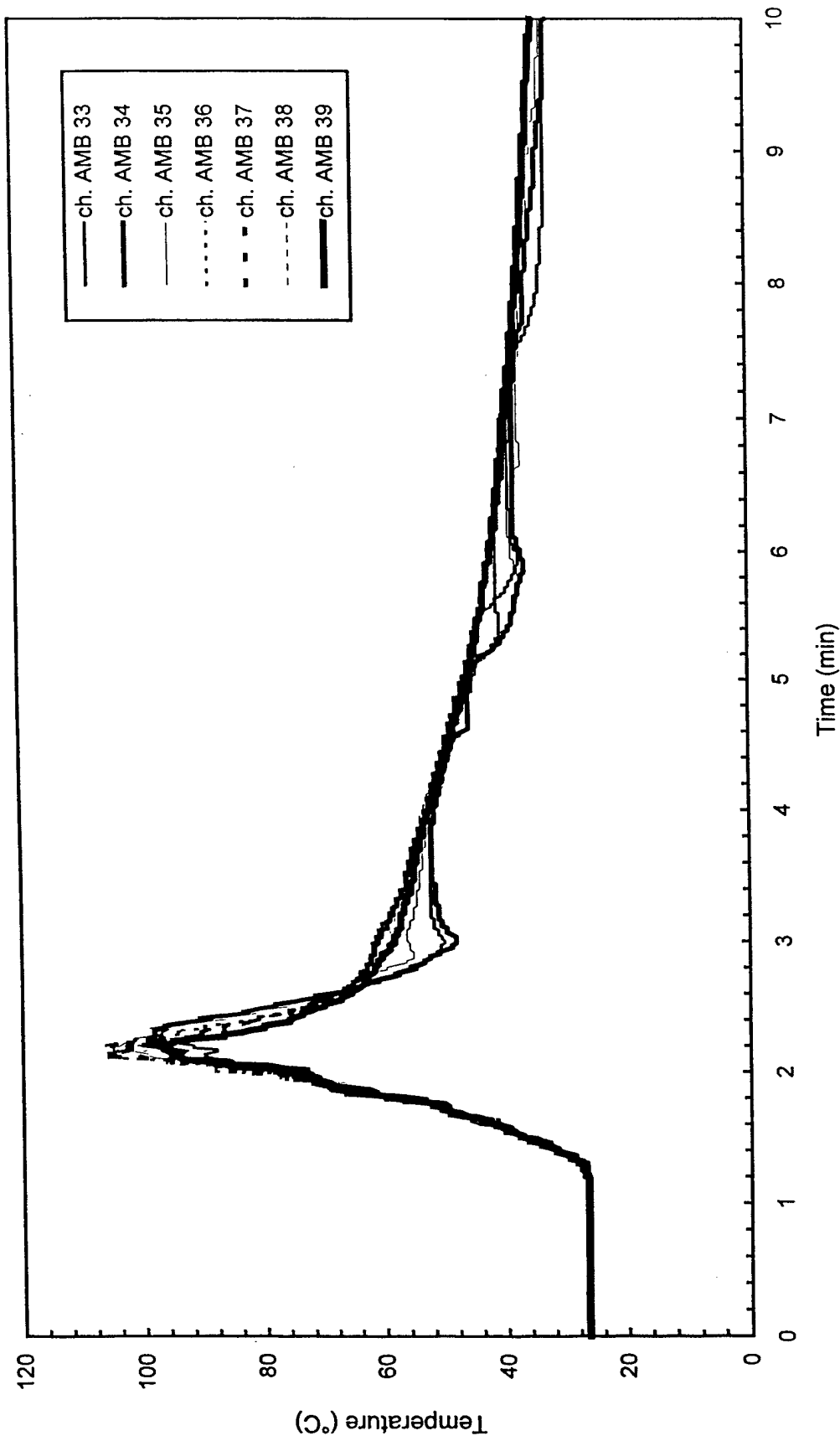


Fig. C69 - Air temperatures around South half of 7.6 m (25 ft) radius from center of pad

Test F5

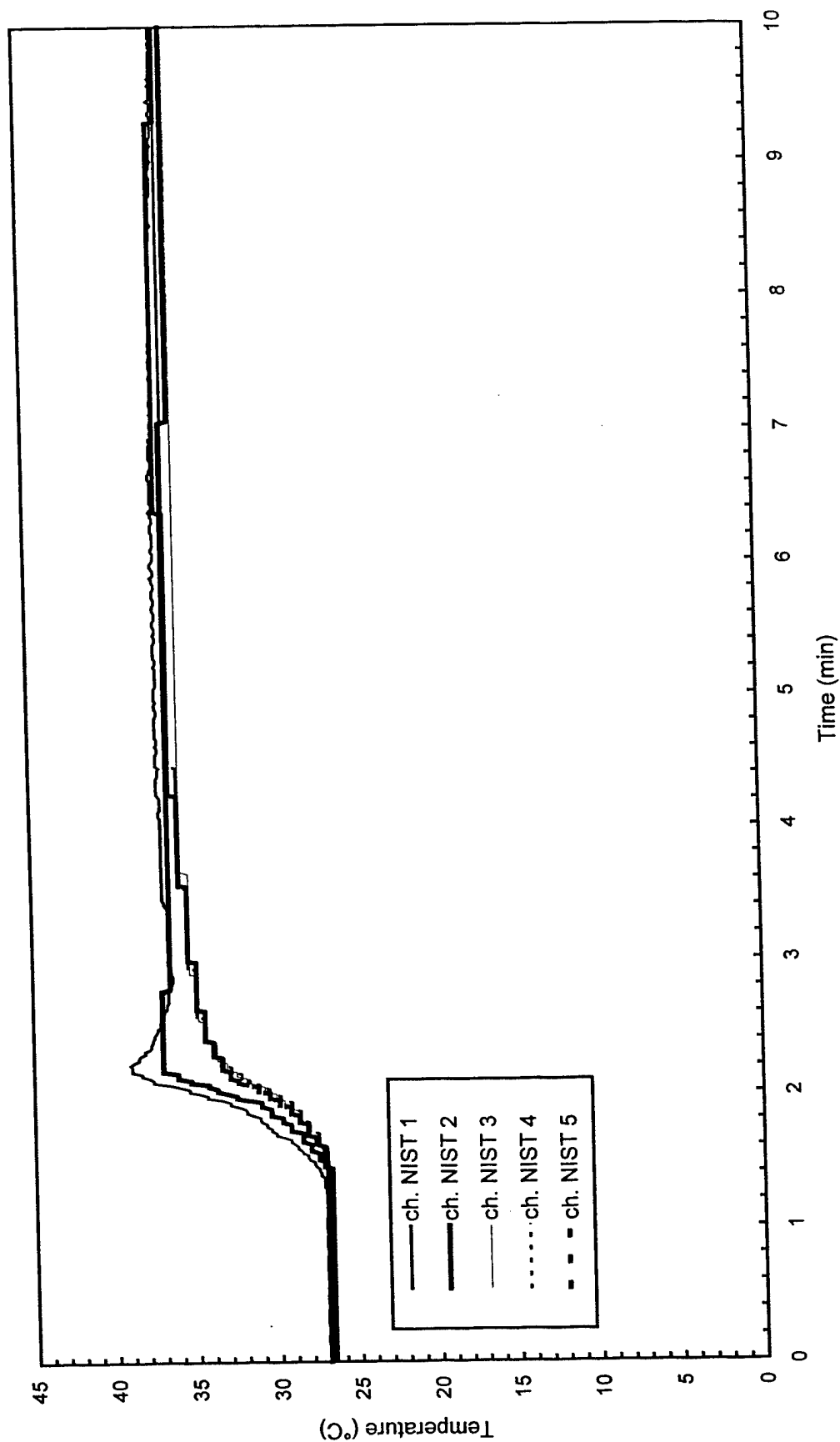


Fig. C70 - Temperature of West steel beam

Test F5

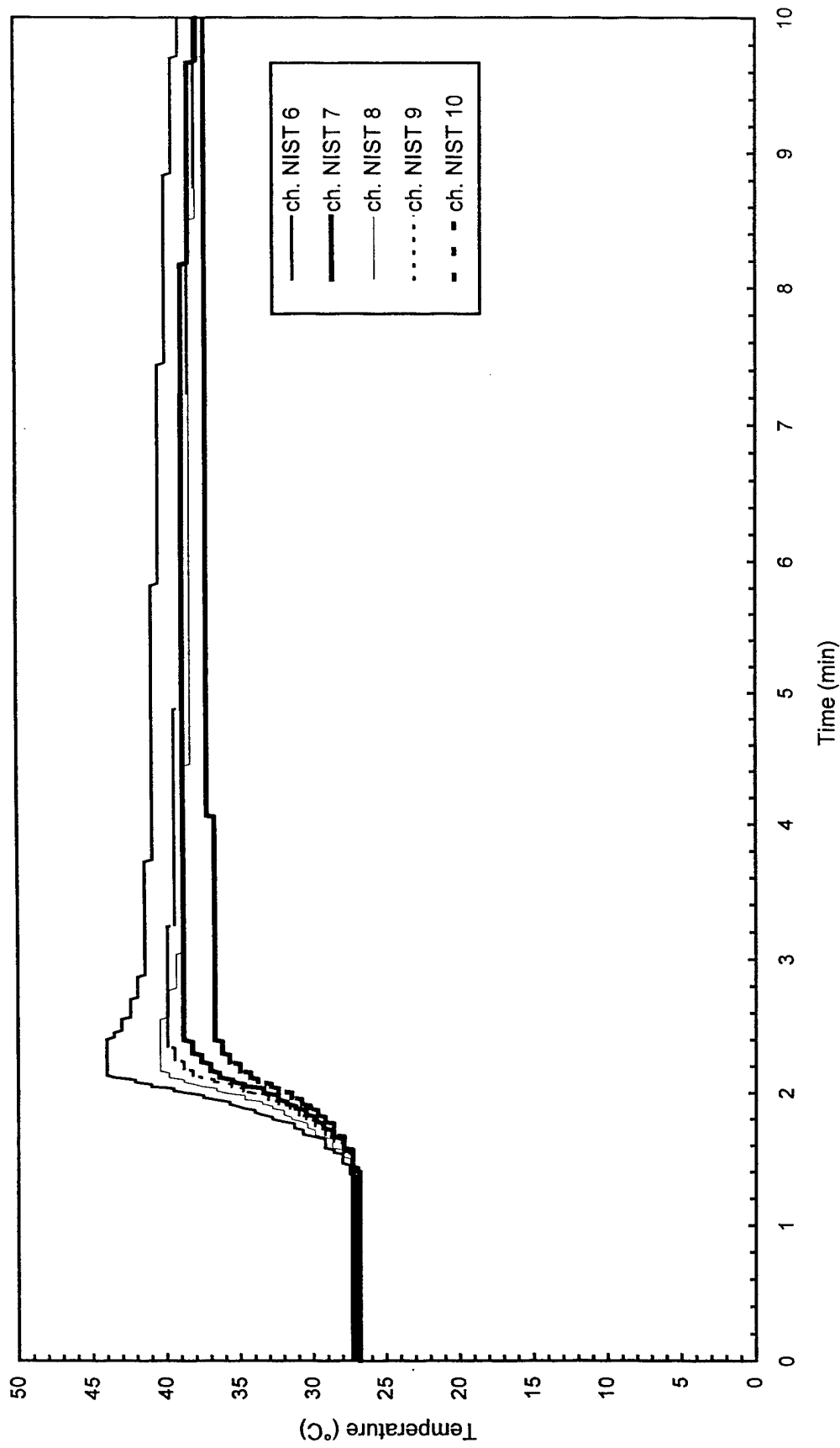


Fig. C71 - Temperature of North steel beam

Test F5

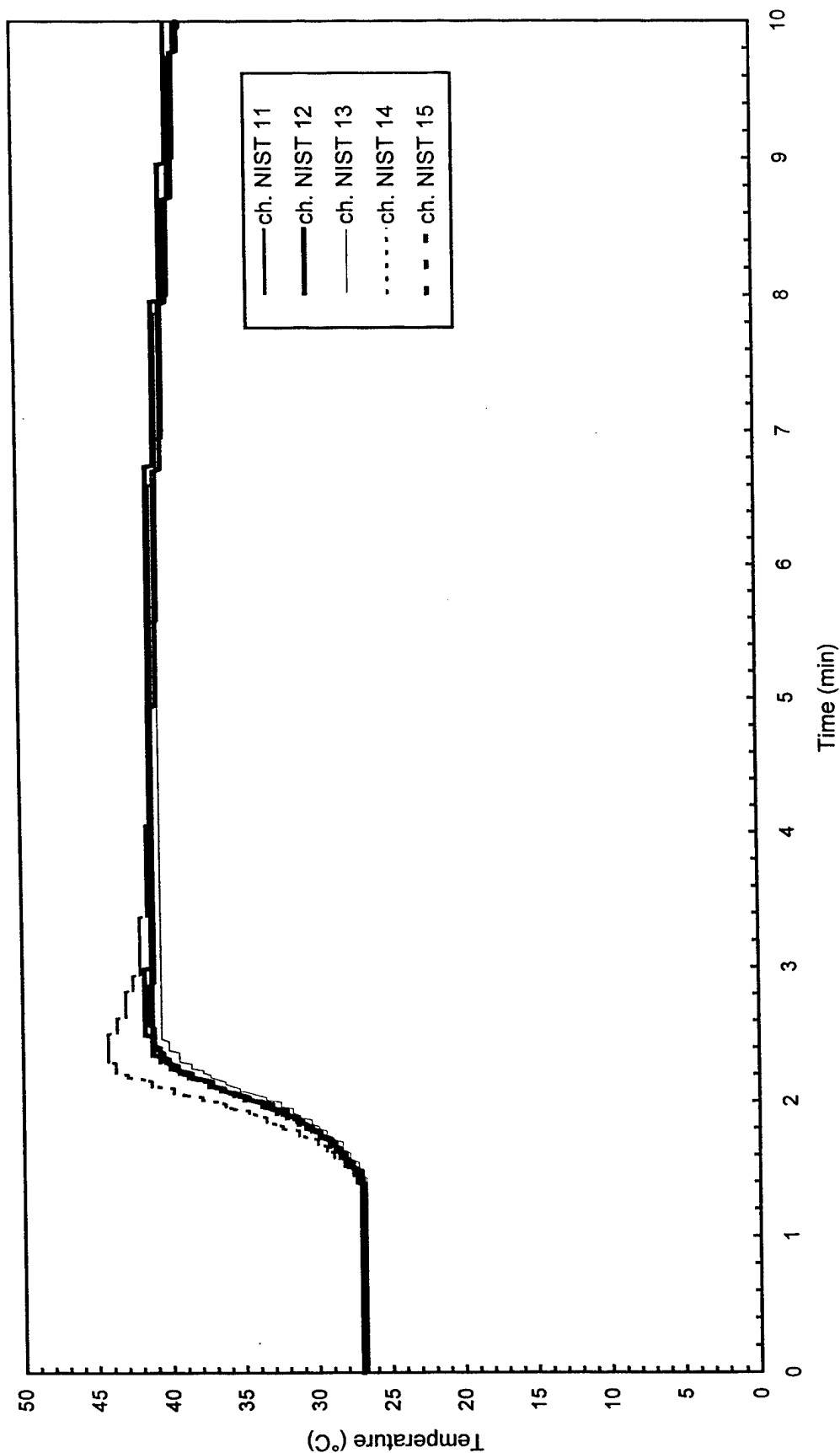


Fig. C72 - Temperature of East steel beam

Test F5

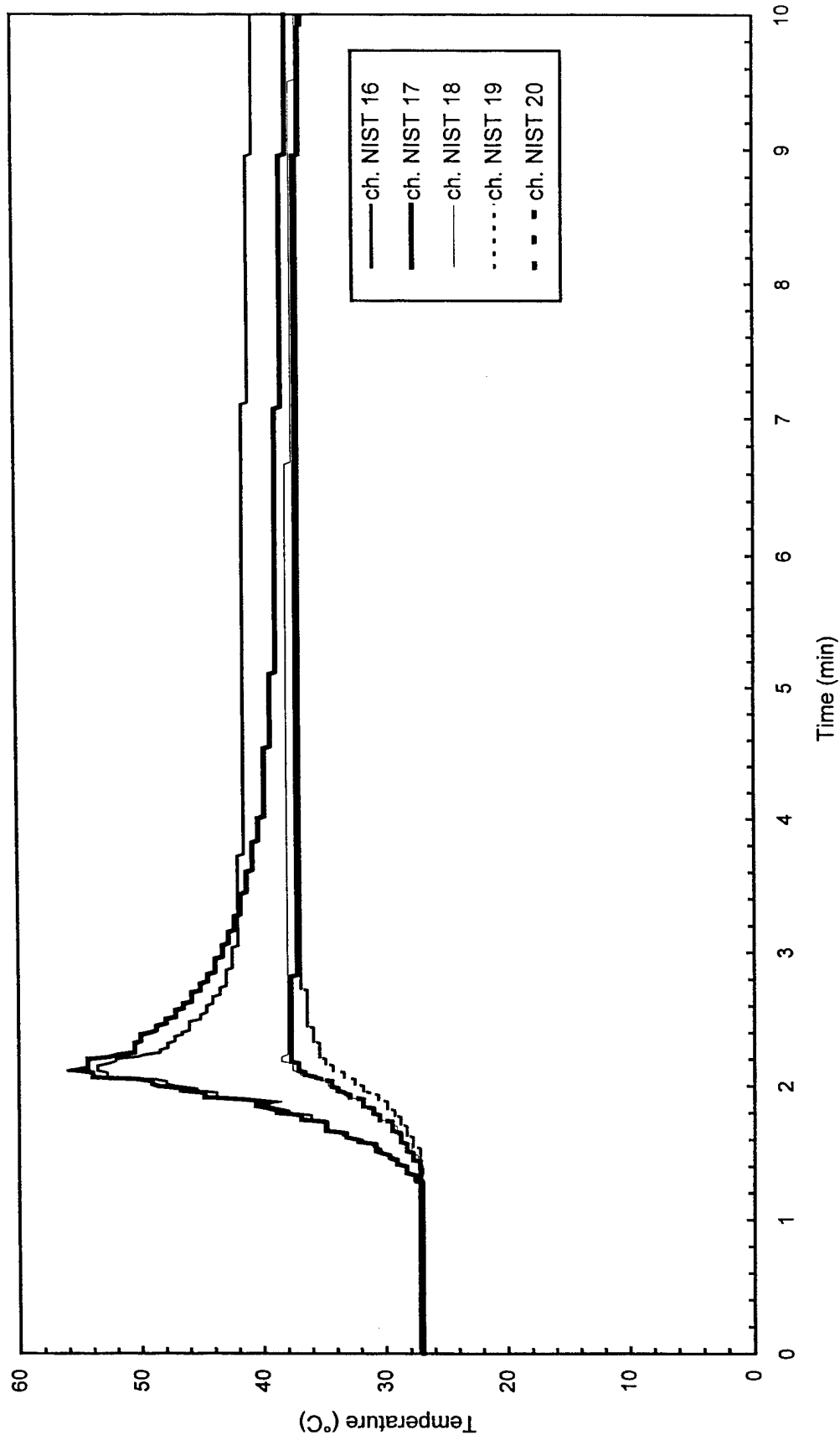


Fig. C73 - Temperature of South steel beam

Test F5

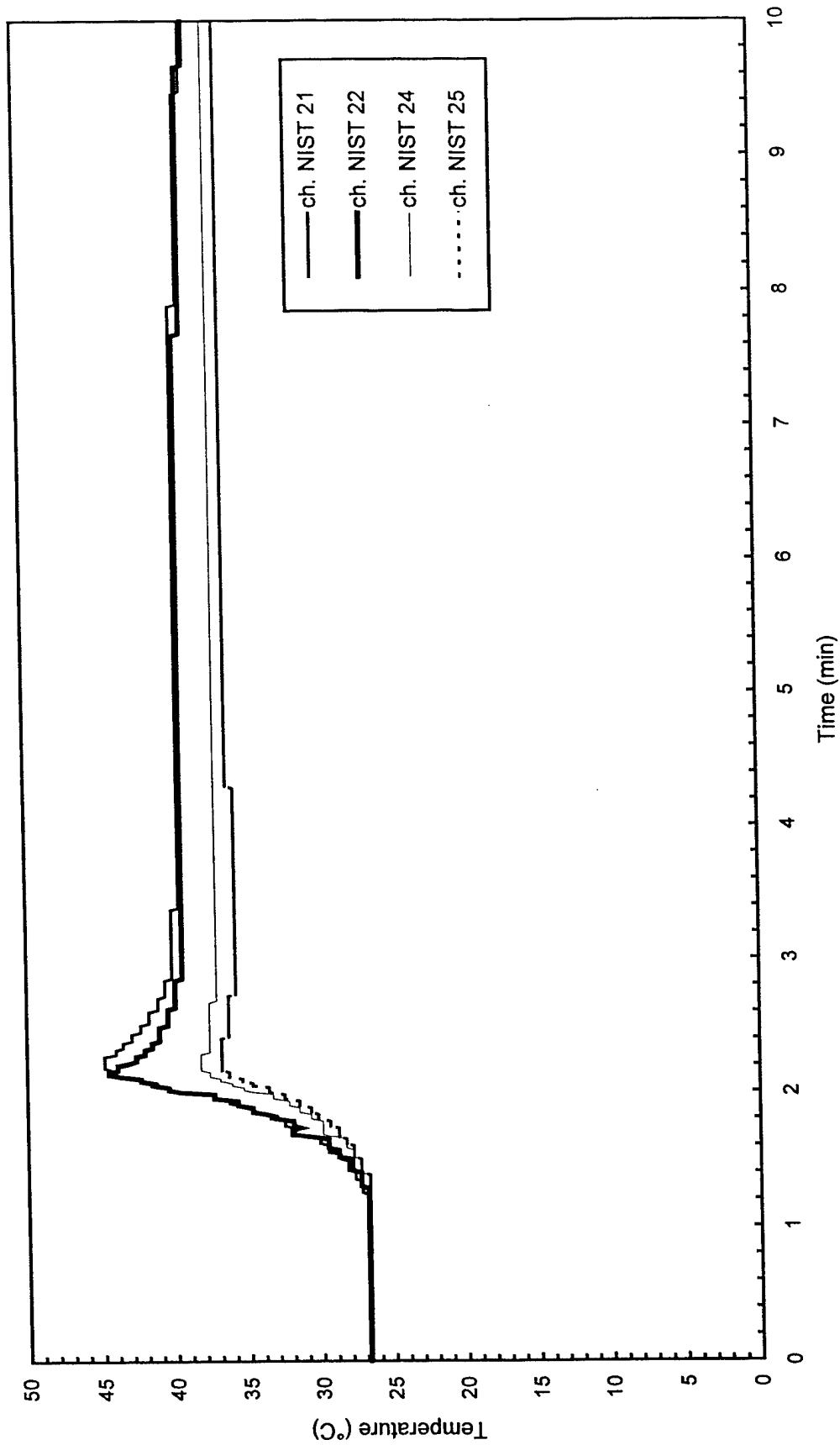


Fig. C74 - Temperature of Northwest steel beam

Test F5

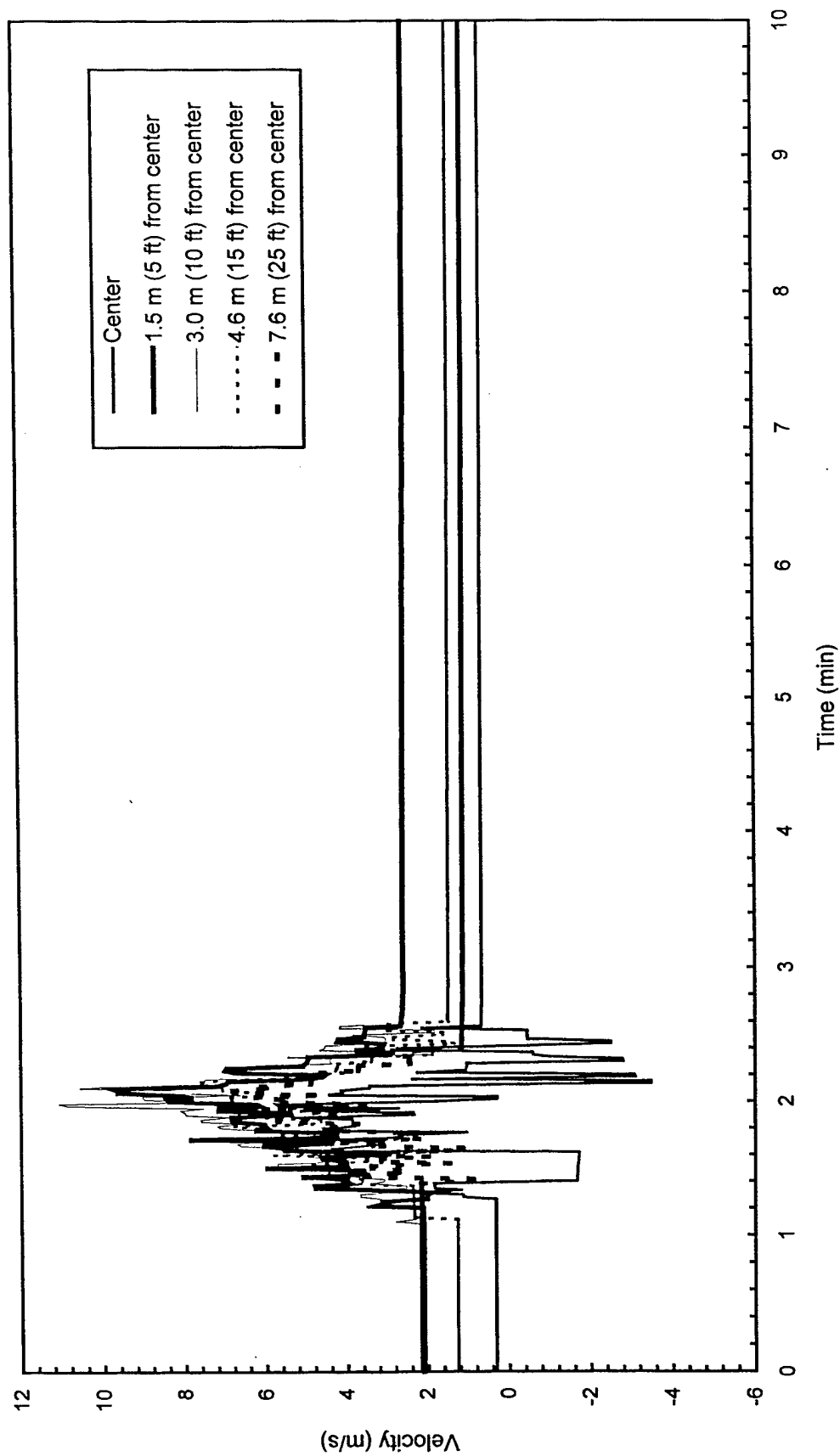


Fig. C75 - Plume and ceiling jet velocities

Test F6

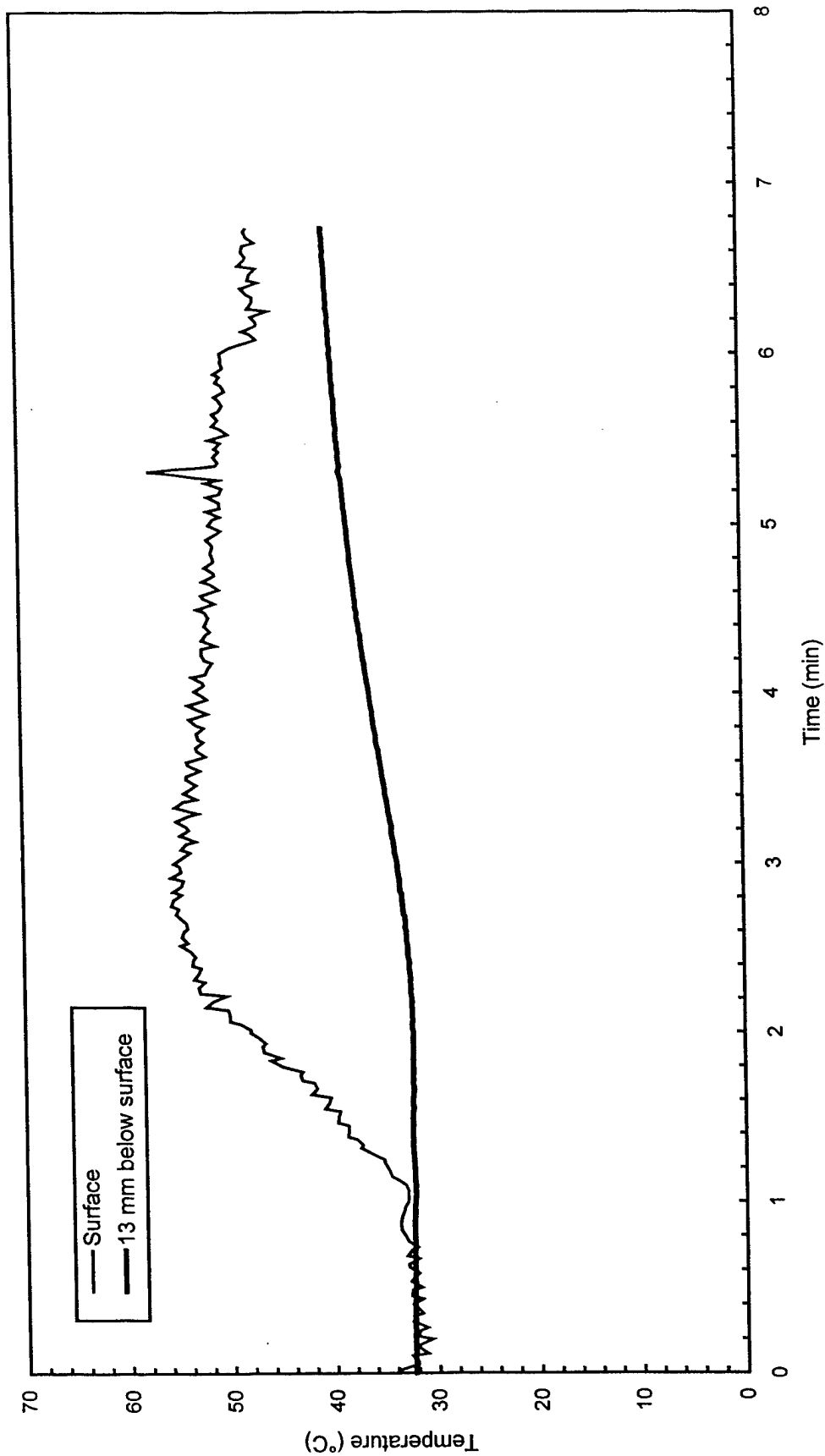


Fig. C76 - Concrete temperatures at center of pad

Test F6

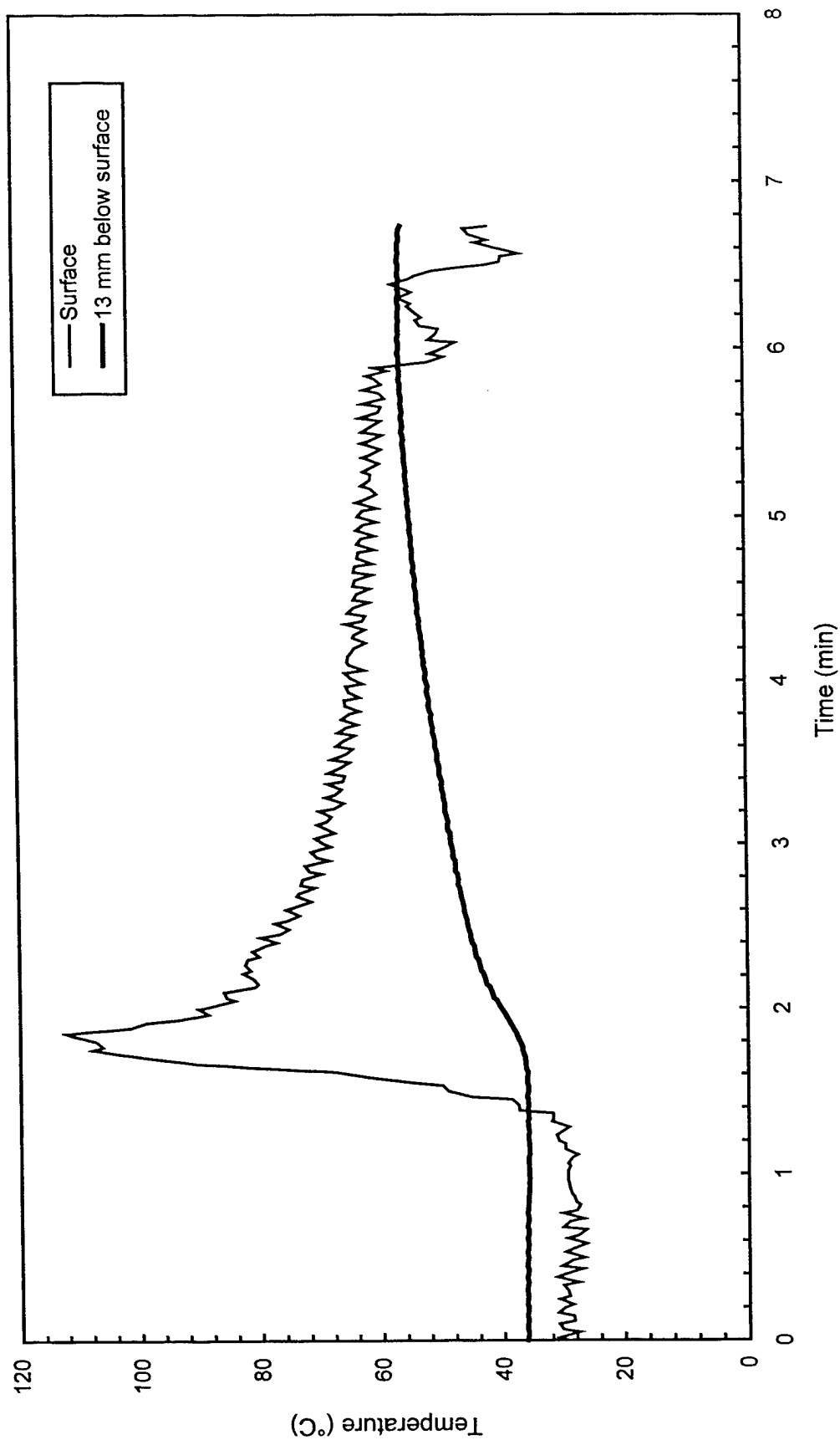


Fig. C77 - Concrete temperatures 3 m (10 ft) East of center of pad

Test F6

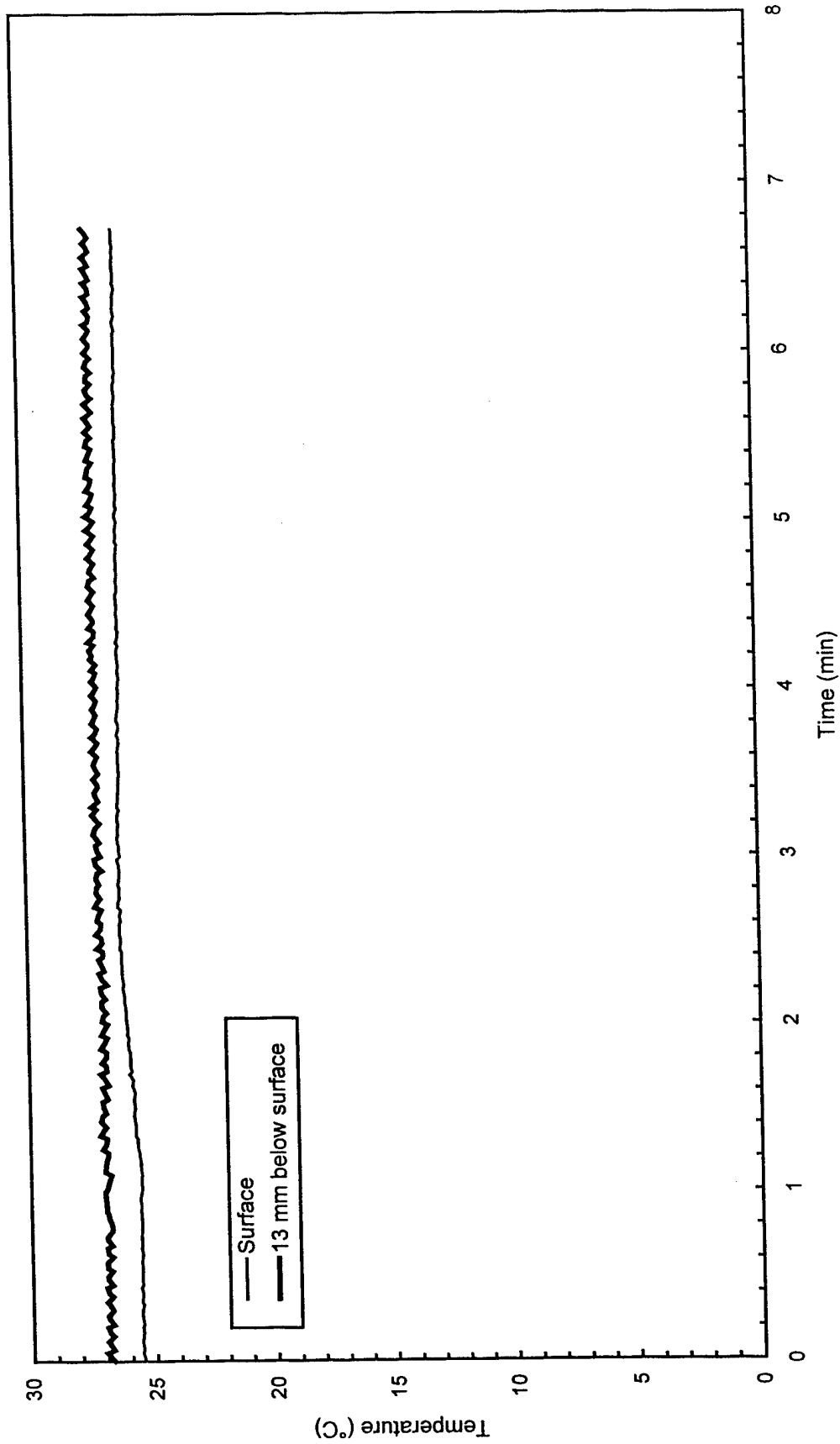


Fig. C78 - Concrete temperatures 3 m (10 ft) West of center of pad

Test F6

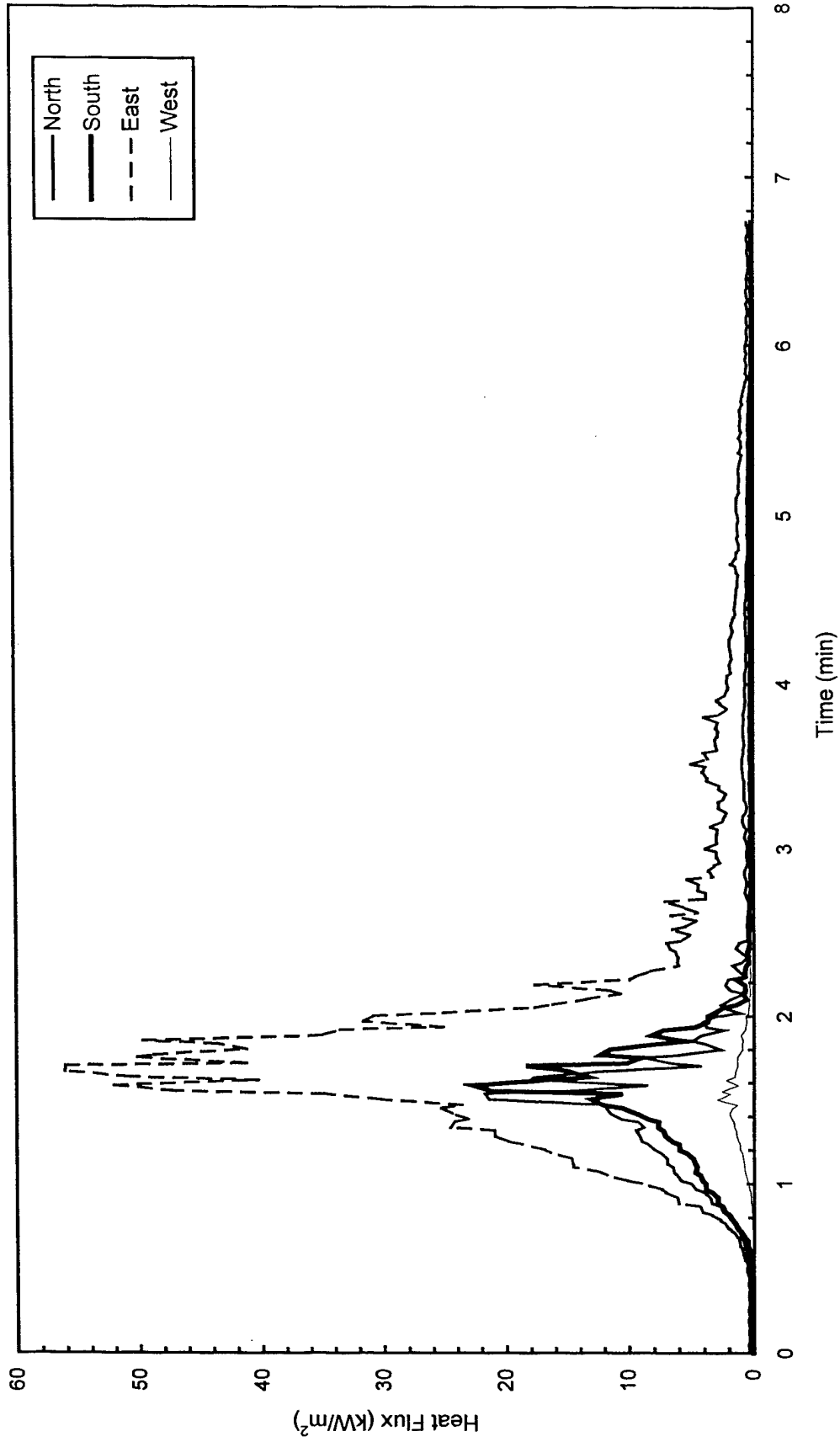


Fig. C79 - Heat flux measured at edge of pad

Test F6

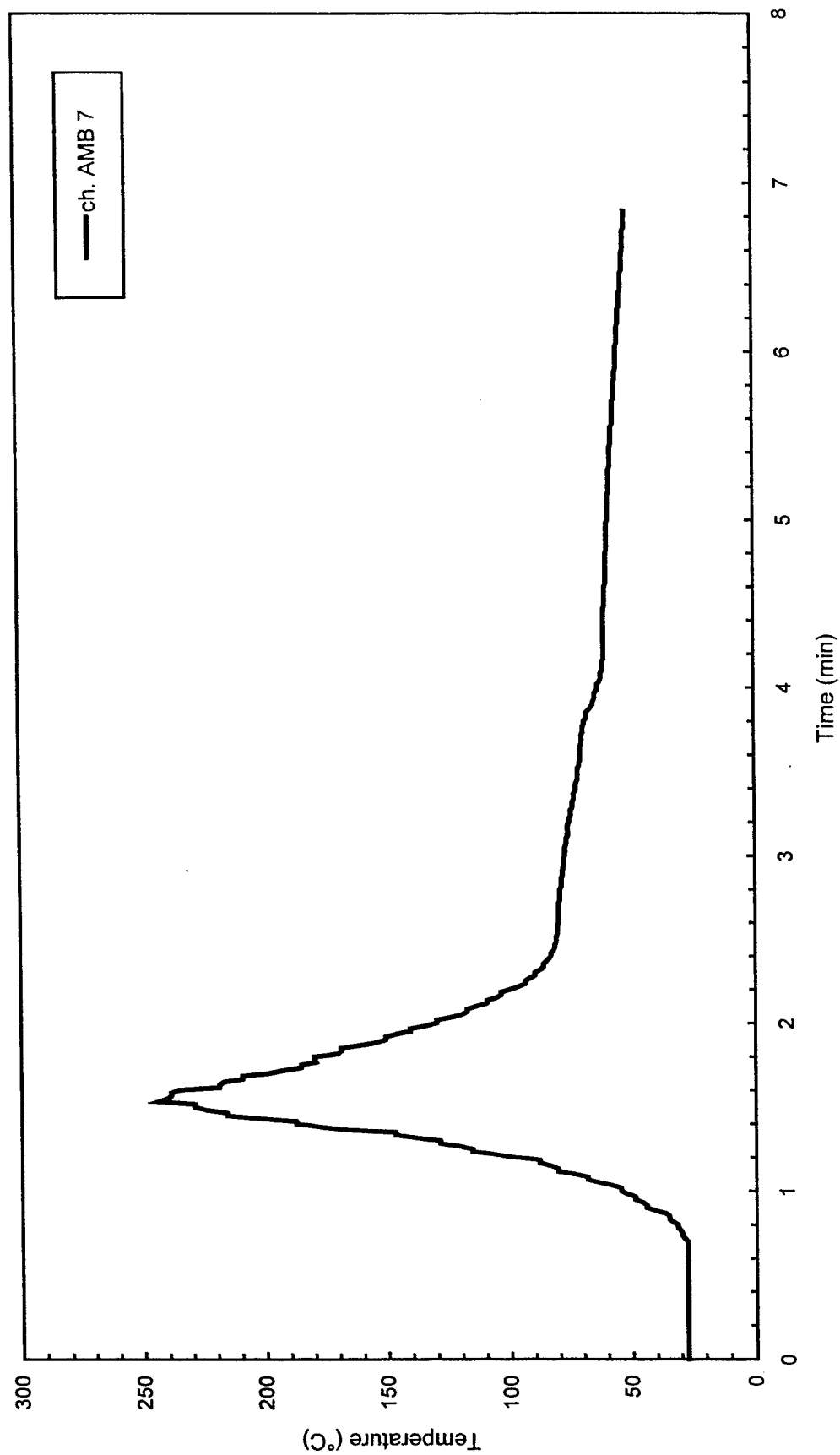


Fig. C80 - Air temperatures over center of pad

Test F6

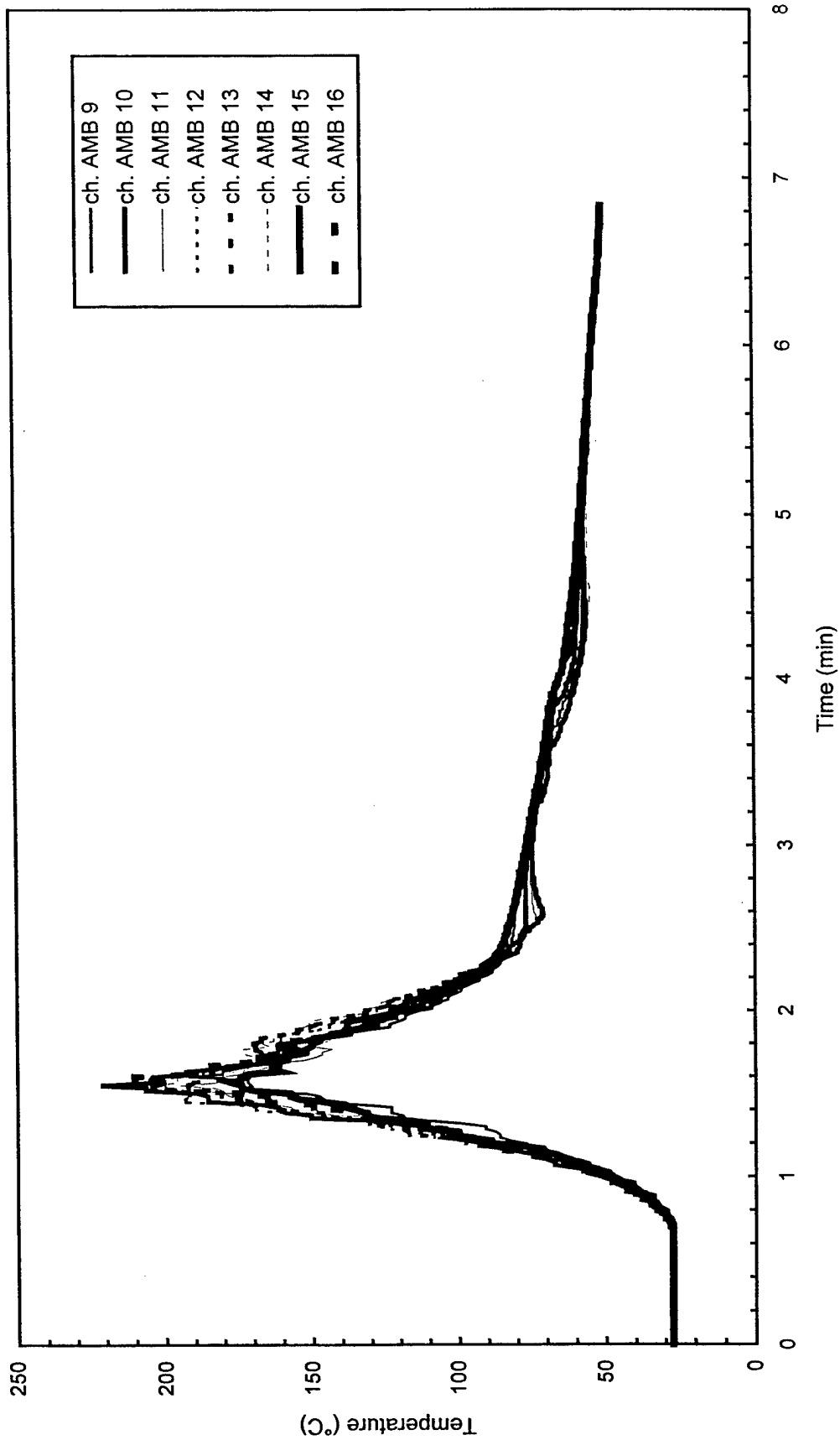


Fig. C81 - Air temperatures around 3 m (10 ft) radius from center of pad

Test F6

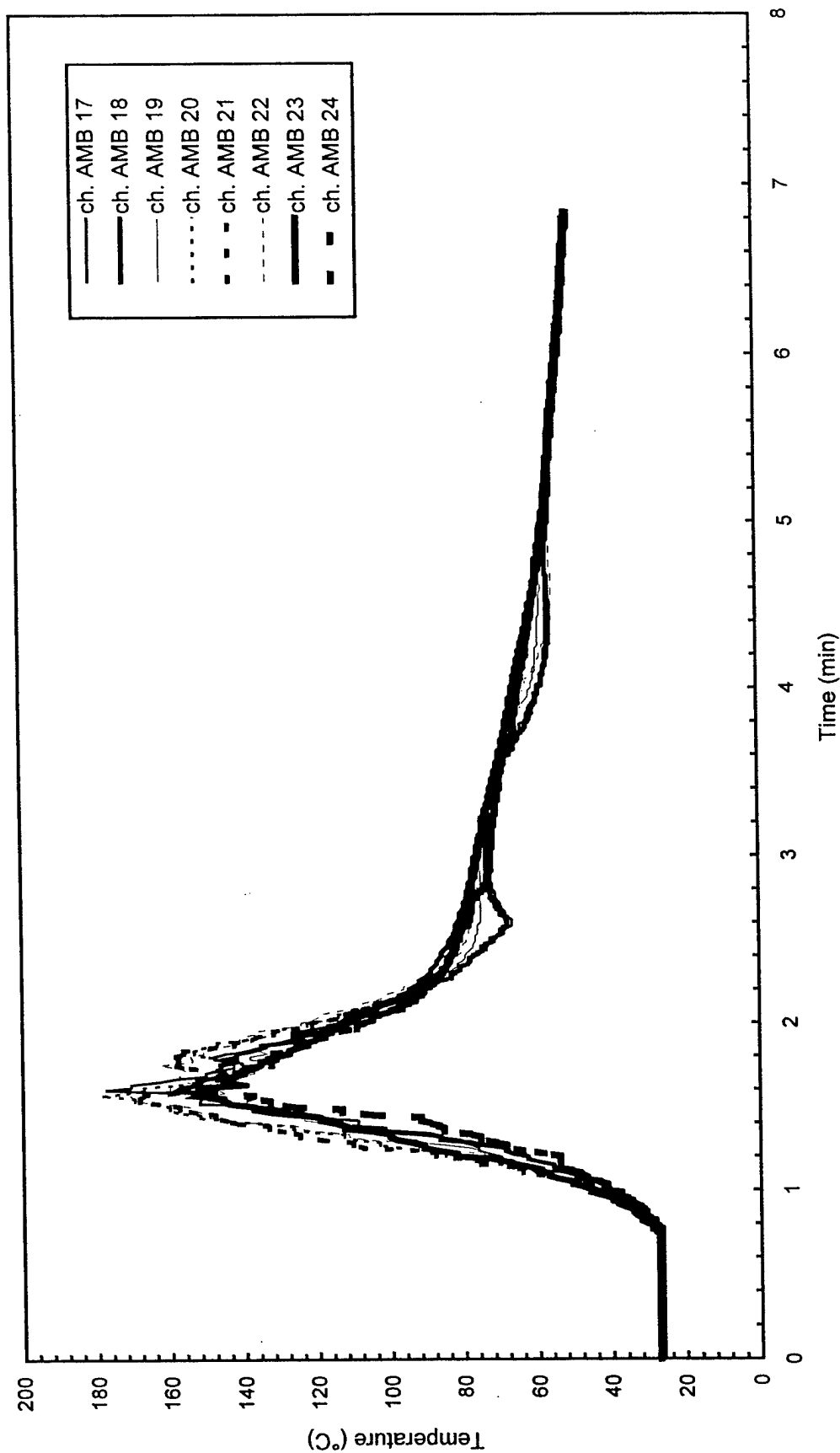


Fig. C82 - Air temperatures around 4.6 m (15 ft) radius from center of pad

Test F6

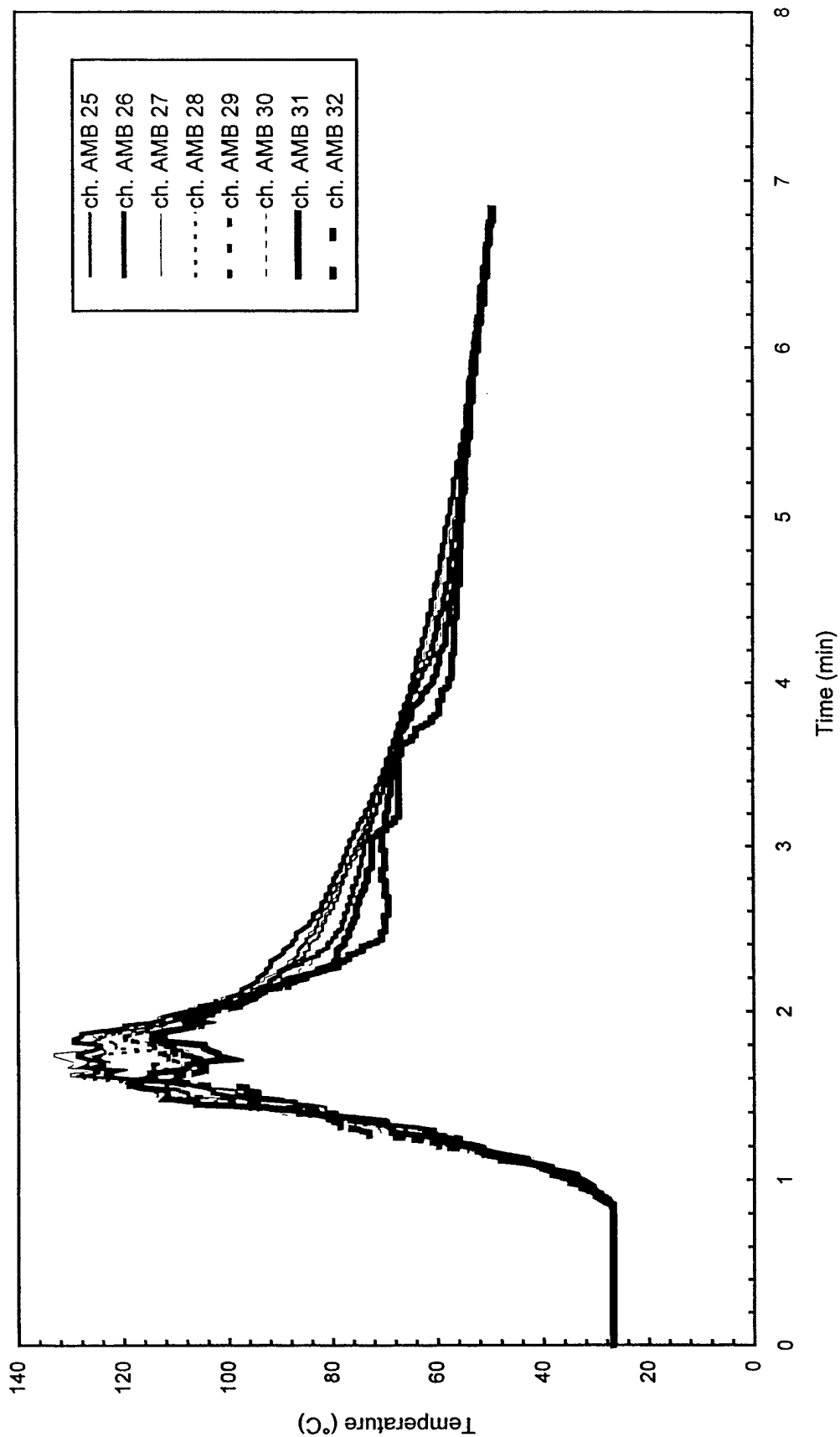


Fig. C83 - Air temperatures around North half of 7.6 m (25 ft) radius from center of pad

Test F6

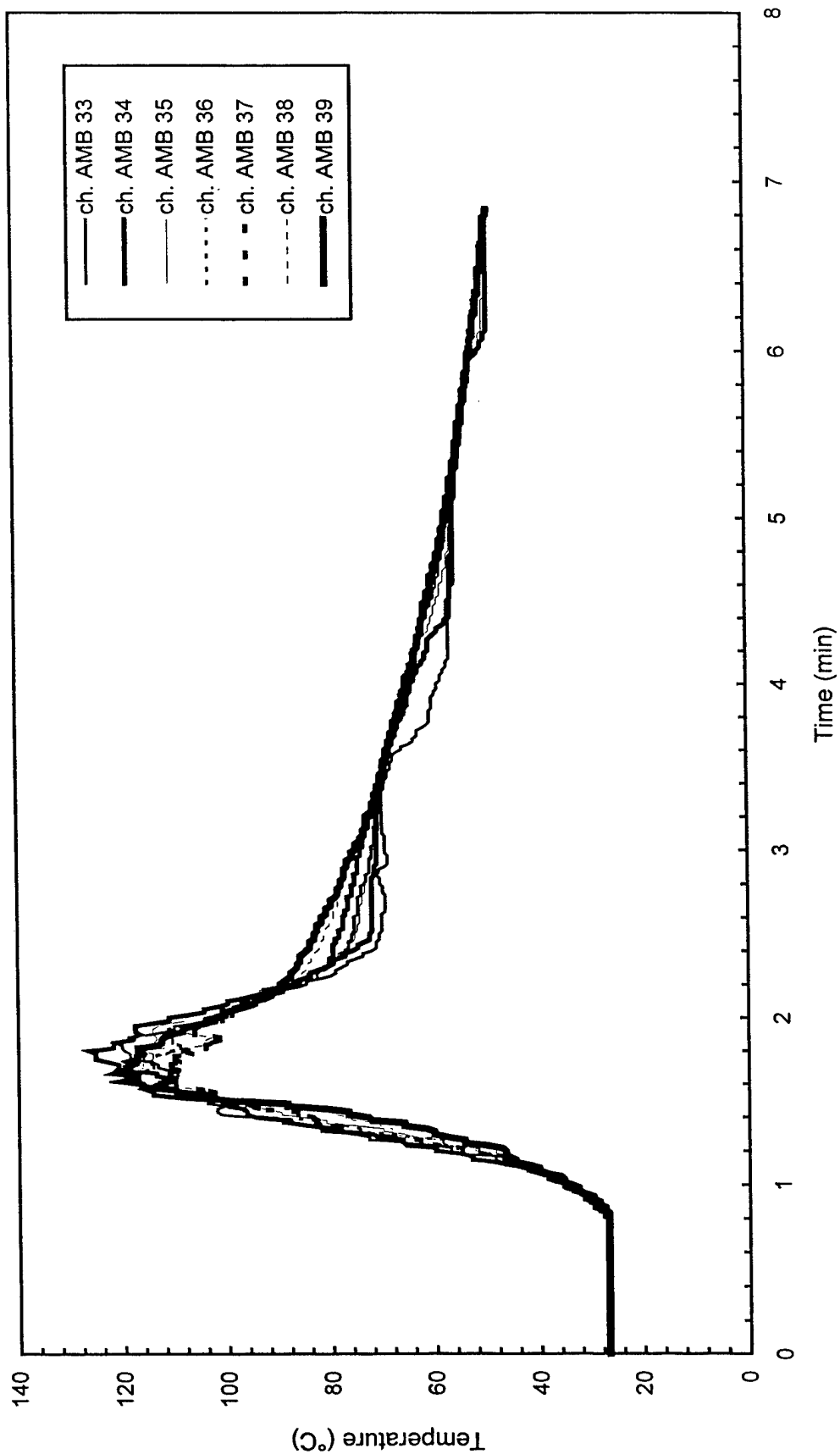


Fig. C84 - Air temperatures around South half of 7.6 m (25 ft) radius from center of pad

Test F6

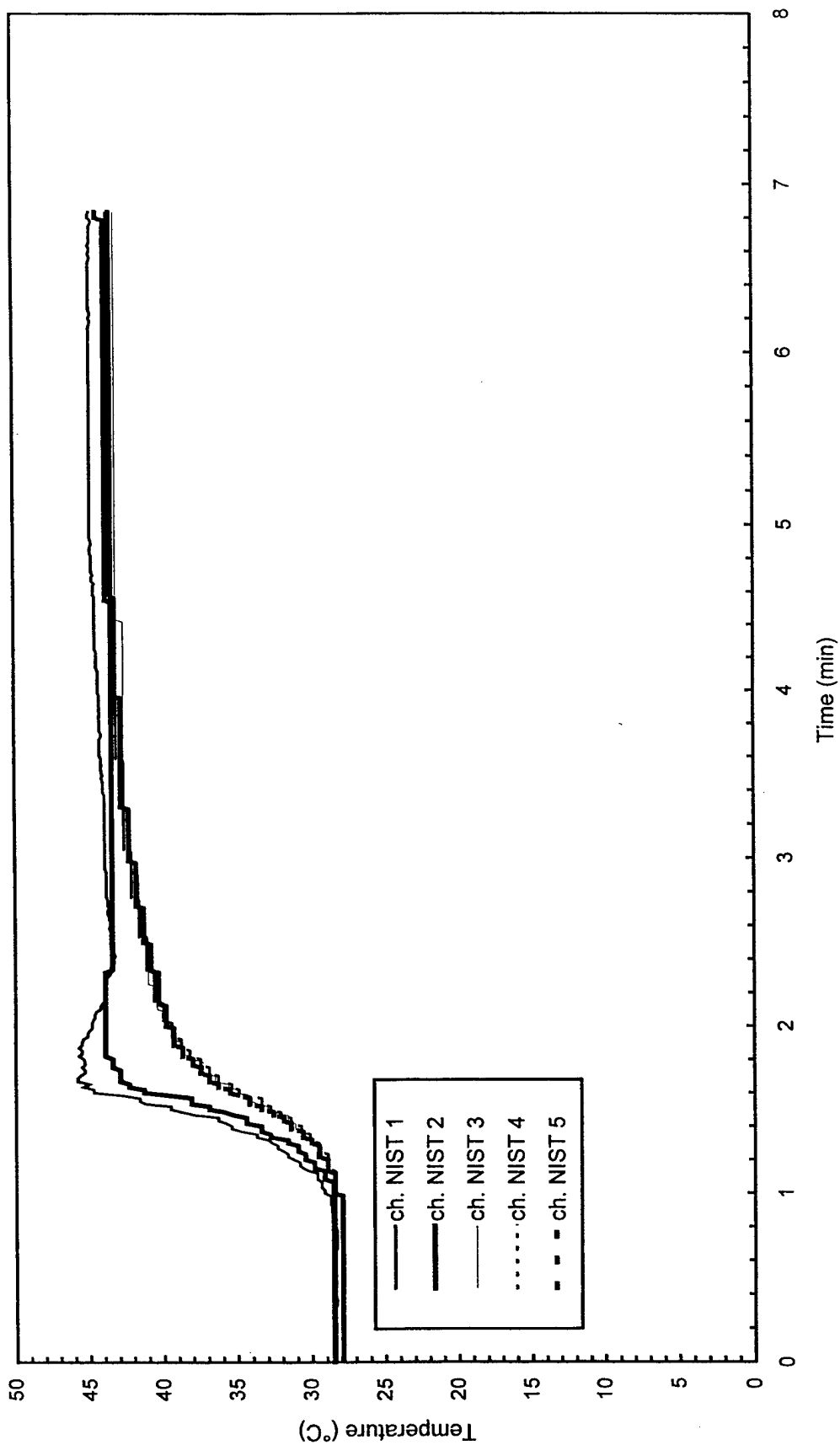


Fig. C85 - Temperature of West steel beam

Test F6

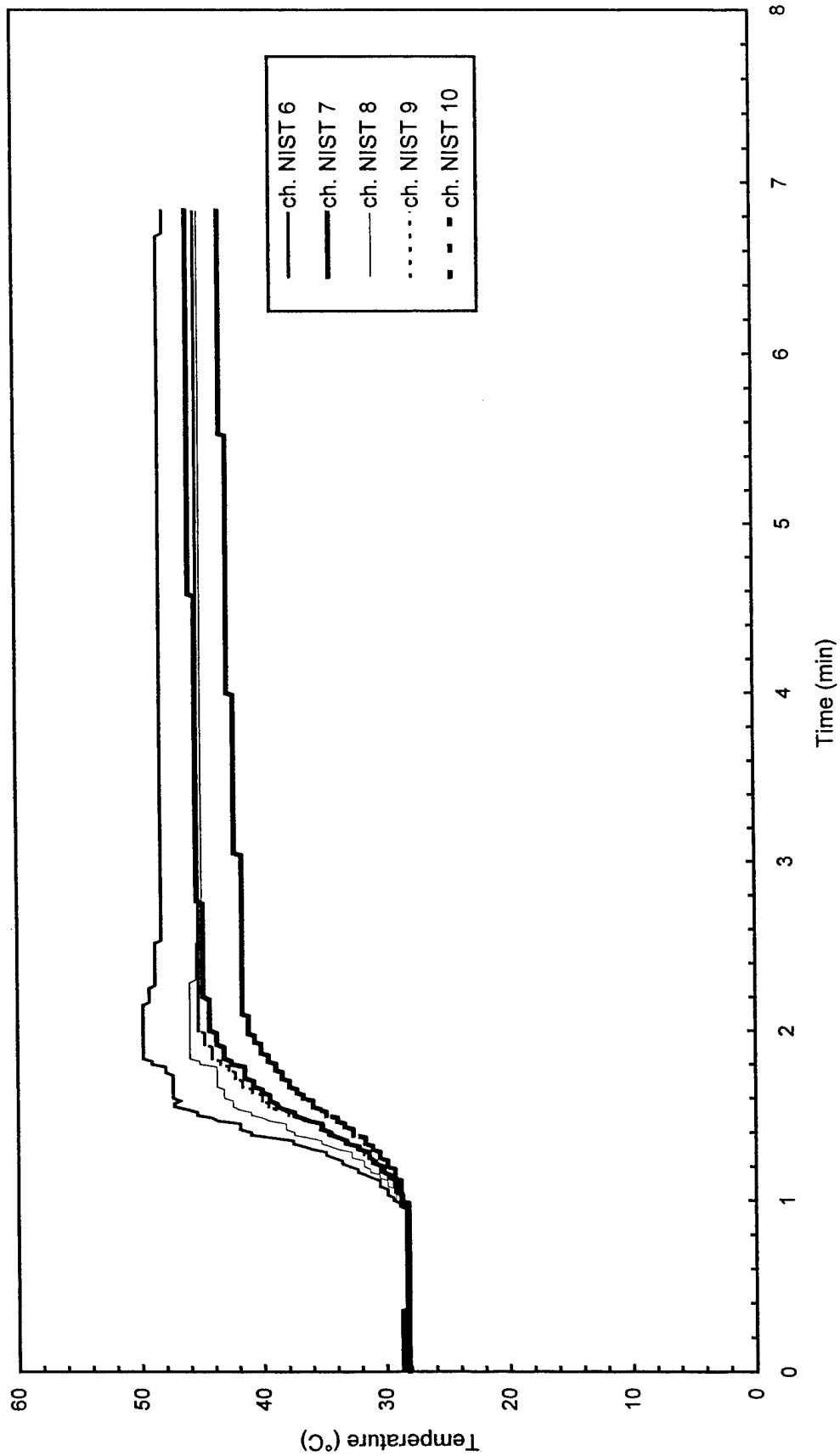


Fig. C86 - Temperature of North steel beam

Test F6

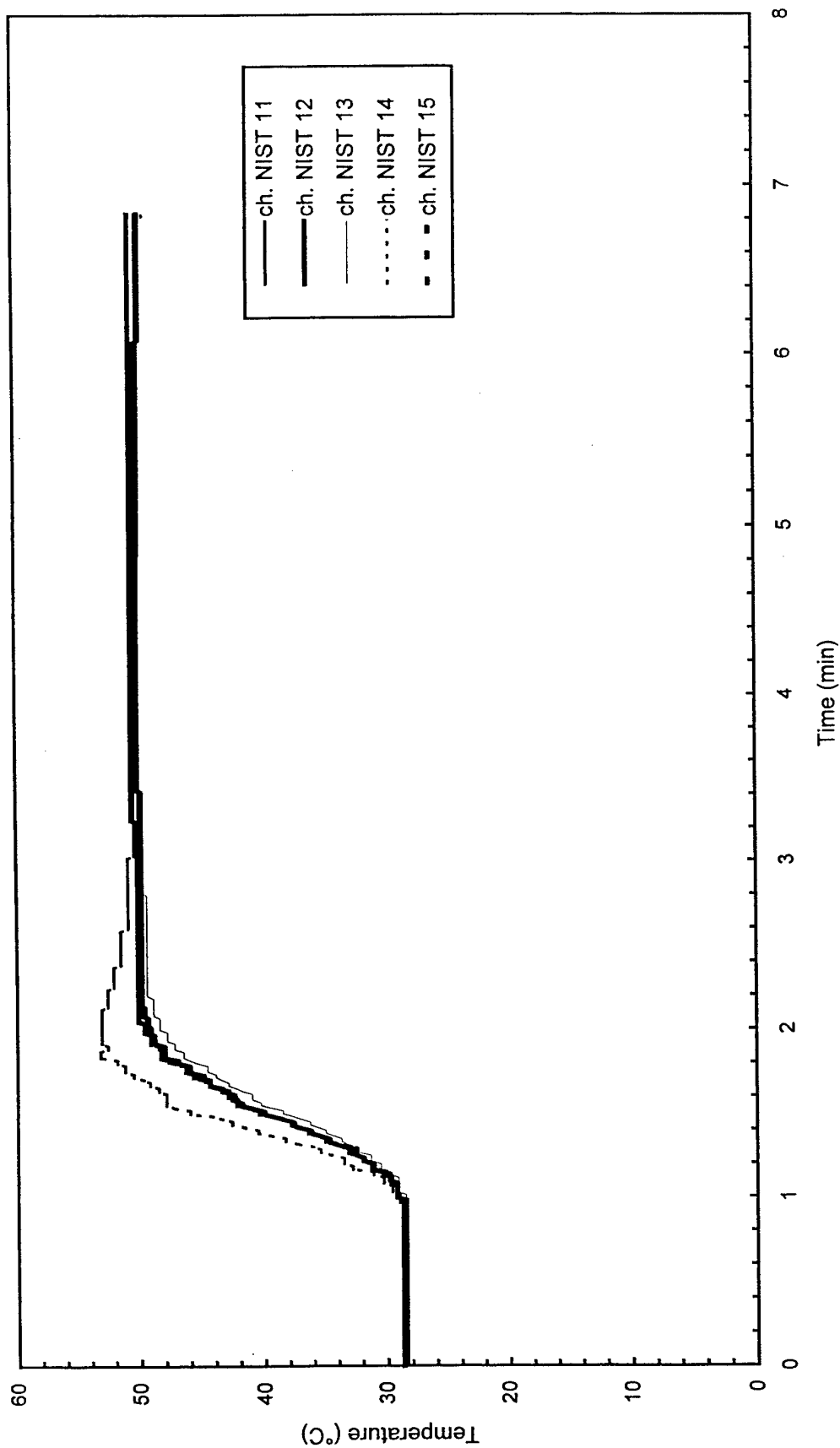


Fig. C87 - Temperature of East steel beam

Test F6

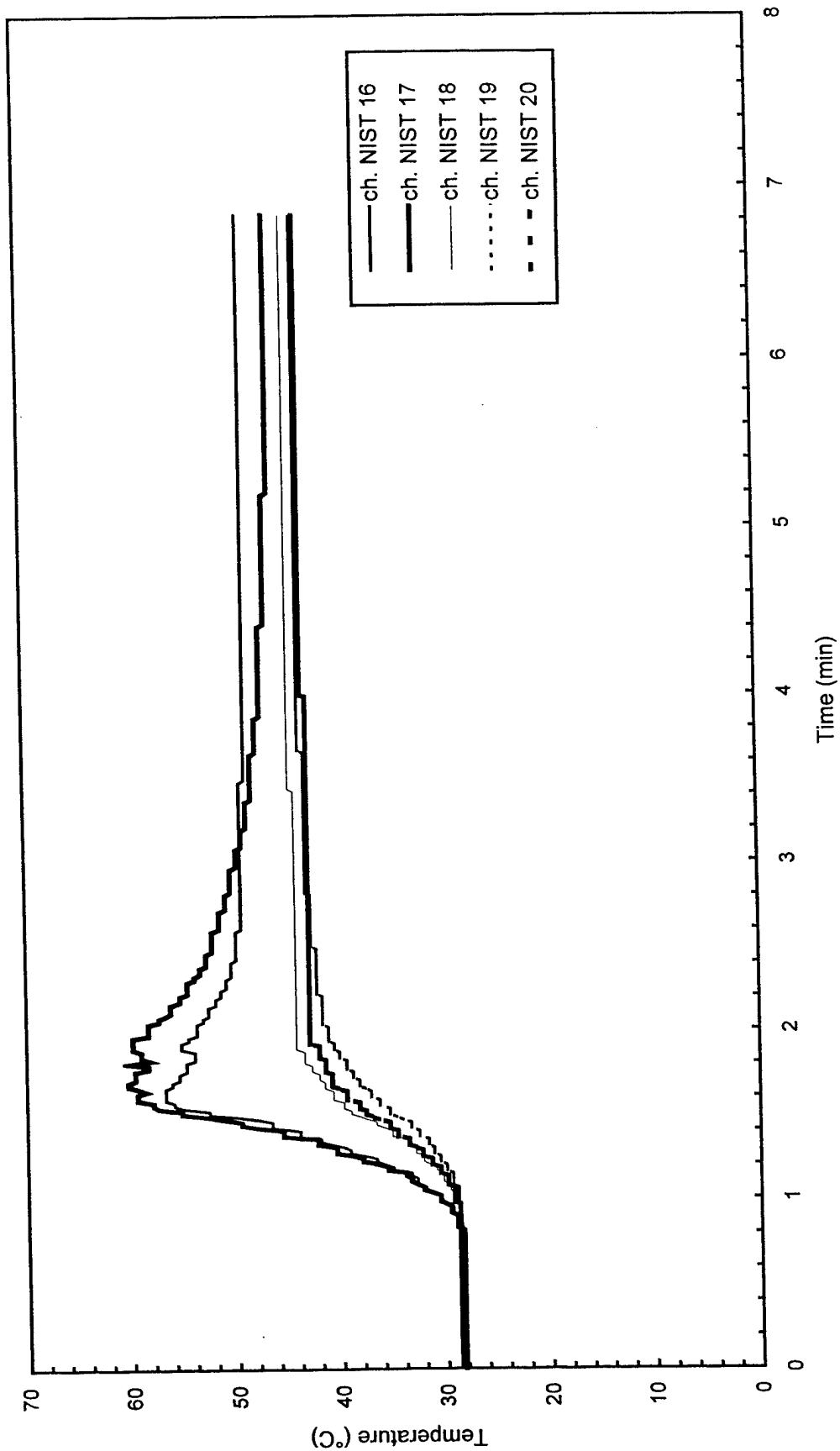


Fig. C88 - Temperature of South steel beam

Test F6

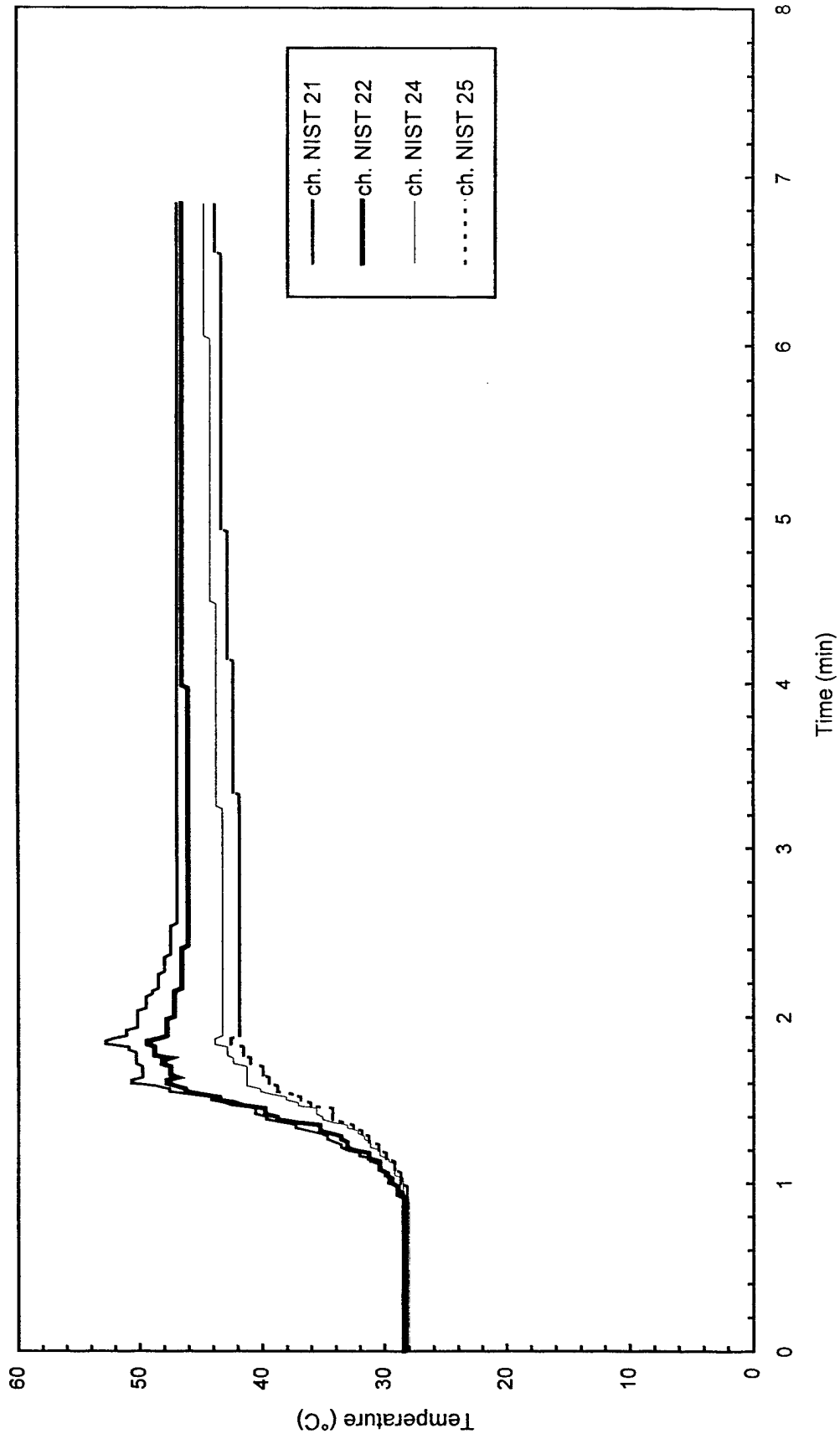


Fig. C89 - Temperature of Northwest steel beam

Test F6

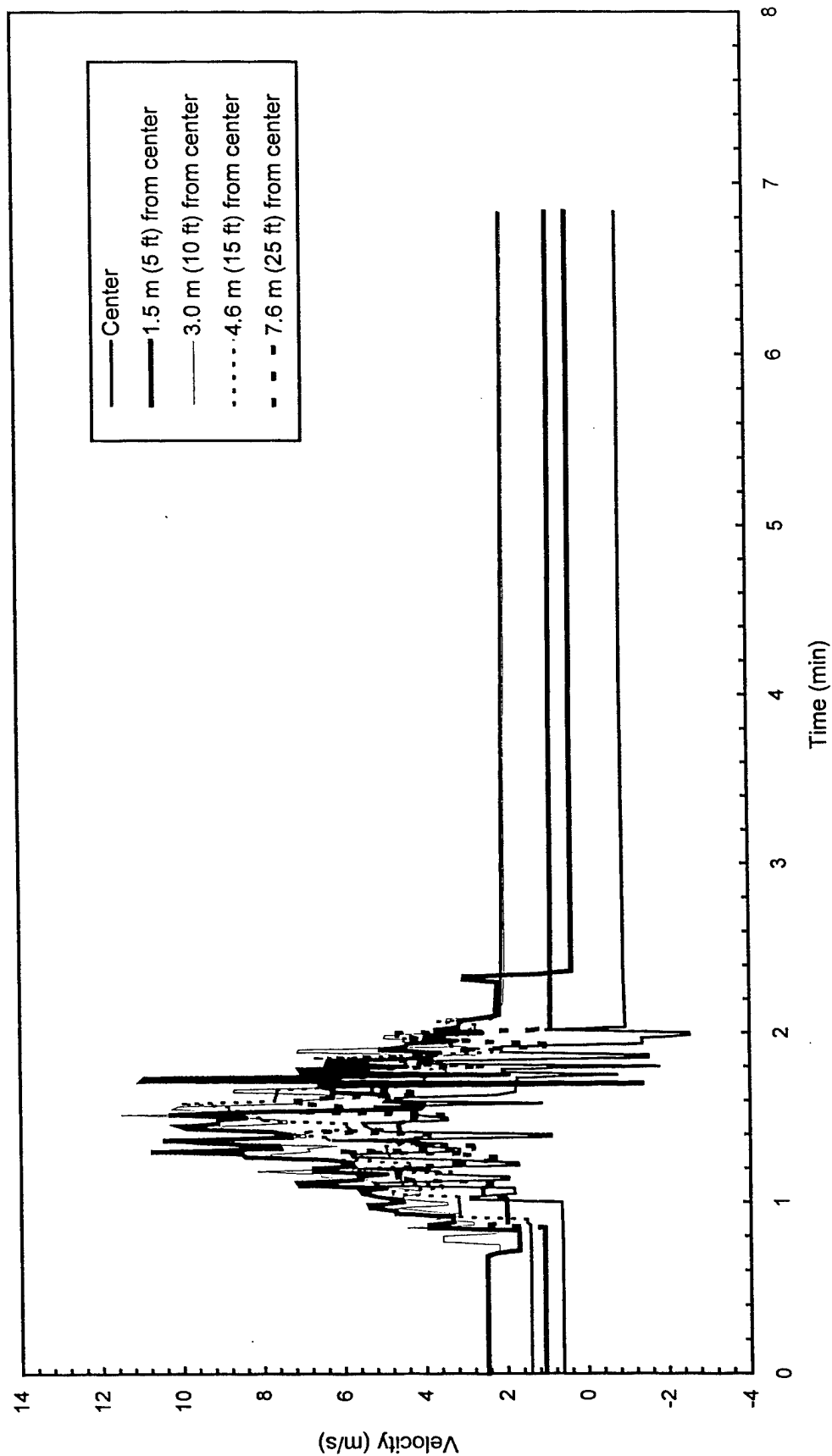


Fig. C90 - Plume and ceiling jet velocities

Test F7

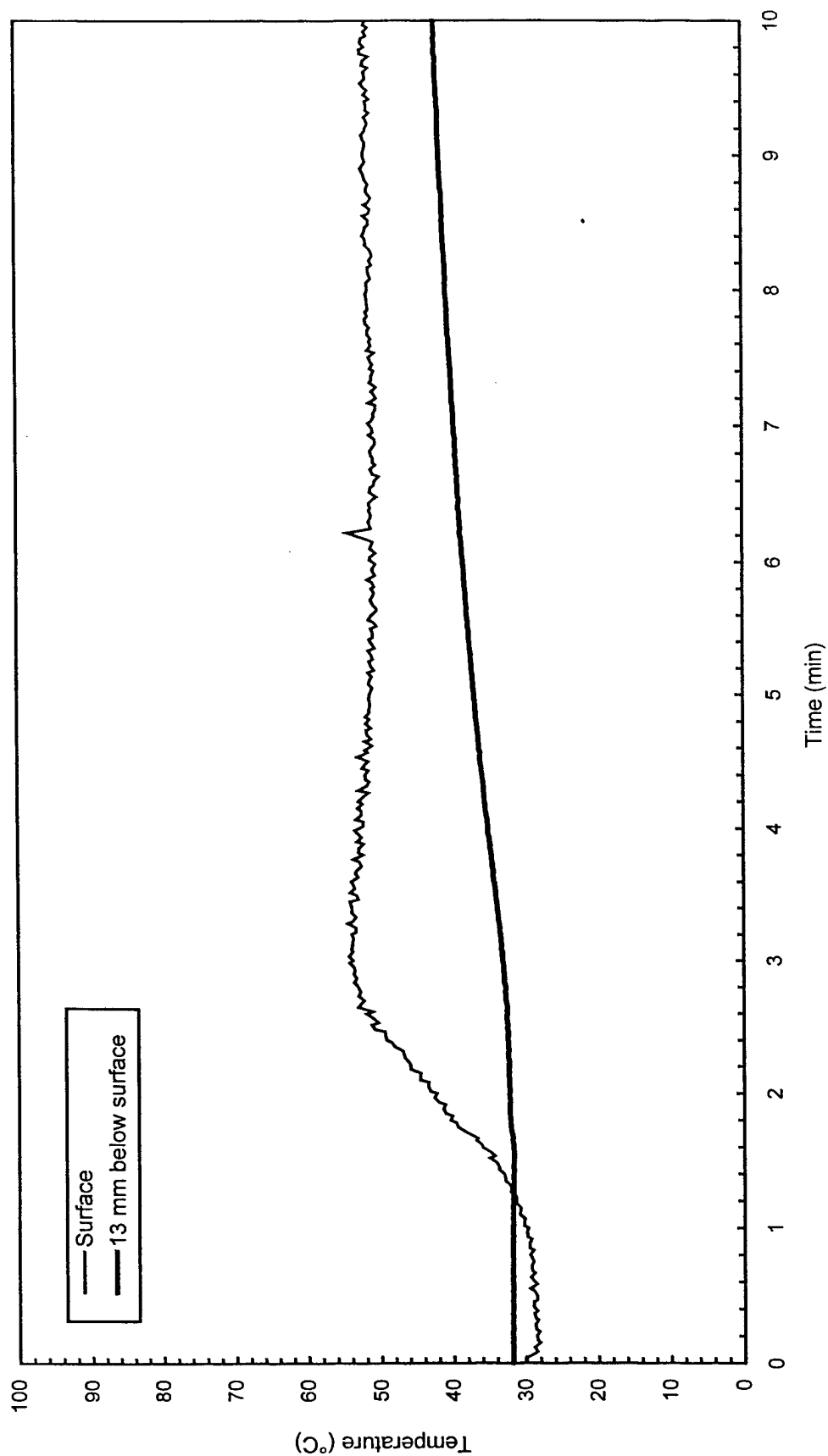


Fig. C91 - Concrete temperatures at center of pad

Test F7

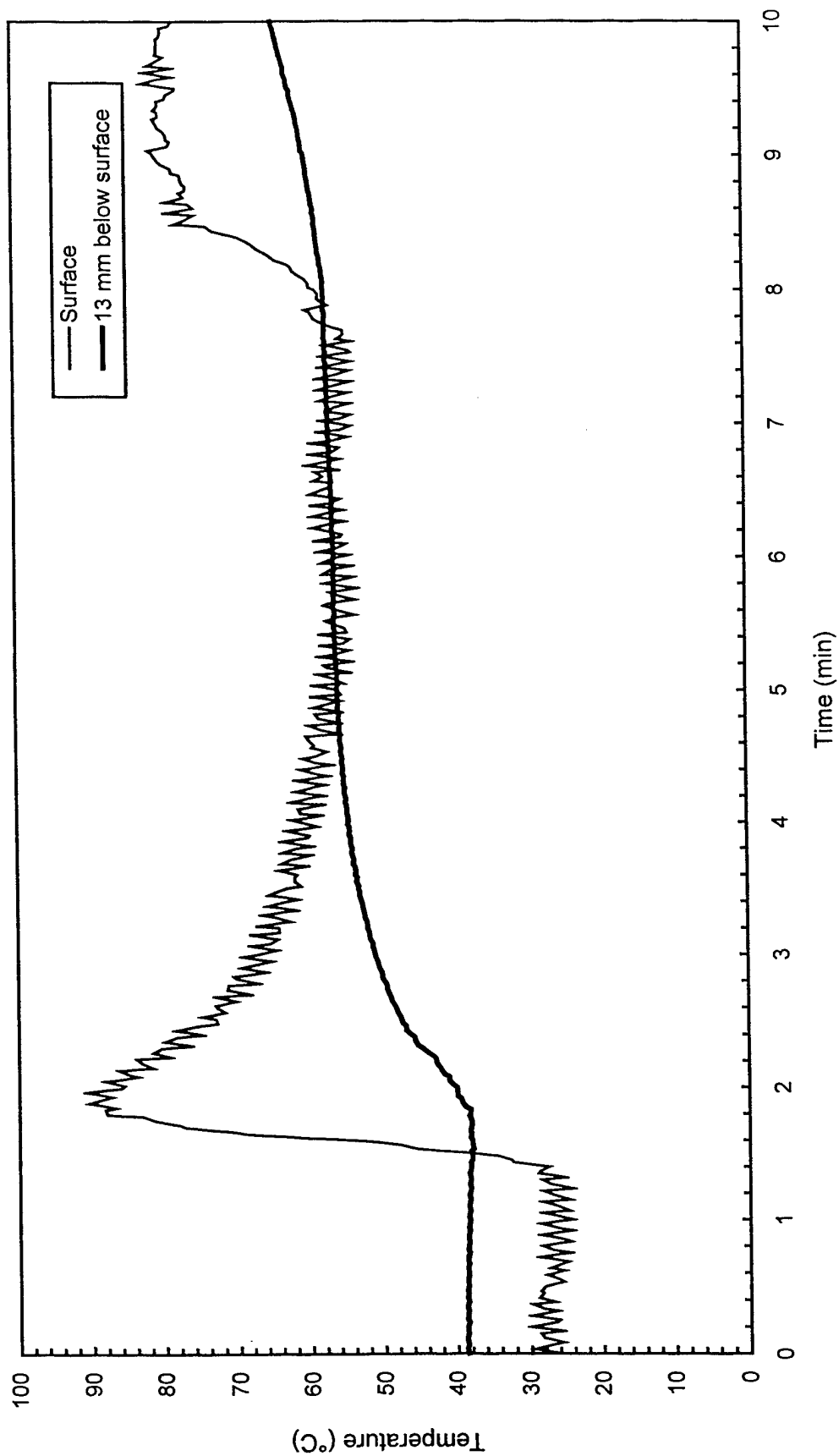


Fig. C92 - Concrete temperatures 3 m (10 ft) East of center of pad

Test F7

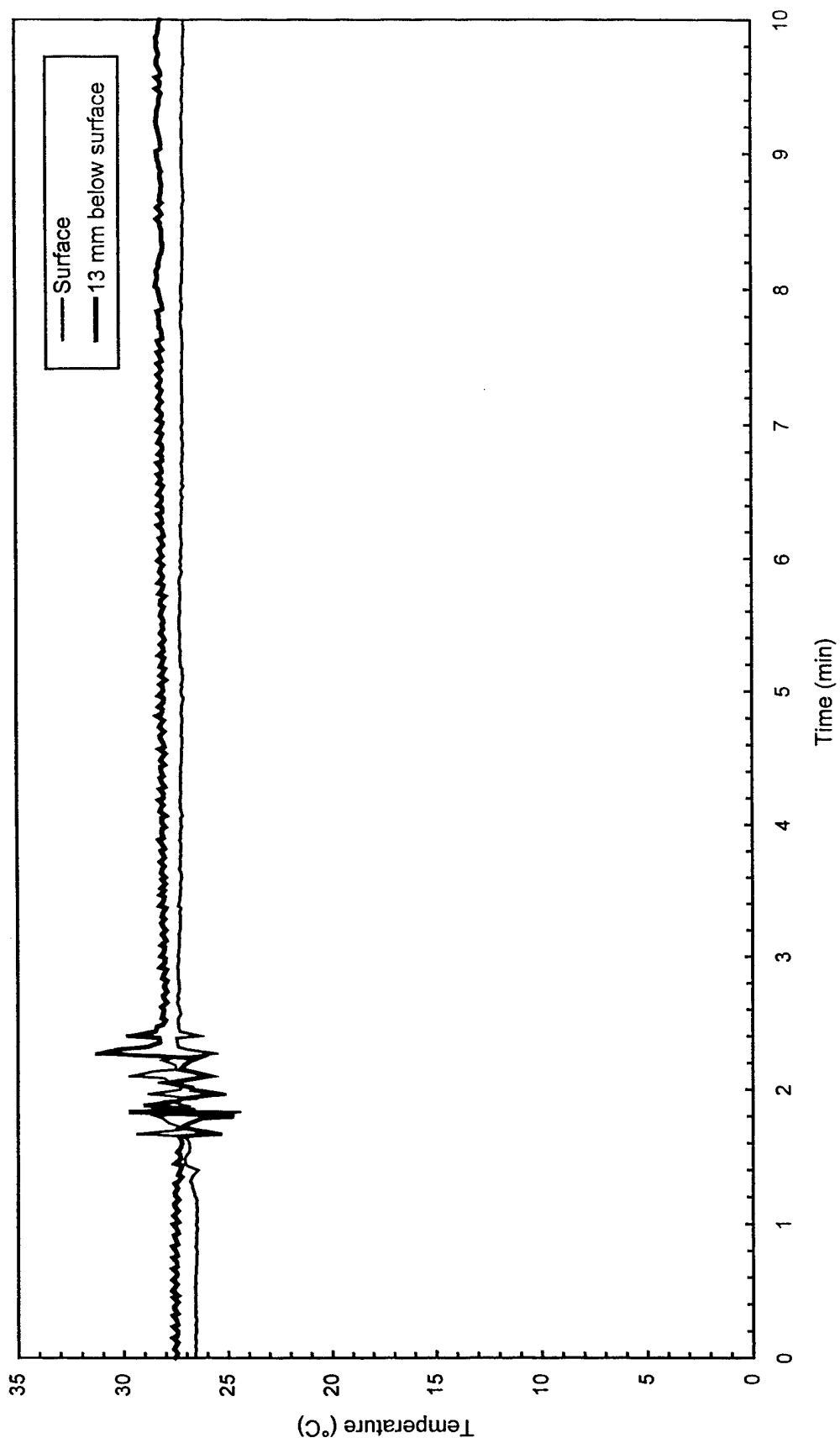


Fig. C93 - Concrete temperatures 3 m (10 ft) West of center of pad

Test F7

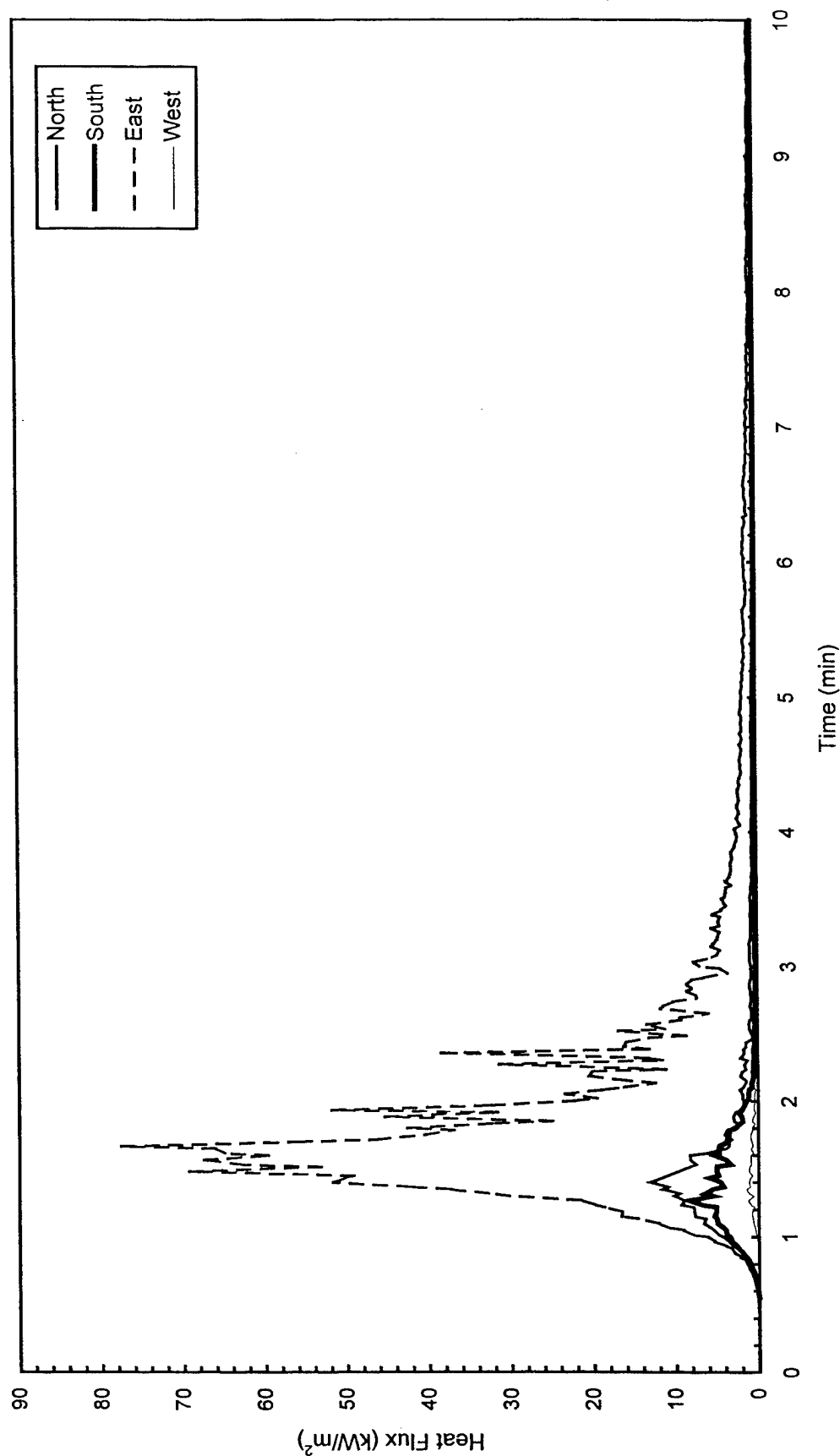


Fig. C94 - Heat flux measured at edge of pad

Test F7

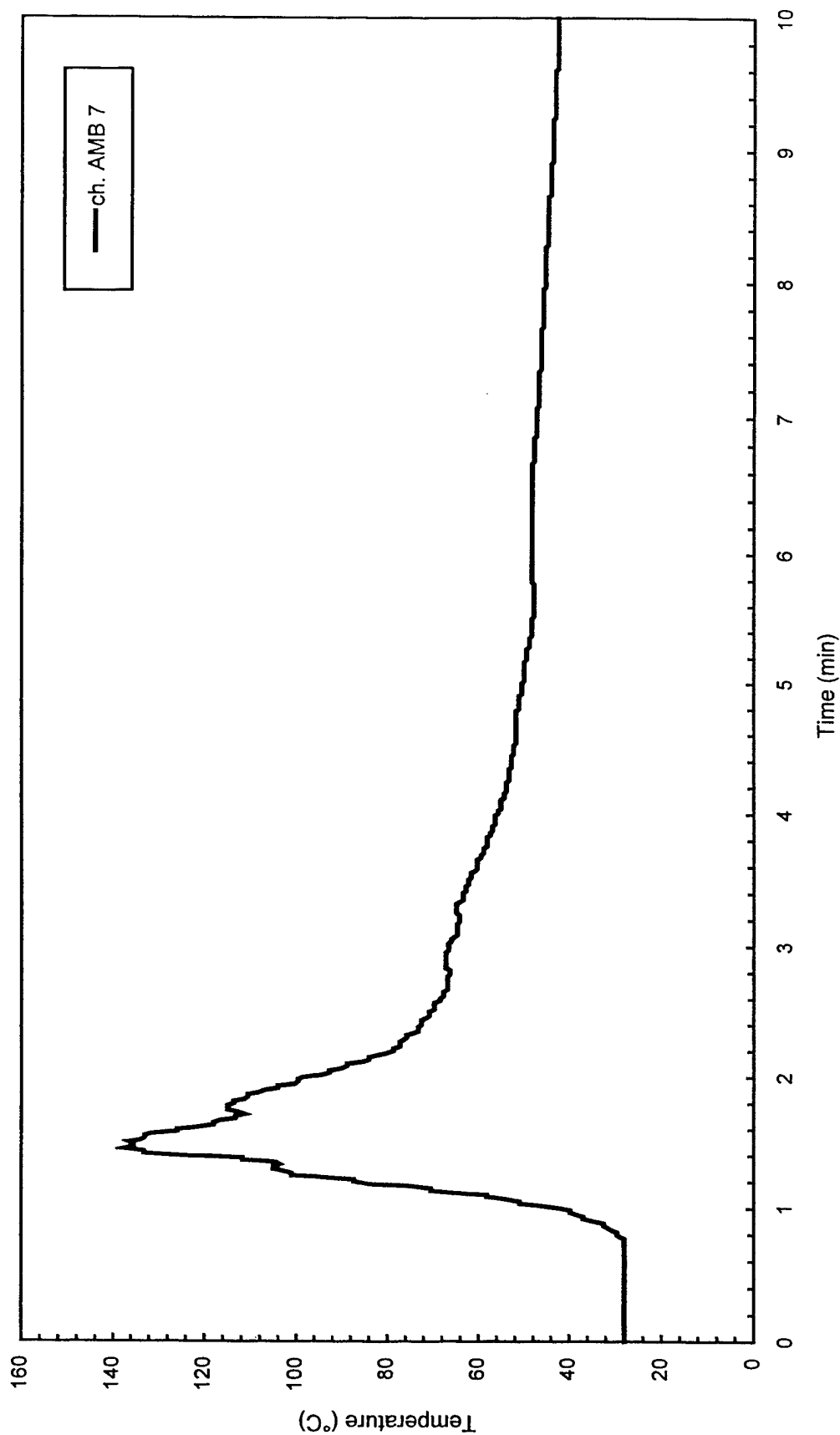


Fig. C95 - Air temperatures over center of pad

Test F7

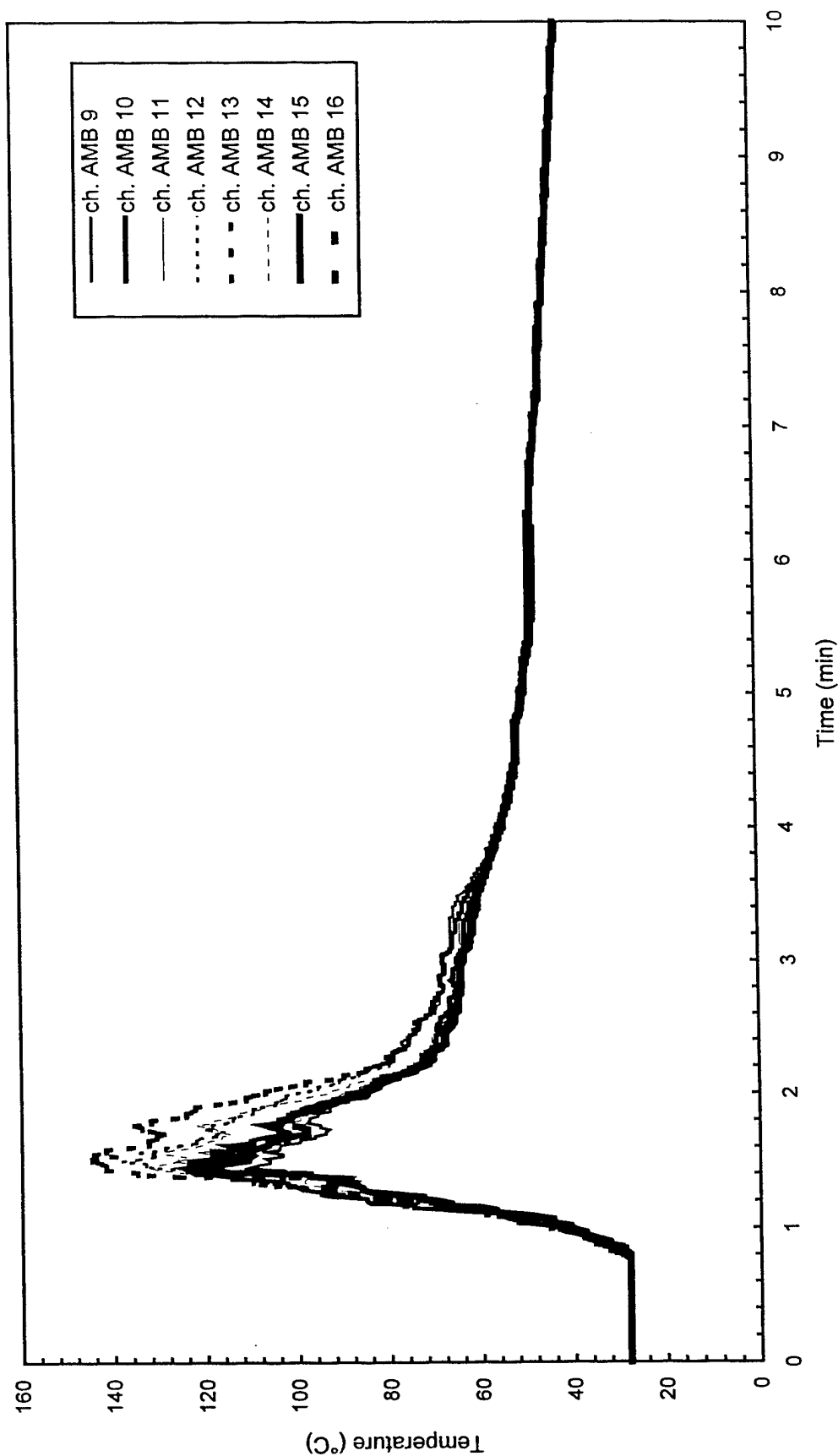


Fig. C96 - Air temperatures around 3 m (10 ft) radius from center of pad

Test F7

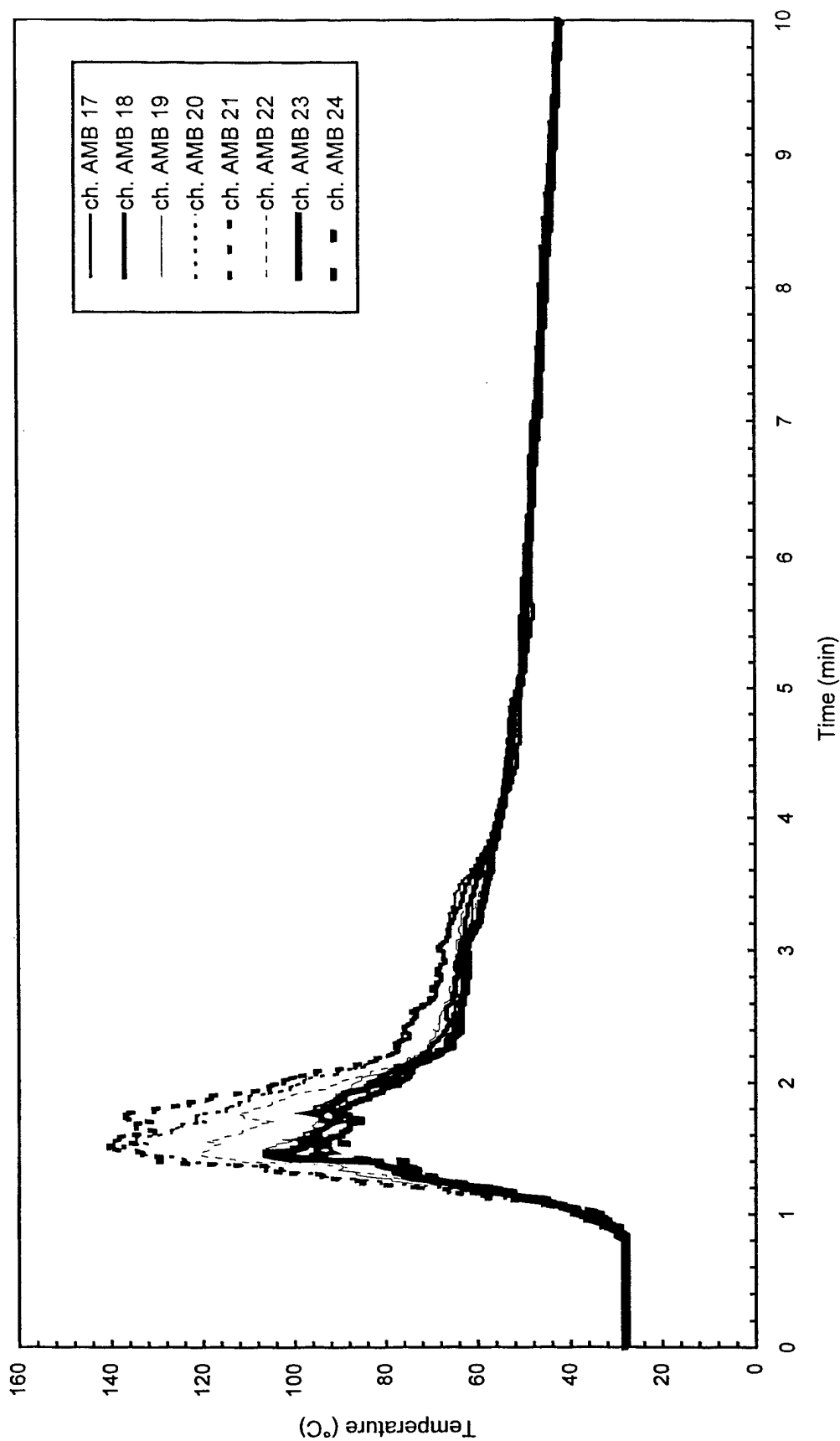


Fig. C97 - Air temperatures around 4.6 m (15 ft) radius from center of pad

Test F7

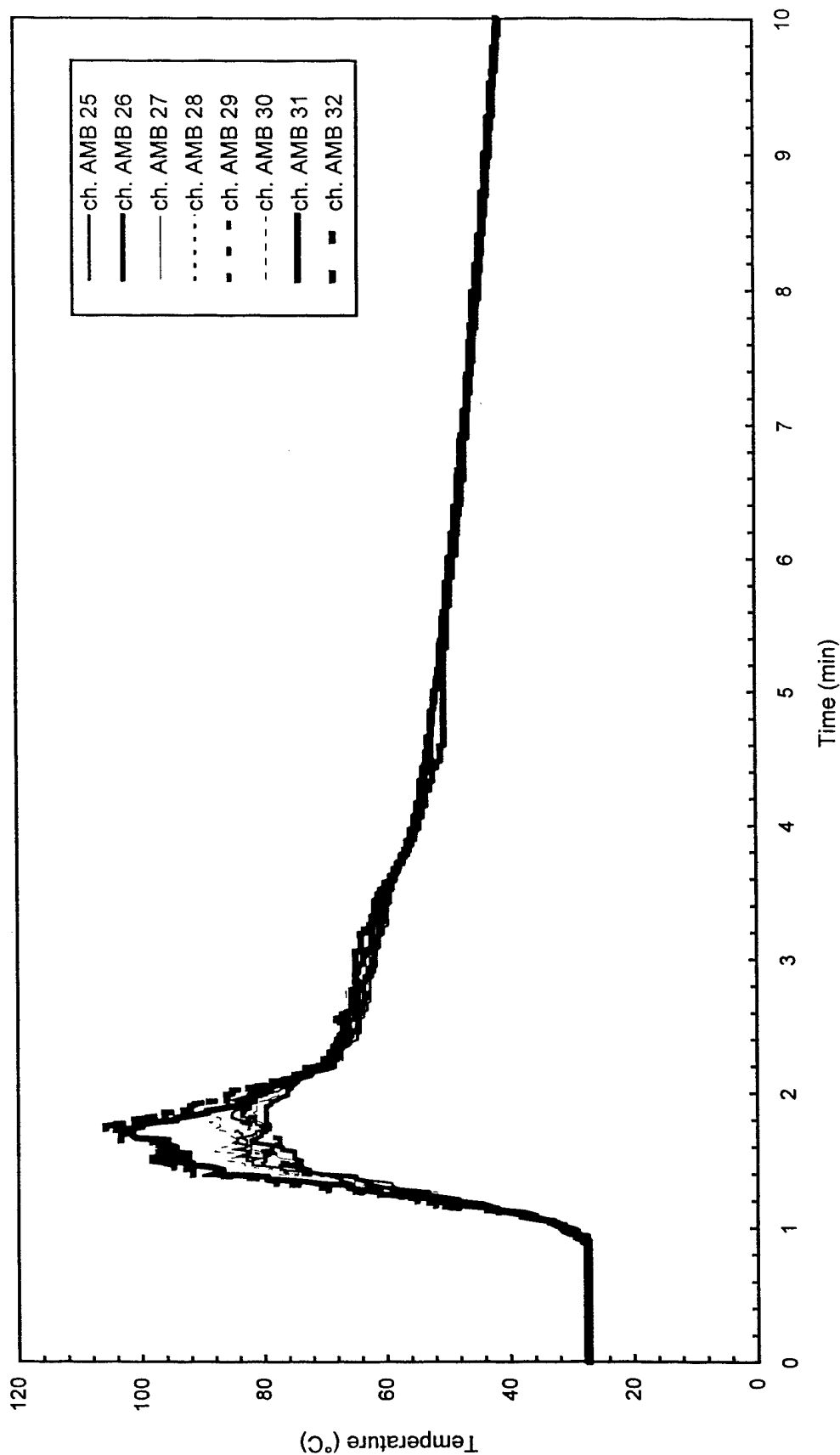


Fig. C98 - Air temperatures around North half of 7.6 m (25 ft) radius from center of pad

Test F7

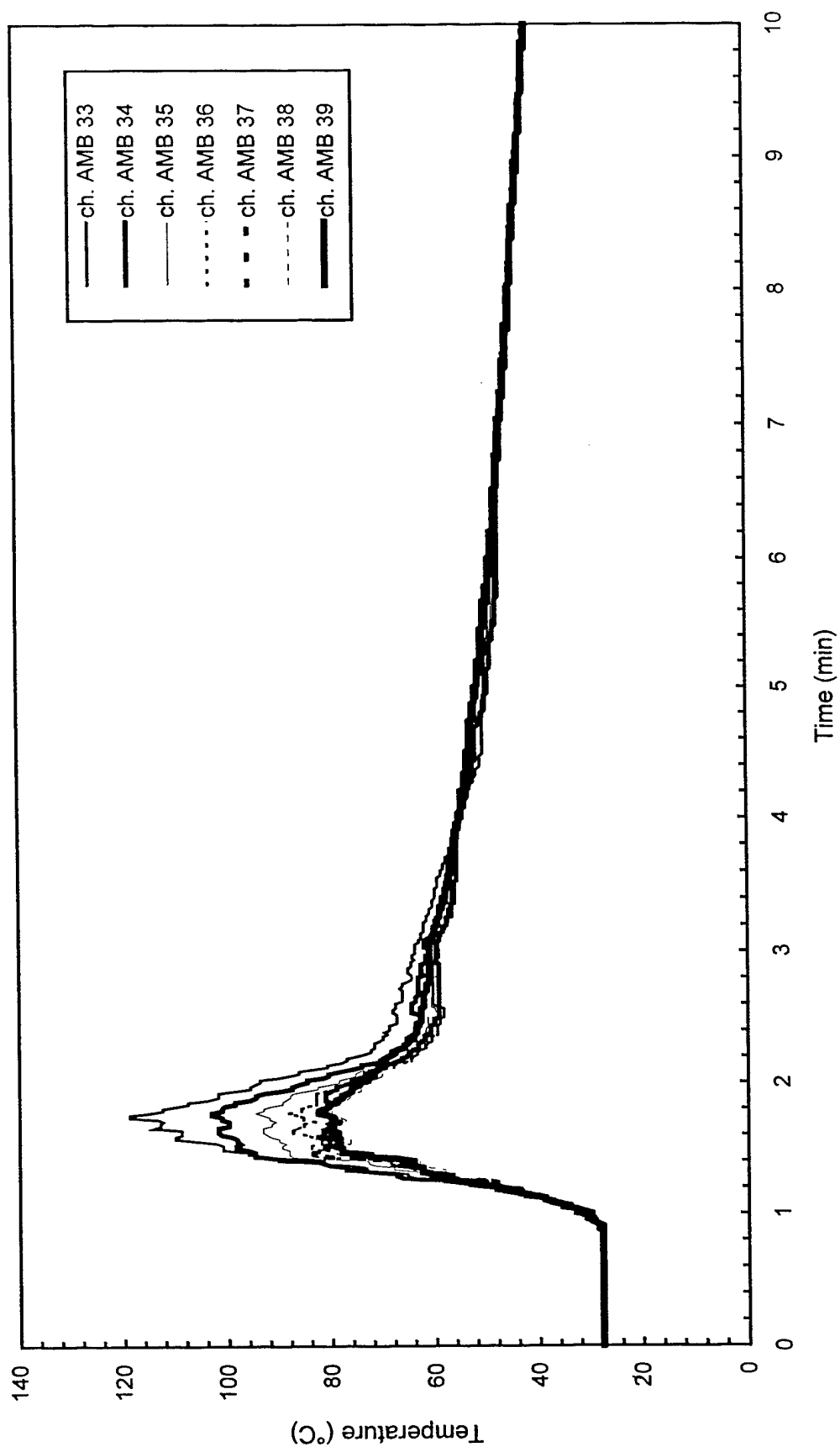


Fig. C99 - Air temperatures around South half of 7.6 m (25 ft) radius from center of pad

Test F7

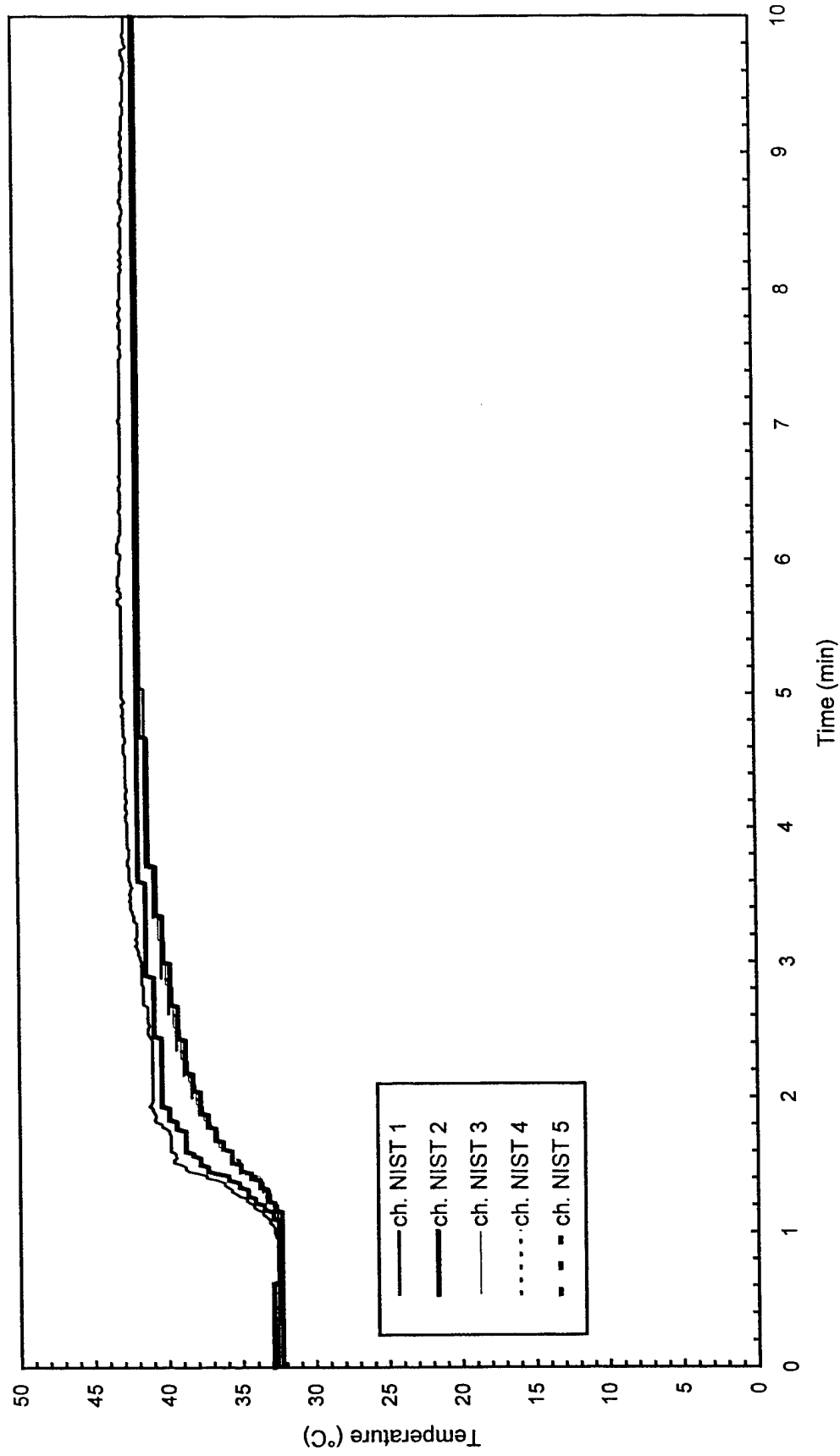


Fig. C100 - Temperature of West steel beam

Test F7

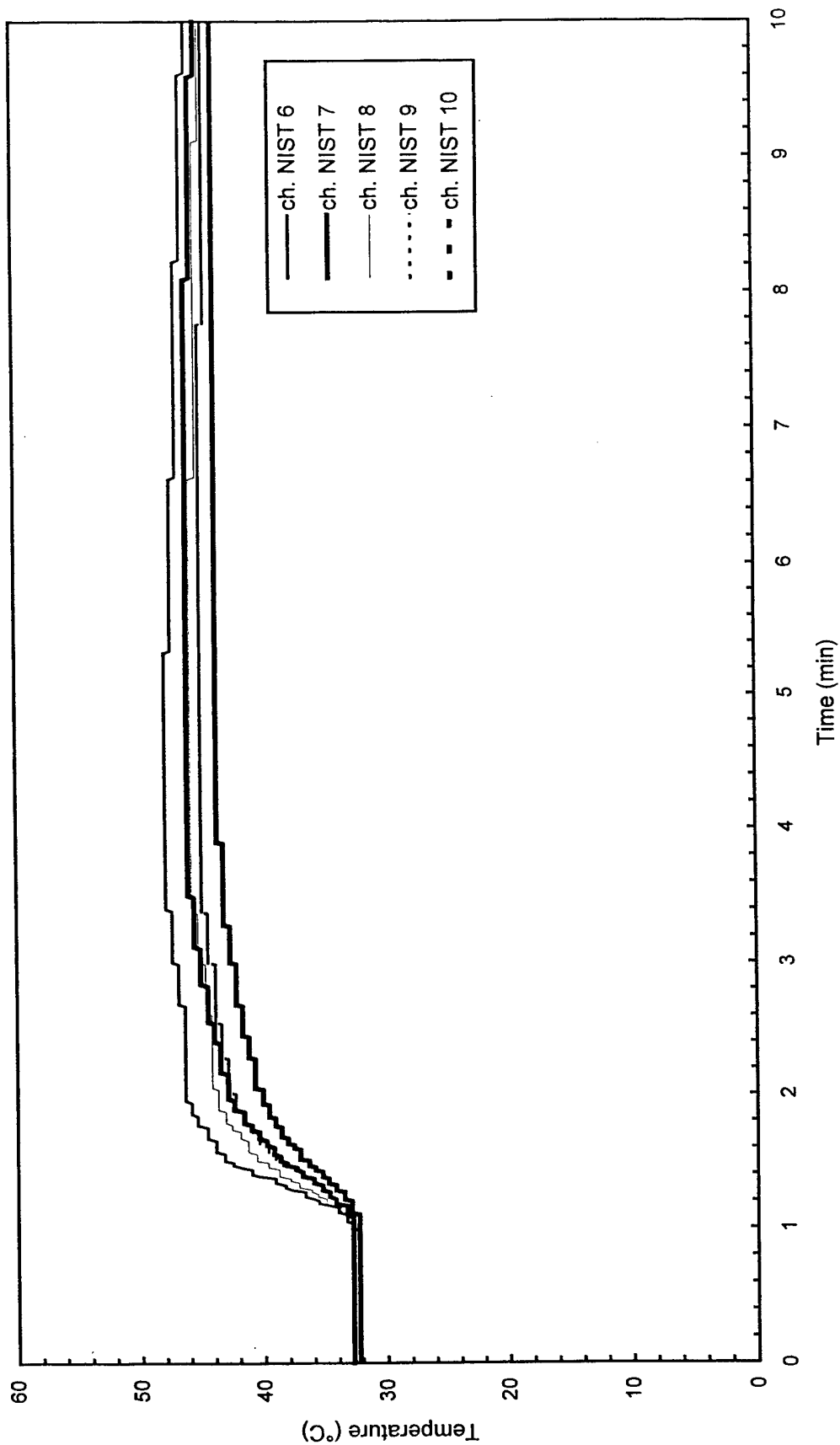


Fig. C101 - Temperature of North steel beam

Test F7

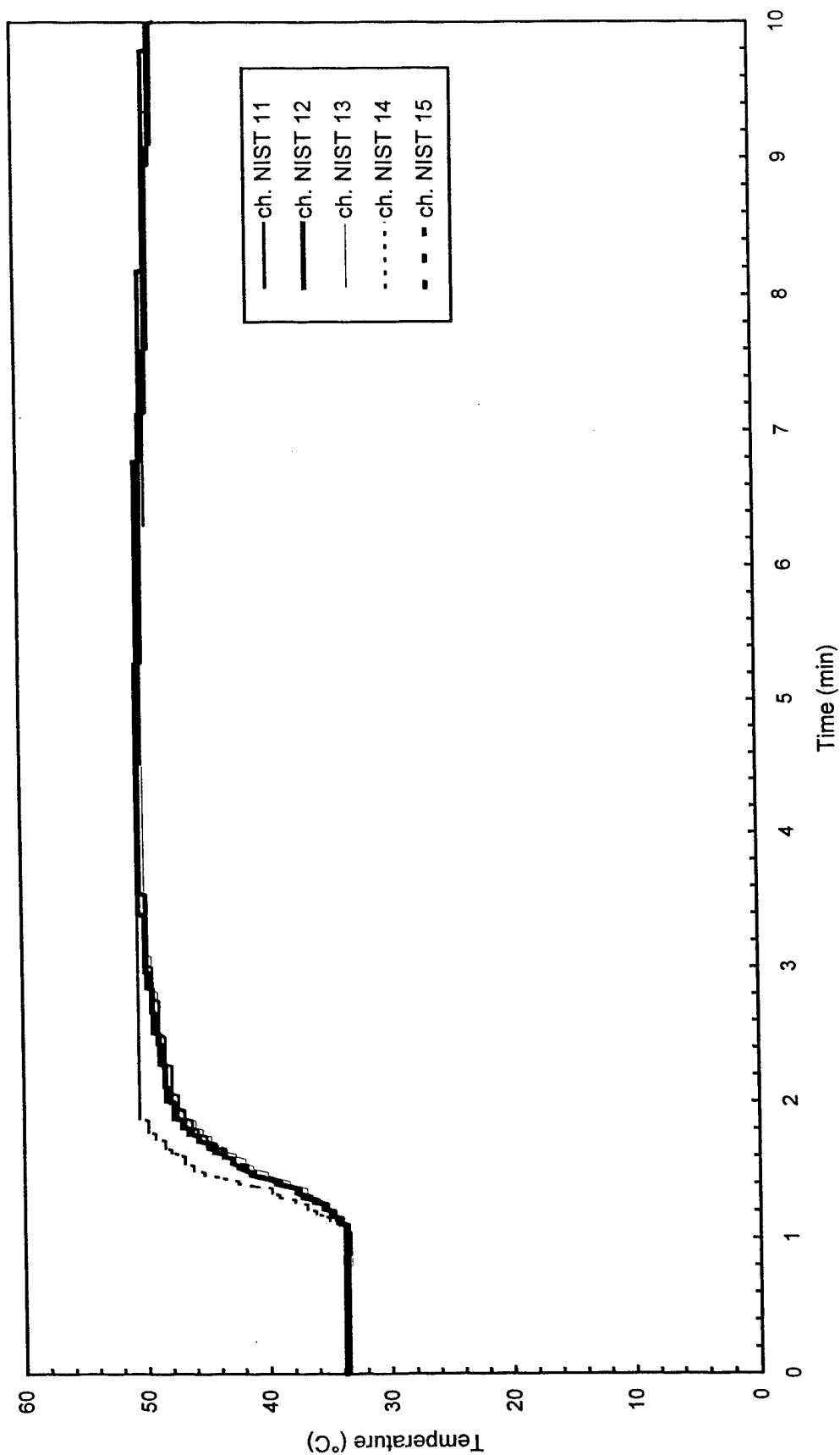


Fig. C102 - Temperature of East steel beam

Test F7

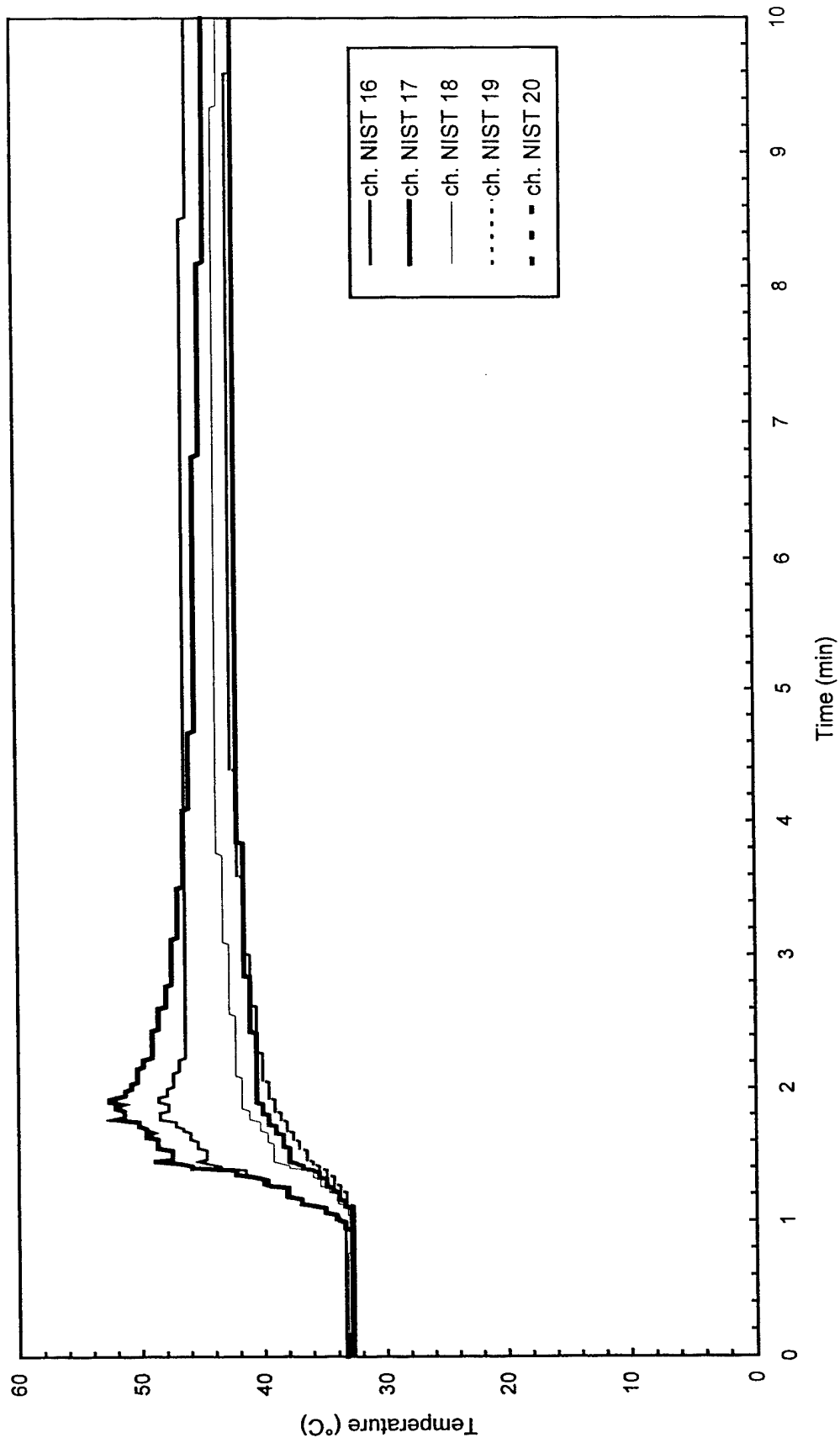


Fig. C103 - Temperature of South steel beam

Test F7

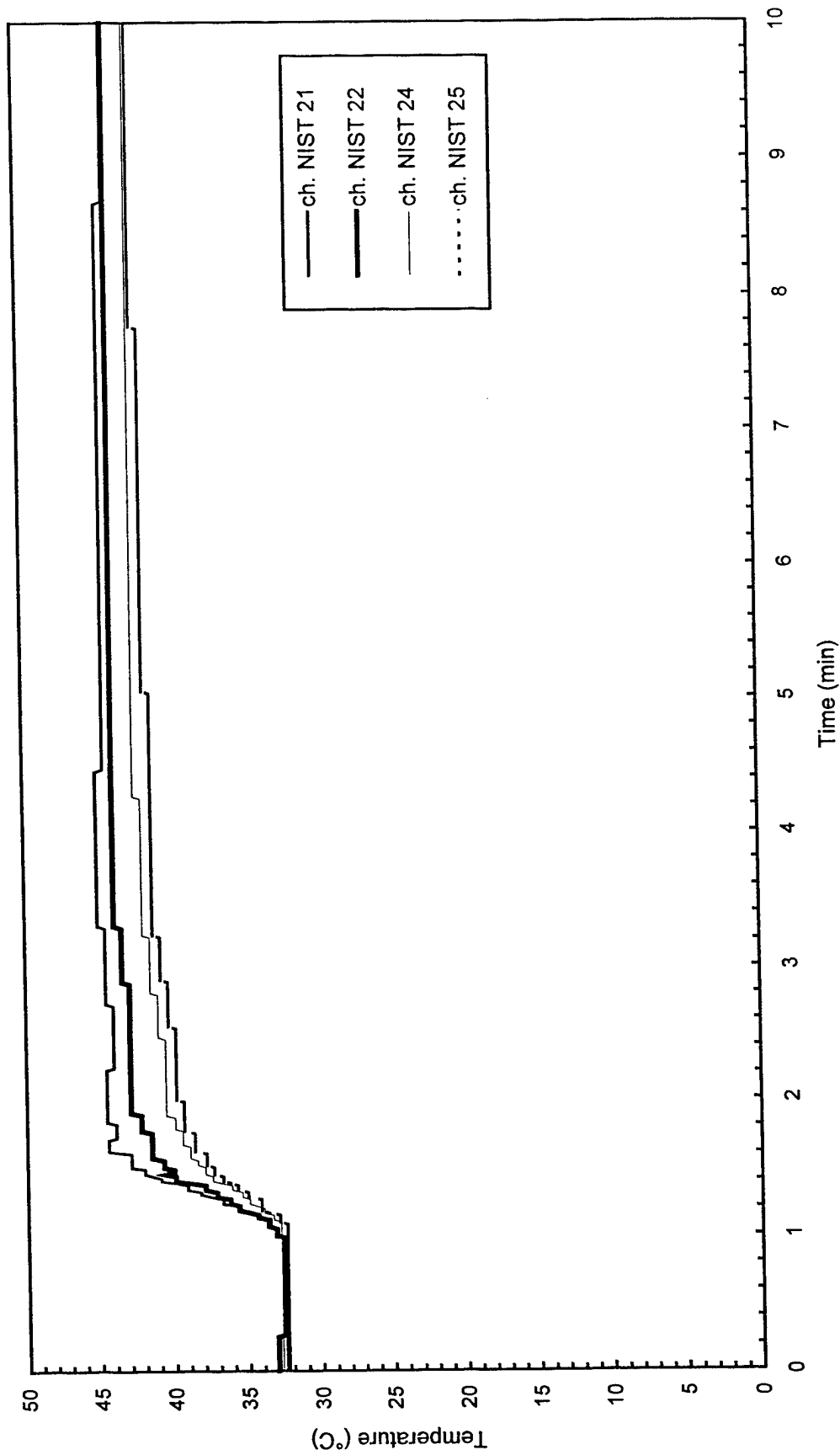


Fig. C104 - Temperature of Northwest steel beam

Test F7

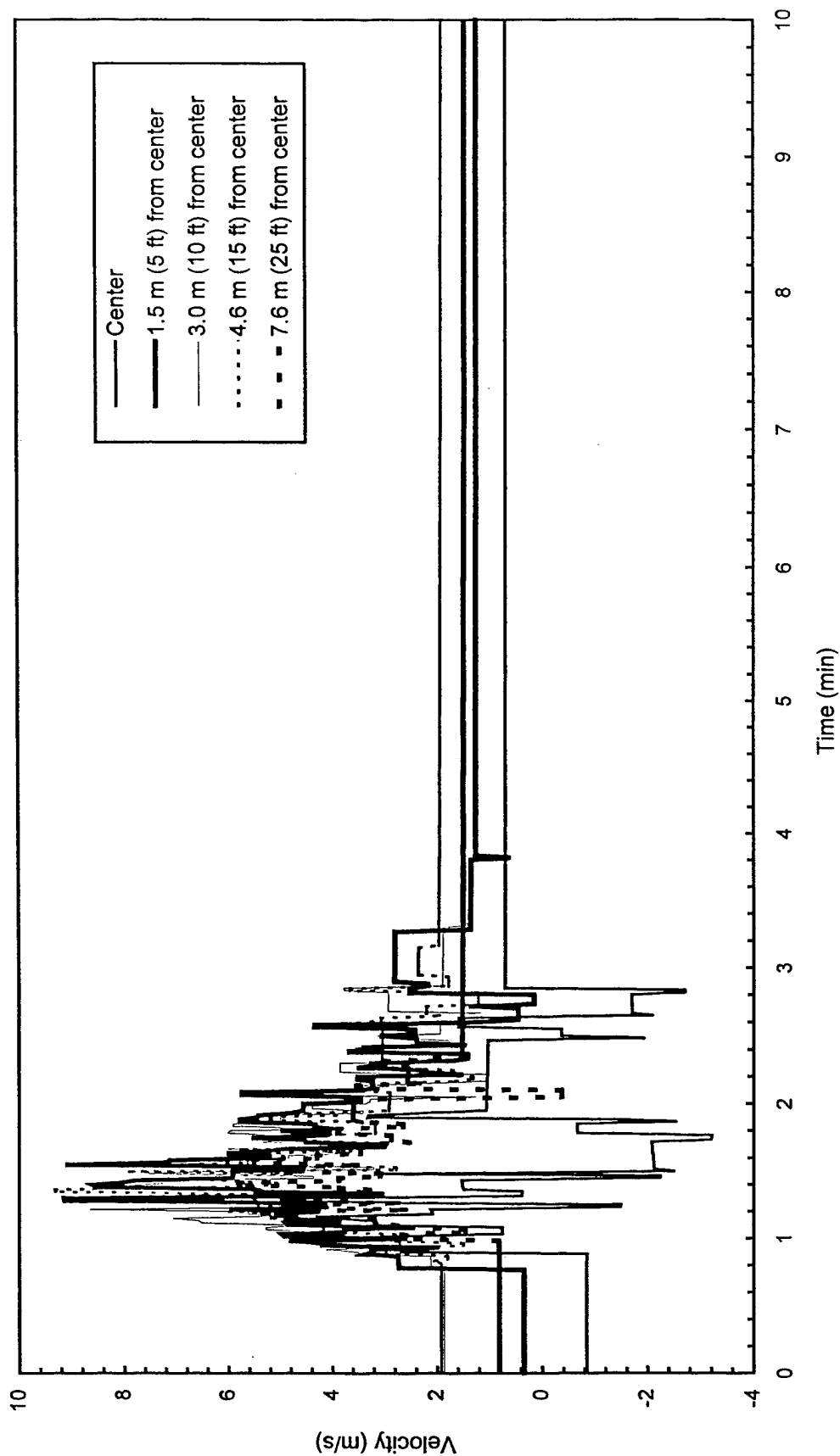


Fig. C105 - Plume and ceiling jet velocities

Test F8

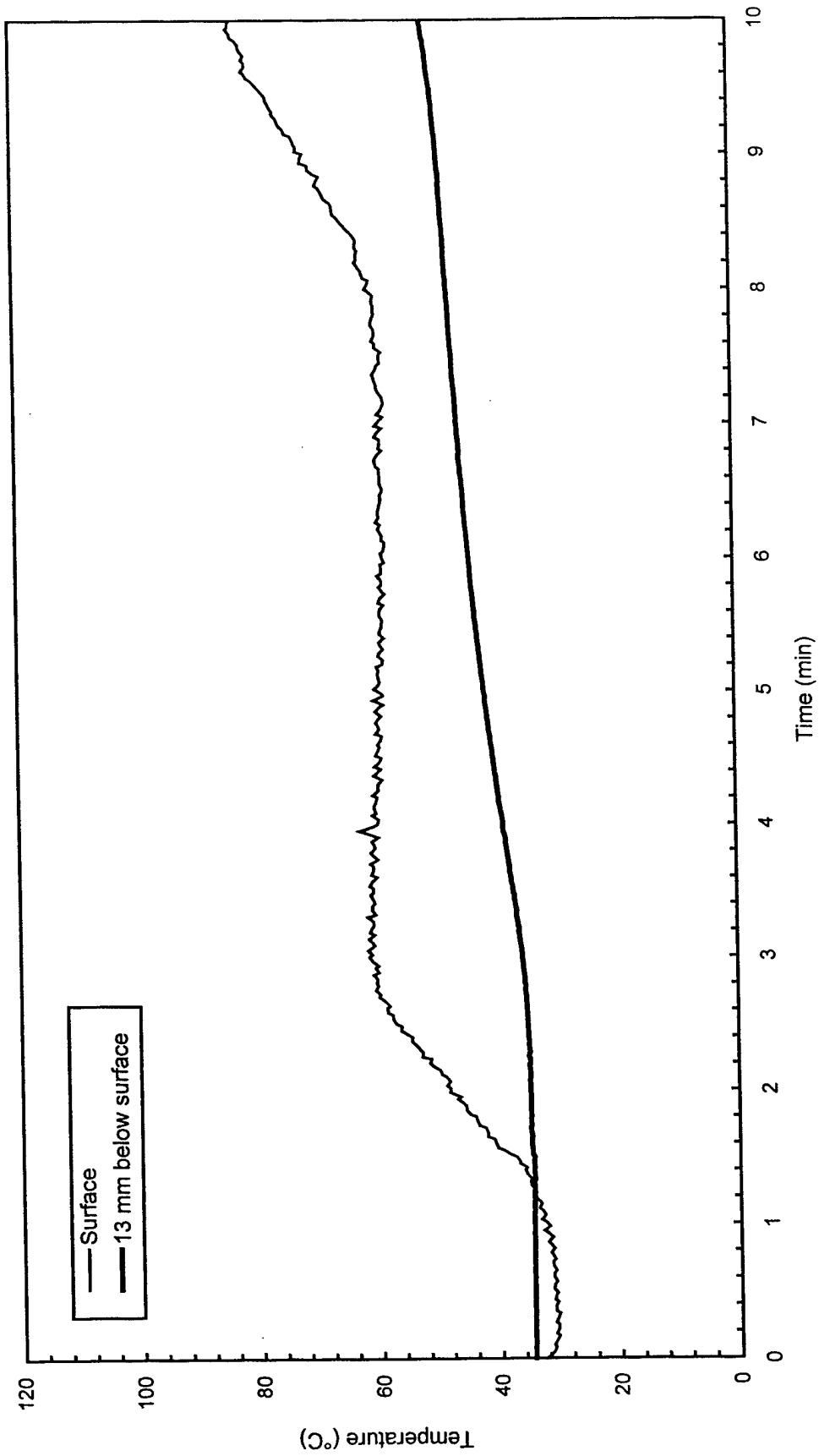


Fig. C106 - Concrete temperatures at center of pad

Test F8

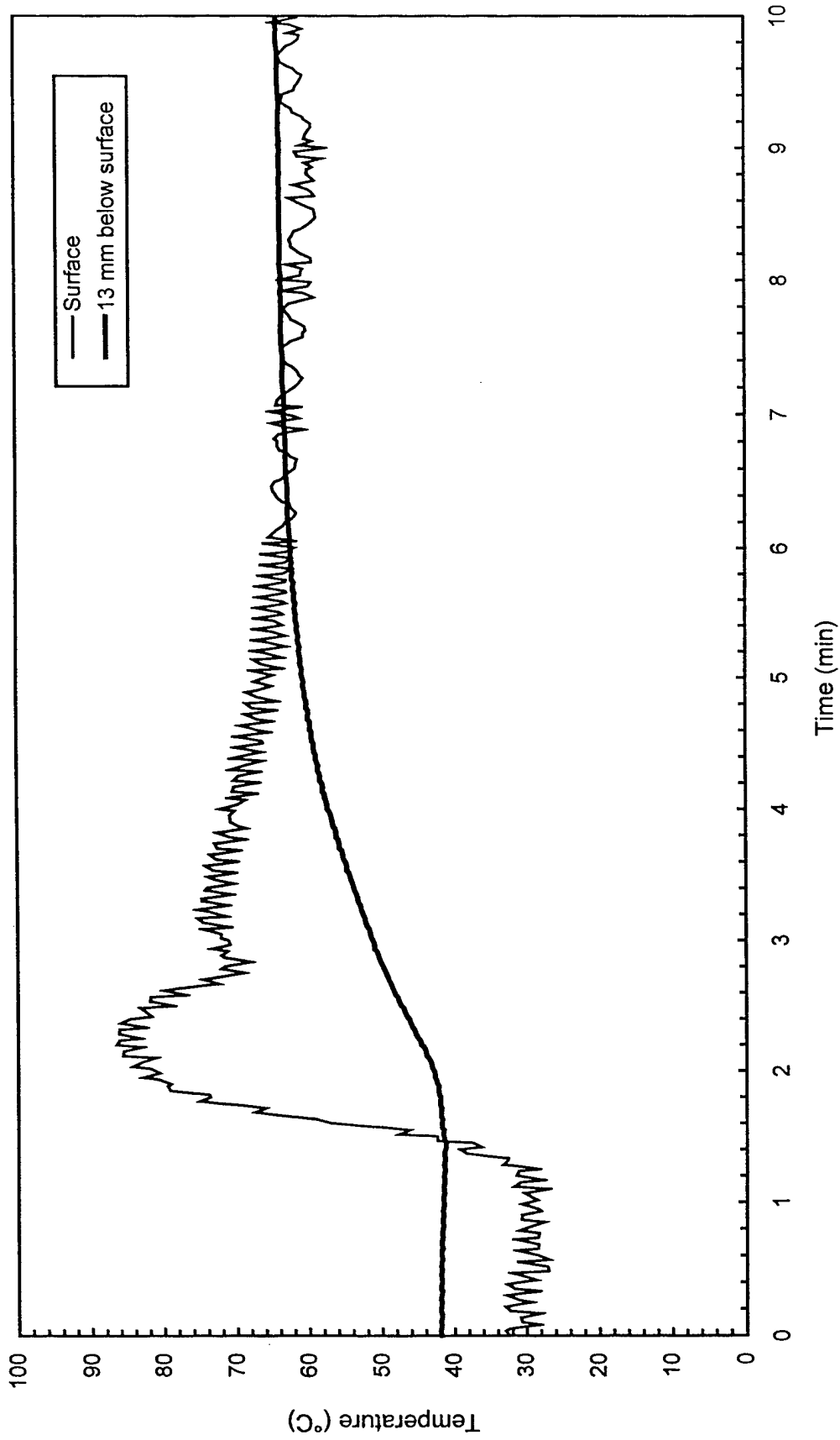


Fig. C107 - Concrete temperatures 3 m (10 ft) East of center of pad

Test F8

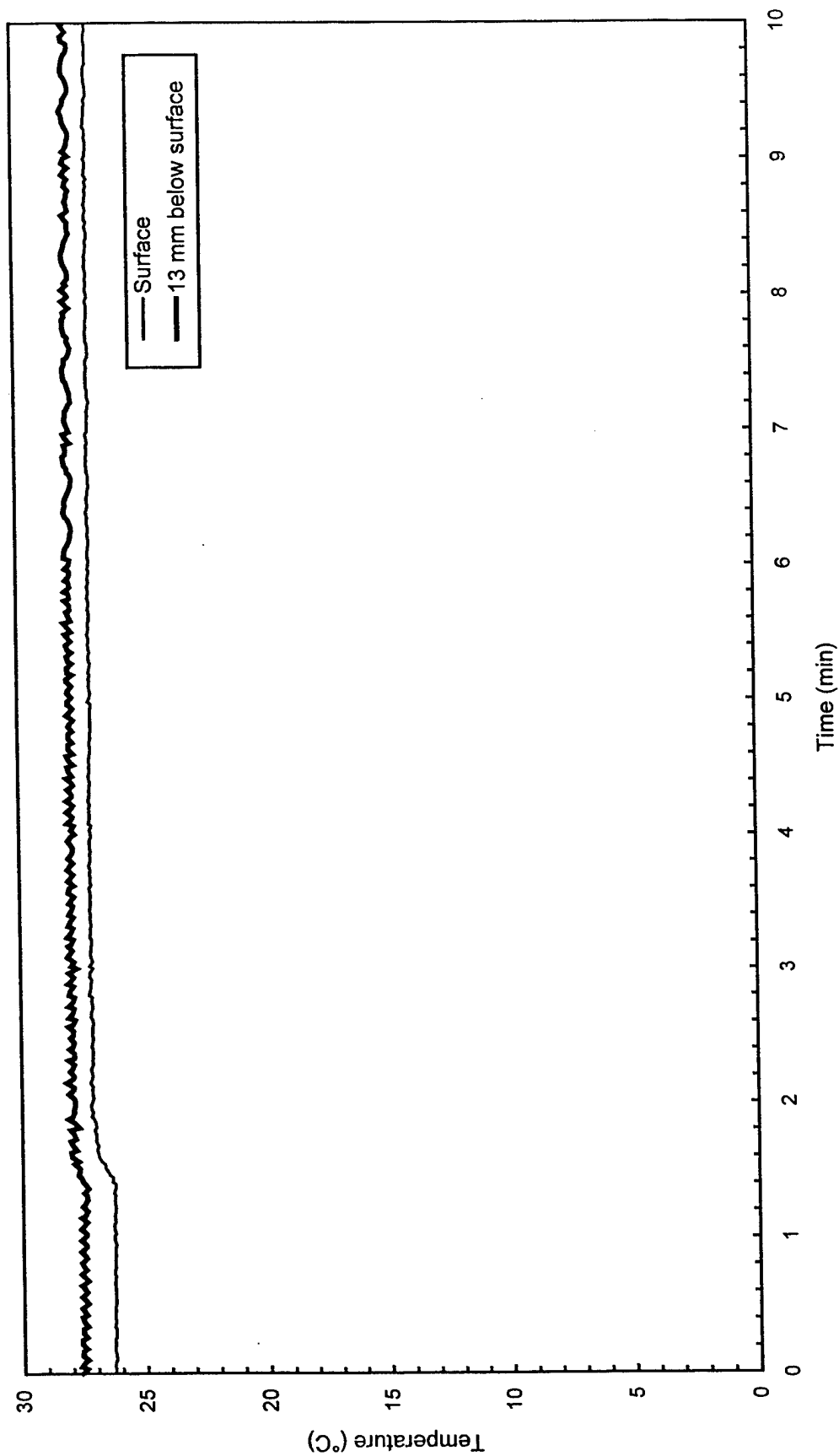


Fig. C108 - Concrete temperatures 3 m (10 ft) West of center of pad

Test F8

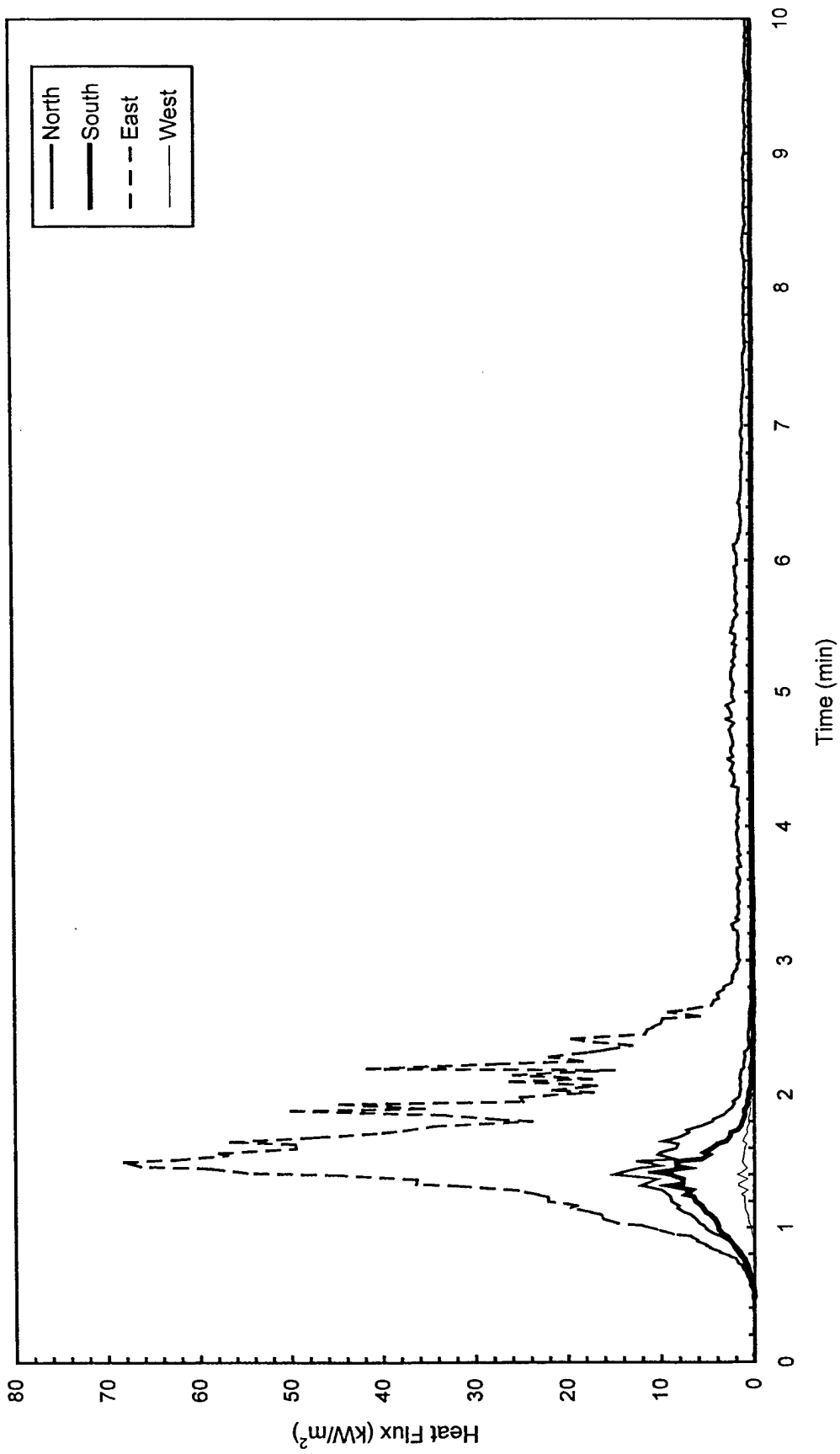


Fig. C109 - Heat flux measured at edge of pad

Test F8

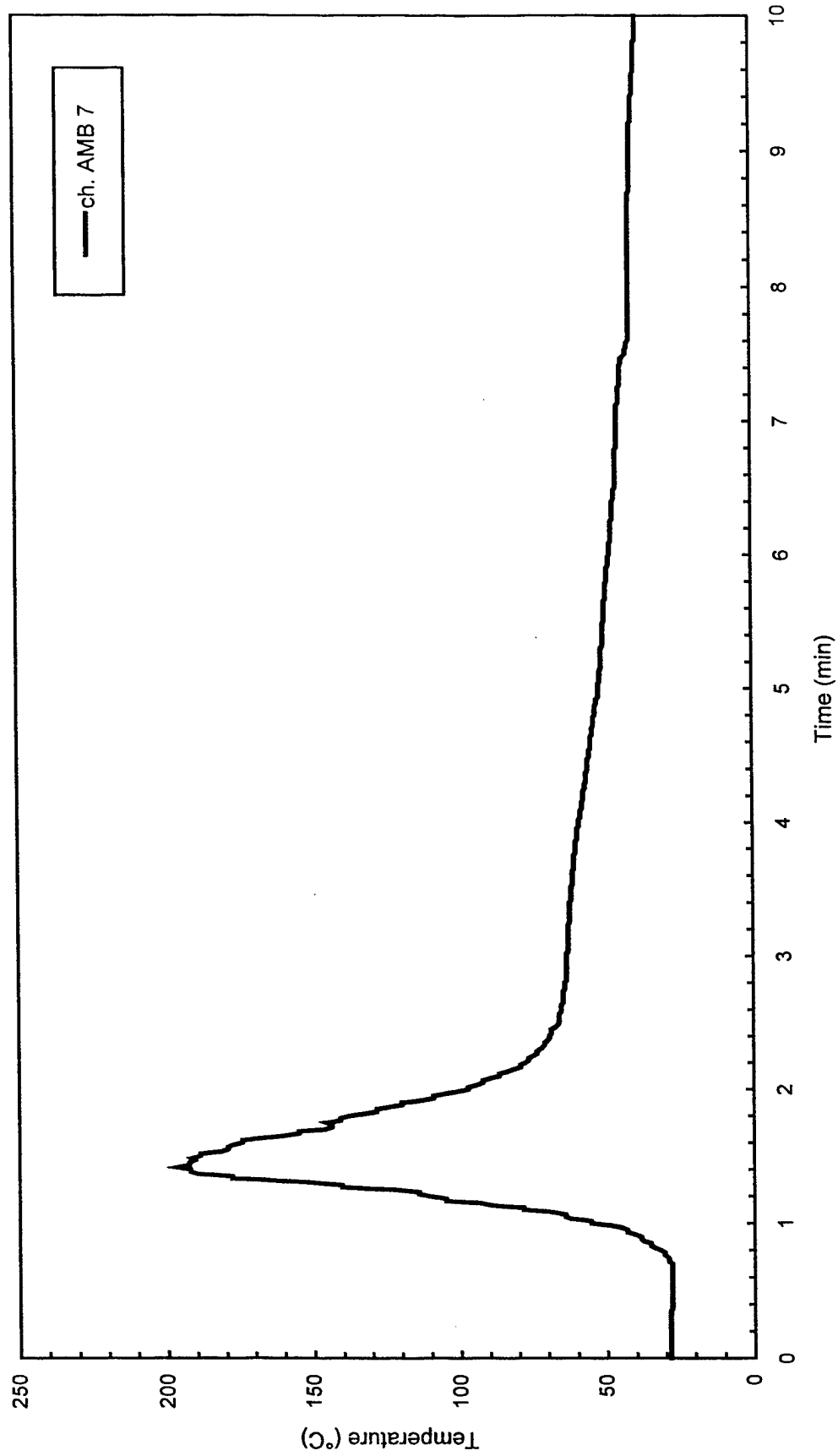


Fig. C110 - Air temperatures over center of pad

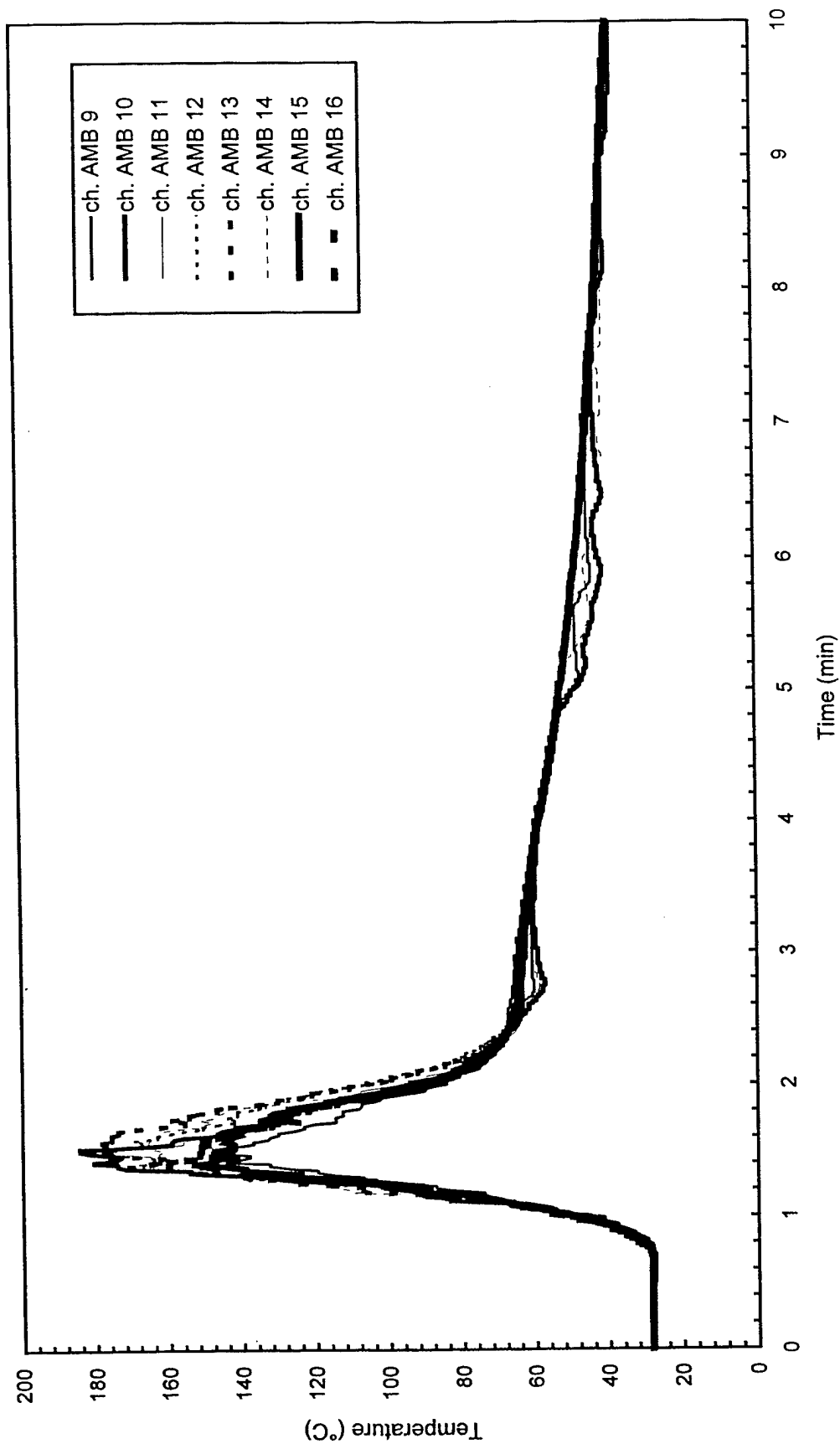


Fig. C111 - Air temperatures around 3 m (10 ft) radius from center of pad

Test F8

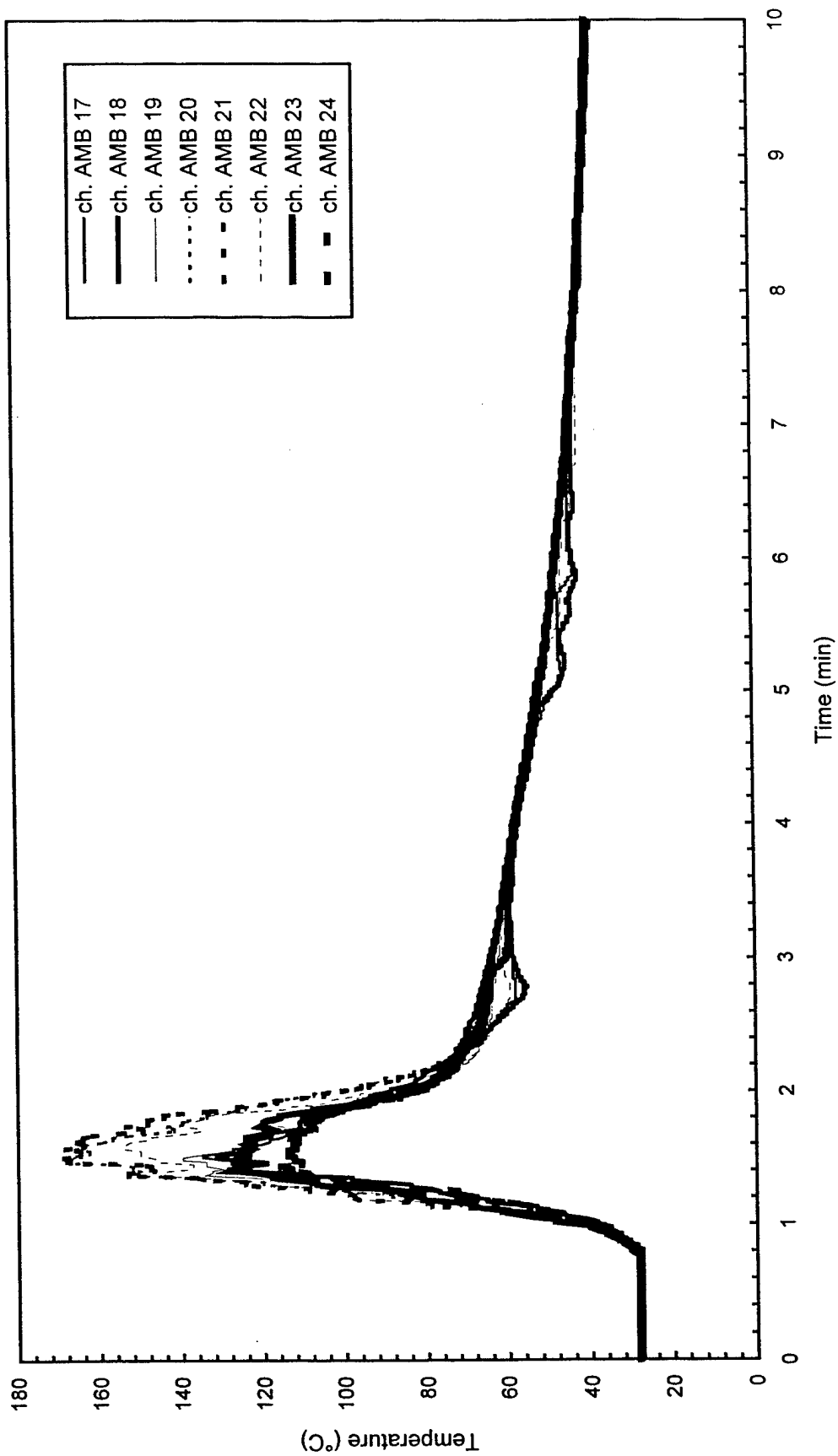


Fig. C112 - Air temperatures around 4.6 m (15 ft) radius from center of pad

Test F8

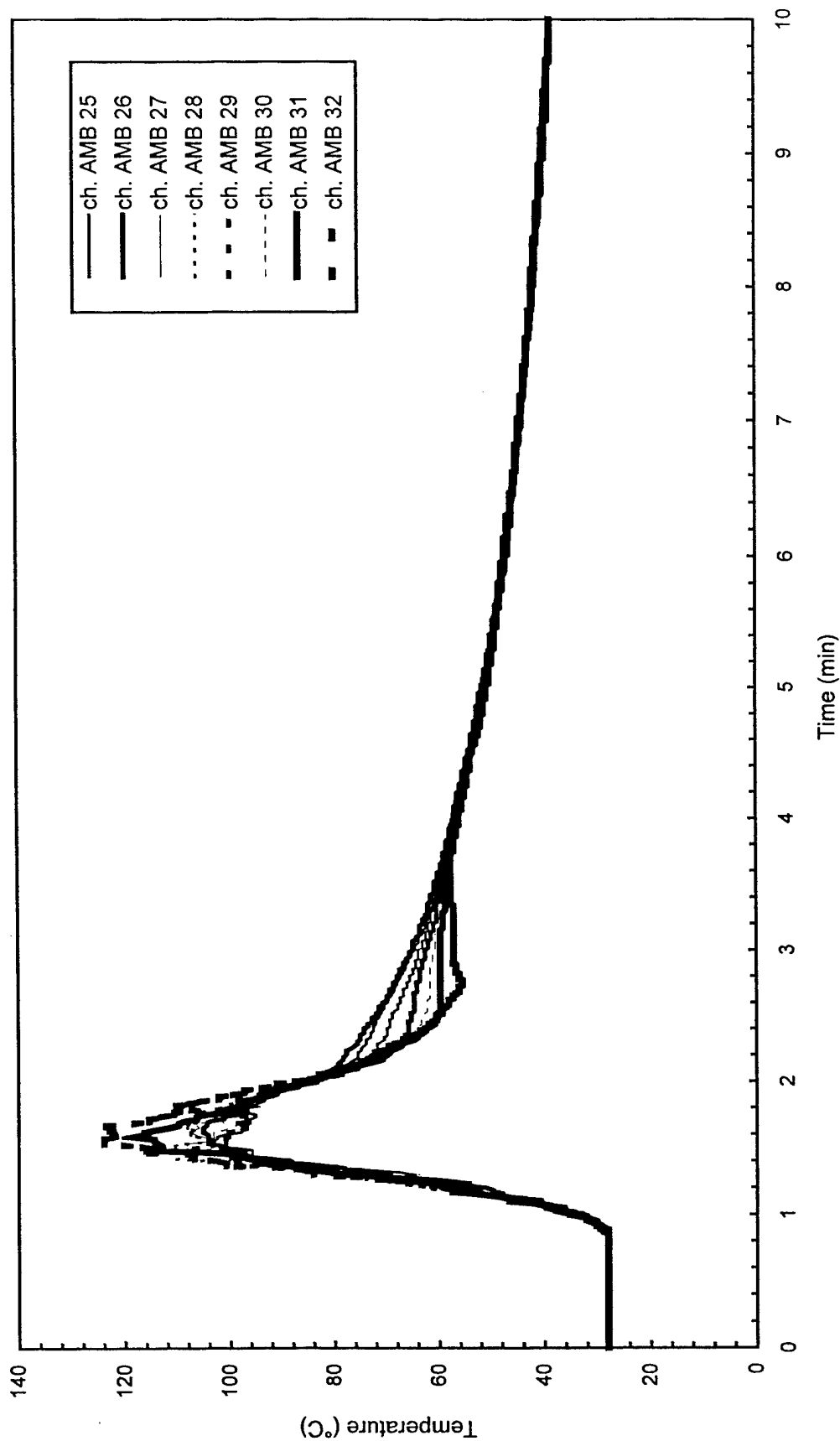


Fig. C113 - Air temperatures around North half of 7.6 m (25 ft) radius from center of pad

Test F8

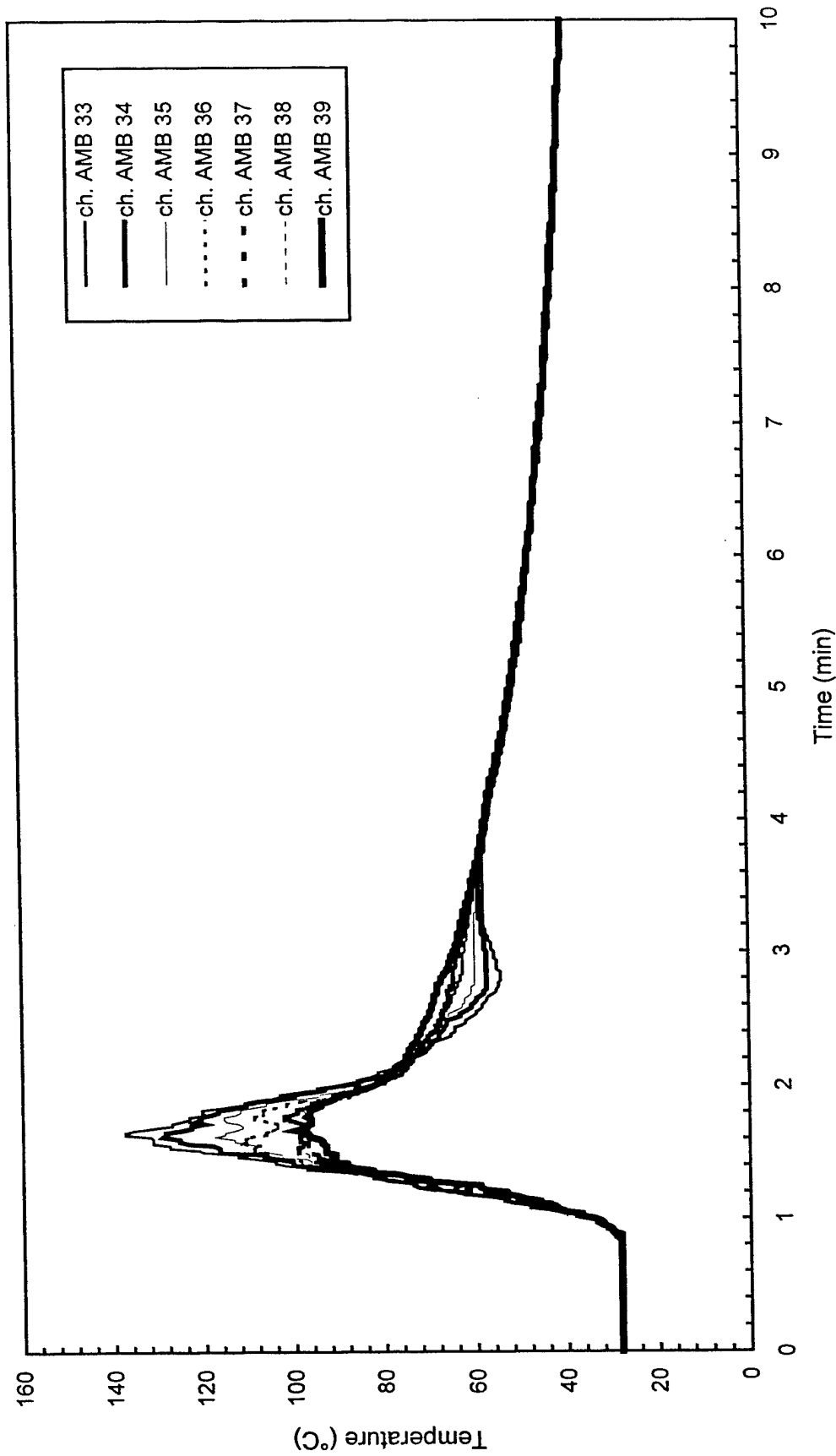


Fig. C114 - Air temperatures around South half of 7.6 m (25 ft) radius from center of pad

Test F8

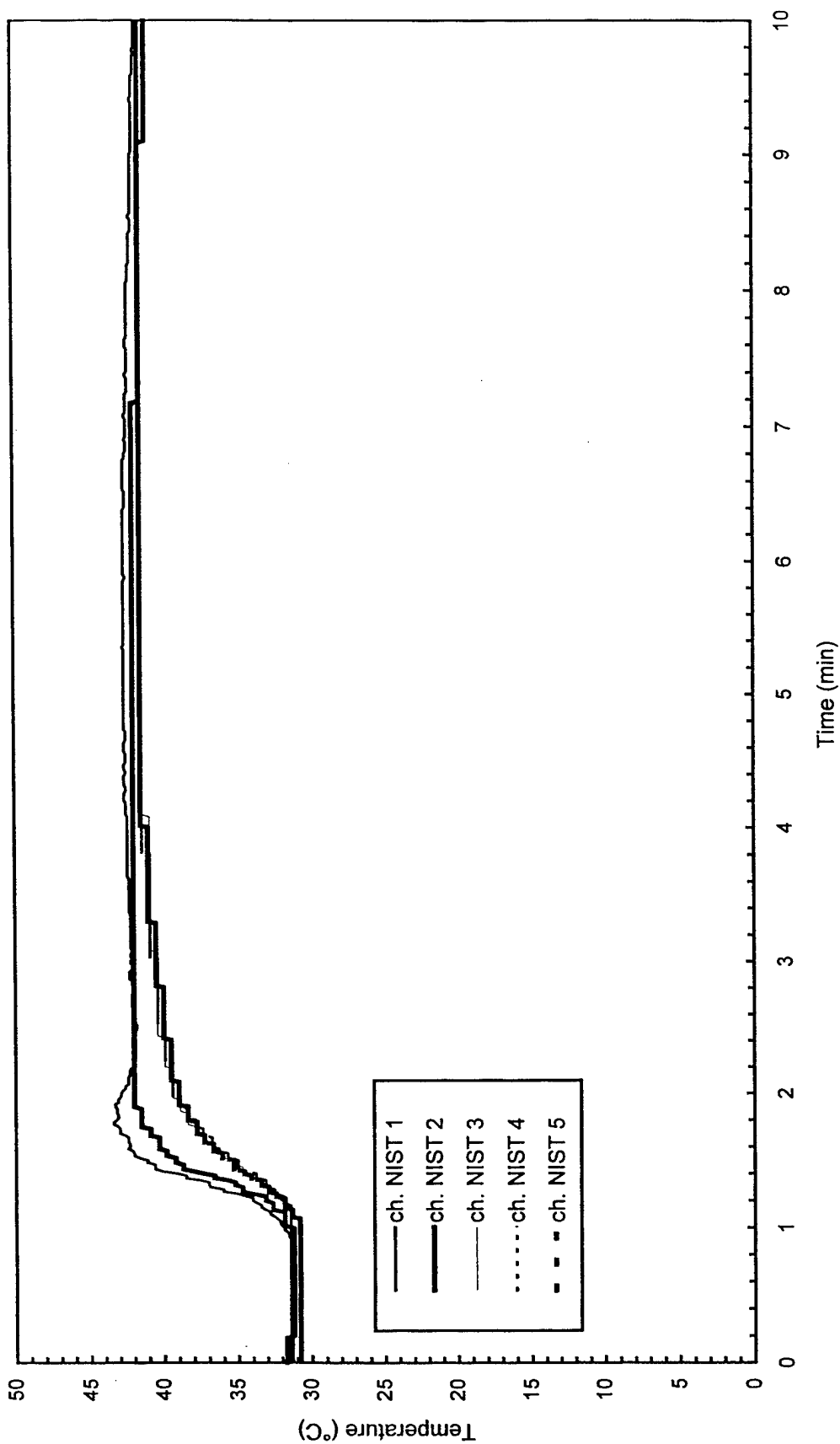


Fig. C115 - Temperature of West steel beam

Test F8

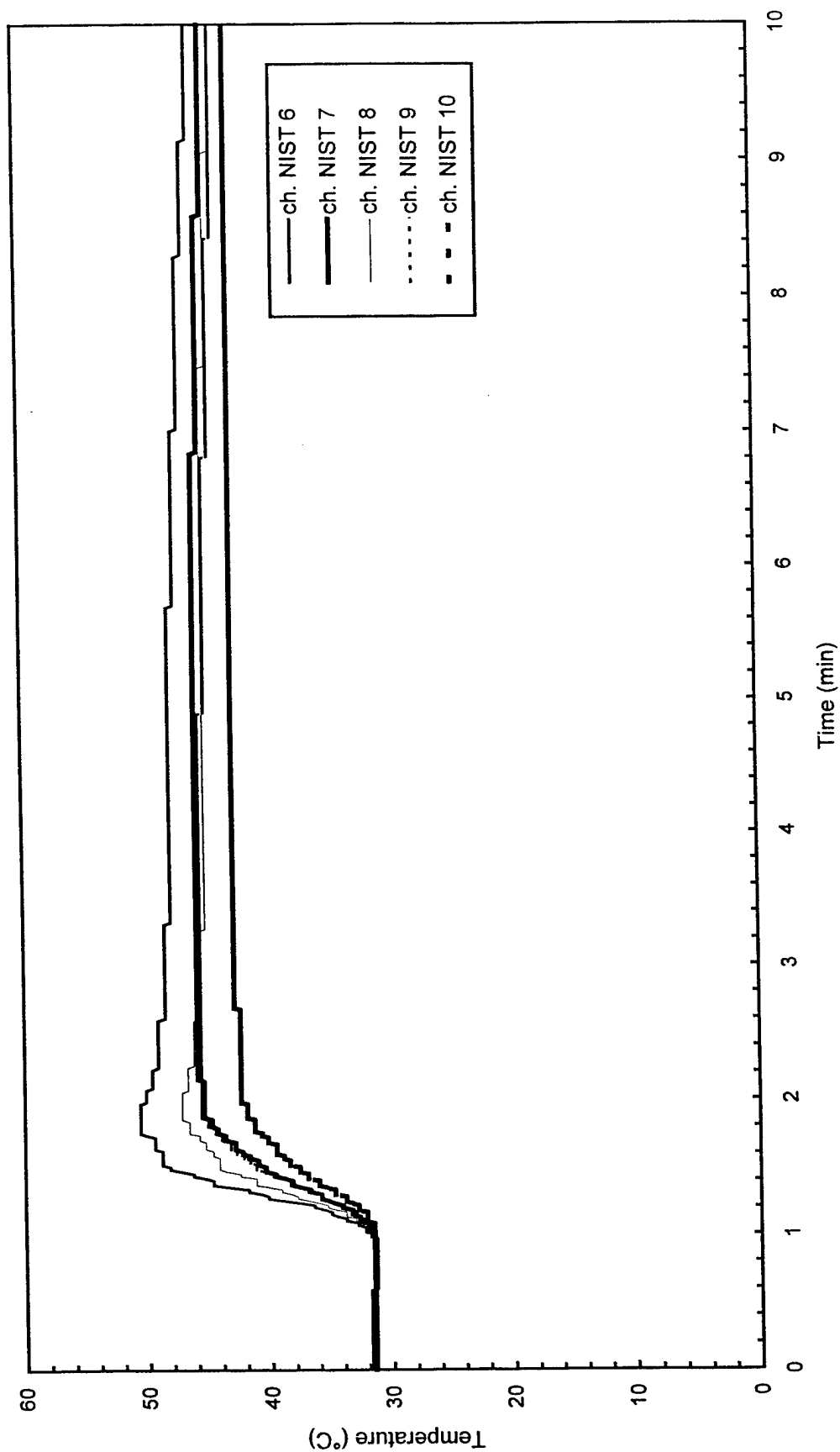


Fig. C116 - Temperature of North steel beam

Test F8

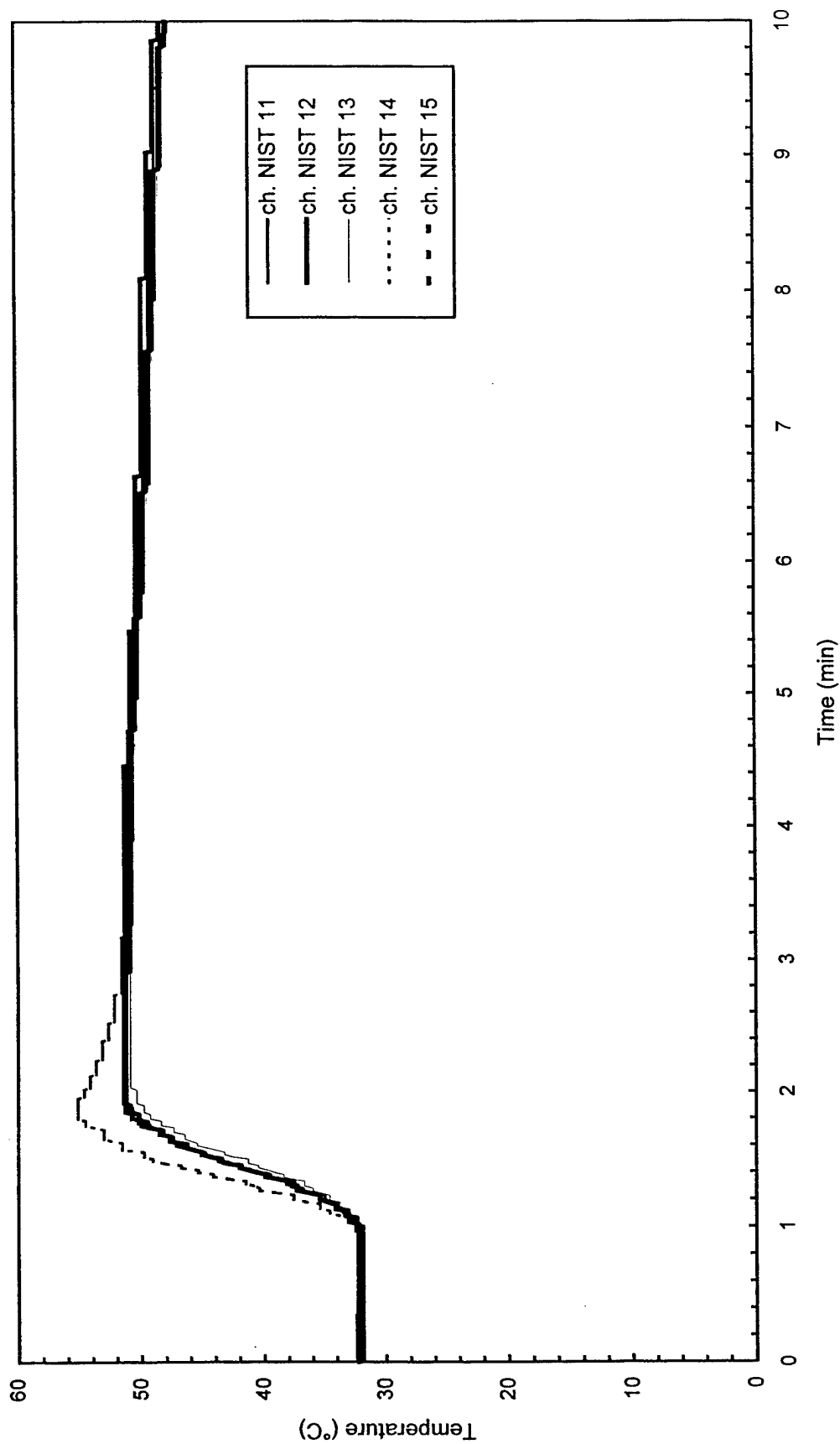


Fig. C117 - Temperature of East steel beam

Test F8

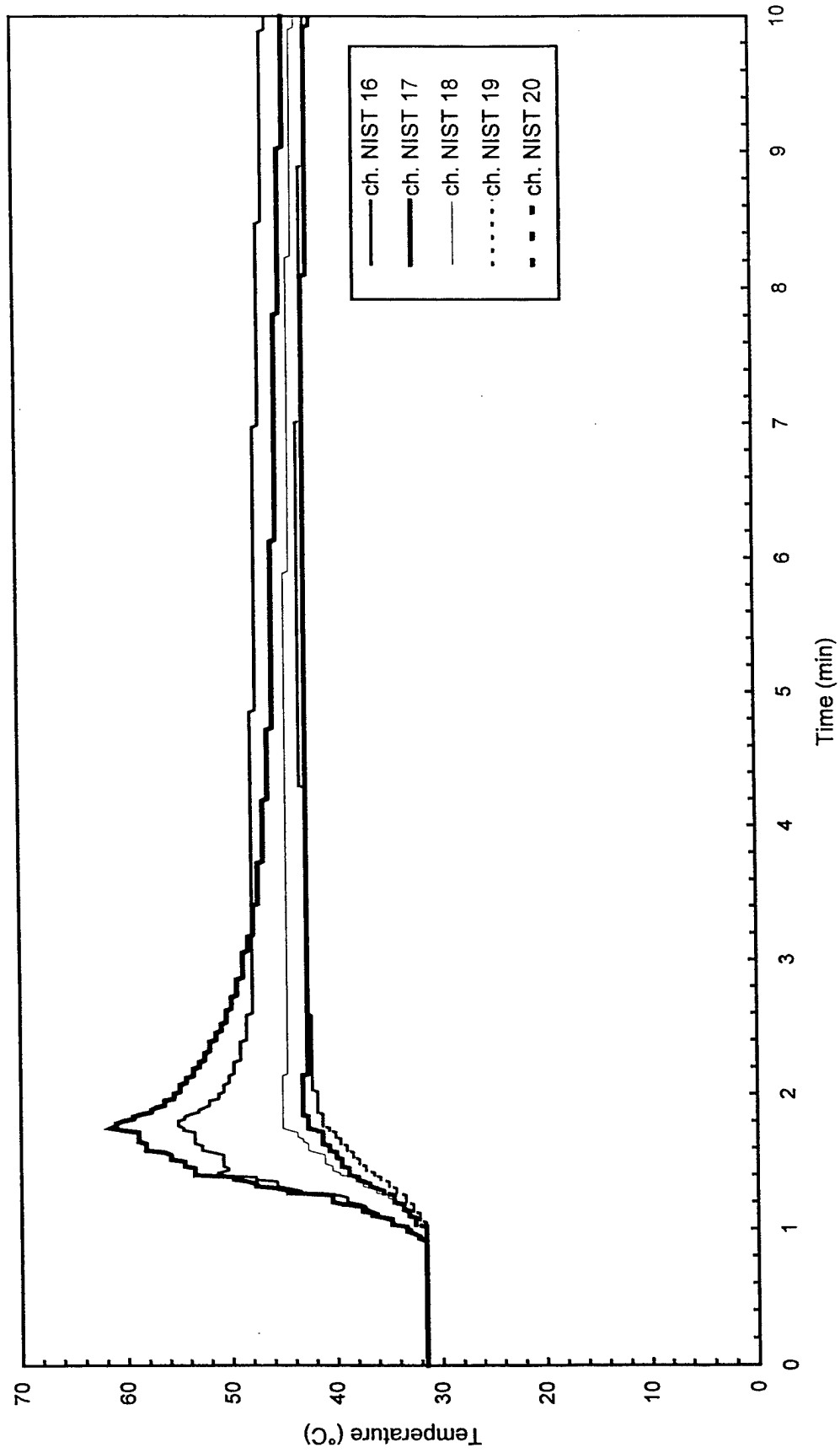


Fig. C118 - Temperature of South steel beam

Test F8

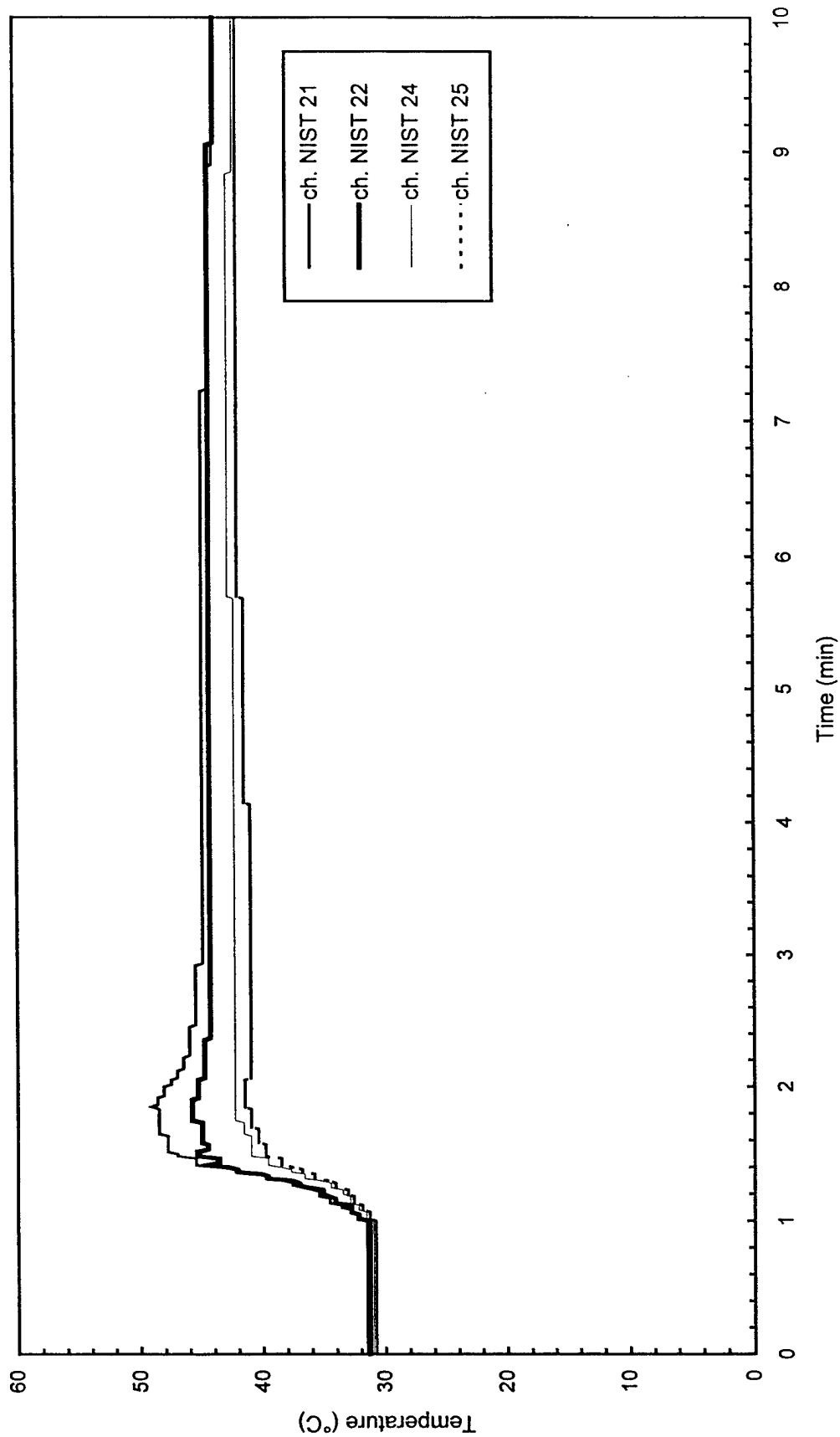


Fig. C119 - Temperature of Northwest steel beam

Test F8

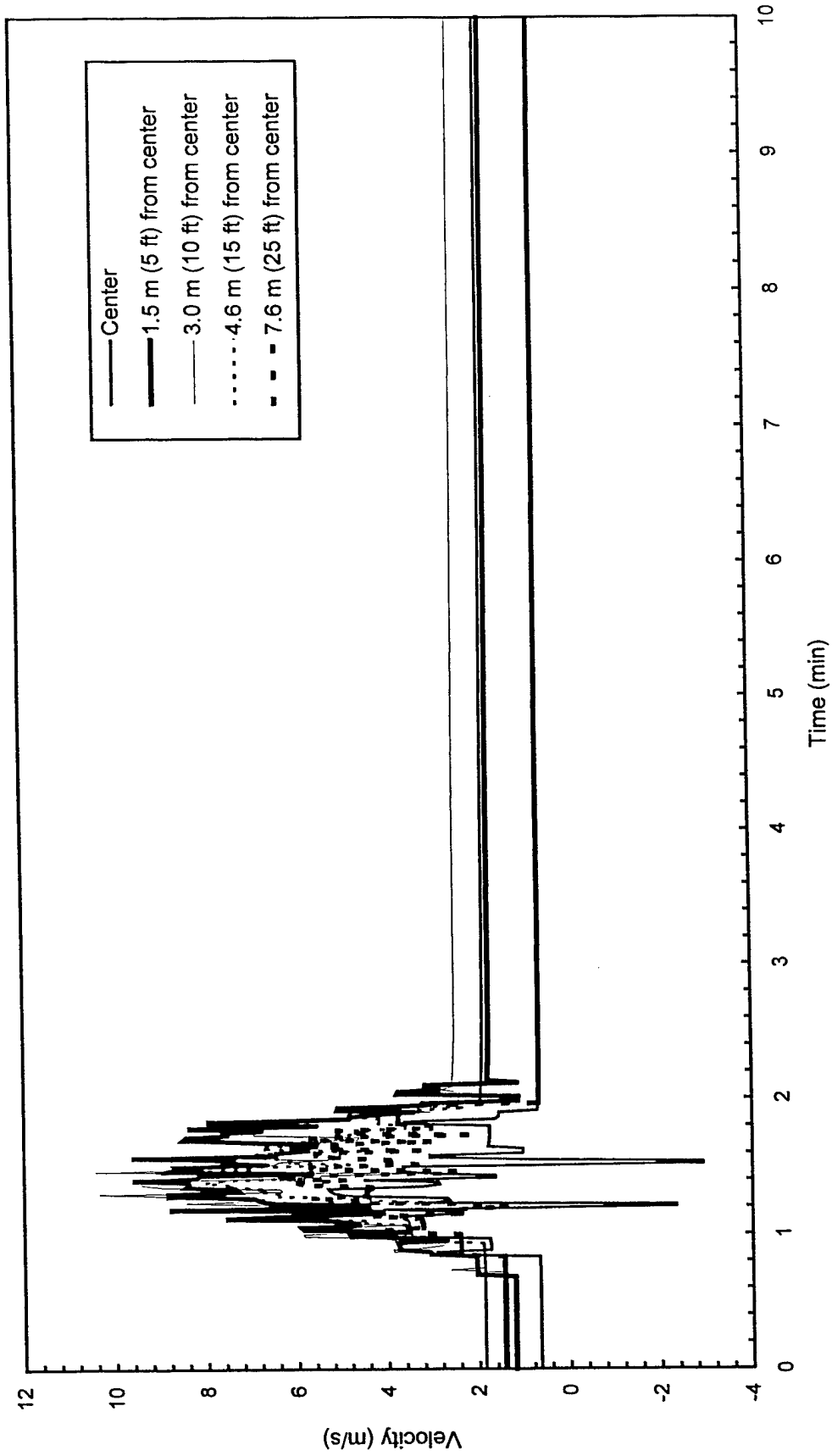


Fig. C120 - Plume and ceiling jet velocities

Test F9

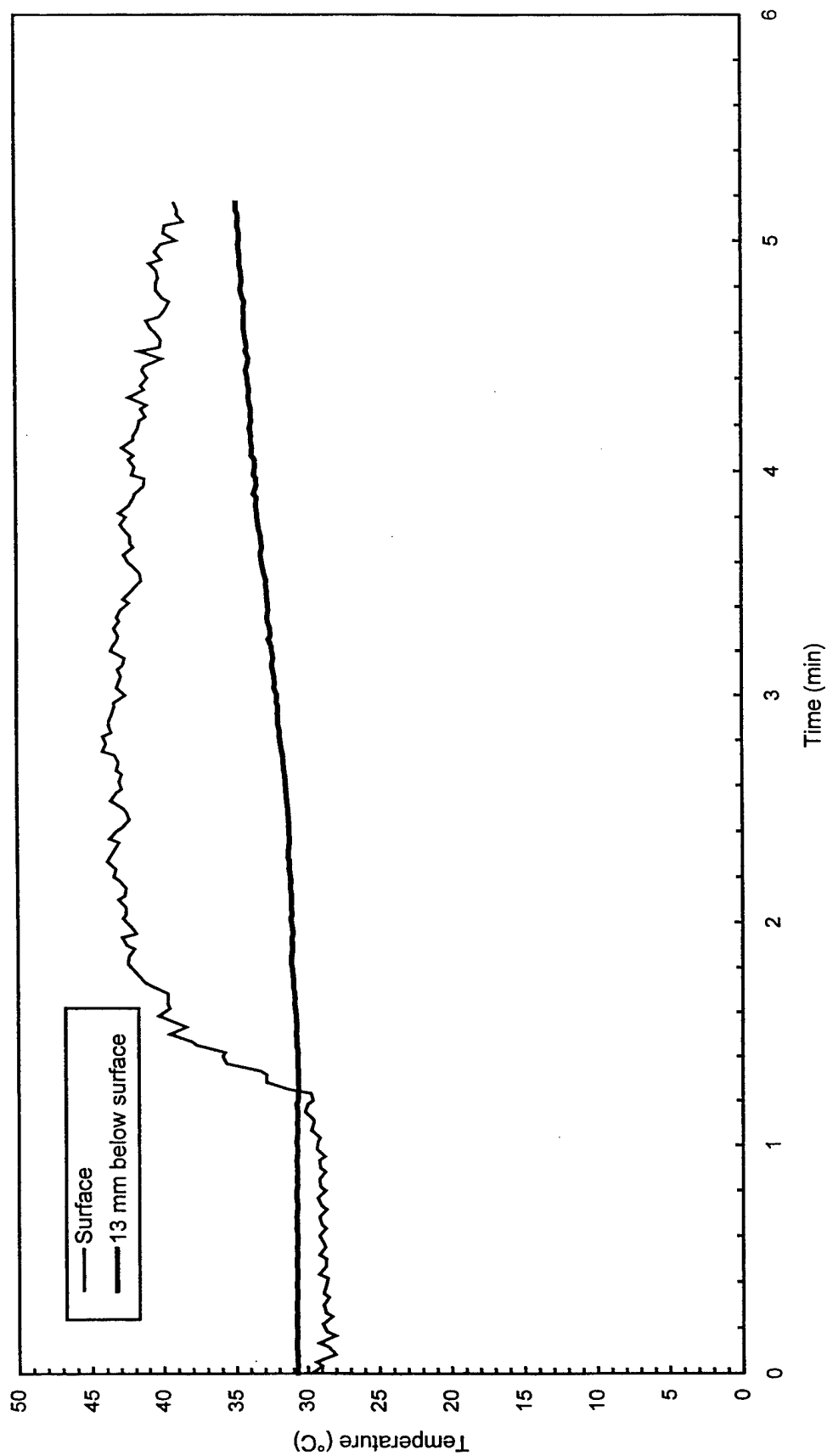


Fig. C121 - Concrete temperatures at center of pad

Test F9

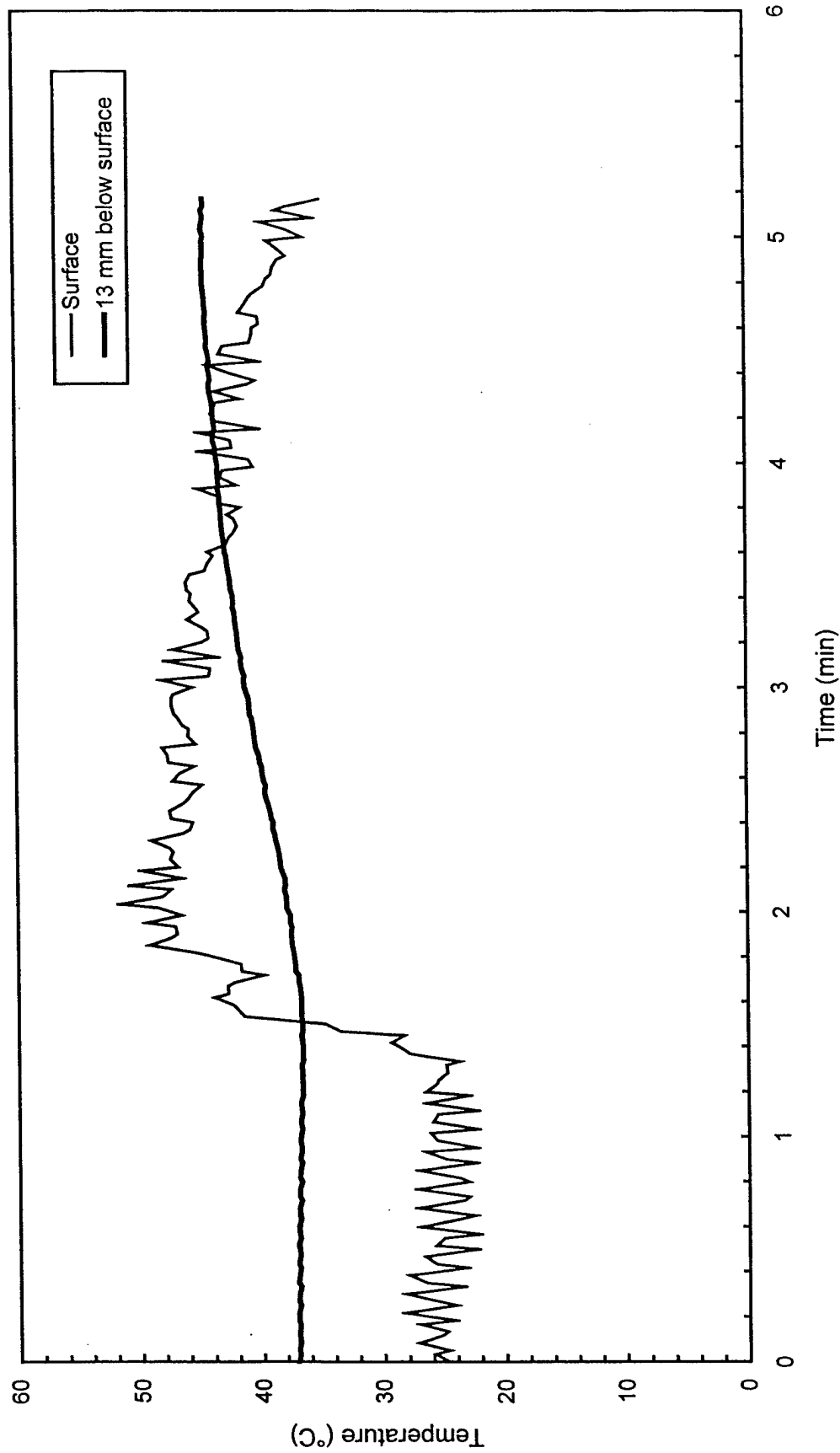


Fig. C122 - Concrete temperatures 3 m (10 ft) East of center of pad

Test F9

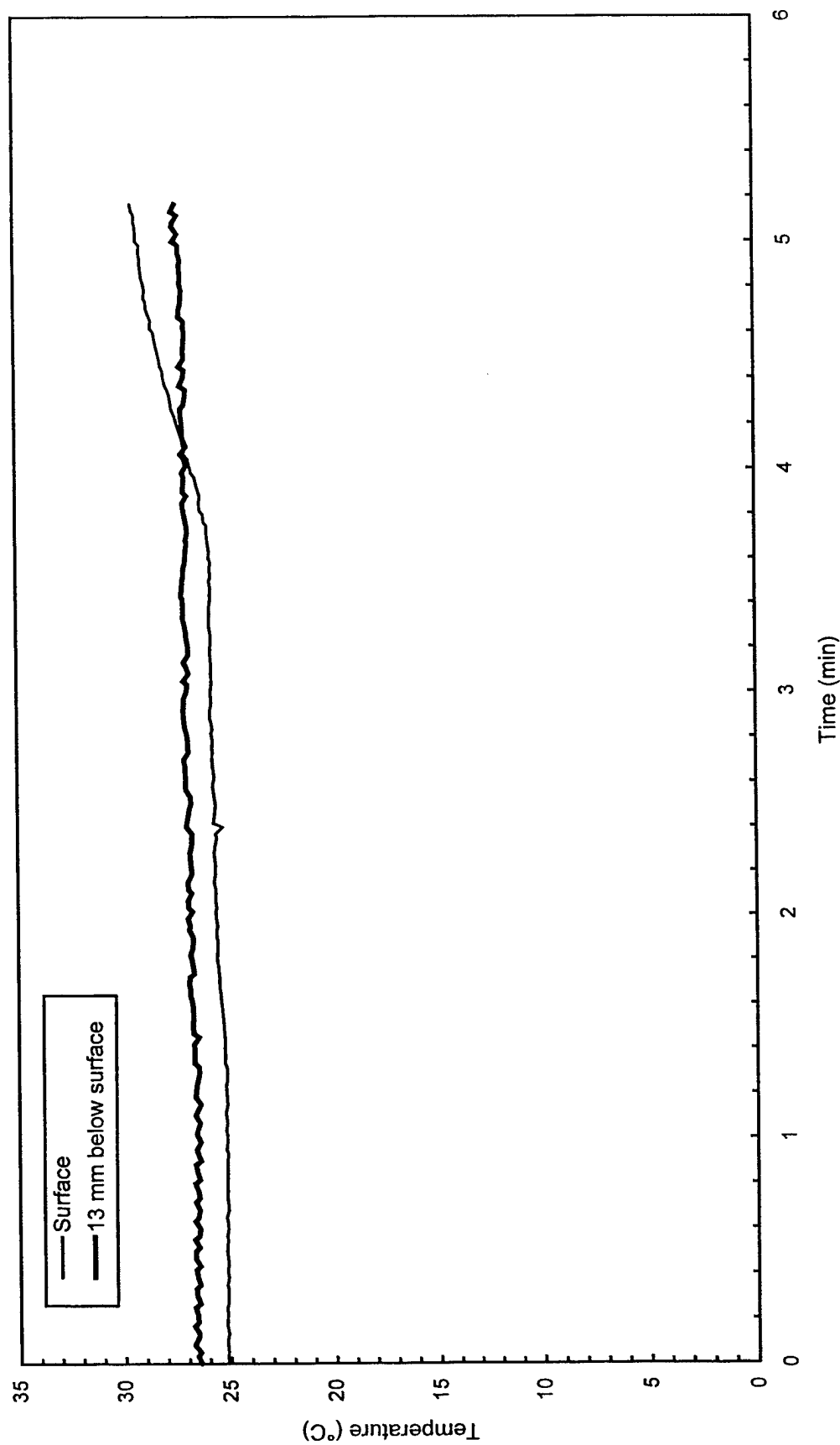


Fig. C123 - Concrete temperatures 3 m (10 ft) West of center of pad

Test F9

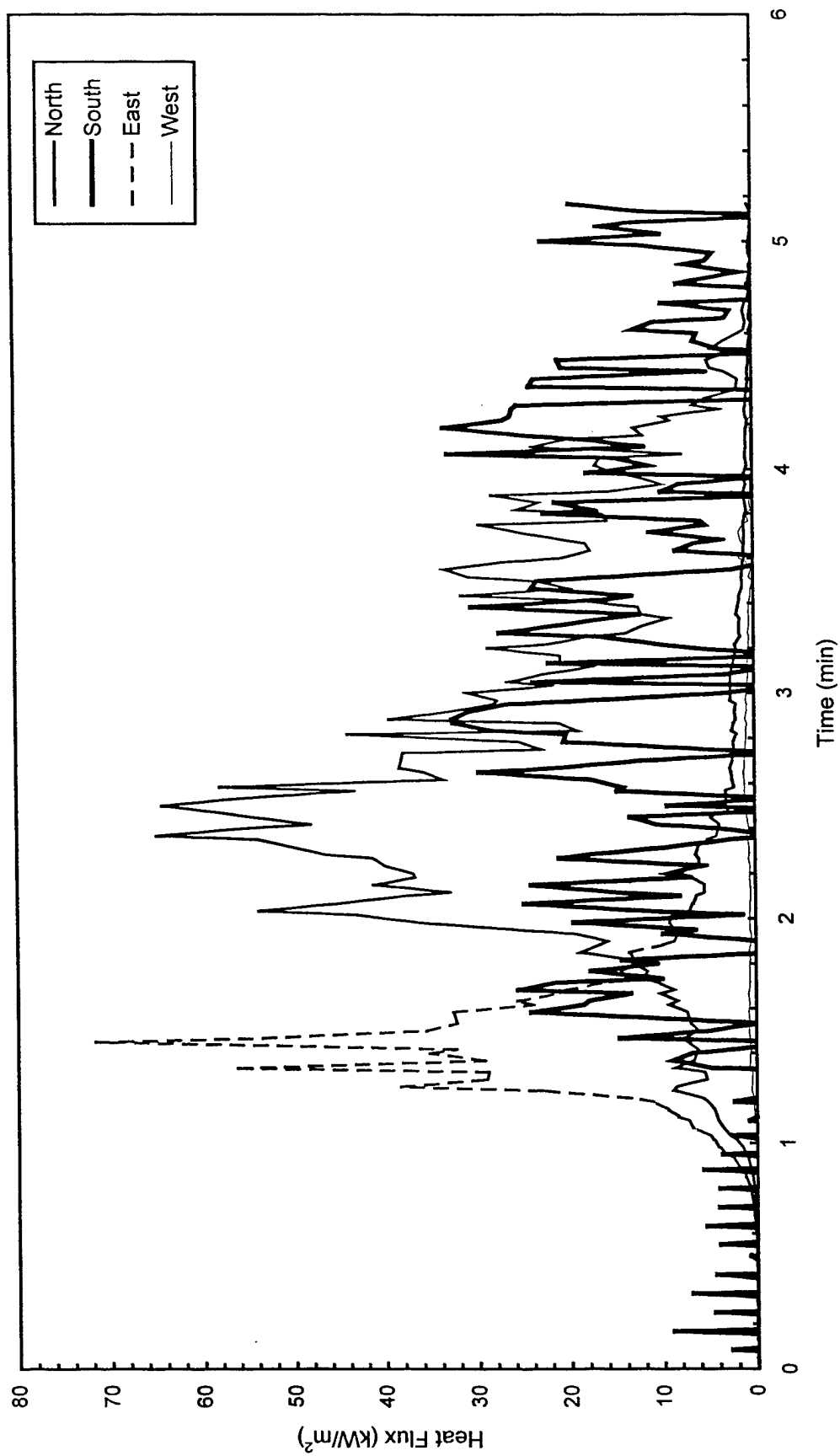


Fig. C124 - Heat flux measured at edge of pad

Test F9

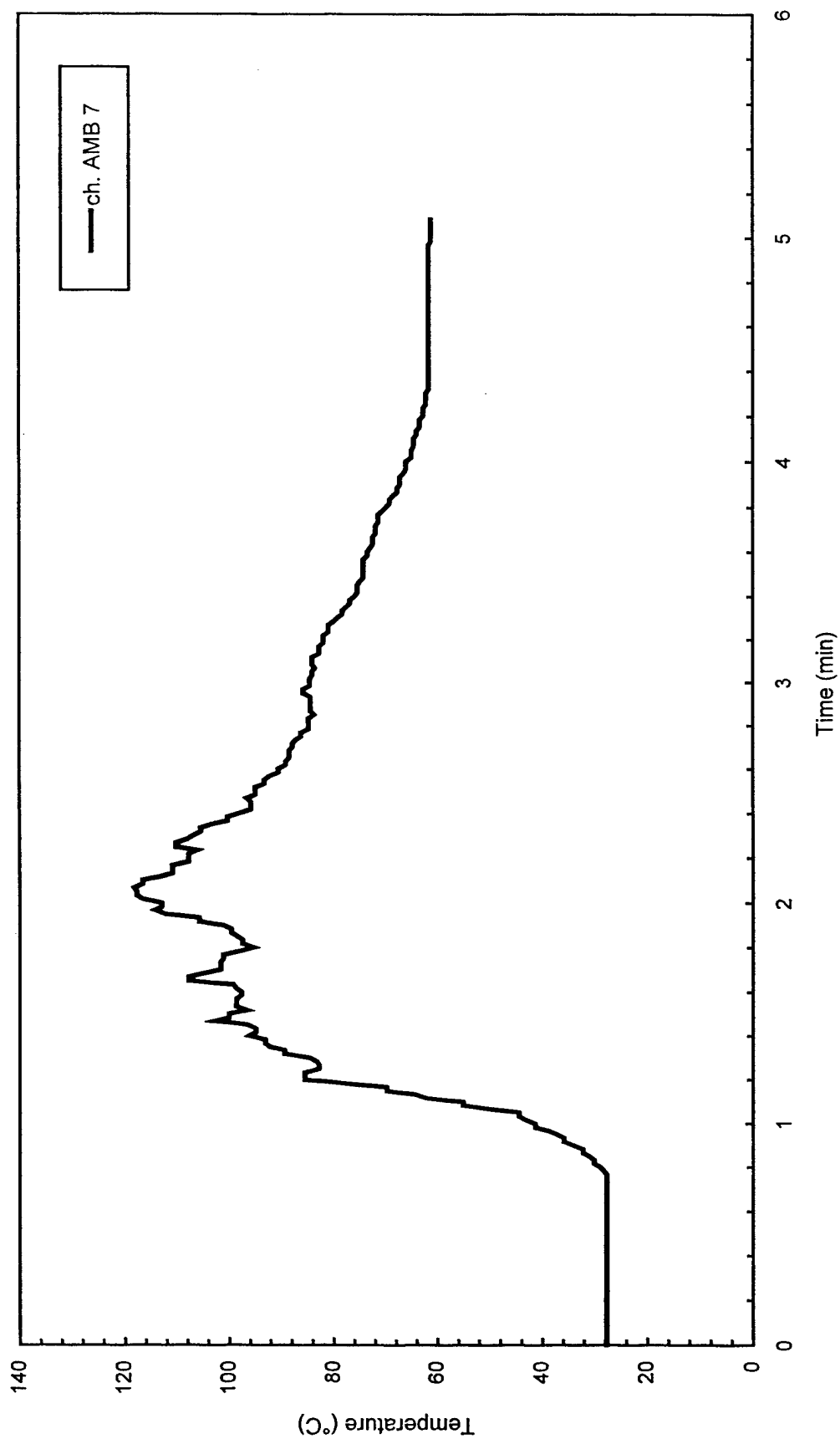


Fig. C125 - Air temperatures over center of pad

Test F9

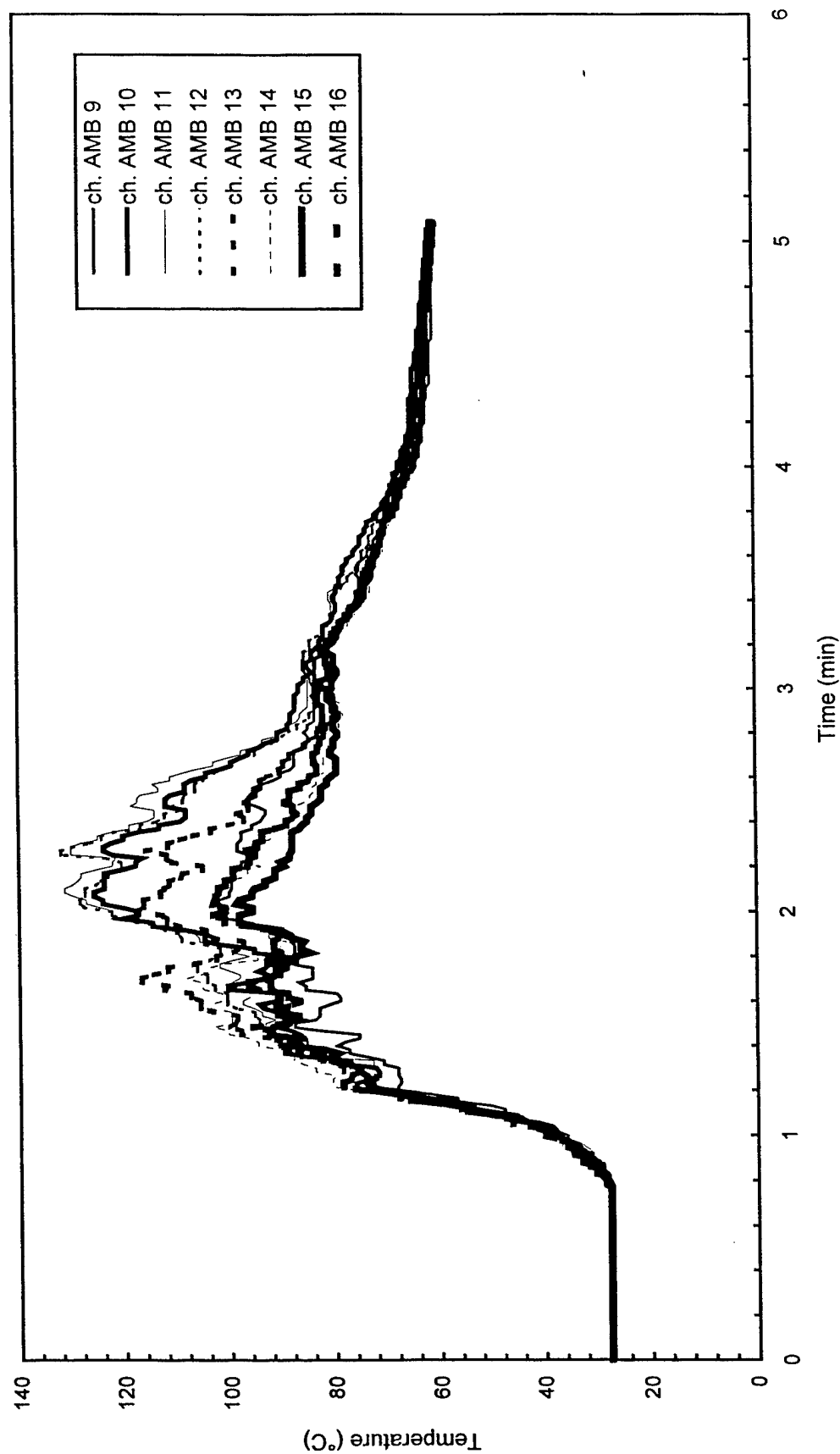


Fig. C126 - Air temperatures around 3 m (10 ft) radius from center of pad

Test F9

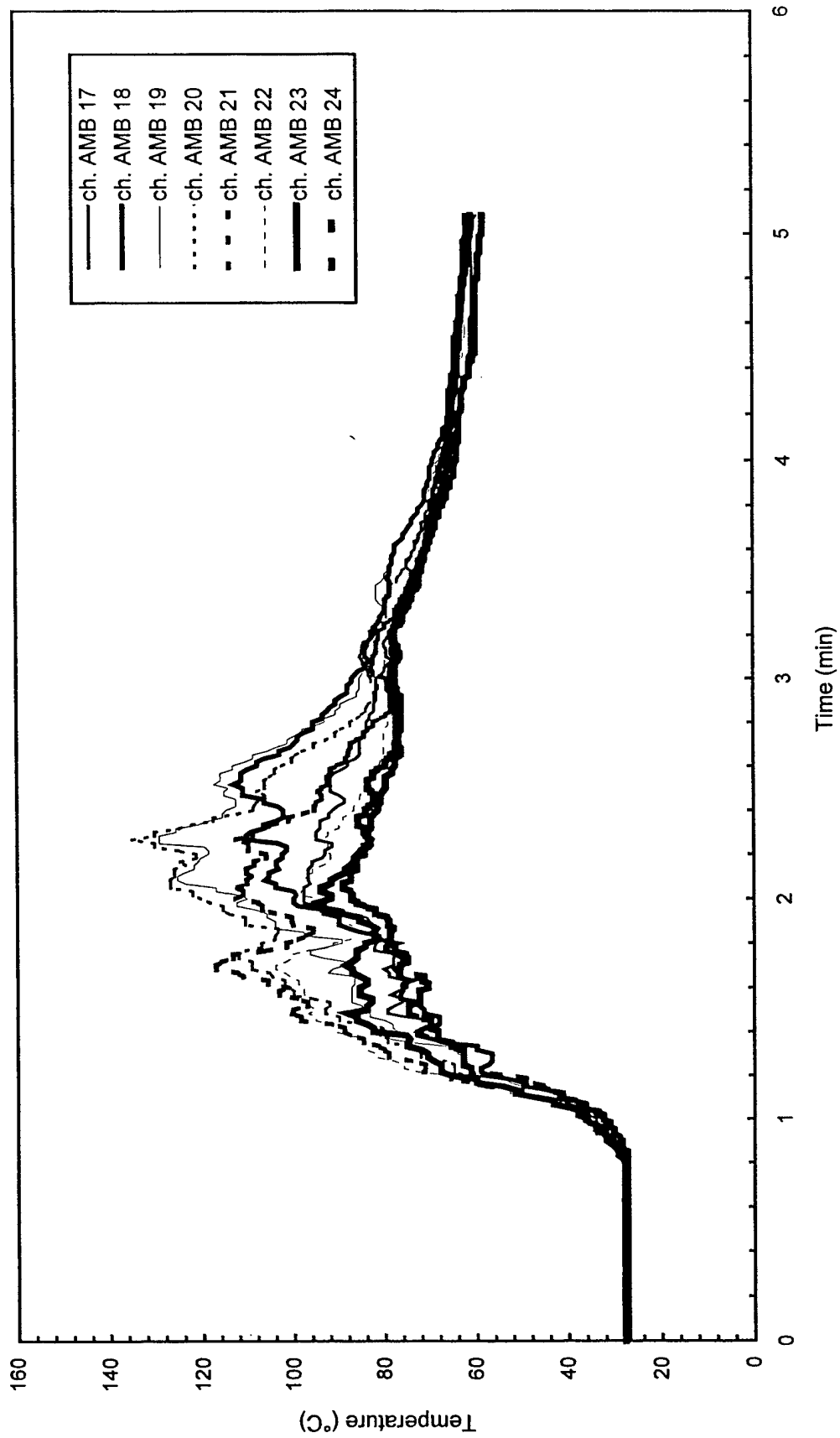


Fig. C127 - Air temperatures around 4.6 m (15 ft) radius from center of pad

Test F9

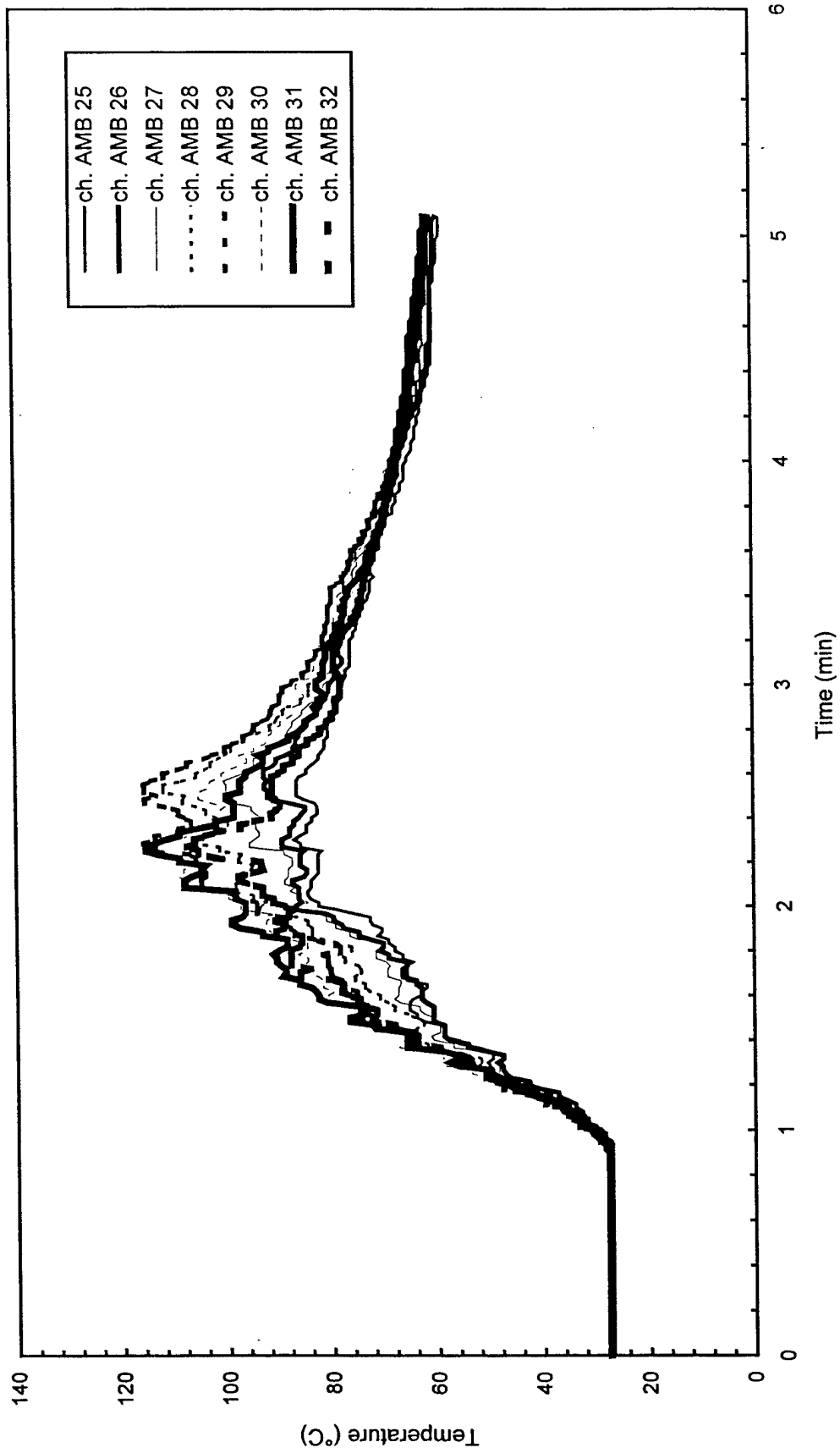


Fig. C128 - Air temperatures around North half of 7.6 m (25 ft) radius from center of pad

Test F9

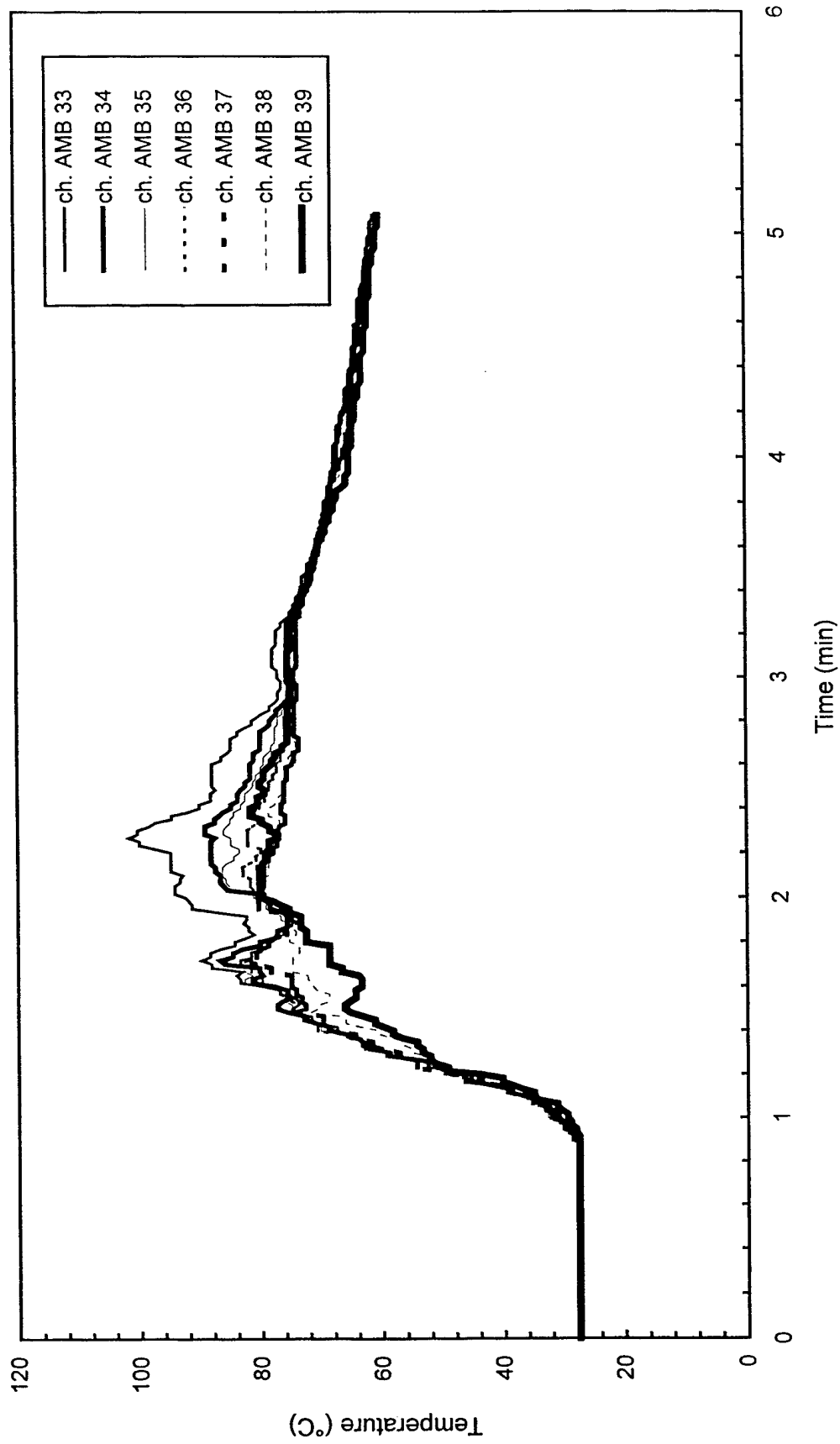


Fig. C129 - Air temperatures around South half of 7.6 m (25 ft) radius from center of pad

Test F9

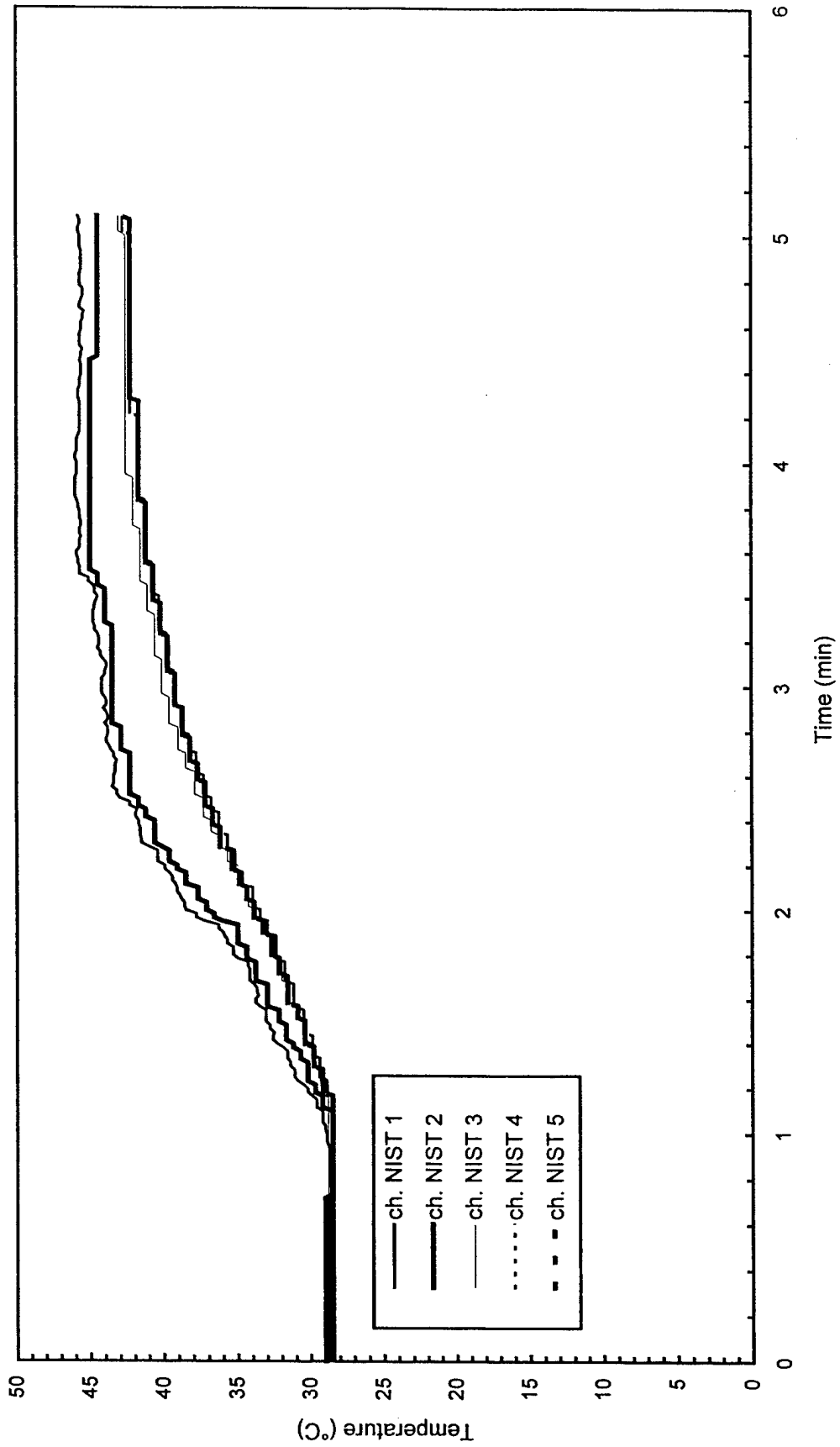


Fig. C130 - Temperature of West steel beam

Test F9

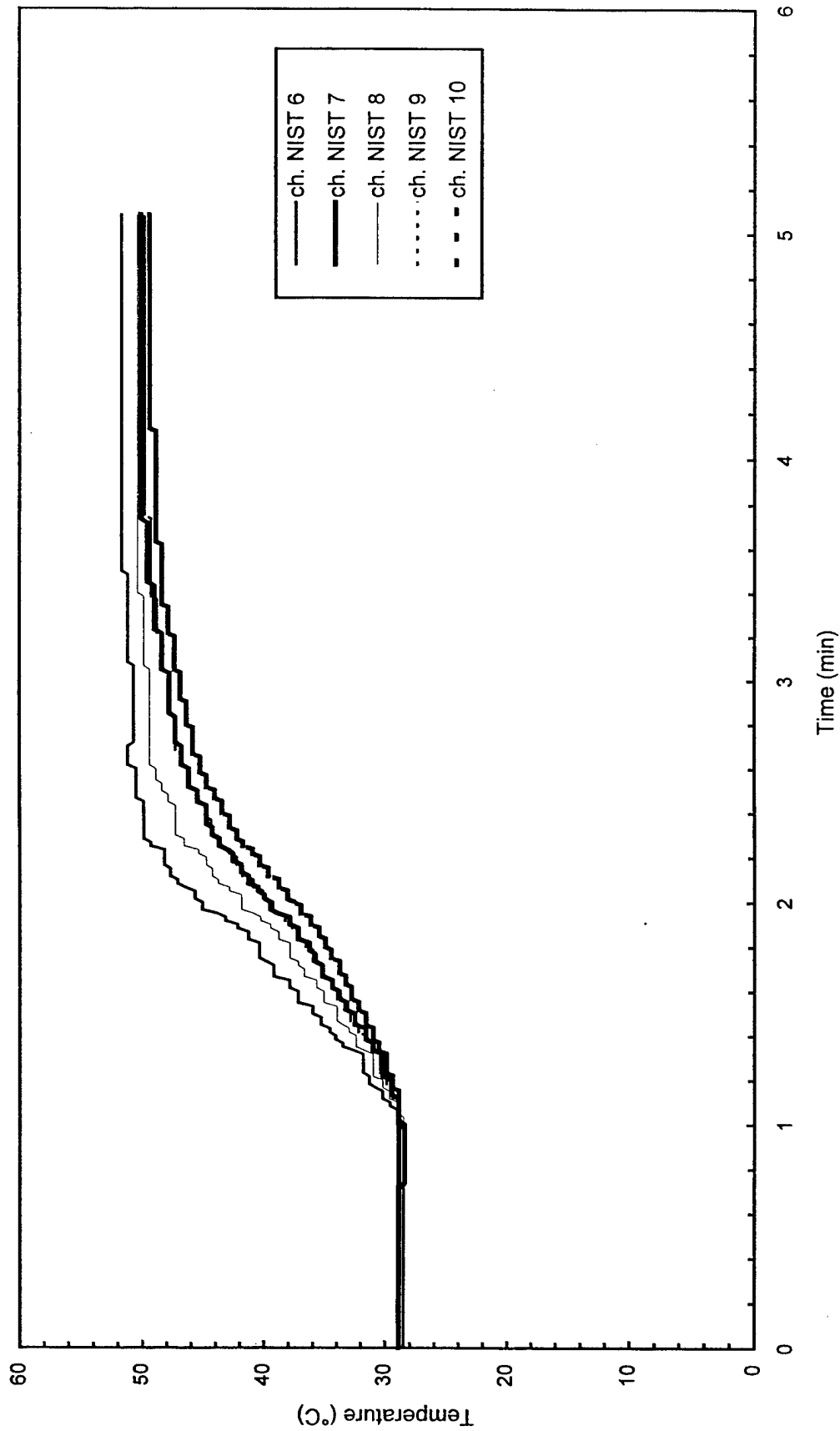


Fig. C131 - Temperature of North steel beam

Test F9

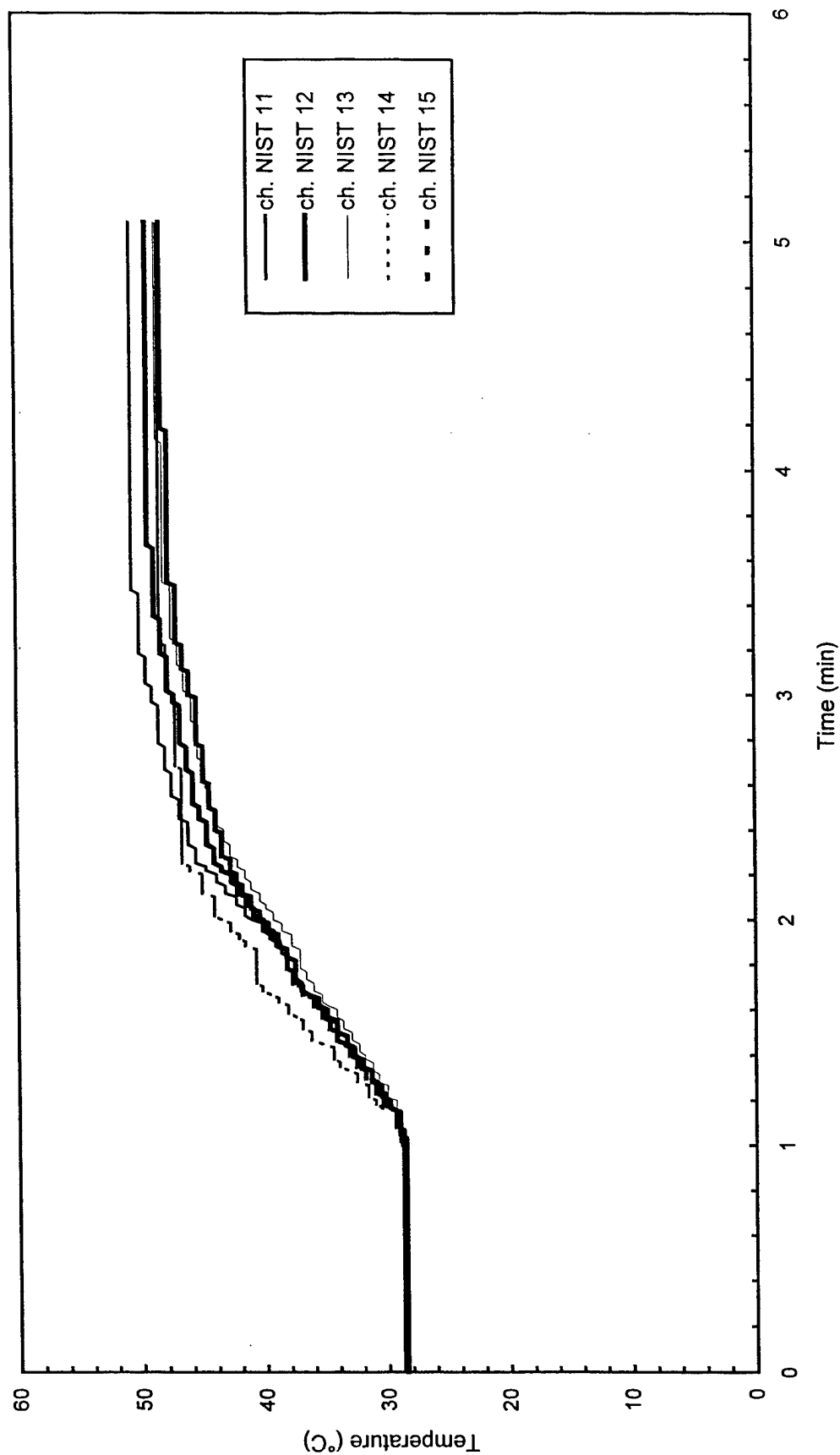


Fig. C132 - Temperature of East steel beam

Test F9

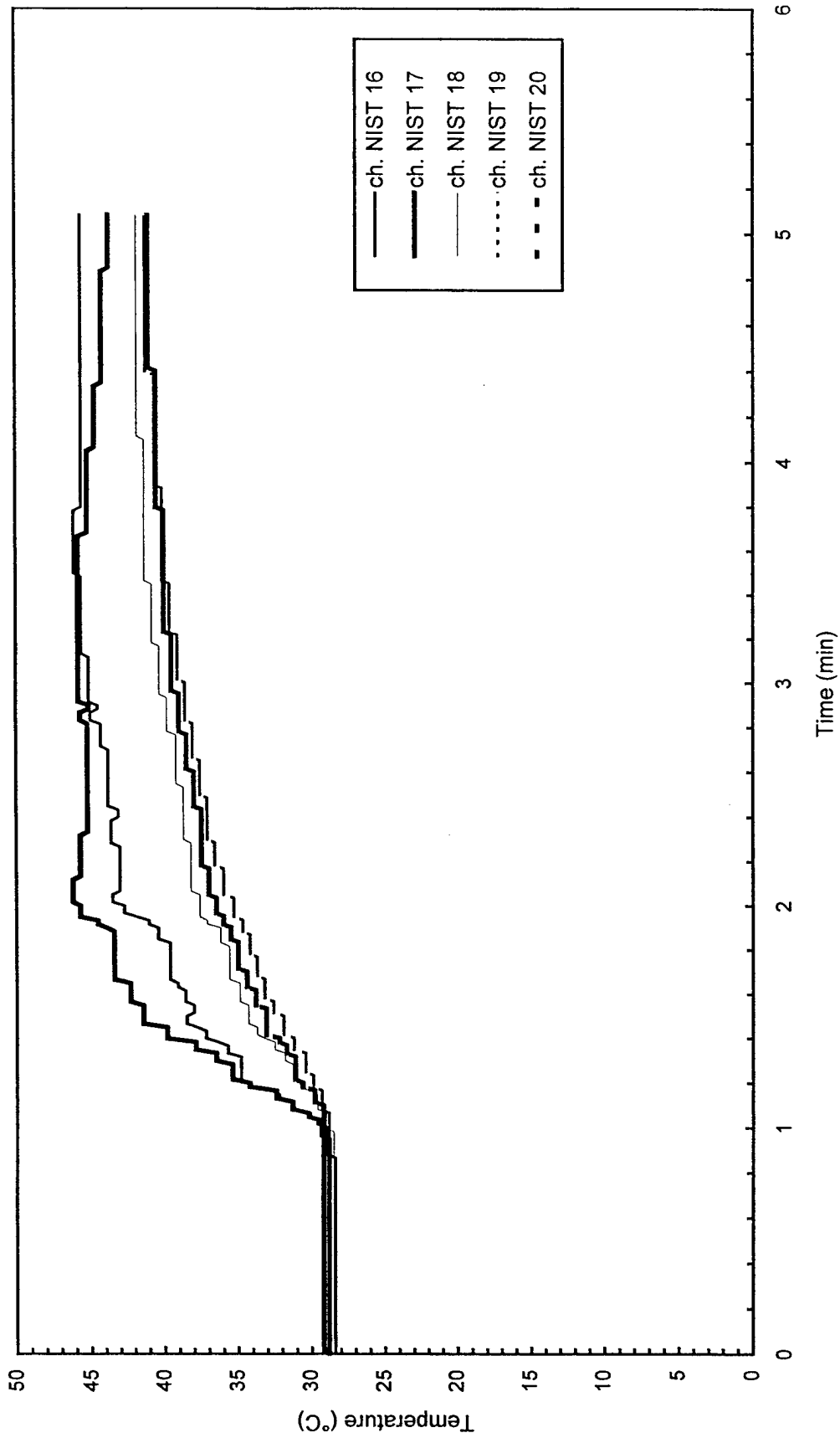


Fig. C133 - Temperature of South steel beam

Test F9

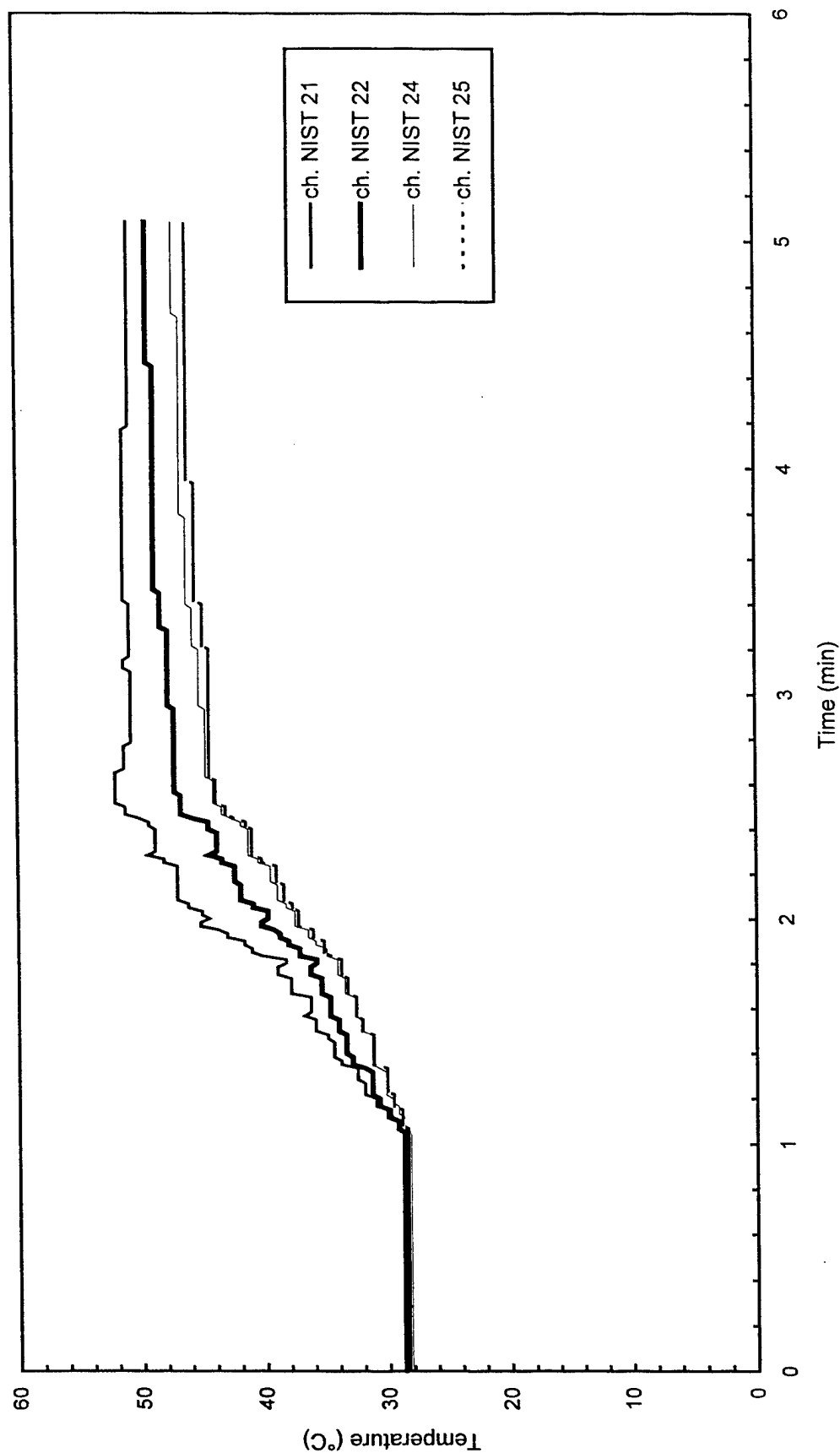


Fig. C134 - Temperature of Northwest steel beam

Test F9

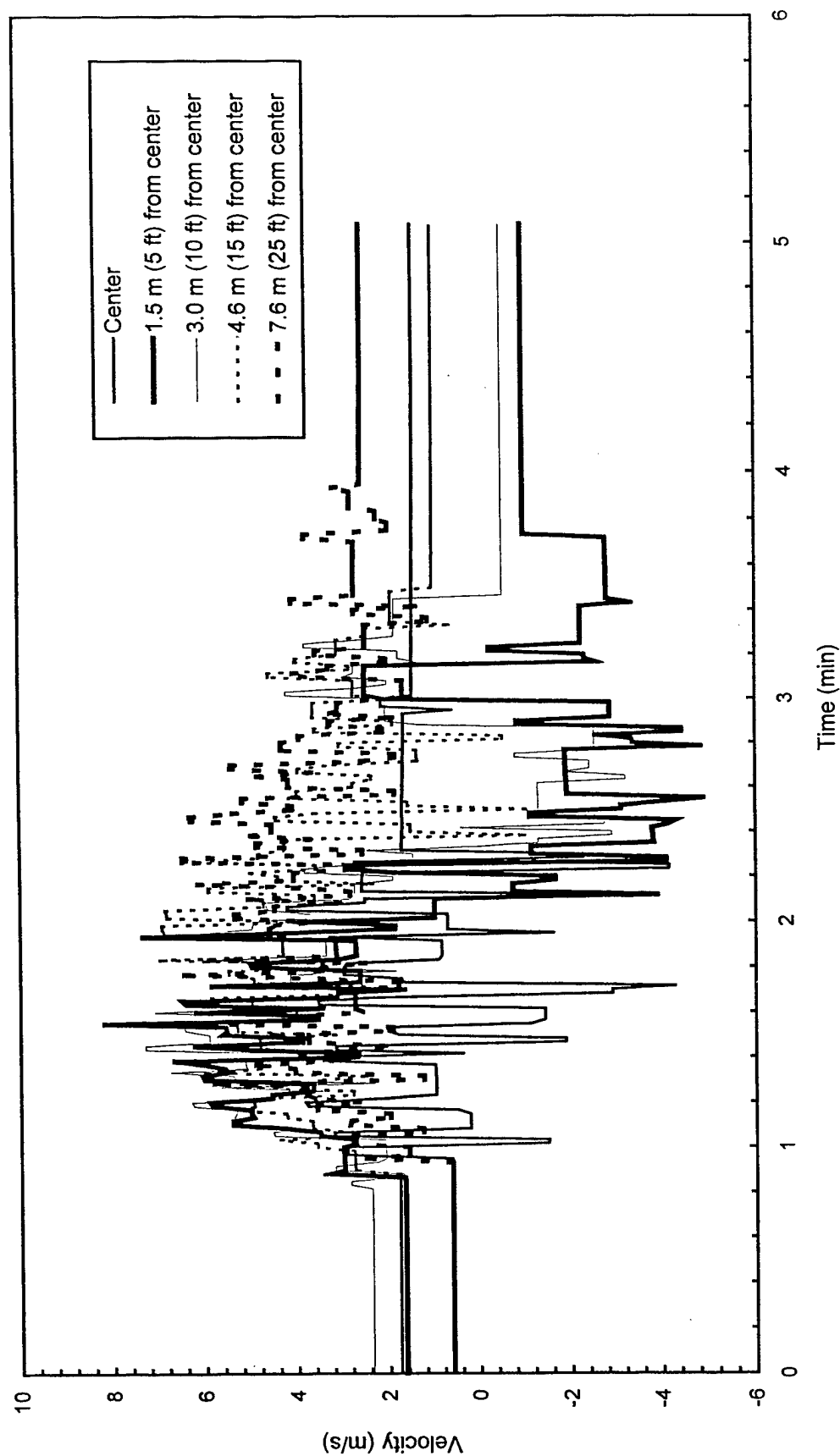


Fig. C135 - Plume and ceiling jet velocities

APPENDIX D

Concept Package For The Use of a
Mobile Automatic Fire Extinguisher
In Aircraft Hangars

CONCEPT PACKAGE FOR THE USE OF A MOBILE AUTOMATIC FIRE EXTINGUISHER IN AIRCRAFT HANGARS

BACKGROUND

To evaluate the potential use of a mobile automatic fire extinguisher in aircraft hangars to replace installed fire protection features, it is necessary to develop a conceptual plan for how such a device might be used. This is a conceptual plan which would require coordination from the civil engineering operations, fire protection operations and the aircraft maintenance communities. This is intended to serve as an example for developing the required design documentation.

PRACTICAL PROTECTION AREA

The total delivery area of the breadboard MCAFFSS unit is on the order of 232 m^2 (2500 ft^2). This is based on a 90° sweep pattern. The total delivery area is 45° on either side of the nozzle centerline by 15 m (50 ft) extension along the centerline. However, to compensate for errors in positioning, the practical delivery area would be limited to 35° on either side of the centerline of the nozzle. This allows for 10° flexibility in positioning. The practical delivery area provided by the system, shown in Figure D1, is 163 m^2 (1750 ft^2). The practical protection area is further divided into an application zone and a practical protection area. The application zone is the first 8 m (25 ft) from the unit. This area must be clear of obstructions. The practical protection area is the zone between 8 m (25 ft) and 15 m (50 ft) from the nozzle. Foam is discharged onto the pad in the application zone and "pushed" into the practical protection area.

AGENT APPLICATION

The MCAFFSS unit delivers 454 L (120 gal) of pre-mix foam agent over the total delivery area of 232 m^2 (2500 ft^2). Total discharge occurs in 1.75 minutes. The application rate is 1.1 Lpm/m^2 (0.027 gpm/ft^2).

CONCEPT OF ACQUISITION

Units will be a commercially available product listed/approved by an independent third party laboratory (UL, FM, etc) to meet specific performance requirements.

Units will be purchased by the installation engineering organization. To provide an adequate number of units, two units will be required for each aircraft hangar parking position plus an additional unit for each 93 m^2 (1000 ft^2) portion of aircraft shadow area over 139 m^2 (1500 ft^2). The installation will also require 10% spare units rounded to the next whole number, to support scheduled maintenance and repairs.

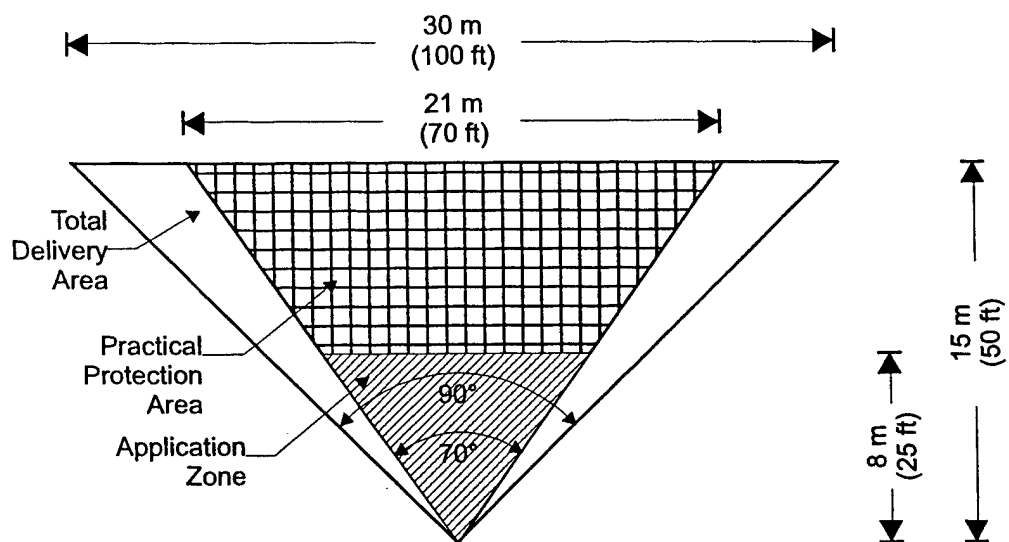


Fig. D1 — MCAFFSS conceptual protection area

CONCEPT OF MAINTENANCE

Maintenance including repair and re-servicing will be accomplished by the base engineering organization in the same manner as portable and flightline fire extinguishers.

Since the unit includes 12 volt automotive batteries on base extinguisher maintenance shops will have to be modified for the safe storage and handling of acid filled batteries including the provision of emergency showers and eye wash stations.

The only special tools required will include:

Floor jacks and stands to permit the replacement of deflated tires and damaged axles.

Nitrogen bottle lift to load and remove the bottle from the unit. The bottles are handled in a vertical configuration and carried on the unit in a horizontal configuration.

Special maintenance such as hydrostatic testing of the main tank (pressure vessel) will be accomplished by an outside contractor.

CONCEPT OF OPERATIONS

The installation fire protection flight will provide annual training to all aircraft hangar maintenance personnel on the positioning, operator maintenance, and manual operation of these units.

The installation fire protection flight and aircraft maintenance personnel must jointly develop a location plan for each aircraft parking position in the hangar.

The installation engineering activity must mark the hangar floor with unit positioning markings for each aircraft parking position. The application zone discharge area must be marked on the floor to prevent obstruction in this critical area.

The installation fire protection flight will deliver the required units to each hangar and provide replacement units when notified by maintenance control of an inoperative unit.

The aircraft maintenance personnel will position the units based on the aircraft serviced.

Move units for each aircraft movement including adjacent units if necessary.

The aircraft maintenance personnel will conduct the daily and operator maintenance on the unit.

Daily - test all units for adequate battery power.

Daily - check nitrogen cylinder pressure.

Daily - inspect unit for damage and/or liquid leaks.

Bi-weekly - move each unit to a safe area, outside the hangar classified electrical area, and re-charge the on-board battery.

The only special tools required by the aircraft maintenance activity are extension cords for recharging the units.